Precision Synthesis of Acrylic Block Copolymers from Neoteric Lactic Acid-Based Solvents and Other Renewable Chemicals

Nabil Bensabeh

UNIVERSITAT ROVIRA i VIRGILI

Precision Synthesis of Acrylic Block Copolymers from Neoteric Lactic Acid-Based Solvents and Other Renewable Chemicals

---

NABIL BENSABEH

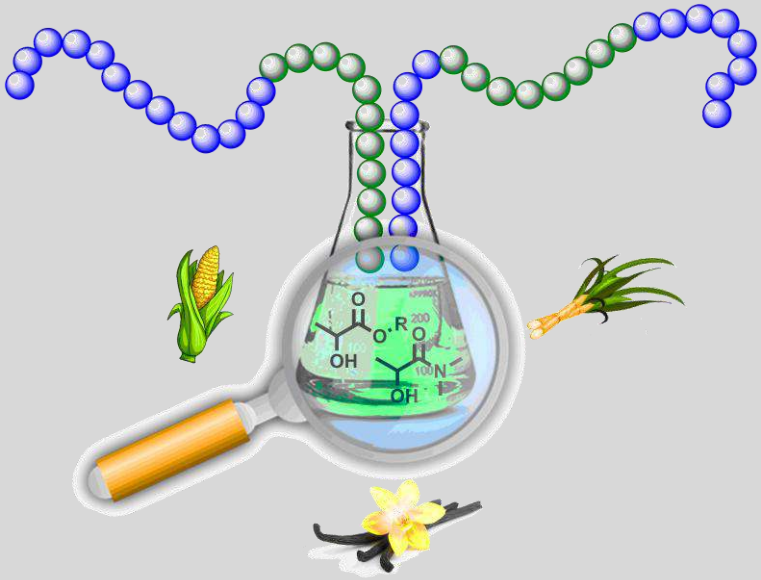

DOCTORAL THESIS
2020

Nabil Bensabeh

Precision Synthesis of Acrylic Block Copolymers from Neoteric Lactic Acid-Based Solvents and Other Renewable Chemicals

PhD-Thesis

Supervised by Dr. Gerard Lligadas Puig

Departament de Química Analítica i Química Orgànica

UNIVERSITAT ROVIRA i VIRGILI

TARRAGONA

November 2020

UNIVERSITAT ROVIRA i VIRGILI

Dr. GERARD LLIGADAS PUIG, Professor Agregat del Departament de Química Analítica i Química Orgànica de la Facultat de Química de la Universitat Rovira i Virgili

FA CONSTAR:

Que aquest treball, titulat "Precision Synthesis of Acrylic Block Copolymers from Neoteric Lactic Acid-Based Solvents and Other Renewable Chemicals", que presenta NABIL BENSABEH per l'obtenció del títol de Doctor, ha estat realitzat sota la meva direcció al Departament de Química Analítica i Orgànica de la Universitat Rovira i Virgili.

Tarragona, novembre de 2020

Gerard Lligadas Puig - DNI 14268536A (AUT)

Firmado digitalmente por Gerard Lligadas Puig - DNI 14268536A (AUT)
Fecha: 2020.12.04 17:14:12 +01'00'

Dr. Gerard Lligadas Puig

Table of contents

Table of contents

Acknowledgements

Parece mentira pero ya ha llegado el momento de terminar una etapa especial que parecía que había empezado justo ayer pero que en realidad han pasado unos cuantos años desde ese momento. Por ello, me gustaría empezar escribiendo las primeras líneas de esta tesis para agradecer el especial papel que tuvieron ciertas personas e instituciones para hacer posible la realización de esta tesis doctoral y que seguramente sin su ayuda no hubiera sido posible realizarla.

Primeramente, quiero empezar agradeciendo a la Universitat Rovira i Virgili por haberme concedido la beca que sin la cual no hubiera llegado hasta este momento tan especial.

En segundo lugar, me gustaría agradecer el gran esfuerzo, paciencia y dedicación recibidos por parte de mi director de tesis, el Dr. Gerard Lligadas. De hecho, gracias a su orientación, consejos y sobretodo sus decisiones de cambiar de estrategias en los momentos en los que más ayuda necesitaba y en los que la química me daba las espaldas, he podido salir adelante consiguiendo resultados satisfactorios. Así que, gracias otra vez Gerard, sin tu ayuda esta tesis no hubiese tenido lugar. Por otra parte, tampoco me olvido de los muy buenos consejos y predisposición de ayudar de los profesores Joan Carlos Ronda, Virginia Cádiz y Marina Galià, y sobre todo por haberme abierto las manos y acogido en su grupo para realizar el trabajo final de grado, posteriormente el de máster y cómo no para realizar esta tesis doctoral. De hecho, echo bastante de menos las diferentes estrategias "innovadoras" diseñadas por ti Ronda utilizando cartuchos de cartón llenos de tamices moleculares cogidos con clavos, de las que por cierto aprendí bastante durante la realización del trabajo final de máster, para intentar eliminar el agua generada durante las malditas reacciones de policondensación. Definitivamente, fue una muy buena experiencia. Muchas gracias Ronda por todos tus esfuerzos y por tu predisposición para resolver los problemas que iba teniendo durante todos estos años. También quiero terminar mis agradecimientos hacia la Prof. Virginia Cádiz por su esfuerzo y dedicación también realizados durante esas tardes que parecían interminables para corregir el trabajo final de máster y a la Prof. Marina Galià por

Acknowledgements

sus consejos constructivos durante los group meatings y también por su predisposición de ayudar en cualquier momento.

También quiero agradecer a todo el personal de la universidad, tanto profesores como técnicos como los diferentes secretarios de los edificios N4, N5 i SRCiT que en algún que otro momento me dieron alguna que otra ayuda. Entre los cuales, quiero dar un especial agradecimiento al Jaume Capdevila, nuestro informático y experto en generar etiquetas de libretas de laboratorio, muchas gracias Jaume por todo el trato que tuviste conmigo y por las sonrisas que nos sacabas a todos en general cuando pasabas por el laboratorio. También quiero dar las gracias a Teresa por su responsabilidad y siempre predisposición de ayudar en cualquier momento así como la buena música que repartía esas mañanas de prácticas de laboratorio, que la verdad se agradecía muchísimo porque generaba un agradable ambiente de trabajo y hacia muy amenas las prácticas. Por otra parte, también quiero dar las gracias a Juan Luis por intentar ayudarme cuando se lo pedía y a la Raquel por ofrecerme una solución infalible cuando necesitaba algún que otro reactivo o disolvente. En cuanto a los técnicos del edificio SRCiT quiero dar también las gracias a Ramón por su profesionalidad y por la resolución de todos los problemas relacionados con RMN. Muchas gracias Ramón por tu trato. Por otra parte tampoco me olvido de Sònia y Irene por su ayuda durante los análisis de masas y tampoco a Carmen por su ayuda cuando intentábamos reanimar de cualquier forma un MALDI-TOF que se veía desde hace muchísimo tiempo que estaba ya en sus últimos momentos de vida. Muchas gracias de nuevo a todos.

I would also express my gratitude to Prof. Virgil Percec's lab from University of Pennsylvania, for all the collaborations we have performed together during these last years. Similarly, my thanks also go to Prof. Steven Howdle from University of Nottingham, Prof. Cesar Rodriguez-Emmenegger from the institute of Technical and Macromolecular Materials (Germany), Prof. Lauri Vares from the Institute of Technology (Estonia) and finally to Olga Abian from Universidad de Zaragoza for their contributions made during this doctoral thesis.

También a mis compañeros de grado y máster (Khalid, Bilal, Alex, Marc, Ester,...) por haber sido excelentes compañeros dignos de recordar y generalmente por haberse cruzado en mi camino durante estos últimos años. Muchas gracias a todos y os deseo todo lo mejor para el futuro.

Por otra parte quiero también agradecer a mis compañeros del laboratorio de azúcares (Albert, Miguel, Isabel, Jordi, Pablo,...) y del laboratorio de polímeros (Adrià (tet), Federico, Franscesco, Daylin,...) por las sonrisas que me sacabais cuando nos encontrábamos tanto en los pasillos como en los laboratorios, así como por los consejos, reactivos y alguna que otra cena que hemos compartido durante estos últimos años.

Ha llegado el momento también de agradecer a toda la gente que ha pasado por los lab. 326/327 y que gracias a su presencia en el lab. hicieron que mi trabajo del día a día fuese bastante más ameno: Ivan, Diego, Lorena... gracias por todos los momentos compartidos. Un especial èmfasis per al meu tet l'Adrià, moltes gracies company per haver-me fet riure tant i per haver compartit jornades llargues de treball durant la realització del teu treball experimental de màster. Et desitjo tot el millor per la teva nova etapa com a estudiant de doctorat. A ti también Pere, muchas gracias por haber sido un compañero responsable, profesional y sobre todo por los consejos y por haber-me ofrecido toda ayuda que necesitaba, te deseo todo lo mejor y toda la suerte en estos últimos días como estudiante de doctorado. Y qué decirte a ti mi querido Aaroncillo, la verdad es que has sido un compañero ejemplar a lo largo de todo este tiempo que hemos coincidido juntos, has sido siempre mi primera opción para resolver mis problemas del laboratorio, sobretodo los informáticos, ya sabes yo y la informática nos entendemos mucho, aunque el problema sea muy fácil de resolver... En fin muchas gracias por todo lo que has hecho por mí y por aguantarme este tiempo, te deseo a ti también todo lo mejor y toda la suerte para afrontar la recta final del PhD, seguro que conseguirás sacarlo todo adelante, todo comienzo tiene un fin. A ti Adrian, decirte que ha sido un placer enorme compartir contigo laboratorio y sobretodo cortar cobre juntos para afrontar las onadas de experimentos que el tet Percec nos enviaba desde

Acknowledgements

el otro lado del charco para reproducir sus experimentos. Sólo decirte que muchas gracias por todo los consejos y generalmente por todo lo que hemos compartidos juntos durante tu estada en Suspol. Y finalmente a ti mi querida Carmen, muchas gracias por haberme asentado como mentora en la nave Suspol durante mi trabajo final de grado y también por compartir muy buenos momentos durante tu estada en el grupo. Tu alegría contagiaba a los demás y eso lo agradecíamos mucho todos los que estábamos cerca de ti. Muchas gracias por todo Carmen.

Finalmente, para terminar me gustaría dedicar un especial agradecimiento hacia unas personas que jugaron un papel enorme a lo lardo de toda mi carrera académica, y que sin su apoyo no hubiera sido capaz de llegar hasta donde estoy, me refiero a mis padres y mis hermanos. Toda la paciencia y la perseverancia que mostré estos últimos años ha sido gracias a ellos y que sin su apoyo no hubiera llegado tan lejos en mis estudios. Muchas gracias por todo lo que habéis hecho por mi.

"As a drop of oil on the sea, you must float,
using intellect and compassion to ride the waves."
-Joseph Campbell-

Abstract

This doctoral thesis focuses on the field of vinyl polymers, a class of polymers that represents approximately more than half of the industrial polymer production. The synthetic approach to this type of materials used in this work has been the use of controlled/living radical polymerization techniques, since they allow to control the molecular weight, the chain-end groups and the architecture of the resulting polymers. In particular, the polymerization methodologies that have been used during this doctoral thesis are SET-LRP (single electron transfer-living radical polymerization), RAFT (reversible addition fragmentation chain transfer) polymerization, and Cu(II)Br_2-mediated photo-initiated polymerization.

Due to the growing environmental concern in modern society, in recent years efforts have been intensified to develop polymer materials derived from renewable raw materials. In order to prepare materials with high-added value, the first part of the thesis focuses on the preparation of block copolymers from vinyl monomers derived from commercial bio-available green solvents such as alkyl lactates (e.g. ethyl and butyl lactate) and *N,N*-dimethyl lactamide. These monomers have been combined with other biobased monomers to prepare AB and ABA block copolymers made up of segments of different nature (e.g. hard/soft or water-soluble/water-insoluble). Specifically, they have been designed and prepared as follows;

(i) Amphiphilic AB polymers capable to self-assemble in water to form micelles or vesicles, depending on their composition.

(ii) ABA polymers with a soft central block and hard end blocks capable to behave as thermoplastic elastomeric materials.

Some of the prepared block copolymers have been shown to have potential technological applications. For example, ABA block copolymers prepared by RAFT polymerization technique from vinyl monomers derived from butyl lactate (soft block) and vanillin or isosorbide (hard block) proved to be competitive pressure sensitive adhesives (PSA), with properties comparable to commercial adhesive tapes. On the other hand, SET-LRP

Abstract

amphiphilic AB block copolymers prepared from vinyl monomers derived from ethyl lactate (hydrophobic block) and glycerol (hydrophilic block), were able to self-assemble into micellar nanostructures capable of solubilising hydrophobic compounds in water. Similarly, it has been shown that amphiphilic AB copolymers prepared through the photopolymerization of vinyl monomers derived from ethyl lactate (hydrophobic block) and *N,N*-dimethyl lactamide (hydrophilic block) can self-assemble into spherical and cylindrical micelles, or vesicles depending on their composition. These micellar systems have been used as nanoreactors to carry out radical emulsion polymerization of industrially relevant monomers such as styrene and methyl methacrylate.

There is no doubt that the popularity of SET-LRP technique has increased considerably during the last decade due to its proven versatility, robustness and efficiency in the preparation of vinyl polymers. It is well-known that a special importance is taken to the role of the solvent and the ligand in the mechanistic aspects of this type of radical polymerization reactions, since they are responsible for promoting the disproportionation of Cu(I)X into Cu(0) (activator) and Cu(II)X_2 (deactivator), and thus ensure the control of radical polymerization by establishing a dynamic balance between the active and dormant polymer chains. The key disproportionation step is favoured in the presence of certain nitrogen-based ligands (generally Me_6-TREN and TREN) and polar solvents (e.g. water, alcohols, DMSO,...). In this context, in the second part of this doctoral thesis, the effect of a "mixed-ligand" system (Me_6-TREN/TREN) during the SET-LRP of methyl acrylate in homogeneous and "programmed" biphasic systems has been studied. The statistical analysis of the kinetic data, together with the control/model experiments, showed that the use of this mixture of ligands accelerates the rate of reaction, increases the monomer conversion, and improves the control over the molecular weight of the final polymer. The greatest effect was observed at a molar ratio of 1/1 Me_6-TREN/TREN, which suggests that, in addition to a rapid exchange between both ligands, a new and unique dynamic ligand generated by hydrogen bonds between them may be responsible for these results.

List of publications

Papers published from the research work presented in this thesis:

1. **Bensabeh, N.** ; Ronda, J. C.; Galià, M.; Cádiz, V.; Lligadas, G. and Percec, V. *Biomacromolecules* **2018**, *19*, 1256-1268.

2. **Bensabeh, N.**; Moreno, A.; Roig, A.; Monaghan, O. R.; Ronda, J. C.; Cádiz, V.; Galià, M.; Howdle, S. M.; Lligadas, G. and Percec, V. *Biomacromolecules* **2019**, *20*, 2135-2147.

3. **Bensabeh, N.**; Moreno, A.; Roig, A.; Rahimzadeh, M.; Rahimi, K.; Ronda, J. C.; Cádiz, V.; Galià, M.; Percec, V.; Rodriguez-Emmenegger, C. and Lligadas, G. *ACS Sustainable Chem. Eng.* **2020**, *8*, 1276-1284.

4. Maurya, D. S.; Malik, A.; Feng, X.; **Bensabeh, N.**; Lligadas, G. and Percec, V. *Biomacromolecules* **2020**, *21*, 1902-1919.

5. Feng, X.; Maurya, D. S.; **Bensabeh, N.**; Moreno, A.; Oh, T.; Luo, Y.; Lejnieks, J.; Galià, M.; Miura, Y.; Monteiro, M. J.; Lligadas, G.; Percec, V. *Biomacromolecules* **2020**, *21*, 250-261.

6. **Bensabeh, N.**; Jiménez-Alesanco, A.; Liblikas, I.; Ronda, J. C.; Cádiz, V.; Galià, M.; Vares, L.; Abian, O.; Lligadas, G. *Molecules* **2020**, *25*, 5740.

Thesis outline

The main goal of this PhD research was the development of AB and ABA acrylic block copolymers based on abundant renewable chemicals to use in high value-added applications, e.g. stabilizers in emulsion polymerization and pressure sensitive adhesives. The present document is organized in five chapters:

- **Chapter 1** provides a general overview covering the significance of controlled/living radical polymerization techniques to synthesize tailor-made vinyl (co)polymers. Special focus is given to single electron transfer-living radical polymerization (SET-LRP). The second part of this chapter emphasizes the importance of biobased vinylic monomers as necessary components for sustainable ABA-type thermoplastic elastomers and amphiphilic block copolymers.

- **Chapter 2** is focused on the design and synthesis of block copolymers derived from alkyl lactate- and lactamide-type solvents. Cu(0)-mediated SET-LRP, Cu(II)Br_2-mediated radical photopolymerization, and reversible addition-fragmentation chain transfer (RAFT) polymerization are examined to afford well-defined lactic acid-derived block copolymers using other vinylic compounds prepared from isosorbide, glycerol, α-pinene, and vanillin as a comonomers. The properties of some of the obtained block copolymers are evaluated as precursors of nanoparticles, stabilizers in emulsion polymerization, and pressure sensitive adhesives.

- **Chapter 3** reports the use of SET-LRP to control the radical polymerization of the hydrophobic (-)-menthyl acrylate in alcoholic solvents at room temperature. The study uses a combination of characterization techniques that include GPC, ^{1}H-NMR, MALDI-TOF MS before and after thioetherification of bromine terminus *via* "thio-bromo" click chemistry, and *in situ* reinitiation copolymerization experiments to demonstrate the near perfect chain end functionality of the synthesized hydrophobic polymers and evaluate their block copolymerization with model monomers.

Thesis outline

- **Chapter 4** deepens on kinetic studies to investigate the role of Me_6-TREN/TREN "mixed-ligand" systems on the SET-LRP of methyl acrylate in "programmed" biphasic reaction mixtures based on aqueous mixtures of the dipolar aprotic solvents such as NMP, DMF, and DMAc as well as in homogeneous systems with DMSO.

- **Chapter 5** presents the most relevant conclusions from this work.

List of acronyms

4BrPr	pentaerythritol tetrakis(2-bromopropionate)
ALA	alkyl lactate acrylate
AIBN	2,2'-azobisisobutyronitrile
AM	acrylamide
AN	acrylonitrile
APC	2-acryloyloxyethyl phosphorylchlorine
ARGET-ATRP	activator regenerated by electron transfer ATRP
ATR	attenuated total reflectance
ATRP	atom-transfer radical polymerization
n-BA	n-butyl acrylate
BCPs	block copolymers
Bypi	2,2'-bypiridine
Bis(EBiB)	ethylene bis(2-bromoisobutyrate)
BL	butyl lactate
BLA	butyl lactate acrylate
BMA	n-butyl methacrylate
BPE	bis(2-bromopropionyl)ethane
BPO	benzoyl peroxide
BTCBA	3,5-Bis(2-dodecylthiocarbonothioylthio-1-oxopropoxy)benzoic acid
C	concentration
CAC	critical aggregation concentration
CBMAAM	(3-methacryloylamino-propyl)-(2-carboxy-ethyl)dimethylammonium
CCD	charge-coupled device
CD	circular dichroism

List of acronyms

$CHBr_3$	bromoform
$CHCl_3$	chloroform
CHI_3	iodoform
CMC	critical micellar concentration
CRP	controlled radical polymerization
CTA	chain transfer agent
Da	Dalton
D1	delay time
DAD	diode-array detection
DCC	dicyclohexylcarbodiimide
DCAP	2,2-dichloroacetophenone
DCM	dicloromethane
DCTB	trans-2-[3-(4-tert-butylphenyl)-2- methyl-2-propenylidene]malononitril
DEGEEA	di(ethylene glycol) 2-ethylhexyl ether acrylate
DEGMEMA	di-(ethylene glycol)methyl ether methacrylate
d_H	hydrodynamic diameter
diNBpy	4,4'-dinonyl-2,2'-bipiridine
DLS	dynamic light scattering
DMA	*N,N*-dimethyl acrylamide
DMAc	dimethylacetamide
DMAEA	*N,N*-dimethylaminoethyl acrylate
DMF	dimethylformamide
DML	*N,N*-dimethyl lactamide
DMLA	*N,N*-dimethyl lactamide acrylate
DMSO	dimethyl sulfoxide

DMTA	dynamic mechanical thermal analysis
DP	degree of polymerization
DTPA	2-(dodecylthiocarbonothioylthio) propionic acid
DSC	differential scanning calorimetry
EA	ethyl acrylate
e-ATRP	electrochemical ATRP
EBiB	ethyl α-bromoisobutyrate
EC	ethylene carbonate
EDC	*N*-(3-dimethylaminopropyl)-*N'*-ethylcarbodiimide
EHA	2-ethylhexyl acrylate
EL	ethyl lactate
ELA	ethyl lactate acrylate
EMA	ethyl methacrylate
EtOH	ethanol
ESI	electrospray ionization
f	chain end functionality
FRP	free radical polymerization
FTIR	fourier-transform infrared spectroscopy
GA	glycerol acrylate
GBLMA	γ-butyrolactone methacrylate
GPC	gel permeation chromatography
HDPE	high-density polyethylene
HEA	2-hydroxyethyl acrylate
HEAGI	2-[(D-glycosamin-2-*N*-yl)carbonil] oxyethyl acrylate
HPLC	high performance liquid chromatography

List of acronyms

HMTETA	1,1,4,7,10,10-hexamethyltriethylenetetramine
HRMS	high resolution mass spectrometry
IA	isosorbide acetate acrylate
ICAR-ATRP	initiators for continuous activator regeneration ATRP
I_{eff}	initiator efficiency
ImPAA	*N*-(3-(1*H*-imidazole-1-yl)-propyl) acrylamide
ISET	inner-sphere electron transfer
IUPAC	International Union of Pure and Applied Chemistry
K_{act}	activation constant
K_{deact}	deactivation constant
K_d	dissociation rate constant
K_{disp}	disproportionation constant
KFTA	potassium trifluoroacetate
K_i	initiation rate constant
K_p	propagation rate constant
K_{tc}	termination by combination rate constant
K_{td}	termination by disproportionation transfer rate constant
K_{tr}	termination by chain transfer rate constant
L	ligand
LAMs	low-activates monomers
LAP	living anionic polymerization
LA	lactic acid
LCMs	large compound micelles
LDPE	low-density polyethylene
LP	living polymerization

LRP	living radical polymerization
M	monomer
MA	methyl acrylate
ML	methyl lactate
MLA	methyl lactate acrylate
MS	mass spectrometry
MAETC	[2-(methacryloxy)ethyl]-trimethylammonium chloride
MALDI	matrix-laser assisted laser desorption/ionization
MAMs	more-activate monomers
MAMA	methyl adamantly methacrylate
MBP	methyl 2-bromopropionate
MCP	methyl-2-chloropropionate
MeCN	acetonitrile
MeOH	methanol
Me-THF	2-methyltetrahydrofuran
Me_6-TREN	tris[2-(dimethylamino)ethyl]amine
MMA	methyl methacrylate
M_n	number-averaged molecular weight
MnA	menthyl acrylate
M(th)	theoretical molecular weight
M_w	weight-averaged molecular weight
MW	molecular weight
MWD	molecular weight distribution
$NaBH_4$	sodium borohydride
NAM	*N*-acryloylmorpholine

List of acronyms

NIPAM	*N*-isopropylacrylamide
Mt	transition metal
NMP	nitroxide mediated polymerization
NMR	nuclear magnetic resonance
NR	nile red
nt	number of scans
NVC	*N*-vinylcarbazole
NVP	*N*-vinylpyrrolidone
OA	octadecyl acrylate
O-ATRP	organic-activated photo-catalyst ATRP
OEOMA	oligo(ethylene oxide) monomethyl ether methacrylate
OEGMEMA	oligo (ethylene glycol) methyl ether methacrylate
OEGMEA	oligo(ethylene oxide) methyl ether acrylate
OFPA	1*H*,1*H*,5*H*-octafluoropentyl acrylate
OFPMA	1*H*,1*H*,5*H*-octafluoropentyl methacrylate
$(OH)_2$EBiB	ethane-1,2-diyl bis(2-bromo-2-methylpropanoate)
OiBBrLac	octa-O-isobutyrylbromide lactose
OSET	outer-sphere electron transfer
PA	α-pinene acrylate
PAN	polyacrylonitrile
PBA	poly (butyl acrylate)
PC	propylene carbonate
PDI	polydispersity index
PDMLA	poly(*N*,*N*-dimethyllactamide acrylate)
PEG	poly(ethylene glycol)

List of acronyms

PELA	poly(ethyl lactate acrylate)
PEI	poly(ethylenimine)
PET	polyethylene terephthalate
PEG-BEBiB	poly(ethylene glycol) bis(2-bromoisobutyrate)
PiBBrGlu	2,3,4,6-penta-O-isobutyryl bromide-α-D-glucose
PISA	polymerization-induced self-assembly
PLA	poly(lactic acid)
PMDETA	*N,N,N',N'',N''*-pentamethyldiethylenetriamine
PMA	poly(methyl acrylate)
PMMA	poly(methyl methacrylate)
Photo-ATRP	photochemical-ATRP
PP	polypropylene
PRE	persistent radical effect
2-PrOH	propan-2-ol
PSt	polystyrene
PVC	polyvinyl chloride
RAFT	reversible addition-fragmentation chain transfer polymerization
RDRP	reversible deactivation radical polymerization
RP	radical polymerization
R_p	polymerization rate
SA	solketal acrylate
SARA-ATRP	supplemental activator and reducing agent ATRP
SET	single electron transfer
SET-DTLRP	single electron transfer-degenerative living radical polymerization
SET-LRP	single electron transfer-living radical polymerization

List of acronyms

SFC	supercritical fluid chromatography
SFRP	stable free radical polymerization
SPMA	1'-(2-methacryloxyethyl)-3',3'-dimethyl-6-nitrospiro-(2H-1-benzopyran2,2')-indoline
St	styrene
$T_{5\%}$	temperature corresponding to the 5% weight loss from TGA
TEA	triethylamine
TEGMEMA	tri(ethylene glycol) methyl ether methacrylate
TEM	transmission electron microscopy
TEMPO	2,2,6,6-tetramethylpiperidinyl-1-oxy
tert-BA	*tert*-butyl acrylate
TFE	2,2,2-trifluoroethanol
$T_3P^{®}$	propylphosphonic anhydride solution
TFP	2,2,3,3-tetrafluoropropanol
T_g	glass transition temperature
TGA	thermogravimetric analysis
THF	tetrahydrofurane
Tmax	maximum weight loss temperature from TGA
TOF	time of flight
TPE	thermoplastic elastomer
TREN	tris(2-aminoethyl)amine
USFDA	United States Food and Drug Administration
UV	ultraviolet
VAc	vinyl acetate
VC	vinyl chloride

Motivation, targets and research significance

Over the last decades, dwindling petrochemical resources and an increasing environmental awareness have motivated the interest for polymer materials based on renewable resources. Controlled/living radical polymerization (RP) is nowadays a powerful tool for preparing tailor-made block copolymers (BCPs) composed of immiscible segments. The possibility to tune monomer composition, polymer molecular weight, and the segment sequence enables the preparation of well-defined nanostructures for a broad range of advanced applications. ABA-type triblock copolymers are one of the very useful examples of this structural tuning because some of these systems are commercialized for many applications as thermoplastic elastomers (TPE). In the same vein, self-assembled nanostructures based on amphiphilic BCPs have been proposed as an interesting approach for the development of advanced drug delivery systems and stabilizers in emulsion polymerization processes.

In this context, the main goal of this PhD thesis was the development of high value-added acrylic BCPs based on abundant bio-available chemicals. The research work was focused on AB and ABA BCPs prepared from vinyl monomers derived from L-lactic acid, L-menthol, isosorbide, α-pinene, glycerol and vanillin, using controlled/living RP processes, such as single electron transfer-living radical polymerization (SET-LRP), copper-catalyzed photoinduced RP, and reversible addition-fragmentation chain transfer (RAFT) polymerization. Among them, special attention has been paid to Cu(0)-catalyzed SET-LRP because it is one of the most facile and versatile systems in terms of its simple reaction set-up, wide monomer scope and sustainability, among the various controls/radical RP systems. At the same time, it was intended to contribute to the development of this technique by investigating “mixed-ligand” effects on model SET-LRP polymerization reactions.

It is expected that this work can contribute to the *novo* design and generation of new families of sustainable BCPs for developing green and functional polymeric materials.

Chapter 1

Introduction

1.1. The importance of radical polymerization in our daily life

Polymers are very large molecules than can be considered giants in the molecular world. They consist of small repeating building blocks, i.e. monomers, covalently joined by a process known as polymerization. Nowadays, both natural and synthetic polymers are an important part of our everyday life and can be found almost everywhere, due to their wide variety of appealing and innumerable targetable properties.[1] Hence, today's society cannot deny the great impact and influence that polymeric materials have brought. The origins of polymer science dates back to 1861, when the British chemist Thomas Graham noted sticky residues after passing through fine filter paper solutions of certain organic compounds such as cellulose.[2] At that time, Graham already thought such substances represented an entirely different class of matter. However, the spread of polymers to every aspect of the modern life was only possible after their fundamentals were laid down during 1920–1930.[3,4] Thus, the discovery of polymeric materials made from either existing natural sources, e.g. vulcanized rubber, or created entirely from chemicals, e.g. bakelite, polystyrene (PSt), polyvinyl chloride (PVC), low and high density polyethylene (LDPE and HDPE, respectively), polypropylene (PP) and polyethylene terephthalate (PET) among others, were crucial steps toward commercialization of polymers, which are commonly called “plastics”. The industrial production of plastic, elastic and also highly cross-linked and hard thermosetting polymers has not stopped growing since 1950s due to their implication on different applications such as clothing made by synthetic fibers, packaging films, blow-molded bottles, adhesives, polymer-based paints, plastic bags, foams, among many others (Figure 1.1a).[5,6] In fact, the production of polymers has increased considerably from just under 1 megatone in 1950 to more than 300 megatons during last years (Figure 1.1b).[7-9] Accordingly, some of the commercial polymeric products are known as "commodity polymers" due to their low cost high production volumes, unbelievable usefulness and versatility, and most importantly because they represent more than ninety percent of the worldwide polymeric material's consumption.[9]

Introduction

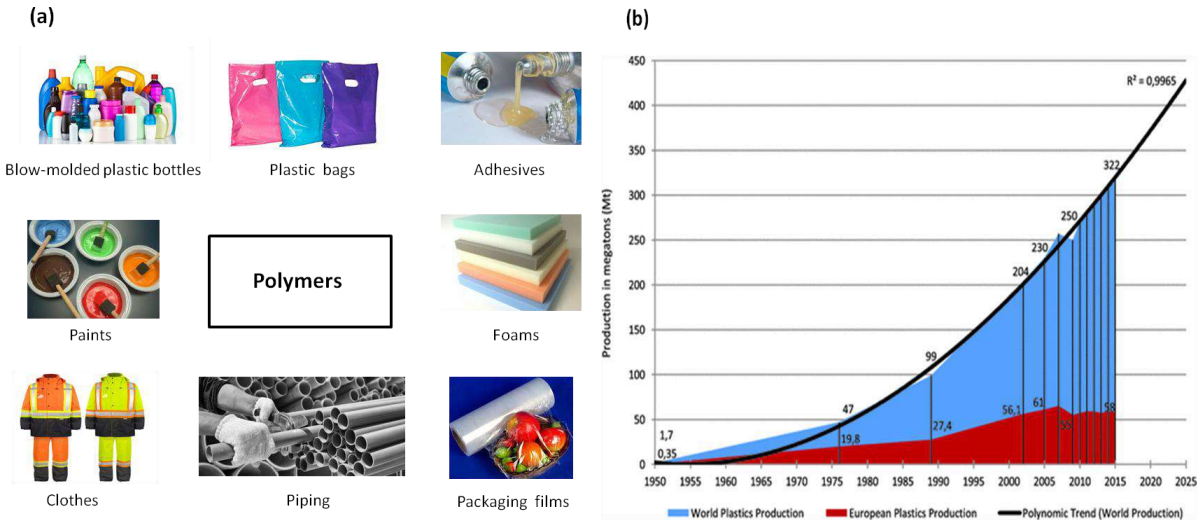

Figure 1.1. (a) Representative examples of polymer-based products used in daily applications and (b) graphical evolution of polymer production from 1950 to early years (adapted from Ref. 9).

However, it is worth to mention that roughly half of all currently produced industrial polymers are prepared by a radical polymerization (RP) process by which the polymer grows by the successive addition of free-radical building blocks. Monomers readily susceptible to polymerize by RP are those containing unsaturated homo or heteronuclear double bonds, dienes, trienes, strained cycloaliphatics, *exo*-methylene-substituted cyclic compounds, or vinylcyclopropanes.[10] However, the industrial gold standards are vinylic compounds where X is primarily X = H or CH_3, and Y = H, Cl, COOH, COOR, $CONH_2$, CN, $OCOCH_3$, C_6H_5, $–CH=CH_2$, which serve as precursors of the corresponding polymers (1 and 2 respectively in Scheme 1.1).

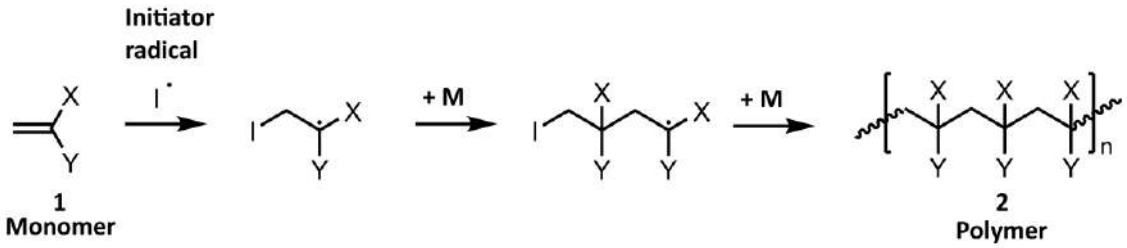

Scheme 1.1. Schematic of the RP of monomers containing C=C (1) to produce the corresponding vinyl polymers (2).

In this context, vinyl-based polymers have been the focus of intensive research over the past few decades and are attractive materials owing to their ease synthesis and their broad diversity of architectures, compositions and functionalities.[11-14] The reason for that interest is the potential of these polymers in higher-added-value and specialty applications.[11,15] Representative examples are found in the microelectronics technology, e.g. positive or negative resists, biomaterials industry, e.g. drug delivery nanocarriers, tissue engineering scaffolds and hydrogels, and adhesive businesses, e.g. hot-melts.[13] However, most of these advanced applications require accessing to vinyl homopolymers with predetermined molar mass, narrow molecular weight distribution (MWD), and high chain-end fidelity or other precisely designed molecular architectures based on block, comb, or star copolymers.[16] However, unfortunately the classic free RP (FRP) technique does not enable such level of efficient macromolecular engineering as will be discussed in the following subchapter.

1.2. Free *versus* living/controlled radical polymerization

Since the pioneer studies of Flory related to FRP in the 1930s,[17] this polymerization technique has became a powerful synthetic tool for the production of industrial polymeric materials such as PSt, poly(methyl methacrylate) (PMMA), and PVC. These and many other vinylic polymers have improved substantially the lives of millions of people. From an industrial point of view, high molecular weight polymers could be obtained by FRP conducted in different media, under relatively undemanding conditions, and without any further purification treatments of the corresponding reactants or solvents.[18-20] FRP mechanistic framework consists of three principal steps; initiation, propagation and termination (Scheme 1.2).[10] The initiation is the key step to perform a FRP process. Thermolysis, photolysis, redox reactions among others, start the homolytic dissociation of the initiator (I_2) to generate a pair of primary radicals ($I^{\bullet}$) as shown in Scheme 1.2, Eq. 1.1 where K_d is the rate constant for the initiator dissociation.

Introduction

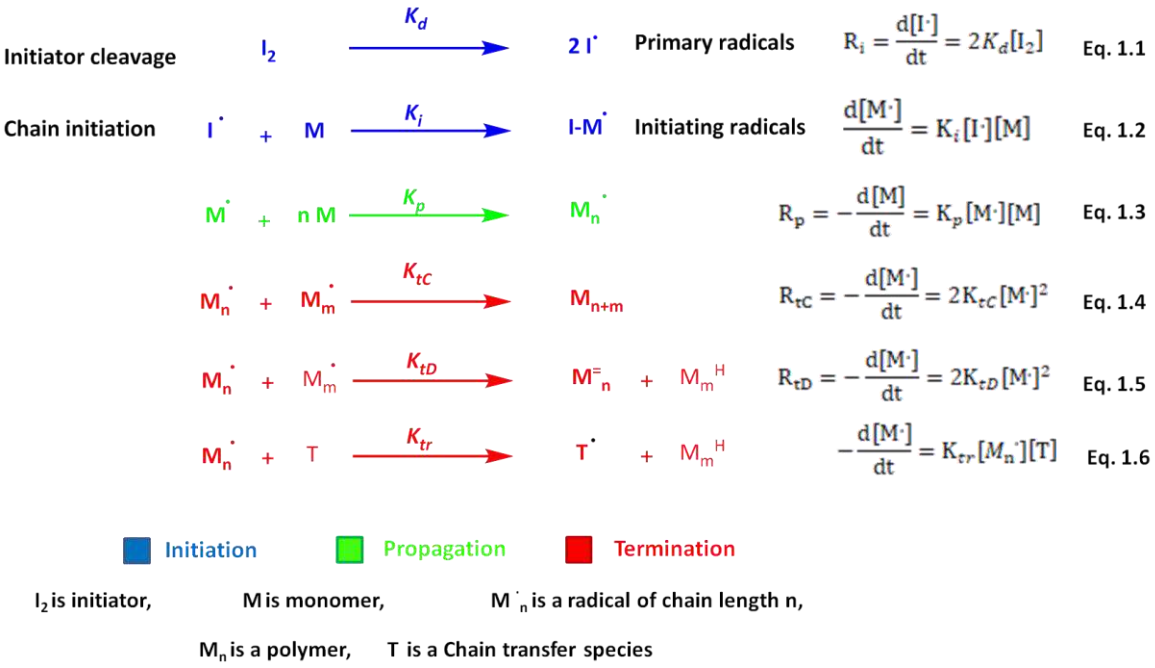

Scheme 1.2. Key mechanistic steps of FRP. Color code: blue refers to initiation, green to propagation and red to termination steps.

Then, the produced primary radicals are added to monomeric molecules (M) to achieve new free macroradical species (I-M$^{\bullet}$) as depicted in Scheme 1.2, Eq. 1.2, where K_i is the rate constant of the initiation step. The propagation step proceeds by the growth of the mentioned free macroradicals through successive additions of a large number of monomer molecules generating new radicals with the same identity as the previous one, except that is larger by one monomeric unit. Generally, the propagation process can be described as shown in Scheme 1.2, Eq. 1.3, where K_p defines the rate constant of propagation. The rate of propagation is in the range of $K_p \sim 10^2$-10^4 $M^{-1}s^{-1}$ and its magnitude depends slightly on the degree of polymerization of the macroradical, at least for the first (~10) propagation steps.[21] The rate consumption of monomer molecules during this step is known to be very fast at the beginning of the reaction due to a dramatic increase of macroradicals concentration.[22-24] Consequently, monomer concentration tends to be minimal at the late stages of the polymerization process, dramatically increasing the probability of side reactions to occur.[25] FRP finishes when the propagating polymeric chains terminate, yielding "dead" polymer

chains in a step known as termination. Termination can generally occur *via* two principal routes known as combination and disproportionation. Combination takes place when two polymeric propagating chains ($M_n^{\bullet}$ and $M_m^{\bullet}$) react with each other by combination (coupling) resulting in a neutral polymeric chains (M_{n+m}). Conversely, termination by disproportionation might occur through the migration of a proton located in *beta* position with respect a radical center to another radical center yielding two neutral polymeric chains, one saturated (M_m^{H}) and another unsaturated ($M_n^{=}$) as is depicted in Scheme 1.2, Eq. 1.4 and 1.5, where K_{tC} and K_{tD} are the rate constant of termination by combination and by disproportionation respectively. It is well-known that the FRP of vinylic monomers such as acrylates, styrene and vinyl chloride tend to terminate by combination[26] while termination by disproportionation dominates the polymerization of methacrylic systems.[27,28] Note also that macroradicals can also terminate by reactions occurring due to the presence of radical species derived from the initiator or oxygen inhibition. Radical chain transfer processes to monomer, solvent, or polymer chains are also common processes (Scheme 1.2, Eq. 1.6). In this context, although FRP enables the polymerization of a myriad of monomers up to full conversion and is useful for a number of applications,[29] uniformity of the polymer chain and control over chain ends represent important limitations when well-defined macromolecules including block copolymers (BCPs) are pursued.[30]

The living polymerization (LP) concept, introduced by Michael Szwarc in 1956 while studying the anionic polymerization of styrene (St) using alkyl lithium initiators in non-polar solvents, enables control over the polymer architecture, which includes molecular weight, MWD, functionality, and composition.[31,32] In this innovation, the initiation step is faster than propagation and therefore ideally, each initiator molecule simultaneously initiates only one polymer chain. This concept enables the elimination of transfer and termination reactions, and consequently polymer molecular weight is expected to increase linearly with time until all monomer is consumed or polymerization is intentionally terminated.[33] Although the anionic polymerization of St was the only example of a living process for more than a decade after its realization, it was subsequently extended to cationic systems.[34] However, it is worth

to mention that living ionic polymerization systems require very strict experimental requisites such as rigorously purified reagents and low temperatures (-78 °C).[35] Accordingly, they have limited application in industrial environments.[35] However, from the 1990s, new methods were developed which enabled an adaptation of the living ionic polymerization concept to living radical polymerization (LRP), also referred to as controlled radical polymerization (CRP). The more popular methodologies to achieve control over RP are: (i) nitroxide-mediated polymerization (NMP),[36] (ii) reversible addition-fragmentation chain transfer (RAFT) polymerization,[37] (iii) atom-transfer radical polymerization (ATRP)[38,39] and (iv) single electron transfer-living radical polymerization (SET-LRP).[40,41] In order to extend the lifetime of the propagating macroradicals and minimize termination processes, all these methods relies on establishing a dynamic equilibrium between active propagating chains and dormant/inactive chains, that are unable to propagate or terminate (Scheme 1.3).[42] Hence, the design concept behind these techniques is also commonly known as reversible deactivation radical polymerization (RDRP).[43]

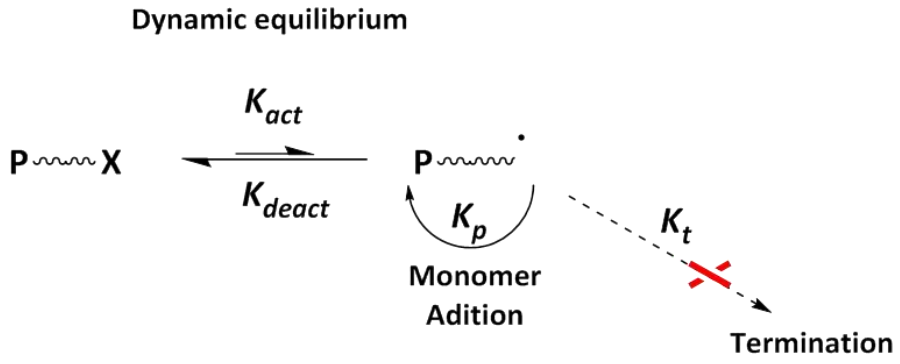

Scheme 1.3. Dynamic equilibrium between dormant and growing polymer chains established in living/controlled RP techniques.

According to the postulates of Quirk and Lee,[44] the requirements that a RP system must fulfill to be considered a living/controlled RP methodology are: (i) the polymerization proceeds until all of the monomer has been consumed and further addition of monomer results in polymerization reinitiation, (ii) the number average molecular weight (M_n) is a

linear function of conversion, (iii) the number of polymer molecules (and active centers) is constant, and independent of conversion, (iv) the molecular weight can be controlled by the stoichiometry of the reaction, and finally (v) narrow MWDs and high chain end fidelity should be accomplished to guarantee that minimal termination processes accurred during the RP.

In light of the ever-increasing breadth of this field, the following four subchapters aim to provide only a general overview of most fundamental living/controlled RP techniques, i.e. NMP, RAFT, ATRP and SET-LRP, and are not intended to be comprehensive. Nevertheless, special attention has been devoted to the SET-LRP technique because it has been used to a greater extend in this thesis.

1.2.1. Nitroxide-mediated polymerization (NMP)

The introduction of stable radicals such as arylazooxyls,[45] substituted triphenyls,[46] verdazyls,[47] triazonilyns,[48] and nitroxides[49] in the field of stable FRP (SFRP) as a radical mediators (deactivators) opened a plethora of possibilities to synthesize polymeric material in a living manner. Among them, the most studied and successful class of compounds are nitroxides and their associated alkylated derivatives, alkoxyamines. The use of nitroxides derived in the 1980s in a new living/controlled RP technique named NMP.[50] The NMP concept was first patented by Solomon and Rizzardo in 1985.[36] Originally, NMP was described as a bimolecular initiating systems using thermal initiators such as 2,2′-azobisisobutyronitrile (AIBN) or benzoyl peroxide (BPO) in combination with 2,2,6,6-tetramethylpiperidinyl-1-oxy (TEMPO), as the stable free nitroxide.[19,51] However, later on, new developments were achieved by designing alkoxyamine initiators that decompose into both the initiating radical and the nitroxide, leading to better control over the molecular weight and MWDs than bimolecular initiating systems.[52] The proposed mechanism for NMP is based on an activation-deactivation dynamic equilibrium between the growing propagating macroradical and the nitroxide, which acts as control agent, yielding macroalkoxyamine as the predominant species (Scheme 1.4).

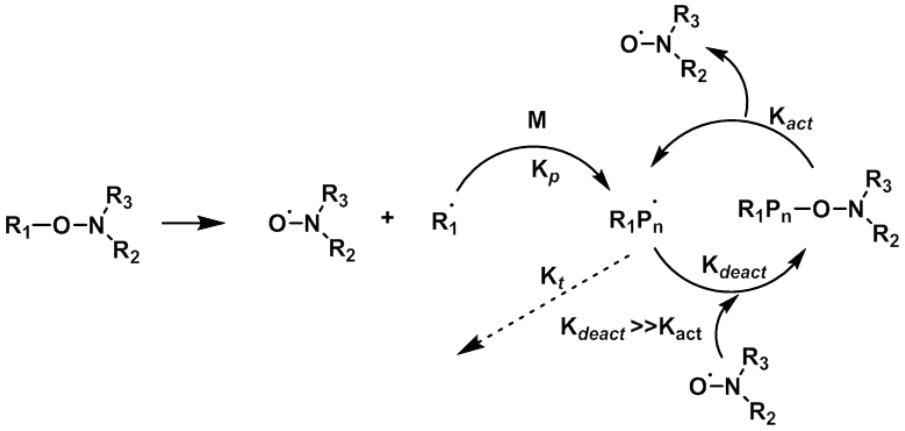

Scheme 1.4. Proposed mechanism for the activation-deactivation equilibrium established in NMP.

The nitroxide and propagating radicals are generated again by this macroalkoxyamine dormant species through a homolytic cleavage upon temperature increase, avoiding the typical termination processes characteristic of FRP. The range of monomers accessible by NMP compresses different vinylic-type building blocks such as St, acrylamides, and 4-vinylpiridine derivatives.[53] However, the limitations of this technique emerge during the polymerization of methacrylic monomers due to β-hydrogen abstraction by nitroxide. In fact, this is one of the most important drawbacks of this technique together with the mandatory use of high temperatures and long reaction times.[54]

1.2.2. Reversible addition-fragmentation chain transfer (RAFT) polymerization

RAFT polymerization is one of the more versatile methods for providing living/controlled characteristics to RP processes.[55-58] The RAFT concept was first patented by Rizzardo, Thang and Moad in 1998.[37] The key feature of this technique is the use of an appropriate thiocarbonylthio compound (RSC(Z))=S), as a chain transfer agent (CTA), to establish a sequence of addition-fragmentation equilibria (Scheme 1.5).

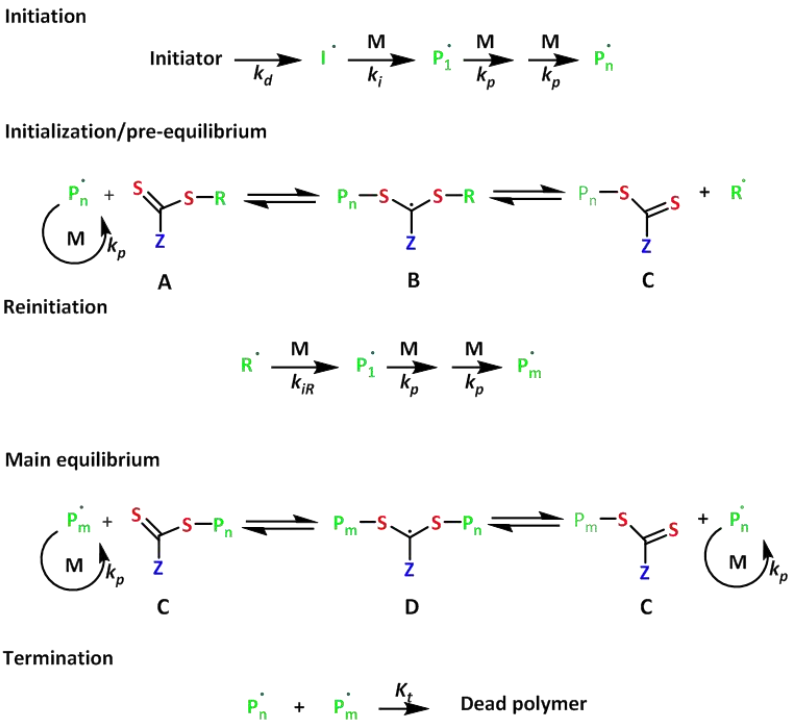

Scheme 1.5. Proposed mechanism for RAFT polymerizations.

The proposed mechanism for RAFT begins with the formation of an initiator derived radical ($I^{\bullet}$) that propagates with monomer (M) to give a polymeric radical ($P_n^{\bullet}$) (see scheme 1.5; initiation step). Next, in an ideal RAFT polymerization the polymeric radical ($P_n^{\bullet}$) reacts with a thiocarbonylthio compound (A) to obtain the intermediate (B) which fragments to quantitatively give the macro-RAFT agent (C) and radical ($R^{\bullet}$), which reinitiates the polymerization reacting with another monomer specie to give new propagating radicals ($P_m^{\bullet}$). The initialization or pre-equilibrium concludes when the original thiocarbonylthio compound (A) and radical $R^{\bullet}$ have been fully consumed. Subsequently, the system moves into the main equilibrium allowing for maximal equilibration of the growing chains, giving polymeric materials with low polydispersity.

Generally, RAFT polymerization technique encompasses a wide range of radically polymerisable monomers which normally are divided into two general classes depending on its ability to react in a free radical process: (i) "more-activated monomers" (MAMs) where

the vinylic group is conjugated to an activating functionalities such carbonyl group, e.g. (meth)acrylates, (meth)acrylamides, or aromatic groups, e.g. styrene, and (ii) "less-activated monomers" (LAMs) where the vinylic group is adjacent to an electron-rich functional group such as oxygen or nitrogen, e.g. vinyl esters or vinyl amides.[59] However, in order to obtain an optimal control over a RAFT polymerization, an appropriate thiocarbonyltio compound with the right R and Z group functionality, depending of the monomer being polymerized, is of prime importance. The nature of the Z group is directly related with the reactivity of the thiocarbonyl group toward radical addition and the rate of fragmentation of the intermediate (B) and (D) (see scheme 1.5). In fact, Z group can be modified with different reactive functionalities leading to a plethora of RAFT agent typologies such as dithioesters, trithiocarbonates, xanthates or dithiocarbamates (Figure 1.2).[60]

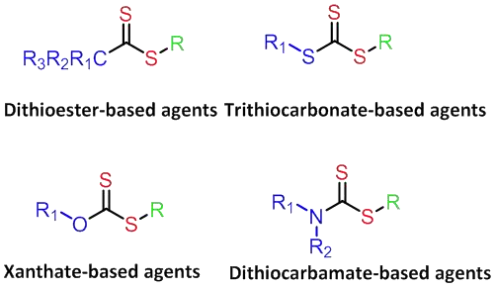

Figure 1.2. General chemical structure of conventional RAFT agents.

In this context, dithioesters and trithiocarbonates provide higher radical addition rates than xanthates and dithiocarbamates. However, electron-withdrawing substituents on Z can enhance the activity of RAFT agents and modify the above reactivity trend.[61-65] Conversely, the R group has to be a good leaving group to fragment as well as has to rapidly reinitiate propagation and ensure all chains are simultaneously initiated to obtain polymers with narrow MWD. Hence, a vast number of both activated and non-activated monomers can be polymerized in a living manner by properly choosing the appropriate R and Z groups (Scheme 1.6).

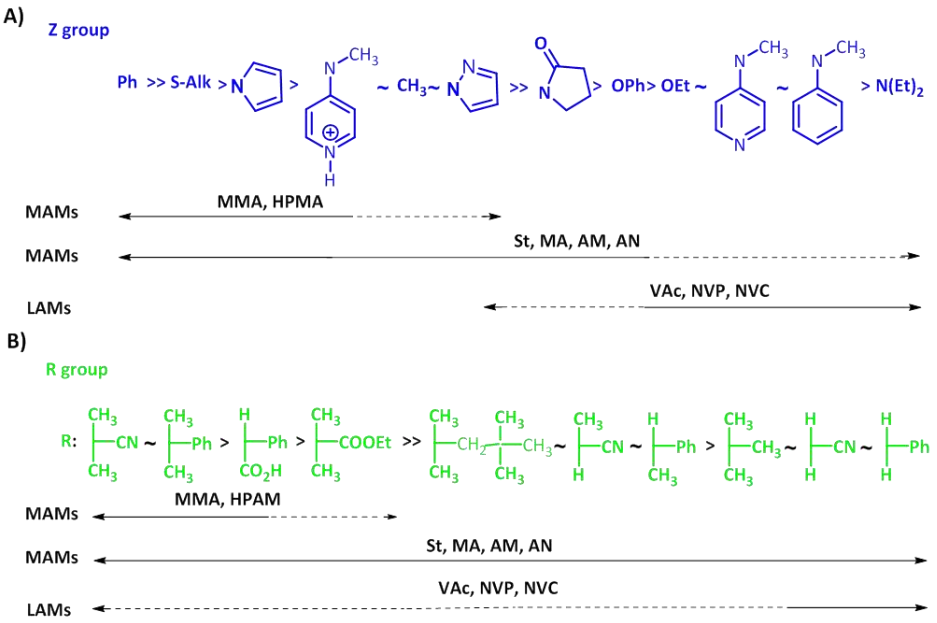

Scheme 1.6. (A) Guidelines to the proper Z-group of RAFT agents for various polymerizations [a]; (B) Guidelines to select the proper R-group of RAFT agents for various polymerizations. (Adapted from Ref 58)[b] Notes: [a] Addition rates decrease and fragmentation rates increase from left to right. A dashed line indicates partial control (i.e., control of molar mass but poor control over dispersity or substantial retardation in the case of LAMs such as VAc or NVP). [b] Fragmentation rates decrease from left to right. A dashed line indicates partial control (i.e., control of molar mass but poor control over dispersity or substantial retardation in the case of VAc, NVC, or NVP). Abbreviations: MMA = methyl methacrylate, HPMA = N-(2-hydroxypropyl)methacrylamide, St = styrene, MA = methyl acrylate, AM = acrylamide, AN = acrylonitrile, VAc = vinyl acetate, NVP =N-vinylpyrrolidone, and NVC = N-vinylcarbazole.

Furthermore, RAFT process is compatible with a wide range of reaction media including protic solvents such as alcohols and water[37,66,67] and other less conventional solvents such as ionic liquids[68] and supercritical carbon dioxide.[69] However, the main drawback of this technique is that the library of commercially available RAFT agents is quite limited and their prices are expensive.

1.2.3. Atom-transfer radical polymerization (ATRP)

ATRP has been widely used in the preparation of polymer materials since the initial developments independently reported by Sawamoto[39] and Mateyjaszewski[38] laboratories in the middle 90s. Since then, a multitude of polymers with predicted molecular weight,

composition, functionality and architecture have been shown to be accessible *via* ATRP.[70-73] From a mechanistic point of view, ATRP proceeds after stablishing a fast dynamic equilibrium between active radicals and dormant alkyl halides favoring the dormant state in order to control the polymerization. In this case, the ATRP equilibrium is regulated by the activator and deactivator forms of the transition metal (Mt) catalyst, Mt^m/L and $X\text{-}Mt^{m+1}/L$, respectively, in which L is typically a nitrogen-based polydentate ligand. The activator Mt^m/L must be sufficiently active to cleave the C-X bond in the halide initiators/dormant macromolecular species (RX/P_nX). Similarly, the $X\text{-}Mt^{m+1}/L$ deactivator complex must quickly trap propagating radicals ($P_n^{\bullet}$) to regenerate again the P_n-X dormant species (Scheme 1.7). In ATRP, small amount of bimolecular termination occurring during the first stages of the process is beneficial to achieve control over the MWD. This phenomenon, known as persistent radical effect (PRE), implies the accumulation of a small excess of deactivator species that shifts the dynamic equilibrium toward dormant species.[74-76]

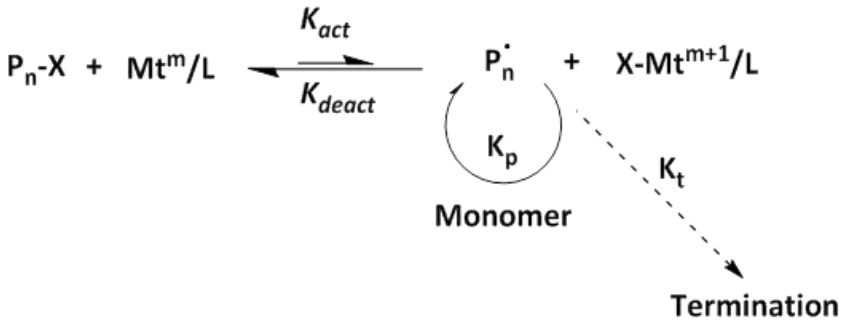

Scheme 1.7. Proposed equilibrium establishes during ATRP.

Being more mechanistically precise, ATRP is proposed to proceed via an inner sphere electron transfer (ISET) process in which the radical and the deactivating species are formed through the homolytic atom transfer of the halogen radical from the dormant species to the active species.[77,78]

Although copper complexes are the most efficient and commonly utilized catalysts in ATRP owing to their availability, low cost, oxidative stability of Cu^{II}, and versatility of the formed

catalytic complexes, ATRP can be conducted with a wide variety of transition metal catalysts such as ruthenium,[79-82] iron,[83-85] nickel,[86-88] palladium,[89] molybdenum,[90,91] osmium[92] and titanium.[93] However, the use of any of these metal catalysts, including copper, at relatively high concentrations have restrained the use of ATRP in the field of industrial and biomedical applications due to contamination issues associated to metals. Consequently, several new approaches have been developed in recent years to reduce the metal concentration and establish catalyst-recycling methodologies. In this context, modified version of classic ATRP methodology such as the activator regenerated by electron transfer ATRP (ARGET-ATRP)[94,95] system, the use of initiators for continuous activator regeneration in ATRP (ICAR-ATRP),[96] electrochemically mediated processes (eATRP)[97] or photo-initiated versions are significant advances.[98-100]

1.2.4. Single electron transfer-living radical polymerization (SET-LRP)

In the last years, the Cu(0)-mediated SET-LRP technique has gained a lot of popularity in the field of polymer synthesis. SET-LRP enables the accelerated preparation of vinyl polymers with well-defined topology and chain end functionality at room temperature or below.[101-103] The origin of this technique dates back to 2002 when Percec laboratory developed a metal-catalyzed living RP for vinyl chloride (VC).[40] It is worth to mention that this monomer could not previously be polymerized in a controlled manner because of the inert nature of -CHClX end groups.[104] The prominent activity of Cu(0) species to reinitiate PVC ends groups made possible the discovery of a new process based on the disproportionation of Cu(I)X into Cu(0) and Cu(II)X_2 in water and in polar media in the presence of specific N-ligands such as tris(2-aminoethyl)amine (TREN) and the branched poly(ethylene imine) (PEI), which evolved into single-electron transfer–degenerative transfer living radical polymerization (SET-DTLRP).[40] In SET-DTLRP, both activation and deactivation steps are controlled by a competition between the single electron transfer (SET) from Cu(0) and degenerative chain-transfer processes (DT) mediated by Cu(II)X_2/L, generated by the disproportionation of Cu(I)X without the need for PRE.[40] Few years later, in 2006, faster activation and deactivation processes than DT were achieved in water, protic solvents,

dipolar aprotic and other solvents in the presence of some N-ligands such as TREN, tris(2-(dimethylamino)-ethyl)amine (Me_6-TREN) and PEI,[105,106] promoting the SET process. Consequently, DT part of SET-DTLRP became negligible leading to a new controlled/living RP techniques that was named by the inventors as SET-LRP.[41]

Fundamental mechanistic aspects of SET-LRP

SET-LRP reaction mechanism is also governed by a dynamic equilibrium between active radicals and dormant species. However, this process takes place in an astonishingly different manner than that above discussed for other copper-mediated living/controlled RP techniques such as ATRP. In SET-LRP, the dissociation of the halide initiator/dormant halide terminated chains (R-X/P_n-X) is promoted by a zero-valent copper catalyst rather than Cu(I)X species. This process is proposed to occur through a heterolytic outer-sphere electron transfer (OSET) process in which the electron donor Cu(0), or other electron-donor species such as Cu_2O, Cu_2S, Cu_2Se, and Cu_2Te, transfer an electron to R-X/P_n-X to furnish a radical anion which degrades in a stepwise or concerted pathway into the propagating specie $R^{\bullet\delta+}$ /$P_n^{\bullet\delta+}$ and X^-.[107] Overall, the mechanistic pathway for SET-LRP is proposed to proceed *via* four fundamental steps: (i) activation of initiator/dormant polymer chains by heterogeneous SET from Cu(0) *via* a stepwise or concerted process, (ii) disproportionation of *in situ* produced or initially provided $Cu^{I}X$/N-ligand that provides self-regulated regeneration of Cu(0) and $Cu^{II}X_2$/N-ligand, (iii) propagation of growing chains, and finally (iv) homogenous deactivation of propagating macroradicals with $Cu^{II}X_2$/N-ligand (Scheme 1.8).

It is well-known that SET-LRP reactions are highly dependent on the solvent and N-ligand typology because this pair of components is crucial to favor a successful disproportionation of $Cu^{I}X$/L into Cu(0) $Cu^{II}X_2L$ and consequently ensure an efficient SET-LRP process.[41] In fact, when poor disproportionation process occurs, the polymerization proceeds through other mechanisms more akin to ATRP, leading to polymers with broad MWDs and limited degree of chain end functionality.[108-111]

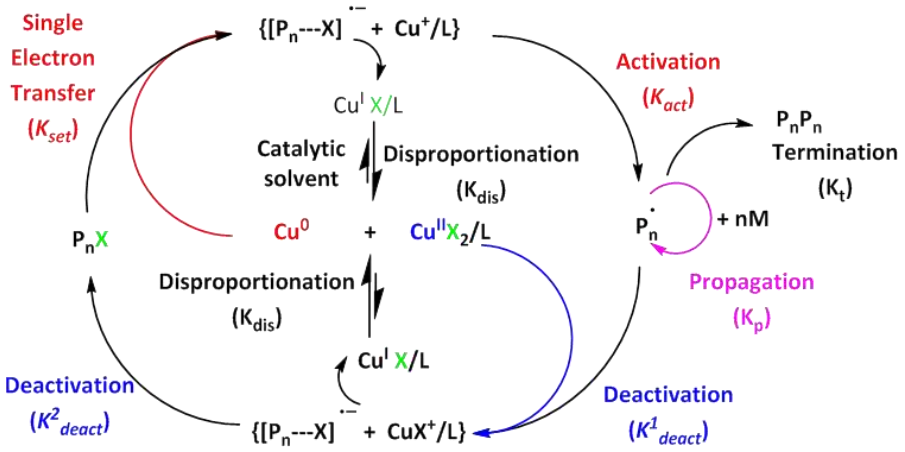

Scheme 1.8. Proposed mechanistic pathway for SET-LRP.

Monomers and initiators compatible with SET-LRP

One of the most important advantages of SET-LRP is that provides an ultrafast and controlled polymerization of a plethora of hydrophilic and hydrophobic monomers including acrylates,[101,112-114] methacrylates,[115-117] acrylamides,[118-122] methacrylamides,[123] and VC.[40,41] Although during the first developments of this technique model acrylic monomers such as methyl acrylate (MA)[112,113] and n-butyl acrylate (n-BA)[114,124] were in the spotlight, the monomer scope of SET-LRP has considerably increased during the last decade. The chemical structure of representative vinylic monomers that have been successfully polymerized under SET-LRP conditions is depicted in Figure 1.3.

The polymerization of any of these monomers requires the selection of an appropriate alkyl halide initiator to obtain well-defined polymeric products.[103,125,126] Methyl 2-bromopropionate (MBP)[127] and ethyl α-bromoisobutyrate (EBiB)[128] are by far the most commonly used mono-functional initiators for acrylic-type monomers. However, a number of functional 2-bromoester derivatives has also been employed as initiators to expand the scope and applications of the technique.

Introduction

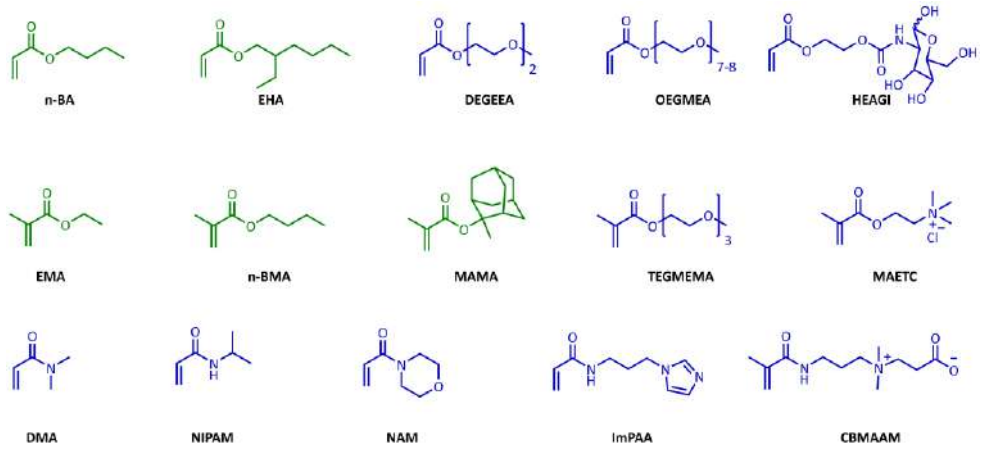

Figure 1.3. Representative vinylic monomers accessible to SET-LRP. Color code: blue as hydrophilic and water-soluble, and green as hydrophobic and water-insoluble. Adapted from Ref. 101.

Selected examples are α-bromoester type initiators bearing phosphate (PBI),[129,130] propargyl (PBIB),[131] azido (mPEG-N_3Br)[132] or hydrophilic moieties (GBMP) are depicted in Figure 1.4a.[103,125,133-137] Furthermore, SET-LRP is also compatible with α-chloroester initiators such as methyl-2-chloropropionate,[123,138] and ethyl 2-chloropropionate.[139] On the other hand, di- and multi-functional initiators have also been used to deliver more complex polymeric materials such as telechelics, star-polymers or dentritic macromolecules (Figure 1.4b).[103,140] Recently, our laboratory has also focused on the design, preparation and use of SET-LRP stimuli-cleavable initiators.[141-143]

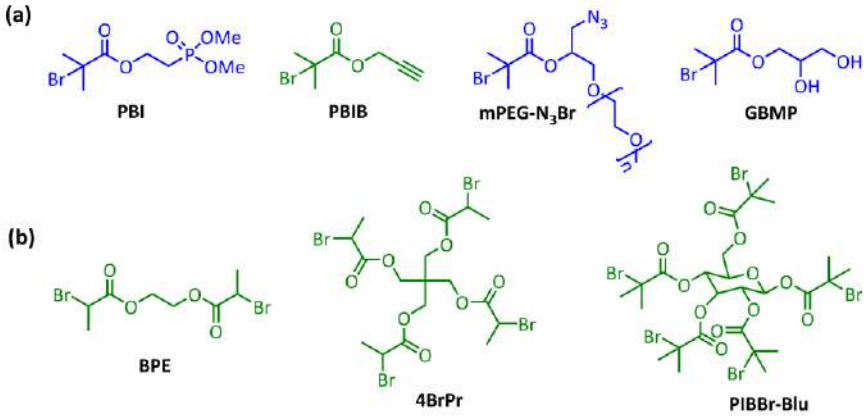

Figure 1.4. Representative mono (a) bi and multi-functional initiators (b) employed in SET-LRP. Color code: blue as hydrophilic and water-soluble, and green as hydrophobic and water-insoluble.

Suitable Cu(0) catalyst forms to practice SET-LRP

Continuous intensive research from different laboratories has evolved into different methodologies to practice SET-LRP based on the use of different Cu(0) forms or different approaches to "in situ" generate Cu(0). The pioneer SET-LRP methodology was based on the use of Cu(0) powder.[108,109] Interestingly, the use of Cu(0) particles of different particle sizes enabled good control over the apparent polymerization rate of SET-LRP reactions.[144] For example, it was reported that a decrease of the Cu(0) particle size from 425 to 0.05 μm (50 nm) increases the rate of polymerization for SET-LRP of MA by almost an order of magnitude. However, experiments conducted using Cu(0) wire provided SET-LRP reactions with greater control of MWD than that of Cu(0) powder.[145] Interestingly, a series of kinetic experiments were used to measure the external rate order for Cu(0) wire catalyst as well as to predict the rate of polymerization for predetermined wire dimensions. The advantages associated with the use of Cu(0) wire-catalyzed SET-LRP methodology include facile catalyst preparation and reaction set-up, handling, and recovery (the wire is usually wrapped around the stirring bar), high level reproducibility, as well as good molecular weight control (Figure 1.5).

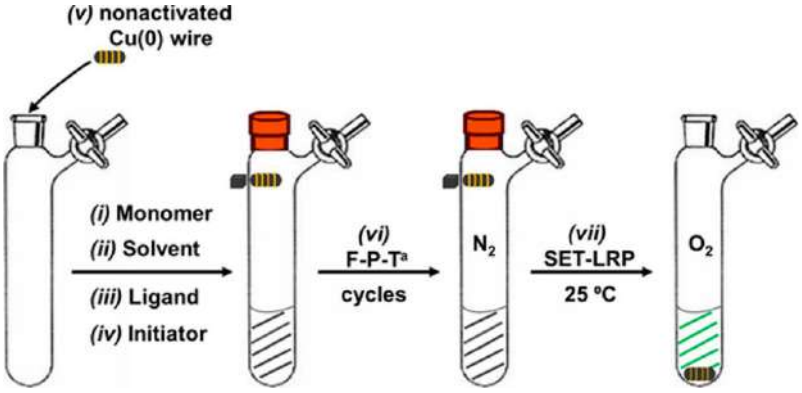

Figure 1.5. General procedure to perform nonactivated Cu(0) wire catalyzed SET-LRP in aqueous or organic media. Adapted from ref. 102.

However, Cu(0) in any form is susceptible to be oxidized to Cu_2O at any time and therefore should be preserved under an anaerobic atmosphere. This is especially important in the case

of "nascent" Cu(0) powder, usually prepared via disproportionation of Cu(I)X.[118] Cu_2O can act as a catalyst for SET-LRP but is known to be less active than Cu(0).[146] In this context, methods for the activation of the Cu(0) wire surface using hydrazine hydrate ($N_2H_4 \cdot H_2O$) treatment[145] or acid dissolution[147] of Cu_2O were also elaborated. Interestingly, self-activation of the Cu(0) wire, following an unknown mechanism, was observed in certain fluorinated alcohols.[148] Colloidal Cu(0) particles, isolated after *in situ* disproportionation of Cu(I)X in the presence of Me_6-TREN in polar solvents and their binary mixtures with water, were also used in SET-LRP. The resulting nanopowder, prepared to mimic the nascent Cu(0) catalyst generated during SET-LRP, provided a faster polymerization than any commercial class of Cu(0) powder, Cu(0) wire, or CuBr. Meanwhile, nascent Cu(0) generated by disproportionation of CuBr/Me_6-TREN in pure water and mixtures of water with other solvents has also been used to mediate the SET-LRP of various hydrophilic acrylamides.[118,120,149] It is also important to highlight that the required Cu(0) catalyst to conduct aqueous SET-LRP has also been generated *in situ* in the reaction mixture by reduction of Cu(II)Br_2 species using sodium borohydride ($NaBH_4$).[150]

The important role of the ligand/solvent pair in SET-LRP

The role of the N-ligand in SET-LRP reactions has been the focus of many studies.[40,125, 151-154] Me_6-TREN[125,151] is the most common option due to its high ability to stabilize Cu(II)X_2 species instead of Cu(I)X promoting the required disproportionation process for an efficient SET-LRP. Me_6-TREN is commercially available but expensive; however, it can easily be synthesized from inexpensive reactants such as TREN, formaldehyde and formic acid.[155] However, N-ligands such as TREN,[40,152,153] *N,N,N',N'',N''*-pentamethyldiethylenetriamine (PMDETA),[154,156] and branched PEI,[40] which are also commercial available and cheaper than Me-TREN, have been also used to mediate the SET-LRP of acrylic monomers both in organic and aqueous media.[157] However, limited success has been obtained until now with ligands such as 1,1,4,7,10,10-hexamethyltriethylenetetramine (HMTETA),[158,159] 2,2'-bypiridine (Bipy)[160] and 4,4'-dinonyl-2,2'-bipiridine (diNBpy)[161] due to their negligible disproportionation ability. The ability of the above mentioned ligands to mediate the disproportionation of Cu(I)X into Cu(0) and Cu(II)X_2

is summarized in Figure 1.6. Note also that the concentration of ligand is also an important parameter when optimizing SET-LRP conditions. In fact, Percec[162] and Haddleton[163] laboratories have demonstrated the existence of a minimum concentration of ligand to obtain an acceptable level of polymerization control.

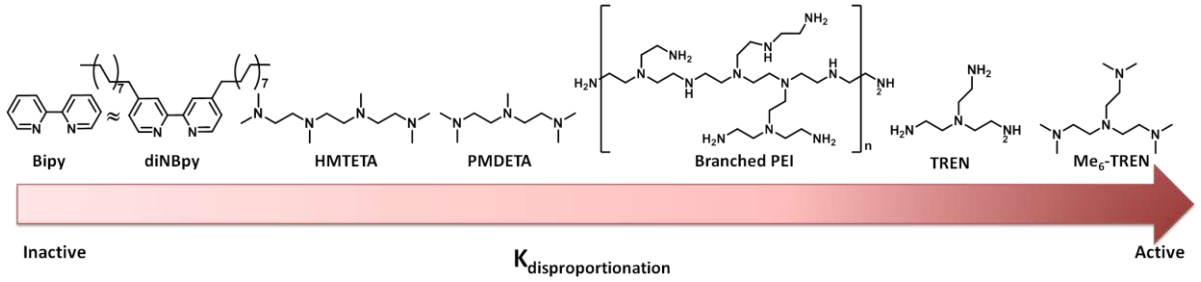

Figure 1.6. Disproportionation ability of commonly used ligands in SET-LRP.

Under disproportionation conditions, the ideal solvent to practice SET-LRP should be capable to stabilize the Cu(0) nanoparticules and dissolve the Cu(II)X_2 species generated during the disproportionation process.[40,41] Combining simple visualization studies with UV-vis measurements, it was demonstrated that in addition to solvents such as DMSO, alcohols and water, other solvents such as dimethylformamide (DMF), dimethyl acetamide (DMAc), ethylene and propylene carbonates (EC and PC, respectively), and also mixtures of two organic disproportionating solvents as well as organic/aqueous mixtures provide efficient reaction media for SET-LRP in homogeneous system.[106,164] Likewise, polyethylene and polypropyleneglycols and their binary mixtures with DMSO and ethanol,[165] as well as ionic liquids,[166] fluorinated alcohols such as 2,2,2-trifluoroethanol (TFE) and 2,2,3,3-tetrafluoropropanol (TFP),[148,167-170] acetic acid[171] and lactic acid (LA) derivatives,[172] phosphate buffer solution,[173] blood serum,[174] as well as alcoholic beverages[175] have also been demonstrated to be successful reaction media. This broad list of solvents supports that almost any polar vinylic polymer is accessible by SET-LRP. However, it was early demonstrated that the SET-LRP performed in polar non-disproportionating, e.g. acetone and acetonitrile, and non-polar solvents was an unsuccessful choice.[109,111] However, the recently

developed biphasic SET-LRP mixtures named "programmed" biphasic systems provided promising perspectives for expanding the scope of solvents. These innovative systems are based on the use of organic solvent and water mixtures. The key point of this system is the unexpected immiscibility of water containing Cu(II)X_2 and ligand in organic solvents, even in water-soluble organic solvents. Under these conditions, the disproportionation step takes place in the aqueous phase and the role of the organic phase becomes a secondary consideration. "Programmed" biphasic SET-LRP systems have been demonstrated to be compatible with a plethora of poor or non-disproportionating solvents, such as acetonitrile,[176,177] acetone,[178] toluene,[179] hexane,[179] ethyl acetate,[179] cyclohexane,[179] anisole,[179] and diethyl carbonate[179] that were incompatible with classical homogeneous reaction mixtures.

1.3. Tailor made biobased BCPs by controlled/living RP

BCPs are an important class of materials fashioned from two or more chemically dissimilar constructs that are covalently-bonded into a single molecule.[180,181] The properties of this special class of polymeric materials can be controlled by designing the length and the nature of their blocky segments, e.g. soft-hard, hydrophilic-hydrophobic and ionic-nonionic segments.[182,183] The linking of constitutionally different units permits the combination of distinct properties within a macromolecule, and enables interesting nanoscale assembly phenomena, and ultimately, unique macroscale behavior that cannot be accessed through simple blending of non-bonded polymer blocks.[184-186] BCPs have experimented an enormous evolution since their early developments more than 60 years ago,[182] and nowadays are considered an expansive class of macromolecules with excellent attributes that confer them exceptional applications in the field of adhesives, blend compatibilizers, nanocarriers and other devices that require phase-separated nanostructures.[182,187] The polymers obtained from any of the above-described controlled/living RP methodologies, e.g. RAFT and SET-LRP, are expected to possess active chain-ends, and therefore can be reinitiated to allow the further block polymerization of other monomers.[37-41] Consequently, controlled/living RP

techniques are attractive tools when aiming to synthesize well-defined BCPs with different compositions and topologies (Figure 1.7).[103,188,189]

In recent years, dwindling petrochemical resources and an increasing environmental awareness have motivated the interest for biobased polymeric materials from renewable sources.[190-193] In this context, controlled/living RP techniques have become increasingly popular and have been applied in the synthesis of BCPs derived from biomass (biobased) for applications ranging from thermoplastic elastomers and pressure-sensitive adhesives to drug delivery vehicles.[194-198]

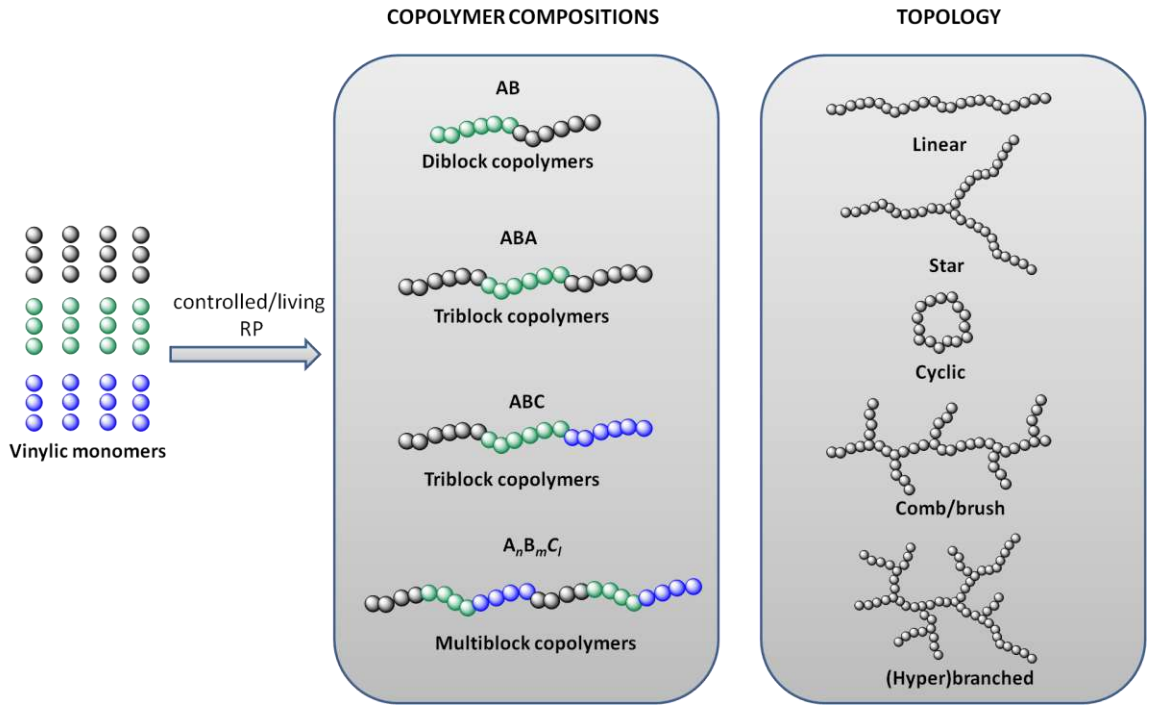

Figure 1.7. Representative examples of BCPs with controlled composition and topology that can be prepared by using controlled/living RP techniques.

Although in most cases, polymerisable vinyl monomers cannot be directly extracted from natural sources, they can be easily prepared from carbohydrates, plant oil derivatives (fatty acids or alcohols), terpenes, amino acids, phenylpropanoids and lignin *via* simple chemical transformation of carboxylic acid-, ester-, or hydroxyl-functional bio-available chemicals with

acrylic, methacrylic or styrenic polymerizable moieties (Scheme 1.9).[199] The possibility to obtain a great variety of biobased vinylic building blocks and subsequently control polymer synthesis by using controlled/living RP methods allows for utilization of sustainable self-assembling BCPs for different advanced applications.[200,201]

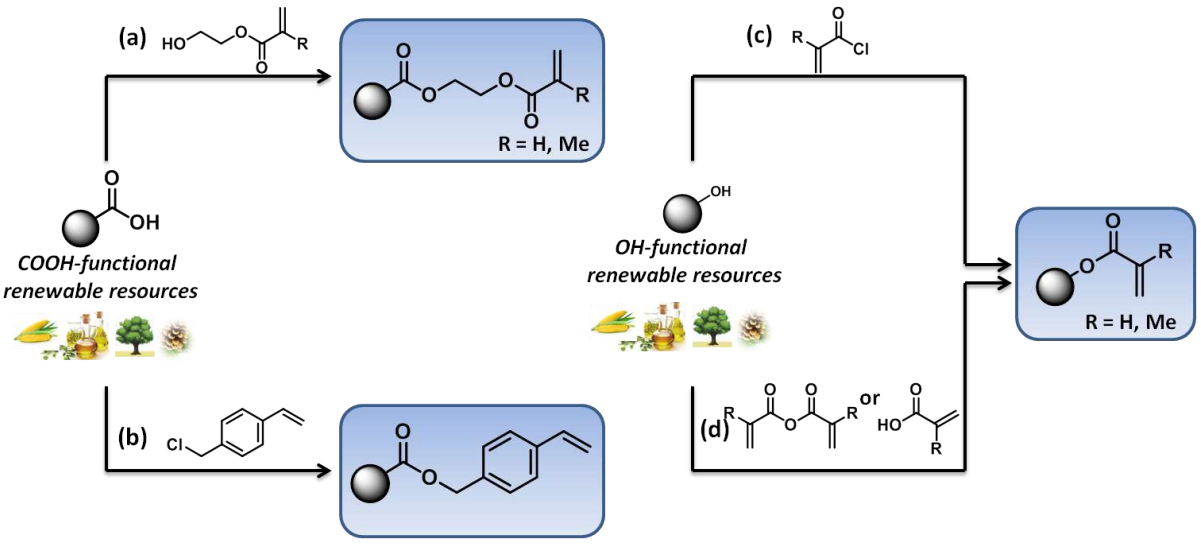

Scheme 1.9. General synthetic routes to prepare vinylic monomers from renewable resources. Carboxylic acid-functional renewable resources have been modified to give polymerizable monomers using (a) *N,N'*-dicyclohexylcarbodiimide (DCC) and 4-dimethylamino pyridine (DMAP) mediated esterification,[202] or (b) esterification using a halogenated compound mediated by 1,1,3,3-tetramethylguanidine (TMG).[203] Alcohol-functional renewable resources have been reacted with (c) (meth)acryloyl chloride in the presence of triethylamine (TEA)[204,205] or (d) (meth)acrylic anhydride or (meth)acrylic acid with DMAP[206] and propylphosphonic anhydride (T3P®)[207] as a catalyst, respectively.

1.3.1. ABA-type biobased thermoplastic elastomers

Combining the service properties of crosslinked elastomers at normal temperature and melt processing properties of thermoplastics at increased temperature, thermoplastic elastomers (TPEs) have found myriad applications in industry, including gaskets, cable insulation, medical devices, sporting goods, automotive bumpers and adhesives.[208-211] The market for TPEs is continuously growing because of their ability of recycling and reprocessing, being beneficial for environmental protection and energy conservation. These

materials often comprise linear ABA triblock copolymers with a soft middle block and hard minority end blocks that phase-separate into hard nanoscale domains, acting as a physically crosslinked junctions, dispersed in a soft matrix (Figure 1.8).[183,212-214]

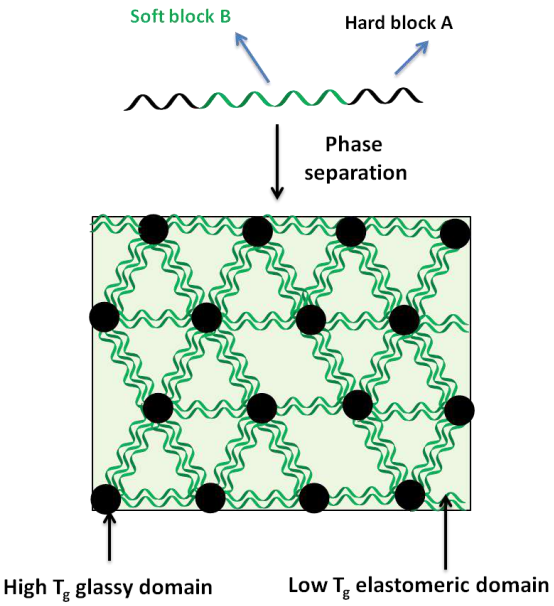

Figure 1.8. Schematic representation of physical cross-linking in ABA-type triblock copolymers.

The resultant physical behavior of these BCPs is that of an elastomeric material that can be recycled. That is, when the material is heated through an order-disorder transition, the disorder state prevails and the material can be readily processed. However, upon cooling, the inverse process occurs in which the order state (and physical crosslinking, providing elastic behavior) is recovered once again. The most widely used engineering TPEs are by far those composed by PSt-*b*-polybutadiene-*b*-PSt or PSt-*b*-polyisoprene-*b*-PSt triblock copolymers. These copolymers have remarkable mechanical properties such as high tensile strengths (up to around 30 MPa) and high elongation at break (up to 800%), similarly to vulcanized rubbers.[213] However, some inconveniences of these materials are: (i) its origin from fossil fuels, (ii) the high UV and oxygen sensibility of polybutadiene and polyisoprene middle blocks,[215] and (iii) the limited upper service temperature (100 °C) of PSt-based systems.[183] These shortcomings have motivated the shift toward innovative sustainable

solutions for high-performance TPEs.[194,216,217] To this end, both soft and hard building blocks based on biobased vinylic monomers are necessary components of a sustainable future that relies minimally on petroleum-based plastics. For instance, reactive monomers derived from fatty acids such as the acrylate monomer M1 shown in Figure 1.9, obtained from soybean oil *via* amidation/esterification,[194,195,217] the lauryl alcohol derivative M2,[196,218,219] amino acids,[220] tetrahydrogeraniol-based acrylate (M3)[216] or itaconic acid esters (M4),[221] available through the fermentation of carbohydrates, represent some examples of vinylic biobased building blocks able to produce well-defined polymers with glass transition temperature (T_g) values well-below room temperature *via* controlled/living RP (Figure 1.9). For example, poly (tetrahydrogeraniol acrylate) of M_n 98500 g/mol prepared by RAFT polymerization shows a T_g ~ -50 °C. Most of these polymers have been used as a constituent soft phase in ABA-type TPEs.[194,217,220,221] For example, the RAFT chain extension of poly(dialkyl itaconate)s with N-aryl itaconimides enabled to realize fully biobased ABA triblock copolymers with a microphase-separated morphology suitable to act as a TPEs with high service temperatures (Figure 1.10).[221]

In the same vein that poly(N-aryl itaconimide)s, several sustainable alternatives for the traditional petroleum-sourced PSt glassy minority end-blocks have also been reported (Figure 1.11).[197,204,221,222] In this case, the hard component of triblock ABA copolymers provide structural integrity and are characterized to have a T_g at around 100 °C being suitable to achieve the common TPE applications.[213]

Biobased monomers such as acetylated acrylic glucose (M5),[204] acetylated acrylic isosorbide (M6),[197] itaconic acid imides (M7),[221] α-methylene-γ-butyrolactone (M8),[222,223] β-pinene acrylate (M9)[224,225] have shown promising results to produce TPEs biomass-derived hard component. Furthermore, biobased phenolic compounds with similar structure to St, including vanillin, ferulic acid, guayacols (M10), syringols (M10), cathecols and other phenolic lignin model compounds have also attracted attention.[208,226-228]

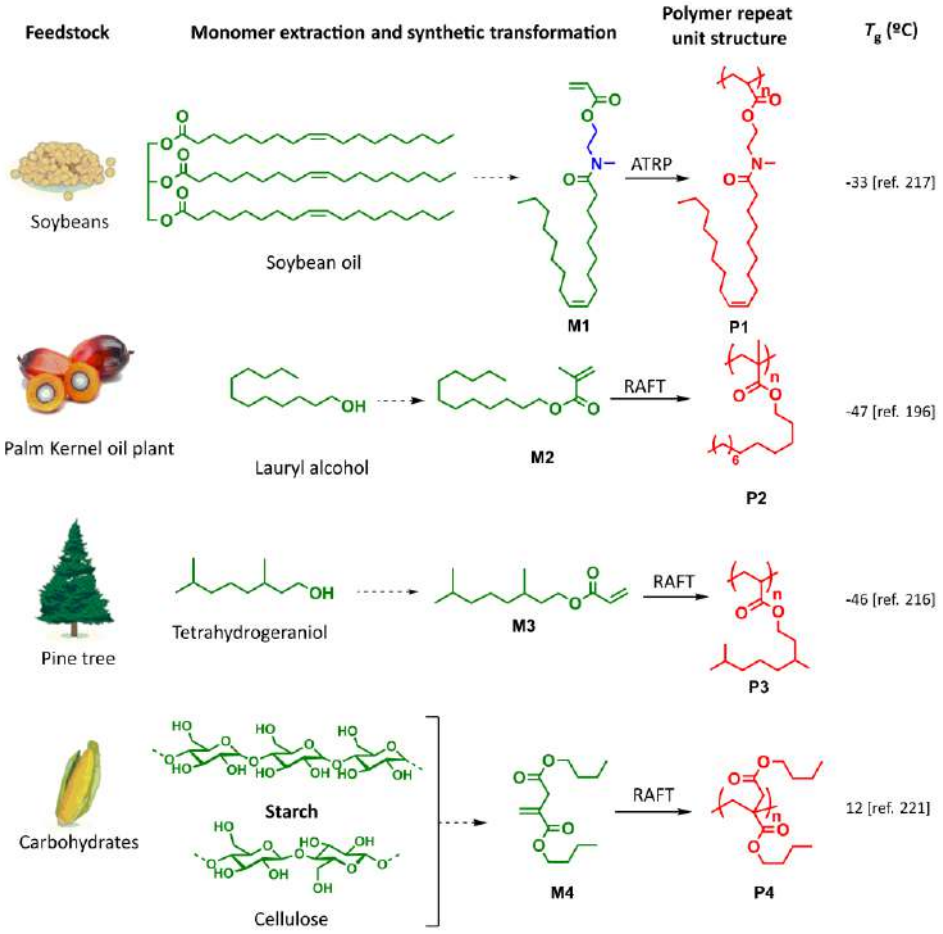

Figure 1.9. Biomass-derived rubbery building blocks for ABA BCPs. Color code: green as biobased and blue as petroleum-based in small molecules, red as rubbery building block in polymers.

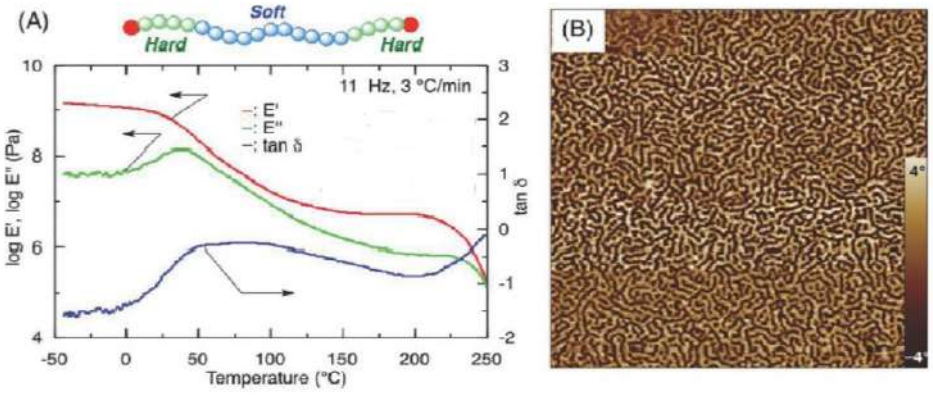

Figure 1.10. Dynamic tensile storage (E') and loss (E") moduli and tan δ (= E"/E´) as a function of temperature (heating rate: 10 °C min^{-1} ; frequency: 11 Hz) (A) and AFM phase images (2 × 2 μ m) for morphologies (B) of the ABA itaconic acid-derived triblock copolymer. Adapted from Ref. 221.

Introduction

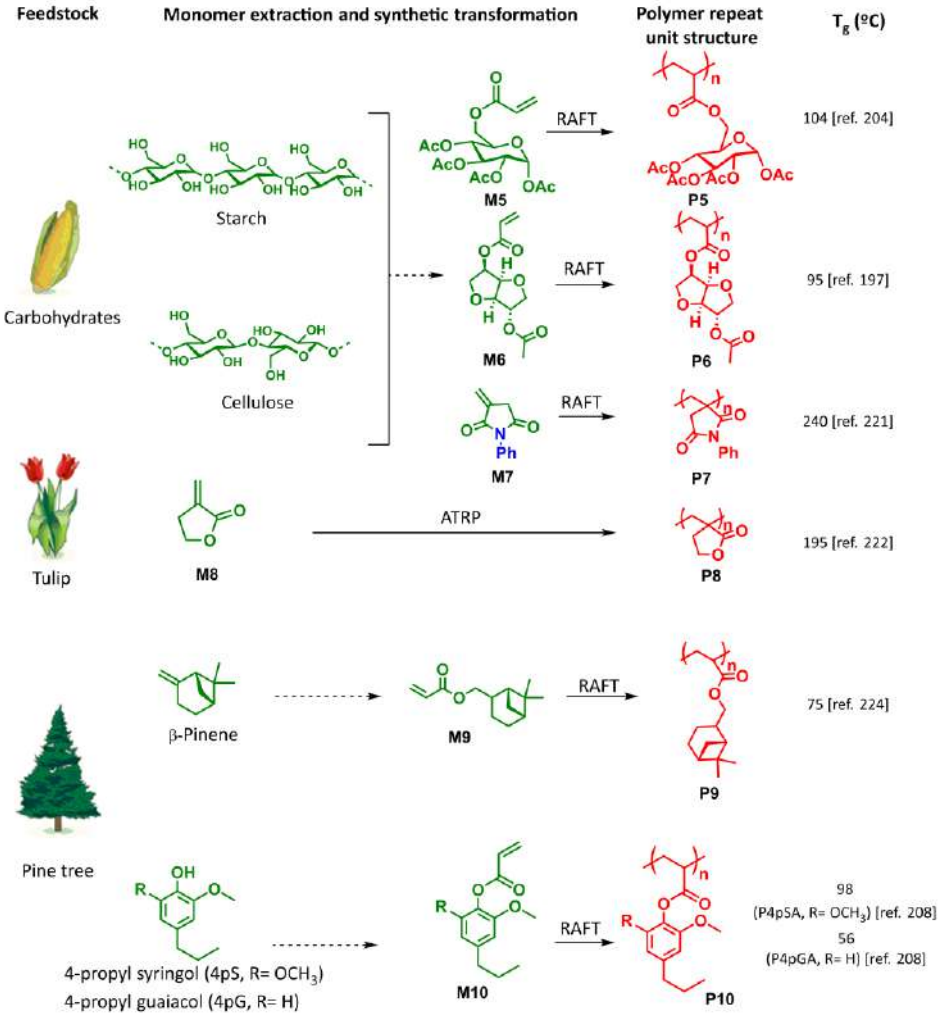

Figure 1.11. Biomass-derived glassy building blocks for ABA BCPs. Color code: green as biobased and blue as petroleum-based in small molecules, red as glassy building block in polymers.

In most of the these studies, innovative biobased hard building blocks were combined with poly(butyl acrylate) (PBA) (T_g ~ -50 °C) as a model soft component.[197,204,208] However, the development of fully biobased ABA-triblock copolymers prepared by controlled/living RP has also been described.[220,221,229] For example, Reineke laboratory recently reported the preparation of ABA triblock copolymers for high-performance pressure-sensitive adhesives (PSAs) from the biorenewable chemicals lauryl acrylate and triacetic acid lactone, which is available from carbohydrates *via* the action of genetically modified yeast (Figure 1.12).[229] As mentioned above, fully biobased itaconic acid-derived triblocks have also been reported.[221]

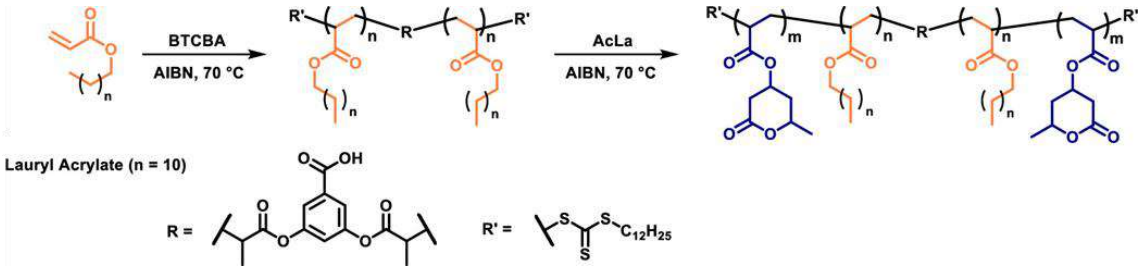

Figure 1.12. Synthesis of ABA Triblock Copolymers *via* RAFT polymerization of lauryl acrylate and triacetic acid lactone acrylate. Adapted from Ref. 229.

These and other approaches have demonstrated that it is possible to utilize biobased chemicals to realize fully sustainable system for high-performance applications based on ABA triblock copolymers.[220,229]

1.3.2. Self-assembly of biobased amphiphilic BCPs

Recently, amphiphilic molecules capable to form different nanosized architectures during a self-assembly process under the appropriate conditions (e.g. temperature, solvent, polymer concentration, etc.) have gained a lot of interest due to its potential in important biomedical and other applications, including drug carriers, imaging agents, catalysis, surfactants, among others.[230-236] Among them, amphiphilic BCPs represent one of the most appealing systems due to the facile control over their self-assembly by simply manipulating their chemical composition, polarity and molecular weight.[237-239] Nanosized architectures are typically obtained from covalently-connected linear AB or ABA amphiphilic BCPs using monomers that ensure both hydrophobic and hydrophilic regions. However, amphiphilic homopolymers and random copolymers have also been used to generate nanosized architectures with promising results.[240-245] When amphiphilic BCPs are exposed to an aqueous environment, different stable self-assembled nanoparticules/nanoaggregates can be formed ranging from simple micelles to complex nanostructures such as vesicles, cylinders, among other morphologies (Figure 1.13).[233]

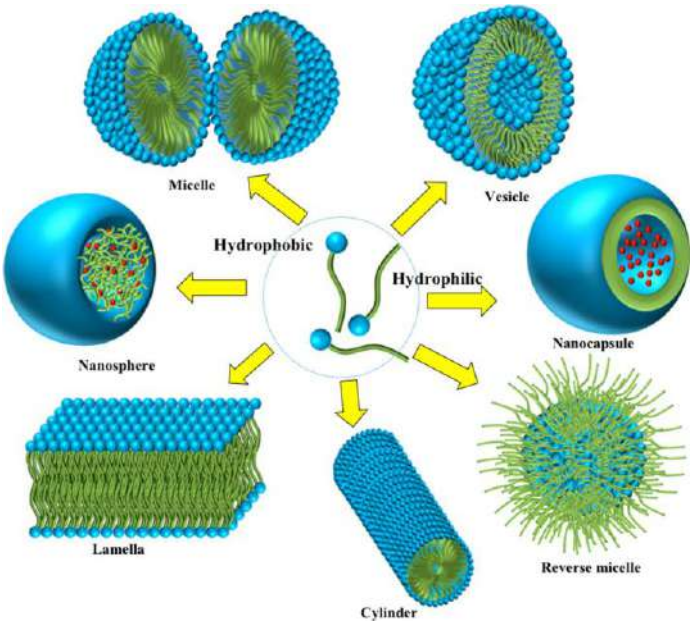

Figure 1.13. Self-assembly of BCP nanostructures. Adapted from ref. 233.

The formation of these nanoaggregates is highly dependent of the critical aggregation concentration (CAC), which is defined as the minimal concentration of an amphiphilic copolymer above which nanoaggregates start to form being stable over time.[233] In the particular case of micelle formation, this parameter is known as the critical micellar concentration (CMC). In this context, in polar solvents (more commonly water), the hydrophilic segments orientate themselves toward solvent maintaining the hydrophobic moieties inside, forming stable regular/normal nanostructures with hydrophobic cores permeable to foreign hydrophobic molecules. However, in apolar solvents, the opposed behavior takes places forming reverse nanostructures. Hence, self-assembled nanostructures have the ability to encapsulate foreign hydrophobic and hydrophilic guest molecules in polar and non-polar solvents, respectively.[141,143] Indeed, they can also be designed with the ability to respond to external stimuli such as temperature, polarity, light or pH by introducing stimuli-cleavage linkages.[246-250] Well-known classical methods for the preparation of BCP nanoassemblies after polymer synthesis are dialysis, oil/water emulsion, solvent evaporation (or film method) and co-solvent evaporation protocols.[251-253] However, it is of a great importance to mention an innovative strategy in which amphiphilic BCP

synthesis and self-assembly occur simultaneously, thus fulfilling great control over the final morphology of the formed aggregates. This method, which is called polymerization-induced self-assembly (PISA), is based on the direct preparation of the BCPs, in a selective solvent using a macroinitiator. Under PISA conditions, polymerization and formation of self-assembled aggregates simultaneously occurs because of the change of the block chain length ratio (driving force).[254-257] This methodology is able to be conducted under dispersion or emulsion polymerization conditions, as well as it has been achieved promising results in a wide range of different solvent systems, including water,[258,259] alcohols,[260,261] ethylene glycol,[262] supercritical carbon dioxide[263,264] and ionic liquids.[265,266] PISA polymerization can be successfully conducted using almost any controlled/living RP techniques such as RAFT,[257,267] NMP, [268,269] ATRP,[270,271] and SET-LRP.[272] It is also important to highlight that this interesting and promising methodology has also been proved under more sustainable conditions using low concentration of catalyst[271] as well as using alternative initiation methods using light which gives low energy requirements, less side reactions and temporal and spatial control over the polymerization process.[273,274]

Considering the imperative role amphiphilic BCPs in the modern era and the crucial need for reducing our dependence on fossil fuel feedstock, current academic efforts have also been devoted to make use of biomass-derived monomers on the preparation of amphiphilic BCPs.[198,201,275-277] In this context, taking advantage of controlled/living RP techniques, the search for innovative hydrophilic biobased vinylic monomers suitable to construct water-soluble polymers has been demonstrated an active area of research (Figure 1.14).[198,275,276]

Introduction

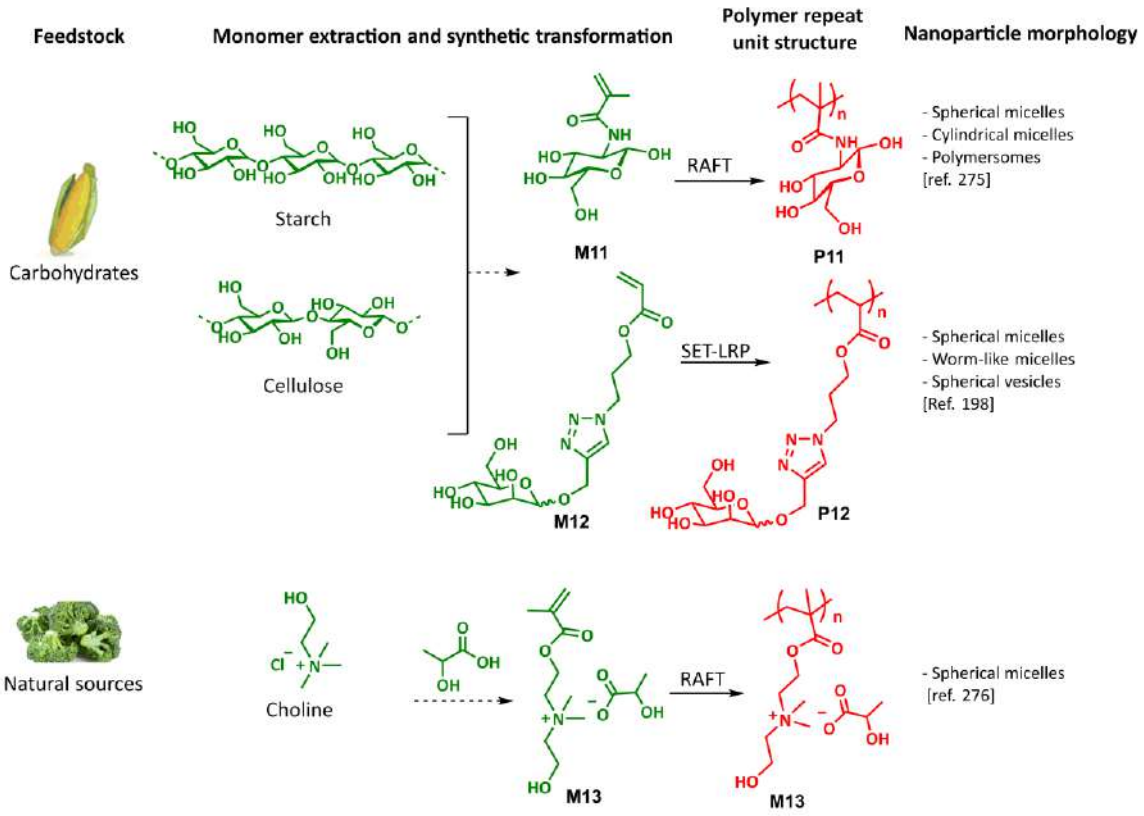

Figure 1.14. Biomass-derived hydrophilic building blocks for amphiphilic BCPs. Color code: green as biobased, red as hydrophilic building block in polymers.

For example, a synthetic hydrophilic glucose-based glycopolymer prepared by RAFT (P11) served as hydrophilic building block for the preparation of amphiphilic AB-type BCPs able to self-assemble into in nanoparticles with morphologies highly dependent on the nature of the hydrophobic segment present in the copolymer.[275] Becer laboratory has also been addressed intensive efforts on the development of glycopolymers based on biobased acrylic glycomonomers.[278-281] As a representative example, amphiphilic SET-LRP polymers based on mannose monomer (M12), MA, and poly(ethylene glycol) (PEG) self-assembled into different morphologies including spherical micelles, worms and vesicles (Figure 1.15).[198] Some of these nanoassemblies containing mannose units in the corona showed excellent lectin binding properties.

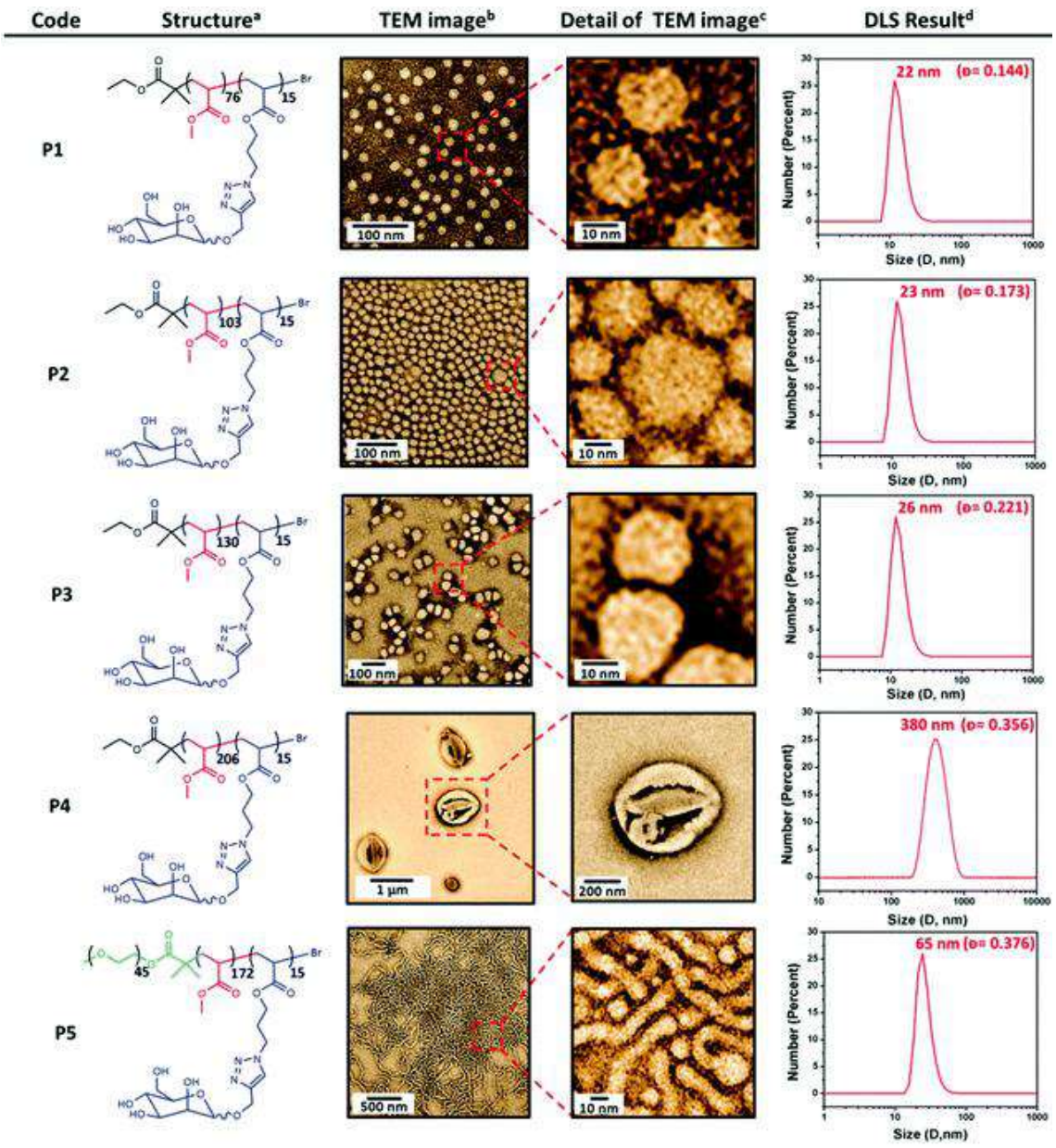

Figure 1.15. Characterization of glycopolymer nanoassemblies containing manose-derived building blocks: (a) chemical structures of polymers, (b) TEM images of glyconanoparticles in selected solvent condition, [c] zoomed in TEM images, and (d) size of glyconanoparticles via DLS. Adapted from Ref. 198.

Last but not at least, innovative amphiphilic AB BCPs based on biobased hydrophilic ionic liquids (M13),[276] composed both from LA and cholinium building blocks, have also been developed. In this case, dynamic light scattering (DLS) measurements revealed the formation

of self-assembled micelles in water, and TEM studies confirmed the presence of spherical nanostructures in dry state having sizes below 17 nm.

In the same vein, several biobased vinylic building blocks have been used to construct the hydrophobic segments of amphiphilic BCPs using controlled/living RP (Figure 1.16). [277,201,282] For example, Oh and coworkers reported a novel rosin-based hydrophobic monomer (M14) that was used to synthesize amphiphilic AB BCPs designed to self-assemble into micellar nanocarriers with positioned disulfide linkages at the interfaces of hydrophobic rosin cores and hydrophilic PEG coronas.[201] These rosin-based nanocarriers exhibited excellent colloidal stability under pseudo-physiological conditions and in the presence of proteins, as well as they offered an enhanced release of encapsulated drugs when *in vitro* cell cultures were performed. Another interesting example is that reported by Stoffelbach *et al.* in which biobased hydrophobic menthyl acrylate monomer (M15), obtained from mentha feedstock, was used for the synthesis of biobased amphiphilic BCPs.[277] In this case, stable spherical nanoparticles were obtained, suggesting that hydrophobic menthyl-based segments could also be used as a candidates for the synthesis of drug-delivery nanocarriers in biomedical applications. Finally, the bile acid-derived vinylic monomer (M16), offers another interesting possibility to synthesize amphiphilic BCPs.[282] This biobased monomer possess both hydrophobic and hydrophilic faces which make it suitable to self-assemble in aqueous solutions to form spherical, vesicular or rod-like aggregates depending on the hydrophobic segments and charge density of facial amphiphilic building blocks as well as the fraction of PEG segments used to balance the amphiphilicity of the final AB BCP.

According to the above described promising results, future challenges must increasingly be addressed to continue expanding the scope of biobased vinylic monomers for developing functional and sustainable materials based on BCPs.

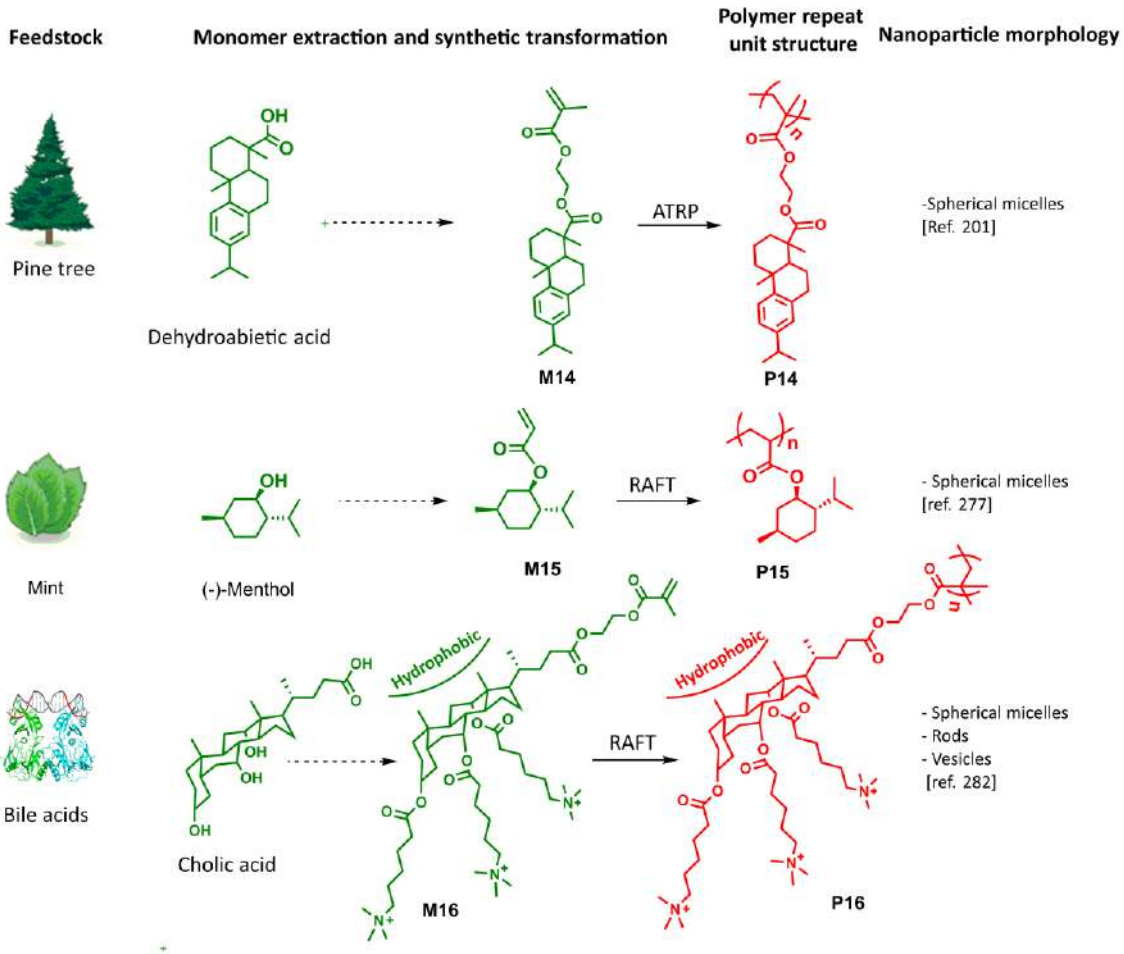

Figure 1.16. Biomass or biologically derived hydrophobic building blocks for amphiphilic BCPs. Color code: green as biobased, red as hydrophilic building block in polymers.

1.4. References

[1] Müllner, M. *Macromol. Rapid Commun.* **2019**, *40*, 1900151.

[2] American Chemical Society. Leo Hendrick Baekeland and the Invention of Bakelite. https://www.acs.org/content/acs/en/education/whatischemistry/landmarks/bakelite.html (consulted on 14 on November, 2020).

[3] American Chemical Society. The Foundation of Polymer Science by Hermann Staudinger (1881-1965): An International Historic Chemical Landmark, Freiburg, Baden-Wurttemberg, April 19, 1999.

[4] Furukawa, Y. In *Chemical Sciences in the 20th Century*; Reinhardt, C., Ed; John Wiley & Sons, Ltd. 2001; pp. 228-245.

[5] Andrady, A.L.; Neal, M.A. *Philos. Trans. R. Soc. Lond. B. Sci.* **2009**, *364*, 1977-1984.

[6] Namazi, H. *BioImpacts* **2017**, *7*, 73-74.

[7] Lebreton, L.; Andrady, A. *Palgrave Commun.* **2019**, *5*, 6.

[8] Thompson, R. C.; Moore, C. J.; vam Saal, F. S.; Swan, S. H. *Phil. Trans. R. Soc. lond B. Sci.* **2009**, *364*, 2153-2166.

[9] Schönmayr, D. In *Automotive Recycling, Plastics, and Sustainability*. Springer, Cham, 2017; pp. 29-77.

[10] Nesvadba, P. In *Encyclopedia of Radicals in Chemistry, Biology and Materials*; John Wiley & Sons, Ltd. 2012, pp. 1-36.

[11] Lessard, J. J.; Garcia, L. F.; Easterling, C. P.; Sims, M. B.; Bentz, K. C.; Arencibia, S.; Savin, D. A.; Sumerlin, B. S. *Macromolecules* **2019**, *52*, 2105-2111.

[12] O'Brien, N.; McKee, A.; Sherrington D. C.; Slarkb, A. T.; Titterton, A. *Polymer* **2000**, *41*, 6027-6031.

[13] Delplace, V.; Nicolas, J. *Nat. Chem.* **2015**, *7*, 771-784.

[14] He, J.; Zhang, Y.; Chen, E. Y.-X. *Synlett* **2014**, *25*, 1534-1538.

[15] Cooker, B. High Added Value Renewable Polymers. https://www.biofuelsdigest.com/bdigest/2017/07/18/high-added-value-renewable-polymers/ (consulted on 07 on November, 2020).

[16] Hart, K. E.; Abbott, L. J.; Lísal, M.; Colina, C. M. *J. Chem. Phys.* **2014**, *141*, 204902.

[17] Flory, P. J. *J. Am. Chem. Soc.* **1937**, *59*, 241-253.

[18] Quin, J.; Guo, W.; Zhang, Z. *Polymer* **2002**, *43*, 1163-1170.

[19] Georges, M. K.; Veregin, R. P. N.; Kazmaier, P. M.; Hamer, G. K. *Macromolecules* **1993**, *26*, 2987-2988.

[20] Molina-Gutiérrez, S.; Ladmiral, V.; Bongiovanni, R.; Caillol, S.; Lacroix-Desmazes, P. *Green Chem.* **2019**, *21*, 36-53.

[21] Nesbadba, P. In *Encyclopedia of Radicals in Chemistry, Biology and Materials*; Chatgilialoglu, C.; Studer, A. Eds; John Wiley & Sons,Ltd. 2012; 4, p. 1701.

[22] Matyjaszewski, K.; Davis, T. P. Eds., *Handbook of Radical Polymerization*, John Wiley & Sons, Inc, Hoboken, NJ, 2002.

[23] Buback, M.; Herk, A. M. Eds., *Radical Polymerization: Kinetics and Mechanism*, Wiley-VCH Verlag GmbH, Weinheim, 2007.

[24] Moad, G.; Solomon, D. Eds. *The Chemistry of Radical Polymerization*, 2nd edn, Elsevier, Oxford, 2006.

[25] Beuermann, S.; Buback, M. *Prog. Polym. Sci.* **2002**, *27*, 191-254.

[26] Schreck, V.; Serelis, A.; Solomon, D. *Aust. J. Chem.* **1989**, *42*, 375-393.

[27] Bizilj, S.; Kelly, D. P.; Serelis, A. K.; Solomon, D. H.; White, K. E. *Aust. J. Chem.* **1985**, *38*, 1657-1673.

[28] Çatalgil-Giz, H.; Öncül-Koç, A. *Polym. Bull.* **1999**, *43*, 215-222.

[29] Washington, R. P.; Steinbock, O. *Polym. News* **2003**, *28*, 303-310.

[30] Odian, G. *Principles of Polymerization*; 4th ed.; Wiley-Interscience, New Jersey, 2004.

[31] Szwarc, M.; Levy, M.; Milkovich, R. *J. Am. Chem. Soc.* **1956**, *78*, 2656-2657.

[32] Szwarc, M. *J. Polym. Sci., Part A: Polym. Chem.* **1988**, *36*, ix-xv.

[33] Quirk, R. P.; Zhuo, Q.; Jang, S. H.; Lee, Y.; Lizarraga, G. *Symp. Ser. Am. Chem. Soc.* **1998**, *696*, 2-27.

[34] (a) Matyjaszewski, K.; Kubisa, P.; Penczek, S. *J. Polym. Sci.: Polym. Chem. Ed.* **1974**, *12*, 1333-1336. (b) Matyjaszewski, K.; Penczek, S. *J. Polym. Sci. Part A: Polym. Chem.* **1974**,

12, 1905-1912. (c) Matyjaszewski, K.; Kubisa, P.; Penczek, S. *J. Polym. Sci. Part A: Polym. Chem.* **1975**, *13*, 763-784.

[35] Frey, H.; Ishizone, T. *Macromol. Chem. Phys.* **2017**, *218*, 1700217.

[36] Solomon, D. H.; Rizzardo, E.; Cacioli, P. US Patent 4581429, 1986.

[37] Le, T. P.; Moad, G.; Rizzardo, E.; Thang, S. H. *Int. Pat.WO 9801478* 1998 [Chem. Abs. 1998, 128, 115390f].

[38] Wang, J.-S.; Matyjaszewski, K. *J. Am. Chem. Soc.* **1995**, *117*, 5614-5615.

[39] Kato, M.; Kamigaito, M.; Sawamoto, M.; Higashimura, T. *Macromolecules* **1995**, *28*, 1721-1723.

[40] Percec, V.; Popov, A. V.; Ramirez-Castillo, E.; Monteiro, M. J.; Barboliu, B.; Weichlod, O.; Asandei, A. D.; Mitchell, C. M. *J. Am. Chem. Soc.* **2002**, *124*, 4940-4941.

[41] Percec, V.; Guliashvili, T.; Ladislaw, J. S.; Wistrand, A.; Stjerndahl, A.; Sienkowska, M. J.; Monteiro, M. J.; Sahoo, S. *J. Am. Chem. Soc.* **2006**, *128*, 14156-14165.

[42] Matyjaszewski, K.; Gaynor, S.; Greszta, D.; Mardare, D.; Shigemoto, T. *J. Phys. Org. Chem.* **1995**, *8*, 306-315.

[43] Jenkins, A. D.; Jones, R. G.; Moad, G. *Pure Appl. Chem.* **2009**, *82*, 483-491.

[44] Quirck, R. P.; Lee, B. *Polym. Int.* **1992**, *27*, 359-367.

[45] Druliner, J. D. *Macromolecules* **1991**, *24*, 6079-6082.

[46] De León-Sáenz, E.; Morales, G.; Guerrero-Santos, R.; Gnanou, Y. *Macromol. Chem. Phys.* **2000**, *201*, 74-83.

[47] Yamada, B.; Nobukane, Y.; Miura, Y. *Polym. Bull.* **1998**, *41*, 539-544.

[48] Steenbock, M.; Klapper, M.; Müllen, K. *Macromol. Chem. Phys.* **1998**, *199*, 763-769.

[49] Puts, R. D.; Sogah, D. Y. *Macromolecules* **1996**, *29*, 3323-3325.

[50] Hawker, C. J.; Bosman, A. W.; Harth, E. *Chem. Rev.* **2001**, *101*, 3661-3688.

[51] Nicolas, J. N.; Guillaneuf, Y.; Lefay, C.; Bertin, D.; Gigmes, D.; Charleux, B. *Prog. Polym. Sci.* **2013**, *38*, 63-235.

[52] Hawker, C. J.; Barclay, G. C.; Orellana, A.; Dao, J.; Devonport, W. *Macromolecules* **1996**, *29*, 5245-5254.

[53] Hawker, C. J. *J. Am. Chem. Soc.* **1994**, *116*, 11185-11186.

[54] Guillaneuf, Y.; Gigmes, D.; Marque, S. R. A.; Astolfi, P.; Greci, L.; Tordo, P.; Bertin, D. *Macromolecules* **2007**, *40*, 3108-3114.

[55] Moad, G; Rizzardo, E.; Thang, S. H. *Polymer* **2008**, *49*, 1079-1131.

[56] Moad, G.; Rizzardo, E.; Thang, S. H. *Aust. J. Chem.* **2012**, *65*, 985-1076.

[57] Perrier, S. S. *Macromolecules* **2017**, *50*, 7433-7447.

[58] Keddie, D. J. *Chem. Soc. Rev.* **2014**, *43*, 496-505.

[59] Benaglia, M.; Chiefari, J.; Chong, Y. K.; Moad, G.; Rizzardo, E.; Thang, S. H. *J. Am. Chem. Soc.* **2009**, *131*, 6914-6915.

[60] Moad, G.; Rizzardo, E.; Thang, S. H. *Aust. J. Chem.* **2009**, *62*, 1402-1472.

[61] Li, Y.; Schadler, L. S.; Benicewicz, B. C. in *Handbook of RAFT Polymerization*; C., Barner-Kowollik, Ed.; Wiley-VCH: Weinheim, 2008; pp. 423-453.

[62] Ladavière, C.; Lacroix-Desmazes, P.; Delolme, F. *Macromolecules* **2009**, *42*, 70-84.

[63] Bathfield, M.; D'Agosto, F.; Spitz, R.; Ladavière, C.; Charreyre, M. T.; Delair, T. *Macromol. Rapid Commun.* **2007**, *28*, 856-862.

[64] Konkolewicz, D.; Hawkett, B. S.; Gray-Weale, A.; Perrier, S. *Macromolecules* **2008**, *41*, 6400-6412.

[65] Konkolewicz, D.; Hawkett, B. S.; Gray-Weale, A.; Perrier, S. *J. Polym. Sci., Part A: Polym. Chem.* **2009**, *47*, 3455-3466.

[66] McCormick, C. L.; Lowe, A. B. *Acc. Chem. Res.* **2004**, *37*, 312-325.

[67] Lowe, A. B.; McCormick, C. L. *Aust. J. Chem.* **2002**, *55*, 367-379.

[68] Perrier, S.; Davis, T. P.; Carmichael, A. J.; Haddleton, D. M. *Chem. Commun.* **2002**, 2226-2227.

[69] Arita, T.; Beuermann, S.; Buback, M.; Vana, P. *E-Polymers* **2004**, *4*, 003.

[70] Siegwart, D. J.; Oh, J. K.; Matyjaszewski, K. *Prog. Polym. Sci.* **2012**, 37, 18-37.

[71] Braunecker, W. A.; Matyjaszewski, K. *Prog. Polym. Sci.* **2007**, *32*, 93-146.

[72] Krys, P.; Matyjaszewski, K. *Eur. Polym. J.* **2017**, *89*, 482-523.

[73] Matyjaszewski, K. *Isr. J. Chem.* **2012**, *52*, 206-220.

Introduction

[74] Fischer, H. *Macromolecules* **1997**, *30*, 5666-5672.

[75] Fischer, H. *J. Polym. Sci., Part A: Polym. Chem.* **1999**, *37*, 1885-1901.

[76] Fischer, H. *Chem. Rev.* **2001**, *101*, 3581-3610.

[77] Lin, C. H.; Coote, M. L.; Gennaro, A.; Matyjaszewski, K. *J. Am. Chem. Soc.* **2008**, *130*, 12762-12774.

[78] Isse, A. A.; Gennaro, A.; Lin, C. Y.; Hodson, J. L.; Coote, M. L.; Guliashvili, T. *J. Am. Chem. Soc.* **2011**, *133*, 6254-6264.

[79] Ando, T.; Kato, M.; Kamigaito, M.; Sawamoto, M. *Macromolecules* **1996**, *29*, 1070-1072.

[80] Nishikawa, T.; Ando, T.; Kamigaito, M.; Sawamoto, M. *Macromolecules* **1997**, *30*, 2244-2248.

[81] Ando, T.; Kamigaito, M.; Sawamoto, M. *Tetrahedron* **1997**, *53*, 15445-15457.

[82] Ueda, J.; Matsuyama, M.; Kamigaito, M.; Sawamoto, M. *Macromolecules* **1998**, *31*, 557-562.

[83] Ando, T.; Kamigaito, M.; Sawamoto, M. *Macromolecules* **1997**, *30*, 4507-4510.

[84] Matyjaszewski, K.; Wei, M.; Xia, J.; McDermott, N. E. *Macromolecules* **1997**, *30*, 8161-8164.

[85] O'Reilly, R. K.; Gibson, V. C.; White, A. J. P.; Williams, D. J. *Polyhedron* **2004**, *23*, 2921-2928.

[86] Uegaki, H.; Kotani, Y.; Kamigaito, M.; Sawamoto, M. *Macromolecules* **1997**, *30*, 2249-2253.

[87] Uegaki, H.; Kotani, Y.; Kamigaito, M.; Sawamoto, M. *Macromolecules* **1998**, *31*, 6756-6761.

[88] Uegaki, H.; Kamigaito, M.; Sawamoto, M. *J. Polym. Sci., Part A: Polym. Chem.* **1999**, *37*, 3003-3009.

[89] Lecomte, P.; Drapier, I.; Dubois, P.; Teyssié, P.; Jérôme, R. *Macromolecules* **1997**, *30*, 7631-7633.

[90] Le Grognec, E.; Claverie, J.; Poli, R. *J. Am. Chem. Soc.* **2001**, *123*, 9513-9524.

[91] Stoffelbach, F.; Haddleton, D. M.; Poli, R. *Eur. Polym. J.* **2003**, *39*, 2099-2105.

[92] Braunecker, W. A.; Itami, Y.; Matyjaszewski, K. *Macromolecules* **2005**, *38*, 9402-9404.

[93] Kabachii, Y. A.; Kochev, S. Y.; Bronstein, L. M.; Blagodatskikh, I. B.; Valetsky, P. M. *Polym. Bull.* **2003**, *50*, 271-278.

[94] Matyjaszewski, K.; Jakubowski, W.; Min, K.; Tang, W.; Huang, J.; Braunecker, W. A.; Tsarevsky, N. V. *Proc. Natl. Acad. Sci.* **2006**, *103*, 15309-15314.

[95] de Vries, A.; Klumperman, B.; de Wet-Roos, D.; Sanderson, R. D. *Macromol. Chem. Phys.* **2001**, *202*, 1645-1648.

[96] Jakubowski, W.; Matyjaszewski, K. *Angew. Chem., Int. Ed.* **2006**, *45*, 4482-4486.

[97] Magenau, A. J. D.; Strandwitz, N. C.; Gennaro, A.; Matyjaszewski, K. *Science* **2011**, *332*, 81-84.

[98] Pan, X.; Tasdelen, M. A.; Laun, J.; Junkers, T.; Yagci, Y.; Matyjaszewski, K. *Prog. Polym. Sci.* **2016**, 62, 73-125.

[99] Wang, G.-X.; Lu, M.; Zhou, M.-J. *J. Macromol. Sci. Part A.* **2018**, 55, 85-89.

[100] Theriot, J. C.; Lim, C.-H.; Yang, H.; Ryan, M. D.; Musgrave, C. B.; Miyake, G. M. *Science* **2016**, *352*, 1082-1086.

[101] Lligadas, G.; Grama, S.; Percec, V. *Biomacromolecules* **2017**, *18*, 1039-1063.

[102] Lligadas, G.; Grama, S.; Percec, V. *Biomacromolecules* **2017**, *18*, 2981-3008.

[103] Anastasaki, A.; Nikolau, V.; Nurumbetov, G.; Wilson, P.; Kempe, K.; Quinn, J. F.; Davis, T. P.; Whittaker, M. R.; Haddleton, D. M. *Chem. Rev.* **2016**, *116*, 835-877.

[104] Queffelec, J.; Gaynor, S. G.; Matyjaszewski, K. *Macromolecules* **2000**, *33*, 8629-8639.

[105] Rosen, B. M.; Percec, V. *J. Polym. Sci., Part A: Polym. Chem.* **2007**, *45*, 4950-4964.

[106] Rosen, B. M.; Jiang, X.; Wilson, C. J.; Nguyen, N. H.; Monteiro, M. J.; Percec, V. *J. Polym. Sci., Part A: Polym. Chem.* **2009**, *47*, 5606-5628.

[107] Guliashvili, T.; Percec, V. *J. Polym. Sci., Part A: Polym. Chem.* **2007**, *45*, 1607-1618.

[108] Lligadas, G.; Rosen, B. M.; Monteiro, M. J.; Percec, V. *Macromolecules* **2008**, *41*, 8360-8364.

[109] Lligadas, G.; Percec, V. *J. Polym. Sci., Part A: Polym. Chem.* **2008**, *46*, 6880-6895.

[110] Nguyen, N. H.; Percec, V. *J. Polym. Sci., Part A: Polym. Chem.* **2011**, *49*, 4227-4240.

Introduction

[111] Nguyen, N. H.; Levere, M. E.; Kulis, J.; Monteiro, M. J.; Percec, V. *Macromolecules* **2012**, *45*, 4606-4622.

[112] Nguyen, N. H.; Rosen, B. M.; Lligadas, G.; Percec, V. *Macromolecules* **2009**, *42*, 2379-2386.

[113] Jiang, X.; Rosen, B. M.; Percec, V. *J. Polym. Sci., Part A: Polym. Chem.* **2010**, *48*, 403-409.

[114] Anastasaki, A.; Waldron, C. J.; Wilson, P.; Boyer, C.; Zetterlund, P. B.; Whittaker, M. R.; Haddleton, D. M. *ACS Macro Lett.* **2013**, *2*, 896-900.

[115] Wang, W.; Zhang, Z.; Wu, Y.; Zhu, J.; Cheng, Z.; Zhou, N.; Zhang, W.; Zhu, X. *J. Polym. Sci., Part A: Polym. Chem.* **2012**, *50*, 711-719.

[116] Fleischmann, S.; Percec, V. *J. Polym. Sci., Part A: Polym. Chem.* **2010**, *48*, 2243-2250.

[117] Hu, X.; Li, J.; Li, H.; Zhang, Z. *J. Polym. Sci., Part A: Polym. Chem.* **2013**, *51*, 4378-4388.

[118] Nguyen, N. H.; Rosen, B. M.; Percec, V. *J. Polym. Sci., Part A: Polym. Chem.* **2010**, *48*, 1752-1763.

[119] Tang, X.; Liang, X.; Yang, Q.; Fan, X.; Shen, Z.; Zhou, Q. *J. Polym. Sci., Part A: Polym. Chem.* **2009**, *47*, 4420-4427.

[120] Anastasaki, A.; Haddleton, A. J.; Zhang, Q.; Simula, A.; Droesbeke, M.; Wilson, P.; Haddleton, D. M. *Macromol. Rapid Commun.* **2014**, *35*, 965-970.

[121] Ding, A.; Lu, H.; Guo, H.; Zheng, X.; Huang, X. *J. Polym. Sci., Part A: Polym. Chem.* **2013**, *51*, 1091-1098.

[122] Deng. Y.; Zhang, J. Z.; Li, Y.; Hu, J.; Yang, D.; Huang, X. *J. Polym. Sci., Part A: Polym. Chem.* **2012**, *50*, 4451-4458.

[123] Nguyen, N. H.; Rodriguez-Emmenegger, C.; Brynda, E.; Sedlakova, Z.; Percec, V. *Polym. Chem.* **2013**, *4*, 2424-2427.

[124] Samanta, S. R.; Percec, V. *Polym. Chem.* **2014**, *5*, 169-174.

[125] Rosen, B. M.; Percec, V. *Chem. Rev.* **2009**, *109*, 5069-5119.

[126] Anastasaki, A.; Nikolaou, V.; Haddleton, D. M. *Polym. Chem.* **2016**, *7*, 1002-1026.

[127] Leng, X.; Nguyen, N. H.; van Buesekom, B.; Wilson, D. A.; Percec, V. *Polym. Chem.* **2013**, *4*, 2995-3004.

[128] Levere, M. E.; Willoughby, I.; O'Donohue, S.; Wright, P. M.; Grice, A. J.; Fidge, C.; Becer, C. R.; Haddleton, D. M. *J. Polym. Sci., Part A: Polym. Chem.* **2011**, *49*, 1753-1763.

[129] Basuki, J. S.; Esser, L.; Duong, H. T. T.; Zhang, Q.; Wilson, P.; Whittaker, M. R.; Haddleton, D. M.; Boyer, C.; Davis, T. P. *Chem. Sci.* **2014**, *5*, 715-726.

[130] Basuki, J. S.; Esser, L.; Zetterlund, P. B.; Whittaker, M. R.; Boyer, C.; Davis, T. P. *Macromolecules* **2013**, *46*, 6038-6047.

[131] Yang, J.; He, W-D.; He, C.; Tao, J.; Chen, S-Q.; Miu, S-M.; Zhu, S-L. *J. Polym. Sci., Part A: Polym. Chem.* **2013**, *51*, 3791-3799.

[132] Xue, X.; Li, F.; Huang, W.; Yang, H.; Jiang, B.; Zheng, Y.; Zhang, D.; Fang, J.; Kong, L.; Zhai, G.; Chen, J. *Macromol. Rapid Commun.* **2014**, *35*, 330-336.

[133] Boyer, C.; Corrigan, N. A.; Jung, K.; Nguyen, D.; Nguyen, T. K.; Adnan, N. N.; Oliver, S.; Shanmugam, S.; Yeow, J. *Chem. Rev.* **2016**, *116*, 1803-1949.

[134] Fan, X.; Wang, Z.; He, C. *J. Mater. Chem. B* **2015**, *3*, 4715–4722.

[135] Zhang, Q.; Nurumbetov, G.; Simula, A.; Zhu, C.; Li, M.; Wilson, P.; Kempe, K.; Yang, B.; Tao, L.; Haddleton, D. M. *Polym. Chem.* **2016**, *7*, 7002-7010.

[136] Bexis, P.; Thomas, A. W.; Bell, C. A.; Dove, A. P. *Polym. Chem.* **2016**, *7*, 7126-7134.

[137] Charan, H.; Kinzel, J.; Glebe, U.; Anand, D.; Garakani, T. M.; Zhu, L.; Bocola, M.; Schwaneberg, U.; Böker, A. *Biomaterials* **2016**, *107*, 115-123.

[138] Lligadas, G.; Percec, V. *J. Polym. Sci., Part A: Polym. Chem.* **2008**, *46*, 4917-4926.

[139] Gu, W.; Jia, Z.; Truong, N. P.; Prasadam, I.; Xiao, Y.; Monteiro, M. J. *Biomacromolecules* **2013**, *14*, 3386-3389.

[140] Simula, A.; Nurumbetov, G.; Anastasaki, A.; Wilson, P.; Haddleton, D. M. *Eur. Polym. J.* **2015**, *62*, 294-303.

[141] Moreno, A.; Jiménez-Alesanco, A.; Ronda, J. C.; Cádiz, V.; Galià, M.; Percec, V.; Abian, O.; Lligadas, G. *Biomacromolecules* **2020**, *21*, 4313-4325.

[142] Moreno, A.; Ronda, J. C.; Cádiz, V.; Galià, M.; Lligadas, G.; Percec, V. *Biomacromolecules* **2019**, *20*, 3200-3210.

Introduction

[143] Moreno, A.; Ronda, J. C.; Cádiz, V.; Galià, M.; Lligadas, G.; Percec, V. *ACS Macro Lett.* **2019**, *8*, 1200-1208.

[144] Lligadas, G.; Rosen, B. M.; Bell, C. A.; Monteiro, M. J.; Percec, V. *Macromolecules* **2008**, *41*, 8365-8371.

[145] Nguyen, N. H.; Percec. *J. Polym. Sci.: Part A: Polym. Chem.* **2010**, *48*, 5109-5119.

[146] Percec, V.; Barboiu, B.; van der Sluis, M. *Macromolecules* **1998**, *31*, 4053-4056.

[147] Nguyen, N. H.; Percec, V. *J. Polym. Sci., Part A: Polym. Chem.* **2011**, *49*, 4241-4252.

[148] Samanta, S. R.; Sun, H. J.; Anastasaki, D. M.; Haddleton, D. M.; Percec, V. *Polym. Chem.* **2014**, *5*, 89-95.

[149] Ree, L.; Kelland, M. A.; Haddleton, D. M.; Alsubaie, F. *Energy Fuels* **2017**, *31*, 1355-1361.

[150] Gavrilov, M.; Zerk, T. J.; Bernhardt, P. V.; Percec, V.; Monteiro, M. J. *Polym. Chem.* **2016**, *7*, 933-939.

[151] Wright, P. M.; Mantovani, G.; Haddleton, D. M. *J. Polym. Sci., Part A: Polym. Chem.* **2008**, *46*, 7376-7385.

[152] Percec, V.; Popov, A. V.; Ramirez-Castillo, E.; Weichold, O. *J. Polym. Sci., Part A: Polym. Chem.* **2003**, *41*, 3283-3299.

[153] Hatano, T.; Rosen, B. M.; Percec, V. *J. Polym. Sci., Part A: Polym. Chem.* **2010**, *48*, 164-172.

[154] Hornby, B. D.; West, A. G.; Tom, J. C.; Waterson, C.; Harrison, S.; Perrier, S. *Macromol. Rapid Commun.* **2010**, *31*, 1276-1280.

[155] Ciampolini, M.; Nardi, N. *Inorg. Chem.* **1966**, *5*, 41-44.

[156] Wang, W.; Zhang, Z.; Zhu, J.; Zhou, N.; Zhu, X. *J. Polym. Sci., Part A: Polym. Chem.* **2009**, *47*, 6316-6327.

[157] Simula, A.; Nikolaou, V.; Alsubaie, F.; Anastasaki, A.; Haddleton, D. M. *Polym. Chem.* **2015**, *6*, 5940-5950.

[158] Ma, J.; Chen, H.; Zhang, M.; Chen, L. *J. Polym. Sci., Part A: Polym. Chem.* **2011**, *49*, 2588-2593.

[159] Fan, L.; Chen, H.; Lv, G.; Gao, J.; Fu, Y. *J. Polym. Sci., Part A: Polym. Chem.* **2013**, *51*, 3233-3239.

[160] Yu, H.; Wu, Y.; Gao, J.; Wang, W.; Zhang, Z.; Zhu, X. *J. Polym. Sci., Part A: Polym. Chem.* **2012**, *50*, 4983-4989.

[161] Tom, J.; Hornby, B.; West, A.; Harrison, S.; Perrier, S. *Polym. Chem.* **2010**, *1*, 420-422.

[162] Nguyen, N. H.; Jiang, X.; Fleischmann, S.; Rosen, B. M.; Percec, V. *J. Polym. Sci., Part A: Polym. Chem.* **2009**, *47*, 5629-5638.

[163] Anastasaki, A.; Waldron, C.; Wilson, P.; McHale, R.; Haddleton, D. M. *Polym. Chem.* **2013**, *4*, 2672-2675.

[164] Levere, M. E.; Nguyen, N. H.; Leng, X.; Percec, V. *Polym. Chem.* **2013**, *4*, 1635-1647.

[165] Shibaeva, O.; Champagne, P.; Cunningham, M. F. *Green Mater.* **2016**, *2*, 104-114.

[166] Ma, J.; Chen, H.; Zhang, M; Yu, M. *J. Polym. Sci., Part A: Polym. Chem.* **2012**, *50*, 609-613.

[167] Samanta, S. R.; Anastasaki, A.; Waldron, C.; Haddleton, D. M.; Percec, V. *Polym. Chem.* **2013**, *4*, 5555-5562.

[168] Samanta, S. R.; Cai, R.; Percec, V. *Polym. Chem.* **2014**, *5*, 5479-5491.

[169] Samanta, S. R.; Anastasaki, A.; Waldron, C.; Haddleton, D. M.; Percec, V. *Polym. Chem.* **2013**, *4*, 5563-5569.

[170] Samanta, S. R.; Levere, M. E.; Percec, V. *Polym. Chem*. **2013**, *4*, 3212-3224.

[171] Fleischmann, S.; Percec, V. *J. Polym. Sci., Part A: Polym. Chem.* **2010**, *48*, 4889-4893.

[172] Moreno, A.; Garcia, D.; Galià, M.; Ronda, J. C.; Cádiz, V.; Lligadas, G.; Percec, V. *Biomacromolecules* **2017**, *18*, 3447-3456.

[173] Zhang, Q.; Wilson, P.; Li, Z.; McHale, R.; Godfrey, J.; Anastasaki, A.; Waldron, C.; Haddleton, D. M. *J. Am. Chem. Soc.* **2013**, *135*, 7355-7363.

[174] Zhang, Q.; Li, Z.; Wilson, P.; Haddleton, D. M. *Chem. Commun.* **2013**, *49*, 6608-6610.

[175] Waldron, C.; Zhang, Q.; Li, Z.; Nikolaou, V.; Nurumbetov, G.; Godfrey, J.; McHale, R.; Yilmaz, G.; Randev, R. K.; Girault, M.; McEwan, K.; Haddleton, D. M.; Droesbeke, M.; Haddleton, A. J.; Wilson, P.; Simula, A.; Collins, J.; Lloyd, D. J.; Burns, J. A.; Summers, C.;

Houben, C.; Anastasaki, A.; Li, M.; Becer, C. R.; Kiviaho, J. K.; Risangud, N. *Polym. Chem.* **2014**, *5*, 57-61.

[176] Enayati, M.; Jezorek, R. L.; Monteiro, M. J.; Percec, V. *Polym. Chem.* **2016**, *7*, 5930-5942.

[177] Jezorek, R. L.; Enayati, M.; Smail, R. B.; Lejnieks, J.; Grama, S.; Monteiro, M. J.; Percec, V. *Polym. Chem.* **2017**, *8*, 3405-3424.

[178] Smail, R. B.; Jezorek, R. L.; Lejnieks, J.; Enayati, M.; Grama, S.; Monteiro, M. J.; Percec, V. *Polym. Chem.* **2017**, *8*, 3102-3123.

[179] Enayati, M.; Smail, R. B.; Grama, S.; Jezorek, R. L.; Monteiro, M. J.; Percec, V. *Polym. Chem.* **2016**, *7*, 7230-7241.

[180] Arslan, H. In *Polymerization*; De Souza Gomez, A., Ed.; IntechOpen. 2012. pp. 279-320.

[181] Jennings, J.; He, G.; Howdle, S. M.; Zetterlund, P. B. *Chem. Soc. Rev.* **2016**, *45*, 5055-5084.

[182] Bates, C. M.; Bates, F. S. *Macromolecules* **2017**, *50*, 3-22.

[183] Epps III, T. H.; O'Reilly, R. K. *Chem. Sci.* **2016**, *7*, 1674-1689.

[184] Matyjaszewski, K.; Shipp, D. A.; McMurtry, G. P.; Gaynor, S. G.; Pakula, T. *J. Polym. Sci., Part A: Polym. Chem.* **2000**, *38*, 2023-2031.

[185] Kowalewski, T.; Tsarevsky, N. V.; Matyjaszewski, K. *J. Am. Chem. Soc.* **2002**, *124*, 10632-10633.

[186] Kowalewski, T.; Tang, C.; Kruk, M.; Dufour, B.; Matyjaszewski, K. *Symp. Ser. Am. Chem. Soc.* **2006**, *944*, 295-310.

[187] Wang, Z.; yuan, L.; Tang, C. *Acc. Chem. Res.* **2017**, *50*, 1762-1773.

[188] Li, M.; Jahed, N. M.; Min, K.; Matyjaszewski, K. *Macromolecules* **2004**, *37*, 2434-2441.

[189] Matyjaszewski, K. *Polym. Int.* **2003**, *52*, 1559-1565.

[190] Yao, K.; Tang, C. *Macromolecules* **2013**, *46*, 1689-1712.

[191] Kamigaito, M.; Satoh, K. In Sustainable Polymers from Biomass, 1st edition; Tang, C.; Ryu, C. Y., Eds; Wiley-VCH Verlag GmbH & Co. KGaA: 2017, pp. 55-90.

[192] Beyazkilic, Z.; Lligadas, G.; Ronda, J. C.; Galià, M.; Cádiz, V. *Polymer* **2015**, *68*, 101-110.

[193] Lluch, C.; Calle, M.; Lligadas, G.; Ronda, J. C.; Galià, M.; Cádiz, V. *Eur. Polym. J.* **2015**, *72*, 64-71.

[194] Yuan, L.; Wang, Z.; Trenor, N. M.; Tang, C. *Macromolecules* **2015**, *48*, 1320-1328.

[195] Yuan, L.; Wang, Z.; Trenor, N. M.; Tang, C. *Polym. Chem.* **2016**, *7*, 2790-2798.

[196] Wang, S.; Ding, W.; Yang, G.; Robertson, M. L. *Macromol. Chem. Phys.* **2016**, *217*, 292-303.

[197] Gallagher, J. J.; Hillmyer, M. A.; Reineke, T. M. *ACS Sustainable Chem. Eng.* **2016**, *4*, 3379-3387.

[198] Yilmaz, G.; Messager, L.; Gleinich, A. S.; Mitchell, D. A.; Battaglia, G.; Becer, C. R. *Polym. Chem.* **2016**, *7*, 6293-6296.

[199] Hatton, F. L. *Polym. Chem.* **2020**, *11*, 220-229.

[200] Gestranius, M.; Otsuka, I.; Halila, S.; Hermida-Merino, D.; Solano, E.; Borsali, R.; Tammelin, T. *Adv. Mater. Interfaces* **2020**, 1901737.

[201] An, S. Y.; Hong, S. H.; Tang, C.; Oh, J. K. *Polym. Chem.* **2016**, *7*, 4751-4760.

[202] Maiti, B.; Haldar, U.; Rajasekhar, T.; De, P. *Chem.– Eur. J.* **2017**, *23*, 15156-15165.

[203] Zhou, J.; Wu, M.; Peng, Q.; Jiang, F.; Pan, H.; Wang, B.; Liu, S.; Wang, Z. *Polym. Chem.* **2018**, *9*, 2880-2886.

[204] Nasiri, M.; Reineke, T. M. *Polym. Chem.* **2016**, *7*, 5233-5240.

[205] Stamm, A.; Tengdelius, M.; Schmidt, B.; Engström, J.; Syrén, P. O.; Fogelström, L.; Malmström, E. *Green Chem.* **2019**, *21*, 2720-2731.

[206] Ray, P.; Hughes, T.; Smith, C.; Simon, G. P.; Saito, K. *ACS Omega* **2018**, *3*, 2040-2048.

[207] Noppalit, S.; Simula, A.; Billon, L.; Asua, J. M. *ACS Sustainable Chem. Eng.* **2019**, *7*, 17990-17998.

[208] Wang, S.; Shuai, L.; Saha, B.; Vlachos, D. G.; Epps III, T. H. *ACS Cent. Sci.* **2018**, *4*, 701-708.

[209] Spontak, R. J.; Pate, N. P. *Curr. Opin. Colloid Interface Sci.* **2000**, *5*, 334-341.

Introduction

[210] Mann, D. M. Inst. M.; Van den Bos, J. C.; Way, A. In Automotive Plastics & Composites: *Worldwide Markets and Trends to 2007*, Second edition; Elsevier Science Ltd: Oxford, 1999; pp. 1-393.

[211] Nurul, H. I.; Mariatti, M. In *Polymer Engineering and Science;* Sadhan, C. J., Ed; Wiley Online Library: 2018; 58.

[212] Jiang, F.; Fang, C.; Zhang, J.; Wang, W.; Wang, Z. *Macromolecules* **2017**, *50*, 6218-6226.

[213] Drobny, J. E. Handbook of Thermoplastic Elastomers, 2nd Ed., Elsevier Inc. San Diego, CA 2014.

[214] Varshney, S. K.; Kesani, P.; Agarwal, N.; Zhang, J. X.; Rafailovich, M. *Macromolecules* **1999**, 32, 235-237.

[215] Xu, J.; Zhang, A.; Zhou, T.; Cao, X.; Xie, Z. *Polym. Degrad. Stab.* **2007**, *92*, 1682-1692.

[216] Noppalit, S.; Simula, A.; Ballard, N.; Callies, X.; Asua, J. M.; Billon, L. *Biomacromolecules* **2019**, *20*, 2241-2251.

[217] Wang, Z.; Yuan, L.; Trenor, N. M.; Vlaminck, L.; Billiet, S.; Sarkar, A.; Du Prez, F. E.; Stefika M.; Tang C. *Green Chem.* **2015**,*17*, 3806-3818.

[218] Chatterjee, D. P.; Mandal, B. M. *Macromolecules* **2006**, *39*, 9192-9200.

[219] Wang, S.; Ding, W.; Yang, G.; Robertson, M. L. *Macromol. Chem. Phys.* **2006**, *217*, 292-303.

[220] Liu, S.; Zhang, X.; Li, M.; Ren, X.; Tao, Y. *J. Polym. Sci. Part A: Polym. Chem.* **2017**, *55*, 349-355.

[221] Satoh, K.; Lee, D. H.; Nagai, K.; Kamigaito, M. *Macromol. Rapid Commun.* **2014**, *35*, 161-167.

[222] Ding, K.; John, A.; Shin, J.; Lee, Y.; Quinn, T.; Tolman, W. B.; Hillmyer, M. A. *Biomacromolecules* **2015**, *16*, 2537-2539.

[223] Shin, J.; Lee, Y.; Tolman, W. B.; Hillmyer, M. A. *Biomacromolecules* **2012**, *13*, 3833-3840.

[224] Sainz, M. F.; Sauto, J. A.; Regentova, D.; Johansson, M. K. G.; Timhagen, S. T.; Irvine, D. J.; Buijsen, P.; Koning, C. E.; Stockman, R. A.; Howdle, S. M. *Polym. Chem.* **2016**, *7*, 2882-2887.

[225] Wang, Z.; Fang, H. In *Sustainable Polymers from Biomass*: first edition; Tang, C.; Y Ryu, C. Eds; Wiley-VCH Verleg GmbH & Co. KGaA.: 2017; pp. 55-90.

[226] Holmberg, A. L., Stanzione III, J. F., Wool, R. P. & Epps III, T. H. *ACS Sustainable Chem. Eng.* **2014**, *2*, 569-573.

[227] Zhou, J., Zhang, H., Deng, J. & Wu, Y. *Macromol. Chem. Phys.* **2016**, *217*, 2402-2408.

[228] Takeshima, H.; Satoh, K.; Kamigaito, M. *Macromolecules* **2017**, *50*, 4206-4216.

[229] Sajjad, H.; Tolman, W. B.; Reineke T. M. *ACS Appl. Polym. Mater.* **2020**, *2*, 2719-2728.

[230] Whitesides, G. M.; Grzybowski, B. *Science* **2002**, *295*, 2418-2421.

[231] Binder, W. H.; Barragan, V.; Menger, F. M. *Angew. Chem., Int. Ed.* **2003**, *42*, 5802-5827.

[232] Zhang, L. F.; Yu, K.; Eisenberg, A. *Science* **1996**, *272*, 1777-1779.

[233] Shivshankar, S. R.; Sathyan, A.; Shunmugam, R. *ACS Appl. Nano Mater.* **2020**, *3*, 2104-2117.

[234] Balmbra, R. R.; Clunie, J. S.; Goodman, J. F. *Nature* **1969**, *222*, 1159-1160.

[235] Israelachvili, J. N. *Intermolecular & Surface Forces*, 2nd ed.; Academic Press: London, 1991; Vol. 1.

[236] Israelachvili, J. N.; Mitchell, D. J.; Ninham, B. W. *J. Chem. Soc., Faraday Trans.* **1976**, *72*, 1525-1568.

[237] Blanazs, A.; Madsen, J.; Battaglia, G.; Ryan, A. J.; Armes, S. P. *J. Am. Chem. Soc.* **2011**, *133*, 16581-16587.

[238] Bang, J.; Jain, S.; Li, Z.; Lodge, T. P.; Pedersen, J. S.; Kesselman, E.; Talmon, Y. *Macromolecules* **2006**, *39*, 5583-5583.

[239] Moughton, A. O.; O'Reilly, R. K. *Chem. Commun.* **2010**, *46*, 1091-1093.

[240] Hill, M. R.; MacKrell, E. J.; Forsthoefel, C. P.; Jensen, S. P.; Chen, M.; Moore, G. A.; He, Z. L.; Sumerlin, B. S. *Biomacromolecules* **2015**, *16*, 1276-1282.

[241] Mane, S. R.; Shunmugam, R. *ACS Macro Lett.* **2014**, *3*, 44-50.

[242] Mane, S. R.; Rao, N. V.; Shunmugam, R. *ACS Macro Lett.* **2012**, *1*, 482-488.

[243] Mane, S. R.; Dinda, H.; Sathyan, S.; Das Sarma, J.; Shunmugam, R. *ACS Appl. Mater. Interfaces* **2014**, *6*, 16895-16902.

Introduction

[244] Bhattacharya, S.; Ganivada, M. N.; Dinda, H.; Das Sarma, J.; Shunmugam, R. *ACS Omega* **2016**, *1*, 108-117.

[245] M., C., Lukowiak; B., N., S., Thota; R., Haag. *Biotechnol. Adv.* **2015**, *33*, 1327-1341.

[246] Zarrintaj, P.; Jouyandeh, M.; Ganjali, M. R.; Hadavand, B. S.; Mozafari, M.; Sheiko, S. S.; Vatankhah-Varnoosfaderani, M.; Gutierrez, T. J.; Saeb, M. R. *Eur. Polym. J.* **2019**, *117*, 402-423.

[247] Moreno, P. S.; de Vicente, J.; Nardecchia, S.; Marchal, J. A.; Boulaiz, H. *Nanomaterials* **2018**, *8*, 935-967.

[248] Li, Q.; Cao, Z.; Wang, G. *Polym. Chem.* **2018**, *9*, 463-471.

[249] Chen, S.; Jiang, F.; Cao, Z.; Wang, G.; Dang, Z. M. *Chem. Commun.* **2015**, *51*, 12633-12636.

[250] Soo, P. L.; Lovric, J.; Davidson, P.; Maysinger, D.; Eisenberg, A. *Mol. Pharmaceutics* **2005**, *2*, 519-527.

[251] Alibadi, H. M.; Lavasanifar, A. *Expert Opin. Drug Deliv.* **2006**, *3*, 139-162.

[252] Jee, J. P.; McCoy, A.; Mecozzi, S. *Pharm. Res.* **2012**, *29*, 69-82.

[253] Gou, M.; Men, K.; Shi, H.; Xiang, M.; Zhang, J.; Song, J.; Long, J.; Wan, Y.; Luo, F.; Zhao, X.; Quian, Z. *Nanoscale* **2011**, *3*, 1558-1567.

[254] Sun, J.-T.; Hong, C.-Y.; Pan, C.-Y. *Soft Matter* **2012**, *8*, 7753-7767.

[255] Karagoz, B.; Esser, L.; Doung, H. T.; Basuki, J. S.; Boyer, C.; Davis, T. P. *Polym. Chem.* **2014**, *5*, 350-355.

[256] Figg, C. A.; Simula, A.; Gebre, K. A.; Tucker, B. S.; Haddleton, D. M.; Sumerlin, B. S. *Chem. Sci.* **2015**, *6*, 1230-1236.

[257] Derry, M. J.; Fielding, L. A.; Armes, S. P. *Prog. Polym. Sci.* **2016**, *52*, 1-18.

[258] Doncom, K. E. B.; Warren, N. J.; Armes, S. P. *Polym. Chem.* **2015**, *6*, 7264-7273.

[259] Sugihara, S.; Ma'Radzi, A. H.; Ida, S.; Irie, S.; Kikukawa, T.; Maeda, Y. *Polymer* **2015**, *76*, 17-24.

[260] Yeow, J.; Xu, J.; Boyer, C. *ACS Macro Lett.* **2015**, *4*, 984-990.

[261] Huo, M.; Ye, Q.; Che, H.; Wang, X.; Wei, Y.; Yuan, J. *Macromolecules* **2017**, *50*, 1126-1133.

[262] Gao, C.; Zhou, H.; Qu, Y.; Wang, W.; Khan, H.; Zhang, W. *Macromolecules* **2016**, *49*, 3789-3798.

[263] Jennings, J.; Beija, M.; Richez, A. P.; Cooper, S. D.; Mignot, P. E.; Thurecht, K. J.; Jack, K. S.; Howdle, S. M. *J. Am. Chem. Soc.* **2012**, *134*, 4772-4781.

[264] Zong, M.; Thurecht, K. J.; Howdle, S. M. *Chem. Commun.* **2008**, 5942-5944.

[265] Zhang, Q.; Zhu, S. *ACS Macro Lett.* **2015**, *4*, 755-758.

[266] Zhang, B.; Yan, X.; Alcouffe, P.; Charlot, A.; Fleury, E.; Bernard, J. *ACS Macro Lett.* **2015**, *4*, 1008-1011.

[267] Rieger, J.; Stoffelbach, F.; Bui, C.; Alaimo, D.; Jerome, C.; Charleux, B. *Macromolecules* **2008**, *41*, 4065-4068.

[268] Qiao, X. G.; Lansalot, M.; Bourgeat-Lami, E.; Charleux, B. *Macromolecules* **2013**, *46*, 4285-4295.

[269] Qiao, X. G.; Dugas, P. Y.; Charleux, B.; Lansalot, M.; Bourgeat-Lami, E. *Macromolecules* **2015**, *48*, 545-556.

[270] Liu, X.; Gao, W. *ACS Appl. Mater. Interfaces* **2017**, *9*, 2023-2028.

[271] Wang, G.; Schmitt, M.; Wang, Z.; Lee, B.; Pan, X.; Fu, L.; Yan, J.; Li, S.; Xie, G.; Bockstaller, M. R.; Matyjaszewski, K. *Macromolecules* **2016**, *49*, 8605-8615.

[272] Kapishon, V.; Whitney, R. A.; Champagne, P.; Cunningham, M. F.; Neufeld, R. J. *Biomacromolecules* **2015**, *16*, 2040-2048.

[273] Tan, J.; Sun, H.; Yu, M.; Sumerlin, B. S.; Hang, L. *ACS Macro Lett.* **2015**, *4*, 1249-1253.

[274] Yeow, J. Y.; Boyer, C. *Adv. Sci.* **2017**, *4*, 1700137.

[275] Levit, M.; Zashikhina, N.; Vdovchenko, A.; Dobrodumov, A.; Zakharova, N.; Kashina, A.; Rühl, E.; Lavrentieva, A.; Scheper, T.; Tennikova, T.; Korzhikova-Vlakh, E. *Polymers* **2020**, *12*, 183.

[276] Isik, M.; Sardon, H.; Saenz, M.; Mecerreyes, D. *RSC Adv.* **2014**, *4*, 53407-53410.

Introduction

[277] Coumes, F.; Balarezo, M.; Rieger, J.; Stoffelbach, F. *Macromol. Rapid Commun.* **2020**, *41*, 2000002.

[278] Yilmaz, G.; Guler, E.; Geyik, C.; Demir, B.; Ozkan, M.; Demirkol, D. O.; Ozcelik, S.; Timur, S.; Becer, C. R. *Mol. Syst. Des. Eng.* **2018**, *3*, 150-158.

[279] Abdouni, Y.; Yilmaz, G.; Becer, C. R. *Macromol. Rapid Commun.* **2017**, 1700212.

[280] Cakir, N.; Hizala, G.; Becer, C. R. *Polym. Chem.* **2015**, *6*, 6623-6631.

[281] Yilmaz, G.; Becer, C. R. *Polym. Chem.* **2015**, *6*, 5503-5514.

[282] Rahman, M. A.; Sha, Y.; Jui, M. S.; Lamm, M. E.; Ma, Y.; Tang, C. *Macromolecules* **2019**, *52*, 9526-9535.

Chapter 2

All-acrylic Biobased Block Copolymers Derived from Lactic Acid-based Solvents

2.1. Polyacrylates derived from bio-based ethyl lactate solvent *via* SET-LRP

2.2. Photoinduced upgrading of lactic acid-based solvents to block copolymer surfactants

2.3. Biosourced all-acrylic ABA block copolymers with lactic acid-based soft phase

The contents of this chapter are published in: Bensabeh, N.; Moreno, A.; Roig, A.; Monaghan, O. R.; Ronda, J. C.; Cádiz, V.; Galià, M.; Howdle, S. M.; Lligadas, G. and Percec, V. *Biomacromolecules* **2019**, *20*, 2135-2147; Bensabeh, N.; Moreno, A.; Roig, A.; Rahimzadeh, M.; Rahimi, K.; Ronda, J. C.; Cádiz, V.; Galià, M.; Percec, V.; Rodriguez-Emmenegger, C. and Lligadas, G. *ACS Sustainable Chem. Eng.* **2020**, *8*, 1276-1284; Bensabeh, N.; Jiménez-Alesanco, A.; Liblikas, I.; Ronda, J. C.; Cádiz, V.; Galià, M.; Vares, L.; Abian, O.; Lligadas, G. *Molecules* **2020**, *25*, 5740.

2.1. Polyacrylates derived from bio-based ethyl lactate solvent *via* SET-LRP

The precise synthesis of polymers derived from alkyl lactate ester acrylates is reported for the first time. Kinetic experiments were conducted to demonstrate that Cu(0) wire-catalyzed single electron transfer-living radical polymerization (SET-LRP) in alcohols at 25 °C provides a green methodology for the LRP of this forgotten class of biobased monomers. The acrylic derivative of ethyl L-lactate solvent and homologous structures with methyl and n-butyl ester (ELA, MLA, and BLA, respectively) were polymerized with excellent control over molecular weight, molecular weight distribution, and chain-end functionality. Kinetics plots in conventional alcohols such as ethanol and methanol were first order in the monomer, with molecular weight increasing linearly with conversion. However, aqueous EL mixtures were found to be more suitable than pure EL to mediate the SET-LRP process. The near-quantitative monomer conversion and high bromine chain-end functionality, demonstrated by matrix-assisted laser desorption ionization time-of-flight analysis, further allowed the preparation of innovative biobased block copolymers containing rubbery poly(ethyl lactate acrylate) poly(ELA) sequences. For instance, the poly(ELA)-*b*-poly(glycerol acrylate) block copolymer self-assembled in water to form stable micelles with chiral lactic acid-derived block-forming micellar core as confirmed by the pyrene-probe-based fluorescence technique. Dynamic light scattering and transmission electron microscopy measurements revealed the nanosize spherical morphology for these biobased aggregates.

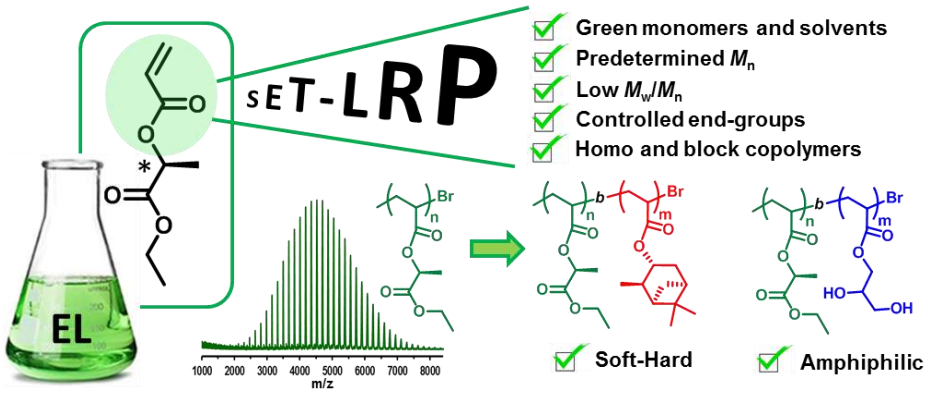

2.1.1. Introduction

Naturally occurring lactic acid (2-hydroxypropionic acid) was first isolated from sour milk by the Swedish chemist Scheele in 1780. Later on, this hydroxycarboxylic acid progressively became an industrial important product due to its versatile functional properties as a flavor agent, pH regulator, and preservative.[1] Currently, about 90% of the enantiomerically pure LA is produced by the fermentation of refined carbohydrates with appropriate microorganisms. [2] However, more convenient bioprocessing technologies based on lignocellulosic raw materials are already consolidated.[3] In recent years, the derivation of polymeric materials from sustainable and annually renewable resources, such as vegetable oils, sugars, terpenes, polysaccharides, rosins and lignin, among others, has attracted increasing interest due to dwindling of fossil oil resources and environmental impact of petroleum manufacturing[4,5] To this end, LA has shown particular promise in production of poly(lactic acid) (PLA), either by its own polycondensation or ring-opening polymerization (ROP) of its cyclic dimer lactide.[6-8]

The preparation of well-defined ABA thermoplastic elastomers illustrates an example on how recent advances in living radical polymerization has started a new era in the preparation of biomass-derived polymers with advanced properties and functions.[9-12] In this regard, SET-LRP has gained great popularity as a facile tool for precision macromolecular engineering. [13 - 19] For example, when conducted in reaction media that facilitates disproportionation of Cu(I)Br into Cu(0) and Cu(II)Br_2[20- 22] this method enables the synthesis of vinylic polymers with nearly 100 % chain end functionality at complete conversion.[23- 26] This has been demonstrated to be feasible even in “programmed” biphasic SET-LRP systems (i.e. aqueous-organic solvent mixtures based on both disproportionating[27-29] and non-disproportionating organic solvents).[30-33] Consequently, benefiting from this and other inherent attributes (e.g. facile set-up, reaction at ambient temperature, oxygen tolerance, compatibility with water and biological media), SET-LRP is an appealing platform to create well-defined bio-based polymers and limitless number of BCPs therefrom. The preparation of sequence controlled multi-block glycopolymers[34,35] and the controlled grafting of natural

polysaccharides[36,37] exemplifies successful efforts. Also, aside from the excellent synergy of SET-LRP with water (H_2O) and conventional alcohols,[17,19] it is compatible with other eco-friendly solvents such as polyethylene glycols,[38] ionic liquids[13,39] and *N,N*-dimethyl lactamide (DML)[40] without detrimentally affecting polymerization. More recently, it was also demonstrated that EL possess interesting features related to SET-LRP,[41] thus expanding the myriad of academic/industrial applications found for this promising bio-sourced solvent.[42-45] Acrylic derivatives of alkyl lactate esters are a forgotten class of sustainable monomers in polymer synthesis which complement the classic alkyl acrylates palette by increasing the density of polar and hydrolysable ester groups per repeat unit. In addition, well-defined poly(alkyl lactate acrylate)s may be important candidates for applications in chiral recognition and enantioselective catalysis because alkyl lactates are chiral syntons. To the best of our knowledge, there is no report on the LRP of such bio-based monomers. Surprisingly, even their free radical polymerization received limited attention.[46-48] Herein, our attention was focused on ELA (Scheme 2.1.1) and investigated Cu(0) wire-catalyzed SET-LRP for the synthesis of well-defined poly(ELA) under mild and environmentally friendly conditions. This method also enables control over the polymerization of homologous monomers with methyl and *n*-butyl ester groups (Scheme 2.1.1). Further, the block copolymerization of poly(ELA) was accomplished with other monomers derived from biomass feedstock resulting in well-defined block copolymers including chiral alkyl lactate acrylate sequences.

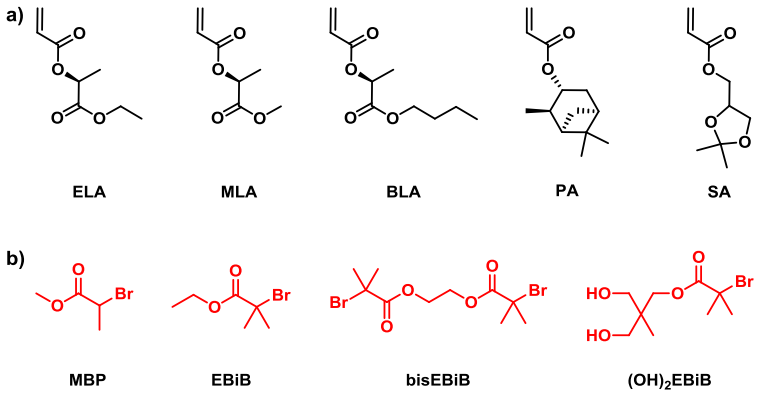

Scheme 2.1.1. Chemical structures of (a) bio-based acrylates and (b) initiators used in this study

2.1.2. Results and discussion

Synthesis of ethyl lactate acrylate

As illustrated in Scheme 2.1.2a, the acryloyl polymerisable functionality was installed on EL, commercially produced from sugarcane by fermentation, by acylation with acryloyl chloride in the presence of triethylamine (TEA) using dichloromethane (DCM) as solvent. ELA was isolated as a colorless liquid after work up and vacuum distillation in the presence of hydroquinone to minimize auto-polymerization (70% yield). The synthesis of the monomer was confirmed by NMR and FTIR spectroscopy (see Annex A, Figures S1-3). The acrylic protons appear in the ^{1}H NMR spectrum between 6.50 and 5.88 ppm, whereas the four characteristic signals of the vinylic and carbonyl carbons appear in the ^{13}C NMR spectrum at 170, 165 and 131, 127 ppm, respectively.

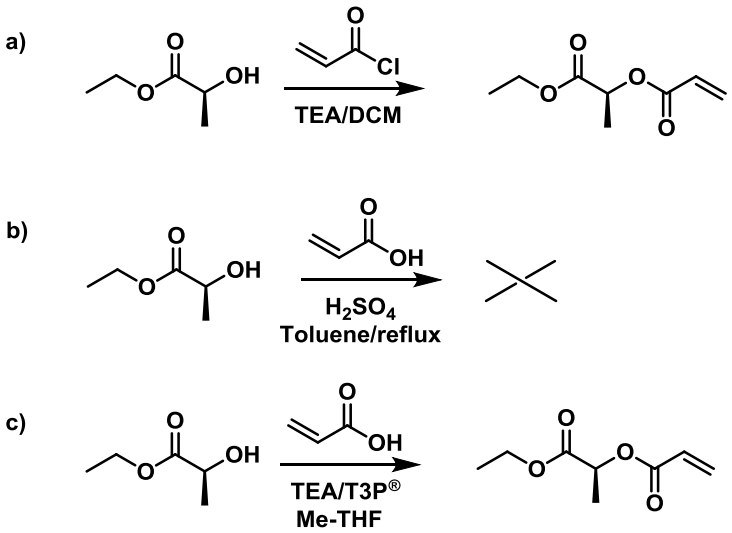

Scheme 2.1.2. Synthetic routes to ELA starting from EL solvent

FTIR spectroscopy showed characteristic absorptions of the two ester moieties at 1748 and 1726 cm^{-1} and the stretching of the acrylate C=C bond at around 1637 cm^{-1}. An additional structure confirmation was provided by high-resolution mass spectrometry (see experimental section). Supercritical fluid chromatography (SFC) was used for analytical chiral separation of the synthesized monomer (Figure S4 in Annex A). On the basis of this analysis

and optical rotation measurements ($[\alpha]_D^{25}$ = -53.9, *c* 1.0 mg/mL, MeCN), ELA employed was L-(-)-ELA with 96.7% enantiomeric excess. Being critical with the sustainability of the above described synthetic procedure, two alternative greener routes were explored in attempt to prepare ELA with the aid of acrylic acid (Scheme 2.1.2b and c). It is worth to mention that with the recent developments toward the commercial production of bio-acrylic acid and the cost-competitive production of bio-ethanol, ELA may be ultimately prepared entirely from biomass derived platform chemicals.[3] Unfortunately, the acrylic acid/EL acid-catalyzed esterification by azeotropic distillation in toluene was low-yielding because extensive oligomerization of EL occurred at high temperature.[46] Conversely, the use of T3P® under milder conditions gave an excellent result.[49] This ester coupling promoter lacks the toxicity and shock sensibility associated with other coupling agents (e.g. DCC and EDC).[50] Moreover, by-products from the coupling are H_2O-soluble and therefore easily separated from the reaction mixture. Using the biomass-derived 2-methyltetrahydrofuran (Me-THF) as solvent and a slight excess of acrylic acid in combination with TEA, ^{1}H NMR analysis confirmed the esterification of EL with acrylic acid. Despite low scale reaction, ELA was purified in this case by flash column chromatography. This route represents a more attractive approach to ELA and other alkyl lactate ester acrylates from a green chemistry point of view.

Selection of initiator for SET-LRP of ELA in DMSO

The polymerization of ELA was investigated employing the simpler SET-LRP methodology which uses Cu(0) wire wrapped around a stirring bar. Our preliminary investigations were devoted to select the optimal initiator for the polymerization of ELA using Me_6-TREN as ligand in DMSO (50 vol %) at 25 °C (Scheme 2.1.3). This powerful dipolar aprotic solvent is always one of the preferred options to practice SET-LRP because promotes extensive disproportionation of Cu(I)X in the presence of *N*-ligands such as Me_6-TREN and TREN.[21, 22] Moreover, it stabilizes the resulting colloidal Cu(0) particles and at the same time is also a good solvent for Cu(II)X_2 ligand complex.[51] Figure 2.1.1a,b depicts kinetic plots and GPC analysis for the polymerization using the monofunctional initiators MBP and EBiB at a targeted degree of polymerization (DP) of 50 (entries 1 and 2 in Table 2.1.1).

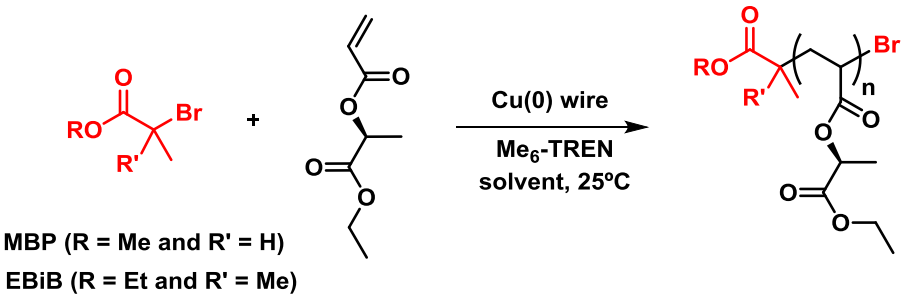

Scheme 2.1.3. Cu(0) wire-catalyzed SET-LRP of ELA initiated with MBP or EBiB using Me_6-TREN ligand in various solvents at room temperature. Solvents used here are DMSO, EtOH, MeOH, 2-PrOH, TFE, EL and aqueous EL mixtures.

^{1}H NMR analysis of regularly withdrawn samples from the homogeneous reaction mixtures was used to monitor monomer consumption during the reaction. Both polymerizations proceeded up to above 90% conversion in 110 min, confirming the generation of propagating radical from initiator. However, GPC analysis showed that there exist important differences between both initiating systems (Figure 2.1.1c). For example, significant deviation between the experimental (M_n (GPC)) and theoretical (M(th)) molecular weight values of the resulting poly(ELA) was observed during the polymerization with MBP up to approximately 30% monomer conversion. Moreover, polydispersity (M_w/M_n) in this case did not decrease below 2.1. These results suggest slow initiator rate when compared with propagation and/or slower rate of deactivation. In stark contrast, molar mass increased monotonically and linearly with theoretical values when using the tertiary initiator EBiB (Figure 2.1.1b, right). In this case, only a subtle molecular weight deviation, probably due to the bimolecular combination reaction between the propagating polymer chains, was observed at high conversion.

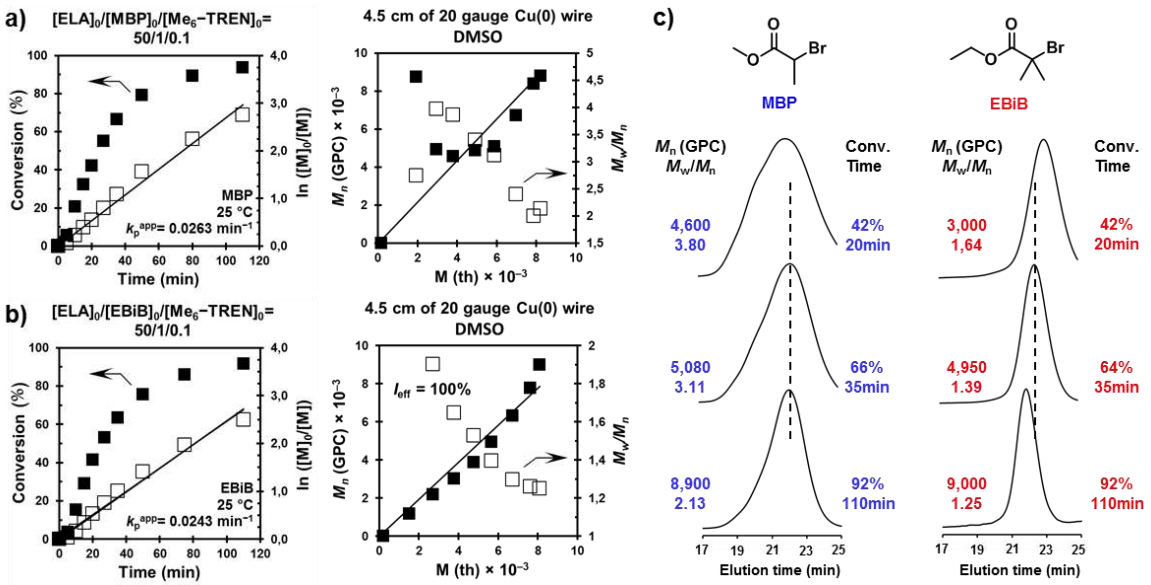

Figure 2.1.1. Monomer conversion, kinetics plots and evolution of experimental M_n (GPC) and M_w/M_n, based on the calibration by PMMA standards, versus theoretical M(th) for the SET-LRP of ELA initiated with MBP (a) and EBiB (b) in DMSO at 25 °C. Reaction conditions: ELA = 1 mL, DMSO = 0.5 mL, $[ELA]_0/[Initiator]_0/[Me_6\text{-}TREN]_0$ = 50/1/0.1 using 4.5 cm of hydrazine-activated Cu(0) wire (20-gauge diameter). (c) GPC traces (normalized to peak height) for the poly(ELA) obtained from kinetic experiments.

Table 2.1.1. Cu(0) Wire-Catalyzed SET-LRP of ELA in DMSO and Conventional Alcohols at 25 °C.[a]

entry	reaction medium	initiator	$[ELA]_0/[Initiator]_0/[Me_6\text{-}TREN]_0$	k_p^{app}	time (min)	conv.[b] (%)	M(th)[c]	M_n[d]	M_w/M_n[d]
1	DMSO	MBP	50/1/0.1	0.0263	110	94	8,225	8.800	2.13
2	DMSO	EBiB	50/1/0.1	0.0243	110	92	8,000	9,000	1.25
3	DMSO	MBP	50/1/0.1[e]	0.0263	110	94	8,225	7,970	1.18
4	EtOH	EBiB	50/1/0.1	0.0315	75	94	8,320	8,400	1.19
5	MeOH	EBiB	50/1/0.1	-	120	96	8,460	9,660	1.20
6	2-PrOH	EBiB	50/1/0.1	-	120	95	8,375	8,560	1.30
7	TFE	EBiB	50/1/0.1	0.0251	110	93	8,150	8,590	1.17
8	EtOH	EBiB	25/1/0.1	-	240	97	4,370	4,120	1.22
9	EtOH	EBiB	100/1/0.2	-	240	94	16,400	18,150	1.22
10	EtOH	EBiB	200/1/0.5	-	240	95	32,700	34,700	1.20
11	EtOH	EBiB	400/1/0.5	-	240	95	65,620	64,300	1.23

[a] Polymerization conditions: ELA = 1 mL, solvent = 0.5 mL (for entries 1-10) or 0.75 mL (for entry 11), 4.5 cm (for entries 1-7 and 9-11) or 0.5 cm (for entry 8) of hydrazine-activated Cu(0) wire (20-gauge diameter). [b] Determined by ^{1}H NMR. [c] M(th) = 172.18 x $[ELA]_0/[EBiB]_0$ x conv. + 195.05. [e] Determined by GPC using PMMA standards.[e] Reaction conducted in the presence of 5 mol % of externally added $Cu(II)Br_2$.

Overall, the tertiary initiator (EBiB) provided much higher degree of control over the MWD resulting in poly(ELA) with narrow M_w/M_n (1.25 compared to 2.13). This result, combined with a linear increase of $\ln[M]_0/[M]$ with time up to high conversion, suggest living polymerization features for the reaction initiated with EBiB. These observations are consistent with the fact that tertiary α-haloester-type initiators are better electronic mimics for conventional acrylates[52] and poly(ELA) provides an excellent example that demonstrates this hypothesis and concept.[52] Notably, the use of MBP initiator in the presence of 5 mol% externally added Cu(II)Br_2 deactivator, with respect to initiator concentration under otherwise identical conditions, yielded an important improvement over the MWD (M_w/M_n = 1.19) (entry 3 in Table 2.1.1 and Figure S5 in Annex A). However, we preferred using EBiB and other mono and bifunctional bromoisobutyrate derivatives, in absence of externally added deactivator, for the rest of this study.

Selection of eco-friendly solvents for SET-LRP of ELA

Ethanol and other conventional alcohols

A more environmentally friendly process for the SET-LRP of ELA was devised through the use of alcohols as solvents because combine both acceptable levels of [Cu(I)(Me_6-TREN)Br] disproportionation and low environmental impact.[17,53-56] We first focused our attention on EtOH, the oldest and most successful bio-sourced chemical solvent. The kinetics of the polymerization for the Cu(0) wire-catalyzed SET-LRP of ELA in EtOH using EBiB was investigated under identical conditions to the experiment in DMSO (entry 4 in Table 2.1.1 and Figure 2.1.2a). Also in this case, the reaction mixture remained homogeneous through the entire reaction course. The time evolution of $\ln([M]_0/[M])$ was linear up to monomer conversion above 90%, which is consistent with a constant concentration of propagating radicals during the homopolymerization reaction. In addition, molecular weights values were in excellent agreement with theoretical predictions (i.e. living polymerization). Surprisingly, the SET-LRP in EtOH was even faster than in DMSO (k_p^{app} = 0.0315 min^{-1} compared to 0.0243 min^{-1}). Indeed, it delivered a polymer with narrower MWD (M_w/M_n = 1.19 compared to 1.25).

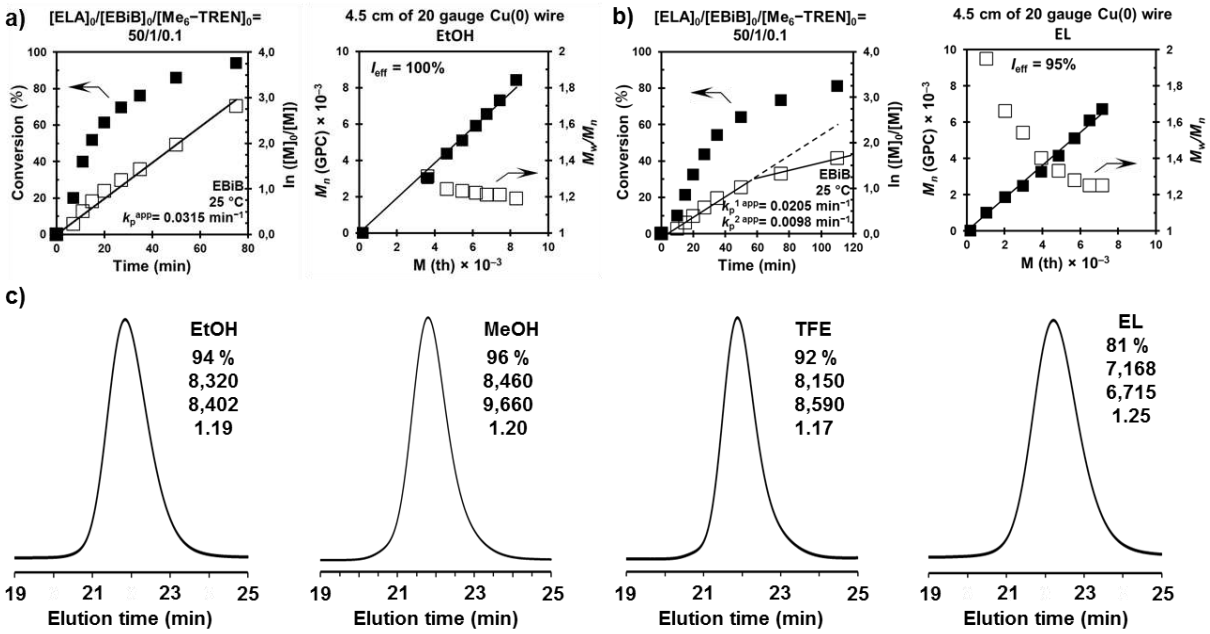

Figure 2.1.2. Monomer conversion, kinetics plots and evolution of experimental M_n (GPC) and M_w/M_n, based on the calibration by PMMA standards, versus theoretical M(th) for the SET-LRP of ELA initiated with EBiB in (a) EtOH and (b) EL at 25 °C. (c) GPC traces (normalized to peak height) for the poly(ELA) isolated after SET-LRP polymerization of ELA in EtOH, MeOH, TFE and EL. Reaction conditions: ELA = 1 mL, alcohol = 0.5 mL, $[ELA]_0/[EBiB]_0/[Me_6\text{-}TREN]_0$ = 50/1/0.1, and 4.5 cm of hydrazine-activated Cu(0) wire (20-gauge diameter). Numbers shown in black in (c) correspond to monomer conversion, M (th), M_n (GPC), and M_w/M_n respectively from the top to bottom.

As shown in Figure 2.1.2c, other conventional alcohols having similar solvent properties such as methanol (MeOH) could also be used to prepare well-defined poly(ELA) (entry 5 in Table 2.1.1). The reaction in propan-2-ol (2-PrOH) furnished a polymer with higher M_w/M_n (entry 6 in Table 2.1.1). However, in a fluorinated alcohol such as 2,2,2-trifluoroethanol (TFE), M_w/M_n was as low as 1.17 (entry 7 in Table 2.1.1 and Figure 2.1.2c). The kinetic plots for the polymerization in TFE also validates the use of fluorinated alcohols (see Annex A, Figure S6).[57-59]

Pushing the envelope of the ethanolic SET-LRP, we further investigated its potential in delivering well-defined poly(ELA) across a broad range of molecular weight while retaining control. Thus, a series of polymerizations were conducted varying the targeted DPs from 25 to 400 (entries 8-11 in Table 2.1.1). In all cases, SET-LRP smoothly proceeded at 25 °C to high

monomer conversions (> 90%), yielding polymers with controlled molecular weight up to 65,000 (Figure 2.1.3).

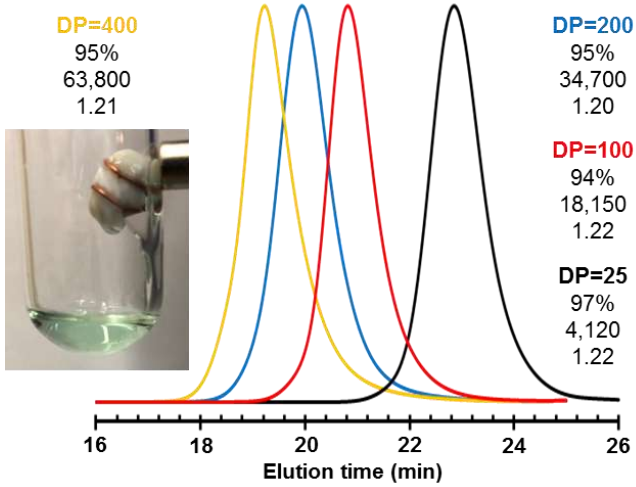

Figure 2.1.3. GPC traces (normalized to peak height) of poly(ELA) with different targeted DPs (see entries 8-11 in Table 2.1.1 for polymerization conditions). The inset shows a digital image of the homogeneous reaction mixture after ethanolic SET-LRP at targeted DP = 400. Numbers shown in black correspond to monomer conversion, M_n (GPC), and M_w/M_n respectively from the top to bottom.

It is worth to mention that the SET-LRP at DP= 400 was still homogeneous at high conversion, suggesting good solubility of poly(ELA) in this protic solvent environment (Figure 2.1.3, inset). Despite using a monofunctional initiator, no shoulders in the GPC curves and $M_w/M_n \approx 1.20$ for all the polymers suggesting minimal side reactions such as bimolecular termination and high end-group fidelity. This was further confirmed by the structural characterization of the lowest molar mass poly(ELA) (M_n = 4,120, M_w/M_n = 1.22).

Unfortunately, bromine end-group functionality could not be evaluated by ^{1}H NMR due to the overlapping of the signal corresponding to both α and ω chain ends with the methylene signal of the pendant ethyl ester groups (see Annex A Figure S7). However, according to MALDI-TOF analysis, the chain-end functionality was well-maintained after the SET-LRP process (Figure 2.1.4). The spectrum of poly(ELA) isolated at near quantitative conversion (> 95%) shows a dominant distribution of peaks, having a peak-to-peak mass increment of 172 Da, which equals to the mass of a single repeating unit (Figure 2.1.4a).

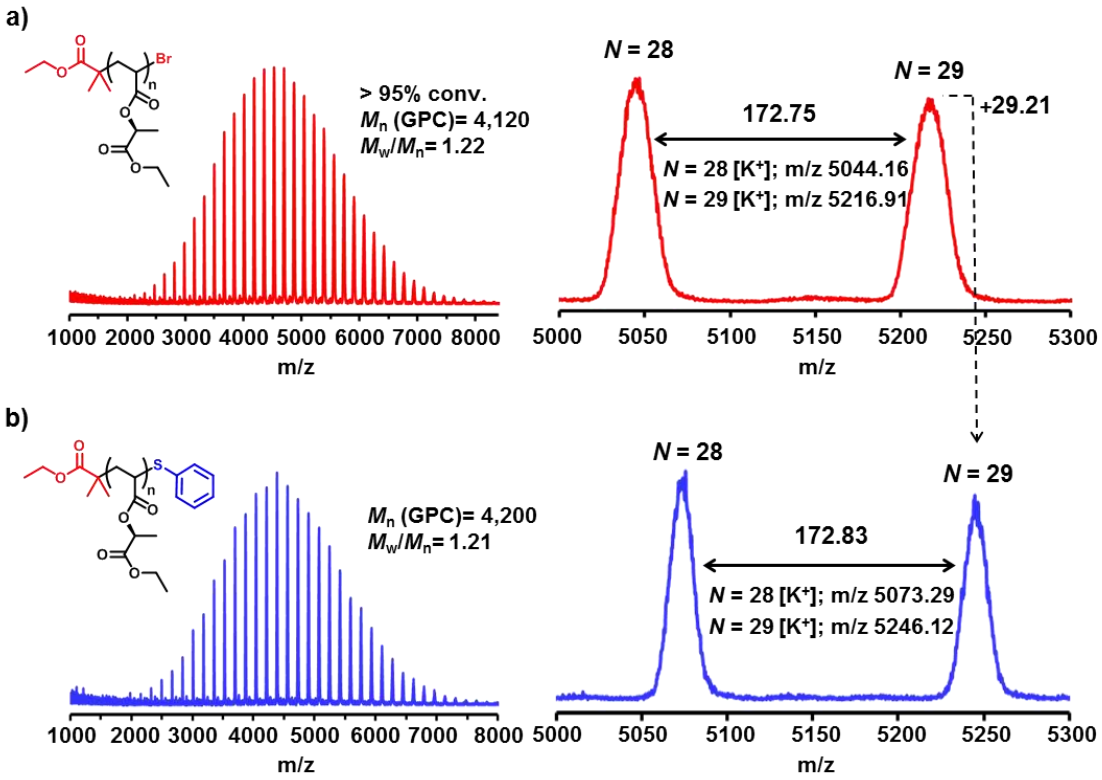

Figure 2.1.4. MALDI-TOF spectra of poly(ELA) obtained at 97 % conversion before and after thio-bromo "click" modification with thiophenol. Magnified regions confirm the expected peak-to-peak spacing for ELA repeating unit and the near perfect bromine chain end functionality of the synthesized polymer.

The *m/z* values of these peaks match the expected $[M+K]^+$ ω-bromo-terminated chains. Moreover, after thio-bromo "click" post-polymerization modification with thiophenol,[60,61] this series completely vanished and meanwhile a new series of peaks emerged 29 Da above (Figure 2.1.4b). This mass difference is consistent with the thioetherification at the ω-bromo chain ends with thiophenol. Overall, MALDI-TOF analysis before and after end-group modification confirmed minimal side reactions and high bromine chain end-group fidelity after SET-LRP, which combined with near quantitative monomer conversions at various DPs is expected to enable the straightforward synthesis of poly(ELA)-derived BCPs by *in situ* sequential addition of a second monomer (*vide infra*).

Ethyl lactate and aqueous ethyl lactate mixtures

Encouraged by these results, the polymerization of ELA was investigated in detail using its bio-sourced synthetic precursor EL as solvent. EL is an economically viable green solvent with effectiveness comparable to some petroleum-based solvents.[42-45] Replacing EtOH by EL, under identical conditions, also furnished poly(ELA) with narrow MWD (entry 1 in Table 2.1.2, and Figure 2.1.2c). However, despite the fact that poly(ELA) was also soluble in this solvent the reaction achieved lower monomer conversion (compare entry 1 in Table 2.1.2 with entry 4 in Table 2.1.1). Unexpectedly, the plot of $\ln([M]_0/[M])$ versus time was linear only up to 50 min (60% monomer conversion) (k_p^{1app} = 0.0205 min^{-1}) (Figure 2.1.2b). After, the polymerization proceeded following a second kinetic domain with a significantly lower rate constant (k_p^{2app} = 0.0098 min^{-1}). According to previous reports, this result may be attributed to rapid activation combined with insufficient disproportionation, which favors bimolecular termination events between growing chains (i.e. loss of bromine chain ends).[62-67] It has been previously demonstrated that the addition of small amount of H_2O to poor disproportionation reaction mixtures can dramatically improve its ability to produce reactive Cu(0) and the needed levels of $Cu(II)X_2$ deactivator to prevent irreversible termination of chains in early stages of SET-LRP reactions.[62,63] Indeed, tuning EL with H_2O and other co-solvents is a common strategy to create ideal conditions in organic synthesis.[68,69]
Inspired by these studies, a series of experiments were conducted in aqueous EL mixtures under the following conditions: $[ELA]_0/[EBiB]_0/[Me_6\text{-TREN}]_0$ = 100/1/0.2 (entries 2-5 in Table 2.1.2). The control experiment in pure EL showed again limited monomer conversion and loss of livingness manifested as kinetic plots with two linear regimes (Figure 2.1.5a).
However, after the addition of 5% H_2O to EL, the polymerization rate of the second linear regime significantly increased (3x). An increase on k_p^{1app} was also observed, but much lower (1.5x) than that determined for k_p^{2app}. To our delight, increasing further the H_2O content completely eliminated k_p^{2app} and generated the characteristic first order kinetic of a LRP processes (Figure 2.1.5b-c).

Table 2.1.2. Cu(0) Wire-catalyzed SET-LRP of ELA initiated with EBiB in EL and aqueous EL mixtures at 25 °C.[a]

entry	reaction medium	k_p^{1app} (min^{-1})	k_p^{2app} (min^{-1})	k_p^{1app} increase[b] (%)	time (min	conv.[c] (%)	M (th)[d]	M_n [e]	M_w/M_n [e]
1	EL	0.0205	0.0098	-	110	81	7,168	6.715	1.25
2	EL	0.0146	0.0035	-	220	81	14,140	14,200	1.26
3	EL/H_2O. (9.5/0.5, v/v)	0.0227	0.0106	55	110	83	14,050	14,330	1.22
4	EL/H_2O. (9/1, v/v)	0.0276	-	89	75	86	14,730	16,500	1.18
5	EL/H_2O. (8.5/1.5, v/v)	0.0344	-	135	75	90	15,520	18,700	1.19

[a] Polymerization conditions: ELA = 1 mL, solvent = 0.5 mL, using 4.5 cm of hydrazine-activated Cu(0) wire (20-gauge diameter), $[ELA]_0/[EBiB]_0/[Me_6\text{-}TREN]_0$ = 50/1/0.1 (for entry 1), $[ELA]_0/[EBiB]_0/[Me_6\text{-}TREN]_0$ = 100/1/0.2 (for entries 2-5). [b] Increase of k_p^{app} with respect to the k_p^{1app} from entry 2. [c] Determined by ^1H NMR. [d] M(th) = 172.18 x $[ELA]_0/[EBiB]_0$ x conv + 195.06. [e] Determined by GPC using PMMA standards.

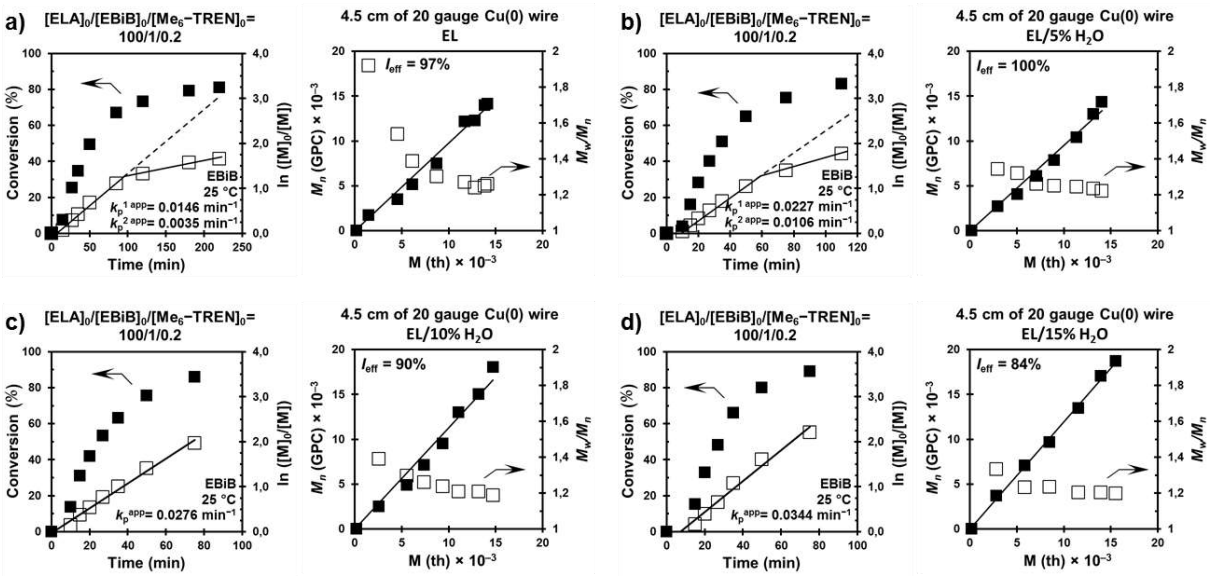

Figure 2.1.5. Monomer conversion, kinetic plots and evolution of molecular weight and polydispersity for the Cu(0) wire-catalyzed SET-LRP of ELA in EL and aqueous EL mixtures initiated with EBiB at 25 °C. (a) EL, (b) EL /5% H_2O, (c) EL /10% H_2O and (d) EL /15% H_2O. Reaction conditions: ELA = 1 mL, (a, b, c, d); EL = 0.5 mL, (a); EL + water = 0.5 mL, (b, c, d), 4.5 cm hydrazine- activated Cu(0) wire and $[ELA]_0/[EBiB]_0/[Me_6\text{-}TREN]_0$= 100/1/0.2.

Figure 2.1.6a-c compares kinetic plots and GPC results for the polymerization in pure EL and EL/H_2O mixture (9/1, v/v). In the latter system, the reaction rate was even faster (1.9x compared to k_p^{1app} obtained in pure EL).The linear increase in k_p^{app} for aqueous EL mixtures is determined by the higher polarity of H_2O (Figure 2.1.6d, close symbols).

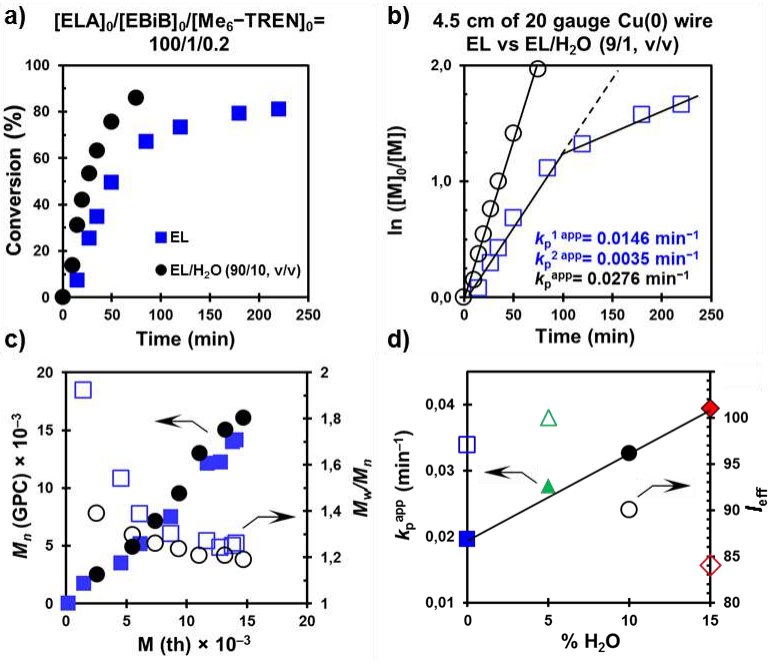

Figure 2.1.6. (a) Monomer conversion vs time, (b) $\ln[M]_0/[M]$ vs time and (c) evolution of experimental M_n (GPC) and M_w/M_n, based on the calibration by PMMA standards, versus theoretical M(th) for the SET-LRP of ELA initiated with EBiB in EL (blue squares) and EL/H_2O (9/1, v/v) (black circles). (d) Dependence of k_p^{app} and I_{eff} with the percentage of H_2O (% H_2O). Reaction conditions: ELA = 1 mL, solvent = 0.5 mL, $[ELA]_0/[EBiB]_0/[Me_6\text{-TREN}]_0$ = 100/1/0.2 using 4.5 cm of hydrazine-activated Cu(0) wire (20-gauge diameter).

Moreover, the high disproportionation constant of Cu(I)Br in H_2O ($K_d = 0.89 \times 10^6$ to 5.8×10^7) is crucial to improve control during initial stages of SET-LRP.[70,71] Notably, GPC traces revealed the disappearance of the high molecular weight tailing observed in pure EL, which tend to indicate insufficient level of Cu(II)Br_2 to mediate an effective deactivation of growing chains, in the presence of H_2O (Figure 2.1.7). Consequently, in the presence of 10%, and even 5% H_2O, better control over the MWD was obtained. Although EL is a good solvent for poly(ELA) and EL/H_2O mixtures are miscible at any composition, the SET-LRP reaction mixture of this series of experiments progressively transitioned from a one phase to a biphasic SET-LRP system by showing increasing turbidity (Figure 2.1.8).

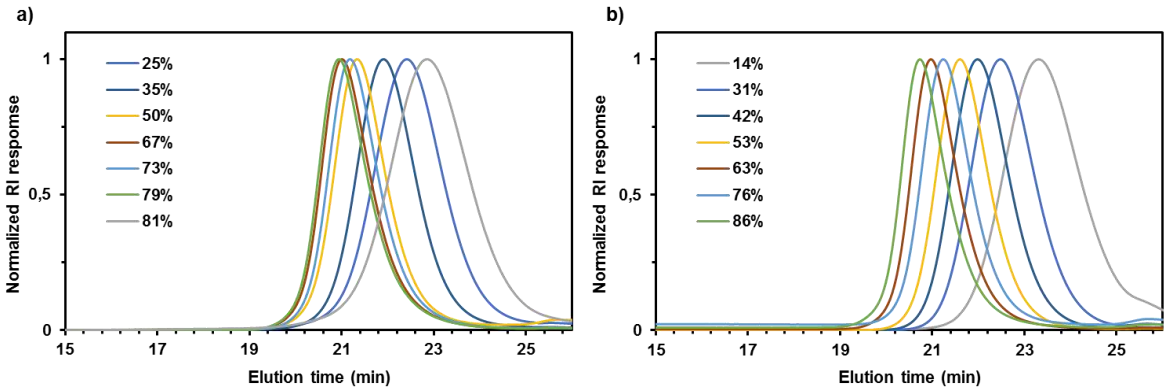

Figure 2.1.7. GPC traces (normalized to peak height) of PELA as a function of monomer conversion obtained during the Cu(0) wire-catalyzed SET-LRP of ELA in EL (a) and an EL/10% H_2O mixture (b) initiated with EBiB at 25 °C. Reaction conditions: ELA = 1 mL, (a, b); EL = 0.5 mL, (a); EL/10% H_2O = 0.5 mL, (b); 4.5 cm hydrazine-activated Cu(0) wire and $[ELA]_0/[EBiB]_0/[Me_6\text{-TREN}]_0$= 100/1/0.2. Conversion measured by ^1H NMR spectroscopy.

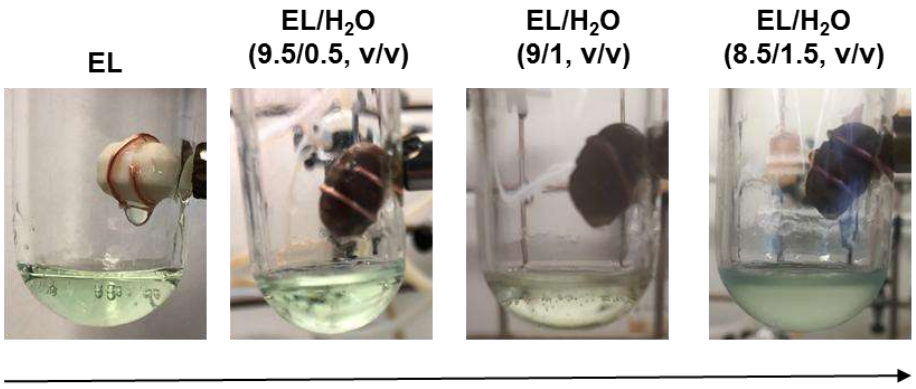

Figure 2.1.8. Digital images of the reaction mixture after the SET-LRP of ELA initiates in EL and aqueous EL mixtures. Reaction conditions: ELA = 1 mL, 4.5 cm hydrazine- activated Cu(0) wire and $[ELA]_0/[EBiB]_0/[Me_6\text{-TREN}]_0$= 100/1/0.2.

However, higher loadings of H_2O only slightly compromise initiator efficiency (I_{eff}) probably due to extremely fast activation and propagation in more polar media and not due to appearance of turbidity (Figure 2.1.6d, open symbols). Note that in the presence of 15% H_2O, reaction rate was accelerated by 135% compared to k_p^{1app} obtained in pure EL (compare entries 2 and 5 in Table 2.1.2 and see Figure 2.1.5d). These results demonstrate that the judicious selection of solvent is critical to practice SET-LRP and highlight the importance of

mixed solvent systems. No influence on the polymer tacticity was observed in different alcohols.

Expanding the range of alkyl lactate ester acrylates

To expand the scope of SET-LRP to other acrylic alkyl lactate ester derivatives, the homopolymerization of MLA and BLA was also investigated *via* ethanolic SET-LRP. Both monomers were synthesized, following the same procedure previously described for ELA, from the corresponding commercially available alkyl lactate ester. The kinetic experiments for $[MLA]_0/[EBiB]_0/[Me_6\text{-TREN}]_0$ = 100/1/0.2 and $[BLA]_0/[EBiB]_0/[Me_6\text{-TREN}]_0$ = 50/1/0.1 are shown in Figure 2.1.9a and b, respectively. In both cases, the Cu(0) wire-catalyzed polymerization initiated by EBiB furnished well-defined polymers with high conversions (entries 1 and 2 in Table 2.1.3).

No significant differences were found between the kinetic data in comparison with ELA (compare entry 2 in Table 2.1.3 with entry 4 in Table 2.1.1). Also in this case, the linear relationship of the semi-logarithmic kinetic plot and the linear increase of molecular weight values throughout the polymerization strongly support that the SET-LRP of these monomers follows a LRP mechanism. Further, the use of difunctional and hydoxyl-functional bromoisobutyrate-type initiators (bisEBiB and $(OH)_2$EBiB, see Scheme 2.1.1) allowed the preparation of well-defined α,ω-dibromo telechelic and α,α-dihydroxy functional polymers (entries 3 and 4 in Table 2.1.3 and Figure 2.1.10a).

MALDI-TOF analysis evidenced the very high end-group fidelity for the poly(BLA) functional polymer (Figure 2.1.10b). These materials could be interesting in the preparation of more complex polymer architectures based on alkyl lactate acrylic polymers including ABA triblocks and AB_2 stars using LRP or other living polymerization reactions in a second step. Results in this line will be discussed in a forthcoming chapter.

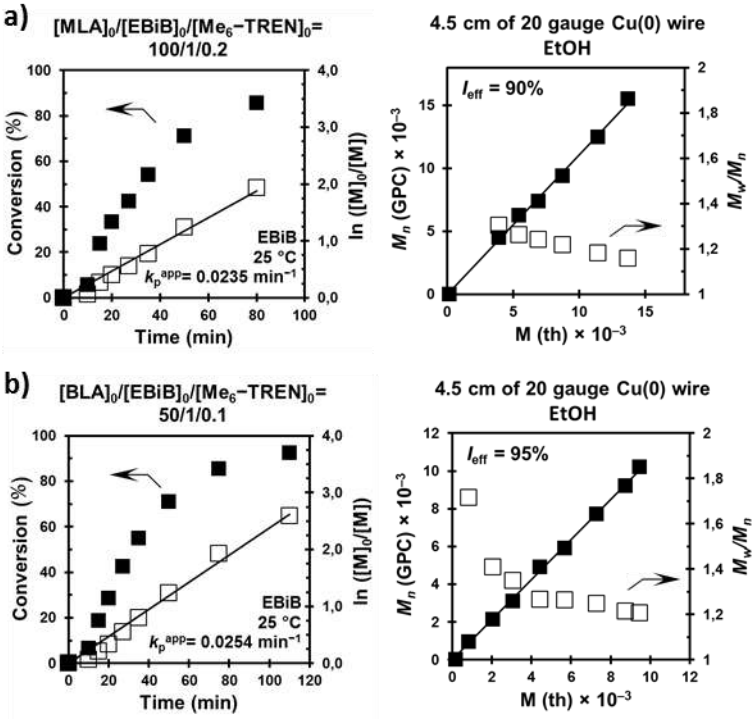

Figure 2.1.9. Monomer conversion, kinetic plots and evolution of molecular weight and polydispersity for the Cu(0) wire-catalyzed SET-LRP of (a) MLA and (a) BLA in EtOH initiated with EBiB at 25 °C. Reaction conditions: monomer = 1 mL, EtOH = 0.5 mL, 4.5 cm hydrazine- activated Cu(0) wire, (a) $[MLA]_0/[EBiB]_0/[Me_6\text{-}TREN]_0$= 100/1/0.2 and (b) $[BLA]_0/[EBiB]_0/[Me_6\text{-}TREN]_0$= 50/1/0.1.

Table 2.1.3. Cu(0) Wire-Catalyzed SET-LRP of MLA and BLA in EtOH at 25 °C.[a]

entry	monomer	initiator	$[M]_0/[Initiator]_0/[Me_6\text{-}TREN]_0$	k_p^{app} (min^{-1})	time (min)	conv.[b] (%)	M (th)[c]	M_n[d]	M_w/M_n[d]
1	MLA	EBiB	100/1/0.1	0.0235	80	87	13,730	15,500	1.18
2	BLA	EBiB	50/1/0.1	0.0254	110	93	9,455	10,200	1.20
3	MLA	bisEBiB	300/1/0.5	-	300	94	44,960	47,620	1.22
4	BLA	$(OH)_2$EBiB	30/1/0.1	-	270	93	6,120	5,000	1.25

[a] Polymerization conditions: monomer = 1 mL, EtOH = 0.5 mL (for entries 1, 2 and 4) and 0.75 mL (for entry 3), 4.5 cm of hydrazine-activated Cu(0) wire (20-gauge diameter). [b] Determined by ^{1}H NMR. [c] M (th) = MW (monomer) x $[M]_0/[Initiator]_0$ x conv + MW (initiator).[d] Determined by GPC using PMMA standards.

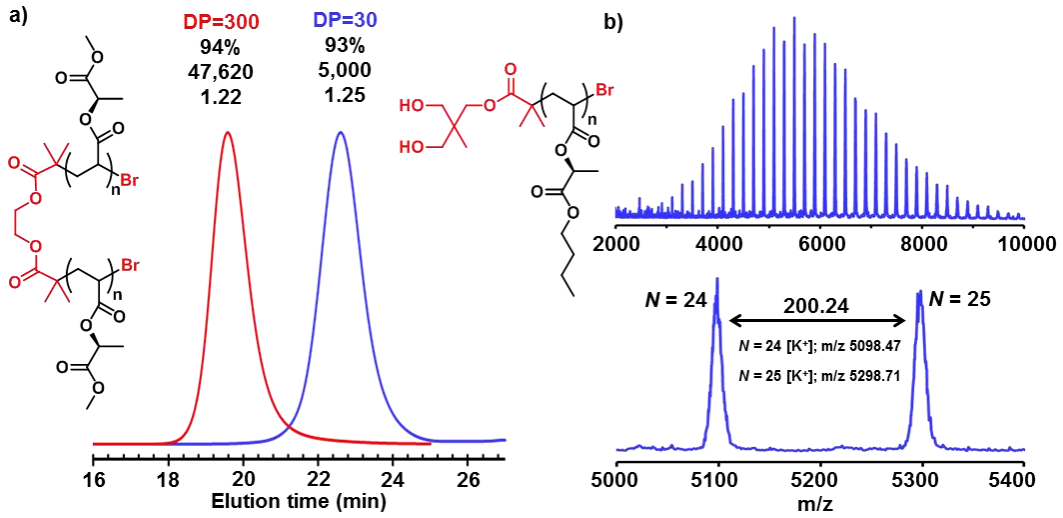

Figure 2.1.10. (a) GPC traces (normalized to peak height) for the poly(ELA) synthesized using bisEBiB and $(OH)_2$EBiB (see entries 3 and 4 in Table 2.1.3 for polymerization conditions). Numbers shown in black above GPC traces correspond to monomer conversion, M_n (GPC), and M_w/M_n respectively from the top to bottom. (b) MALDI-TOF spectrum of poly(BLA) synthesized by SET-LRP using $(OH)_2$EBiB initiator. Magnified region in (b) confirms the expected peak-to-peak spacing for BLA repeating unit and the near perfect bromine chain end functionality of the synthesized polymer.

Block copolymerization of poly(ethyl lactate acrylate) with bio-based α-pinene (αPA) and solketal acrylates (SA)

Poly(alkyl lactate acrylate)s are amorphous hydrophobic polymers with T_g below ambient temperature and thermal stability comparable to conventional alkyl acrylates (see discussion in supplementary information in Annex A, Figure S8a,b). Also appealing is the chiroptical activity of these bio-based polymers (Annex A Figure S9 and Table S1). Boosted by the near-perfect retention of bromine chain-ends at high conversion in ethanolic SET-LRP, we investigated the block copolymerization of poly(ELA) by sequential addition of a second vinylic monomer. Two diblock copolymers of ELA were targeted using αPA,[49] which is derived from one of the most abundant turpentine components, and the glycerol-derived SA[72] as a comonomers. Preliminary experiments were conducted to confirm for the first time that well-defined poly(αPA) is also accessible by SET-LRP in EtOH. Despite the polymerization of this bulky and hydrophobic monomer occurred through a self-generated biphasic

system,[55] kinetic plots evidenced living character and MALDI-TOF analysis confirmed near-perfect end group fidelity (see Annex A Figures S10-13). The *in situ* Cu(0) wire-catalyzed SET-LRP chain-extension of poly(ELA) at high conversion (> 95%) with equivalent amount of αPA (DP= 50) and twice as much SA (DP=100) was successful at synthesizing the corresponding AB BCPs. In both cases, GPC curve of the first block shifted to lower retention time while retaining narrow MWD after chain extension, thus hinting successful chain-growing from the ω-bromo terminal of poly(ELA) (Figure 2.1.11).

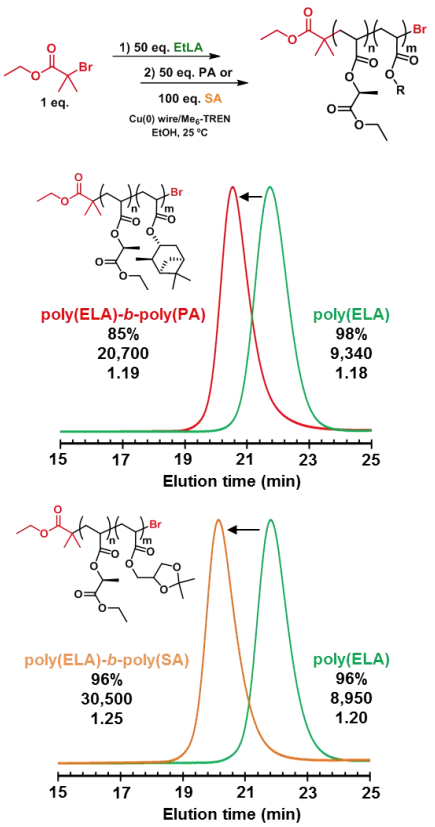

Figure 2.1.11. GPC traces for the *in situ* block copolymerization of ELA with αPA and SA. Initial conditions for block copolymerization: $[ELA]_0/[EBiB]_0/[Me_6\text{-TREN}]$ = 50/1/0.1, ELA:EtOH = 2:1 (v/v), 4.5 cm of hydrazine-activated Cu(0) wire (20 gauge). Block copolymerization achieved by addition of αPA (50 equiv.) and Me_6-TREN (0.1 equiv) in EtOH (αPA:EtOH = 2:1 (v/v)) and SA (100 equiv.) and Me_6-TREN (0.1 equiv) in EtOH (SA:EtOH = 2:1 (v/v)).

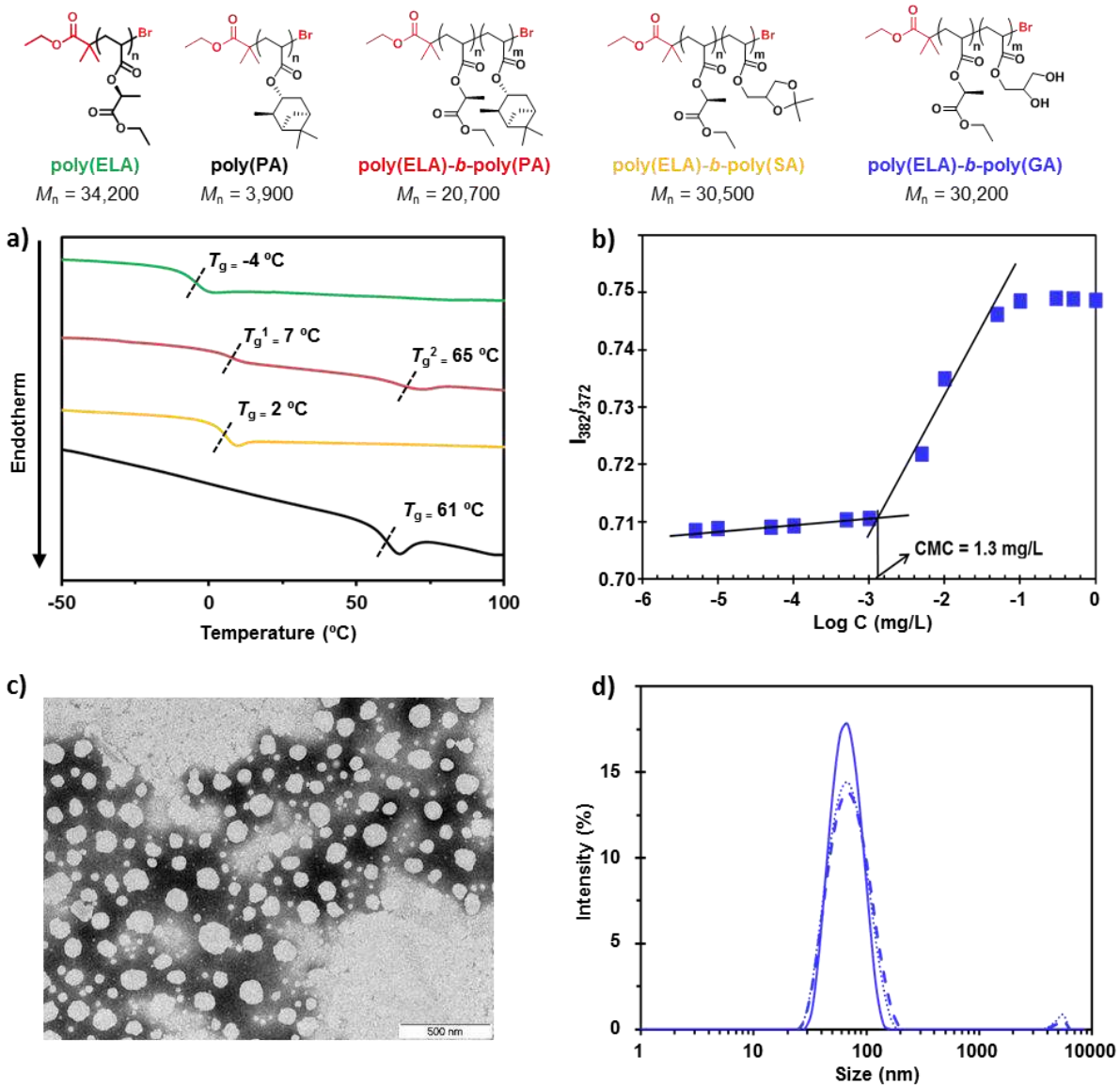

Figure 2.1.12. (a) DSC analysis of various homopolymers and block copolymers obtained by Cu(0) wire-catalyzed SET-LRP in EtOH. Characterization of poly(ELA)-b-poly(GA) micelles: (b) plot of the fluorescence intensity ratio (I_{382}/I_{372}) for pyrene *vs* the log of micelle concentration, (c) TEM image and (d) DLS size distribution.

Differential scanning calorimetry (DSC) analysis of poly(ELA)-*b*-poly(αPA) reveled the existence of two distinct T_gs (Figure 2.1.12a, red trace). These T_gs can be ascribed to those of the poly(ELA) and poly(αPA) segments (green and black traces, respectively), suggesting immiscibility between the poly(ELA) segments with the bulky poly(αPA). The existence of

microphase separated morphology in this system could be exploited in the preparation of innovative ABA sustainable thermoplastic elastomers.[9-12] Conversely, poly(ELA)-*b*-poly(glycerol acrylate (GA)) showed only one T_g at 2 °C (Figure 2.1.12a, yellow trace) but the hydrolysis of the acetal protecting group of SA segments in acidic media afforded a novel BCP poly(ELA)-*b*-poly(GA) (Figure 2.1.13).[72-74]

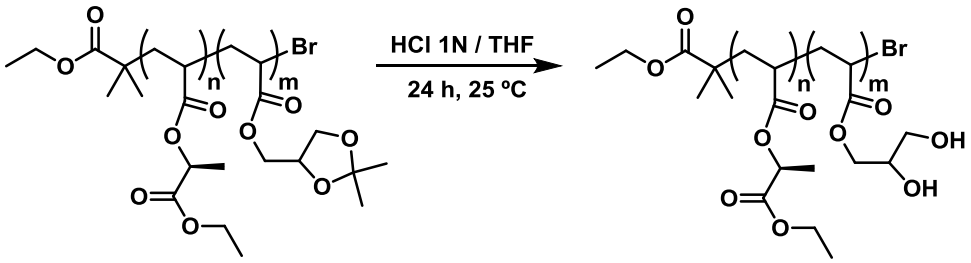

Figure 2.1.13. Deprotection of block copolymer poly(ELA)-*b*-poly(SA) with HCl to afford an amphiphilic copolymer poly(ELA)-*b*-poly(GA).

FTIR-ATR analysis was used to confirm the complete removal of isopropylidene acetal groups and consequently the preparation of a new copolymer which is amphiphilic in nature with poly(GA) as the hydrophilic segment and poly(ELA) being hydrophobic (Figure 2.1.14). Stable micellar aggregates in aqueous solution could be simply prepared by nanoprecipitation method. The formation of micelles was first proved by tracking fluorescence intensity of pyrene as a function of the polymer concentration.

The change of fluorescence emission intensity of pyrene in poly(ELA)-*b*-poly(GA) aqueous solutions at different concentrations is depicted in Figure 2.1.15. In spite of the constant pyrene concentration, the fluorescence intensity increased and an obvious intensity variation occurred for fluorescence emission peaks at 382 and 372 nm as the polymer concentration increased from 1.0×10^{-9} to 1.0×10^{-3} g L^{-1}. This phenomenon was attributed to the formation of micelles in the system and the movement of pyrene probe from the polar aqueous environment into the hydrophobic micelles core where much stronger fluorescence is shown.

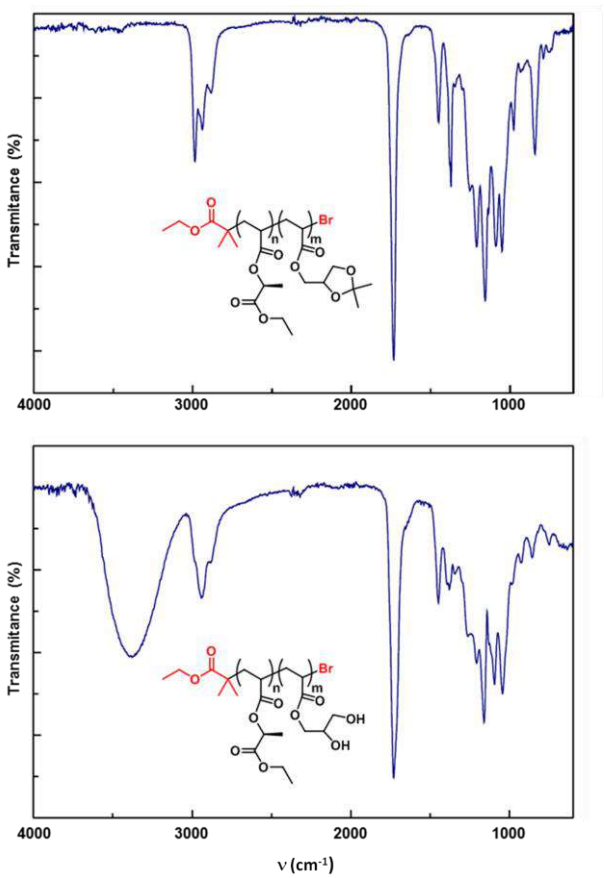

Figure 2.1.14. FTIR-ATR spectra before and after the deprotection of block copolymer poly(ELA)-*b*-poly(SA) with HCl to afford an amphiphilic copolymer poly(ELA)-*b*-poly(GA).

The excitation intensity ratio of I_{382}/I_{372} was plotted against the logarithmic concentration (log c) of copolymer and the concentration corresponding to the intersection of the two tangential lines was considered the CMC value (Figure 2.1.12b). The CMC of poly(ELA)-*b*-poly(GA) was determined to be 1.3 mg/L, which is comparable with other BCPs used as drug delivery systems.[75-77] Further, shape and size of the micelles were determined using transmission electron microscopy (TEM) and dynamic light scattering (DLS). As can be seen in Figure 2.1.12c, micelles from poly(ELA)-*b*-poly(GA) displayed spherical morphology. Finally, z-average hydrodynamic diameter (d_H) of the micelles was determined to be 67 ± 1.6 nm (PDI = 0.19) by DLS (Figure 2.1.12d). Collectively, these results suggest that that amphiphilic block copolymers with hydrophilic poly(GA) shells and poly(ELA) in the hydrophobic core could potentially be used as hydrophobic drug carriers.[78]

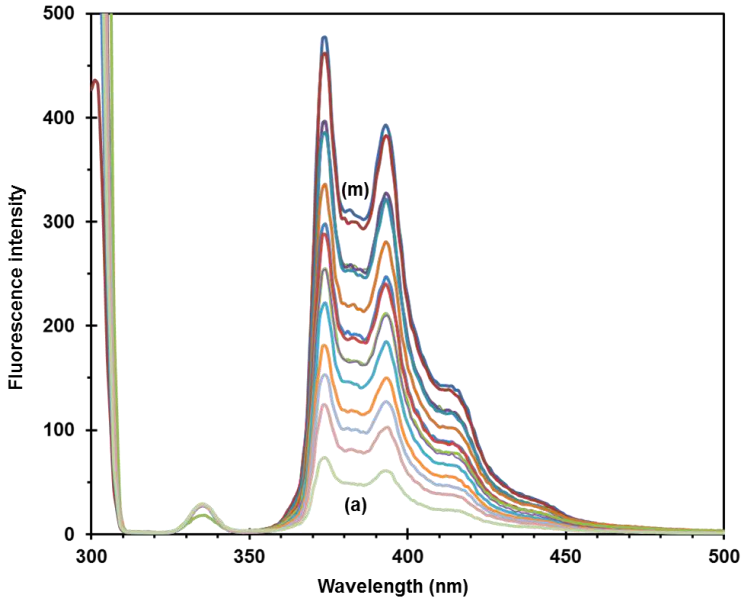

Figure 2.1.15. Emission spectra of pyrene in poly(ELA)-*b*-poly(GA) aqueous solutions from 1.0 x 10^{-9} (a) to 1.0 x 10^{-3} g L^{-1} (m) (λ_{ex} = 300 nm).

Moreover, due the chiral nature of the lactic acid synthon, other potential applications of poly(ELA)-based amphiphilic copolymers could be as enantioselective sensors or chiral catalysts for asymmetric synthesis.[79-82]

2.1.3. Conclusions

The synthesis of polymers by LRP of alkyl lactate ester acrylates was reported here for the first time. Two different methods were elaborated for the synthesis of the bio-based forgotten acrylate monomers based on EL, and of homologous structures based on methyl- and *n*-butyl- acrylates. Their SET-LRP in alcohols, in mixtures of alcohols and water, and in biphasic mixtures of alcohols with water provided excellent control of their molecular weight, polydispersity and chain end functionality that creates the basis for the synthesis of polymers with more complex architecture. As a proof-of-concept, poly(ELA) soft blocks have been shown suitable for the preparation of BCPs with phase-separated morphology using pinene-derived polyacrylate as model hard block. Moreover, a block copolymer of poly(ELA)-b-poly(glycerol acrylate) was shown to form micellar assemblies in water and thus demonstrated that SET-LRP methods for the monomers elaborated here could be used to

design and synthesize a large diversity of new complex biomaterials based on these and other bio-based monomers. SET-LRP of the corresponding methacrylates can be performed under conditions reported recently for related methacrylates.[83] SET-LRP tolerates both air[53, 84] and radical inhibitors.[84] Therefore, the synthesis of complex biomacromolecules from biobased monomers in biobased solvents by SET-LRP provides an ideal methodology for their preparation.[17]

2.1.4. Experimental section

Materials

The following chemicals were purchased from Sigma-Aldrich and were used as received: methyl 2-bromopropionate (MBP, 98%), ethyl α-bromoisobutyrate (EBiB, 98%), α-bromoisobutyryle bromide (98%), acryloyl chloride (≥ 97%), dowex® 50WX4 hydrogen form, tris[2-(dimethylamino)ethyl]amine (Me_6-TREN, 97%), copper(II) bromide (Cu(II)Br_2, 99%), propylphosphonic anhydride solution (T3P®, ≥ 50 wt. % in ethyl acetate), pyrene (≥ 99%), hydrazine hydrate (60% hydrazine), DL-1,2-isopropylideneglycerol (≥ 99%, 2-methyltetrahydrofuran (2-Me-THF, ≥ 99%), thiophenol (PhSH, ≥ 99%), dimethylsulfoxide (DMSO, ≥99.7%), *trans*-2-[3-(4-*tert*-butylphenyl)-2-methyl-2-propenylidene]malononitrile (DCTB ≥ 98%) and potassium trifluoroacetate (KTFA, 98%). 1,1,1-Tris(hydroxymethyl)ethane was received from Alfa Aesar. Acrylic acid (stabilised with hydroquinone monomethyl ether, for synthesis), 2,2,2-trifluoroethanol (TFE ≥ 99%) and HPLC grade acetonitrile were obtained from Merck. HPLC grade methanol (MeOH) and ethanol (96%) were purchased from Scharlab and VWR Chemicals, respectively. Acetone (synthesis grade) was also purchased from Scharlab. The radical inhibitor of methyl acrylate (MA, 99%, Sigma Aldrich) was removed by passing the monomer through a short column of basic Al_2O_3 prior to use. Deuterated chloroform ($CDCl_3$) was purchased from Eurisotop. Ethyl lactate (EL, natural, ≥ 98%), methyl L-lactate (ML, 98%) and butyl L-lactate (BL, ≥ 99%) were purchased from Sigma-Aldrich and distilled prior to use. Triethylamine (TEA, ≥ 99%, Merck) and dichloromethane (DCM, reagent grade, Scharlab) were distilled from CaH_2. Propan-2-ol (2-

PrOH, >97.7%) was passed through a short column of basic Al_2O_3 and freshly distilled before to use. Ethylene glycol (≥ 99%, Sigma-Aldrich) was dried by azeotropic distillation before to use and stored under inert atmosphere. Ethylene bis(2-bromoisobutyrate) (bisEBiB)[85] and ethane-1,2-diyl bis(2-bromo-2-methylpropanoate) ($(OH)_2$EBiB)[86] initiators and both solketal[87] and α-pinene[49] acrylates (SA and αPA, respectively) were prepared according to literature procedures. Copper(0) wire 99.9% pure of 20 gauge diameter, received from Creating Unkamen, was activated using hydrazine following a procedure developed in our laboratory.[88]

Methods

Proton (^{1}H NMR) and carbon (^{13}C NMR) nuclear magnetic resonance spectra were recorded on a 400 MHz (for ^{1}H) and 100.6 MHz (for ^{13}C) Varian VNMR-S400 NMR instrument at 25 °C in $CDCl_3$. All chemical shifts are quoted on the δ scale in ppm using the residual solvent as internal standard (^{1}H NMR: $CDCl_3$ = 7.26 and ^{13}C NMR: $CDCl_3$ = 77.16). Infrared (IR) spectra were recorded on a FTIR-680PLUS spectrophotometer with a resolution of 4 cm^{-1} in the transmittance mode. An attenuated total reflection (ATR) devise with thermal control and a diamond crystal (Golden Gate heated single-reflection diamond ATR, Specac-Teknokroma) was used. Absorption maxima (ν_{max}) are reported in wavenumbers (cm^{-1}). Fluorescence spectra were obtained on an RF-5301 PC Shimatzu fluorescence spectrometer with a RFPC software with emission using excitation slit widths of 5 nm. Supercritical fluidic chromatography (SFC) analysis was performed on a supercritical CO_2 chromatograph UPC2 from Waters equipped with Chiralpak IC (100x4.6 mm, 3 µm) column coupled with a DAD detector. CO_2/2-PrOH (98:2) was used as eluent at a flow rate of 3.0 mL/min with the control ABPR pressure set at 1500 psi. Electrospray ionization mass spectrometry (ESI-MS) analysis were run on a chromatographic system Agilent G3250AA liquid chromatography coupled to 6210 time of flight (TOF) mass spectrometer from Agilent Technologies with an ESI interface. Nominal and exact *m*/*z* values are reported in Daltons (Da). Optical rotations measurements were conducted on a Perkin-Elmer 241 MC polarimeter with a path length of 10 cm and are reported with implied units of 10^{-1} deg cm^2 g^{-1}. Molecular weight analysis was performed *via*

gel permeation chromatography (GPC) using an Agilent 1200 series system equipped with three serial columns (PLgel 3 μm MIXED-E, PLgel 5 μm MIXED-D and PLgel 20 μm from Polymer Laboratories) and an Agilent 1100 series refractive-index detector. Tetrahydrofuran (THF) (Panreac, HPLC grade) was used as eluent at a flow rate of 1.0 mL/min. The calibration curves for GPC analysis were obtained with PMMA standards purchased from PSS Polymer Standards Service GmbH. The molecular weights were calculated using the universal calibration principle and Mark-Houwink parameters. Matrix-assisted laser desorption ionization TOF (MALDI-TOF) analysis was performed on a Voyager DE (Applied Biosystems) instrument with a 337-nm nitrogen laser (3-ns pulse width). For all polymers, the accelerating potential was 25 kV, the grid voltage was 93.5%, the laser power was 1700 units, and a positive ionization mode was used. The analysis was performed with DCTB as matrix. THF solutions of the matrix (30 mg/mL), KTFA as cationization agent (10 mg/mL), and polymer (10 mg/mL) were prepared separately. The solution for MALDI-TOF analysis was obtained by mixing the matrix, polymer and salt solutions in a 9/1/1 volumetric ratio. Then 1 μL portions of the mixture were deposited onto three wells of a sample plate and dried in air at room temperature before being subjected to MALDI-TOF analysis. Differential scanning calorimetry (DSC) measurements were carried out on a Mettler DSC3+ instrument using N_2 as a purge gas (50 mL/min) at scanning rate 20 °C/min in the -80 to 150 °C temperature range. Calibration was made using an indium standard (heat flow calibration) and an indium-lead-zinc standard (temperature calibration). Thermal stability studies were carried out on a Mettler TGA2 /LF/1100 with N_2 as a purge gas at flow rate of 50 mL/min. The studies were performed in the 30-600 °C temperature range at a heating rate of 10 °C/min. Transmission electron microscopy (TEM) was performed using a JEOL JEM-1011 TEM microscope. Before the measurement, a drop of solution was placed on a copper grid which was allowed to dry at room temperature. Dynamic light scattering (DLS) measurements were carried out at room temperature using Zetasizer Nano ZS (Model ZEN3500) from Malvern Instruments equipped with a He-Ne laser. Chiral polymers were characterized on a Chirascan circular dichroism spectrometer from Applied Photophysics. The contact angle of deionised water

against polymer surfaces was measured by the water drop method (3 μL) at 25 °C, using the OCA15EC contact angle setup (Neurtek Instruments).

Synthesis of alkyl lactate acrylate monomers

This procedure is generic for all the alkyl lactate monomers synthesized herein. The synthesis of ELA is described. EL (20.0 g, 0.17 mol) and anhydrous TEA (26.5 g, 0.26 mol) were dissolved in dry DCM (50 mL) under a positive flow of argon. The solution was stirred for 30 min at 0-5 °C before adding dropwise acryloyl chloride (18.4 g, 0.20 mol) dissolved in dry DCM (50 mL). The reaction was allowed to proceed for 24 h at room temperature. The mixture was then filtered and then washed with HCl 1 M (150 mL) and saturated $NaHCO_3$ solution (150 mL). The organic layer was rinsed with brine solution and dried over anhydrous $MgSO_4$. The final residue was purified by vacuum distillation in the presence of 5 (w/w%) of hydroquinone to afford ELA (20.4 g, 70 %) as a colorless liquid. $[\alpha]_D^{20}$ −53.9 (1.0 mg/mL, MeCN). ^{1}H NMR (400MHz, $CDCl_3$, δ): 6.48 (dd, 1H), 6.19 (dd, 1H), 5.89 (dd, 1H), 5.15 (q, 1H), 4.21 (q, 2H), 1.53 (d, 3H), 1.28 (t, 3H); ^{13}C NMR (100.6 MHz, $CDCl_3$, δ): 170.72, 165.43, 131.86, 127.78, 68.85, 61.42, 17.01, 14.14. FTIR–ATR (neat, ν_{max}): 2989, 1748, 1726, 1637, 1406, 1179, 809. HRMS (TOF ES$^+$) *m/z* : $[M+H]^+$ calcd for $C_8H_{13}O_4^+$, 173.0808 , found, 173.0809.

Methyl lactate acrylate (MLA): ^{1}H NMR (400MHz, $CDCl_3$, δ): 6.48 (dd, 1H), 6.19 (dd, 1H), 5.91 (dd, 1H), 5.17 (q, 1H), 3.76 (s, 3H), 1.54 (d, 3H); ^{13}C NMR (100.6 MHz, $CDCl_3$, δ): 171.00, 165.18, 131.78, 127.57, 68.55, 52.20, 16.84. FTIR–ATR (neat, ν_{max}): 2995, 2956, 1749, 1725, 1637, 1406, 1178, 808. HRMS (TOF ES$^+$) *m/z* : $[M+H]^+$ calcd for $C_7H_{11}O_4^+$, 159.0652, found, 159.0656.

n-Butyl lactate acrylate (BLA): ^{1}H NMR (400MHz, $CDCl_3$, δ): 6.48 (dd, 1H), 6.19 (dd, 1H), 5.90 (dd, 1H), 5.16 (q, 1H), 4.16 (m, 2H), 1.63 (m, 2H), 1.53 (d, 3H), 1.38 (m, 2H), 0.93 (t, 3H); ^{13}C NMR (100.6 MHz, $CDCl_3$, δ): 170.72, 165.34, 131.74, 127.71, 68.78, 65.13, 30.51, 18.99, 16.96, 13.62. FTIR–ATR (neat, ν_{max}): 2961, 2875, 1750, 1723, 1637, 1406, 1179, 807. HRMS (TOF ES$^+$) *m/z* : $[M+H]^+$ calcd for $C_{10}H_{17}O_4^+$, 201.1121, found, 201.1119.

Synthesis of ELA with the aid of acrylic acid

Acrylic acid (0.70 mL, 10.18 mmol), TEA (3.65 mL, 26.19 mmol) and T3P® (6.73 g, 10.58 mmol) were added to a solution of EL (1mL, 8.72 mmol) in 2-Me-THF (50 mL). The mixture was stirred for 48 h at room temperature. The reaction was monitored by ^{1}H NMR. After 48 h, the reaction was diluted with water (30 mL) and the aqueous phase was extracted with diethyl ether (3x30 mL). The combined organic layers were rinsed with aqueous HCl 1 M (30 mL), saturated aqueous solution of $NaHCO_3$ (30 mL), brine (20 mL) and finally dried with $MgSO_4$. The resulting solution was concentrated under reduced pressure, and the residue was purified by column chromatography (9:1 hexanes/ethyl acetate) to afford ELA (0.9 g, 60%) as a colorless liquid.

Cu(0)-catalyzed SET-LRP of alkyl lactate acrylates at 25 °C

This procedure is generic for all the polymerizations conducted herein. The polymerization of ELA with EBiB in EtOH under the following conditions: $[ELA]_0/[EBiB]_0/[Me_6\text{-}TREN]_0$ = 50/1/0.1 is described. ELA (1 mL, 6.23 mmol), EtOH (0.5 mL), Me_6-TREN (3.3 μL, 0.01 mmol) and EBiB (18.3 μL, 0.12 mmol) were introduced into a 25 mL Schlenk tube. The solution was deoxygenated by applying four freeze-pump (~ 1 min)-thaw cycles. After that, a Teflon-coated stirring bar wrapped with 4.5 cm of hydrazine-activated Cu(0) wire of 20 gauge was loaded under positive argon pressure. Then, two additional freeze-pump (~ 1 min)-thraw cycles were applied before placing the flask in a water bath at 25 °C and introducing the stirring bar wrapped with the Cu(0) wire catalyst into the reaction mixture. To monitor the monomer conversion, the side arm of the tube was purged with argon before it was opened to remove two drops of sample using an airtight syringe. Samples were dissolved in $CDCl_3$ and quenched by air bubbling. After that, the monomer conversion was determined by ^{1}H NMR spectroscopy and M_n and M_w/M_n values by GPC using PMMA standards. Finally, to stop the reaction, the Schlenk flask was opened to air, and the polymerization mixture was dissolved in 2 mL of CH_2Cl_2. Next, the resulting solution was precipitated twice in 100 mL of hexane with vigorous stirring. The solvent was removed by filtration, and the final polymer was dried under vacuum until constant weight.

Thio-bromo "click" modification of poly(ELA) using thiophenol

A solution of polymer (0.3 g, M_n^{th} = 4370 g/mol) in MeCN (1 mL) was prepared in a 10 mL vial equipped with a rubber septum. Then, thiophenol (23.3 μL, 0.227 mmol) and TEA (31.7 μL, 0.227 mmol) were added. The reaction was allowed to proceed for 4 h at room temperature and then added dropwise into 10 mL of hexanes with vigorous stirring. The resulting modified poly(ELA) was washed twice with fresh solvent and dried under vacuum until constant weight before MALDI-TOF analysis.

In situ block copolymerization of poly(ELA) by Cu(0)-catalyzed SET-LRP in ethanol

This procedure was used for both copolymerizations with SA and αPA. The block copolymerization of poly(ELA) ($[ELA]_0/[EBiB]_0/[Me_6\text{-TREN}]_0$ = 50/1/0.1) with αPA (50 equiv) is described. A solution of the ELA (1 mL, 6.23 mmol), EtOH (0.5 mL), Me_6TREN (3.3 μL, 0.01 mmol) and EBiB (18.3 μL, 0.12 mmol) was prepared in a 25 mL Schlenk tube. After following the deoxygenation procedure described above, Cu(0) catalyst (4.5 cm of gauge 20 wire, wrapped around a Teflon-coated stir bar) was introduced into the flask under positive pressure of argon. Next, two additional freeze-pump (~ 1 min)-thaw cycles were applied before placing the flask in a water bath at 25 °C and introducing the stirring bar wrapped with the catalyst into the reaction mixture. After 3 h the side arm of the tube was purged with argon before it was opened to determine monomer conversion and introduce a degassed solution containing the αPA (1.3 mL, 6.27 mmol) in EtOH (0.7 mL) containing Me_6-TREN (3.3 μL, 0.01 mmol) *via* cannula. After stirring the polymerization mixture for 24 h at 25 °C, conversion of the second monomer was determined by ^{1}H NMR and the polymerization mixture was dissolved in the minimum DCM and precipitated in cold methanol. The final copolymer poly(ELA)-*b*-poly(αPA) was dried under vacuum until constant weight.

Preparation and characterization of amphiphilic BCP poly(ELA)-*b*-poly(GA) micelles

Polymer micelles were prepared by nanoprecipitation as follows: 1 mg of poly(ELA)-b-poly(GA) copolymer was first dissolved in acetone (1 mL). This solution was added dropwise

into 10 mL of deionized water via a syringe. The colloidal dispersion was sonicated for 4 h at room temperature to remove the organic solvent. The CMC was determined by using pyrene as a fluorescence probe by monitoring the emission peaks at 382 and 372 nm. The concentration of block copolymer was ranging from 1.0×10^{-9} to 1.0×10^{-3} g L^{-1} and the pyrene concentration was fixed at 6.0×10^{-7} M.

2.1.5. References

[1] Rodrigues, C.; Vandenberghe, L. P. S.; Woiciechowski, A. L.; de Oliveira, J.; Letti, L. A. J.; Soccol, C. R. In *Current Developments in Biotechnology and Bioengineering*, 1st ed.; Pandey, A.; Negi, S.; Soccol, C. R., Eds.; Elsevier, Academic Press, 2017; pp. 543-556.

[2] Mäki-Arvela, P.; Simakova, I. L.; Salmi, T.; Murzin, D. Y. *Chem. Rev.* **2014**, *114*, 1909-1971.

[3] Isikgora, F. H.; Becer, C. R. *Polym. Chem*. **2015**, *6*, 4497-4559.

[4] Zhu, Y.; Romain, C.; Williams, C. K. *Nature* **2016**, *540*, 354-362.

[5] Schneiderman, D. H.; Hillmyer, M. A. *Macromolecules* **2017**, *50*, 3733-3749.

[6] Nagarajan, V.; Mohanty, A. K.; Misra, M. *ACS Sustainable Chem. Eng*. **2016**, *4*, 2899-2916.

[7] Raquez, J. M.; Habibi, Y.; Murariu, M.; Dubois, P. *Prog. Polym. Sci.* **2013**, *38*, 1504-1542.

[8] Inkinen, S.; Hakkarainen, M.; Albertsson, A. C.; Södergård, A. *Biomacromolecules* **2011,** *12*, 523-532.

[9] Ding, W.; Wang, S.; Yao, K.; Ganewatta, M. S.; Tang, C.; Robertson, M. L. *ACS Sustainable Chem. Eng*. **2017**, *5*, 11470-11480.

[10] Satoh, K.; Lee, D. H.; Nagai, K.; Kamigaito, M. *Macromol. Rapid Commun.* **2014**, *35*, 161-167.

[11] Nasiria, M.; Reineke, T. M. *Polym. Chem*. **2016**, *7*, 5233-5240.

[12] Gallagher, J. J.; Hillmyer, M. A.; Reineke, T. M. *ACS Sustainable Chem. Eng*. **2016**, *4*, 3379-3387.

[13] Percec, V.; Guliashvili, T.; Ladislaw, J. S.; Wistrand, A.; Stjerndahl, A.; Sienkowska, M. J.; Monteiro, M. J.; Sahoo, S. *J. Am. Chem. Soc.* **2006**, *128*, 14156-14165.

[14] Percec, V.; Popov, A. V.; Ramirez-Castillo, E.; Monteiro, M.; Barboiu, B.; Weichold, O.; Asandei, A. D.; Mitchell, C. M. *J. Am. Chem. Soc.* **2002**, *124*, 4940-4941.

[15] Rosen, B. M.; Percec, V. *Chem. Rev.* **2009**, *109*, 5069-5119.

[16] Zhang, N.; Samanta, S. R.; Rosen, B. M.; Percec, V. *Chem. Rev.* **2014**, *114*, 5848-5958.

[17] (a) Lligadas, G.; Grama, S.; Percec, V. *Biomacromolecules* **2017**, *18*, 2981-3008. (b) Lligadas, G.; Grama, S.; Percec, V. *Biomacromolecules* **2017**, *18*, 1039-1063.

[18] Boyer, C.; Corrigan, N. A.; Jung, K.; Nguyen, D.; Nguyen, T. K.; Adnan, N. N.; Oliver, S.; Shanmugam, S.; Yeow, J. *Chem. Rev.* **2016**, *116*, 1803-1949.

[19] Anastasaki, A.; Nikolaou, V.; Nurumbetov, G.; Wilson, O.; Kempe, K.; Quinn, J. F.; Davis, T. P.; Whittaker, M. R.; Haddleton, D. M. *Chem. Rev.* **2016**, *116*, 835-877.

[20] Nguyen, N. H.; Levere, M. E.; Kulis, J.; Monteiro, M. J.; Percec, V. *Macromolecules* **2012**, *45*, 4606-4622.

[21] Rosen, B. M.; Jiang, X.; Wilson, C. J.; Nguyen, N. H.; Monteiro, M. J.; Percec, V. *J. Polym. Sci., Part A: Polym. Chem.* **2009**, *47*, 5606-5628.

[22] Levere, M. E.; Nguyen, N. H.; Leng, X.; Percec, V. *Polym. Chem.* **2013**, *4*, 1635-1647.

[23] Lligadas, G.; Percec, V. *J. Polym. Sci., Part A: Polym. Chem.* **2007**, *45*, 4684–4695.

[24] Nguyen, N. H.; Lenga, X.; Percec, V. *Polym. Chem.* **2013**, *4*, 2760-2766.

[25] Boyer, C.; Zetterlund, P. B.; Whittaker, M. R. *J. Polym. Sci., Part A: Polym. Chem*. **2014**, *52*, 2083-2098.

[26] Alsubaie, F.; Anastasaki, A.; Wilson, P.; Haddleton, D. M. *Polym. Chem.* **2015**, *6*, 406-417.

[27] Enayati, M.; Smail, R. B.; Grama, S.; Jezorek, R. L.; Monteiro, M. J.; Percec, V. *Polym. Chem*. **2016**, *7*, 7230-7241.

[28] Enayati, M.; Jezorek, R. L.; Monteiro, M. J.; Percec, V. *Polym. Chem.* **2016**, *7*, 3608-3621.

[29] Moreno, A.; Liu, T.; Ding, L.; Buzzacchera, I.; Galià, M.; Möller, M.; Wilson, C. J.; Lligadas, G.; Percec, V. *Polym. Chem*. **2018**, *9*, 2313-2327.

[30] Moreno, A.; Galià, M.; Lligadas, G.; Percec, V. *Biomacromolecules* **2018**, *19*, 4480-4491.

[31] Moreno, A.; Jezorek, R. L.; Liu T.; Galià, M.; Lligadas, G.; Percec, V. *Polym Chem*. **2018**, *9*, 1885-1899.

[32] Moreno, A.; Liu, T.; Galià, M.; Lligadas, G.; Percec, V. *Polym Chem*. **2018**, *9*, 1961-1971.

[33] Grama, S.; Lejnieks, J.; Enayati, M.; Smail, R. B.; Ding, L.; Lligadas, G.; Monteiro, M. J.; Percec, V. *Polym. Chem*. **2017**, *8*, 5865-5874.

[34] Zhang, Q.; Wilson, P.; Anastasaki, A.; McHale, R.; Haddleton, D. M. *ACS Macro. Lett.* **2014**, *3*, 491-495.

[35] Zhang, Q.; Collins, J.; Anastasaki, A.; Wallis, R.; Mitchell, D. A.; Becer, C. R.; Haddleton, D. M. *Angew. Chem. Int. Ed.* **2013**, *52*, 4435-4439.

[36] Voepel, J.; Edlund, U.; Albertsson, A. C.; Percec, V. *Biomacromolecules* **2011**, *12*, 253-259.

[37] Edlund, U.; Albertsson, A. C. *J. Polym. Sci., Part A: Polym. Chem*. **2012**, *50*, 2650-2658.

[38] Shibaeva, O.; Champagne, P.; Cunningham, M. F. *Green Mater.* **2016**, *2*, 104-114.

[39] Ma, J.; Chen, H.; Zhang, M.; Yu, M. *J. Polym. Sci., Part A: Polym. Chem.* **2012**, *50*, 609-613.

[40] Bertrand, O.; Wilson, P.; Burns, J. A.; Bell, G. A.; Haddleton, D. M. *Polym. Chem.* **2015**, *6*, 8319-8324.

[41] Moreno, A.; Garcia, D.; Galià, M.; Ronda, J. C.; Cádiz, V.; Lligadas, G.; Percec, V. *Biomacromolecules* **2017**, *18*, 3447-3456.

[42] Pereira, C. S. M.; Silva, V. M. T. M.; Rodrigues, A. E. *Green Chem.* **2011**, *13*, 2658-2671.

[43] Paul, S.; Pradhan, K.; Das, A. R. *Curr. Org. Chem.* **2016**, *3*, 111-118.

[44] Jessop, P. G. *Green Chem*. **2011**, *13*, 1391-1398.

[45] Gu, Y.; Jérôme, F. *Chem. Soc. Rev.* **2013**, *42*, 9550-9770.

[46] Purushothaman, M.; Krishnan, P. S. G.; Nayak, S. K. *J. Appl. Polym. Sci.* **2014**, *131*, 40962.

[47] Purushothaman, M.; Krishnan, P. S. G.; Nayak, S. K. *J. Renew. Mater.* **2015**, *3*, 292-301.

[48] Purushothaman, M.; Krishnan, P. S. G.; Nayak, S. K. *J. Macromol. Sci. A.* **2014**, *51*, 470-480.

[49] Sainz, M. F.; Souto, J. A.; Regentova, D.; Johansson, M. K. G.; Timhagen, S. T.; Irvine, D. J.; Buijsen, P.; Koning, C. E.; Stockman, R. A.; Howdle, S. M. *Polym. Chem.* **2016**, *7*, 2882-2887.

[50] Waghmare, A. A.; Hindupur, R. M.; Pati, H. N. *Rev. J. Chem.* **2014**, *4*, 53-131.

[51] Levere, M. E.; Nguyen, N. H.; Sun, H. J.; Percec, V. *Polym. Chem.* **2013**, *4*, 686-694.

[52] Nguyen, N. H.; Rosen, B. M.; Percec, V. *J. Polym. Sci., Part A: Polym. Chem.* **2011**, *49*, 1235-1247.

[53] Nguyen, N. H.; Percec, V. *J. Polym. Sci., Part A: Polym. Chem.* **2011**, *49*, 4756-4765.

[54] Nguyen, N. H.; Rosen, B. M.; Percec, V. *J. Polym. Sci., Part A: Polym. Chem.* **2010**, *48*, 1752-1763.

[55] Boyer, C.; Atme, A.; Waldron, C.; Anastasaki, A.; Wilson, P.; Zetterlund, P. B.; Haddleton, D. M.; Whittaker, M. R. *Polym. Chem.* **2013**, *4*, 106-112.

[56] Lligadas, G.; Percec, V. *J. Polym. Sci., Part A: Polym. Chem.* **2008**, *46*, 2745-2754.

[57] Samanta, S. R.; Cai, R.; Percec, V. *Polym. Chem.* **2014**, *5*, 5479-5491.

[58] Samanta, S. R.; Levere, M. E.; Percec, V. *Polym. Chem*. **2013**, *4*, 3212-3224.

[59] Bensabeh, N.; Ronda, J. C.; Galià, M.; Cádiz, V.; Lligadas, G.; Percec, V. *Biomacromolecules* **2018**, *19*, 1256-1268.

[60] Rosen, B. M.; Lligadas, G.; Hahn, C.; Percec, V. *J. Polym. Sci., Part A: Polym. Chem.* **2009**, *47*, 3931-3939.

[61] Rosen, B. M.; Lligadas, G.; Hahn, C.; Percec, V. *J. Polym. Sci., Part A: Polym. Chem.* **2009**, *47*, 3940-3948.

[62] Nguyen, N. H.; Percec, V. *J. Polym. Sci., Part A: Polym. Chem.* **2011**, *49*, 4227-4240.

[63] Nguyen, N. H.; Rosen, B. M.; Jiang, X.; Fleischmann, S.; Percec, V. *J. Polym. Sci., Part A: Polym. Chem.* **2009**, *47*, 5577-5590.

[64] Jiang, X.; Fleischmann, S.; Nguyen, N. H.; Rosen, B. M.; Percec, V. *J. Polym. Sci., Part A: Polym. Chem.* **2009**, *47*, 5591-5605.

[65] Nguyen, N. H.; Levere, M. E.; Kulis, J.; Monteiro, M. J.; Percec, V. *Macromolecules* **2012**, *45*, 4606-4622.

[66] Lligadas, G.; Percec, V. *J. Polym. Sci., Part A: Polym. Chem*. **2008**, *46*, 6880-6895.

[67] Lligadas, G.; Rosen, B. M.; Monteiro, M. J.; Percec, V. *Macromolecules* **2008**, *41*, 8360-8364.

[68] Zhang, M.; Fu, Q. Y.; Gao, G.; He, H. Y.; Zhang, Y.; Wu, Y. S.; Zhang, Z. H. *ACS Sustainable Chem. Eng*. **2017**, *5*, 6175-6182.

[69] Bennett, J. S.; Charles, K. L.; Miner, M. R.; Heuberger, C. F.; Spina, E. J.; Bartelsa, M. F.; Foremana, T. *Green Chem.*, **2009**, *11*, 166-168.

[70] Ahrland, S.; Rawsthorne, J. *J. Acta Chem. Scand.* **1970**, *24*, 157-172.

[71] Ciavatta, L.; Ferri, D.; Palombari, R. *J. Inorg. Nucl. Chem.* **1980**, *42*, 593-598.

[72] Pham, P. D.; Monge, S.; Lapinte, V.; Raoul, Y.; Robin, J. J. *Eur. J. Lipid Sci. Technol.* **2013**, *115*, 28-40.

[73] Whittaker, M. R.; Urbani, C. N.; Monteiro, M. J. *J. Polym. Sci., Part A: Polym. Chem.* **2008**, *46*, 6346-6357.

[74] Anastasaki, A.; Nikolaou, V.; Simula, A.; Godfrey, J.; Li, M.; Nurumbetov, G.; Wilson, P.; Haddleton, D. M. *Macromolecules* **2014**, *47*, 3852-3859.

[75] Danafar, H.; Rostamizadeh, K.; Davaran, S.; Hamidi, M. *Pharm. Dev. Technol*. **2017**, *22*, 947-957.

[76] Li, F.; Danquah, M.; Mahato, R. I. *Biomacromolecules* **2010**, *11*, 2610-2620.

[77] Yan, L.; Miller, J.; Yuan, M.; Liu, J. F.; Busch, T. M.; Tsourkas, A.; Cheng, Z. *Biomacromolecules* **2017**, *18*, 1836-1844.

[78] Bodratti, A. M.; Alexandridis, P. *Expert Opin. Drug Deliv.* **2018**, *15*, 1085-1104.

[79] Skey, J.; O'Reilly, R. K. *J. Polym. Sci., Part A: Polym. Chem.* **2008**, *46*, 3960-3702.

[80] La Sorella, G.; Strukul, G.; Scarso, A. *Green Chem.* **2015**, *17*, 644-683.

[81] Ladmiral, V.; Charlot, A.; Semsarilar, M.; Armes, S. P. *Polym. Chem.* **2015**, *6*, 1805-1816.

[82] Bloksma, M. M.; Hoeppener, S.; D'Haese, C.; Kempe, K.; Mansfeld, U.; Paulus, R. M.; Gohy, J. F.; Schubert, U. S.; Hoogenboom, R. *Soft Matter* **2012**, *8*, 165-172.

[83] Moreno, A.; Bensabeh, N.; Parve, J.; Ronda, J. C.; Cádiz, V.; Galià, M.; Vares, L.; Lligadas, G.; Percec, V. *Biomacromolecules* **2019**, *20*, 1816-1827.

[84] (a) Fleischmann, S.; Rosen, B. M.; Percec, V. *J. Polym. Sci., Part A: Polym. Chem.* **2010**, *48*, 1190-1196. (b) Nguyen, N. H.; Leng, X.; Sun, H.-J.; Percec, V. *J. Polym. Sci., Part A: Polym. Chem.* **2013**, *51*, 3110-3122. (c) Fleischmann, S.; Percec, V. *J. Polym. Sci., Part A: Polym. Chem.* **2010**, *48*, 2243-2250. (d) Lligadas, G.; Percec, V. *J. Polym. Sci., Part A: Polym.*

Chem. **2008**, *46*, 3174-3181. (e) Liarou, E.; Whitfield, R.; Anastasaki, A.; Engelis, N. G.; Jones, G. R.; Velonia, K.; Haddleton, D. M. *Angew. Chem., Int. Ed.* **2018**, *57*, 8998-9002.

[85] Kavitha, A. A.; Singha, N. K. *Macromolecules* **2010**, *43*, 3193-3205.

[86] Gavrilov, M.; Zerk, T. J.; Bernhardt, P. V.; Percec, V.; Monteiro, M. J. *Polym. Chem.* **2016**, *7*, 933-939.

[87] Oguchi, K.; Sanui, K.; Ogata, N.; Takahashi, Y.; Nakada, T. *Polym. Eng. Sci.* **1990**, *30*, 449-452.

[88] Enayati, M.; Jezorek, R. L.; Percec, V. *Polym. Chem.* **2016**, *7*, 4549-4558.

2.2. Photoinduced upgrading of lactic acid-based solvents to block copolymer surfactants

We report a new strategy toward the development of BCP surfactants from chemicals of the LA family. A particularly unique aspect of this work is the use of green solvents as biobased platform chemicals to generate well-defined and nanostructure-forming materials. Herein, efficient functionalization of EL and DML solvents with acrylate groups generated monomers that could be polymerized by the photoinduced copper-catalyzed living radical polymerization process to yield polymeric materials with different water solubilities. These LA-derived monomers were used as a major component in well-defined diblock copolymers composed of poly(EL acrylate) and poly(DML acrylate) segments as hydrophobic and hydrophilic building blocks, respectively. The resulting amphiphilic copolymers could self-assemble in aqueous solution to form nanoparticles with different morphologies (e.g., large-compound micelles and vesicles). Subsequently, the formed amphiphilic polymers were employed as efficient stabilizers in the emulsion polymerization of MMA and St, offering a facile method for the synthesis of well-defined and stable polymer latexes in the range of 100–200 nm, demonstrating the practical significance of these biobased polymers in nanomaterial synthesis.

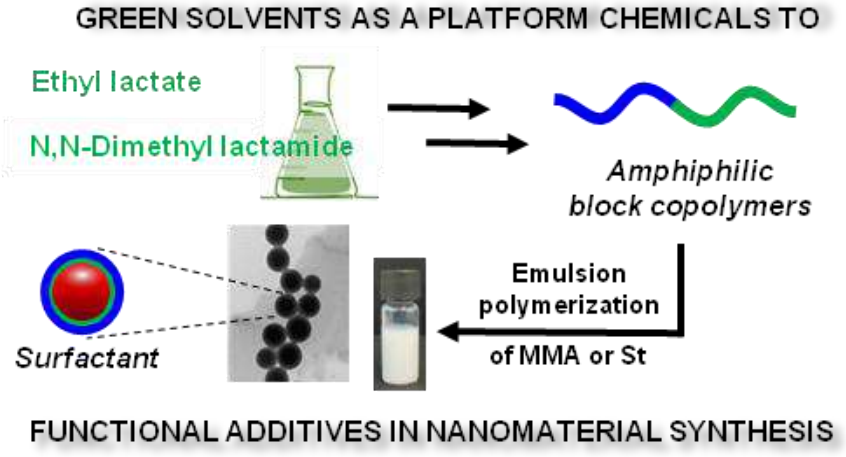

2.2.1. Introduction

Biomass-derived platform chemicals are gaining momentum in both industry and academia due to dwindling of fossil fuel resources and environmental concerns.[1-4] In this regard, LA is one of the top feedstocks given its ready availability from renewable carbohydrates *via* fermentation or chemocatalytic routes,[5,6] and its facile conversion into a number of important derivatives such as fine and commodity chemicals, biodegradable polymers, and fuel precursors.[7-10] Among them, EL[11] and DML[12] are in portfolio of bio-available green solvents suitable to replace traditional chemicals because offer an appealing combination of properties including high boiling point, high solvency power, negligible toxicity and 100% biodegradability that translate into important environmental benefits and performance advantages.[13-16] The use of EL, for example, enabled to improve the green angle of numerous organic transformations such as olefin metathesis,[17] cycloadditions[18] reactions. The instability of Cu(I)X/N-ligand complexes towards disproportionation in DML[19] and EL[20] also facilitated their application as efficient green reaction media in Cu(0)-mediated SET-LRP reactions.[21,22] However, the potential of these simple and cheap LA derivatives[23] goes beyond their academic use as have been used in many industrial applications including the preparation of agrochemical[24] and cleaning formulations,[25] polymeric membranes in a safe workplace,[26] among others.[13,27-29]

The chemical structure of EL and DML is also of great appeal to expand the scope of potential application of these green solvents as sustainable feedstock for sustainable polymer synthesis.[30 - 32] Their secondary alcohol offers a simple access to monovinyl derivatives for use in either free or living radical chain growth polymerizations (FRP and LRP, respectively). In this regard, few publications reported that acrylic and methacrylic derivatives of LA esters (i.e. methyl, ethyl, butyl) are suitable to polymerize by FRP to yield water-insoluble rubbery polymers.[33-36] It was demonstrated in the previous chapter that well-defined polymers derived from this toolbox of monomers are easily accessible by Cu(0) wire-mediated SET-LRP.[37, 38] However, vinylic derivatives of N-alkyl lactamides and polymers thereof are only reported in the old patent literature,[39] and no study on their physical

properties, LRP as well as block copolymer (BCP) synthesis is yet available to the best of our knowledge.

Herein, we sought to enable the development of advanced materials such as BCPs[40-42] using EL and DML green solvents as a bio-based platform molecules by synthesizing and polymerizing the corresponding acrylic derivatives. The different water solubility demonstrated by the corresponding homopolymers, i.e. poly(EL acrylate) (PELA) is hydrophobic and water-insoluble and poly(DML acrylate) (PDMLA) is the hydrophilic and water-soluble, drove our interest to study the overall ability of the resulting sustainable BCPs to undergo self-assembly under aqueous conditions. The innovative sustainable amphiphilic copolymers reported in this study showed promise as polymeric surfactants in the aqueous emulsion polymerization of commodity monomers such as MMA and St.

2.2.2 Results and discussion

Synthesis of ELA and DMLA

As reported in the previous chapter,[37] EL solvent was used as a biobased-platform chemical to synthesize its acrylic derivative (ELA, Scheme 2.2.1). ELA was synthesized using an environmentally-friendly approach using acrylic acid as a main reagent and T3P® as an ester coupling promoter in the presence of TEA.[43] To maximize the green angle of the process, a solvent with low environmental impact such as 2-Me-THF was used. After a simple work up method with no chromatographic purification, ELA was obtained in 52% yield. Unfortunately, although research to improve this procedure continues to be in progress, at this time this attractive procedure was not employed to install the acrylate functionality on DML solvent (*vide infra*). Therefore, the acylation of DML with acryloyl chloride in the presence of TEA afforded the corresponding optically active ($[\alpha]_D^{25}$ = +8.0, *c* 1.0 mg/mL, MeCN) acrylic ester-amide monomer (DMLA) as a colorless liquid after vacuum distillation (70% yield). Although EL solvent is miscible with water and common organic solvents, the corresponding acrylic derivative (ELA) turned insoluble in water. However, switching the ethyl ester moiety to a *N,N*-dimethyl substituted amide resulted in a water-soluble vinylic monomer (DMLA) that, as will be discussed lately, enabled us to prepare new amphiphilic

BCPs from these two LA-derived monomers. Unfortunately, the water-solubility of DMLA compromised the isolation of this monomer after synthesis *via* T3P® promoted esterification with acrylic acid.

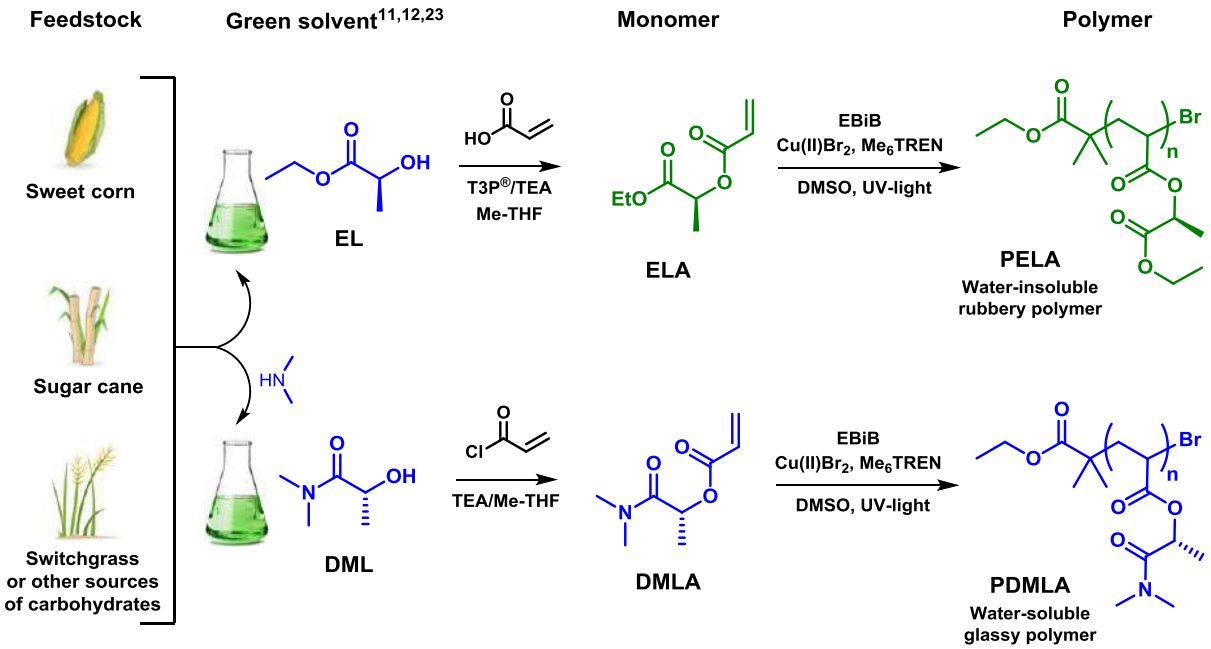

Scheme 2.2.1. Synthesis of ELA and DMLA monomers from the corresponding green solvents and subsequent Cu(II)-mediated radical photopolymerization. Color code: blue, hydrophilic and water-soluble and green, hydrophobic and water-insoluble.

The structure of both monomers was verified by NMR and high-resolution mass spectrometry (Figure S1-4 in Annex B). Previously, our group and others demonstrated that ELA is prone to polymerize either by FRP or LRP to deliver a water-insoluble rubbery polymers (i.e. PELA).[33, 34-37] The ability of DMLA to polymerize by FRP using AIBN as initiator was confirmed by ^{1}H NMR and GPC. ^{1}H NMR analysis indicated 96% monomer conversion after 8 h at 90 °C. The resulting polymer, named thereafter PDMLA, was soluble at 10 wt% in polar organic solvents such as THF, CH_2Cl_2, $CHCl_3$, acetone, and DMF but also in water. This hydrophilic polymer could also be dissolved in DML and EL. Compared to ^{1}H NMR spectrum of the monomeric precursor, the ^{1}H NMR spectrum of PDMLA recorded in D_2O revealed the successfully formation of the saturated polymer backbone by the absence of the olefinic

protons and the appearance of the characteristic signals at 1.35-2.65 ppm corresponding to the polymer backbone (Figure 2.2.1).

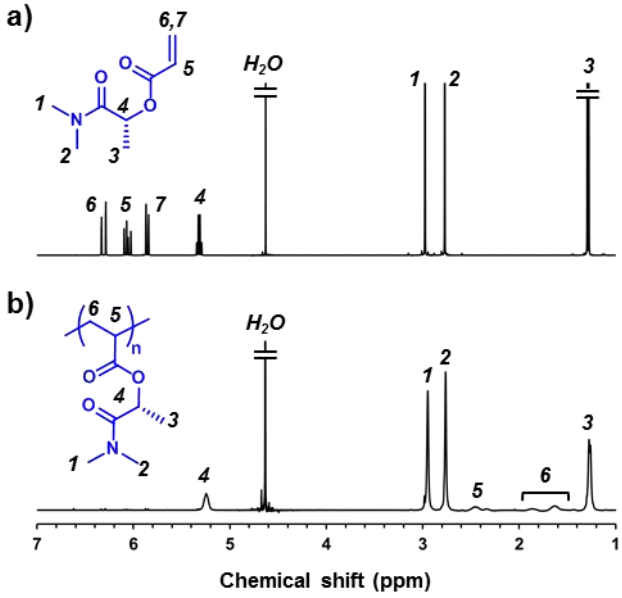

Figure 2.2.1. ^{1}H NMR spectra in D_2O of (a) DMLA monomer and (b) the corresponding polymer prepared by bulk FRP at 70 °C.

GPC analysis in DMF (0.1 wt% LiBr) was used to determine M_n = 27,300 g mol^{-1} and M_w/M_n = 2.9 (Figure S5 in Annex B). Next, the thermal properties of PDMLA were investigated by DSC and TGA techniques. The only thermal event that was detected in the DSC curve was an endothermal baseline shift, associated with the T_g, at a remarkably high temperature (75 °C) which is in accordance to the solid appearance of the polymer at room temperature (Figure S6 in Annex B). The T_g of this amorphous polymer is significantly higher than that previously reported for PELA prepared by FRP (T_g = -27 °C).[33] It is believed that polar *N,N*-dimethyl amide side groups leads to stronger intermolecular attractive interactions between chains which hinders molecular motion thus causing an increase in T_g. TGA analysis revealed that after an initial weight loss, associated with some humidity absorbed, the thermal degradation of PDMLA side groups and backbone has a well-defined one-step degradation profile with a maxima at 353 °C (Figure S7 in Annex B).

Photoinduced LRP of DMLA and ELA

Considering the potential of photopolymerization techniques on the way for a green and sustainable polymerization processes, the living photopolymerization of DMLA and ELA was investigated. To provide an effective route for the synthesis of well-defined polymers, copper-catalyzed photoinduced radical polymerization was employed in this study.[44-49] Initially, the polymerization of DMLA was performed at ambient temperature using catalytic Cu(II)Br_2 (2 mol % with respect to the initiator) and an aliphatic amine ligand, Me_6-TREN, in the presence of UV light ($\lambda_{max} \approx$ 365 nm) (Scheme 2.2.1). The polymerization of DMLA was initiated from EBiB acting as a monofunctional initiator. When the degree of polymerization (DP) was targeted at 50 using DMSO as a non-toxic green solvent,[50] ^{1}H NMR analysis revealed near quantitative conversion after 3 h according to disappearance of the vinyl signals between 5.8 ppm and 6.4 ppm (Figure S8 in Annex B). Molecular weight analysis of the resulting polymer by GPC revealed a symmetrical monomodal peak (M_w/M_n = 1.26) (Figure S9 in Annex B). Moreover, the experimental number average molecular weight of the polymer (M_n^{GPC} = 10,000 g·mol^{-1}) determined using PMMA standards was in good agreement with the theoretical value (M_n^{th} = 8,800 g·mol^{-1}) calculated from the monomer/initiator ratio and the monomer conversion. Note that the photopolymerization of DMLA in its solvent precursor (i.e. DML) also reached high monomer conversion (conv. > 99%) and delivered a well-defined polymer (M_w/M_n = 1.26) (Figure S10 in Annex B).

Next, the living character of the photoinitiated radical polymerization of DMLA in DMSO was investigated in detail *via* kinetic analysis. As can be seen in Figure 2.2.2a (left panel), more than 90% DMLA conversion was reached within 120 min including an initial induction period of 30 min. Following this induction period, kinetic analysis revealed a linear increase of $\ln([M]_0/[M])$-time plot, which is in agreement with a constant number of propagating chains throughout the polymerization.

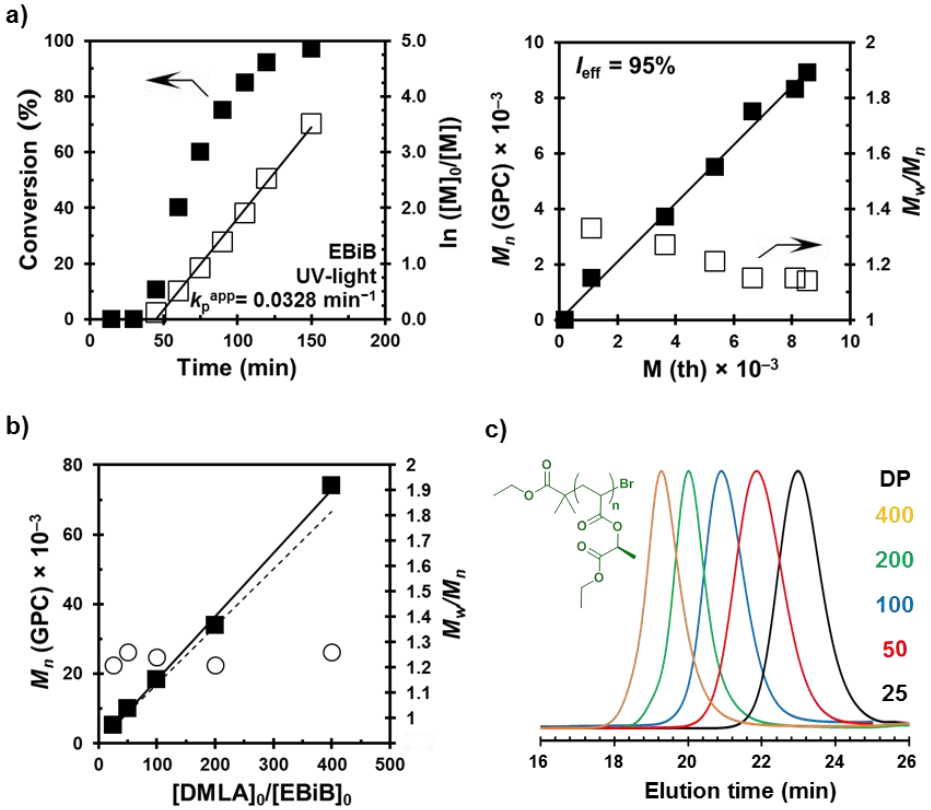

Figure 2.2.2. (a) Kinetics plots and evolution of experimental M_n (GPC) and M_w/M_n versus theoretical M_n^{th} for the Cu(II)-mediated living photopolymerization of DMLA in DMSO. Reaction conditions: $[DMLA]_0/[EBiB]_0/[Me_6\text{-}TREN]_0/[Cu(II)Br_2]_0$= 50/1/0.12/0.02. (b) Dependence of experimental M_n (GPC) and M_w/M_n on $[DMLA]_0/[EBiB]_0$ ratio for the photopolymerization of DMLA in DMSO. (c) GPC traces (normalized to peak height) of PELA with different targeted DPs (25-400).

Moreover, GPC analysis at different polymerization times clearly illustrated the linear increase of molar mass with theoretical values and symmetrical unimodal GPC traces (M_w/M_n = 1.35-1.12) throughout the polymerization process (right panel).

Under identical conditions, the polymerization was conducted at different M/I ranging from 25 to 400 (Figure 2.2.2b and S11 in Annex B). Results are summarized in Table 2.2.1. In all cases these experiments proceeded up to high monomer conversion (> 95%) which is along the lines of the Green Chemistry principles. GPC analysis revealed increasing molecular weights when targeting higher DPs, with narrow MWD (M_w/M_n = 1.19-1.26).

Table 2.2.1. Cu(II)-mediated radical photopolymerization of DMLA.[a]

entry	$[DMLA]_0/[EBiB]_0$	conv.[b] (%)	M_n^{th} [c]	M_n [d]	M_w/M_n [d]
1	25/1	99	4,500	5,300	1.19
2	50/1	99	8,800	10,000	1.26
3	100/1	98	17,000	18,300	1.24
4	200/1	97	33,400	33,900	1.21
5	400/1	97	64,600	74,000	1.25

[a] Polymerization conditions: DMLA = 1 mL, DMSO = 0.5 mL, UV-light irradiation for 2.5 h. [b] Determined by ^{1}H NMR. [c] M(th) = 171.19 x $[DMLA]_0/[EBiB]_0$ x conv. + 195.05. [d] Determined by GPC in DMF (0.1 wt % LiBr) using PMMA standards.

Moreover, good agreement between M_n^{th} and M_n^{GPC} was maintained up to approximately 75,000 g·mol^{-1}. As expected, the resulting PDMLA homopolymers were glassy (T_g ~ 65 °C) and water-soluble at room temperature (Figure 2.2.3).

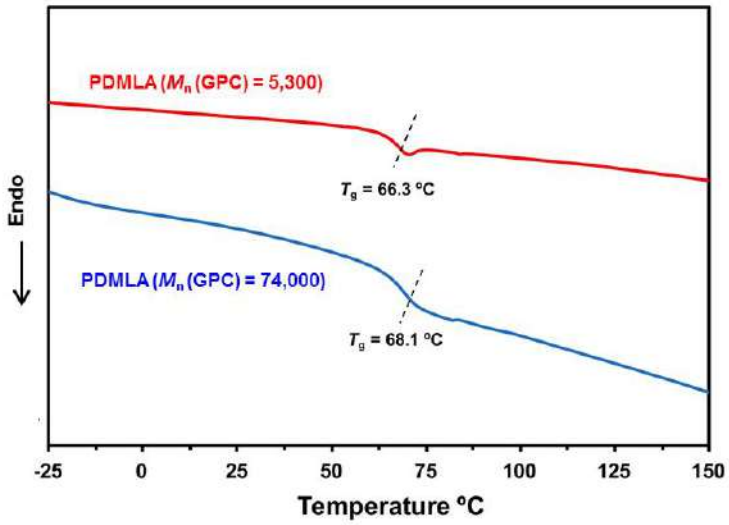

Figure 2.2.3. DSC analysis of PDMLA samples of low and high molecular weight isolated after $Cu(II)Br_2$-mediated radical photopolymerization of DMLA using EBiB as an initiator at a targeted DP = 25 and 400, respectively.

Importantly, PDMLA polymers exhibited a significant chiral amplification ($[\alpha]_D^{25}$ = +25.7 for M_n = 10,000 and $[\alpha]_D^{25}$ = +28.5 for M_n = 74,000) compared to the corresponding monomer ($[\alpha]_D^{25}$ = +8.0). This kind of increase suggests that the optical activity of the polymer not only arises due to the configurational chirality in the side chain but also from a conformational

chirality, most likely a secondary helical arrangement of the main chain.[51] Note that no chiral amplification was previously observed for PELA.[37]

With the hydrophilic building block in our hands, this efficient synthetic methodology was also applied to the hydrophobic and water-insoluble ELA monomer. Under strictly identical reaction conditions, a series of polymerizations were conducted in DMSO targeting DPs from 25 to 400 (Figure 2.2.2c and Table 2.2.2).

Table 2.2.2. Cu(II)-mediated radical photopolymerization of ELA.[a]

entry	$[ELA]_0/[EBiB]_0$	conv.[b] (%)	M_n^{th} [c]	M_n [d]	M_w/M_n [d]
1	25/1	98	4,400	4,000	1.21
2	50/1	99	8,700	8,200	1.24
3	100/1	99	17,250	17,400	1.23
4	200/1	94	32,600	34,700	1.19
5	400/1	94	64,700	66,500	1.19

[a] Polymerization conditions: ELA = 1 mL, DMSO = 0.5 mL, UV-light irradiation for 2.5 h. [b] Determined by ^{1}H NMR. [c] M(th) = 172.18 x $[ELA]_0/[EBiB]_0$ x conv. + 195.05. [d] Determined by GPC in THF using PMMA standards.

Irrespective of the targeted DP, the Cu(II)-mediated photoinduced polymerizations of ELA reached almost quantitative conversions within 2 hours. All the polymerizations were found to proceed under homogeneous conditions with a high degree of control (M_w/M_n = 1.19-1.24) (Figure 2.2.2c and Table 2.2.2). A representative kinetic experiment demonstrated that the photopolymerization of ELA is also fast and shows the expected features for a LRP technique (Figure 2.2.4).

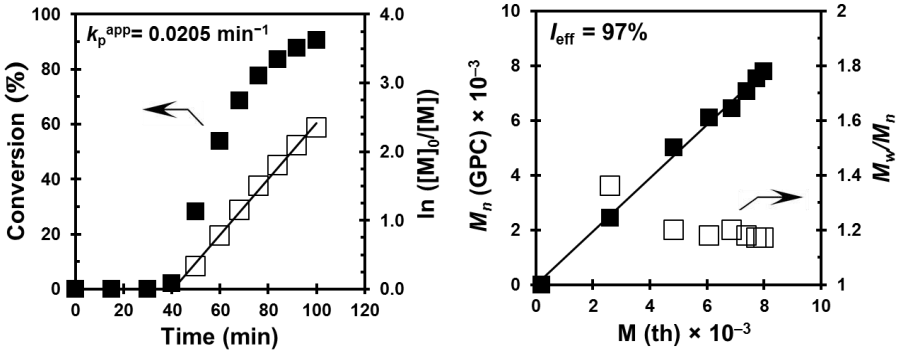

Figure 2.2.4. Kinetics plots and evolution of experimental M_n (GPC) and M_w/M_n versus theoretical M_n^{th} for the Cu(II)Br_2-mediated living photopolymerization of ELA in DMSO. Reaction conditions: 1 mL ELA, 0.5 mL DMSO, $[ELA]_0/[EBiB]_0/[Me_6\text{-TREN}]_0/[Cu(II)Br_2]_0$= 50/1/0.12/0.02.

Note that there is no significant difference on the Cu(II)-mediated photopolymerization kinetics of ELA and DMLA monomers in comparison with a commercially available model acrylate such as methyl acrylate (compare Figure 2.2.2a, 2.2.4 and S12 in Annex B). The photopolymerization of ELA in its solvent precursor proceeded up to high conversion (conv. = 95%) and furnished a narrow molecular weight polymer (M_w/M_n = 1.30) (Figure S13 in Annex B). Finally, the excellent control over the polymerization and high chain-end functionality attained in both systems was proved by MALDI-TOF MS analysis of the lowest molar mass PDMLA and PELA samples before and after thio-bromo "click" thiotherification of bromine chain ends with thiophenol (Figure 2.2.5).[52, 53]

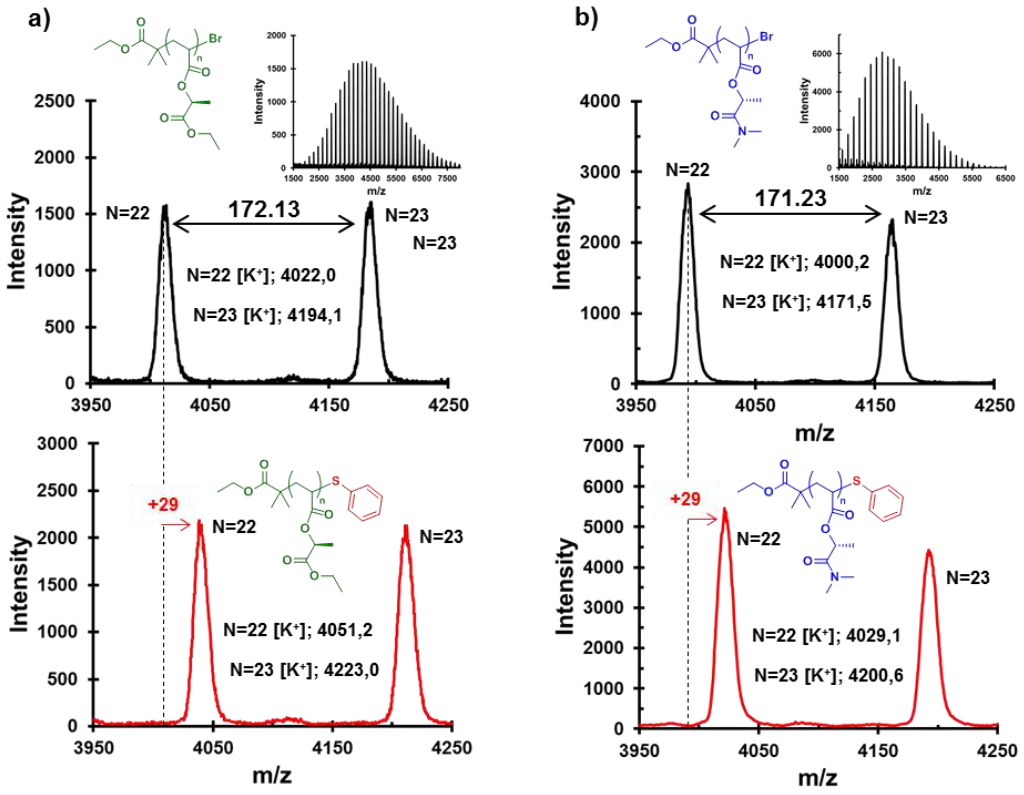

Figure 2.2.5. MALDI-TOF MS confirmation of the high chain end fidelity of PELA and PDMLA synthesized by Cu(II)-mediated radical photopolymerization. MALDI-TOF MS spectra of (a) PELA and (b) PDMLA before (upper spectrum) and after (lower spectrum) thio-bromo "click" thioetherification with thiophenol. Both polymers were synthesized targeting a DP=25 and isolated at near quantitative monomer conversion.

The presence of a dominant distribution with a peak-to-peak mass increment, which equals to the mass of a single repeating unit, vanishing after thio-bromo "click" thiotherification of bromine chain ends with thiophenol, supports the high end group fidelity of the synthesized polymers. The new series of peaks emerging after the chemical modification at polymer chain ends appears 29 mass units above. This mass difference is consistent with the replacement of –Br (80) with –SPh (109) at the ω-chain ends of both polymers.

Synthesis and thermal properties of amphiphilic BCPs

After demonstrating the facile preparation of well-defined homopolymers from ELA and DMLA with very different water solubility, we pursued synthesizing amphiphilic diblock copolymers with PELA and PDMLA segments as hydrophobic and hydrophilic building blocks, respectively. In this study, we were interested to obtain BCPs able to self-assemble into various nanostructures in aqueous solution. As a proof of concept, two different PELA-PDMLA copolymers were synthesized using a one-pot polymerization approach (i.e. *in situ* chain extension of the first block prepared at near quantitative monomer conversion) (Figure 2.2.6a). Initially, a BCP with hydrophilic/hydrophobic ratio of 50/50 (mol/mol), named thereafter BCP1, was targeted to favor the formation of spherical micelles in water. First, the hydrophobic core block was synthesized by Cu(II)-mediated living radical photopolymerization of ELA under conditions $[ELA]_0/[EBiB]_0/[Me_6\text{-}TREN]_0/[Cu(II)Br_2]_0$ =50/1/0.12/0.02 irradiating with UV-light (conversion 99 %, M_n = 9,250, M_w/M_n = 1.23). The near-quantitative monomer conversion enabled the *in situ* chain extension, avoiding intermediate purification of the first block, with DMLA (DP=50) in the second step (98% DMLA conversion) to produce PELA-*b*-PDMLA (BCP1, M_n = 18,200, M_w/M_n = 1.13).

As shown in Figure 2.2.7, the successful formation of a di-block copolymer was demonstrated by a clear shift of GPC trace toward higher molecular weights relative to the respective macroinitiator, without significant shoulders or tailing. Both blocks were grown in a controlled fashion as indicated by the close agreement between the measured M_n^{GPC} and the M_n^{th} calculated from the monomer conversions and narrow molecular weight distribution of the resulting copolymer.

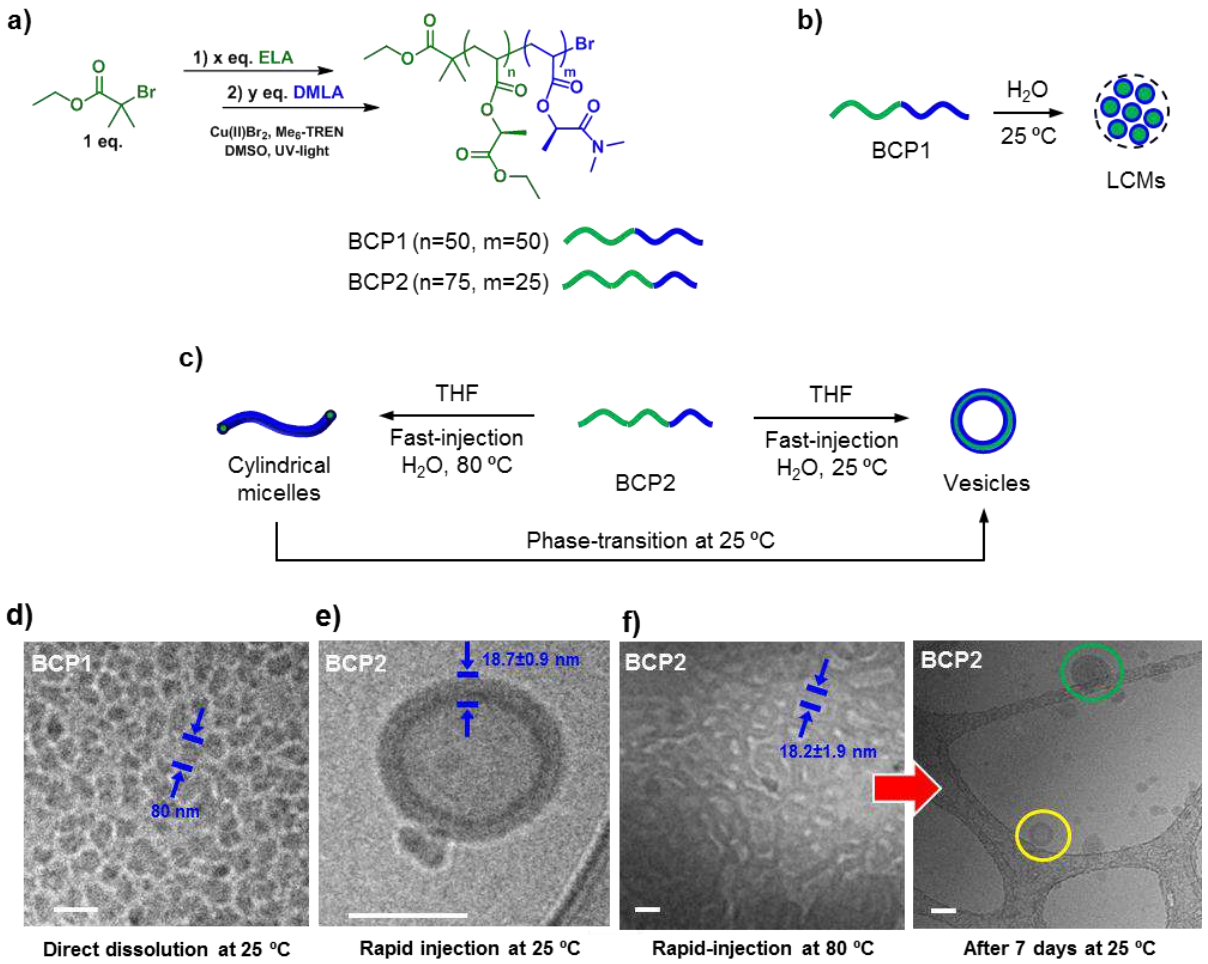

Figure 2.2.6. Schematic representations for: (a) synthesis of amphiphilic BCPs from ELA and DMLA *via* Cu(II)-mediated radical photopolymerization using a one-pot polymerization approach, (b) BCP1 micelles self-assemble in water at 25 °C, (c) BCP2 vesicles self-assemble when the copolymer is injected into water at 25 °C but BCP2 worm-like micelles self-assemble when the injection is carried out at 80 °C. The worm-like micelles transform into vesicles after some days at 25 °C. Cryo-TEM images for (d) BCP1 self-assembled in water by direct dissolution and (e) BCP2 self-assembled by fast injection of the copolymer (dissolved in THF) into water at 25 °C. (f) Cryo-TEM images recorded 30 min after self-assembly of BCP2 by fast injection of the copolymer (dissolved in THF) into hot water (80 °C) (left image) and after 7 days at 25 °C (right spectrum). Scale bars are 100 nm.

Note that the reverse block sequence (PDMLA-PELA) was also successful but with major discrepancy between experimental and theoretical M_n values of the resulting copolymer (Figure S14 in Annex B). Next, with the aim to deliver an amphiphilic block copolymer which could self-assemble to vesicles, the molar ratio of $[ELA]_0/[DMLA]_0$ was

varied to deliver an amphiphilic diblock copolymer with a higher hydrophobic content (BCP2, Figure 2.2.6a).

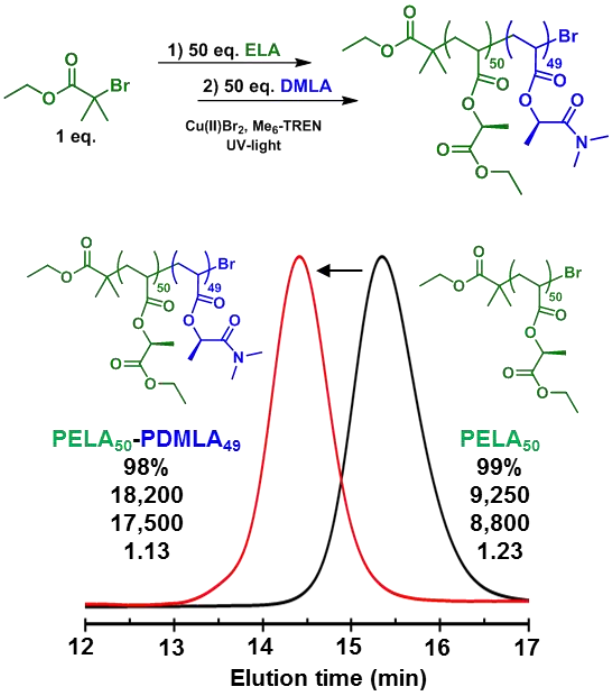

Figure 2.2.7. GPC analysis of the *in situ* block copolymerization *via* Cu(II)-mediated photopolymerization of PELA with DMLA to synthesize BCP1. Reaction conditions for the synthesis of PELA macroinitiator: $[ELA]_0/[EBiB]_0/[Me_6\text{-TREN}]_0/[Cu(II)Br_2]_0$= 50/1/0.12/0.02 in DMSO (50 vol %) followed by the addition of deoxygenated DMLA (50 equiv.) in DMSO *in situ*. Numbers shown together with the GPC traces correspond to monomer conversion, M_n (GPC), M_n^{th}, and M_w/M_n respectively from the top to bottom.

In this case, a PELA macroinitiator was synthesized using a $[ELA]_0/[EBiB]_0$ = 75 under otherwise identical conditions to yield PELA with M_n = 12,640 and M_w/M_n = 1.17 which was chain-extended *in situ* with DMLA (DP=25). GPC analysis after each of the two synthesis stages showed the expected growth in molar mass (Figure 2.2.8).

The targeted BCPs were recovered by dialysis on small scale against acetone (MWCO 2000) to minimize solvent waste and further analyzed by ^{1}H NMR. As an example, the analysis of BCP1 is shown in Figure 2.2.9.

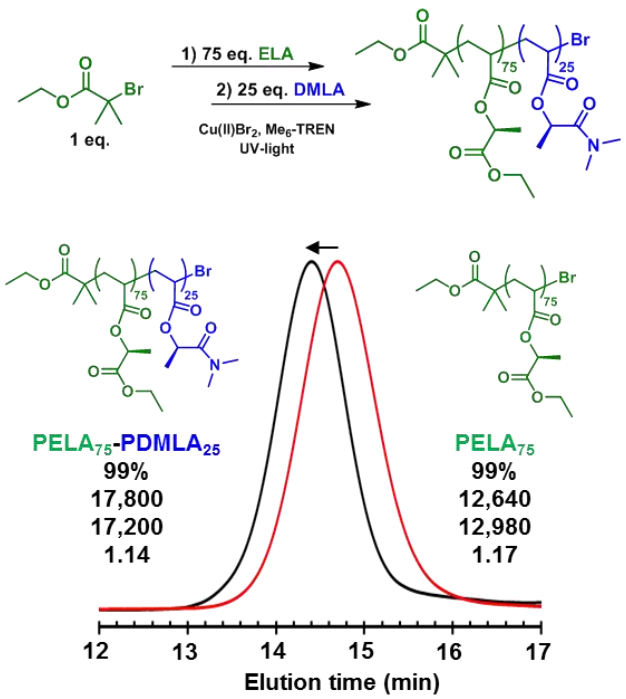

Figure 2.2.8. GPC analysis of the *in situ* block copolymerization *via* Cu(II)Br_2-mediated photopolymerization of PELA with DMLA to synthesize BCP2. Reaction conditions for the synthesis of PELA macroinitiator: $[ELA]_0/[EBiB]_0/[Me_6\text{-TREN}]_0/[Cu(II)Br_2]_0$= 75/1/0.12/0.02 in DMSO (50 vol%) followed by the addition of deoxygenated DMLA (25 equiv) in DMSO *in situ*.

^{1}H NMR analysis using a solvent such as $CDCl_3$, which is a good solvent for the PELA and PDMLA blocks, revealed the characteristic resonances of PELA (e.g. δ_8 = 5.00 ppm and δ_{10} = 4.17 ppm) and PDMLA (e.g. δ_{12} = 5.4 ppm) segments. The copolymer composition was calculated from the integrated signal of PELA CH-O group proton (δ = 5.0 ppm) with respect to the same signal of PDMLA (δ = 5.4 ppm). According to the targeted DPs, ^{1}H NMR analysis indicated a PELA/PDMLA copolymer composition of 0.51/0.49 for BCP1 and 0.80/0.20 for BCP2.

Importantly, when BCP1 was dissolved in D_2O, which is a good solvent only for the PDMLA block, no precipitate was observed and only the resonances attributed to the hydrophilic PDMLA block could be detected in the ^{1}H NMR spectrum (Figure 2.2.9b), whereas those stemming from PELA cannot be detected since the block is collapsed and the solvent excluded.

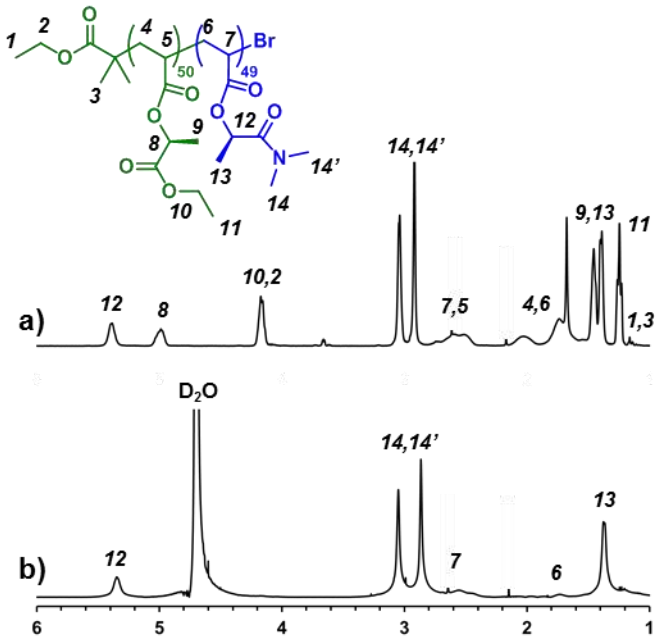

Figure 2.2.9. ^{1}H NMR spectrum of BCP1 recorded in (a) $CDCl_3$ and (b) D_2O.

Overall, these observations are consistent with the formation of self-assembled structures of BCP1 in water (e.g. micelles, vesicles) with an external hydrophilic PDMLA shell and an internal hydrophobic PELA portion with restricted motion. Microphase separation behavior of the synthesized copolymers in the bulk state, but with the possibility of partial mixing of the two constitutive segments, was also proved by DSC and TEM (Figure 2.2.10). In this case, BCP1 exhibited two glass transition temperatures (T_gs), i.e., 4 and 56 °C, which can be ascribed to those of the PELA and PDMLA segments, respectively, suggesting two-phase morphology. The T_g value of the PELA phase was in agreement with that of the corresponding copolymer. In contrast, the T_g value of the PDMLA phase decreased from 72 °C to 56 °C. These observations suggest partial phase mixing between PELA and PDMLA. On the other hand, BCP2 containing much lower PDMLA content showed a T_g corresponding to the soft block at about 8 °C and no signals corresponding the T_g of the PDMLA hard and hydrophilic block. However, the TEM imaging of a solvent cast sample of BCP2, stained with uranyl acetate, showed segregation (i.e. microphase separation) between hydrophilic and

hydrophobic segments of BCP2 with DPs of 75 and 25 for PELA and PDMLA blocks, respectively.

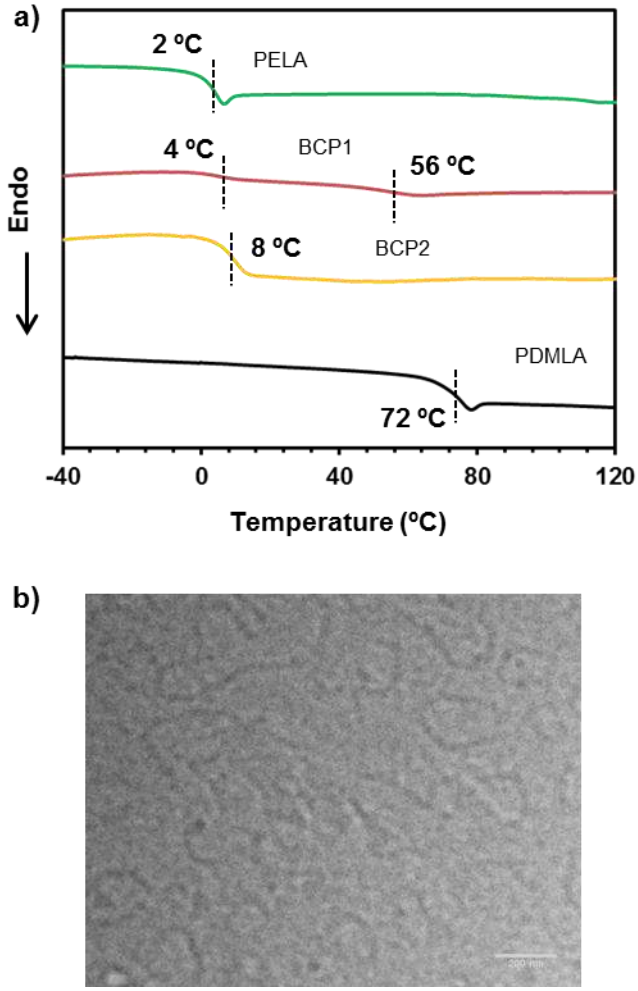

Figure 2.2.10. (a) DSC analysis of homopolymers PELA and PDMLA as well as copolymers BCP1 and BCP2: PELA (M_n (GPC) = 17,400), BCP1 (M_n (GPC) = 18,200), BCP2 (M_n (GPC) = 17,800), and PDMLA ((M_n (GPC) = 18,300). (b) TEM image showing segregation between hydrophilic and hydrophobic segments in BCP2.

Overall these results indicated that both copolymers are microphase separated in bulk, but with the possibility of partial mixing of the two constitutive segments.

Self-assembly studies of amphiphilic BCPs in water

With two PELA-PDMLA copolymers with different compositions in-hand, their self-assembly abilities in water were first evaluated by measuring the critical aggregation

concentration (CAC) using nile red (NR) as the fluorescence probe. The fluorescence quantum yield of this molecule is much higher in an apolar environment than polar. As can be seen in Figure 2.2.11, the fluorescence intensity of NR increases rapidly through a critical polymer concentration, indicating the formation of nanoaggregates of BCP1 and BCP2 with apolar pockets.

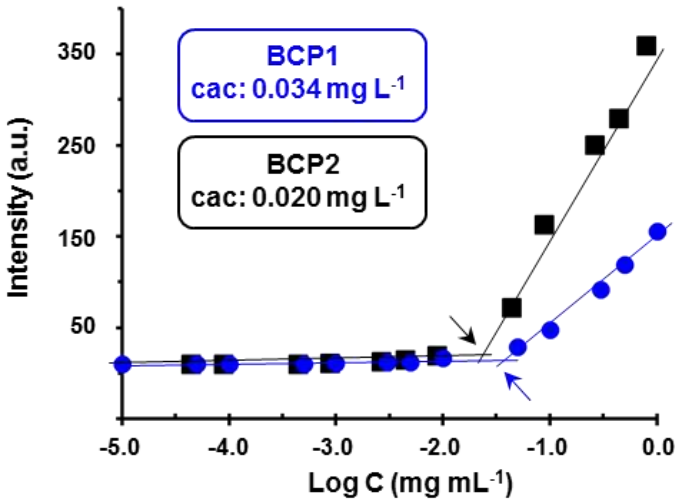

Figure 2.2.11. CAC of BCP1 and BCP2 determined using NR as a fluorescent probe. The relatively faster increase in intensity of BCP2 compared to BCP1 can be ascribed to the larger proportion of hydrophobic polymer in the former. It is the net volume of the hydrophobic block what determines the amount of NR sequestered above the CAC.

The CAC determined at the onset of slope change, indicated that BCP1 acts as a container for NR above a concentration of approximately 0.034 mg L^{-1}. However, BCP2 with higher fraction of PELA hydrophobic segment promoted aggregation to a greater extent as indicated by a lower experimental CAC value (0.020 mg L^{-1}). This is in line with stronger interaction energy ($N \cdot \chi$) for a longer block. Some intensity could be observed below the CAC which correspond with the existence of monomolecular micelles. The hydrodynamic size and morphologies of the self-assembled structures was further investigated by DLS and cryo-TEM. BCP2 was added to water in a concentration above the CAC (0.5 mg mL^{-1}). A slightly turbid solution was obtained, indicating the formation of aggregates in solution (Figure S15 in Annex B). BCP1 consists of two blocks with identical DP. However, while the hydrophobic

block (ELA) is collapsed in water, the hydrophilic block (DMLA) is fully expanded. Thus, low packing parameters (conical shape) corresponding to micelles were expected. DLS analysis revealed an average size of 78 nm with a dispersity of 0.224 for the nanoparticules (Figure S16a in Annex B). However, the size of these particles was larger than one should expect for single spherical micelles of BCP1. The hydrophobic part of BCP1 has only DP = 50 and its contour length is smaller than half the diameter of the aggregates. The larger size could result from further aggregation of single spherical micelles due to the existence of secondary interactions, bridging, between the hydrophilic swollen micellar coronas,[54] leading to large compound micelles (LCMs) (Figure 2.2.6b). Such attractive interactions may be supported by hydrogen bonding and dipole-dipole. The cryo-TEM analysis confirmed the presence of a large number of clustered particles of about 80 nm size (Figure 2.2.6d and Figure S17 in Annex B), in agreement with the DLS measurement. The nonuniformity of the clusters confirms that they could not be simple micelles. The higher hydrophobic character of BCP2 required a modified approach to study its self-assembly in water. A dilute solution of BCP2 in THF (5 mg mL^{-1}) was injected into water at room temperature (final concentration 0.5 mg mL^{-1}) (Figure 2.2.6c, right). In this case, a cloudy suspension was obtained, indicating the formation of larger aggregates in water (Figure S15 in Annex B) that strongly scatter light. Accordingly, DLS measurements showed a narrow size distribution centered at 148 nm (Figure S16b in Annex B). The self-assembly of amphiphilic BCP2 was visualized with cryo-TEM (Figure 2.2.6e). The majority of the particles were unilamelar vesicles with a diameter of 50-150 nm. The clear contrast between the dark periphery and the hollow center indicates that these spheres are vesicular. Vesicles with higher lamellarity cannot be excluded by the injection method but were found in minimal proportion.

The differences in lyothropic assembly between BCP1 and BCP2 are in agreement with their molecular structure. In BCP2 the ratio of hydrophobic to hydrophilic block is increased, thus bilayer type of assembly that closed into vesicles is expected.[55] Cryo-TEM image shown in Figure 2.2.12 was used to evaluate the membrane thickness, which statistically yields a thickness of 19 ± 0.9 nm.

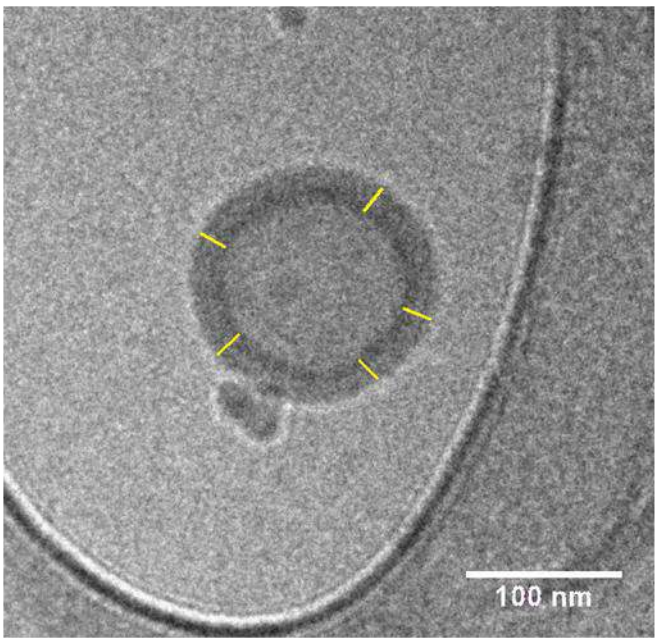

Measurement	Membrane thickness (nm)
1	18.6
2	19.6
3	17.2
4	18.6
5	19.3

Figure 2.2.12. Membrane thickness measurement of vesicles self-assembled from BCP2 by fast-injection of polymer solution (THF) into water at 25 °C.

Interestingly, a different morphology was obtained when injecting the organic solution of the copolymer into hot water (80 °C) and cooling down to room temperature (Figure 2.2.6c, left). The assembly temperature is selected to be higher than the highest T_g of each block as observed in the thermal analysis by DSC (Figure 2.2.10). In this case, the cryo-TEM grid was prepared 30 min after sample preparation, thus giving short time for structure evolution. Cryo-TEM revealed aggregates consistent with the formation of worm-like micelles with a diameter of approximately 18 nm were obtained (Figure 2.2.6f left and 2.2.13). This diameter is in agreement with the thickness of the membrane in unilamellar vesicle. The formation of cylindrical micelles on BCP2 when injection was carried out at high temperature can be explained by a higher swelling of the hydrophilic block.

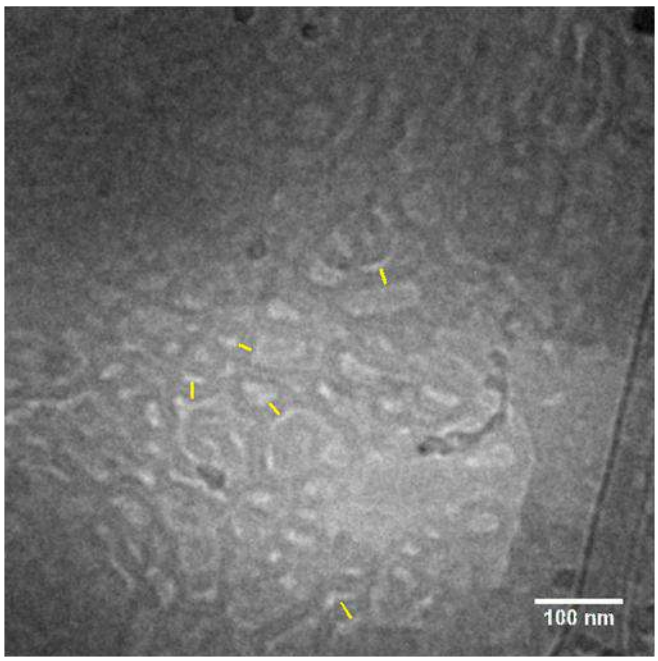

Measurement	Membrane thickness (nm)
1	16.9
2	18.6
3	15.6
4	19.0
5	20.7

Figure 2.2.13. Membrane thickness measurement of worm-like micelles self-assembled from BCP2 by fast-injection of polymer solution (THF) into water at 80 °C.

The larger hydrophilic volume causes that the ratio of hydrophilic interfacial area becomes larger than the cross section of the hydrophobic block shifting the packing parameter to the range of worm-like micelles at 80 °C. Because of the high molecular weight and low mobility of the chains in the aggregate the worm-like micelles did not evolve to vesicles after 30 min at 25 °C. But is this system dynamic enough to observe a phase transition between lyotropic phases? To prove the dynamic self-assembly behavior of the system, the same sample was analyzed again after 7 days at room temperature (Figure 2.2.6f, right). After this time, cryo-TEM imaging showed unilamellar (yellow circle) and onion-like vesicles (green circle) but no cylindrical micelles could be found. Hence, we observed an interesting phase transition from cylindrical micelles to unilamellar vesicles as, after some days, the hydrophilic block size and

consequently packing parameter goes back to what it is when the injection is done at room temperature. Overall, these results demonstrate that PELA-PDMLA amphiphilic copolymer can self-assemble into different morphologies such as LCMs, worm-like micelles, and unilamellar or onion-like vesicles depending on the relative block length of the constitutive homopolymers and the preparation method of the self-assemblies.

PELA-PDMLA amphiphilic BCPs as stabilizers in emulsion polymerization

Aqueous emulsion radical polymerization processes are industrially relevant in large-scale synthesis of vinyl polymers.[56,57] A basic emulsion polymerization system involves the use of a monomer or a mixture of monomers, typically in water and in the presence of a surface active agent (surfactant). Commonly, low molecular, short-chain stabilizers are used. However, the use of amphiphilic BCP surfactants impart several advantages to the properties of the resulting emulsion because exhibit unique properties in aqueous solution owing their low CAC and low diffusion coefficient compared to those of conventional low molecular weight surfactants.[58,59]

As a proof of concept test procedure, the emulsion polymerization of MMA and St were investigated using 1.0 wt% of either BCP1 or BCP2 as macromolecular stabilizer with respect to the monomer (Figure 2.2.16a). Both reactions were performed at a monomer content of 6 wt% using potassium persulfate as an initiator at 75 °C.

Under these conditions, no stable latexes were obtained using BCP2 as a macromolecular surfactant. However, BCP1 was found to be an efficient stabilizer for both commodity monomers because no coagulum was observed during the polymerization process up to high conversion. DLS analysis revealed the formation of well-defined PSt and PMMA nanoparticles according to low PDI values although the average diameter for PSt particles was larger (190 nm versus 98 nm) (Figure 2.2.14b). As can be seen in the Figure S18 in Annex B, the smaller particle size distribution after polymerization than the initial droplet-size distribution is consistent with a predominant emulsion polymerization mechanism. Uniform and spherical latex particles were visualized by TEM (Figure 2.2.14c and Figure S19 in Annex B). Both PSt and PMMA latex particles stabilized with BCP1 remained stable for at

least 30 days at room temperature. The stability of the PMMA latex particles was investigated under various conditions (Figure 2.2.14d,e).

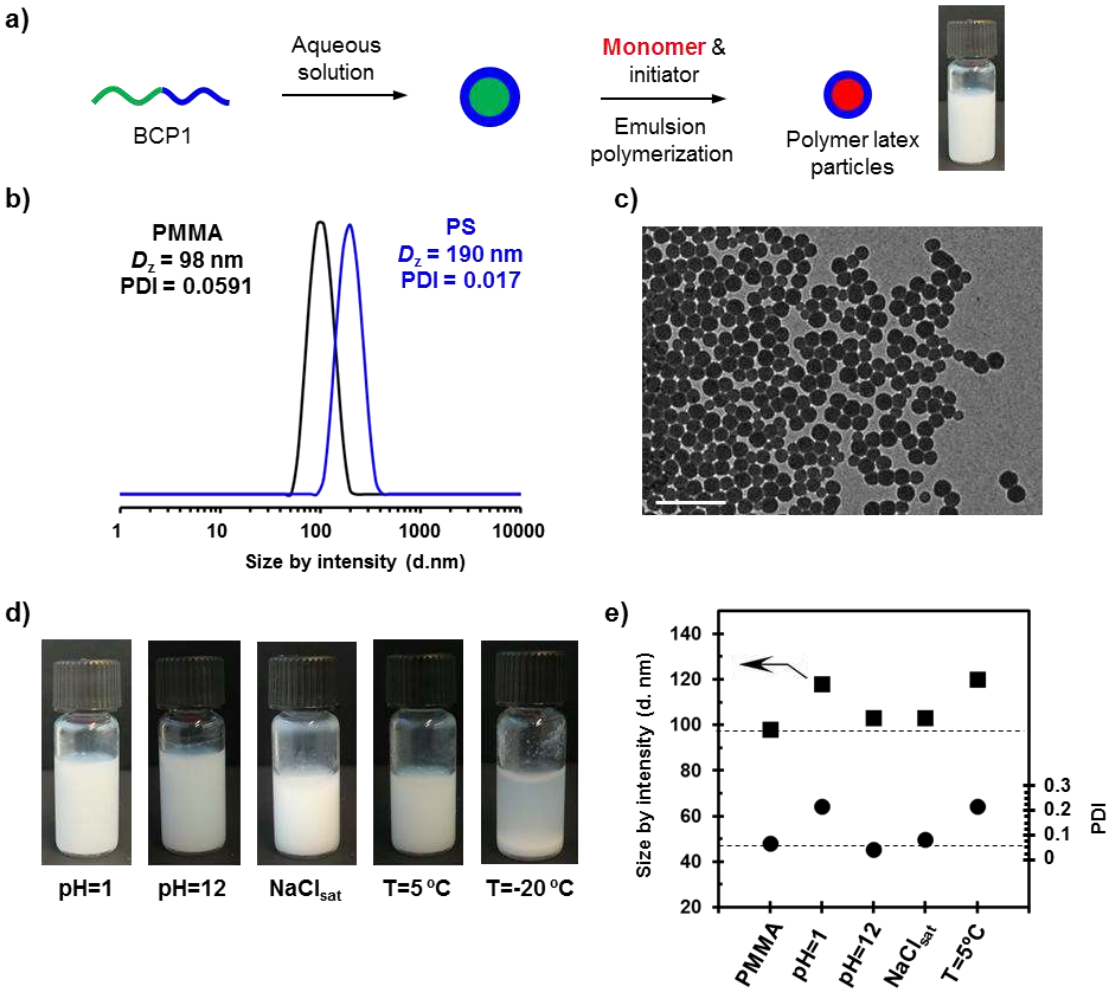

Figure 2.2.14. (a) Schematic representation of the aqueous emulsion radical polymerization of MMA and S using BCP1 as stabilizer. (b) DLS size distribution by intensity of PMMA and PS latexes stabilized by BCP1. (c) TEM image of the PMMA latex (scale bar is 100 nm). (d,e) Digital images and DLS analysis of PMMA latex under various storage conditions.

The non-ionic nature of the BCP1 endowed excellent pH stability to the system. PMMA latex was stable when the pH was increased to 14. When the pH of the system was decreased to 1, no coagulation took place and DLS analysis after 24 h revealed only a slight increase on diameter and PDI. A similar behavior was observed after storing the PMMA suspension for 24 h in the fridge (5 °C). However, it broken after cooling at -20 °C for 24 h and thaw at room

temperature (Figure 2.2.14d, right image). A promising stability to electrolyte addition was also demonstrated as PMMA latex stabilized by BCP1 was stable even after increasing the NaCl concentration until saturation.

2.2.3. Conclusions

In conclusion, our study demonstrate that environmentally friendly solvents can be upgraded to functional amphiphilic BCPs, suitable for applications as surfactants in nanofabrication. Efficient and sustainable functionalization of EL and DMLA green solvents with acrylate moieties generated monomers well-behaved under Cu(II)-mediated photoinduced LRP to deliver narrow and highly-end functional homopolymers at near-quantitative monomer conversion. Most importantly, EL-based polymer is hydrophobic and water-insoluble but switching the ethyl ester moiety to a N,N-dimethyl substituted amide, resulted in a water-soluble vinylic polymer (PDMLA). Thus, we focused our attention on the preparation of well-defined amphiphilic diblock copolymers, combining both building blocks in one material. Several green chemistry principles apply to this approach: (i) monomer synthesis is conducted using minimal energy in a biomass-derived solvent such as 2-Me-THF avoiding chromatographic purification, (ii) photoinduced Cu(II)-catalyzed polymerizations, conducted under mild conditions using a simple reaction setup, offer near-quantitative monomer conversions that enable block copolymerization with no intermediate purification of the first block, (iii) polymer purification protocols involves dialysis on a small scale to minimize solvent waste. The synthesized copolymers could self-assemble in water to generate nanoaggregates with different morphologies such as LCMs, worm-like micelles and vesicles. In this regard, they exhibited efficient performance as non-ionic surfactants in the preparation of well-defined PMMA and PSt latexes *via* aqueous emulsion polymerization, demonstrating their practical significance for technological applications.

2.2.4. Experimental section

Materials

The following chemicals were purchased from Merck and used as received: ethyl α-bromoisobutyrate (EBiB, 98%), methyl acrylate (MA, 99%), acryloyl chloride (≥ 97%), tris[2-(dimethylamino)ethyl]amine ligand (Me_6-TREN), copper (II) bromide (Cu(II)Br_2, 99%), propylphosphonic anhydride solution (T3P®, ≥50 wt.% in ethyl acetate), thiophenol (PhSH, ≥ 99%), dimethylsulfoxide (DMSO, ≥ 99.7%), trans-2-[3-(4-tert-butylphenyl)-2-methyl-2-propenylidene] malononitrile (BTCB, ≥ 98%), potassium trifluoroacetate (KTFA, 98%), natural ethyl lactate (EL, 98%), acetonitrile (HPLC grade), potassium persulfate ($K_2S_2O_8$, 98%), dialysis tube benzoylated (MWCO 2000), and 9-diethylamino-5-benzo[α]phenoxazinone (Nile Red). Methyl methacrylate (MMA, >99%) and styrene (St), also purchased from Merch, were de-inhibited by passing them through a small basic alumina pipette just before polymerization. Acetone (synthesis grade) was purchased from Scharlab. Deuterated chloroform ($CDCl_3$) and water (D_2O) were purchased from Eurositop. Triethylamine (TEA, ≥ 99%, Merck) and 2-methyltetrahydrofuran (2-Me-THF, Merck, 99.5%) were distilled prior to use from CaH_2 and sodium/benzophenone, respectively. α,α'-Azoisobutyronitrile (AIBN, >98%, Fluka) radical initiator for FRP was recrystallized from methanol before use. DMLA was kindly donated by Corbion, Gorinchem (Netherlands) and used as received.

Methods

^{1}H and ^{13}C NMR analyses were performed on a 400 MHz (for ^{1}H) and 100.6 MHz (for ^{13}C) Varian VNMR-S400 NMR instrument at 25°C using deuterated solvents. All chemical shifts are quoted on the δ scale in ppm using the residual solvent as internal standard. Molecular weight analysis for PELA samples were performed via gel permeation chromatography (GPC) using an Agilent 1200 series system equipped with three columns (PLgel 3 μm MIXED-E, PLgel 5 μm and PLgel 20 μm from Polymer Laboratories) and an Agilent 1100 series refractive-index factor detector. THF (Scharlab, HPLC grade) was used as eluent at

1.0 mL/min of flow rate and toluene as a flow rate marker. In the case of PDMLA samples the GPC analyses were performed on an Agilent 1200 series system, equipped with two serial columns (PLgel 5 μm MIXED-D) and an Agilent 1100 series refractive detector. Dimethylformamide (DMF) (Scharlab, HPLC grade with 0.1 wt% LiBr) and toluene were used as eluent at flow 1.0 mL/min and flow rate marker, respectively. In both cases, the weight-average (M_w) and number-average (M_n) molecular weights of the analyzed polymers samples were determined using a PMMA standards from American PSS Polymer Standards Service GmbH. Matrix-assisted laser desorption ionization-time of flight mass spectrometry (MALDI-TOF MS) analyses were performed on a Voyager-DE (Applied Biosystems) instrument with a 337 nm nitrogen laser (3 ns pulse width). For all the samples, the accelerating potential was 25 kV, the grid voltage was 93.5%, the laser power was 1700 units and a positive ionization mode was used. Samples were prepared as follows: independent solutions of the matrix (30 mg/mL), KTFA (10 mg/mL) and polymer (10 mg/mL) in THF were prepared and used to obtain a fourth solution at a volumetric ratio 9/1/1 that was used for MALDI-TOF analysis. After that, 5 x 1 μL of this solution were deposited onto five wells of MALDI-TOF sample plate and dried in air at room temperature before being subject to the analysis. Optical rotation measurements were conducted on a Perkin-Elmer 241 MC polarimeter with a path length of 10 cm and are reported with implied units of 10^{-1} deg cm^2 g^{-1}. Differential scanning calorimetry (DSC) measurements were carried out on a Mettler DSC3+ instrument using N_2 as a purge gas (50 mL/min) at a scanning rate of 10 °C/min with a -80 to 150 °C of temperature range. Calibration was made using an indium standard (heat flow calibration) and an indium-lead-zinc standard (temperature calibration). Thermal stability studies were carried out on a Mettler TGA2/LF/1100 with N_2 as a purge gas at a flow rate of 50 mL/min. The studies were performed in the 30-600 °C temperature range at a heating rate of 10 °C/min. Fluorescence spectra were obtained on an RF-5301 PC Shimadzu fluorescence spectrometer with RFPC software with emission using excitation slit widths of 5 nm. Fluorescence emission spectra of Nile red were recorded fixing the excitation wavelength at 550 nm and the emission spectra was recorded from 560-720 nm. Transmission electron microscopy (TEM) was performed using JEOL JEM-1011 TEM

microscope. Cryogenic transmission electron microscopy (Cryo-TEM) was performed on a Carl Zeiss Libra 120 Microscope operated at 120 kV at a temperature of -168 °C. Samples were prepared by rapid vitrification of 4 μL droplet of aqueous solution deposited on a plasma-treated lacey grid. The preparation was performed using a FEI Vibrot system. The vitrified specimens were then transferred to a 910-Gatan cryo-holder. Cryo-TEM micrographs were taken on a Carl Zeiss Libra 120 microscope (Oberkochen, Germany) operated at 120 kV at a temperature of -168 °C. The images were recorded using an in-column Omega energy filter and a CCD detector. Dynamic light scattering (DLS) measurements were carried out at room temperature using Zetasizer Nano ZS (model ZEN3500) from Malvern Instruments equipped with He-Ne laser. The Cu(II)-mediated radical photopolymerization reactions conducted herein were carried out in a Promed UV-365 nail lamp equipped with four 9W UV-lamps (λ=365 nm).

Synthesis of ELA monomer

Acrylic acid (13.6 mL, 0.19 mol), TEA (70.9 mL, 0.50 mol) and T3P® (65.4 g, 0.20 mol) were added to a solution of (L)-(-)-ethyl lactate (10 g, 0.17 mol) in MeTHF (200 mL). The mixture was stirred for 48 h at room temperature. The reaction was monitored by ^{1}H NMR. After 48 h, the reaction was diluted with water (100 mL) and the aqueous phase was extracted with diethyl ether (3x100 mL). The combined organic layers were rinsed with aqueous HCl 1 M (100 mL), saturated aqueous solution of $NaHCO_3$ (100 mL), brine (100 mL) and finally dried with $MgSO_4$. The resulting solution was concentrated under reduced pressure, and the residue was purified by vacuum distillation in the presence of 5 (w/w%) of hydroquinone to afford ELA (15.2 g, 52%) as a colorless liquid. $[\alpha]_D^{20}$ +53.9 (1.0 mg/mL, MeCN). ^{1}H NMR (400 MHz, CDCl3, δ): 6.48 (dd, 1H), 6.19 (dd, 1H), 5.89 (dd, 1H), 5.15 (q, 1H), 4.21 (q, 2H), 1.53 (d, 3H), 1.28 (t, 3H); ^{13}C NMR (100.6 MHz, $CDCl_3$, δ): 170.72, 165.43, 131.86, 127.78, 68.85, 61.42, 17.01, 14.14. HRMS (TOF ES$^+$) m/z: $[M+H]^+$ calcd for $C_8H_{13}O_4^+$, 173.0808, found, 173.0809.

Synthesis of DMLA monomer

The same procedure was used to synthesize ELA and DMLA monomers from the corresponding lactic acid-based solvent precursor (Scheme 2.2.1). The synthesis of DMLA is described: (D)-(+)-*N*,*N*-dimethyl lactamide (DML) (20.0 g, 0.17 mol) and anhydrous TEA (26.4 g, 0.26 mol) were dissolved in anhydrous 2-Me-THF (50 mL) under a positive flow of argon. The solution was stirred for 30 min at 0-5 °C before adding dropwise acryloyl chloride (18.2 g, 0.20 mol) dissolved in anhydrous 2-Me-THF (50 mL). The reaction was allowed to proceed for 24 h at room temperature. The reaction mixture was then filtered and Me-THF was removed under reduced pressure. The final residue was purified by vacuum distillation in the presence of 5 (w/w%) of hydroquinone to afford DMLA (20.5 g, 70%) as a colorless liquid. $[\alpha]_D^{20}$ +7.9 (1.0 mg/mL, MeCN). ^{1}H NMR (400 MHz, $CDCl_3$, δ): 6.48 (dd, 1H), 6.19 (dd, 1H), 5.89 (dd, 1H), 5.47 (q, 1H), 3.08 (s, 3H), 2.98 (s, 3H), 1.48 (d, 3H); ^{13}C NMR (100.6 MHz, $CDCl_3$, δ): 170.10, 165.65, 131.70, 127.84, 67.04, 36.80, 35.93, 16.65. HRMS (TOF ES^+) m/z: $[M+H]^+$ calcd for $C_8H_{14}NO_3^+$, 172.0968; found, 172.0969.

FRP of DMLA

DMLA (1 g, 5.8 mmol) and AIBN (1.85 mg, 0.011 mmol) were introduced into a Schlenk-flask equipped with a rubber septum. After bubbling argon through the reaction mixture during 30 min, the flask was placed in a thermostatic bath at 90 °C during 9 h. Next, the monomer conversion was determined by ^{1}H NMR spectroscopy. The resulting polymer was purified through dialysis against acetone.

Cu(II)Br_2-mediated radical photopolymerization of DMLA and ELA

This procedure is generic for all the photohomopolymerizations conducted herein. The polymerization of ELA initiated from EBiB in DMSO under the conditions: $[ELA]_0/[EBiB]_0/[Cu(II)Br_2]/[Me_6\text{-TREN}]_0$= 50/1/0.02/0.12 is described. ELA (1 mL, 6.23 mmol) and Me_6-TREN (2 µL, 0.015 mmol) were introduced into a vial containing a small Teflon-

coated stirring bar followed by the addition of 1 mL of stock solution containing EBiB (91.5 μL, 0.6 mmol) and Cu(II)Br_2 (2.8 mg, 0.012 mmol) in DMSO. After sealing the flask with a rubber septum and bubbling argon through the reaction mixture during 15 min, the vial was placed under UV light irradiation (4 x 9 W, λ= 365 nm) while stirring. The reaction was allowed to proceed during 2.5 h at room temperature. Next, it was quenched by bubbling air during 5 minutes and the monomer conversion was determined by ^{1}H NMR spectroscopy. The final polymer was purified through dialysis against acetone and dried under vacuum until constant weight. M_n and M_w/M_n values of the resulting polymer was determined by GPC using PMMA standards.

General procedure for chain-end modification of PELA and PDMLA via thio-bromo "click" reaction

In a 5 mL round-bottomed flask equipped with a Teflon-coated stirring bar and a rubber septum, thiophenol (0.06 equiv.) and distilled triethylamine (0.06 equiv.) were added into a solution of polymer (0.01 equiv.) in acetonitrile (2 mL) under argon flow. The reaction mixture was stirred at room temperature for 3 hours. Then, the resulting modified polymer was dialyzed against acetone and dried under vacuum until constant weight before analysis by MALDI-TOF MS.

General procedure for the *in situ* Cu(II)-mediated radical block photocopolymerization of ELA and DMLA

The procedure is generic for all the BCPs prepared herein. The block copolymerization of ELA ($[ELA]_0/[EBiB]_0/[Cu(II)Br_2]_0/[Me_6TREN]_0$ = 50/1/0.02/0.12) with DMLA (50 equiv.) is described. ELA (0.5 mL, 3.11 mmol) and Me_6TREN (2 μL, 0.0075 mmol) were added in a vial containing a small Teflon-coated stirring bar. Afterwards, 0.5 mL of stock solution containing EBiB (36.6 μL, 0.062 mmol) and Cu(II)Br_2 (1.12 mg, 0.0013 mmol) in DMSO was introduced to the reaction mixture. After sealing the flask with a rubber septum and bubbling argon through the reaction mixture during 15 min, the vial was placed under UV light irradiation

while stirring. After 2.5 h, the reaction mixture was sampled using an airtight syringe under positive pressure of argon to determine ELA conversion by ^{1}H NMR spectroscopy. After that, a solution of DMLA (0.44 mL, 3.11 mmol) and Me_6TREN (2 μL, 0.0075 mmol) in DMSO (0.44 mL), previously deoxygenated, was injected into the polymerization mixture *via* cannula. The reaction mixture was placed again under UV light and allowed to proceed for additional 2.5 h. Finally, the DMLA conversion was determined by ^{1}H NMR spectroscopy and M_n and M_w/M_n values by GPC using PMMA standards. The obtained copolymer was purified through dialysis against acetone and dried under vacuum until constant weight. The CAC of selected copolymers was determined by using NR as a fluorescence probe by monitoring the emission peaks at 585 nm. A copolymer concentration ranging from 1.0 x 10^{-9} g·L^{-1} to 1.0 g·L^{-1} was used. NR concentration was fixed at 6.0 x 10^{-7} M.

Self-assembly of BCPs

BCP1 nanoassemblies were prepared by direct dissolution of 0.5 mg of copolymer in 10 mL of milli Q water. BCP2 nanoassemblies were prepared by two different methods: (i) fast injection of a solution of copolymer in THF (5 mg·mL^{-1}) to milli Q water at room temperature and (ii) fast injection of the same solution to milli Q water at 80 °C.

Critical aggregation concentration (CAC)

The aggregate dispersions of BCP1 (2 mg/mL) were prepared by direct dissolution of the copolymer in water under sonication overnight. This stock dispersion was used to prepare the different polymer concentrations ranging from 1.0x10^{-6} to 1.0 mg/mL. For the fluorescence analysis, 85 μL of Nile red (NR) solution in acetone (0.35 mM) was added into a 50 mL flask to obtain a final concentration of 6.7 x 10^{-7} M, followed by the evaporation of acetone under vacuum (30 minutes). To the flask containing NR, different volumes of the stock dispersion were added to achieve the desired concentrations and were diluted to 50 mL with water. The obtained solutions were incubated overnight in a shaker. After that, the excitation spectra of the polymer dispersions were recorded from 560-570 nm on a RF-

5301 PC Shimadzu fluorescence spectrometer with an excitation wavelength of 550 nm and a scanning rate of 100 nm/min at 25 °C. Both excitation and emission slit were fixed to 5 nm. The CAC was determined by monitoring the evolution of fluorescence emission intensity (NR, λem = 617 nm) at different concentrations of BCP1.

The aggregate dispersions of BCP2 (2 mg/mL) were prepared by solvent exchange methodology. Briefly, BCP2 (20 mg) was dissolved in acetone (300 μL). This solution was added dropwise into a water solution (5 mL) and the solution was sonicated during 3 hours to ensure the complete evaporation of acetone, then to achieve the desired final concentrations the solutions were diluted to 10 mL with water. This stock dispersion was used to prepare the different polymer concentrations ranging from $1.0x10^{-6}$ to 1.0 mg/mL. For the fluorescence analysis and CAC determination the same aforementioned protocol applied for BCP1 was conducted.

General emulsion polymerization procedure using BCP1 as stabilizer

The procedure is generic for the emulsion polymerizations of MMA and St conducted herein. The emulsion polymerization of MMA is described: 6 mL of deionized water were added to a 10 mL round-bottomed flask containing a Teflon-coated stirring bar. Next, 4 mg of BCP1 (1 wt% based on MMA) dissolved in 300 μL of acetone were injected to promote the self-assembly of the copolymer. After that, the flask was sealed with a rubber septum and was deoxygenated with argon during 30 minutes. Then, it was placed in a thermostatic bath at 65 °C. After 10 minutes, the addition of MMA (0.4 g over 2 h) with a syringe pump was started. After completing the addition, the temperature was fixed at 75 °C and the polymerization was started by the addition of an aqueous solution of potassium persulfate (1 wt% based on MMA, 4 mg, 0.024 mol/L). The polymerization was allowed to proceed for 2 hours. Monomer conversion was determined gravimetrically, after quenching 500 μL of emulsion solution with hydroquinone (4 mg), and by drying at 85 °C under vacuum. In all

cases, high conversion (> 95%) were determined. Size number and TEM analysis from latex solutions were conducted on diluted solutions by a factor of 200.

2.2.5. References

[1] Bozell, J.; Petersen, G. *Green Chem.* **2010**, *12*, 539-554.

[2] Gunukula, S.; Pendse, H. P.; DeSisto, W. J.; Wheeler, M. C. *ACS Sustainable Chem. Eng.* **2018**, *6*, 5533-5539.

[3] Rinaldi, R.; Jastrzebski, R.; Clough, M. T.; Ralph, J.; Kennema, M.; Bruijnincx, P. C. A.; Weckhuysen, B. M. *Angew. Chem. Int. Ed.* **2016**, *55*, 8164-8215.

[4] Isikgora, F. H.; Becer, C. R. *Polym. Chem.* **2015**, *6*, 4497-4559.

[5] Wang, Y.; Deng, W.; Wang, B.; Zhang, Q.; Wan, X.; Tang, Z.; Wang, Y.; Zhu, C.; Cao, Z.; Wang, G.; Wan, H. *Nat. Commun.* **2013**, *4*, 2141.

[6] Cubas-Cano, E.; González-Fernández, C.; Ballesteros, M.; Tomás-Pejó, E. *Biofuels Bioprod. Bioref.* **2018**, *12*, 290-303.

[7] Dusselier, M.; Wouwe, P. V.; Dewaele, A.; Makshina, E.; Sels, B. F. *Energy Environ. Sci.* **2013**, *6*, 1415-1442.

[8] Mäki-Arvela P.; Simakova, I. L.; Salmi, T.; Murzin, D. Y. *Chem. Rev.* **2014**, *114*, 1909-1971.

[9] Chen, G. Q.; Patel, M. K. *Chem. Rev.* **2012**, *112*, 2082-2099.

[10] Yee, G. M.; Hillmyer, M. A.; Tonks, I. A. *ACS Sustainable Chem. Eng.* **2018**, *6*, 9579-9584.

[11] Galaster EL 98.5 FCC, Galasolv 003, PURASOLV ELECT, and VertecBio EL are examples of commercial ethyl lactate solvents produced by Galactic, Corbion, or Vertec Biosolvents.

[12] N,N-Dimethyl lactamide solvent is marketed by BASF under the product name AGNIQUE AMD 3L.

[13] Pereira, C. S. M.; Silva, V. M. T. M.; Rodrigues, A. E. *Green Chem.* **2011**, *13*, 2658-2671.

[14] Paul, S.; Pradhan, K.; Das, A. R. *Curr. Green. Chem.* **2016**, *3*, 111-118.

[15] European Chemicals Agency https://www-echa-europa-eu.sabidi.urv.cat/web/guest/substance-information/-/substanceinfo/100.132.568 (accessed Oct 31, 2019).

[16] Material Safety Data Sheet MSDS AGNIQUEAMD 3L, BASF SE, 67056 Ludwigshafen, Germany (accessed Oct 31, 2019).

[17] Planer, S.; Jana, A.; Grela, K. *ChemSusChem* **2019**, *12*, 4655-4661.

[18] Dandia, A.; Jain, A. K.; Laxkar, A. K. *Tetrahedron Lett*. **2013**, *54*, 3929-3932.

[19] Bertrand, O.; Wilson, P.; Burns, J. A.; Bell, G. A.; Haddleton, D. M. *Polym. Chem.* **2015**, *6*, 8319-8324.

[20] Moreno, A.; Garcia, D.; Galià, M.; Ronda, J. C.; Cádiz, V.; Lligadas, G.; Percec, V. *Biomacromolecules* **2017**, *18*, 3447-3456.

[21] Lligadas, G.; Grama, S.; Percec, V. *Biomacromolecules* **2017**, *18*, 2981-3008.

[22] Zhang, N.; Samanta, S. R.; Rosen, B. M.; Percec, V. *Chem. Rev*. **2014**, *114*, 5848-5958.

[23] EL is produced by the esterification reaction of ethanol and lactic acid whereas DML can be easily synthesized either from the reaction of lactic acid esters or lactide with dimethyl amine.

[24] Bell, G. A.; Tovey, I. D. WO2007/107745 A2, Sep 27, 2007.

[25] Henneberry, M.; Snively, J.; Vasek, G.; Datta, R. U. S. Patent US 2003/0171241 A1, Sep 11, 2003.

[26] Gronwald, O.; Weber, M. *J. Appl. Polym. Sci.* **2019**, *136*, 48419.

[27] Sobieski, R. T. WO Patent 2005/049719 A2, June 2, 2005.

[28] Nikles, S. M.; Piao, M.; Lanea, A. M.; Nikles, D. E. *Green Chem.* **2001**, *3*, 109-113.

[29] Sen, R.; Sivarajan, R.; Rueckes, T.; Segal, B. M. WO Patent 2006/007206 A3, Jan 19, 2006.

[30] Llevot, A.; Dannecker, P. K.; von Czapiewski, M.; Over, L. C.; Söyler, Z.; Meier, M. A. R. *Chem. Eur. J.* **2016**, *22*, 11510-11521.

[31] Zhu, Y.; Romain, C.; Williams, C. K. *Nature* **2016**, *540*, 354-362.

[32] Schneiderman, D. H.; Hillmyer, M. A. *Macromolecules* **2017**, *50*, 3733-3749.

[33] Purushothaman, M.; Krishnan, P. S. G.; Nayak, S. K. *J. Appl. Polym. Sci.* **2014**, *131*, 40962.

[34] Purushothaman, M.; Krishnan, P. S. G.; Nayak, S. K. *J. Renew. Mater.* **2015**, *3*, 292-301.

[35] Purushothaman, M.; Krishnan, P. S. G.; Nayak, S. K. *J. Macromol. Sci. A.* **2014**, *51*, 470-480.

[36] Purushothaman, M.; Krishnan, P. S. G.; Gopala, S.; Nayak, S. K. *Mater. Focus* **2018**, *7*, 101-107.

[37] Bensabeh, N.; Moreno, A.; Roig, A.; Monaghan, O. R.; Ronda, J. C.; Cádiz, V.; Galià, M.; Howdle, S. M.; Lligadas, G.; Percec, V. *Biomacromolecules* **2019**, *20*, 2135-2147.

[38] Moreno, A.; Bensabeh, N.; Parve, J.; Ronda, J. C.; Cádiz, V.; Galià, M.; Vares, L.,; Lligadas, G.; Percec, V. *Biomacromolecules* **2019**, *20*, 1816-1827.

[39] Reynolds, D. D.; Kenyon, W. O. U.S. Patent 2,458,420 A, Jan 4, 1949.

[40] Holmberg, A. L.; Reno, K. H.; Wool, R. P.; Epps III, T. H. *Soft Matter* **2014**, *10*, 7405-7424.

[41] Brown, H. R.; Krappe, U.; Stadler, R. *Macromolecules* **1996**, *29*, 6582-6588.

[42] Ruzette, A. V.; Leibler, L. *Nat. Mater.* **2005**, *4*, 19-31.

[43] Sainz, M. F.; Souto, J. A.; Regentova, D.; Johansson, M. K. G.; Timhagen, S. T.; Irvine, D. J.; Buijsen, P.; Koning, C. E.; Stockman, R. A.; Howdle, S. M. *Polym. Chem*. **2016**, *7*, 2882-2887.

[44] Anastasaki, A.; Nikolaou, V.; Zhang, Q.; Burns, J.; Samanta, S. R.; Waldron, C.; Haddleton, A. J.; McHale, R.; Fox, D.; Percec, V.; Wilson, P.; Haddleton, D. M. *J. Am. Chem Soc.* **2014**, *136*, 1141-1149.

[45] Jones, G. R.; Whitfield, R.; Anastasaki, A.; Haddleton, D. M. *J. Am. Chem. Soc.* **2016**, *138*, 7346-7352.

[46] Anastasaki, A.; Nikolaou, V.; Nurumbetov, G.; Truong, N. P.; Pappas, G. S.; Engelis, N. G.; Quinn, J. F.; Whittaker, M. R.; Davis, T. P.; Haddleton, D. M. *Macromolecules* **2015**, *48*, 5140-5147.

[47] Laun, J.; Vorobii, M.; de los Santos Pereira, A.; Pop-Georgievski, O.; Trouillet, V.; Welle, A.; Barner-Kowollik, C.; Rodriguez-Emmenegger, C.; Junkers, T. *Macromol. Rapid Commun.* **2015**, *36*, 1681-1686.

[48] Vorobii, M.; de los Santos Pereira, A.; Pop-Georgievski, O.; Kostina, N. Y.; Rodriguez-Emmenegger, C.; Percec, V. *Polym. Chem.* **2015**, *6*, 4210-4220.

[49] Vandenbergh, J.; Reekmans, G.; Adriaensens, P.; Junkers, T. *Chem. Sci.* **2015**, *6*, 5753-5761.

[50] Marti, M.; Molina, L.; Aleman, C.; Armelin, E. *ACS Sustainable Chem. Eng*. **2013**, *1*, 1609-1618.

[51] Bauri, K.; De, P.; Shah, P. N.; Li, R.; Faust, R. *Macromolecules* **2013**, *46*, 5861-5870.

[52] Rosen, B. M.; Lligadas, G.; Hahn, C.; Percec, V. *J. Polym. Sci., Part A: Polym. Chem.* **2009**, *47*, 3940-3948.

[53] Rosen, B. M.; Lligadas, G.; Hahn, C.; Percec, V. *J. Polym. Sci., Part A: Polym. Chem.* **2009**, *47*, 3931-3939.

[54] Israelachvili, J. N. *Intermolecular and Surface Forces* 2nd Ed., Academic Press: London, UK, 1992.

[55] Smart, T.; Lomas, H.; Massignani, M.; Flores-Merino, M. V.; Perez, L. R.; Battaglia, G. *Nano Today* **2008**, *3*, 38-46.

[56] Asua, J. M. *J. Polym. Sci., Part A: Polym. Chem.* **2004**, *42*, 1025-1041.

[57] Rigoussen, A.; Verge, P.; Raquez, J. M.; Dubois, P. *Chemistry and Technology of Emulsion Polymerisation*. John Wiley & Sons Ltd: Oxford, UK, 2013, vol. 6.

[58] Raffa, P.; Wever, D. A. Z.; Picchioni, F.; Broekhuis, A. A. *Chem. Rev*. **2015**, *115*, 8504-8563.

[59] George, S.; Champagne-Hartley, R.; Deeter, G.; Campbell, D.; Reck, B.; Urban, D.; Cunningham, M. *Macromolecules* **2015**, *48*, 8913-8920.

2.3. Biosourced all-acrylic ABA block copolymers with lactic acid-based soft phase

LA is one of the key biobased chemical building blocks given its readily availability from sugars through fermentation and facile conversion into a range of important chemical intermediates and polymers. Herein, well-defined rubbery polymers derived from BL solvent were successfully prepared by RAFT polymerization of the corresponding monomeric acrylic derivative. Good control over molecular weight and molecular weight distribution was achieved in bulk using either monofunctional or and difunctional trithiocarbonate-type chain transfer agents. Subsequently, poly(butyl lactate acrylate) (PBLA) having a relative low T_g (-20 °C), good thermal stability (5 wt.% loss at 340 °C) as well as low toxicity was evaluated as sustainable middle block in all-acrylic ABA copolymers using isosorbide and vanillin-derived glassy polyacrylates as representative end blocks. Thermal, morphological and mechanical properties of copolymers containing hard segment contents < 20 wt% were evaluated to demonstrate suitability of rubbery poly(alkyl lactate) building blocks for developing functional sustainable materials. Noteworthy, 180° peel adhesion measurements showed that the synthesized biosourced all-acrylic ABA copolymers possess competitive performance when compared with commercial pressure-sensitive tapes.

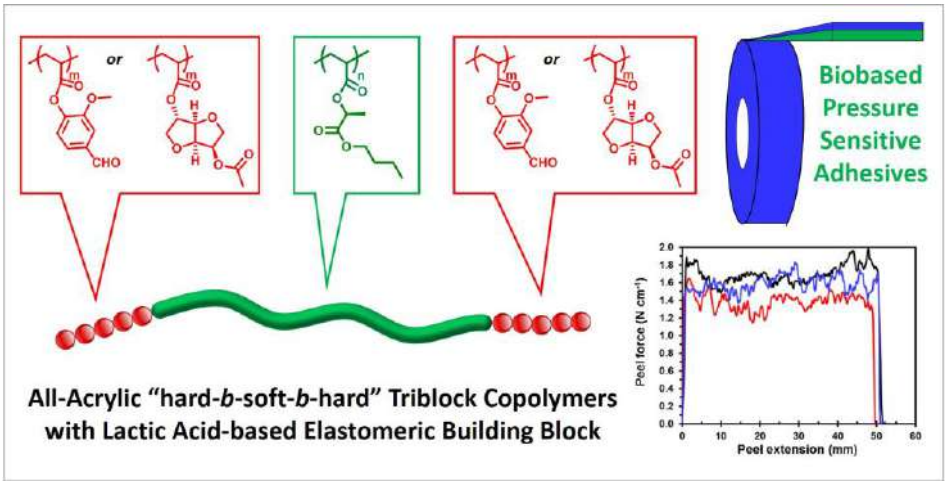

2.3.1. Introduction

Nature uses molecular self-assembly to create precision nanostructures and build large constructs through hierarchical assembly.[1,2] Inspired by these motifs, considerable efforts have been undertaken to recreate such concepts using synthetic BCPs fashioned from two or more chemically dissimilar components that are covalently-bonded into a single molecule.[3] Linear ABA BCPs with a soft middle block and hard minority end blocks are of high utility and interest for a wide variety of applications, ranging from adhesives to clothing, automotive, and biomedical components due to their remarkable (re)processable structures.[4] Among them, all-acrylic systems offer advantages to the current gold-standard systems based on poly(St-block-isoprene-block-St) and poly(St-block-butadiene-block-St) copolymers, in terms of wider service temperature range, improved optical transparency and stability to UV-light.[5,6] In addition, acrylate-based triblocks may exhibit excellent performance as pressure sensitive adhesives (PSAs) even without the incorporation of additives such as tackifiers and plastisizers.[7]

Making the most of reversible deactivation radical polymerizations techniques,[8] the rich assortment of (meth)acrylate monomers from biosourced feedstocks offers an attractive palette of rubbery and glassy polymers for the design of innovative sustainable all-acrylic ABA-type thermoplastic elastomers (TPEs) with competitive properties. For instance, poly(lauryl methacrylate) (T_g ~ -46 °C) as the rubbery segment, and poly(acetylsalicylic ethyl metacrylate) (T_g ~ 53 °C) as the glassy segment were combined to build up ABA copolymer architectures exhibiting elastomeric behavior at room temperature.[9] Biosourced acrylic monomers derived from glucose,[10] isosorbide,[11] itaconic acid imides,[12] rosin,[13] as well as aromatic lignin derivatives,[14] have been shown to provide useful glassy components for developing sustainable elastomeric and adhesive materials based on ABA BCPs. In most of these studies, PBA (T_g ~ -50 °C) was chosen as the rubbery midblock, since it is a conventional component of acrylic ABA copolymers with tunable properties according to block lengths and molecular composition. Although it is feasible to derive nBA from bio-sourced acrylic acid and butan-1-ol,[15] the search for alternative rubbery blocks from

biobased feedstocks represents a key step forward towards improving the material's sustainability. In this regards, fatty acids acrylic derivatives,[16] dialkyl itaconates[12] and tetrahydrogeraniol derivatives[17] are only selected examples on how to create renewable triblock copolymers with biobased soft phase without compromising performance.

LA is one of the top value added biomass derived platform chemicals, given its ready availability from sugars through fermentation and its facile conversion into a number of important derivatives.[18-20] Among them, polylactide, most commonly synthesized by the ring-opening polymerization of the cyclic dimer of LA, is a good alternative replacement for the traditional petroleum-sourced PSt glassy end-blocks in ABA TPEs, due to their high modulus characteristics.[21] The potential of alkyl lactate esters, e.g., methyl, ethyl, butyl, goes beyond their well-recognized use as ecofriendly solvents,[22] as their secondary alcohol offers a simple access to monovinyl derivatives prone to polymerization by radical mechanisms.[23-26]

In this regard, in chapter 2.1 it has demonstrated that poly(alkyl lactate ester) (meth)acrylates with controlled molecular weight, narrow molecular weight distribution and high end-group fidelity are also easily accessible by Cu(0) wire-mediated single-electron transfer living radical polymerization (SET-LRP).[27,28] In a more recent effort, the different water solubility of poly(ethyl lactate acrylate)s (hydrophobic and water-insoluble) and poly(*N,N*-dimethyl lactamide acrylate) (hydrophilic and water-soluble) was exploited to design amphiphilic AB block copolymers from neoteric lactic acid-based solvents, i.e., EL and DML, that could self-assemble in aqueous solution to form nanoparticles with different morphologies including large-compound micelles and vesicles (Chapter 2.2).[29]

Herein, we report on the preparation of all-acrylic ABA copolymers with LA acrylic derivative as elastomeric building block. A biobased acrylic monomer, L-butyl lactate acrylate (BLA) has been synthesized from the corresponding alkyl lactate, which is used as a solvent and a dairy-related flavoring agent approved as a food additive by the US Food and Drug Administration. This monomer was conceived to impart a LA-based sustainable soft segment into ABA-type BCPs. RAFT polymerization of the BLA monomer allowed the preparation of fine-tuned all-acrylic triblock copolymers combining soft poly(BLA) segments with isosorbide and vanillin-derived glassy end blocks. The ABA architecture were investigated for the

fidelity of phase-separation in the bulk, and were initially examined for their mechanical and adhesion properties. The results reported here demonstrate that biosourced and non-toxic acrylic derivatives of alkyl lactate esters can complement the classic alkyl acrylate palette for developing sustainable materials with assembly properties that can be utilized in a wide variety of applications.

2.3.2. Results and discussion

BLA monomer synthesis and RAFT polymerization model studies

As reported in previous publications, alkyl lactate solvents are appealing chemicals to prepare biorenewable acrylic/methacrylic polymers.[23-29] Here, BLA was prepared from L-butyl lactate (BL) by acylation with acryloyl chloride in the presence of base using a solvent with low environmental impact such as Me-THF (Figure 2.3.1). After vacuum distillation in the presence of hydroquinone to minimize polymer formation, BLA was isolated as a colorless liquid in high yield (75%). The structure of BLA was verified by NMR spectroscopy. Figure 2.3.2a shows ^{1}H NMR spectrum of BLA, in which the three acrylic protons appear between 6.5 and 5.8 ppm. The characteristic BL methine proton [$CH(CH_3)O$], at around 4.3 ppm, shifted to 5.6 ppm after the formation of the ester group. The ^{13}C NMR spectrum was also consistent with that expected for BLA (see experimental section).

After monomer synthesis, we investigated its controlled polymerization by using the RAFT technique, on account of its ability to form polymers with predicted molecular weight and relatively low molecular weight distribution (MWD) in a green fashion.[30] Figure 2.3.1 depicts the RAFT polymerization of BLA at 70 °C in bulk, using 2,2'-azobisisobutyronitrile (AIBN) and 2-(dodecylthiocarbonothioylthio)propionic acid (DTPA) as radical initiator and chain transfer agent (CTA), respectively. A series of polymerizations were conducted at different $[BLA]_0/[DTPA]_0$ ratios (50 to 400) to target various polymer chain lengths. PBLAs grown in one direction, defined as PBLA-Z, with polydispersity (M_w/M_n) ranging from 1.22–1.27 and gel permeation chromatography (GPC)-determined molecular weight ($M_{n,GPC}$) as high as $M_{n,GPC}$ = 80,300 g/mol could be obtained after 2 h (Figure 2.3.3a).

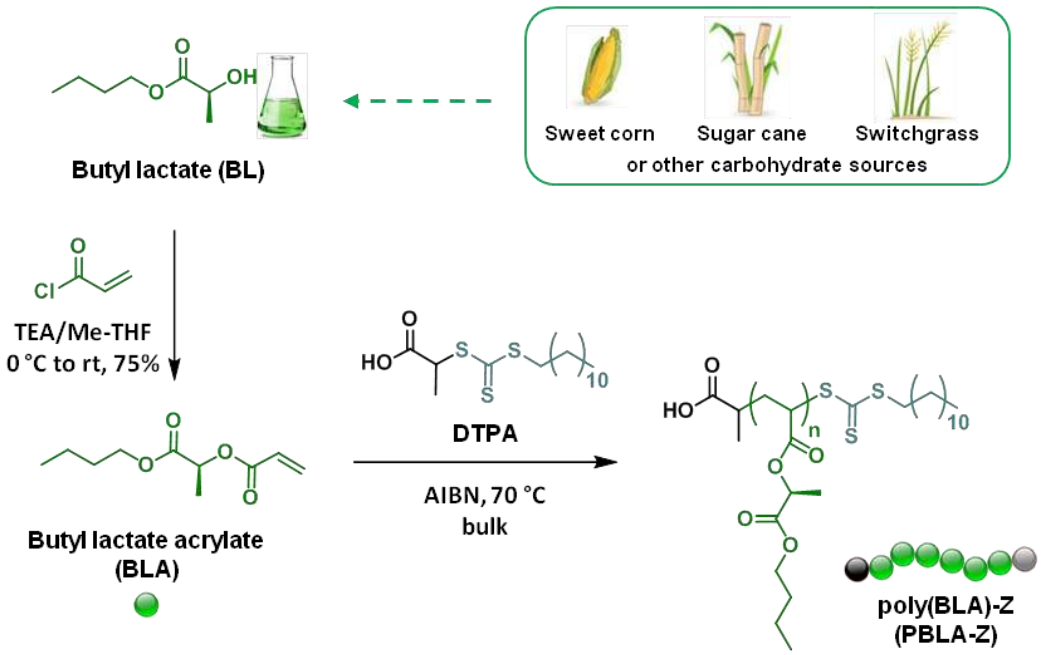

Figure 2.3.1. Synthesis of BLA from biorenewable BL solvent and their bulk RAFT polymerization using a monofunctional CTA, namely 2-(dodecylthiocarbonothioylthio)propionic acid (DTPA) to yield PBLA-Z.

In all cases, the bulk RAFT process proceeded to high monomer conversions (>90%) and yielding polymers with $M_{n,GPC}$ close to the theoretical values ($M_{n,th}$), calculated from monomer conversion assuming complete consumption of CTA. The small discrepancy in the $M_{n,GPC}$ and $M_{n,th}$ data may be attributed to differences in hydrodynamic volume between PBLA-Z and PMMA standards used for calibration. As a representative example, purified low molar mass PBLA-Z prepared at degree of polymerization (DP) of 50 ($M_{n,GPC}$ = 10,900 Da, M_w/M_n = 1.24) was characterized by ^{1}H NMR (Figure 2.3.2b).

After polymerization, the olefinic protons, i.e., 5.8–6.5 ppm, in the BLA monomer were incorporated into the backbone of the new vinylic polymer (i.e., 1.9–3.0 ppm). Moreover, the peak at ≈ 3.3 ppm, attributed to the CH_2-S protons of RAFT CTA groups located at the ω-chain end of the polymer, supports the "livingness" of the synthesized polymer. Next step, we further investigated the kinetics of the polymerization at a DP of 200. As can be seen in Figure 2.3.3b (left panel), after a 10 min induction period attributed to the difficulty in

deoxygenating a highly viscous reaction mixture, the polymerization achieved ≈ 90% conversion in less than 1 h.

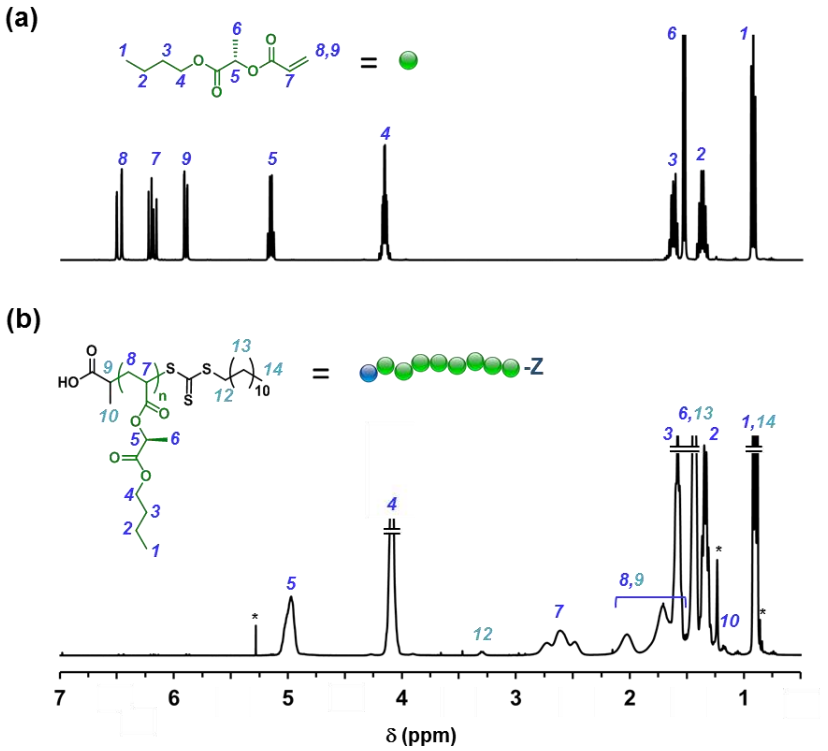

Figure 2.3.2. ^{1}H NMR spectra of (a) BLA and (b) PBLA-Z ($M_{n,GPC}$ = 10,900, M_w/M_n = 1.24) in $CDCl_3$. ^{1}H NMR resonances from "grease" impurities are indicated with *.

The linear evolution of $\ln[M]_0/[M]$ versus reaction time suggested a constant concentration of active species throughout the entire RAFT process. Moreover, as expected for a controlled polymerization, molecular weights increased linearly with conversion retaining narrow MWD (M_w/M_n ≈ 1.25) even at high values (right panel).

Prior to conducting block copolymerization studies, we evaluated the cytotoxic effect of PBLA-Z RAFT homopolymer by treating HeLa, HT-29 and MIA-Pa-Ca-2 cell lines with different doses of the homopolymer dissolved in the culture medium (Figure 2.3.4). Figure 2.3.4a depicts the CellTiter plates for different concentrations of PBLA-Z ($M_{n,GPC}$ = 11,000 Da, M_w/M_n = 1.23) for HeLa cells culture. CellTiter colorimetric assay was used for determining cell viability and cellular proliferation after the addition of test RAFT polymer.

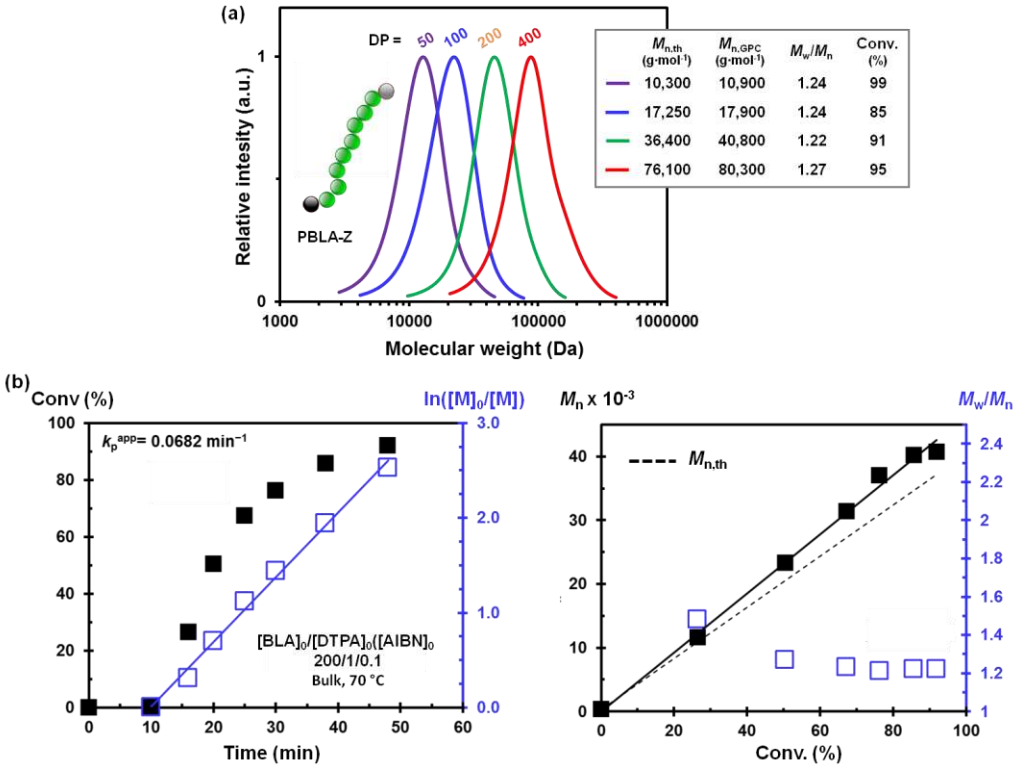

Figure 2.3.3. Bulk RAFT polymerization of BLA with DTPA at 70 °C. (a) GPC traces of PBLA-Z prepared at different DPs, ranging from 50 to 400. The inset contains $M_{n,th,}$ $M_{n,GPC,}$ M_w/M_n, and monomer conversion values; and (b) evolution of monomer conversion and semilogarithmic kinetic plot of $\ln([M]_0/[M])$ versus time (left panel) and evolution of experimental $M_{n,GPC}$ and M_w/M_n, based on the calibration by PMMA standards, with the monomer conversion (right panel). Reaction conditions for (b): BLA = 1 mL, $[BLA]_0/[DTPA]_0/[AIBN]_0$ = 200/1/0.1 at 70 °C.

This assay determines the number of viable cells due to the bioreduction of the MTS tetrazolium compound (Owen's reagent) into a colored formazan product accomplished by NADPH or NADH produced by dehydrogenase enzymes in metabolically active cells. Therefore, color formation can be a useful marker of viable cells. Notably, the cytotoxicity analysis using the CellTiter assay showed that 24 h exposure of the cells to up to 100 mg·mL^{-1} at 37 °C did not reduce cell viability. Hence, these results further support the use of PBLA polymers as a soft and hydrophobic building block in well-defined copolymer synthesis employed in a wide range of applications, including biomedical devices and adhesives.[31]

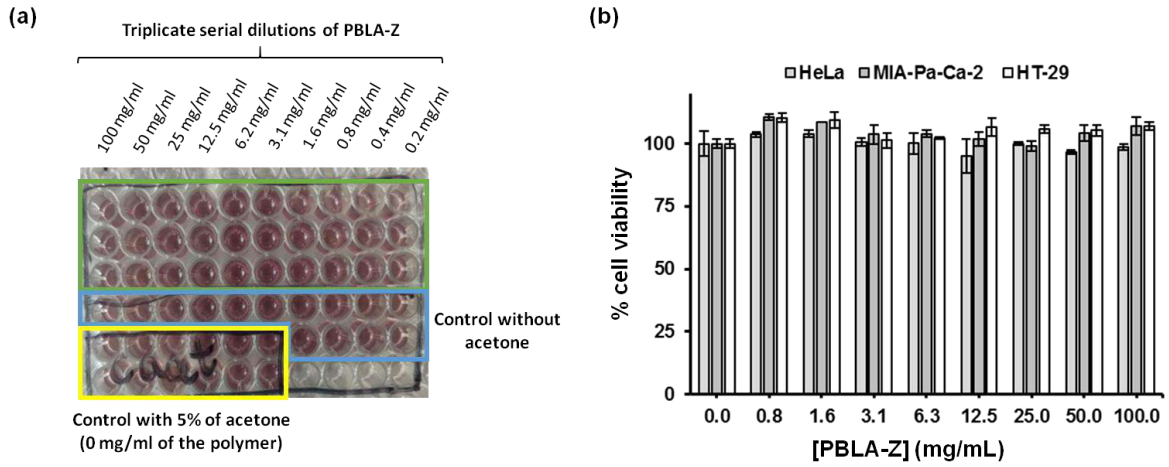

Figure 2.3.4. (a) The plates for cytotoxic assays of PBLA-Z ($M_{n,GPC}$ = 11,000 Da, M_w/M_n = 1.23) tested in HeLa cells; and (b) CellTiter cell viability assay results for the same polymer at different concentrations assessed in HeLa, MIA-Pa-Ca-2 and HT-29 cell lines.

Bifunctional PBLA macro-CTA *via* bulk RAFT polymerization

With the final goal to prepare ABA block copolymers with PBLA as the soft middle block, we used a commercially available bifunctional CTA, namely 3,5-bis(2-dodecylthiocarbonothioylthio-1-oxopropoxy)benzoic acid (BTCBA), to prepare bifunctional PBLA macroCTAs (defined as PBLA-2Z) through divergent RAFT polymerization of BLA at 70 °C in bulk (see first reaction step in Figure 2.3.5a). Initially, we targeted a low molar mass polymer (DP = 50, $M_{n,th}$ = 10,830 g·mol^{-1}) to collect structural information about the "livingness" of the system when performing divergent chain growth. Under these conditions, the RAFT polymerization of BLA achieved 99% monomer conversion in 2 h. BTCBA controlled the polymerization of BLA and yielded PBLA-2Z macroinitiator with $M_{n,GPC}$ of 10,500 and M_w/M_n of 1.24 (Figure S1 in Annex C). ^{1}H NMR analysis of the isolated polymer clearly revealed the presence of CTA residues at both the polymer core and chain ends, e.g., signals 7.68 and 7.13 ppm for aryl mid group protons and 3.33 ppm for the α methylene protons of the trithiocarbonate end groups (Figure 2.3.6). Hence, the ratio of integration of these signals to the methylene (CH_2-O) peak of the BL repeating units enabled to determine $M_{n,NMR}$ (11,200 g·mol^{-1}) which was in good agreement with $M_{n,th}$ and $M_{n,GPC}$ (11,700 g·mol^{-1}

and 11,000 g·mol^{-1}, respectively). Note that the $M_{n,NMR}$ was only about 5% above $M_{n,th}$. Thus, within the experimental error of ^{1}H NMR measurement, these results support good control of the bulk RAFT polymerization. Next, we pushed this polymerization system to higher DPs (100–400) under strictly identical reaction conditions, as higher molar mass polymers are required to prepare ABAs with competitive performance. Also in this case, high conversions (>90%) were achieved. As shown in Figure 2.3.7a, the successful synthesis of PBLA-2Z macro-CTAs with molecular weight as high as $M_{n,GPC}$ = 78,150 g·mol^{-1} was demonstrated by unimodal GPC traces and $M_{n,GPC}$ values very close to the theoretical values and narrow M_w/M_n values (<1.25).

Good candidates for the soft middle block in triblock TPEs must have a T_g lower than their application temperature, in order to provide flexibility or tacky characteristics to the final materials. DSC analysis of PBLA-2Z ($M_{n,GPC}$ = 78,150) revealed a T_g value (indicated by dashed line in the green trace) well below room temperature (T_g = −21 °C) (Figure 2.3.7b).

The reduction of molar mass from $M_{n,GPC}$ = 78,150 g·mol^{-1} to $M_{n,GPC}$ = 20,000 g·mol^{-1} did not significantly influence the value of T_g (data not shown). Note that the T_g value for PBLA-2Z is 23 °C above that of PBA of approximately the same M_n prepared by RAFT (Figure 2.3.7b). This result can be attributed to the presence of two polar carbonyl units per repeating unit, which decreases segmental motion. TGA also revealed that PBLA-2Z is also highly competitive in terms of thermal stability (Figure 2.3.7b). The thermal stability of PBLA-2Z was slightly higher, with a 5% degradation temperature of 340 °C (327 °C for PBA). Overall, these results support the use of PBLA as an innovative candidate soft block in triblock copolymer-based ABA-type TPEs.

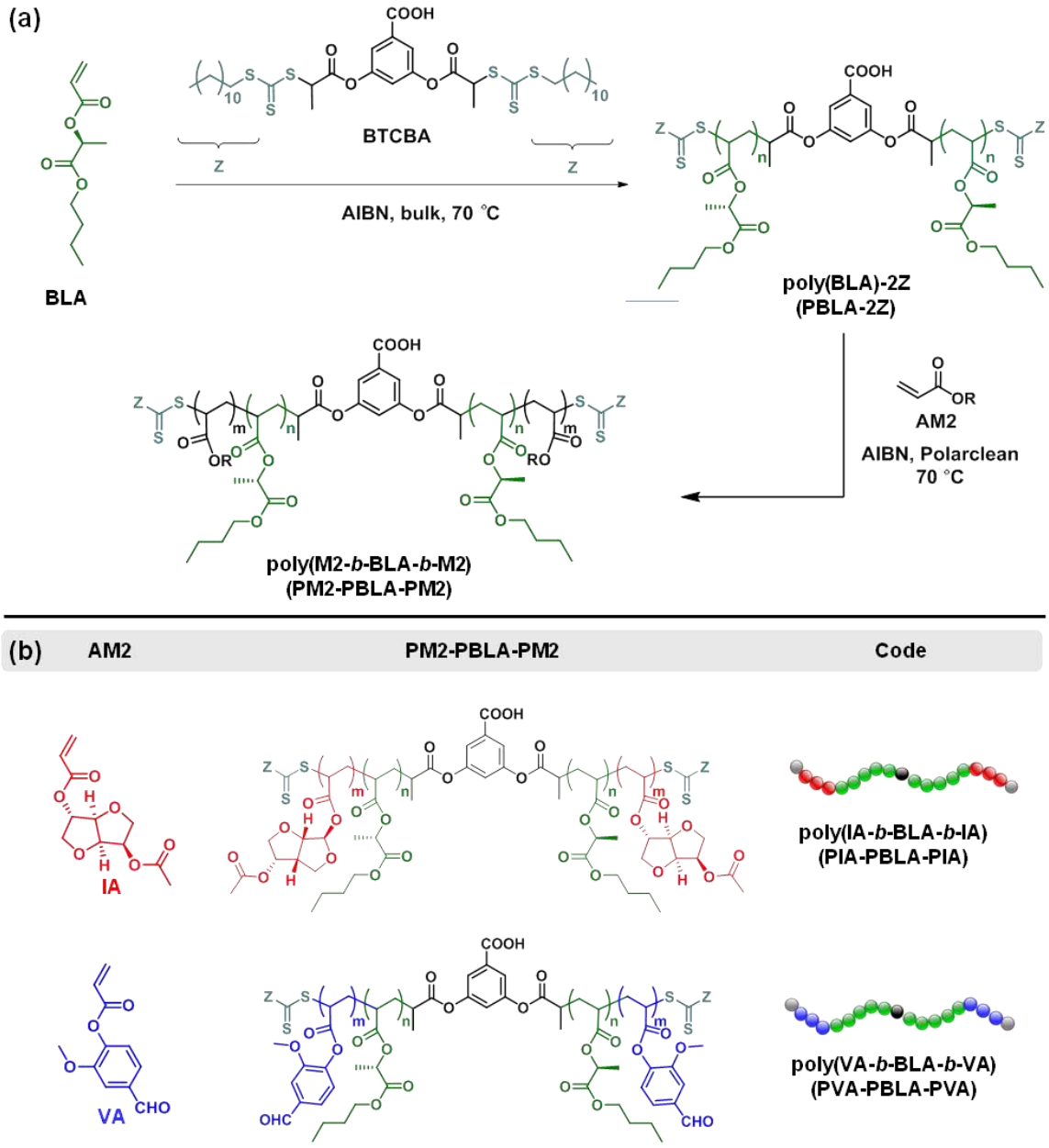

Figure 2.3.5. (a) Two-step RAFT synthesis of ABA BCPs with LA-based middle block using AM2 monomer to build up end blocks and BTCBA as a CTA. (b) Chemical structures of AM2 acrylic monomers (IA and VA) and ABA block copolymers (PIA-PBLA-PIA and PVA-PBLA-PVA) studied herein.

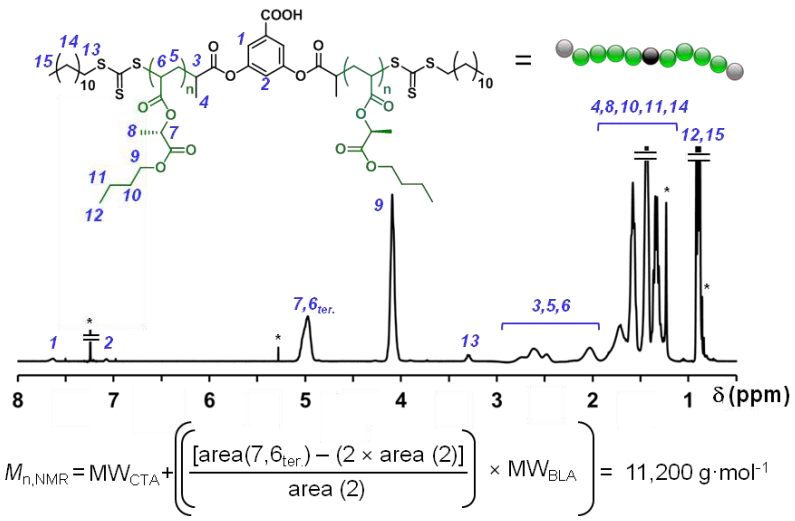

Figure 2.3.6. ^{1}H NMR spectrum PBLA-2Z ($M_{n,GPC}$ = 10,900, M_w/M_n = 1.24) in $CDCl_3$. ^{1}H NMR resonances from "grease" impurities and residual solvents are indicated with *.

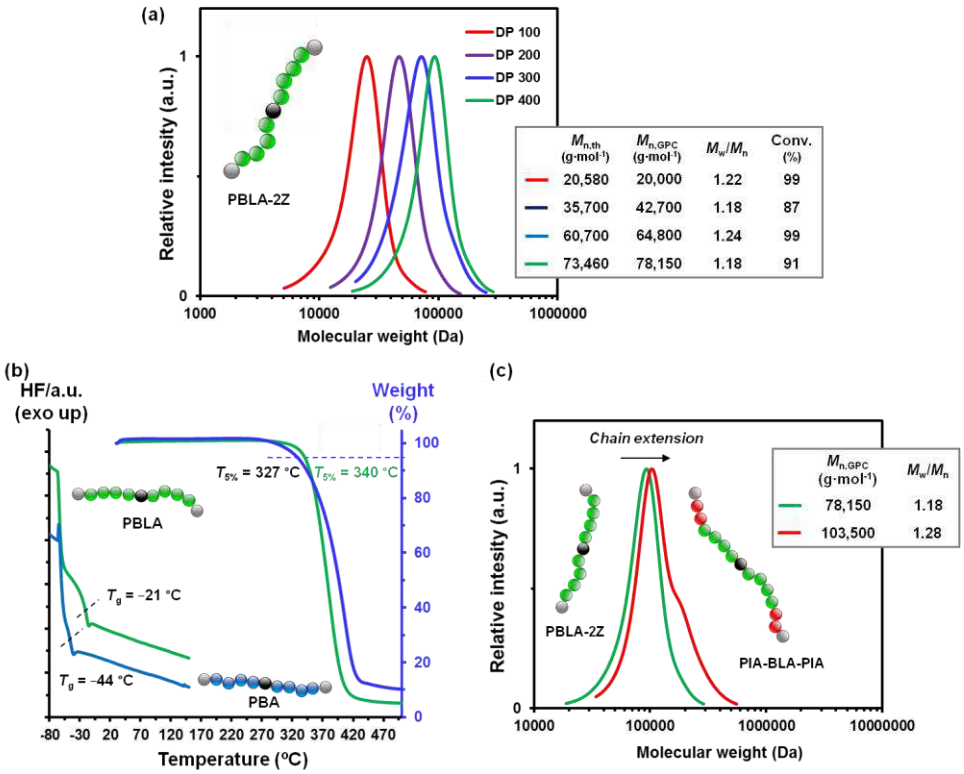

$M_{n,th}$ (g·mol^{-1})	$M_{n,GPC}$ (g·mol^{-1})	M_w/M_n	Conv. (%)
20,580	20,000	1.22	99
35,700	42,700	1.18	87
60,700	64,800	1.24	99
73,460	78,150	1.18	91

$M_{n,GPC}$ (g·mol^{-1})	M_w/M_n
78,150	1.18
103,500	1.28

Figure 2.3.7. (a) GPC traces of PBLA-2Z prepared at different DPs ranging from 50 to 400 by the bulk RAFT polymerization of BLA with BTCBA at 70 °C (The inset contains $M_{n,th}$, $M_{n,GPC}$, M_w/M_n, and monomer conversion values); (b) thermal characterization by DSC and TGA analyses of PBLA-2Z ($M_{n,GPC}$ = 78,150 g·mol^{-1}) and PBA ($M_{n,GPC}$ = 97,900 g·mol^{-1}); and (c) GPC traces of the chain extension of PBLA-2Z macro-RAFT agent with IA monomer at 70 °C in Rhodiasolv® PolarClean solvent. The inset contains $M_{n,GPC}$ and M_w/M_n values.

ABA BCPs *via* RAFT in Rhodiasolv® PolarClean solvent

Using PBLA-2Z ($M_{n,GPC}$ = 78,150 g·mol^{-1}) as macroCTA, we subsequently studied the incorporation of glassy external segments at the chain ends of PBLA in a divergent fashion *via* RAFT polymerization with a second acrylic monomer AM2 (see the second reaction step in Figure 2.3.5a,b). Two sustainable triblock copolymers were targeted using poly(vanillin acrylate) (PVA) and a poly(isosorbide acrylate) (PIA) as hard blocks. The chemical structure of both biosourced acrylic monomers (IA, i.e., isosorbide 2-acrylate-5-acetate, and VA, i.e., vanillin acrylate) and the targeted ABA BCPs (PVA-PBLA-PVA and PIA-PBLA-PIA) is shown in Figure 2.3.5b. IA and VA were prepared from isosorbide and vanillin, respectively, using previously reported synthetic procedures.[32-34] Unfortunately, the chain extension step required the use of solvent to build the pursued triblocks, as reaction mixtures were not homogeneous at the polymerization temperature (70 °C). Although recent advances in waterborne processes are highly attractive,[35] the search for eco-friendly solvents as an alternative to conventional petroleum-derived solvents is also desirable. For this purpose, after control experiments that will be reported in a forthcoming publication, BCP synthesis were performed in ethyl-5-(dimethylamido)-2-methyl-5-oxopentanoate (Rhodiasolv® PolarClean).[36] To our knowledge, this eco-friendly water-soluble and polar solvent was never used as green reaction media in controlled radical polymerization. Hence, chain extension of PBLA-2Z ($M_{n,GPC}$ = 75,340 g·mol^{-1}) with IA at 70 °C under the reaction conditions of $[IA]_0/[PBLA\text{-}2Z]_0/[AIBN]_0$ = 109/1/0.2 in PolarClean was afforded the PIA-PBLA-PIA triblock. The conversion of IA monomer was calculated to be 86%, using ^{1}H NMR analysis prior to purification of the polymer (Figure S2 in Annex C). A clear shift to higher molar masses in the SEC trace indicated successful chain extension (Figure 2.3.7c). Note that a high molar mass shoulder was present in the GPC trace of the ABA copolymer, likely due to termination by combination at high conversion. Nevertheless, the molar mass distribution was relatively narrow (M_w/M_n = 1.28) suggesting that the chain extension occurs, retaining substantial control. As depicted in Figure S3 in Annex C, chain extension PBLA-2Z with VA also resulted in success to furnish PVA-PBLA-PVA triblock (78% conversion, $M_{n,GPC}$ = 110,150 g·mol^{-1}). Both

triblocks were subsequently characterized by ^{1}H NMR to determine their compositions (Figure 2.3.8).

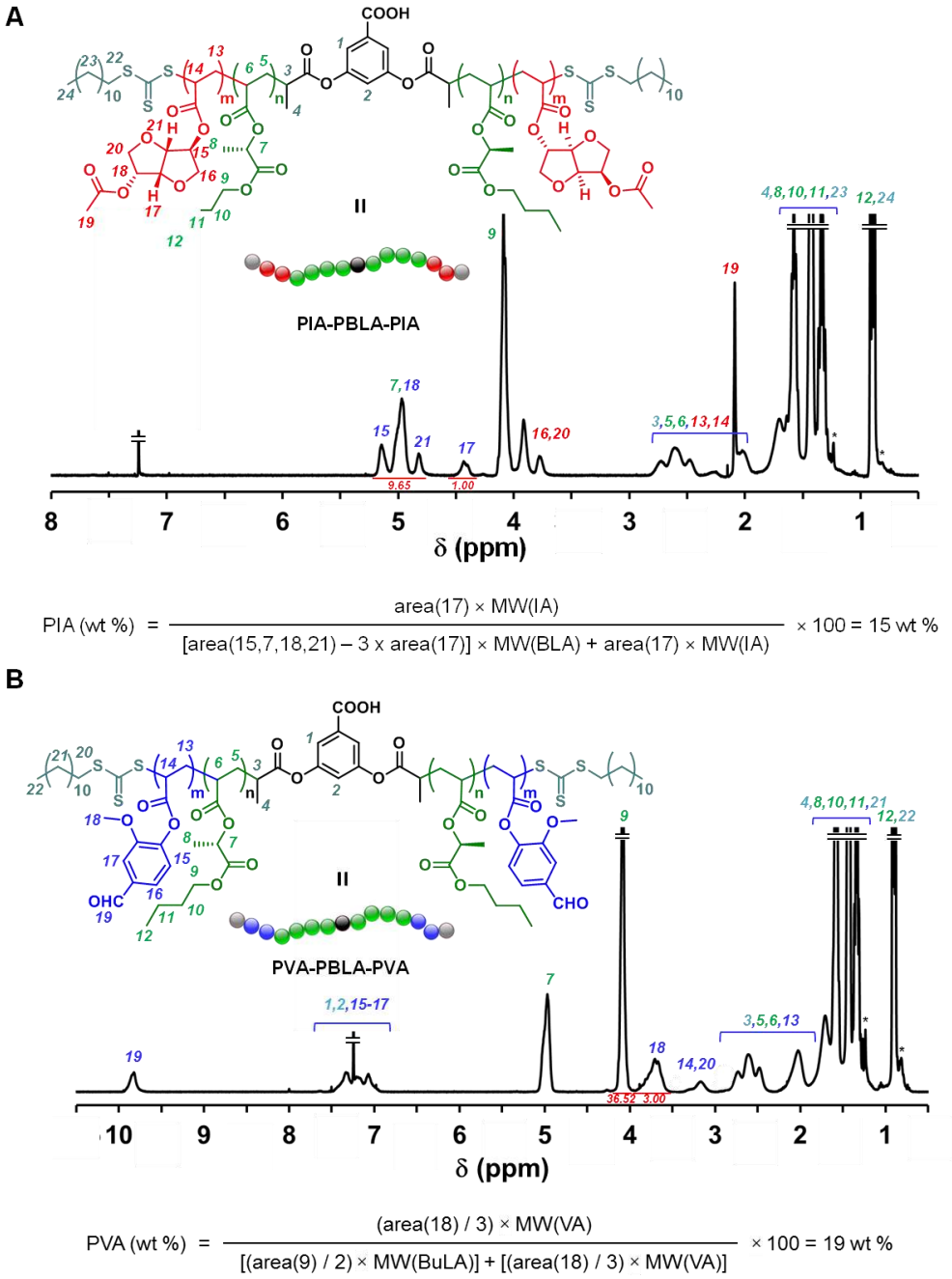

Figure 2.3.8. ^{1}H NMR spectra of: (a) PIA-PBLA-PIA ($M_{n,GPC}$ = 103,500 g·mol^{-1}, M_w/M_n = 1.28); and (b) PVA-PBLA-PVA ($M_{n,GPC}$ = 110,150 g·mol^{-1}, M_w/M_n = 1.38) triblocks in $CDCl_3$. ^{1}H NMR resonances from "grease" impurities are indicated with *.

For instance, as indicated in Figure 2.3.8a, the composition of BCP PIA-PBLA-PIA could be determined from the integration of signals at 4.3–4.5 ppm from H17 corresponding to PIA units and the integration of the signals at 4.7–5.3 ppm from PBLA units, after subtracting the peak area contributed by the PIA units (H15, H18, and H21) in this region. Thus, the obtained PIA-PBLA-PIA triblock had a PIA (hard block) weight percentage of 15 wt%, as determined *via* ^{1}H NMR spectroscopy, which is comparable to the theoretical 18 wt% value determined from monomer conversion. As depicted in Figure 2.3.8b, the hard block content for the PVA-PBLA-PVA copolymer was slightly higher (19 wt% PVA), but also comparable with the theoretical value calculated from conversion (21 wt%). Note that the hard block content in these representative copolymers is consistent with typical hard block composition for triblock copolymers used for pressure-sensitive adhesive (PSA) applications, where high tacky materials are pursued.[10,14]

ABA BCPs characterization: thermal, mechanical, morphological, and adhesive properties

The microstructure and viscoelastic properties of the synthesized triblock copolymers were studied by DSC and dynamic mechanical thermal analysis (DMTA). DSC analysis of both synthesized triblocks revealed a low T_g for the PBLA midblock at about −20 °C, although no discernible signals corresponding to the T_g of the glassy end blocks were observed, likely due to the lack of a DSC signal based on the low weight fraction of hard block (Figure S4 in Annex C).[9-11,14] However, the presence of midblock T_g near that of the homopolymer suggests that PBLA segment is not mixed with either PIA or PVA segments. Note that the T_g of PIA and PVA homopolymer glassy blocks was expected to appear around 80 °C, as indicated DSC analysis of model homopolymers also prepared by RAFT (dashed lines in Figure S4 in Annex C). Next, both copolymers were submitted to DMTA (Figures 2.3.9a and S5 in Annex C). DMTA revealed a relaxation process at around 0 °C, corresponding to the glass-rubber transition of the PBLA soft phase in PIA-PBLA-PIA and PVA-PBLA-PVA triblocks, as indicated by a stepwise decrease in the storage (E') and loss (E'') moduli, as well as a peak in tan δ. The presence of a second tan δ peaks at around 100 °C in the case of PIA-PBLA-PIA triblock, and at 130 °C for

the copolymers integrating PVA, which confirmed the soft-hard-soft microstructure configuration of the synthesized triblock copolymers.[37] Note also that E' (25 °C) for PVA-PBLA-PVA triblock was slightly higher than that observed for PIA-PBLA-PIA (1.3 MPa versus 1.0 MPa). This can be attributed to the higher weight percentage of hard block for PVA-PBLA-PVA (19 wt% of PVA) in comparison to PIA-PBLA-PIA (15 wt% of PVA).

Next step, mechanical properties of both triblocks were measured by monotonic tensile tests on polymer films prepared by a hot-press technique (Figure 2.3.9b). Both systems exhibited comparable elongation at a break at around 250%. However, PVA-PBLA-PVA with 19 wt% hard block content demonstrated improved tensile strength (0.83 versus 0.33 MPa). Nevertheless, it is noteworthy that the relatively low tensile strength (<1 MPa) of these materials points toward good adhesion performance (*vide infra*).[10] TGA was used to evaluate the thermal stability of the synthesized copolymers (Figure S6 in Annex C), and no significant differences were found between them. TGA under an inert atmosphere showed 5 wt% loss temperatures of PVA-PBLA-PVA and PIA-PBLA-PIA to be 386 °C and 389 °C, respectively. Hence, these polymers can be processes at elevated temperatures without degradation, and could therefore be used in practical applications demanding high temperatures, e.g., hot melt adhesives.[37] Finally, the adhesion properties of the synthesized all-acrylic ABA block biopolymers with a LA-based elastomeric phase were evaluated. A 30 wt% solution of PVA-PBLA-PVA and PIA-PBLA-PIA was spread on a polyethylene terephthalate (PET) film.[10,14] After complete evaporation of the solvent at room temperature, the coated PET films were adhered onto a stainless steel plate, and the peel resistance was measured by pulling the adhered films off the plate at an angle of 180° (Figure 2.3.9c). Data for both polymers is presented in Figure 2.3.9d, and compared with a commercial Scotch 508 tape.

The 180° peel strength for PVA-PBLA-PVA and PIA-PBLA-PIA was about 1.5 $N \cdot cm^{-1}$, which is comparable to the tested commercial tape. All the investigated samples had adhesive failure, leaving no residue on the adherend. It is important to mention that both synthesized triblock copolymers were tested without the addition of tackifier or additive.

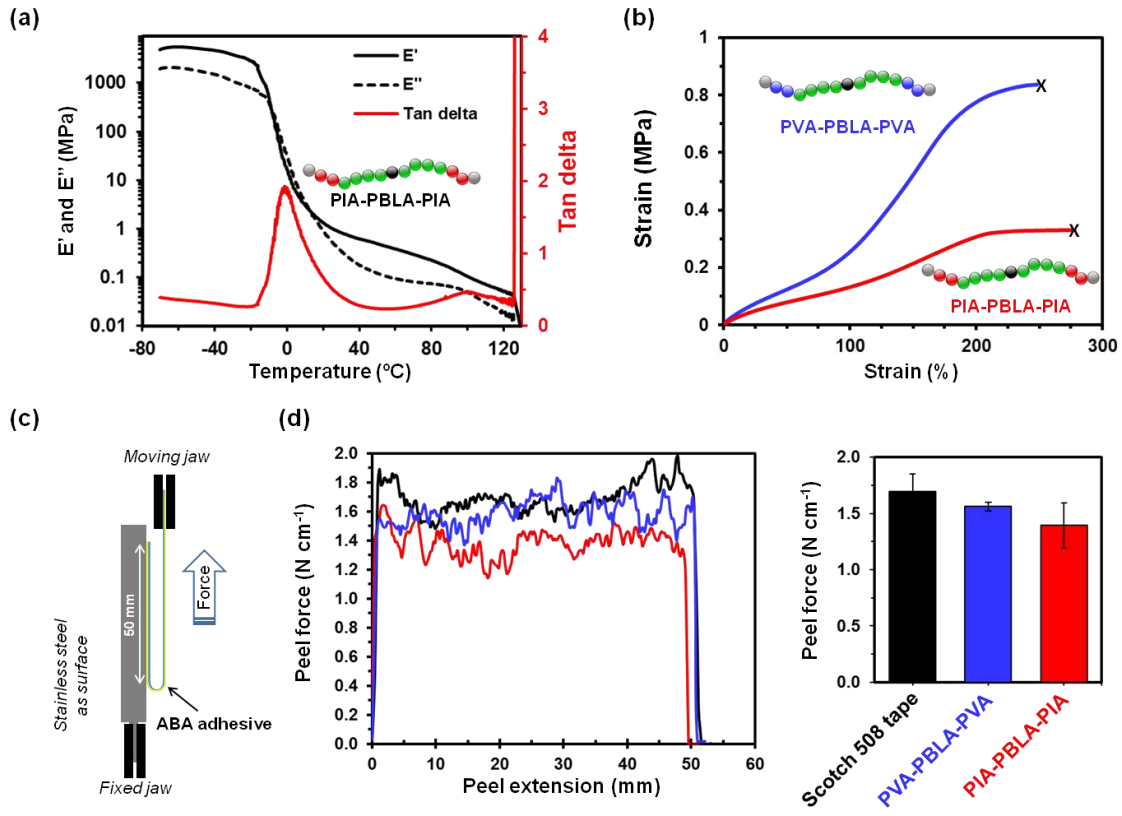

Figure 2.3.9. (a) Dynamic tensile storage (E') and loss (E'') moduli and tan (δ = E''/E') as a function of temperature of PIA-PBLA-PIA triblock; (b) stress-strain curves of PIA-PBLA-PIA and PVA-PBLA-PVA; (c) schematic design of 180° peel test; and (d) 180° peel force of PIA-PBLA-PIA, PVA-PBLA-PVA and Scotch 508 tape.

Hence, taking into account that no optimization studies were conducted, these results suggest that the all-acrylic ABA copolymers with a LA-based elastomeric building block are promising materials for PSA applications, and open the door to further investigations in this line.

2.3.3. Conclusions

In summary, our study demonstrates that L-BL solvent can be upgraded to well-defined tacky triblock copolymers, suitable for applications as PSAs. The functionalization of BL with an acrylate moiety generated a monomer well behaved under RAFT polymerization. Good control over molecular weight and MWD was achieved in bulk, using either monofunctional and bifunctional trithiocarbonate-type CTAs. Subsequently, poly(BLA), with a relative low

T_g (−20 °C), good thermal stability (5% wt. loss at 340 °C) and low toxicity in the cell cultures assessed was evaluated as sustainable elastomeric core block in all-acrylate ABA copolymers using isosorbide and vanillin-derived glassy polyacrylates as representative end blocks. Materials with a low content of hard building block (<20 wt%) were targeted, pursuing the preparation of materials with high tack. The thermal and mechanical properties of the prepared copolymers were evaluated to demonstrate suitability of rubbery poly(alkyl lactate) building blocks for developing innovative sustainable materials. As is noteworthy, 180° peel adhesion measurements showed that the synthesized biosourced all-acrylic ABA copolymers possess competitive performance when compared with commercial pressure-sensitive tapes. The significance of developing innovative adhesives based on renewable resources combining good thermal stability and low cytotoxicity is that these materials are promising for a broad range of applications, including both biomedical and technological fields.

2.3.4. Experimental section

Materials

3,5-Bis(2-dodecylthiocarbonothioylthio-1-oxopropoxy)benzoic acid (BTCBA, 98%), 2-(Dodecylthiocarbonothioylthio)propionic acid (DTPA, 98%), acryloyl chloride (≥97%), triethylamine (TEA, ≥99%), 2-methyltetrahydrofuran (Me-THF, 99.5%), n-Butyl acrylate (BA, 99%), butyl L-lactate (98%) were all purchased from Merck KGaA (Darmstadt, Germany) and used as received unless otherwise specified. Thus, BA was passed through a short column of basic Al_2O_3 prior to use in order to remove the radical inhibitor and both TEA and Me-THF were distilled prior to use from CaH_2 and sodium/benzophenone, respectively. 2,2'-Azobis(2-methylpropionitrile) [AIBN, ≥98%, Fluka (Buchs, Switzerland] was recrystallized three times from methanol before further use. Deuterated chloroform ($CDCl_3$) was purchased from Eurisotop, and ethyl-5-(dimethylamido)-2-methyl-5-oxopentanoate (Rhodiasolv® PolarClean) was kindly donated by Solvay (Aubervilliers, France). Isosorbide acetate, i.e., isosorbide 2-acrylate-5-acetate and vanillin acrylate monomers were prepared following previously reported synthetic procedures.[32-34]

Methods

400 MHz (for ^{1}H) and 100.6 MHz (for ^{13}C) NMR spectra were recorded on a Varian VNMR-S400 NMR instrument at 25 °C in $CDCl_3$ with tetramethylsilane (TMS) as an internal standard. The number-average molecular weight (M_n) and polydispersity (M_w/M_n) of the synthesized polymers were obtained via GPC using an Agilent 1200 series system [Agilent Technologies Inc., Santa Clara (CA), USA] equipped with three serial columns (PLgel 3 µm MIXED-E, PLgel 5 µm MIXED-D and PLgel 20 µm from Polymer Laboratories) and an Agilent 1100 series refractive-index detector. THF HPLC grade (Panreac Química S.L.U., Barcelona, Spain) was used as eluent at a flow rate of 1.0 mL/min. The calibration curves for GPC analysis were obtained with poly(methyl methacrylate) (PMMA) standards purchased from American Polymer Standards (Mentor, OH, USA). The molecular weights were calculated using the universal calibration principle and Mark-Houwink parameters. The glass transition temperature (T_g) of all polymers was determined on the second heating/cooling ramps using DSC measurements conducted on a Mettler DSC3+ thermal analyzers (Mettler-Toledo S.A.E., Barcelona, Spain) using N_2 as a purge gas (50 mL/min) at scanning rate 20 °C/min in the −80 to 150 °C temperature range. Calibration was based on an indium standard (heat flow calibration) and an indium-lead-zinc standard (temperature calibration). Thermal stability studies were carried out on a Mettler TGA2/LF/1100 (Mettler-Toledo S.A.E., Barcelona, Spain) with N_2 as a purge gas at flow rate of 50 mL/min. The studies were performed in the 30–600 °C temperature range at a heating rate of 10 °C/min. ESI MS were run on a chromatographic system Agilent G3250AA liquid chromatography coupled to 6210 Time of Flight (TOF) mass spectrometer from Agilent Technologies Inc. [Santa Clara (CA), USA] with an ESI interface. Dynamic mechanical analysis of all polymers was performed on a DMA Q800 (TA Instruments, New Castle, DE, USA) in tension configuration. Rectangular-shaped specimens (5 mm length, 5 mm width, 0.12 mm thickness) were prepared by compression molding into a rectangular steel mould (20 mm 5 mm 1.2 mm) between two parallel steel plates on a Specac Atlas Manual Hydraulic Press (Specac Ltd, Orpington, UK) at 100 °C, with an applied load of 4 tons for 30 min. Then, the rectangular specimen was further heated in

the range of −70 to 200 °C using a heating rate of 3 °C/min and a fixed frequency of 1 Hz. For tensile testing, the lower grip was stationary, and the upper grip was raised at a force ramp rate of 1 N/min to obtain tensile strength and elongation at break of polymer at 27 °C. The peel strength analysis was performed on an Instron 5965 (Instron, Bucks, UK) at a peel rate of 300 $mm \cdot min^{-1}$.

Synthesis of BLA monomer

Butyl L-lactate (20.0 g, 0.14 mol) and anhydrous triethylamine (21.4 g, 0.21 mol) were dissolved in dry 2-methyltetrahydrofuran (Me-THF; 50 mL) under a constant flow of argon. After the solution was stirred for 30 min at 0-5 °C, acryloyl chloride (14.8 g, 0.16 mol) dissolved in dry Me-THF (50 mL) was added dropwise. The reaction was allowed to proceed for 24 h at room temperature. The reaction mixture was then filtered and Me-THF was removed under reduced pressure. The resulting residue was dissolved in 150 mL of diethyl ether and subsequently the solution was washed with HCl 1M (150 mL) and saturated $NaHCO_3$ solution (150 mL). The organic layer was rinsed with a brine solution and dried over anhydrous $MgSO_4$. The final residue was purified by vacuum distillation in the presence of 5 (w/w %) of hydroquinone to afford BLA (20.5 g, 75 %) as a colorless liquid. ^{1}H NMR (400MHz, $CDCl_3$, δ): 6.48 (dd, 1H), 6.19 (dd, 1H), 5.90 (dd, 1H), 5.16 (q, 1H), 4.16 (m, 2H), 1.63 (m, 2H), 1.53 (d, 3H), 1.38 (m, 2H), 0.93 (t, 3H); ^{13}C NMR (100.6 MHz, $CDCl_3$, δ): 170.72, 165.34, 131.74, 127.71, 68.78, 65.13, 30.51, 18.99, 16.96, 13.62. HRMS (TOF ES^+) m/z: $[M+NH_4]^+$ calcd for $C_{10}H_{20}NO_4^+$, 218.1392 found, 218.1393 $[M+H]^+$ calcd for $C_{10}H_{17}O_4^+$, 201.1127, found, 201.1119; $[M+Na]^+$ calcd for $C_{10}H_{16}NaO_4^+$, 223.0946, found, 223.0942.

General procedure for the RAFT polymerization of BLA monomer

The synthesis of poly(L-butyl lactate acrylate) (PBLA) macro-CTA was performed in bulk. A representative procedure is described as follows: AIBN (2.07 mg, 0.01 mmol) 3,5-Bis(2-dodecylthiocarbonothioylthio-1-oxopropoxy)benzoic acid (BTCBA) (or DTPA) (103.3 mg, 0.13 mmol) and L-butyl lactate acrylate (10.0 g, 50.40 mmol) were mixed in a 25 mL Schlenk tube equipped with a teflon stirring bar. The reaction mixture was degassed by bubbling

argon for 30 min and subsequently submerged into a preheated, stirring oil bath maintained at 70 °C. To monitor the monomer conversion, the side arm of the tube was purged with argon before it was opened to remove two drops of sample using an airtight syringe. Samples were quenched by immediately placing them into liquid nitrogen exposed to air. After that, samples were dissolved in $CDCl_3$ and the monomer conversion was measured by ^{1}H NMR spectroscopy. The Mn and M_w/M_n values were determined by GPC calibrated with Poly(methyl methacrylate) (PMMA) standards. Finally, to stop the reaction, the Schlenk flask was placed into nitrogen liquid and opened to air. The final polymerization mixture was dissolved in the minimal volume of DCM and precipitated in 400 mL of cold hexane and isolated by decanting off the supernatant fluid. The procedure was repeated three times and the final polymer was dried under a vacuum for 24 h at room temperature to lead a viscous yellowish liquid. Model homopolymers prepared from butyl, isosorbide acetate and vanillin acrylates were prepared following the same procedure.

General procedure for RAFT block copolymerization experiments

An illustrative example is provided. CTA-poly(BLA)-CTA (1.0 g, 0.013 mmol), isosorbide acetate acrylate (0.26 g, 1.06 mmol), AIBN (0.47 mg, 2.86 µmol) (from a dilute stock solution), and 3 mL of ethyl-5-(dimethylamido)-2-methyl-5-oxopentanoate (Rhodiasolv® PolarClean) were added to a Schlenk flask equipped with a teflon stirring bar. The flask was sealed and degassed by bubbling argon for 45 min, and then submerged in a preheated oil bath at 70 °C. After stirring vigorously for 24 h, the flask was immediately submerged into liquid nitrogen and opened to air. Two drops of sample were dissolved in $CDCl_3$, and a monomer conversion was determined by ^{1}H NMR. The polymerization mixture was dissolved in the minimum of DCM, and precipitated three times in cold methanol (3 × 200 mL). The final copolymer was then dried in a vacuum at room temperature for 24 h.

Cell cultures

HT-29 (human colon adenocarcinoma), HeLa (human cervix epithelioid carcinoma) and MIA-Pa-Ca-2 (human Caucasian pancreatic carcinoma) cells were obtained from ATCC and

maintained in Dulbecco's Modified Eagle's Medium (DMEM) (PAN-Biotech GmbH, Germany) supplemented with 10% FBS (Fetal Bovine Serum), 1% P/S (Penicillin/Streptomycin) and 1% NEAAs (Non-Essential Amino Acids) at 37 °C with 5% CO_2.

Cell viability assays

The cellular cytotoxicity of selected polymers was assessed in three cell lines: HT-29, HeLa and MIA-Pa-Ca-2 cells. The cell viability experiments were carried out by serial dilutions of PBLA-Z, which was diluted in acetone.

Cells were plated in 96-well plates (8000 cells/95µL/well in HeLa and MIA-Pa-Ca-2 cells; 9000 cells/95µL/well in HT-29 cells) with supplemented DMEM without phenol red. Forty-eight hours later, 5 µL of each serial dilutions of the polymer were added to the cells. 100 mg/mL was the maximum tested concentration of the polymer in the cells (poly(butyl lactate acrylate) stock: 2 g/mL). The borders of the plates were in presence of 100 µL of PBS, in order to prevent evaporation-related problems caused by acetone.

The cells were in the presence of the polymer during 24 h and after this period the cytotoxicity was checked by adding the CellTiter reagent. The CellTiter 96® AQueous One Solution Cell Proliferation Assay Kit (Promega, Madrid, Spain) provides a convenient and sensitive procedure for determining the number of viable cells in cytotoxicity assays. 20 µL of CellTiter reagent (1/4 dilution in DMEM without phenol red) were added into each well of the 96-well assay plates containing the samples. The plates were incubated at 37 °C for 2 h in a humidified, 5% CO_2 atmosphere and later the absorbance was recorded at 490 nm (background correction at 800 nm). Each experiment was performed in triplicate and repeated at least twice.

General procedure for 180° peel adhesion tests

The samples for 180° peel adhesion tests were prepared by dissolving the polymer in ethyl acetate to obtain a 30% solid content solution. As a representative example, 200 mg of triblock copolymer was dissolved in 520 µL ethyl acetate. The solution was solvent-cast on a polyethylene terephthalate (PET) film of 19 mm width using a standard laboratory

drawdown rod. The film was allowed to dry under ambient conditions open to air in a chemical fume hood for 4 h. The resultant coated film strips were approximately 5 cm long. The peel strength analyses were performed on an Instron 5965 at a peel rate of 300 mm·min^{-1}. 5 cm-wide strips of the coated PET films were placed on a clean stainless steel panel, as an adherend. The coated film was gently pressed against steel plate by manually rolling in order to develop good contact between the adhesive and the steel plate. The strip was then peeled from the stainless steel panel. The reported average peel force and standard deviation values were acquired from at least three replicates. Adhesion testing on commercially available scotch 805 PSA was also performed for comparison under identical conditions.

2.3.5. References

[1] Bates, C. M.; Bates, F. S. *Macromolecules* **2017**, *50*, 3-22.

[2] Epps III, T. H.; O'Reilly, R. K. *Chem. Sci.* **2016**, *7*, 1674-1689.

[3] Ruzette, A. V.; Leibler, L. *Nat. Mater.* **2005**, *4*, 19-31.

[4] Holden, G.; Kricheldorf, H. R.; Quirk, R. P. Thermoplastic Elastomers 3rd ed.; Hanser Publishers: Munich, Germany, 2004.

[5] Shipp, D. A.; Wang, J. L.; Matyjaszewski, K. *Macromolecules* **1998**, *31*, 8005-8008.

[6] Jeusette, M.; Leclère, Ph.; Lazzaroni, R.; Simal, F.; Vaneecke, J.; Lardot, Th.; Roose, P. *Macromolecules* **2007**, *40*, 1055-1065.

[7] Nakamura, Y.; Adachi, M.; Tachibana, Y,M Sakai, Y.; Nakano, S.; Fujii, S.; Sasaki, M.; Urahama, Y. *Int. J. Adhes. Adhes.* **2009**, *29*, 806-811.

[8] Corrigan, N.; Jung, K.; Moad, G.; Hawker, C. J.; Matyjaszewski, K.; Boyer, C. *Prog. Polym. Sci.* **2020**, 101311.

[9] Wang, S.; Ding, W.; Yang, G.; Robertson, M. L. *Macromol. Chem. Phys.* **2016**, *217*, 292-303.

[10] Nasiri, M.; Reineke, T. M. *Polym. Chem.* **2016**, *7*, 5233-5240.

[11] Gallagher, J. J.; Hillmyer, M. A.; Reineke, T. M. *ACS Sustainable Chem. Eng.* **2016**, *4*, 3379-3387.

[12] Satoh, K.; Lee, D. H.; Nagai, K.; Kamigaito, M. *Macromol. Rapid Commun.* **2014**, *35*, 161-167.

[13] Ding, W.; Wang, S.; Yao, K.; Ganewatta, M. S.; Tang, C.; Robertson, M. L. *ACS Sustainable Chem. Eng.* **2017**, *5*, 11470-11480.

[14] Wang, S.; Shuai, L.; Saha, B.; Vlachos, D. G.; Epps, T. H. *ACS Cent. Sci.* **2018**, *4*, 701-708.

[15] Vendamme, R.; Schüwer, N.; Eevers, W. *J. Appl. Polym. Sci.* **2014**, *131*, 40669.

[16] Hussnain Sajjad, William B. Tolman, Theresa M. Reineke. *ACS Appl. Polym. Mater.* **2020**, *2*, 2719-2728.

[17] Noppalit, S.; Simula, A.; Ballard, N.; Callies, X.; Asua, J. M.; Billon, L. *Biomacromolecules* **2019**, *20*, 2241-2251.

[18] Wang, Y.; Deng, W.; Wang, B.; Zhang, Q.; Wan, X.; Tang, Z.; Wang, Y.; Zhu, C.; Cao, Z.; Wang, G.; Wan, H. *Nat. Commun.* **2013**, *4*, 2141.

[19] Cubas-Cano, E.; González-Fernández, C.; Ballesteros, M.; Tomás-Pejó, E. *Biofuels Bioprod. Bioref.* **2018**, *12*, 290-303.

[20] Yee, G. M.; Hillmyer, M. A.; Tonks, I. A. *ACS Sustainable Chem. Eng.* **2018**, *6*, 9579-9584.

[21] Kim, H. J.; Jin, K.; Shim, J.; Dean, W.; Hillmyer, M. A.; Ellison, C. J. *ACS Sustainable Chem. Eng.* **2020**, *8*, 12036-12044.

[22] Galaster EL 98.5 FCC, Galasolv 003, PURASOLV ELECT/BL/ML, and VertecBio EL are examples of commercial ethyl lactate solvents produced by Galactic, Corbion, or Vertec Biosolvents.

[23] Purushothaman, M.; Krishnan, P. S. G.; Nayak, S. K. *J. Appl. Polym. Sci.* **2014**, *13*1, 40962.

[24] Purushothaman, M.; Krishnan, P. S. G.; Nayak, S. K. *J. Renew. Mater.* **2015**, *3*, 292-301.

[25] Purushothaman, M.; Krishnan, P. S. G.; Nayak, S. K. *J. Macromol. Sci. A.* **2014**, *51*, 470-480.

[26] Purushothaman, M.; Krishnan, P. Santhana Gopala; Nayak, S. K. *Mater. Focus* **2018**, *7*, 101-107.

[27] Bensabeh, N.; Moreno, A.; Roig, A.; Monaghan, O. R.; Ronda, J. C.; Cádiz, V.; Galià, M.; Howdle, S. M.; Lligadas, G.; Percec, V. *Biomacromolecules* **2019**, *20*, 2135-2147.

[28] Moreno, A.; Bensabeh, N.; Parve, J.; Ronda, J. C.; Cádiz, V.; Galià, M.; Vares, L.; Lligadas, G.; Percec, V. *Biomacromolecules* **2019**, *20*, 1816-1827.

[29] Bensabeh, N.; Moreno, A.; Roig, A.; Rahimzadeh, M.; Rahimi, K.; Ronda, J. C.; Cádiz, V.; Galià, M.; Percec, V.; Rodriguez-Emmenegger, C.; Lligadas, G. *ACS Sustainable Chem. Eng.* **2020**, *8*, 1276-1284.

[30] Semsarilar, M.; Perrier, S. *Nat. Chem.* **2010**, *2*, 811-820.

[31] Holmberg, A. L.; Reno, K. H.; Wool, R. P.; Epps III, T. H. *Soft Matter* **2014**, *10*, 7405-7424.

[32] Matt, L.; Parve, J.; Parve, O.; Pehk, T.; Pham, T. H.; Liblikas, I.; Vares, L.; Jannasch, P. *ACS Sustainable Chem. Eng.* **2018**, *6*, 17382-17390.

[33] Zhang, P.; Liu, T.; Xin, J.; Zhang, J. *J. Appl. Polym. Sci.* **2020**, *137*, 48281.

[34] Zhou, J.; Zhang, H.; Deng, J.; Wu, Y. *Macromol. Chem. Phys.* **2016**, *217*, 2402-2408.

[35] Noppalit, S.; Simula, A.; Billon, L.; Asua, J. M. *ACS Sustainable Chem. Eng.* **2019**, *7*, 17990-17998.

[36] Cseri, L.; Szekely, G. *Green. Chem.* **2019**, *21*, 4178-4188.

[37] Lu, W.; Wang, Y.; Wang, W.; Cheng, S.; Zhu, J.; Xu, Y.; Hong, K.; Kang, N.G.; Mays, J. *Polym. Chem.* **2017**, *8*, 5741-5748.

Chapter 3

SET-LRP of the Hydrophobic Biobased (-)-Menthyl Acrylate

The contents of this chapter are published in: Bensabeh, N. ; Ronda, J. C.; Galià, M.; Cádiz, V.; Lligadas, G. and Percec, V. *Biomacromolecules* **2018**, *19*, 1256-1268.

3. SET-LRP of the Hydrophobic Biobased (-)-Menthyl Acrylate

Cu(0) wire-catalyzed SET-LRP of (−)-menthyl acrylate, a biobased hydrophobic monomer, was investigated at 25 °C in ethanol, isopropanol, ethyl lactate, 2,2,2-trifluoroethanol (TFE), and 2,2,3,3-tetrafluoropropanol (TFP). All solvents are known to promote, in the presence of N-ligands, the mechanistically required self-regulated disproportionation of Cu(I)Br into Cu(0) and Cu(II)Br_2. Both fluorinated alcohols brought out their characteristics of universal SET-LRP solvents and showed the proper polarity balance to mediate an efficient polymerization of this bulky and hydrophobic monomer. Together with the secondary alkyl halide initiator, methyl 2-bromopropionate (MBP), and the tris(2-dimethylaminoethyl)amine (Me_6-TREN) ligand, TFE and TPF mediated an efficient SET-LRP of MnA at room temperature that proceeds through a self-generated biphasic system. The results presented here demonstrate that Cu(0) wire-catalyzed SET-LRP can be used to target polyMnA with different block lengths and narrow molecular weight distribution at room temperature. Indeed, the use of a combination of techniques that include GPC, ^{1}H NMR, MALDI-TOF MS performed before and after thioetherification of bromine terminus via “thio–bromo” click chemistry, and in situ reinitiation copolymerization experiments supports the near perfect chain end functionality of the synthesized biobased hydrophobic polymers. These results expand the possibilities of SET-LRP into the area of renewable resources where hydrophobic compounds are widespread.

SET-LRP of the Hydrophobic Biobased (-)-Menthyl Acrylate

3.1. Introduction

During the past decade, many methodologies to practice SET-LRP have been developed because of intensive research efforts undertaken in different laboratories.[1-7] The continuous evolution of this technique, which evolved from studies on the metal-catalyzed LRP of VC,[8-10] has made available today a diversity of methodologies that differ in the way to present Cu(0) catalyst to the rest of reagents (i.e. monomer, initiator, ligand, and solvent).[1] Nowadays, SET-LRP practitioners not only can use almost any form of Cu(0) (e.g. powder,[11] nanopowder,[12] activated[13,14] and non-activated[15] wire,[16] coins,[17] and bars[18]), but also Cu(0) nanoparticles prepared *via* disproportionation of Cu(I)Br and used *ex situ* and *in situ*.[19-23] Cu(0) nanoparticules can also be prepared *in situ* from the reduction of $Cu(II)Br_2$ by sodium borohydride ($NaBH_4$)[24,25] or alternative reducing agents.[26]

Studies and developments on the key-role of solvent on SET-LRP have also constituted an indisputable step forward.[27-34] SET-LRP requires the use of solvents favoring the disproportionation of Cu(I)X into Cu(0) and $Cu(II)X_2$. Originally, the success of this LRP technique was thought to be contingent upon the solubility of targeted monomers and polymers in polar solvents (e.g. DMSO, DMF, alcohols, and water). Such solvents in the presence of ligands such as Me_6-TREN, TREN and PEI, that destabilize Cu(I)X *via* preferentially binding to $Cu(II)X_2$,[35,36] promote the mechanistically required disproportionation of Cu(I)X into Cu(0) activator and $Cu(II)X_2$ deactivator.[29] In fact, in the presence of polar and non-polar non-disproportionating solvents such as MeCN and specially toluene, in which both Cu(I)X and $Cu(II)X_2$ are not sufficiently soluble, a significant loss of chain-end functionality is observed as the conversion increases.[27] However, good molecular weight control, high-level retention of chain end functionality and high monomer conversions has been observed in "self-generated" SET-LRP systems in which polymer phase-separates from the homogeneous reaction mixture above or after reaching a certain molecular weight.[37-43] The first "self-generated" biphasic system was first observed during the synthesis of PMA with M_n = 1,600,000 g/mol in DMSO.[42] The same phenomenon was also observed during the polymerization of BA in the same solvent.[43] Later, polymers with

highly hydrophobic character such as poly(lauryl acrylate), and poly(stearyl acrylate) could be obtained with high level of control via "self-generated" biphasic systems in *iso*-propanol (^{i}PrOH).[37,39] A biphasic system also evolved from the SET-LRP of 2-ethylhexyl acrylate in TFE.[38] All these reports inspired the elaboration organic solvent/water "programmed" biphasic systems that relies on the unexpected immiscibility between a solution of water containing Cu(II)Br_2 and a ligand with organic solvents, including water miscible organic solvents, containing monomer and polymer.[44-50] Of particular interest are combinations of polar and/or non-polar non-disproportionating solvents with water because they overcome the inherent SET-LRP requirements to use polar disproportionating solvents.[45,47]

Since its invention, SET-LRP has been widely used by researchers working at the interface of polymer science with biology and medicine.[3,7] The derivation of renewable resources to well-defined polymers has recently experienced a remarkable resurgence to meet contemporary sustainability challenges.[51,52] In this context, SET-LRP has been demonstrated as a very efficient LRP technique to produce well-defined glycopolymers[53-55] as well as to prepare graft-copolymers from natural polysaccharides[56,57] and polymer-protein conjugates.[58-60] As mentioned above, it has also been used to deliver well-defined polymers up to 10,000 g/mol from biobased lauryl and stearyl acrylates.[37,39] However, the polymerization of highly hydrophobic and bulky monomers derived from terpenes, terpenoids and rosin has not been investigated so far.[61] In this chapter, we report the SET-LRP of the hydrophobic and biobased (-)-menthyl acrylate (MnA) in a series of alcohols, i.e EtOH,[31,44,50,62] ^{i}PrOH,[37,39,63] EL,[64] TFE,[38,65-68] and TFP[65-69]) that previously demonstrated promising properties as SET-LRP solvents. Among them, the two fluorinated alcohols demonstrated the best performance using hydrazine-activated Cu(0) wire as catalyst, the secondary alkyl halide initiator, MBP and the Me_6-TREN ligand. The controlled polymerization of this terpenoid-derived monomer is reported for the first time and proceeds through a self-generated biphasic reaction mixture without compromising the creation of well-defined polymers with near perfect chain end functionality.

3.2. Results and discussion

3.2.1. Selection of solvent for SET-LRP of MnA

Finding a solvent with a proper polarity balance to both promote disproportionation of Cu(I)X, whilst retaining high solubility/swelling properties with respect to poly(menthyl acrylate) (polyMnA) was anticipated to be a key-point to succeed with the SET-LRP of MnA. The monomer was synthesized by esterification of the corresponding alcohol with acryloyl chloride in the presence of triethylamine (TEA) (Scheme 3.1a).[70]

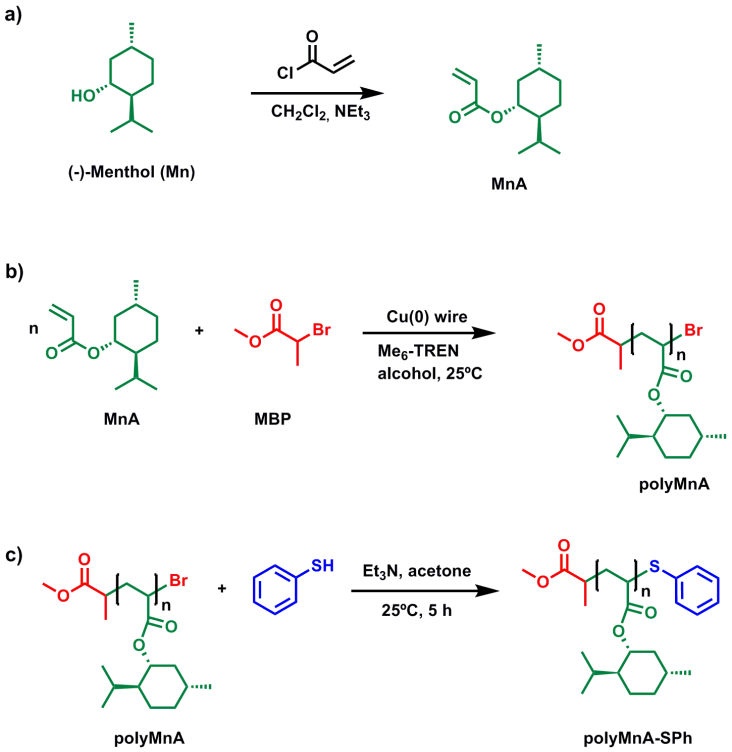

Scheme 3.1. SET-LRP of the hydrophobic MnA: (a) synthesis of MnA, (b) SET-LRP of MnA initiated with MBP and catalyzed by Cu(0) wire/Me_6-TREN in alcohols, (c) "thio-bromo click" thioetherification of polyMnA using thiophenol.

This Mn-derived monomer is highly hydrophobic, and thus classic polar SET-LRP solvents are not expected to be a good choice to deliver an efficient SET-LRP process at 25 °C. After discarding dipolar aprotic solvents such as DMSO and DMF because of their undesirable

health, safety, environmental problems and high price, we focused our attention to alcohols because are the most attractive SET-LRP solvents from a sustainability viewpoint.[62] Besides being most of them non-toxic, they have lower boiling points than dipolar aprotic solvents and are miscible with water at any composition and therefore can evolve into either homogeneous[38,63,71] or biphasic SET-LRP systems.[44,50] MeOH, the least expensive commercially available organic solvent, was unfortunately unable to solubilize MnA at room temperature. However, the good solubility of this biobased monomer in EtOH (MnA:EtOH = 2/1, v/v) encouraged us to first test the SET-LRP in this alcohol. Using MBP as monofunctional initiator, the polymerization was held over 8 h at room temperature under the following conditions: $[MnA]_0/[MBP]_0/[Me_6\text{-TREN}]_0$ = 50/1/0.1, MnA = 1 mL, EtOH = 0.5 mL and 4.5 cm of hydrazine-activated Cu(0) wire of 20 gauge (Scheme 3.1b, Table 3.1 entry 1). Polymerization of MnA occurred, as indicated by a high monomer conversion (92%). However, despite the low targeted $[M]_0/[I]_0$, EtOH was not able to either solubilize or swell polyMnA. As can be seen in the image shown in Figure 3.1a, the polymer separated as a white solid from a green ethanolic solution, containing residual monomer and catalyst. GPC analysis revealed poor control of the molecular weight distribution (M_w/M_n = 3.40) and brought out clear evidences of radical bimolecular coupling processes (see shoulder peak at higher molecular weight position in Figure 3.1a, bottom). Inspired by previous reports from our laboratory and others, EL[64] and ^{i}PrOH[37,39,63] were tested as solvents for the SET-LRP of MnA under identical conditions.

We recently reported that EL is an attractive environmentally friendly solvent for the SET-LRP of both hydrophilic and hydrophobic monomers.[64] ^{i}PrOH has also been widely used to practice the SET-LRP of a variety of vinyl monomers under homogeneous conditions as well as challenging long chain hydrophobic monomers such as lauryl and stearyl acrylates through “self-generated” biphasic systems. [37,39,63]

SET-LRP of the Hydrophobic Biobased (-)-Menthyl Acrylate

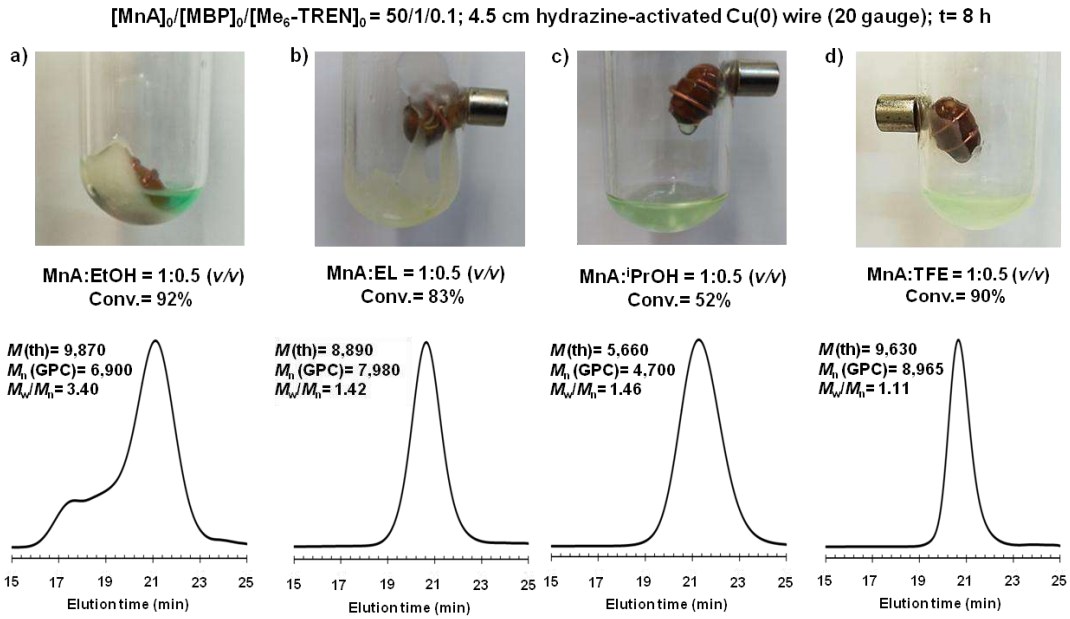

Figure 3.1. Visualization of the reaction mixture, monomer conversion and GPC chromatograms after the SET-LRP of MnA initiated with MBP in (a) EtOH, (b) EL, (c) ^{i}PrOH, and (d) TFE. Reaction conditions: MnA = 1 mL, solvent = 0.5 mL, $[MnA]_0/[MBP]_0/[Me_6\text{-TREN}]$ = 50/1/0.1 using 4.5 cm of hydrazine-activated Cu(0) wire (20 gauge), reaction time = 8 h.

Table 3.1. SET-LRP of MnA initiated with MBP using 4.5 cm of hydrazine-activated Cu(0) wire (20 gauge) in various alcohols at 25 °C. Reaction conditions: MnA = 1 mL, solvent = 0.5 mL.

entry	solvent	$[M]_0/[I]_0/[L]_0$	k_p^{app} (min^{-1})	time (min)	conv. (%)	M (th) (g mol^{-1})	M_n (NMR)[c] (g mol^{-1})	M_n (GPC) (g mol^{-1})	M_w/M_n (GPC)
1	EtOH	50/1/0.1	-	480	92	9,870	-	6,900	3.40
2	EL	50/1/0.1	-	480	83	8,890	-	7,980	1.42
3	^{i}PrOH	50/1/0.1	-	480	52	5,660	-	4,700	1.46
4	TFE	50/1/0.1	-	480	90	9,630	-	8,965	1.11
5[a,b]	TFE	50/1/0.1	0.0058	400	82	8,680	-	7,312	1.13
6[b]	TFE	50/1/0.1	0.0052	310	80	8,580	9,246	7,880	1.10
7	TFE	100/1/0.1	0.0031	400	67	14,280	-	13,530	1.23
8	TFE	100/1/0.2	0.0042	300	73	15,600		14,325	1.15
9	TFE	100/1/0.5	0.0060	327	88	18,590	18,901	17,930	1.14
10	TFE	200/1/1	0.0037	410	78	32,980	33,850	32,220	1.17
11	TFE	25/1/0.1	0.0089	270	90	4,900	4,934	4,690	1.14
12	TFP	50/1/0.1	0.0071	276	84	9,000	-	8,900	1.14

[a] Non-activated Cu(0) wire (20 gauge) was used. [b] MnA:TFE = 1:1, v/v was used. [c] From end group analysis.

On one hand, Cu(0) wire-catalyzed SET-LRP in EL reached 83% conversion in 8 h (Table 3.1 entry 2). The GPC analysis of the resulting polymer was symmetric with no tailing or shoulder peak (Figure 3.1b, bottom). However, M_w/M_n was quite far from the expected value for a well-defined polymer (M_w/M_n = 1.42). PolyMnA did not precipitate in this agrochemical solvent but the reaction mixture showed slight opaqueness at the end of the process (Figure 3.1b, up). Nevertheless, EL was able to swell polyMnA and no sign of precipitation was observed. On the other hand, the reaction mixture in ^{i}PrOH was a green one-phase solution with no visual sign of insolubility (Figure 3.1c, up). Unfortunately, the polymerization of MnA in this alcohol achieved only 52% conversion after 8 h under these conditions (Table 3.1 entry 3). GPC analysis revealed the formation of polyMnA with M_n = 4,700 g/mol and M_w/M_n = 1.46 (Figure 3.1c, bottom).

Fluorinated alcohols such as TFE and TFP have been coined "universal solvents" for SET-LRP, as they open the possibility of polymerizing a broad polarity spectrum of monomers.[38,65-69] In fact, the SET-LRP of MnA in TFE provided encouraging results (Figure 3.1d). The polymerization of MnA in TFE resulted in polyMnA with M_n = 8,965 g/mol at 90% conversion (Table 3.1 entry 4). The final polymer was well-defined as indicated by a perfectly symmetric GPC peak (M_w/M_n = 1.11) regardless the reaction mixture was greenish with some turbidity at the end of the SET-LRP process. This aspect will be discussed in detail later in this chapter. These solvent screening experiments provided an initial starting point to study on the SET-LRP of MnA in TFE.

3.2.2. SET-LRP of MnA in TFE catalyzed by Cu(0) wire

Both TFE and TFP are unique SET-LRP solvents because activate *in situ* commercial Cu(0) wire by themselves.[68] It is well-known that Cu(0) wire is more reactive without its characteristic oxide layer and different activation protocols are usually applied to practice with this SET-LRP methodology.[1] The Cu_2O/CuO layer on the surface of any commercial Cu(0) wire is responsible, in most of the cases, of the induction periods reported for SET-LRP reactions. Hence, the first kinetic experiments to study in-depth the SET-LRP of MnA in TFE was carried out using commercially available non-activated Cu(0) wire (4.5 cm of 20 gauge

wire) under the following conditions $[MnA]_0/[MBP]_0/[Me_6\text{-TREN}]_0$ = 50/1/0.1. Despite using MnA:TFE =1:1, v/v, the SET-LRP showed an induction period of approximately 90 min with no reaction after which, the polymerization proceeded fulfilling all the expected characteristics for a LRP process (Figure 3.2a). Thus, the $\ln[M]_0/[M]$ increases linearly up to approximately 80% conversion suggesting that concentration of propagating radicals remains constant throughout the entire process. Moreover, a linear evolution of molecular weight with conversion and the formation of a polyMnA with narrow molecular weight was also observed.

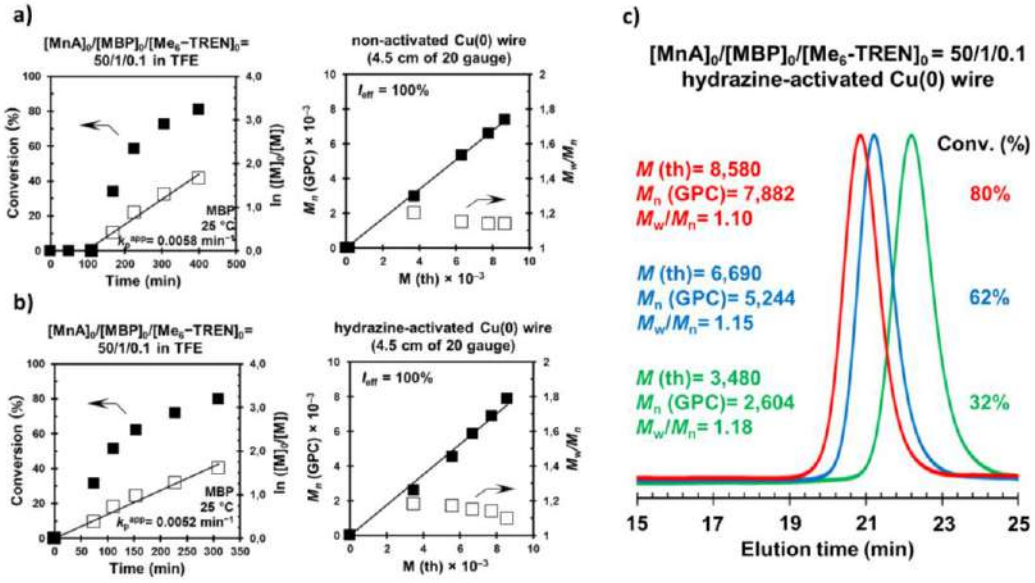

Figure 3.2. Conversion and $\ln([M]_0/[M])$ *vs* time kinetic plots and experimental M_n (GPC) and M_w/M_n *vs* theoretical M(th) in SET-LRP of MnA in TFE initiated with MBP and catalyzed by (a) non-activated Cu(0) wire and (b) hydrazine-activated Cu(0) wire. (c) Representative GPC chromatograms of polyMnA obtained from kinetic experiment shown in (b). Reaction conditions: MnA = 1 mL, TFE = 1 mL, $[MnA]_0/[MBP]_0/[Me_6\text{-TREN}]$ = 50/1/0.1 using 4.5 cm of Cu(0) wire (20 gauge).

Consistently with the results presented in the previous subsection, well-defined polyMnA with M_n = 7,312 g/mol and M_w/M_n = 1.13 was obtained at 82% conversion (Table 3.1, entry 5).

Upon switching to hydrazine-activated Cu(0) wire the long induction period disappeared (Figure 3.2b). It is important to note that polymerization proceeded over 80% conversion in

300 min with strictly the same k_p^{app} (k_p^{app} = 0.052 min^{-1}) to the experiment with the non-activated Cu(0) counterpart (k_p^{app} = 0.058 min^{-1}) (Table 3.1, entries 5 and 6). We do not know the reason for this induction period although this result may suggest that the activation of Cu(0) wire by TFE is not effective in highly hydrophobic reaction mixtures. Again, the kinetic and molecular weight/dispersity evolution plots together with chain end analysis, that will be discussed in another subsection, are consistent with a LRP process. As previously noted, the reaction mixture was turbid and opaque at the end of the polymerization. As can be seen in Figure 3.3a-d, turbidity progressively appeared with increasing conversion, suggesting that phase separation occurs during polymerization of MnA in TFE. SET-LRP systems in which growing polymer chains precipitate out of the initially homogeneous mixture to generate a biphasic system consisting of a solvent swollen polymer-rich phase and a second organic phase containing the solvent, monomer and soluble Cu(II)X_2 species were named "self-generated" biphasic systems by Whittaker and Haddleton laboratories.[41] Our group and others observed this phenomenon during the polymerization of various hydrophobic monomers (i.e. BA, 2-ethylhexyl acrylate (EHA), lauryl acrylate in various solvents such as DMSO,[37,41,43] TFE,[38] ^{i}PrOH,[37,39] EL,[64] and DML.[40] Here, after centrifugation in air, the biphasic nature of the reaction mixture is clearly visible with an upper layer containing polyMnA swelled in TFE and a lower layer containing the residual monomer, ligand and Cu(II)Br_2 dissolved in the remaining TFE. Despite the formation of a biphasic system, GPC analysis during the polymerization of MnA in TFE revealed the formation of polyMnA with narrow molecular weight distribution at all conversions, as indicated by low dispersity values (M_w/M_n = 1.2 – 1.10) (Figure 3.2c). Experimental molecular weight values (M_n (GPC)), as determined by GPC analysis with against PMMA standards, and theoretical values (M_n (th)) were in good agreement.

PolyMnA with M_n(NMR) = 9,246 g/mol, isolated after precipitation in MeOH, is a glassy white solid (Figure 3.4). This polymer is soluble in THF, CH_2Cl_2, and acetone but insoluble in DMSO, MeCN, and EtOH. Because the glass transition temperature (T_g) of polyMnA is at

around 55 °C, this biobased polymer could be used as biocompatible glassy minority end-block in sustainable ABA thermoplastic elastomers.[72-79]

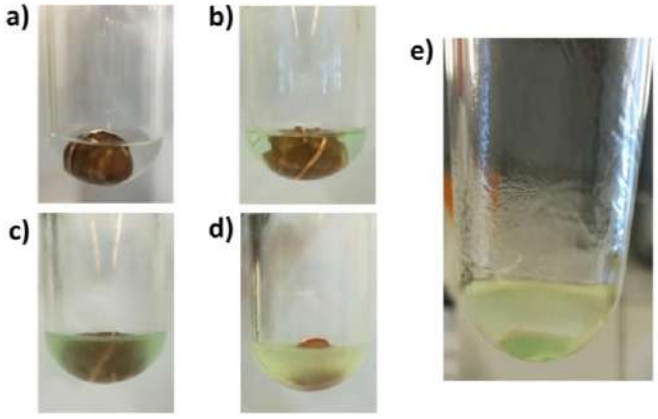

Figure 3.3. (a-d) Visualization of the progressive formation of a biphasic reaction mixture thorough the SET-LRP of MnA in TFE. Digital images were captured at 0% conv. (0 min), 40% conv. (100 min), 75% conv. (200 min) and 90% conv. (300 min). Reaction conditions: MnA = 1 mL, TFE = 0.5 mL, $[MnA]_0/[MBP]_0/[Me_6\text{-TREN}]$ = 50/1/0.1 using 4.5 cm of hydrazine-activated Cu(0) wire (20 gauge). (e) Digital image of the "self-generated" biphasic system at 94% conv. captured after centrifugation in air.

The relatively high T_g of polyMnA is attributed to reduced polymer flexibility caused by structural rigidity and limited "free volume" of the pendant menthyl groups.

Thermoplastic elastomers with hard-block T_g as low as 50 °C are appealing for biomedical applications because the upper service temperatures of these materials is well above the body temperature.

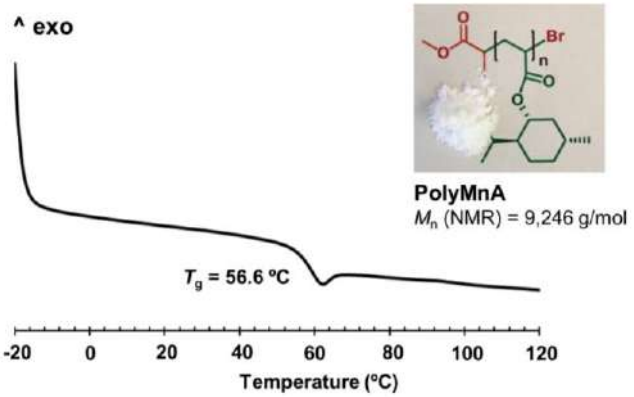

Figure 3.4. DSC analysis of PolyMnA with M_n (NMR) = 9,246 g/mol isolated after precipitation in MeOH (inset: digital image of the polymer).

3.2.3. Synthesis of high molecular weight polyMnA

We were interested in pushing the limits of this polymerization system by targeting higher molecular weight polymers. First, SET-LRP of MnA at $[M]_0/[I]_0$ = 100 was performed under the following conditions: $[MA]_0/[MBP]_0/[Me_6\text{-TREN}]_0$ = 100/1/0.1, MnA = 1 mL, TFE = 0.5 mL using 4.5 cm of hydrazine-activated wire. However, using 10 mol% with respect to the initiator, the polymerization reached a plateau below 70% conversion (Table 3.1 entry 7).

Next, the SET-LRP of MnA at $[M]_0/[I]_0$ = 100 was performed increasing the ligand concentration with respect to the MBP to 20 mol% and 50 mol%. While polymerization in the presence of 0.2 equivalents of Me_6-TREN did still not exceed 75 % conversion, with 0.5 equivalents of Me_6-TREN the $\ln[M]_0/[M]$ kinetic plot was linear up to almost 90% conversion (k_p^{app} = 0.0060 min^{-1}) (Figure 3.5a, Table 3.1 entries 8 and 9).

The reason because higher molecular weight target requires higher concentration of ligand can be related to specific interactions between soluble copper species and TFE. These interactions, which are in competition with those with Me_6-TREN, may lead to bimolecular termination and limited conversion due to ineffective deactivation events. In previous publications, the use of concentrations of ligand higher than 10 mol% respect to the initiator was also necessary for the SET-LRP of N-(2-hydroxypropyl)methacrylamide[80] and 2-hydroxyethyl acrylate[81] in H_2O and MeOH, respectively. Note that in our study, the high ionizing power and strong hydrogen bond donating ability of TFE may increase this effect. In fact, the SET-LRP of 2-ethylhexyl acrylate[38] and di(ethylene glycol) 2-ethylhexyl ether acrylate[82] in TFE also required the use of higher concentration of Me_6-TREN to achieve optimum results.

Thus, we were able to obtain polyMnA with M_n just below 20,000 g/mol and M_w/M_n = 1.14 (Figure 3.5a). At $[M]_0/[I]_0$ = 200, increasing the concentration of ligand from 0.5 to 1 equivalents with respect to the MBP, the polymerization also exhibited a linear first order kinetic plot reaching 80% conversion in less than 7 h (Figure 3.5b, Table 3.1 entry 10).

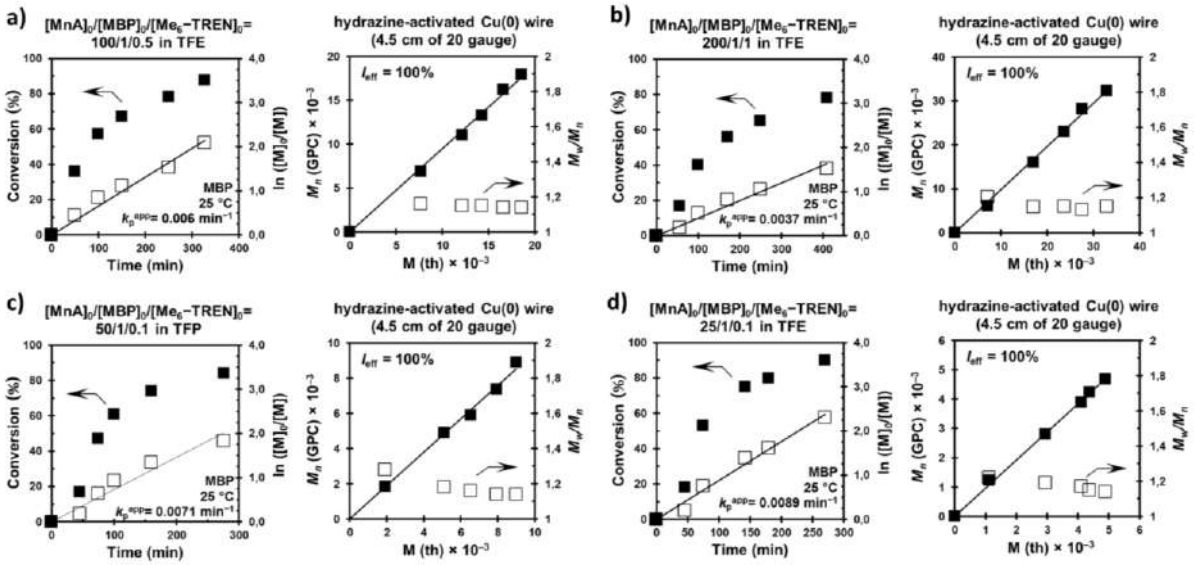

Figure 3.5. Conversion and ln([M]$_0$/[M]) *vs* time kinetic plots and experimental M_n (GPC) and M_w/M_n *vs* theoretical *M*(th) in SET-LRP of MnA in TFE or TFP initiated with MBP and catalyzed by hydrazine-activated Cu(0) wire. (a) [MnA]$_0$/[MBP]$_0$/[Me$_6$-TREN] = 100/1/0.5 in TFE, (b) [MnA]$_0$/[MBP]$_0$/[Me$_6$-TREN] = 200/1/1 in TFE, (c) [MnA]$_0$/[MBP]$_0$/[Me$_6$-TREN] = 50/1/0.1 in TFP, and (d) [MnA]$_0$/[MBP]$_0$/[Me$_6$-TREN] = 25/1/0.1 in TFE. Reaction conditions: MnA = 1 mL, solvent = 0.5 mL, 4.5 cm of Cu(0) wire (20 gauge).

These results demonstrate that molecular weight control of this system is not just limited to low target molecular weight. Higher molecular weight polyMnA isolated from these experiments were also characterized by DSC. The T_g value of polyMnA increased slightly with molecular weight. DSC analysis of the polymers with M_n (NMR) = 18,901 g/mol and M_n(NMR) = 33,850 g/mol showed T_g values at 60.1 °C and 62.3 °C, respectively.

3.2.4. SET-LRP of MnA in TFP

As mentioned above, both TFE and TFP are excellent SET-LRP solvents for the polymerization of both hydrophilic and hydrophobic acrylates.[38,65-69] Well-defined polyMnA could also be prepared in TFP. However, the use of TFE is more suitable because is less expensive and has a lower boiling point (73.6 °C *vs* 107-109 °C). The polymerization of MnA in TFP using MBP as initiator and catalyzed by 4.5 cm of Cu(0) wire activated with hydrazine reached 84% conversion after 4.5 h (Figure 3.5c, Table 3.1 entry 12). The polymerization

rate was similar that that obtained using TFE as solvent (k_p^{app}= 0.0071 min^{-1} *vs* 0.0052 min^{-1}). A linear increase in M_n with conversion and narrow molecular weight distribution indicated the SET-LRP of MnA in TFP was well-controlled. The formation of a biphasic reaction mixture also occurred in this case. Low, medium, and high conversion GPC chromatograms are shown in Figure 3.6b.

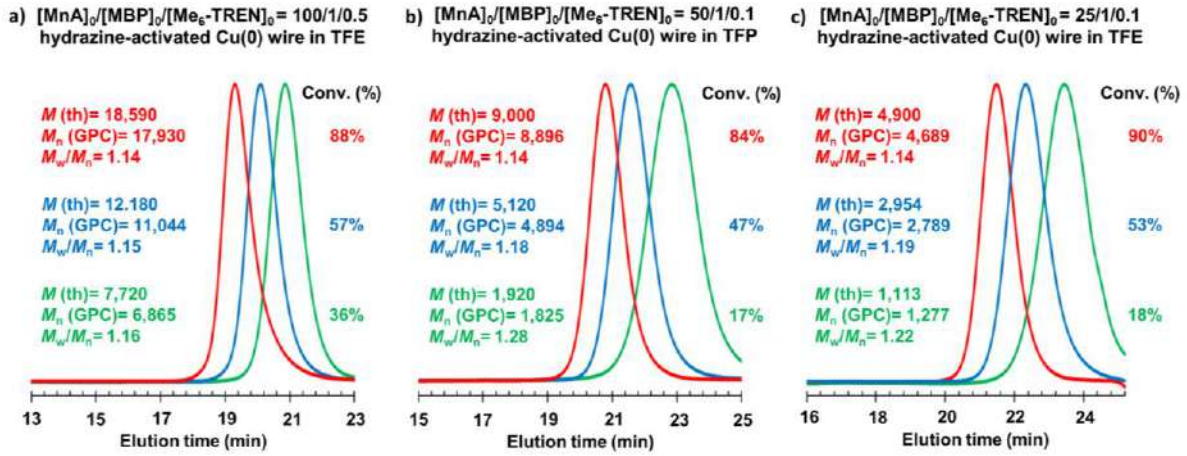

Figure 3.6. Representative GPC chromatograms of polyMnA from kinetic plots in SET-LRP of MnA in TFE or TFP initiated with MBP and catalyzed by hydrazine-activated Cu(0) wire. (a) $[MnA]_0/[MBP]_0/[Me_6\text{-TREN}]$ = 100/1/0.5 in TFE, (b) $[MnA]_0/[MBP]_0/[Me_6\text{-TREN}]$ = 50/1/0.1 in TFP, and (c) $[MnA]_0/[MBP]_0/[Me_6\text{-TREN}]$ = 25/1/0.1 in TFE. Reaction conditions: MnA = 1 mL, solvent = 0.5 mL, 4.5 cm of Cu(0) wire (20 gauge).

3.2.5. Chain-end analysis of polyMnA prepared by SET-LRP of MnA in TFE

To explore in detail the degree of control attained for the SET-LRP of MnA in TFE, polyMnA with theoretical degree of polymerization of 25 at 100% conversion was prepared to have a sample with molecular weight suitable for a precise determination of the percentage of the chain-end functionality by ^{1}H NMR analysis. At [M]/[I] = 25, kinetic and molecular weight dispersity plots were consistent with previous experiments and showed the typical features of a LRP process (Figure 3.5d). Despite the formation, also in this case, of a biphasic reaction mixture, GPC chromatograms at different conversions were symmetric without high/low molecular weight tailing (Figure 3.6c). The structural analysis of the final sample, isolated at 90% conversion by precipitation in MeOH, was carried out by ^{1}H NMR

spectroscopy and MALDI-TOF MS spectrometry. The fraction of polyMnA chains that are capped with bromine atoms at the ω-terminus was determined to be 96% by the ratio between characteristic signals of both α and ω polymer terminus (see Figure 3.7).

Within the experimental error of the ^{1}H NMR measurement, this result supports the perfect or near-perfect retention of chain-end functionality achieved by this SET-LRP system. End-group analysis of the final product by ^{1}H NMR was also used to determine the molecular weight M_n (NMR) (Figure 3.7). M_n (NMR) was also calculated for higher molecular weight samples (Table 3.1, entries 6, 9, and 10). In all cases, M_n (NMR) values are in good agreement with theoretical values and M_n (GPC) values determined using PMMA standards. MALDI-TOF MS analysis before and after modifying the polyMnA bromine terminus with thiophenol via "thio−bromo" click chemistry[83,84] leaves no doubt about the outstanding degree of control attained by the SET-LRP of this bulky hydrophobic monomer in TFE (Scheme 3.1c and Figure 3.8). PolyMnA isolated after SET-LRP shows a single distribution of peaks attributable to polyMnA-Br/K^+ species separated by 210.4 mass units (see Figure 3.8a, inset expansion). Delightfully, with the reaction of polyMnA with thiophenol in the presence of NEt_3 the original distribution completely vanishes, and a new series of well-defined and symmetrical peaks emerge 29 units above the parent distribution (Figure 3.8b).

This value is consistent with the increase in mass after the reaction of thiophenol at ω-polymer chain end. It should be noted that this reaction at the ω-polymer terminus was performed in acetone because polyMnA was not soluble in MeCN, the common solvent used for the "thio−bromo" click modification of conventional polyacrylates.[83,84] As an additional proof of the high chain ends fidelity of the synthesized polyMnA, *in situ* chain extension experiments from a low molecular weight polyMnA were carried out using BA. Figure 3.9a shows that the addition via cannula of a deoxygenated solution of BA and Me_6-TREN in TFE led to a clear and neat displacement of the polyMnA GPC curve while maintaining low dispersity. In another experiment, two successive *in situ* chain extensions were carried out via sequential addition of two aliquots of BA and MnA to deliver multiblock poly(MnA)-*b*-poly(BA)-*b*-poly(MnA) with M_n = 21,520 g/mol and M_w/M_n = 1.22 (Figure 3.9b).

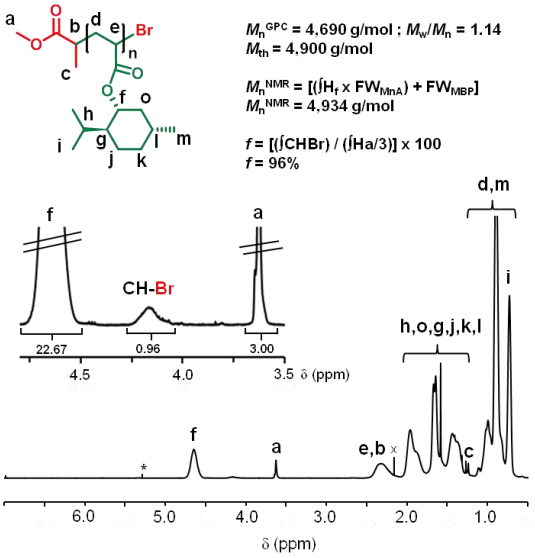

Figure 3.7. ^{1}H NMR spectrum (400 MHz) of polyMnA isolated at 90% conversion (M_n ^{GPC} = 4690 Da, M_w/M_n = 1.14) from SET-LRP of MnA in TFE. Reaction conditions: MnA = 1 mL, solvent = 0.5 mL, and $[MnA]_0/[MBP]_0/[Me_6\text{-TREN}]$ = 25/1/0.1 using 4.5 cm of Cu(0) wire (20 gauge). ^{1}H NMR resonances from residual CH_2Cl_2 and acetone are indicated with ∗ and x, respectively.

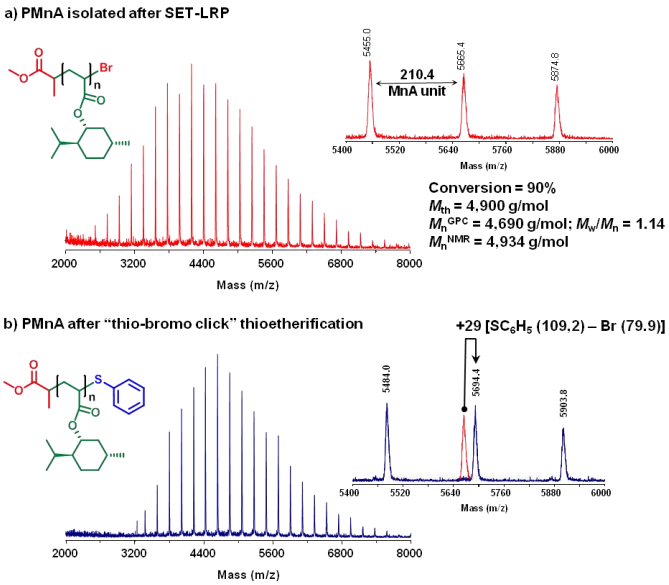

Figure 3.8. MALDI-TOF of polyMnA isolated at 90 % conversion (M_n GPC = 4,690 g/mol, M_w/M_n = 1.14) from SET-LRP of MnA in TFE (a) before and (b) after "thio–bromo click" reaction. Reaction conditions: MnA = 1 mL, solvent = 0.5 mL, and $[MnA]_0/[MBP]_0/[Me_6\text{-TREN}]$ = 25/1/0.1 using 4.5 cm of Cu(0) wire (20 gauge). Red line in the expansion after modification shows the original peak corresponding to the bromo-terminated polyMnA.

SET-LRP of the Hydrophobic Biobased (-)-Menthyl Acrylate

Despite the compounds synthesized are not really strict AB or ABA block copolymers, these results open up new avenues to investigate the SET-LRP of other terpene derived hydrophobic monomers[85,86] with the final goal to prepare innovative sustainable ABA thermoplastic elastomers from renewable resources or other multiblock structures with menthol units.[72-79] Experiments along these lines will be reported in due time.

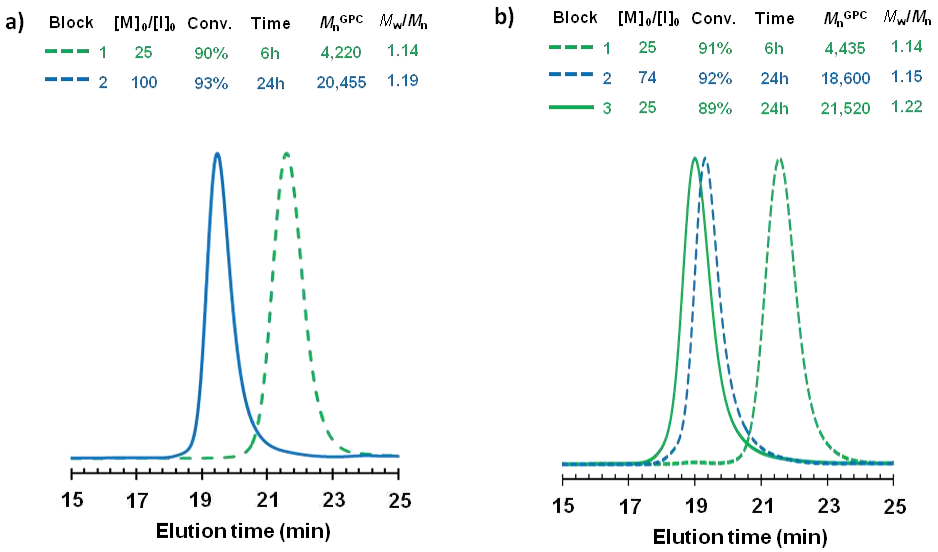

Figure 3.9. *In situ* chain extension from polyMnA. Initial conditions for block copolymerization: $[MnA]_0/[MBP]_0/[Me_6\text{-TREN}]$ = 25/1/0.1, MnA:TFE = 2:1 (v/v), and 4.5 cm of hydrazine activated Cu(0) wire (20 gauge). Block copolymerization achieved by addition of (a) BA (100 equiv) and Me_6-TREN (0.1 equiv) in TFE (BA:TFE = 2:1 (v/v)) and (b) BA (75 equiv) and Me_6-TREN (0.1 equiv) in TFE (BA:TFE = 2:1 (v/v)) and MnA (25 equiv) and Me_6-TREN (0.1 equiv) in TFE (MnA:TFE = 2:1 (v/v)).

3.2.6. Controlled LRP of MnA: SET-LRP *vs* ATRP

Hydrophobic and bulky compounds such as (-)-Mn are widespread in the realm of renewable resources. Although significant efforts have made in the past to create polymers from terpene-, terpenoid-, and rosin-derived monomers, the precise synthesis of well-defined polymers is receiving increasing attention.[86-88] In recent years, the popularity of SET-LRP has raised exponentially due to the possibility to deliver polymers with nearly 100% chain end fidelity at high conversion.[1] This is possible because only in SET-LRP, and not in

ATRP, Cu(II)X_2 deactivator is produced *via* disproportionation without the need for bimolecular termination.[1,5-7] However, the SET-LRP of MnA was anticipated to be challenging due to its high hydrophobicity and bulkiness. In fact, hydrophobic monomers/polymers have been until recently the Achilles' heel of SET-LRP. Results reported here demonstrate that the use of fluorinated alcohols such as TFE in combination with a secondary alkyl halide initiator (MBP) and Me_6-TREN ligand allows the preparation of polyMnA with a range of targeted degrees of polymerization (DP = 25-200, M_n^{th} = 5,400-42,200) at room temperature. In spite of the appealing characteristics of MnA (e.g. optically active biomass-derived monomer) and the potential applications of the corresponding polymer,[70,89,90] according to our knowledge, the controlled LRP of this monomer received scarce attention until now. Only the Cu(I)X-mediated ATRP of MnA was previously investigated in anisole, a solvent with poor disproportionating properties, using various catalytic systems based on the air-sensitive Cu(I)Br.[91] The use of Cu(0) wire in SET-LRP is much more convenient because offers an easier catalyst handling and recovery/recycling. In addition, Cu(0) wire-catalyzed SET-LRP tolerates oxygen from air,[92-95] because Cu(0) catalyst consumes the O_2 from the reaction mixture, and therefore can be practiced using simple N_2 sparging in a test tube[96] or even without deoxygenation protocols.[97] Best results for the ATRP of MnA were obtained using also Me_6-TREN as ligand and a secondary alkyl halide initiator (i.e. ethyl 2-bromopropionate). However, optimum ATRP polymerization conditions required much higher temperature (95 °C) than the SET-LRP system (25 °C). Unfortunately, detailed structural analysis of the polyMnA products prepared by ATRP was not reported, and it is expected to be not better than that obtained in toluene[27] or in other nondisproportionating solvents.[1-5,27,28,30,33,98] ATRP is based on the persistent radical effect, and therefore it requires at least 10% bimolecular termination. Conversely, the combination of ^{1}H NMR and MALDI-TOF MS before/after "thio-bromo" click chemistry as well as reinitiation copolymerization experiments presented here supports the near perfect chain end functionality of the polyMnA synthesized by SET-LRP.

Therefore, the SET-LRP system offers an environmentally friendly methodology operating at room temperature for the preparation of block, multiblock and more complex architectures based on this monomer and thus expand the already described medical applications of (-)-Mn. Moreover, they will expand the possibilities of SET-LRP into the area of renewable resources where hydrophobic compounds are widespread and will provide new opportunities for their application in the area of medicine and biomacromolecules. Although the use of fluorinated alcohols such as TFE and TFP can be questioned from an economic and sustainability viewpoint, TFE can be easily removed from reaction mixtures by distillation and recycled due to its low boiling point. Moreover, "self-generating" biphasic SET-LRP offer important advantages respect to homogeneous systems in terms of *in situ* purification of the polymer from soluble copper species and the suppression of bimolecular termination.[37,39] Finally, the use of "programmed biphasic systems based on mixtures of these alcohols and water are expected to provide faster reactions.[44-50,99]

3.3. Conclusions

Pushing the limits of fluorinated alcohols as solvents for SET-LRP, here we report the hydrazine-activated Cu(0) wire-mediated SET-LRP of the biobased (-)-menthyl acrylate at room temperature. TFE and TFP showed much better performance than other alcohols such as EtOH, iPrOH, and EL in terms of conversion and molecular weight control. The monofunctional initiator MBP and the Me_6-TREN ligand were used to initiate the polymerization and mediate the mechanistically required disproportionation of Cu(I)Br into Cu(0) and Cu(II)Br_2. Regardless of the bulkiness and hydrophobicity of this biobased monomer, SET-LRP successfully created polyMnA with a range of targeted degrees of polymerization (DP = 25-200, M_n^{th} = 5,400-42,200 g/mol) in moderate reaction times (<7 h). In all cases, polymerization kinetics were used to demonstrate a perfect living polymerization behavior as indicated by linear time evolution of $\ln([M]_0/[M])$ and M_n^{GPC} *vs* M_n^{th} plots. The hydrophobicity of this monomer forced SET-LRP in TFE and TFP to proceed through a self-generated biphasic system. However, this does not compromise the achievement of outstanding control of molecular weight and narrow molecular weight

distribution. The high-end group fidelity of these biobased polyacrylates is supported by a combination of ^{1}H NMR, MALDI-TOF MS performed before and after modification of bromine terminus *via* "thio-bromo" click chemistry, and *in situ* reinitiation copolymerization experiments. Well-defined polyacrylates, including telechelics, macromonomers, branched, hyperbranched, and dendrimers,[84] from any of the eight existing stereoisomers of menthol are expected to be accessible by this methodology, so that optically active polymers and copolymers can be targeted. Moreover, the high chain end functionality of the synthesized polymers can help to expand the already described medical applications of Mn[100]-[105] *via* the preparation of well-defined bioconjugates. Menthol has also been used to mediate and monitor supramolecular polymerization,[106] and its polyacrylates are expected to bring a new dimension to this concept. Last but not least, these results are envisioned to encourage the use of SET-LRP in the preparation of well-defined and functional polymers with complex architecture with new biomedical applications biobased on this and other hydrophobic biobased monomers.

3.4. Experimental section

3.4.1. Materials

(-)-Menthol (Mn, ≥ 99 %, Sigma Aldrich), acryloyl chloride (96%, Sigma Aldrich), methyl 2-bromopropionate (MBP, 98%, Sigma Aldrich), tris[2-(dimethylamino)ethyl]amine (Me_6-TREN, 97%, Sigma Aldrich), hydrazine hydrate (60%, hydrazine, Sigma Aldrich), *trans*-2-[3-(4-*tert*-butylphenyl)-2-methyl-2-propenylidene]malononitril (DCTB, ≥ 98%, Sigma Aldrich, 98%), potassium trifluoroacetate (KTFA, Sigma Aldrich), 2,2,2-trifluoroethanol (TFE, ≥ 99%, Merck), 2,2,3,3-tetrafluoropropanol (TFP, 99%, Molekula), dimethylsulfoxide (DMSO, ≥ 99.7%, Sigma Aldrich) and methanol (MeOH, HPLC grade Scharlab) were used as received. *n*-Butyl acrylate (BA, 99%, Sigma Aldrich) was passed through a short column of basic Al_2O_3 prior to use in order to remove the radical inhibitor. EL (ethyl 2-hydroxypropionate, natural >98%, Sigma Aldrich) was passed through a short column of basic Al_2O_3 before to use in order to remove the peroxide residues.[107] Triethylamine (≥ 99% , Scharlab), was distilled

before to use under calcium hydride. Other solvents were purchased from Panreac and used as received except dichloromethane (DCM) that was freshly distilled on calcium hydride. Copper(0) wire 99.9% pure of 20 gauge, purchased from Creating Unkamen, was activated using a deoxygenated solution of hydrazine hydrate in DMSO following a previously reported procedure.[13] Menthyl acrylate (MnA) was synthesized by esterification of the corresponding alcohol with acryloyl chloride in the presence of trimethylamine (TEA) following a reported procedure (Scheme 3.1a).[70]

3.4.2. Methods

400 MHz ^{1}H-NMR spectra were recorded on a Varian VNMR-S400 NMR instrument at 25 °C in $CDCl_3$ with tetramethylsilane as an internal standard. For chain end analysis of low molecular weight polyMnA by ^{1}H-NMR, a delay time (D1) of 10 s and a minimum number of 150 scans (nt) were used. Gel permeation chromatography (GPC) analysis was carried out with an Agilent 1200 series system equipped with three columns (PLgel 3 μm MIXED-E, PLgel 5 μm MIXED-D and PLgel 20 μm) from Polymer Laboratories) and an Agilent 1100 series refractive-index detector. THF (Panreac, HPLC grade) was used as eluents at a flow rate of 1.0 mL/min. The calibration curves for GPC analysis were obtained using PSS ReadyCal PMMA standards. MALDI-TOF analysis was performed on a Voyager DE (Applied Biosystems) instrument with a 337-nm nitrogen laser (3-ns pulse width) using the following parameters in a linear ionization mode: accelerating potential = 25 kV, grid voltage = 93.5% and laser power = 1500 units. The analysis was performed using DCTB as matrix and KTFA as cationization agent. Samples for MALDI-TOF analysis were prepared as follows: THF solutions of DCTB (30 mg/mL), KTFA (10 mg/mL), and polyMnA (10 mg/mL) were prepared separately. The solution for MALDI-TOF analysis was obtained by mixing the matrix, polymer and salt solutions in a 9/1/1 volumetric ratio. Then five 2 μL drops of the mixture were spotted onto a MALDI plate and dried at room temperature before being subjected to analysis. Calorimetric studies were carried out on a Mettler DSC3+ thermal analyzers using N_2 as a purge gas (100 mL/min at scanning rate 20 °C/min in the -80 to 120 °C temperature

range. Calibration was made using an indium standard (heat flow calibration) and an indium-lead-zinc standard (temperature calibration).

3.4.3. General procedure for the SET-LRP of MnA in TFE

A solution of MnA (1 mL, 4.5 mmol), TFE (0.5 mL), Me_6-TREN (10.1 μL, 0.090 mol) and MBP (2.4 μL, 0.0090 mmol) was prepared in a 25 mL Schlenk flask. Then the removal of oxygen was accomplished by applying 4 freeze-pump (~1 min)-thraw cycles. After that, 4.5 cm of hydrazine-activated Cu(0) wire of 20 gauge wrapped around a Teflon-coated stirring bar was loaded under positive argon pressure. An additional freeze-pump (~1 min)-thraw cycle was applied before placing the flask in a water bath thermostated at 25 °C with stirring. To monitor the monomer conversion, the side arm of the tube was purged with argon before it was opened to remove two drops of sample using an airtight syringe. Samples were dissolved in $CDCl_3$ to determine the monomer conversion by ^{1}H NMR spectroscopy. The M_n and M_w/M_n values were determined by GPC with polystyrene standards. Finally, to stop the reaction the Schlenk flask was opened to air and the polymerization mixture was dissolved in 2 mL of CH_2Cl_2. Then, the resulting solution was precipitated twice in 100 mL MeOH with vigorous stirring. Solvent was removed by filtration, and the final glassy white polymer was dried under vacuum until constant weight.

3.4.4. General procedure for the chain-end modification of polyMnA *via* "thio-bromo" click reaction

A solution of polyMnA (0.2 g, M_n^{th} = 4841 g/mol) in acetone (1 mL) was prepared in a 10 mL vial equipped with a rubber septum. Next, thiophenol (12.5 μL, 0,123 mmol) and triethylamine (NEt_3, 17.1 μL, 0,123 mol) were added and the reaction mixture was stirred at room temperature over 5 h. Finally, polyMnA-SPh was isolated by precipitation into 10 mL of MeOH with vigorous stirring and washed twice with fresh solvent. The final polymer was died under vacuum until constant weight before MALDI-TOF analysis.

SET-LRP of the Hydrophobic Biobased (-)-Menthyl Acrylate

3.4.5. General procedure for the *in-situ* chain extension of polyMnA with BA

A solution of the monomer (MnA, 1 mL, 4.5 mmol), solvent (0.5 mL), Me_6-TREN (4.81 μL, 0.018 mmol) and initiator (MBP, 20.10 μL, 0.18 mmol) was prepared in a 25 mL Schlenk tube. The reaction mixture was deoxygenated as described above by 4 freeze-pump (~1 min)-thaw cycles. Hydrazine-activated Cu(0) wire (4.5 cm of 20 gauge wire) wrapped around a Teflon-coated stirring bar was added under positive pressure of argon. After an additional freeze-pump (~1 min)-thaw cycle, the flask was placed in a water bath thermostated at 25 °C with stirring. The SET-LRP was left to proceed for 5 h, and then the monomer conversion was determined by ^{1}H NMR after sampling the reaction with an airtight syringe. Next, a deoxygenated solution containing 2.58 mL BA (0.018 mol) and 4.8 μL Me_6-TREN (0.018 mmol) in 1.3 mL TFE was injected. After 24 h, the conversion of BA was determined and the polymerization mixture was dissolved in 2 mL of CH_2Cl_2 before precipitating the final copolymer in 100 mL MeOH with vigorous stirring. The solvent was decanted off and the final sticky polymer was dried under vacuum until constant weight.

3.5. References

[1] Lligadas, G.; Grama, S.; Percec, V. *Biomacromolecules* **2017**, *18*, 2981-3008.

[2] Anastasaki, A.; Nikolaou, V.; Nurumbetov, G.; Wilson, O.; Kempe, K.; Quinn, J. F.; Davis, T. P.; Whittaker, M. R.; Haddleton, D. M. *Chem. Rev.* **2016**, *116*, 835-877.

[3] Boyer, C.; Corrigan, N. A.; Jung, K.; Nguyen, D.; Nguyen, T. K.; Adnan, N. N.; Oliver, S.; Shanmugam, S.; Yeow, J. *Chem. Rev.* **2016**, *116*, 1803-1949.

[4] Anastasaki, A.; Nikolaou, V.; Haddleton, D. M. *Polym. Chem.* **2016**, *7*, 1002-1026.

[5] Rosen, B. M.; Percec, V. *Chem. Rev.* **2009**, *109*, 5069-5119.

[6] Zhang, N.; Samanta, S. R.; Rosen, B. M.; Percec, V. *Chem. Rev.* **2014**, *114*, 5848-5958.

[7] Lligadas, G.; Grama, S.; Percec, V. *Biomacromolecules* **2017**, *18*, 1039-1063.

[8] Asandei, A. D.; Percec, V. *J. Polym. Sci., Part A: Polym. Chem*. **2001**, *39*, 3392–3418.

[9] Percec, V.; Popov, A. V.; Ramirez-Castillo, E.; Monteiro, M.; Barboiu, B.; Weichold, O.; Asandei, A. D,; Mitchell, C. M. *J. Am. Chem. Soc.* **2002**, *124*, 4940-4941.

[10] Percec, V.; Popov, A. V.; Ramirez-Castillo, E.; Weichold, O. *J. Polym. Sci., Part A: Polym. Chem.* **2003**, *41*, 3283–3299.

[11] Lligadas, G.; Ladislaw, J. S.; Guliashvili, T.; Percec, V. *J. Polym. Sci., Part A: Polym. Chem*. **2008**, *46*, 278–288.

[12] Lligadas, G.; Rosen, B. M.; Bell, C. A.; Monteiro, M. J.; Percec, V. *Macromolecules* **2008**, *41*, 8365-8371.

[13] Nguyen, N. H.; Percec, V. *J. Polym. Sci., Part A: Polym. Chem.* **2010**, *48*, 5109-5119.

[14] Enayati, M.; Jezorek, R. L.; Percec, V. *Polym. Chem.* **2016**, *7*, 4549-4558.

[15] Nguyen, N. H.; Rosen, B. M.; Lligadas, G.; Percec, V. *Macromolecules* **2009**, *42*, 2379-2386.

[16] Jiang, X.; Rosen, B. M.; Percec, V. *J. Polym. Sci., Part A; Polym. Chem.* **2010**, *48*, 2716-2721.

[17] Aksakal, R.; Resmini, M.; Becer, C. R. *Polym. Chem*. **2016**, *7*, 6564-6569.

[18] Dax, D.; Xu, C.; Langvik, O.; Hemming, J.; Backman, P.; Willfor, S. *J. Polym. Sci., Part A: Polym. Chem.* **2013**, *51*, 5100-5110.

[19] Nguyen, N. H.; Rosen, B. M.; Percec, V. *J. Polym. Sci., Part A: Polym. Chem.* **2010**, *48*, 1752–1763.

[20] Zhang, Q.; Wilson, P.; Li, Z.; McHale, R.; Godfrey, J.; Anastasaki, A.; Waldron, C.; Haddleton, D. M. *J. Am. Chem. Soc.* **2013**, *135*, 7355-7363.

[21] Jiang, X.; Rosen, B. M.; Percec, V. *J. Polym. Sci., Part A: Polym Chem.* **2010**, *48*, 403-409.

[22] Sun, F.; Feng, C.; Liu, H.; Huang, X. *Polym. Chem.* **2016**, *7*, 6973-6979.

[23] Cui, Y.; Jiang, X.; Feng, C.; Gu, G.; Xu, J.; Huang, X. *Polym. Chem.* **2016**, *7*, 3156-3164.

[24] Gavrilov, M.; Zerk, T. J.; Bernhardt, P. V.; Percec, V.; Monteiro, M. J. *Polym. Chem.* **2016**, *7*, 933-939.

[25] Gavrilov, M.; Jia, Z.; Percec, V.; Monteiro, M. J. *Polym. Chem.* **2016**, *7*, 4802-4809.

[26] Gawande, M. B.; Goswami, A.; Felpin, F. X.; Asefa, T.; Huang, X.; Silva, R.; Zou, X.; Zboril, R.; Varma, R. S. *Chem. Rev.* **2016**, *116*, 3722-3811.

[27] Nguyen, N. H.; Levere, M. E.; Kulis, J.; Monteiro, M. J.; Percec, V. *Macromolecules* **2012**, *45*, 4606-4622.

[28] Lligadas, G.; Percec, V. *J. Polym. Sci., Part A: Polym. Chem*. **2008**, *46*, 6880-6895.

[29] Levere, M. E.; Nguyen, N. H.; Leng, X.; Percec, V. *Polym. Chem.* **2013**, *4*, 1635-1647.

[30] Nguyen, N. H.; Percec, V. *J. Polym. Sci. A Polym. Chem.* **2011**, *49*, 4227–4240.

[31] Nguyen, N. H.; Rosen, B. M.; Jiang, X.; Fleischmann, S.; Percec, V. *J. Polym. Sci., Part A: Polym. Chem.* **2009**, *47*, 5577–5590.

[32] Jiang, X.; Fleischmann, S.; Nguyen, N. H.; Rosen, B. M.; Percec, V. *J. Polym. Sci., Part A: Polym. Chem*. **2009**, *47*, 5591–5605.

[33] Nguyen, N. H.; Levere, M. E.; Percec, V. *J. Polym. Sci., Part A: Polym. Chem*. **2012**, *50*, 860–873.

[34] Nguyen, N. H.; Kulis, J.; Sun, H. J.; Jia, Z.; van Beusekom, B.; Levere, M. E.; Wilson, D. A.; Monteiro, M. J.; Percec, V. *Polym. Chem.* **2013**, *4*, 144-155.

[35] Rosen, B. M.; Percec, V. *J. Polym. Sci., Part A: Polym. Chem.* **2007**, *45*, 4950-4964.

[36] Rosen, B. M.; Jiang, X.; Wilson, C. J.; Nguyen, N. H.; Monteiro, M. J.; Percec, V. *J. Polym. Sci., Part A: Polym. Chem.* **2009**, *47*, 5606-5628.

[37] Waldron, C.; Anastasaki, A.; McHale, R.; Wilson, P.; Li, Z.; Smith, T.; Haddleton, D. M. *Polym. Chem.* **2014**, *5*, 892-898.

[38] Samanta, S. R.; Levere, M. E.; Percec, V. *Polym. Chem*. **2013**, *4*, 3212-3224.

[39] Anastasaki, A.; Waldron, C.; Nikolaou, V.; Wilson, P.; McHale, R.; Smith, T.; Haddleton, D. M. *Polym. Chem.* **2013**, *4*, 4113-4119.

[40] Bertrand, O.; Wilson, P.; Burns, J. A.; Bell, G. A.; Haddleton, D. M. *Polym. Chem.* **2015**, *6*, 8319-8324.

[41] Boyer, C.; Atme, A.; Waldron, C.; Anastasaki, A.; Wilson, P.; Zetterlund, P. B.; Haddleton, D. M.; Whittaker, M. R. *Polym. Chem.* **2013**, *4*, 106-112.

[42] Percec, V.; Guliashvili, T.; Ladislaw, J. S.; Wistrand, A.; Stjerndahl, A.; Sienkowska, M. J.; Monteiro, M. J.; Sahoo, S. *J. Am. Chem. Soc.* **2006**, *128*, 14156-14165.

[43] Lligadas, G.; Percec, V. *J. Polym. Sci., Part A: Polym. Chem.* **2007**, *45*, 4684-4695.

[44] Enayati, M.; Smail, R. B.; Grama, S.; Jezorek, R. L.; Monteiro, M. J.; Percec, V. *Polym. Chem*. **2016**, *7*, 7230-7241.

[45] Smail, R. B.; Jezorek, R. L.; Lejnieks, J.; Enayati, M.; Grama, S.; Monteiro, M. J.; Percec, V. *Polym. Chem.* **2017**, *8*, 3102-3123.

[46] Jezorek, R. L.; Enayati, M.; Smail, R. B.; Lejnieks, J.; Grama, S.; Monteiro, M. J.; Percec, V. *Polym. Chem.* **2017**, ***8,*** 3405-3424.

[47] Enayati, M.; Jezorek, R. L.; Monteiro, M. J.; Percec, V. *Polym. Chem*. **2016**, *7*, 5930-5942.

[48] Grama, S.; Lejnieks, J.; Enayati, M.; Smail, R. B.; Ding, L.; Lligadas, G.; Monteiro, M. J.; Percec, V. *Polym. Chem*. **2017**, *8*, 5865-5874.

[49] Moreno, A.; Grama, S.; Liu, T.; Galià, M.; Lligadas, G.; Percec, V. *Polym. Chem.* **2017**, *8*, 7559-7574.

[50] Enayati, M.; Jezorek, R. L.; Monteiro, M. J.; Percec, V. *Polym. Chem*. **2016**, *7*, 3608-3621.

[51] Zhu, Y.; Romain, C.; Williams, C. K. *Nature* **2016**, *540*, 354-362.

[52] Schneiderman, D. H.; Hillmyer, M. A. *Macromolecules* **2017**, *50*, 3733-3749.

[53] Yilmaz, G.; Messager, L.; Gleinich, A. S.; Mitchell, D. A.; Battaglia, G.; Becer, C. R. *Polym. Chem.* **2016**, *7*, 6293-6296.

[54] Zhang, Q.; Anastasaki, A.; Li, G. Z.; Haddleton, A. J.; Wilson, P.; Haddleton, D. M. *Polym. Chem.* **2014**, *5*, 3876-3883.

[55] Zhang, Q.; Collins, J.; Anastasaki, A.; Wallis, R.; Mitchell, D. A.; Becer, C. R.; Haddleton, D. M. *Angew. Chem. Int. Ed.* **2013**, *52*, 4435-4439.

[56] Voepel, J.; Edlund, U.; Albertsson, A. C.; Percec, V. *Biomacromolecules* **2011**, *12*, 253-259.

[57] Edlund, U.; Albertsson, A. C. *J. Polym. Sci., Part A: Polym. Chem*. **2012**, *50*, 2650-2658.

[58] Jones, W. J.; Gibson, M. I.; Mantovani, G.; Haddleton, D. M. *Polym. Chem*. **2011**, *2*, 572-574.

[59] Collins, J.; Tanaka, J.; Wilson, P.; Kempe, K.; Davis, T. P.; McIntosh, M. P.; Whittaker, M. R.; Haddleton, D. M. *Bioconjugate Chem*. **2015**, *26*, 633-638.

[60] Wilson, P.; Anastasaki, A.; Owen, M. R.; Kempe, K.; Haddleton, D. M.; Mann, S. K.; Johnston, A. P. R.; Quinn, J. F.; Whittaker, M. R.; Hogg, P. J.; Davis, T. P. *J. Am. Chem. Soc.* **2015**, *132*, 4215-4222.

[61] Wilbon, P. A.; Chu, F.; Tang, C. *Macromol. Rapid Commun*. **2013**, *34*, 8-37.

[62] Lligadas, G.; Percec, V. *J. Polym. Sci., Part A: Polym. Chem.* **2008**, *46*, 2745–2754.

[63] Whitfield, R.; Anastasaki, A.; Nikolaou, V.; Jones, G. R.; Engelis, N. G.; Discekici, E. H.; Fleischmann, C.; Willenbacher, J.; Hawker, C. J.; Haddleton, D. M. *J. Am. Chem. Soc.* **2017**, *131*, 1003-1010.

[64] Moreno, A.; Garcia, D.; Galià, M.; Ronda, J. C.; Cádiz, V.; Lligadas, G.; Percec, V. *Biomacromolecules*, **2017**, *18*, 3447-3456.

[65] Samanta, S. R.; Anastasaki, A.; Waldron, C.; Haddleton, D. M.; Percec, V. *Polym. Chem.,* **2013**, *4*, 5563-5569.

[66] Samanta, S. R.; Cai, R.; Percec V. *Polym. Chem.,* **2014**, *5*, 5479-5491.

[67] Samanta, S. R.; Percec, V. *Polym. Chem.* **2014**, *5*, 169-174.

[68] Samanta, S. R.; Sun, H. J.; Anastasaki, A.; Haddleton, D. M.; Percec, V. *Polym. Chem.,* **2014**, *5*, 89-95.

[69] Samanta, S. R.; Anastasaki, A.; Waldron, C.; Haddleton, D. M.; Percec, V. *Polym. Chem*. **2013**, *4*, 5555-5562.

[70] Baek, S. S.; Hwang, S. H. *Polym. Bull.* **2016**, *73*, 687-701.

[71] Samanta, S. R.; Anastasaki, A.; Waldron, C.; Haddleton, D. M.; Percec, V. *Polym. Chem*. **2013**, *4*, 5555-5562.

[72] Bolton, J. M.; Hillmyer, M. A.; Hoye, T. R. *ACS Macro Lett*. **2014**, *3*, 717-720.

[73] Satoh, K.; Lee, D. H.; Nagai, K.; Kamigaito, M. *Macromol. Rapid Commun.* **2014**, *35*, 161-167.

[74] Chatterjee, D. P.; Mandal, B. M. *Macromolecules* **2006**, *39*, 9192-9200.

[75] Liu, S.; Zhang, X.; Li, M.; Ren, X.; Tao, Y. *J. Polym. Sci., Part A: Polym. Chem.* **2017***, 55*, 349-355.

[76] Olsén, P.; Borke, T.; Odelius, K.; Albertsson, A. C. *Biomacromolecules* **2013**, *14*, 2883-2890.

[77] Ding, K.; John, A.; Shin, J.; Lee, Y.; Quinn, T.; Tolman, W. B.; Hillmyer, M. A. *Biomacromolecules* **2015**, *16*, 2537-2539.

[78] Shin, J.; Lee, Y.; Tolman, W. B.; Hillmyer, M. A. *Biomacromolecules* **2012**, *13*, 3833-3840.

[79] Martello, M. T.; Schneiderman, D. K.; Hillmyer, M. A. *ACS Sustainable Chem. Eng.* **2014**, *2*, 2519-2526.

[80] Nguyen, N. H.; Rodriguez-Emmenegger, C.; Brynda, E.; Sedlakova, Z.; Percec, V. *Polym. Chem*. **2013**, *4*, 2424-2427.

[81] Leng, X.; Nguyen, N. H.; van Beusekom, B.; Wilson, D. A.; Percec, V. *Polym. Chem.* **2013**, *4*, 2995-3004.

[82] Samanta, S. R.; Cai, R.; Percec, V. *J. Polym. Sci., Part A: Polym. Chem.* **2015**, *53*, 294–303.

[83] Rosen, B. M.; Lligadas, G.; Hahn, C.; Percec, V. *J. Polym. Sci., Part A: Polym. Chem.* **2009**, *47*, 3931-3939.

[84] Rosen, B. M.; Lligadas, G.; Hahn, C.; Percec, V. *J. Polym. Sci., Part A: Polym. Chem.* **2009**, *47*, 3940-3948.

[85] Sainz, M. F.; Souto, J. A.; Regentova, D.; Johansson, M. K. G.; Timhagen, S. T.; Irvine, D. J.; Buijsen, P.; Koning, C. E.; Stockman, R. A.; Howdle, S. M. *Polym. Chem.* **2016**, *7*, 2882-2887.

[86] Thomsett, M. R.; Storr, T. E.; Monaghan, O. R.; Stockman, R. A.; Howdle, S. M. *Green Mater.* **2016**, *4*, 115-134.

[87] Wilbon, P. A.; Chu, F.; Tang, C. *Macromol. Rapid Commun*. **2013**, *34*, 8-37.

[88] Satoh, K. *Polym. J.* **2015**, *47*, 527-536.

[89] Turos, E.; Mahzamani, F. S.; Bachman, A. B.; Flore, K. L. *US Patent* US 2017/9,533,051-B2, **2017**.

[90] Gries, K.; Bubel, K.; Wohlfahrt, M.; Agarwal, S.; Koert, U.; Greiner, A. *Macromol. Chem. Phys.* **2011**, *212*, 2551−2557.

[91] Liu, S.; Mishra, M. K. *Macromolecules* **2007**, *40*, 867-871.

[92] Nguyen, N. H.; Leng, X.; Sun, H. J.; Percec, V. *J. Polym. Sci., Part A: Polym. Chem.* **2013**, *51*, 3110-3122.

[93] Fleischmann, S.; Rosen, B. M.; Percec, V. *J. Polym. Sci., Part A: Polym. Chem.* **2010**, *48*, 1190–1196.

[94] Nguyen, N. H.; Percec, V. *J. Polym. Sci., Part A: Polym. Chem.* **2011**, *49*, 4756-4765.

[95] Fleischmann, S.; Percec, V. *J. Polym. Sci., Part A: Polym. Chem.* **2010**, *48*, 2243-2250.

[96] Lligadas, G.; Enayati, M.; Grama, S.; Smail, R.; Sherman, S. E.; Percec, V. *Biomacromolecules* **2017**, *18*, 2610-2622.

[97] Hatano, T.; Rosen, B. M.; Percec, V. *J. Polym. Sci., Part A: Polym. Chem.* **2010**, *48*, 164–172.

[98] Nyström, F.; Soeriyadi, A. H.; Boyer, C.; Zetterlund, P. B.; Whittaker, M. R. *J. Polym. Sci., Part A: Polym. Chem.* **2011**, *49*, 5313-5321.

[99] Moreno, A.; Liu, T.; Ding, L.; Buzzachera, I.; Galia, M.; Möller, M.; Wilson, C. J.; Lligadas, G.; Percec, V. *Chem.* **2017**, *8*, 7559-7574.

[100] Lin, J. P.; Lu, H. F.; Lee, J. H.; Lin, J. G.; Hsia, T. C.; Wu, L. T.; Chung, J. G. *Anticancer Res.* **2005**, *25* , 2069-2074.

[101] Li, Q.; Wang, X.; Yang, Z.; Wang, B.; Li, S. *Oncology* **2009**, *77*, 335-341.

[102] Nazıroğlu, M.; Blum, W.; Josvay, K.; Çiğ, B.; Henzi, T.; Oláh, Z.; Vizler, C.; Schwaller, B.; Pecze, L. *Redox Biol.* **2018**, *14*, 439-449.

[103] Peier, A. M.; Moqrich, A.; Hergarden, A. C.; Reeve, A. J.; Andersson, D. A.; Story, G. M.; Earley, T. J.; Dragoni, I.; McIntyre, P.; Bevan, S.; Patapoutian, A. *Cell* **2002**, *108*, 705-715.

[104] Parashar, G.; Parashar, N. C.; Capalash, N. *Asian Pac. J. Cancer Prev*. **2017**, *18*, 1365–1370.

[105] Uyar, T.; Nur, Y.; Hacaloglu, J.; Besenbacher, F. *Nanotechnology* **2009**, *20*, 125703-125712.

[106] Percec, V.; Imamm, M. R.; Peterca, M.; Wilson, D. A.; Graf, R.; Spiess, H. W.; Balagurusamy, V. S. K.; Heiney, P. A. *J. Am. Chem. Soc.* **2009**, *131*, 7662-7677.

[107] Muse Jr, J.; Colvin, H. A. *US Patent* US 2005/0287179-A1, 2005.

Chapter 4

Mixed-Ligand Effect During Cu(0)-mediated SET-LRP :

4.1. Replacing Cu(II)Br_2 with Me_6-TREN in biphasic Cu(0)/TREN catalyzed SET-LRP reveals the mixed-ligand effect

4.2. Me_6-TREN/TREN mixed-ligand effect during SET-LRP in the catalytically active DMSO revitalizes TREN into an excellent ligand

The contents of this chapter are published in: Feng, X.; Maurya, D. S.; Bensabeh, N.; Moreno, A.; Oh, T.; Luo, Y.; Lejnieks, J.; Galià, M.; Miura, Y.; Monteiro, M. J.; Lligadas, G.; Percec, V. *Biomacromolecules* **2020**, *21*, 250-261; Maurya, D. S.; Malik, A.; Feng, X.; Bensabeh, N.; Lligadas, G. and Percec, V. *Biomacromolecules* **2020**, *21*, 1902-1919.

4.1. Replacing Cu(II)Br_2 with Me_6-TREN in biphasic Cu(0)/TREN catalyzed SET-LRP reveals the mixed-ligand effect

The mixed-ligand system consisting of tris(2-aminoethyl)amine (TREN) and tris(2-dimethylaminoethyl)amine (Me_6-TREN) during the Cu(0) wire-catalyzed single electron transfer-living radical polymerization (SET-LRP) of methyl acrylate (MA) in "programmed" biphasic mixtures of the dipolar aprotic solvents NMP, DMF, and DMAc with H_2O is reported. Kinetic and chain end analysis studies by NMR and MALDI-TOF before and after thio-bromo "click" reaction demonstrated that Me_6-TREN complements and makes the less expensive TREN a very efficient ligand in the absence of externally added Cu(II)Br_2. Statistical analysis of the kinetic data together with control experiments demonstrated that this mixed-ligand effect enhanced the apparent rate constant of propagation, monomer conversion, and molecular weight control. The most efficient effect was observed at a 1/1 molar ratio between these two ligands, suggesting that in addition to a fast exchange between the two ligands, a new single dynamic ligand generated by hydrogen bonding may be responsible for the mixed ligand effects observed.

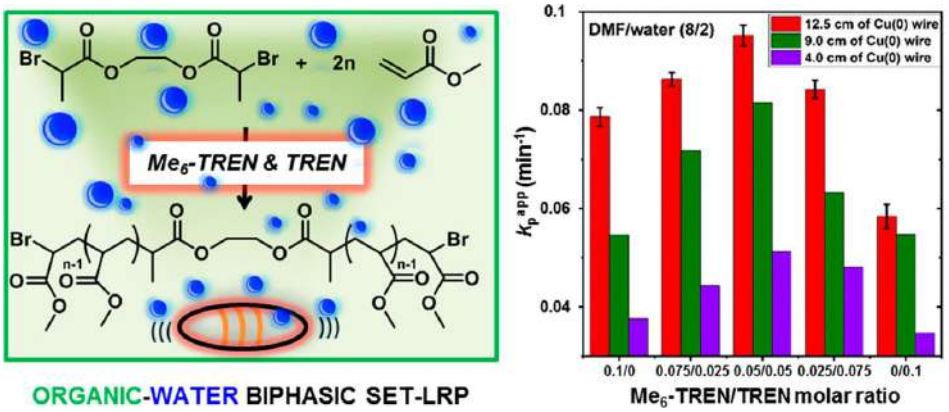

Mixed-Ligand Effect During Cu(0)-mediated SET-LRP

4.1.1. Introduction

The concept of mixed-ligand systems emerged as an efficient and simple methodology to obtain superior catalytic activity in transition-metal-catalyzed enantioselective reactions.[1] Nearly at the same time, Feringa's laboratory reported that hetero-combinations of chiral monodentate ligands were more effective than homo-combinations for Rh-catalyzed C–C cross-coupling reactions.[2] This concept was also employed for Pd-catalyzed C-N[3,4] and C-S[5] cross-coupling reactions as well as for Ni-catalyzed Suzuki-type cross-coupling and borylation reactions.[6] However, the benefits of using mixed-ligand catalysts have only been noted so far in few metal-catalyzed polymerization experiments.[7-9]

The use of an appropriate solvent/N-ligand combination is important in Cu(0)-mediated single electron transfer-living radical polymerization (SET-LRP),[10-17] since it can either promote or disfavor the mechanistically fundamental disproportionation reaction of Cu(I)X into Cu(0) atomic species and Cu(II)X_2.[18,19] Tris(2-dimethylaminoethyl)amine (Me_6-TREN) is frequently employed as ligand in SET-LRP,[10,11,14] because it favors the disproportionation process by preferentially binding Cu(II)X_2 rather than Cu(I)X.[20] However, the use of its precursor, tris(2-aminoethyl)amine (TREN),[11,21-23] which is about 80 times less expensive, and poly(ethylene imine) (PEI)[10] also proved successful for the polymerization of vinyl chloride (VC) during the first days of SET-LRP. Likewise, TREN[24-26] and *N,N,N′,N″,N*′-pentamethyldiethylenetriamine (PMDETA)[10,27,28] are also alternative ligands to Me_6-TREN for the Cu(0) wire-catalyzed SET-LRP of acrylates and methacrylates in homogeneous SET-LRP.

Unfortunately, the replacement of Me_6-TREN with TREN was not so successful in aqueous-organic "programmed" biphasic systems using Cu(0) wire catalyst,[29,30-33] although is very efficient in single phase SET-LRP experiments. In biphasic organic solvent-water systems, the external addition of Cu(II)Br_2 was necessary to complement the performance of TREN and retain living character. In this complex system, SET-LRP is an interfacial process in which disproportionation and activation events take place independently in the aqueous and

organic compartments, respectively, whereas the "self-controlled" reversible deactivation occurs at the interface.[34] The Cu(0)-mediated polymerization in "programmed" bi(multi)phasic mixtures of organic solvents with water has been proven to be valuable in various organic solvents regardless of their ability to mediate or not disproportionation of Cu(I)X/N-ligand.[35-39] Thus, this designed biphasic organic solvent-H_2O programmed biphasic systems resolved the incompatibility of SET-LRP with polar non-disproportionating solvents and non-polar non-disproportionating solvents, thus expanding the library of accessible solvents.

In this chapter, we report that replacing Cu(II)Br_2 additive with Me_6-TREN in "programmed" biphasic Cu(0)-mediated SET-LRP using TREN revealed a mixed-ligand effect which increased the rate of polymerization, monomer conversion and molecular weight control. This preliminary study demonstrates the systematic occurrence of this unexpected synergic effect between Me_6-TREN and TREN during the nonactivated Cu(0) wire-mediated SET-LRP of MA in various "programmed" biphasic systems based on mixtures of NMP, DMF, and DMAc with H_2O. The experiments reported here demonstrate for the first time the superior activity of mixed-ligand systems of these two N-ligands that are widely used independently in SET-LRP.

4.1.2. Results and discussion

The mixed-ligand effect during the biphasic SET-LRP of MA in NMP-water mixture using Me_6-TREN and TREN as ligands

To the best of our knowledge, the use of mixed-ligand systems of Me_6-TREN and TREN was not employed before in SET-LRP or any other metal-catalyzed LRP technique. Hence, in the first series of experiments reported here we sought to investigate their performance by mediating the "programmed" biphasic SET-LRP of MA in NMP-water mixtures (8/2, v/v). This dipolar aprotic solvent is not one of the most efficient SET-LRP solvents in homogeneous solution,[40] but becomes excellent in biphasic systems with water.[29,39] The chemical structure

of both ligands and a schematic illustration for the Cu(0) wire-catalyzed SET-LRP of MA initiated from the bifunctional initiator bis(2-bromopropnionyl)ethane (BPE) are depicted in Scheme 4.1.1. Triplicate kinetic experiments were performed under the following reaction conditions: $[MA]_0/[BPE]_0/[L]_0$ = 222/1/0.1 using 9.0 cm of nonactivated Cu(0) wire. The molar ratio between Me_6-TREN and TREN was varied from 1:0 to 0:1 while maintaining the total amount of ligand, relative to initiator, constant at 10 mol%.

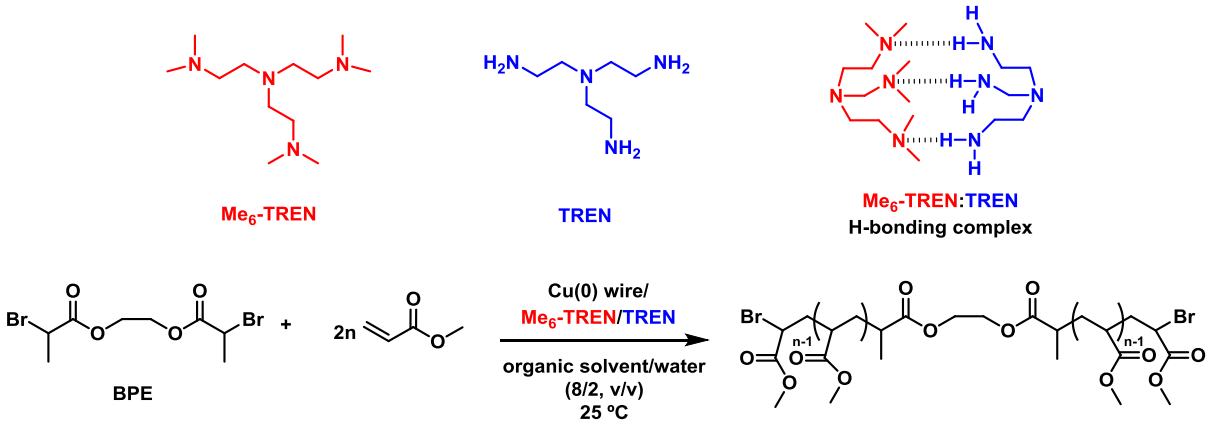

Scheme 4.1.1. Biphasic SET-LRP of MA initiated from BPE and catalyzed with nonactivated Cu(0) wire using various molar combinations of Me_6-TREN and TREN. Organic solvents investigated herein are NMP, DMF, and DMAc.

Interestingly, any of the tested mixed ligand compositions provided higher k_p^{app} values than those obtained in the control experiments performed in the presence of either Me_6-TREN or TREN (Figure 4.1.1 and 4.1.2a). For example, the replacement of 2.5 mol% of Me_6-TREN with TREN increased the k_p^{app} from 0.068 min^{-1} (Figure 4.1.1a) to 0.078 min^{-1} (Figure 4.1.1b), while retaining first-order kinetics. Similar trends were observed using the inverse ligand composition (Figure 4.1.1d). Moreover, in both cases a slight increase in monomer conversion was also noted (Figure S1a in Annex D). Nevertheless, the superior catalytic activity was observed wherein 1:1 molar combinations of both ligands.

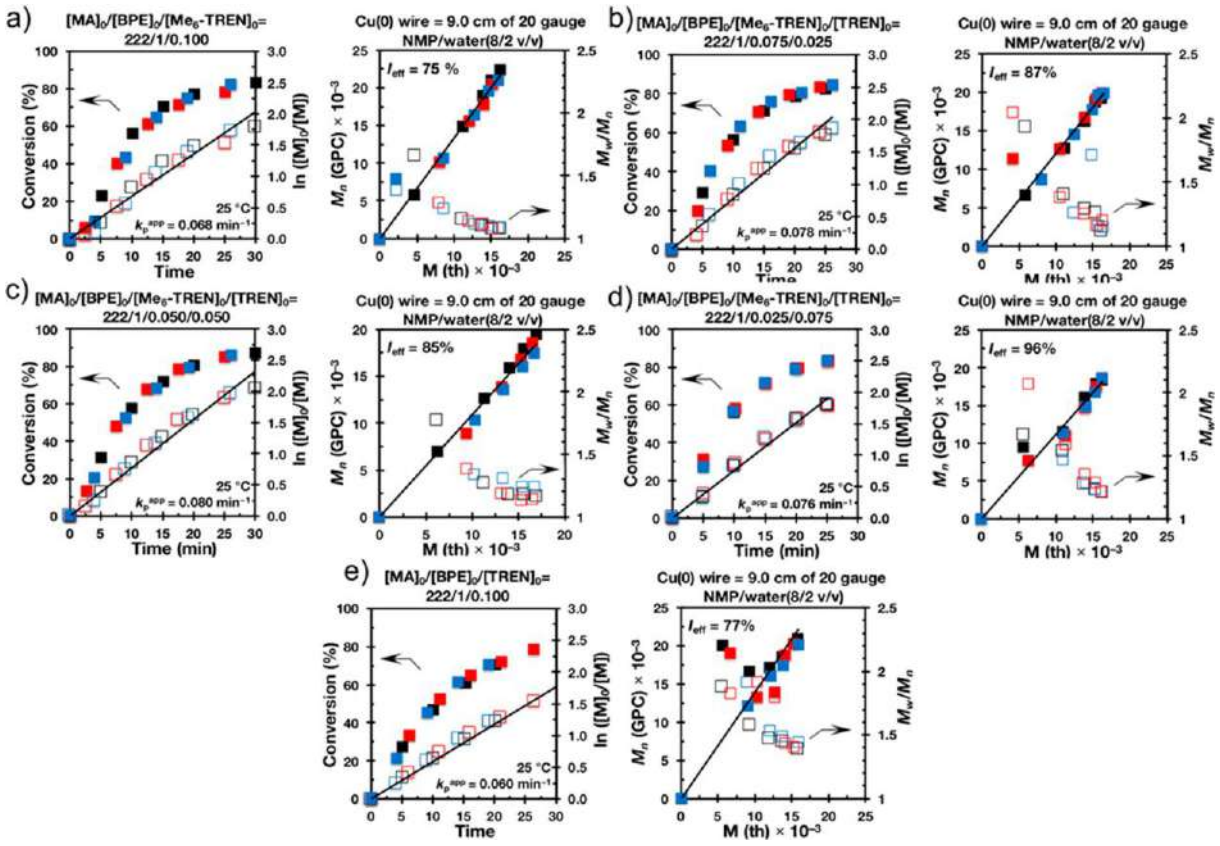

Figure 4.1.1. Kinetic plots, molecular weight, and polydispersity evolution for the SET-LRP of MA in NMP/water mixture (8/2, v/v) initiated with BPE and catalyzed by the 9.0 cm nonactivated Cu(0) wire at 25 °C. Experimental data in different colors were obtained from different kinetics experiments sometimes performed by different researches. k_p^{app} and I_{eff} are the average values of three experiments. Reaction conditions: MA = 1 mL, NMP = 0.4 mL, water = 0.1 mL, $[MA]_0/[BPE]_0/[L]_0$ = 222/1/0.1.

Under these conditions, the SET-LRP of MA proceeded approximately 1.2 and 1.3-fold faster than control experiments with Me_6-TREN and TREN, respectively.

This particular mixed-ligand system also enabled the highest monomer conversion (Figure S1a in Annex D). In addition, the synergic effect between both ligands also improved the control over molecular weight distribution attained by SET-LRP.

Mixed-Ligand Effect During Cu(0)-mediated SET-LRP

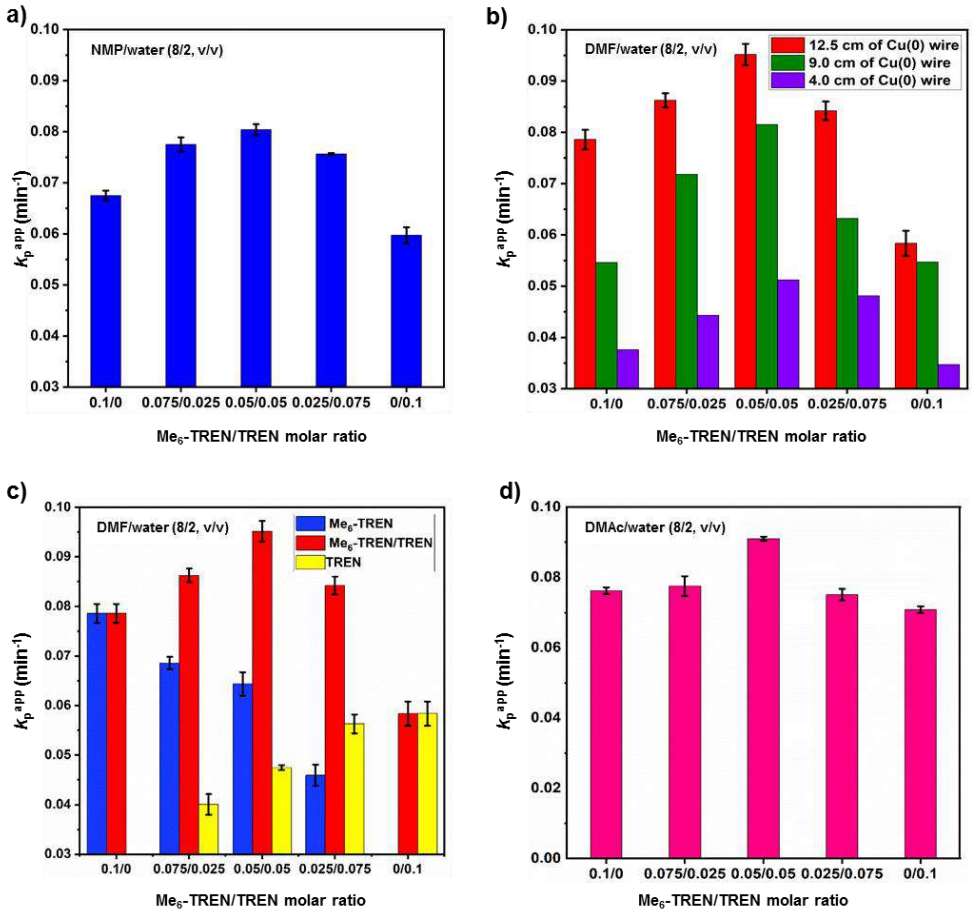

Figure 4.1.2. Evolution of k_p^{app} for the SET-LRP of MA initiated with BPE in various "programmed" biphasic reaction mixtures at 25 °C. (a) NMP/water mixture (8/2, v/v) using 9.0 cm nonactivated Cu(0) wire as catalyst. (b) DMF/water mixture (8/2, v/v) using 12.5 cm, 9.0 cm, and 4.0 cm of nonactivated Cu(0) wire as catalyst. (c) DMF/water mixture (8/2, v/v) using 9.0 cm of nonactivated Cu(0) wire as catalyst, and (d) DMAc/water mixture (8/2, v/v) using 9.0 cm of nonactivated Cu(0) wire as catalyst. Reaction conditions: MA = 1 mL, organic solvent = 0.4 mL, water = 0.1 mL, and $[MA]_0/[BPE]_0/[L]_0$ = 222/1/0.1 (a,b, and d) $[MA]_0/[BPE]_0/[L]_0$ = 222/1/0.1-0.0 (c).

Representative GPC data shown in Figure 4.1.3 illustrate the evolution of molecular weight as a function of conversion during these experiments. GPC chromatograms revealed monomodal polymer peak distributions shifting to higher molecular weight while increasing conversion. However, significantly higher than expected M_n^{GPC} values were obtained at low conversion for the control experiment using TREN without Me_6-TREN (Figure 4.1.3e). Accordingly, using the 0:1 molar combination of ligands a nonlinear evolution of molecular

weight was detected during the early stages of the polymerization (right panel of Figure 4.1.1e). Likewise, the broadest PMA at ultimate monomer conversion was obtained under these conditions (M_w/M_n=1.39 at 81% conversion). In previous publications, the addition of Cu(II)Br_2 additive was used to significantly improve molecular weight control under these conditions.[29-33] In this case, GPC analysis revealed that Me_6-TREN was complementary and made TREN a very efficient ligand without using the externally added Cu(II)Br_2. As can be seen in Figure S1a in Annex D, replacing only 2.5 mol% of TREN with Me_6-TREN improved significantly the molecular weight distribution evolution throughout polymerization (compare panels e and d of Figure 4.1.1). As expected, increasing further the amount of hexamethylated ligand resulted in a better-defined polymer (Figure S1a in Annex D).

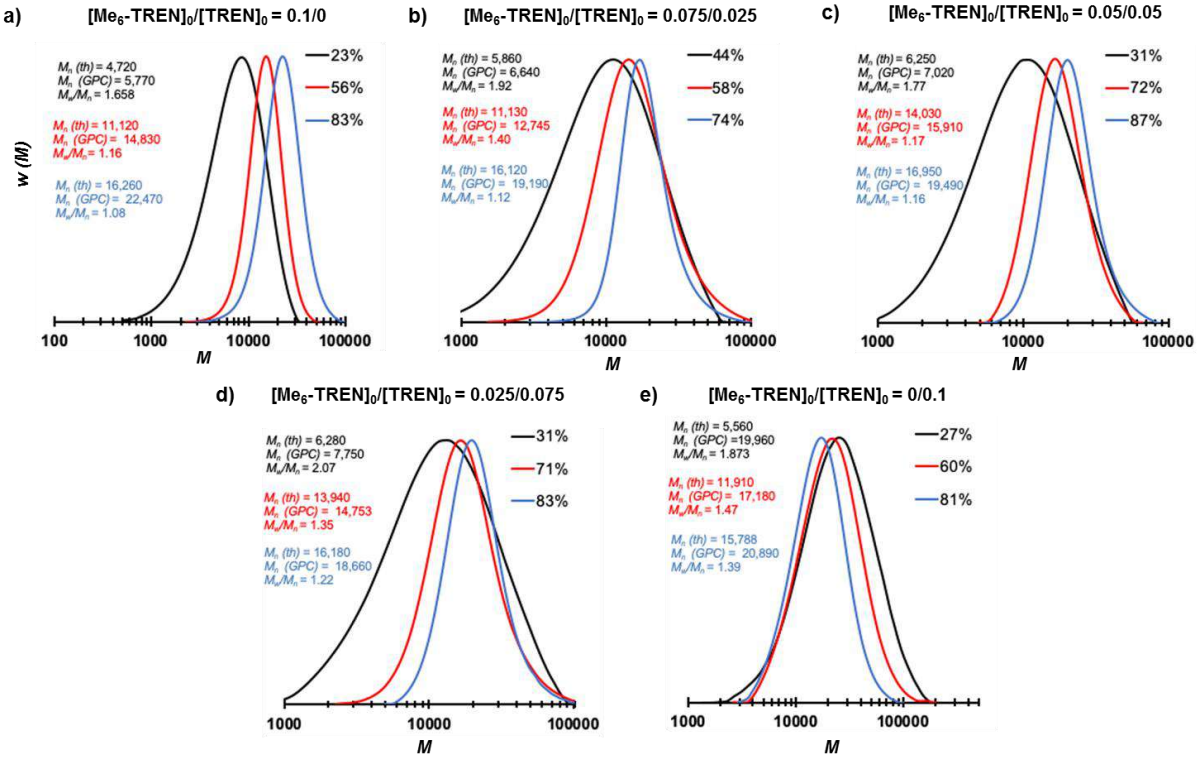

Figure 4.1.3. Representative GPC traces of the evolution of molecular weight as a function of conversion for the SET-LRP of MA in a mixture of NMP/water (8/2, v/v) and catalyzed by the 9.0 cm nonactivated Cu(0) wire at 25 °C in the presence of various ligand compositions. Reaction conditions: MA = 1 mL, NMP = 0.4 mL, water = 0.1 mL, $[MA]_0/[BPE]_0/[L]_0$ = 222/1/0.1.

Note that the average M_w/M_n was below 1.2 using the equimolar combination of ligands. Meanwhile, whereas initiator efficiency (I_{eff}) was around 75% for both control experiments, the use of mixed-ligand systems enhanced significantly this value. Again, the most important effect was observed at 1:1 molar ratio between ligands. In this case, the I_{eff} was determined to be above 90%. Overall, these results demonstrate that the mixed-ligand catalytic system consisting of nonactivated Cu(0) wire and Me_6-TREN/TREN is an effective catalyst for the SET-LRP of MA under biphasic reaction conditions.

The mixed-ligand effect during the biphasic SET-LRP of MA in DMF-water mixture using Me_6-TREN and TREN as ligands and various Cu(0) wire lengths

The accuracy of the trend disclosed above was tested with an additional set of control experiments using different Cu(0) wire lengths in a DMF-water mixture (8/2, v/v). Thus, the SET-LRP of MA was investigated using wire lengths of 12.5 cm, 9.0 cm, and 4.0 cm while maintaining the rest of the polymerization conditions unchanged. Figures S2-4 in Annex D show the corresponding kinetic plots and evolution of experimental M_n and M_w/M_n versus theoretical M_{th}. Kinetic experiments using 9.0 cm of nonactivated Cu(0) wire showed the same trend (Figure 4.1.2b, green columns) as in the case of Figure 4.1.2a. The biphasic SET-LRP of MA in a DMF/water (8/2, v/v) mixture was faster using mixed-ligand systems. However, again, the highest k_p^{app} and I_{eff} values were observed at 1:1 molar ratio of Me_6-TREN and TREN. Under these conditions, SET-LRP was approximately 1.5-fold faster than the control experiment with either Me_6-TREN or TREN. Indeed, monomer conversion was also slightly improved when the mixed-ligand systems 0.075/0.025 (87%) and 0.05/0.05 (85%) were used. Mixed-ligand effects were also noted for the polymerization using 12.5 cm and 4.0 cm of Cu(0) wire. Previous reports demonstrated that SET-LRP catalysts utilize a surface-mediated activation.[41,42] Accordingly, the use of 12.5 cm of Cu(0) wire provided the faster series of polymerizations whereas with the shortest wire length reactions were slower (Figure 4.1.2b, red and purple columns, respectively). For example, at the 1:1 molar ratio between ligands the k_p^{app} values decreases as follows, 0.095 min^{-1} (12.5 cm), 0.082 min^{-1}

(9.0 cm), and 0.052 min^{-1} (4.0 cm). Nevertheless, the evolution k_p^{app} values as a function of ligand ratio reiterates again the benefit of employing a combination of both ligands. These results suggest the existence of an optimum molar ratio between ligands. Accordingly, both monomer conversion and I_{eff} also showed higher values in the mixed-ligand systems for the polymerization using 4.0 cm of Cu(0) wire. However, the highest amount of catalyst did not provide a clear trend (compare Figure S1b,c with S1d in Annex D).

An additional set of control experiments were performed to highlight the occurrence of fast exchange between the two ligands at all compositions (Figure 4.1.2c). The SET-LRP of MA was investigated using decreasing ligand loading using either Me_6-TREN or TREN and no coligand. The corresponding kinetic plots are shown in Figure S5 in Annex D, panels a-c (Me_6-TREN) and Figure S5 in Annex D, panels d-f (TREN). The control experiments from Figure 4.1.2c demonstrate both for the case of TREN (yellow colored experiments) and of Me_6-TREN (blue colored experiments) a continuous decrease of the rate of polymerization as the concentration of the ligand decreases. These experiments contrast the experiments in which mixed-ligand with identical compositions as the single ligands are used (see red colored experiments). In these series of experiments an increase in rate is obtained as the ration between the two ligands tends to approach the 1/1 ratio. This trend demonstrates the mixed-ligand effect. The fact that the most important effects have been systematically observed at 1/1 molar ratio suggests that in addition to a fast exchange between the two ligands, a new single dynamic ligand generated by H-bonding should be considered in future mechanistic investigations (Scheme 4.1.1). The interaction between both ligands was confirmed by ^{1}H NMR analysis of their equimolar mixture prepared in DMF-d_7. Figure 4.1.4 shows that signal corresponding to amine protons of TREN shifts downfield (0.15 ppm) and becomes broader in the presence of Me_6-TREN suggesting the formation of a more rigid complex than TREN or Me_6-TREN.

Mixed-Ligand Effect During Cu(0)-mediated SET-LRP

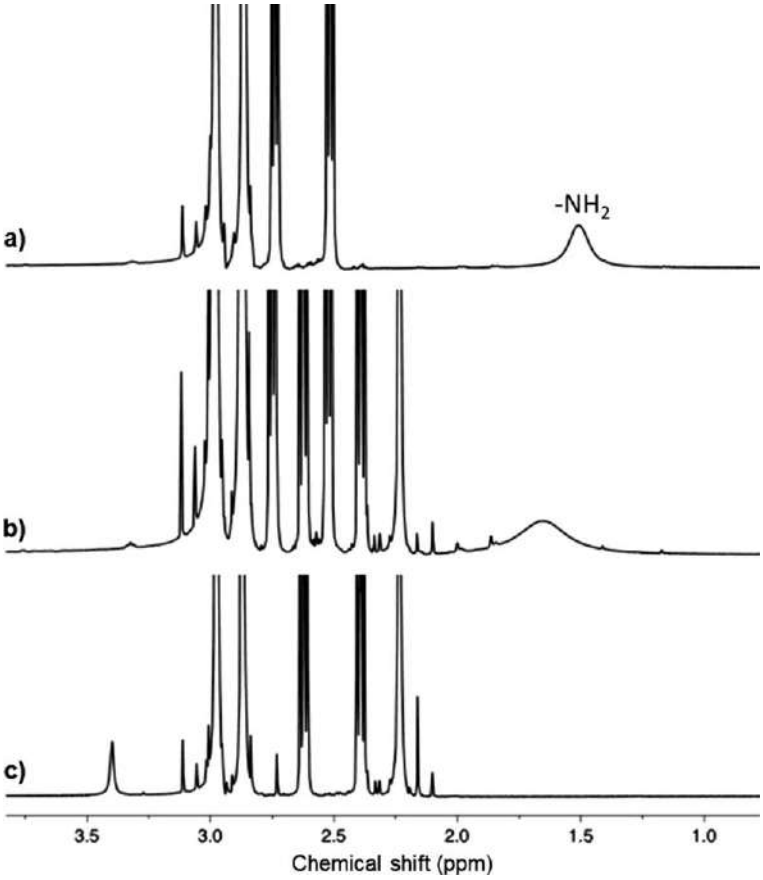

Figure 4.1.4. ^{1}H NMR spectra at 400 MHz of (a) TREN, (b) 1:1 molar ratio mixture of TREN and Me_6-TREN, and (c) Me_6-TREN in DMF-d_7 at 25 °C.

The mixed-ligand effect during the biphasic SET-LRP of MA in DMAc-water mixture using Me_6-TREN and TREN as ligands

In the last series of kinetics we examined the solvent screening with a DMAc-water mixture also at 8/2 (v/v). The SET-LRP of MA was investigated using only 9.0 cm of nonactivated Cu(0) wire. In this case, all the tested compositions showed two first-order kinetic regimes with a slower second domain (Figure S6 in Annex D). The same behavior was previously observed during the homogeneous SET-LRP of MA in DMAc with lower loadings of water.[40] On the basis of previous reports, this result may be attributed to rapid activation combined with insufficient disproportionation, which favors bimolecular termination events

between growing chains. Nevertheless, even under these conditions, the 1:1 molar ratio of Me_6-TREN and TREN provided the fastest polymerization (Figure 4.1.2d). Moreover, I_{eff} values also were higher for mixed-ligand systems but not clear trend was observed on monomer conversion (Figure S1e in Annex D). As in all previously tested systems, with the transition from TREN to Me_6-TREN the resulting PMA showed narrower molecular weight distribution.

Visualization of the reaction mixtures at the end of the polymerization: how biphasic SET-LRP takes place?

NMP, DMF and DMAc are dipolar aprotic solvents miscible with water. However, irrespective of the ligand or mixture of ligands used, the SET-LRP of MA in aqueous mixtures of these solvents containing 20% water proceeds under biphasic reaction conditions as can be seen in the series of digital images recorded at the end of the polymerizations (Figure 4.1.5).

Note that these biphasic reaction mixtures are "programmed" by the partition of the Cu(I)Br/mixed-ligand generated during the activation step in the organic phase, to the water phase, where it disproportionates into atomic Cu(0) and Cu(II)Br_2. Under these conditions, dissociation of I-X and P_n-X is achieved in the organic phase through a heterolytic outer-sphere SET-process wherein the outer sphere electron donor Cu(0) transfer an electron to I-X/P_n-X resulting, depending of the structure of the initiator, in a radical anion $[P_n/P\text{-}X]^{\bullet -}$, which degrades in a step-wise or concerted pathway to $P_n^{\bullet \delta +}$ and X^- (Scheme 5.1.2).[12-14] Detailed mechanism and definitions by both IUPAC Organic Division and Electrochemistry Division were discussed in previous reviews.[12-14]

Subsequently, Cu(I)X species generated during or after the SET event, are partitioned from the organic phase into the aqueous phase associated with an N-ligand. This process is determined by the much higher solubility of Cu(I)X/L in the aqueous phase rather in organic phase. In water phase Cu(I)X/L species quantitatively disproportionate (equilibrium constant for disproportionation, $K_{disp} = 0.89 \times 10^6\text{-}5.8 \times 10^7$)[43,44] to generate the atomic Cu(0) activator and Cu(II)X_2/L deactivator. While water is miscible with dipolar aprotic solvents, the solution

of Cu(II)Br_2/L in water is not miscible with the solution dipolar aprotic solvent containing MA.

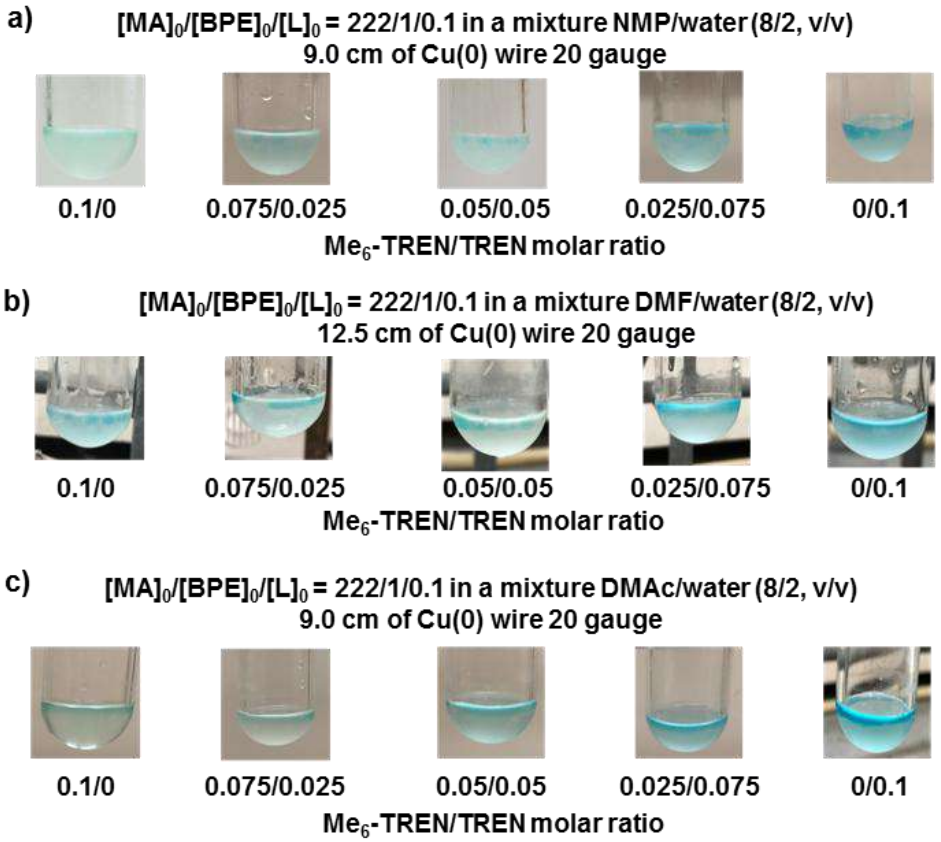

Figure 4.1.5. Visualization of the reaction mixture after the biphasic SET-LRP of MA initiated with BPE using various ligand compositions. (a) NMP/water (8/2, v/v), (b) DMF/water (8/2, v/v), and (c) DMAc/water (8/2, v/v). Reaction conditions: MA = 1 mL, organic solvent = 0.4 mL, water = 0.1 mL, $[MA]_0/[BPE]_0/[L]_0$ = 222/1/0.1.

This immiscibility is responsible for the transition from a single-phase reaction mixture to a biphasic reaction mixture. Cu(0) atomic species activate the dormant species and the excess of Cu(0) nucleates and grows on the existing Cu(0) surface (e.g. powder, wire, plates, etc)[45] increasing its area and therefore, the reactivity of the original Cu(0) surface. Propagation takes place in the organic phase *via* the addition of the monomer to the growing radicals. However, the Cu(II)X_2-mediated deactivation of the propagating macroradicals is thought to

occur at the interphase between organic and aqueous phase *via* reverse outer-sphere oxidation of $P_n^{\bullet}$ to P_n-X (Scheme 4.1.2).

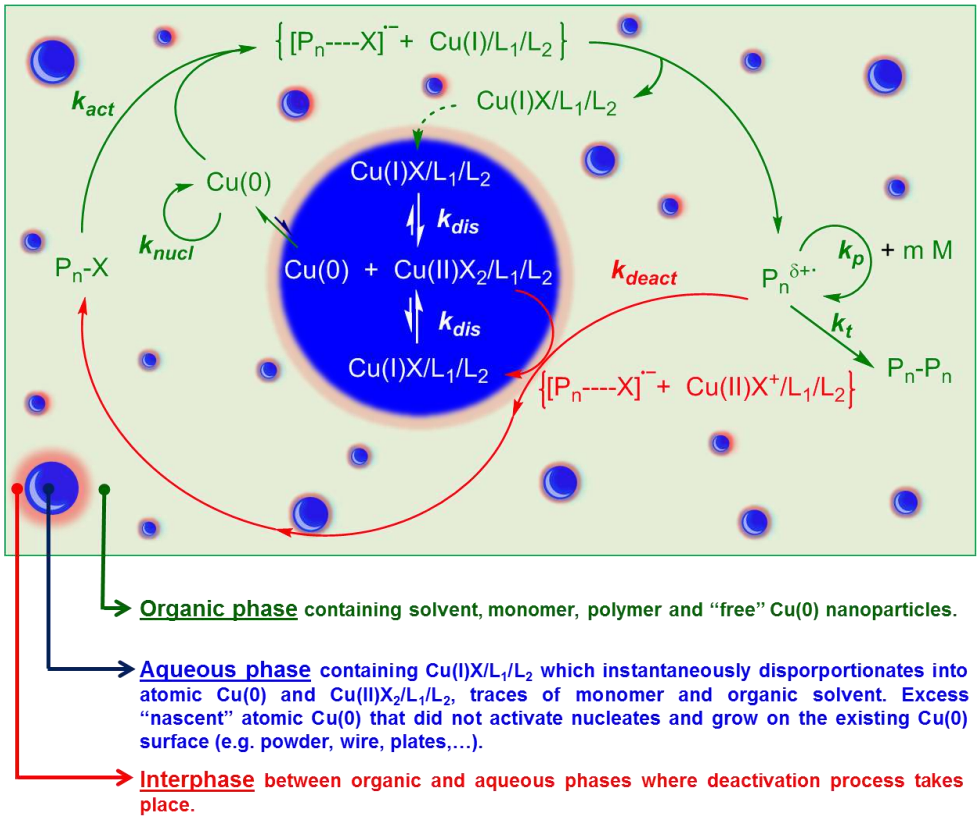

Scheme 4.1.2. Schematic representation of Cu(0)-catalyzed SET-LRP in organic-water "programmed" biphasic reaction mixtures.[a] Notes: [a]color code: organic phase, green; aqueous phase, blue; interphase, red.

According, after SET-LRP the organic phase consisting mainly of PMA and residual monomer dissolved in the organic solvent was almost colorless, whereas the water droplets were bluish because they contain Cu(II)Br_2/L complexes with only some traces of organic solvent and monomer (Figure 4.1.5). The images in Figure 4.1.5 also revealed a slight increase in the blue color of the water phase as the concentration of TREN increases. This trend may indicate a negligible increase in the extent of bimolecular termination that is too low to be detected by NMR and MALDI-TOF analysis experiments. This effect will be investigated in more details and it will be reported elsewhere. A similar color change going from Me_6-TREN

to TREN was observed during the control experiments using ethyl acetate instead of MA (Figure S7 in Annex F). $[EA]_0$ in Figure S7 in Annex D refers to ethyl acetate that has been used as a non-reactive model for methyl acrylate.

Structural analysis of PMA before and after thio-bromo "click" functionalization

A combination 400 MHz ^{1}H NMR and MALDI-TOF measurements before and after reacting -Br end-groups of PMA with thiophenol *via* thio-bromo "click" reaction[46,47] were used to assess the livingness of polymers prepared using various molar ratios between Me_6-TREN and TREN. Low molar mass polymers were prepared using the three above investigated "programmed" biphasic mixtures targeting SET-LRP of MA at a $[MA]_0/[BPE]_0 = 60$. Figure 4.1.6 shows representative ^{1}H NMR spectra of PMA samples isolated at high conversion after biphasic SET-LRP in DMF/water mixture (8/2, v/v) using 1:0, 1:1, and 0:1 molar ratios of Me_6-TREN and TREN.

Within the experimental error, the integral of signal *c*, corresponding to the CH_3- groups of the middle-chain initiator residue, and signal *a,k*, corresponding to the middle-chain CH_2 groups and CH-Br end-groups, did not provide any evidence of termination events. Irrespective of the ligand composition, the bromine chain-end functionality was in all cases >98% at monomer conversion >90%.

The chain-end functionality of PMA calculated after thio-bromo "click" reaction with thiophenol also supports the near perfect functionality of the synthesized PMA (Figure S8 in Annex D). The MALDI-TOF analysis of the prepared samples was also consistent with these results. Figure 4.1.7 depicts representative MALDI-TOF spectra of PMA synthesized using equimolar amounts of Me_6-TREN and TREN analyzed before and after the thioetherification reaction. The polymer isolated after SET-LRP showed one distribution which can be assigned to the corresponding bromine-terminated polyacrylate chains ionized with Na^+.

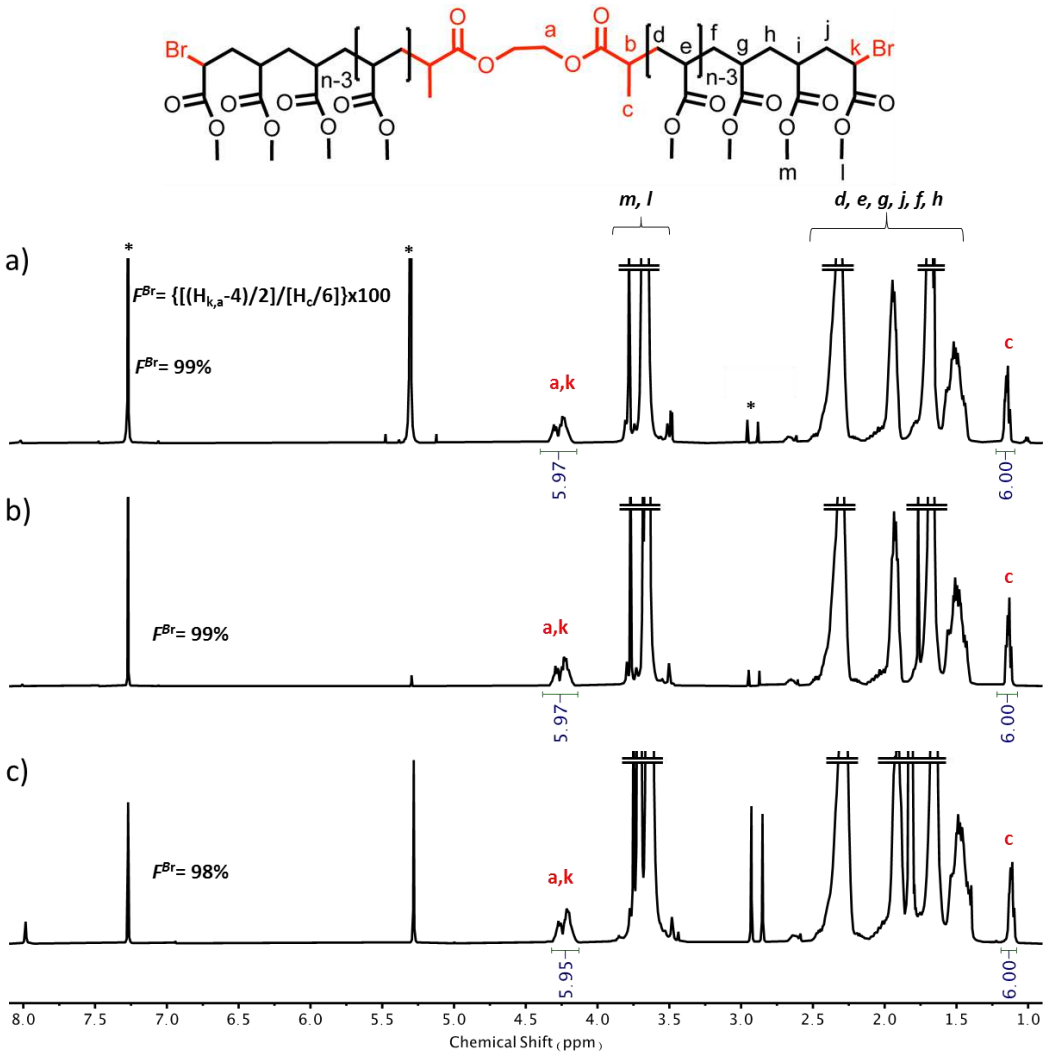

Figure 4.1.6. ^{1}H NMR spectra at 400 MHz of α,ω-di(bromo)PMA at (a) 93% conversion (M_n= 6,480 and M_w/M_n= 1.14) ([MA]$_0$/[BPE]$_0$/[Me$_6$-TREN]$_0$ = 222/1/0.1); (b) 91% conversion (M_n = 6,100 and M_w/M_n= 1.25) ([MA]$_0$/[BPE]$_0$/[Me$_6$-TREN]$_0$/[TREN]$_0$ = 222/1/0.05/0.05); (c) 94% conversion (M_n= 4,990 and M_w/M_n =1.25) ([MA]$_0$/[BPE]$_0$/[TREN]$_0$ = 222/1/0.1). Polymerization conditions: MA = 1 mL, DMF = 0.4 mL, water = 0.1 ml using 12.5 cm of nonactivated Cu(0) wire 20-gauge wire. ^{1}H NMR resonances from residual solvents are indicated with *.

After thioetherification with thiophenol, the original series of peaks vanished and appeared 59 mass units above. This is the expected mass difference value considering the replacement of -Br atoms (2 x 79.9) by -SPh moieties (2 x 109.2) at both polymer chain-ends. MALDI-TOF analysis of PMA prepared using Me$_6$-TREN and TREN showed also high levels of

chain end functionality (Figures S9 and S10 in Annex D, respectively). Likewise, equivalent samples prepared in NMP/water and DMAc/water (8/2, v/v) mixtures provided also evidence of chain-end functionality close to 100% in all cases (see Figures S11-20 in Annex D).

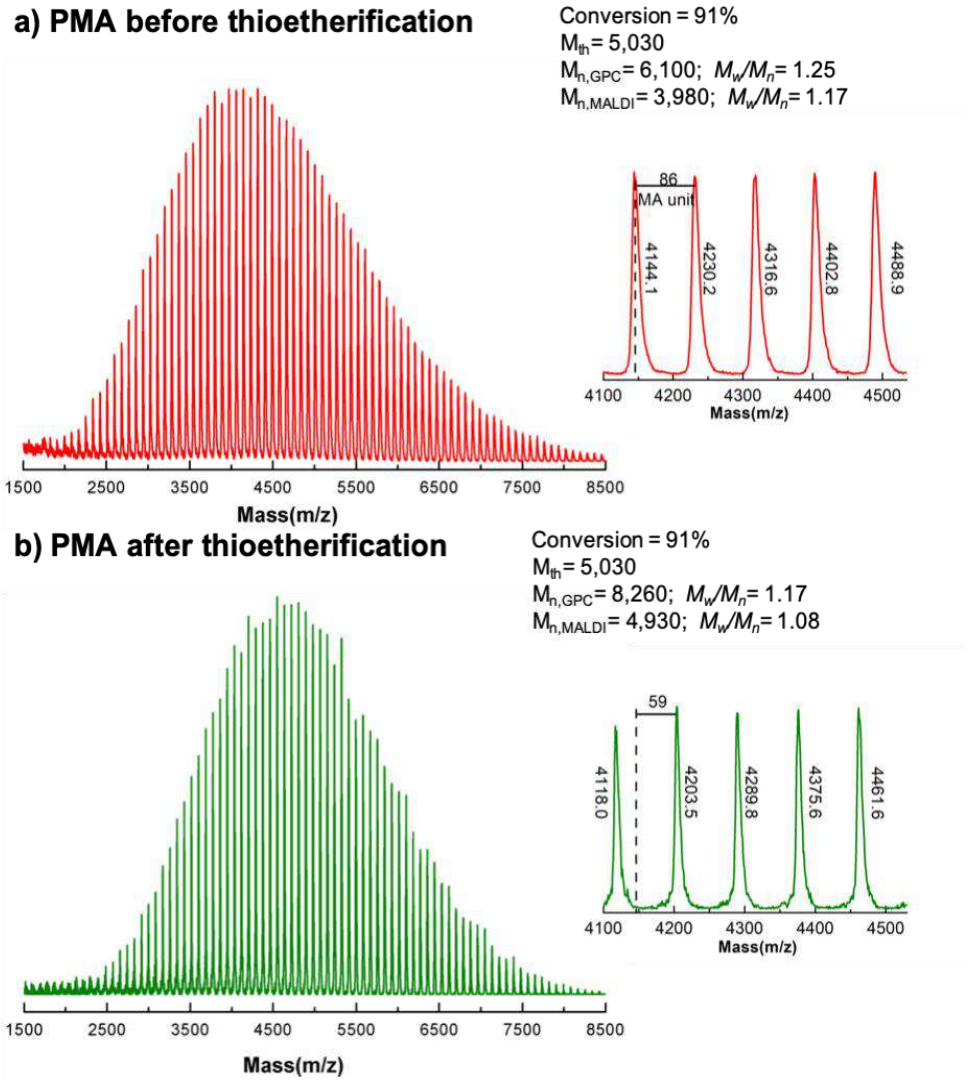

Figure 4.1.7. MALDI-TOF of α,ω-di(bromo)PMA isolated at 94% from SET-LRP of MA in DMF/water (8/2, v/v) mixture initiated with BPE and catalyzed by nonactivated Cu(0) wire at 25 °C: (a) before and (b) after "thio-bromo "click". Polymerization conditions: MA = 1 mL, DMF = 0.4 mL, water = 0.1 ml using 12.5 cm of nonactivated Cu(0) wire 20-gauge wire ($[MA]_0/[BPE]_0/[TREN]_0$ = 60/1/0.05/0.05). The dotted line in expansion after thioetherification shows the original peak from before thioeterification, while 58 represents the increase in molar mass after thioeterification i.e., 2x[SPh (109. 2) - Br (79.9)] = 58.57 for each chain end.

Brief comments on SET-LRP mechanism and on significance for the field of biomacromolecules

SET-LRP catalyzed by Cu(0) wire, powder, coins and other objects occurs in disproportionating solvents and provides polymers with unexpectedly high chain end functionality for a living radical polymerization process.[26,48] This includes, within the limits of NMR experimental error, 100% chain end functionality.[26,48] In non-disproportionating solvents including polar solvents like acetonitrile[41] and non-polar solvents like toluene,[48] the chain end functionality of the resulting polymers is much lower. Best chain end functionality is observed in the absence $Cu(II)X_2$ and could be obtained either with TREN or Me_6-TREN[26] or in the presence of very small amount of $Cu(II)X_2$.[26,48] Larger amounts of $Cu(II)X_2$ additive decrease the chain end functionality of the resulting polymers, although it remains the highest chain end functionality of any LRP prepared polymers.[26,48,49] Details of chain end functionality as a function of the concentration of externally added $Cu(II)X_2$ were discussed in previous publications.[26, 48] Under these conditions, the lower chain end functionality values can also be explained by the $Cu(II)Br_2$ mediated oxidation of radicals to carbocations that subsequently provide chain end double bonds by proton transfer to the basic components of the reaction mixture.[50-52] Terminal double bond chain ends have been reported in polyacrylates obtained by SET-LRP in the presence of $Cu(II)X_2$.[49] The unusually high chain end functionality observed under SET-LRP reaction conditions was attributed to the polymer adsorption on the surface of Cu(0) that decreases the reactivity of the growing radicals in bimolecular termination events but not in the propagation reactions.[53,54] This high chain end functionality contrasts with the much lower chain end functionality observed in ATRP, where the persistent radical effect (PRE)[55] is responsible for the production of $Cu(II)X_2$.[56,57] Activation of the alkyl halides by Cu(0) objects occurs by the most active site of their face centered crystal (FCC) that is 111.[58] Both powder[41] and wire[42] experiments demonstrated that objects produced from Cu(0) crystals have a reactivity that is surface dependent. Moreover, this reactivity increases when Cu(0) atoms are produced by disproportionation followed by activation, nucleation and growth on the original surface of

Cu(0).[19,59] Nucleation and growth has been demonstrated to occur during SET-LRP on the surface of the wire.[45] Colloidal Cu(0) particles were also demonstrated during SET-LRP.[60] However the highest activity of Cu(0) is as atoms. Cu(0) atoms are more reactive that Cu(I)X and are classic and well-established SET catalysts.[61] This diversity of catalytic Cu(0) species are all involved in the SET-LRP process but they could not be observed to reduce $Cu(II)X_2$ to Cu(I)X species during the SET-LRP process;[62] however, it cannot be excluded to occur in the absence of activation. This brief mechanistic discussion demonstrates that the reduction of the amount of $Cu(II)X_2$ during SET-LRP can contribute to a better control of the chain ends and to a lower amount of contamination of the product with Cu species. Since this polymerization proceeds in biphasic systems containing water, the mixed ligand process elaborated here is expected to impact the field of biomacromolecules at a much higher level than SET-LRP performed with externally added $Cu(II)Br_2$ or ATRP also in the presence of externally added $Cu(II)Br_2$.

4.1.3. Conclusions

The use of TREN and Me_6-TREN mixed-ligand system to mediate the Cu(0) wire-catalyzed SET-LRP MA in various “programmed” biphasic mixtures based on dipolar aprotic solvents and water is reported. Kinetic data and chain end analysis demonstrate that Me_6-TREN can complement and make TREN a very efficient ligand in the absence of externally added $Cu(II)B_2$. During the SET-LRP of MA in 8/2 (v/v) aqueous mixtures of NMP, DMF and DMAc with H_2O the use of the mixed-ligand system demonstrated an enhanced rate of polymerization, monomer conversion and molecular weight control. The fact that the most important effect is observed at 1/1 molar ratio between ligands suggests that in addition to a fast exchange between the two ligands, a new single dynamic ligand generated by hydrogen-bonding should be considered in future mechanistic investigations. The rate of polymerization at 1/1 molar ratio between the two ligands is higher than that obtained with each of the individual ligand at the same molar concentration. At the same time, SET-LRP experiments performed in biphasic systems with H_2O do not require the use of the activated

Cu(0) wire. The high chain end functionality generated in the absence of externally added Cu(II)Br_2 makes the SET-LRP in the presence of the mixed-ligand the method of choice for the synthesis of biomacromolecules.

4.1.4. Experimental section

Materials

Methyl acrylate (MA) (99%, Acros) was passed over a short column of basic Al_2O_3 before use in order to remove the radical inhibitor. Tris(2-aminoethyl)amine (TREN) (99%, Acros), Cu(0) wire (20 gauge wire, 0.812 mm diameter from Fisher) and dimethylformamide (DMF) (99.8%, Sigma Aldrich) were used as received. *N*,*N*-Dimethylacetamide anhydrous (DMAc) (99.8%, Sigma Aldrich), and N-methylpyrrolidone (NMP) (99%, Sigma Aldrich) were distilled before use. Deionized water was used in all SET-LRP experiments. Triethylamine (NEt_3) (>99.5% Chemimpex) was distilled under N_2 over CaH_2. Bis(2-bromopropionyl)ethane (BPE) was synthesized by esterification of ethylene glycol with 2-bromopropionyl bromide in the presence pyridine according to our previously reported method.[63] Hexamethylated tris(2-aminoethyl)amine (Me_6-TREN) was synthesized according to a literature procedure.[64]

Methods

400 MHz ^{1}H-NMR spectra were recorded on a Bruker AVANCE NEO 400 NMR instrument at 27 °C in $CDCl_3$ containing tetramethylsilane (TMS) as internal standard. Gel permeation chromatography (GPC) analysis of the polymer samples was performed using a Shimadzu LC-20AD high-performance liquid chromatograph pump, a PE Nelson Analytical 900 Series integration data station, a Shimadzu RID-10A refractive index (RI) detector, and three AM gel columns (a guard column, 500 Å, 10 µm and 104 Å, 10 µm). THF (Fisher, HPLC grade) was used as eluent at a flow rate of 1 mL min^{-1}. The number-average (M_n) and weight-average (M_w) molecular weights of PMA samples were determined with PMMA standards purchased from American Polymer Standards. MALDI-TOF spectra were obtained on a Voyager DE (Applied Biosystems) instrument with a 337 nm nitrogen laser (3 ns pulse

width). For all polymers, the accelerating potential was 25 kV, the grid was 92.5, the laser power was 2200-2500, and a positive ionization mode was used. The sample analysis was performed with 2-(4-hydroxyphenylazo) benzoic acid as the matrix. Solutions of the matrix (25 mg/mL in THF), NaCl (2 mg/mL in deionized H_2O), and polymer (10 mg/mL) were prepared separately. The solution for MALDI-TOF analysis was obtained by mixing the matrix, polymer, and salt solutions in a 5/1/1 volumetric ratio. Then 0.5 µL portions of the mixture were deposited onto three wells of sample plate and dried in air at room temperature before subjected to MALDI- TOF analysis.

Typical procedure for SET-LRP of MA in "programmed" biphasic mixtures using mixed-ligand systems

Stock solutions of different ligand ratio (Me_6-TREN/TREN as 0.05 M/0 M, 0.0375 M/0.0125 M, 0.025 M/0.025 M, 0.0125 M/0.0375 M, 0 M/0.05 M) in water were prepared. The monomer (MA, 11.1 mmol, 1.00 mL), organic solvent (DMF, DMAc, or NMP, 0.4 mL), water stock solution (0.005mmol Ligand, 0.1 mL), and initiator (BPE, 0.05 mmol, 16.6 mg) were added to a 25-mL Schlenk tube. The reaction mixture was then deoxygenated by six freeze–pump–thaw cycles. After these cycles, the Schlenk tube was opened under a positive flow of nitrogen to add the Cu(0) wire wrapped around a Teflon-coated stir bar. Two more freeze–pump–thaw cycles were carried out while holding the stir bar above the reaction mixture using an external magnet. After that, the Schlenk tube was filled with N_2 and the reaction mixture was placed in a water bath at 25 °C. Then, the stir bar wrapped with the Cu(0) wire was dropped gently into the reaction mixture. The introduction of the Cu(0) wire defines t = 0. Samples were taken at different reaction times by purging the side arm of the Schlenk tube with nitrogen for 2 min using a deoxygenated syringe and stainless steel needles. The collected samples were dissolved in $CDCl_3$ and quenched by air bubbling. After that, the monomer conversion was measured by ^{1}H-NMR spectroscopy. In order to determine the molecular weight and polydispersity of the samples, the solvent and the residual monomer were removed under vacuum. Finally, samples were dissolved in THF and passed through a short and small basic Al_2O_3 chromatographic column to remove any

residual copper and subsequently were analyzed by GPC. The resulting PMA was precipitated in cold methanol and dried under vacuum until constant weight to perform chain end analysis by ^{1}H-NMR spectroscopy, before and after the thioetherification reaction.

General procedure for the chain end modification of PMA *via* thio-bromo "click" reaction

In a 10 mL test tube sealed with a rubber septum, thiophenol (0.05 equiv.) and distilled triethylamine (NEt_3, 0.05 equiv.) were added into a solution of the corresponding polymer (0.01 equiv.) in acetonitrile (1 mL) under a nitrogen flow. The reaction mixture was stirred at room temperature for 3 h. Then, the resulting modified PMA was precipitated in cold methanol and washed with methanol several times. The resulting modified polymers were dried under vacuum until constant weight.

4.1.5. References

[1] Reetz, M. T.; Sell, T.; Meiswinkel, A.; Mehler, G. *Angew. Chem. Int. Ed.* **2003**, *42*, 790-793.

[2] Duursma, A.; Hoen, R.; Schuppan, J.; Hulst, R.; Minnaard, A. J.; Feringa, B. L. *Org. Lett.* **2003**, *5*, 3111-3113.

[3] Fors, B. P.; Buchwald, S. L. *J. Am. Chem. Soc.* **2010**, *132*, 15914-15917.

[4] Fan, Y.; Xia, Y.; Tang, J.; Ziarelli, F.; Qu, F.; Rocchi, P.; Iovanna, J. L.; Peng, L. *Chem. Eur. J.* **2012**, *18*, 2221-2225.

[5] Cong, M.; Fan, Y.; Raimundo, J. M.; Xia, Y.; Liu, Y.; Quéléver, G.; Qu, F.; Peng, L. *Chem. Eur. J.* **2013**, *19*, 17267-17272.

[6] (a) Percec, V.; Golding, G. M.; Smidrkal, J.; Weichold, O. *J. Org. Chem.* **2004**, *69*, 3447-3452. (b) Wilson, D. A.; Wilson, C. J.; Rosen, B. M.; Percec, V. *Org. Lett*. **2008**, *10*, 4879-4882. (c) Moldoveanu, C.; Wilson, D. A.; Wilson, C. J.; Corcoran, P.; Rosen, B. M.; Percec, V. *Org. Lett.* **2009**, *11*, 4974-4977. (d) Wilson, D. A.; Wilson, C. J.; Moldoveanu, C.; A. M. Resmerita; Corcoran, P.; Hoang, L. M.; Rosen, B. M.; Percec, V. *J. Am. Chem. Soc.* **2010**, *132*, 1800-1801. (e) Leowanawat, P.; Resmerita, A. M.; Moldoveanu, C.; Liu, C.; Zhang, N.; Wilson, D. A.; Hoang, L. M.; Rosen, B. M.; Percec, V. *J. Org. Chem.* **2010**, *75*, 7822-7828. (f) Moldoveanu, C.; Wilson, D. A.; Wilson, C. J.; Leowanawat, P.; Resmerita, A. M.; Liu, C.; Rosen, B. M.; Percec, V. *J. Org. Chem*. **2010**, *75*, 5438-5452. (g) Leowanawat, P.; Zhang, N.; Resmerita, A.-M.; Rosen, B. M.; Percec, V. *J. Org. Chem.* **2011**, *76*, 9946-9955. (h) Leowanawat, P.; Zhang, N.; Safi, M.; Hoffman, D. J.; Fryberger, M. C.; George, A.; Percec, V. *J. Org. Chem*. **2012**, *77*, 2885-2892. (i) Leowanawat, P.; Zhang, N.; Percec, V. Nickel Catalyzed Cross-Coupling of Aryl C–O Based Electrophiles with Aryl Neopentylglycolboronates. *J. Org. Chem.* **2012**, *77*, 1018-1025. (j) Zhang, N.; Hoffman, D. J.; Gutsche, N.; Gupta, J.; Percec, V. *J. Org. Chem*. **2012**, *77*, 5956-5964. (k)

Leowanawat, P.; Zhang, N.; Safi, M.; Hoffman, D. J.; Fryberger, M. C.; George, A.; Percec, V. *J. Org. Chem*. **2012**, *77*, 2885-2892. (l) Malineni, J.; Jezorek, R. L.; Zhang, N.; Percec, V. *Synthesis* **2016**, *48*, 2795-2807. (m) Malineni, J.; Jezorek, R. L.; Zhang, N.; Percec, V. *Synthesis* **2016**, 48, 2808-2815.

[7] Li, K.-T.; Shieh, D.C. *Ind. Eng. Chem. Res.* **1994**, *33*, 1107-1112.

[8] Matyjaszewski, K.; Wei, M.; Xia, J.; McDermott, N. E. *Macromolecules* **1997**, *30*, 8161-8164.

[9] Iizuka, E.; Wakioka, M.; Ozawa, F. *Macromolecules* **2015**, *48*, 2989-2993.

[10] Percec, V.; Guliashvili, T.; Ladislaw, J. S.; Wistrand, A.; Stjerndahl, A.; Sienkowska, M. J.; Monteiro, M. J.; Sahoo, S. *J. Am. Chem. Soc.* **2006**, *128*, 14156-14165.

[11] Percec, V.; Popov, A. V.; Ramirez-Castillo, E.; Monteiro, M.; Barboiu, B.; Weichold, O.; Asandei, A. D.; Mitchell, C. M. *J. Am. Chem. Soc.* **2002**, *124*, 4940-4941.

[12] Rosen, B. M.; Percec, V. *Chem. Rev.* **2009**, *109*, 5069-5119.

[13] Zhang, N.; Samanta, S. R.; Rosen, B. M.; Percec, V. *Chem. Rev.* **2014**, *114*, 5848-5958.

[14] Lligadas, G.; Grama, S.; Percec, V. *Biomacromolecules* **2017**, *18*, 2981-3008.

[15] Boyer, C.; Corrigan, N. A.; Jung, K.; Nguyen, D.; Nguyen, T. K.; Adnan, N. N.; Oliver, S.; Shanmugam, S.; Yeow, J. *Chem. Rev.* **2016**, *116*, 1803-1949.

[16] Anastasaki, A.; Nikolaou, V.; Nurumbetov, G.; Wilson, O.; Kempe, K.; Quinn, J. F.; Davis, T. P.; Whittaker, M. R.; and Haddleton, D. M. *Chem. Rev.* **2016**, *116*, 835-877.

[17] Anastasaki, A.; Nikolaou, V.; Haddleton, D. M. *Polym. Chem.* **2016**, *7*, 1002-1026.

[18] Rosen, B. M.; Jiang, X.; Wilson, C. J.; Nguyen, N. H.; Monteiro, M. J.; Percec, V. *J. Polym. Sci., Part A: Polym. Chem.* **2009**, *47*, 5606-5628.

[19] Levere, M. E.; Nguyen, N. H.; Leng, X.; Percec, V. *Polym. Chem.* **2013**, *4*, 1635-1647.

[20] Rosen, B. M.; Percec, V. *J. Polym. Sci., Part A: Polym. Chem.* **2007**, *45*, 4950-4964.

[21] Sienkowska, M. J.; Rosen, B. M.; Percec, V. *J. Polym. Sci., Part A: Polym. Chem.* **2009**, *47*, 4130-4140.

[22] Hatano, T.; Rosen, B. M.; Percec, V. *J. Polym. Sci., Part A: Polym. Chem.* **2010**, *48*, 164-172.

[23] Percec, V.; Popov, A. V.; Ramirez-Castillo, E.; Weichold, O. *J. Polym. Sci., Part A: Polym. Chem.* **2003**, *41*, 3283-3299.

[24] Nguyen, N. H., Levere, M. E. and Percec, V. *J. Polym. Sci., Part A: Polym. Chem.* **2012**, *50*, 35-46.

[25] Nicol, E.; Derouineau, T.; Puaud, F.; Zaysev, A. *J. Polym. Sci., Part A: Polym. Chem.* **2012**, *50*, 3885-3894.

[26] Nguyen, N. H.; Levere, M. E.; Percec, V. *J. Polym. Sci., Part A: Polym. Chem.* **2012**, *50*, 860-873.

[27] Voorhaar, L.; Wallyn, S.; Du Prez, F. E.; Hoogenboom, R. *Polym. Chem.* **2014**, *5*, 4268-4276.

[28] Simula, A.; Nikolaou, V.; Alsubaie, F.; Anastasaki, A.; Haddleton, D. M. *Polym. Chem.* **2015**, *6*, 5940-5950.

[29] Moreno, A.; Grama, S.; Liu, T.; Galià, M.; Lligadas, G.; Percec, V. *Polym. Chem*. **2017**, *8*, 7559-7574.

[30] Moreno, A.; Galià, M.; Lligadas, G.; Percec, V. *Biomacromolecules* **2018**, *19*, 4480-4491.

[31] Moreno, A.; Liu, T.; Galià, M.; Lligadas, G.; Percec, V. *Polym Chem*. **2018**, *9*, 1961-1971.

[32] Moreno, A.; Jezorek, R. L.; Liu, T.; Galià, M.; Lligadas, G.; Percec, V. *Polym Chem*. **2018**, *9*, 1885-1899.

[33] Moreno, A.; Liu, T.; Ding, L.; Buzzacchera, I.; Galià, M.; Möller, M.; Wilson, C. J.; Lligadas, G.; Percec, V. *Polym. Chem*. **2018**, *9*, 2313-2327.

[34] Jezorek, R. L.; Enayati, M.; Smail, R. B.; Lejnieks, J.; Grama, S.; Monteiro, M. J.; Percec, V. *Polym. Chem*. **2017**, *8*, 3405-3424.

[35] Smail, R. B.; Jezorek, R. L.; Lejnieks, J.; Enayati, M.; Grama, S.; Monteiro, M. J.; Percec, V. *Polym. Chem*. **2017**, *8*, 3102-3123.

[36] Enayati, M.; Jezorek, R. L.; Monteiro, M. J.; Percec, V. *Polym. Chem*. **2016**, *7*, 5930-5942.

[37] Enayati, M.; Smail, R. B.; Grama, S.; Jezorek, R. L.; Monteiro, M. J.; Percec, V. *Polym. Chem*. **2016**, *7*, 7230-7241.

[38] Enayati, M.; Jezorek, R. L.; Monteiro, M. J.; Percec, V. *Polym. Chem.* **2016**, *7*, 3608-3621.

[39] Grama, S.; Lejnieks, J.; Enayati, M.; Smail, R. B.; Ding, L.; Lligadas, G.; Monteiro M. J.; Percec, V. *Polym. Chem*. **2017**, *8*, 5865-5874.

[40] Nguyen, N. H.; Rosen, B. M.; Jiang, X.; Fleischmann, S.; Percec, V. *J. Polym. Sci., Part A: Polym. Chem.* **2009**, *47*, 5577-5590.

[41] Lligadas, G.; Rosen, B. M.; Bell, C. A.; Monteiro, M. J.; Percec, V. *Macromolecules* **2008**, *41*, 8365-8371.

[42] Nguyen, N. H.; Rosen, B. M.; Lligadas, G.; Percec, V. *Macromolecules* **2009**, *42*, 2379-2386.

[43] Ahrland, S.; Rawsthorne, J. *Acta Chem. Scand.* **1970**, *24*, 157-172.

[44] Ciavatta, L.; Ferri, D.; Palombari, R. *Chem.* **1980**, ***42***, 593-598.

[45] Nguyen, N. H.; Hao-Jan, S.; Levere, M. E.; Fleischmann, S.; Percec, V. *Polym. Chem.* **2013**, *4*, 1328-1332.

[46] Rosen, B. M., Lligadas, G., Hahn, C. and Percec, V. *J. Polym. Sci., Part A: Polym. Chem.* **2009**, *47*, 3931–3939.

[47] Rosen, B. M.; Lligadas, G.; Hahn, C.; Percec, V. *J. Polym. Sci., Part A: Polym. Chem.* **2009**, *47*, 3940-3948.

[48] Nguyen, N. H.; Levere, M. E.; Kulis, J.; Monteiro, M. J.; Percec, V. *Macromolecules* **2012**, *45*, 4606-4622.

[49] Nyström, F.; Soeriyadi, A. H.; Boyer, C.; Zetterlund, P. B.; Whittaker, M. R. *J. Polym. Sci., Part A: Polym. Chem.* **2011**, *49*, 5313-5321.

[50] Jenkins, C. L.; Kochi, J. K. *J. Am. Chem. Soc.* **1972**, *94*, 856-865.

[51] Cohen, H.; Meyerstein, D. *Inorg. Chem*. **1974**, *13*, 2434-2443.

[52] Bower, B. K.; Tennent, H. G. *J. Am. Chem. Soc.* **1972**, *94*, 2512-2514.

[53] Samanta, S. R.; Nikolaou, V.; Keller, S.; Monteiro, M. J.; Wilson, D. A.; Haddleton, D. M.; Percec, V. *Polym. Chem*. **2015**, *6*, 2084-2097.

[54] Nguyen, N. H.; Kulis, J.; Sun, H. J.; Jia, Z.; van Beusekom, B.; Levere, M. E.; Wilson, D. A.; Monteiro, M. J.; Percec, V. *Polym. Chem*. **2013**, *4*, 144-155.

[55] Fischer, H. *J. Polym. Sci., Part A: Polym. Chem.* **1999**, *37*, 1885-1901.

[56] Lutz, J. F.; Matyjaszewski, K. *J. Polym. Sci., Part A: Polym. Chem.* **2005**, *43*, 897-910.

[57] Jakubowski, W.; Kirci-Denizli, B.; Gil, R. R.; Matyjaszewski, K. *Macromol. Chem. Phys.* **2008**, *209*, 32-39.

[58] Enayati, M.; Jezorek, R. L.; Percec, V. *Polym. Chem.* **2016**, *7*, 4549-4558.

[59] Jiang, X.; Rosen, B. M.; Percec, V. *J. Polym. Sci., Part A: Polym Chem.* **2010**, *48*, 403-409.

[60] Levere, M. E.; Nguyen, N. H.; Sun, H. J.; Percec, V. *Polym. Chem*. **2013**, *4*, 686-694.

[61] (a) Negrel, J. C.; Gony, M.; Chanon, M.; Lai, R. *Inorg. Chim. Acta.* **1993**, *207*, 59-63. (b) Julliard, M.; Chanon, M. *Chem. Scr.* **1894**, *4*, 11-21. (c) Timms, P. L. *Proc. R. Soc. Lond. A.* **1984**, *396*, 1-19. (d) Klabunde, K. J. *Acc. Chem. Res.* **1975**, *8*, 393-399. (e) Klabunde, K. J.; Li, Y. X.; Tan, B. J. *Chem. Mater.* **1991**, *3*, 30-39.

[62] Levere, M. E.; Nguyen, N. H.; Percec, V. *Macromolecules* **2012**, *45*, 8267-8274.

[63] Lligadas, G.; Percec, V. *J. Polym. Sci., Part A: Polym. Chem.,* **2007**, *45*, 4684-4695.

[64] Ciampolini, M.; Nardi, N. *Inorg. Chem.*, **1966**, *5*, 41-44.

4.2. Me_6-TREN/TREN mixed-ligand effect during SET-LRP in the catalytically active DMSO revitalizes TREN into an excellent ligand

A mixed-ligand effect was observed for mixtures of Me_6-TREN with TREN ligands during Cu(0) wire-catalyzed, SET-LRP of MA initiated with BPE in DMSO. The external order of reaction of SET-LRP both in the presence of Me_6-TREN, TREN and of the mixed-ligand Me_6-TREN/TREN, in DMSO, demonstrated a catalytic activity for DMSO similar to that reported in the presence of Cu(0) powder. The catalytic activity of DMSO, with close to 100% chain-end functionality, facilitates the much less expensive TREN to act as a very efficient ligand that is competitive with Me_6-TREN and with the mixed-ligand and revitalizes TREN into an excellent ligand. The highest activity of the mixed-ligand at 1/1 ratio between ligands suggests that in addition to a fast exchange between these two ligands, a new single dynamic ligand stabilized by hydrogen-bonding, may generate these results.

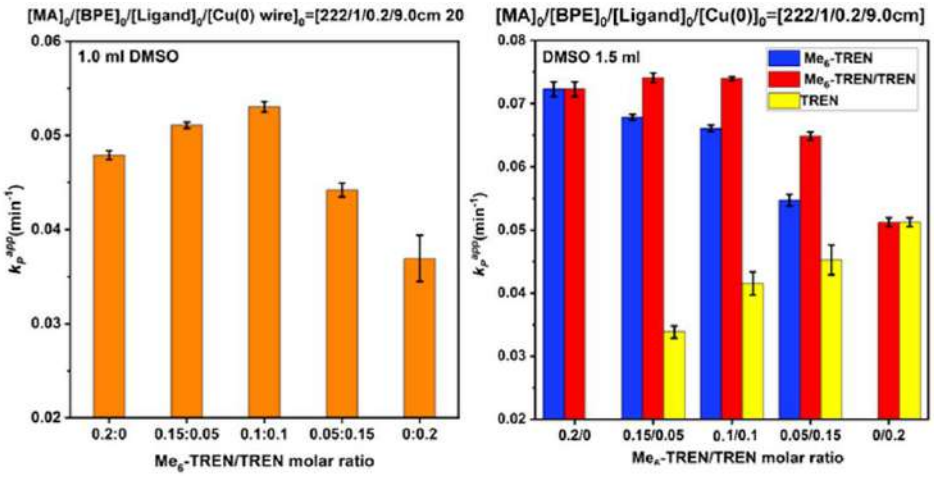

Mixed-Ligand Effect During Cu(0)-mediated SET-LRP

4.2.1. Introduction

The mixed-ligand concept represents an inexpensive but extremely efficient methodology to design new catalytic systems without synthetic efforts.[1] Almost simultaneously with its development, Feringa reported heterocombinations of chiral monodentate ligands as more efficient than homocombinations in Rh-catalyzed C–C cross-coupling.[2] At the same time the mixed-ligand strategy was expanded to Pd-catalyzed C–N[3,4] and C–S[5] cross-coupling and to Ni-mediated Suzuki cross-coupling and borylation.[6] The advantages of the mixed-ligand catalytic systems have been observed only in several polymerization reactions.[7-9]

A suitable solvent/N-ligand mixture is demanded for Cu(0)-catalyzed SET-LRP[10-17] in order to facilitate the disproportionation of Cu(I)X into Cu(0) and Cu(II)X_2.[18,19] Me_6-TREN is a common ligand used in SET-LRP,[10,11,14] since it favors the disproportionation by preferentially binding Cu(II)X_2 rather than Cu(I)X.[20] Nevertheless, the precursor of Me_6-TREN, TREN[11,21-23] that is about 80× less expensive than Me_6-TREN, and poly(ethylene imine) (PEI)[10] was also used for SET-LRP of VC, acrylates, and methacrylates during the first days of SET-LRP. Likewise, TREN[24-26] and *N,N,N′,N″,N‴*-pentamethyldiethylenetriamine (PMDETA)[10,27,28] were also employed in SET-LRP.

The replacement of Me_6-TREN with TREN was not very successful in biphasic SET-LRP complex systems catalyzed by Cu(0) wire that we call "programmed,"[29-33] although TREN is known for its efficiency in single-phase SET-LRP. Biphasic organic solvent–water SET-LRP complex systems demand the addition of Cu(II)Br_2 in order to retain the living character when TREN is used as a ligand. In this particular case, SET-LRP is an interfacial process that was discussed in more details in previous publications.[34] The Cu(0)-mediated SET-LRP in bi(multi)phasic mixtures of organic solvents with water is very important and opens new methodologies since the organic solvent does not have to facilitate the disproportionation of Cu(I)X/N-ligand, as in the classic SET-LRP.[35-39] The first mixed-ligand effect in a SET-LRP system was observed in the water–organic solvent "programmed" biphasic systems when

Me_6-TREN was successfully employed to replace the externally added Cu(II)X_2 with Me_6-TREN.[10b]

In this chapter, we first report experiments that demonstrate the catalytic activity of DMSO solvent in both Me_6-TREN and TREN and in the mixed-ligand Me_6-TREN/TREN-mediated SET-LRP of MA initiated with BPE at 25 °C and catalyzed with nonactivated Cu(0) wire. The catalytic activity of DMSO was discovered previously when Cu(0) powder was employed as catalyst,[11a] but was not used to improve the synthetic capabilities of SET-LRP. Subsequently, the mixed-ligand effect of Me_6-TREN/TREN was investigated at two different concentrations of the DMSO solvent. Statistical analysis of the kinetics and of the control experiments together with the determination of the chain-end functionality of the resulting polymers by a combination of NMR and MALDI-TOF before and after thio-bromo "click" reaction demonstrated that the catalytic activity of DMSO can be employed to improve the efficiency of the inexpensive TREN ligand. Therefore, we can conclude that the catalytic activity of DMSO was employed to revitalize the long-neglected TREN and transform it into an excellent ligand. Since TREN is 80× less-expensive than Me_6-TREN, numerous new applications, including in the field of biomacromolecules, will evolve from the series of experiments reported here.

4.2.2. Results and discussion

Determination of the external order of reaction in DMSO during SET-LRP catalyzed with nonactivated Cu(0) wire in DMSO

A close to first order external order of reaction in the DMSO used as solvent was observed when Cu(0) powder was employed as catalyst in SET-LRP.[11a,40-45] This external first order of reaction in DMSO demonstrated the catalytic activity of DMSO when SET-LRP was performed in DMSO as solvent. Three series of experiments were carried out with nonactivated Cu(0) wire as catalyst, MA as monomer, and Me_6-TREN, TREN, and mixtures of

Mixed-Ligand Effect During Cu(0)-mediated SET-LRP

Me_6-TREN/TREN in different concentrations of DMSO at 25 °C. BPE was used as initiator in all cases.

The structures of the two ligands and an equation of the Cu(0) wire-catalyzed SET-LRP of MA initiated with BPE are outlined in Scheme 4.2.1. Duplicate and triplicate kinetics were carried out under the following conditions: $[MA]_0/[BPE]_0/[L]_0$ = 222/1/0.2 using 9.0 cm of nonactivated Cu(0) wire.

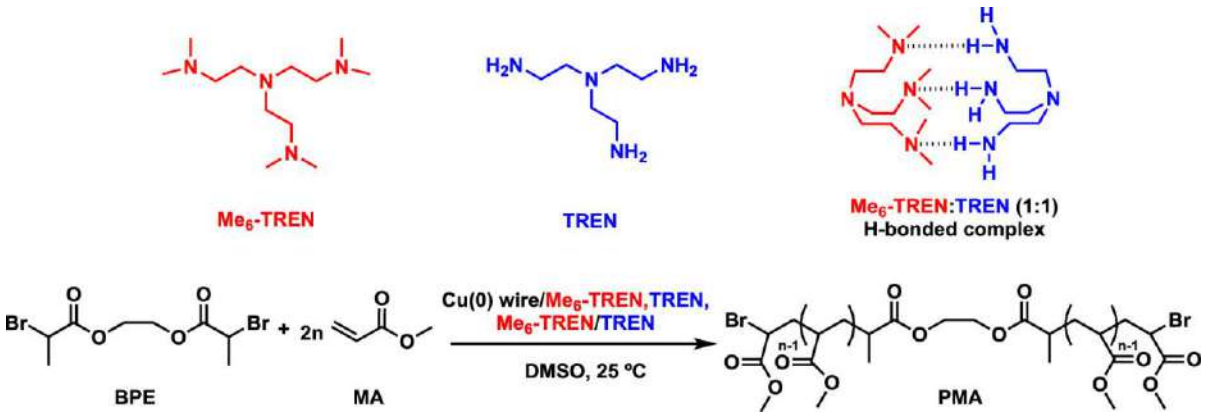

Scheme 4.2.1. SET-LRP of MA initiated with BPE and catalyzed with nonactivated Cu(0) wire by employing various ratios of Me_6-TREN and TREN in the catalytically active DMSO at 25 °C.

Figure 4.2.1a reports the kinetic data for the experiments performed with Me_6-TREN as ligand, Figure 4.2.1b shows the data obtained with TREN, while Figure 4.2.1c shows the data obtained with the mixed-ligand system Me_6-TREN/TREN. Selected kinetic experiments from which these external orders of reaction in DMSO were obtained for Me_6-TREN (Figure 4.2.2a,c,e) and TREN (Figure 4.2.2b,d,f) as ligands are reported in Figures 4.2.2 when the DMSO concentration was varied from 1.0 to 1.5 and to 1.8 mL of DMSO with 2 mL of MA. Kinetic experiments with all other DMSO concentrations employed in Figure 4.2.1a–c are shown in Supporting Information, Figures S1–S5 in Annex E. First order reaction kinetics in monomer were observed for all DMSO concentrations from Figures 4.2.2 and Supporting Information Figures S1–S5 in Annex E. A continuous increase in the rate of polymerization and of the corresponding apparent rate constant, k_p^{app}, as the concentration of the DMSO

increased or the overall concentration of the MA decreased was observed in all cases (Figures 4.2.2 and Supporting Information, Figures S1–S5 in Annex E).

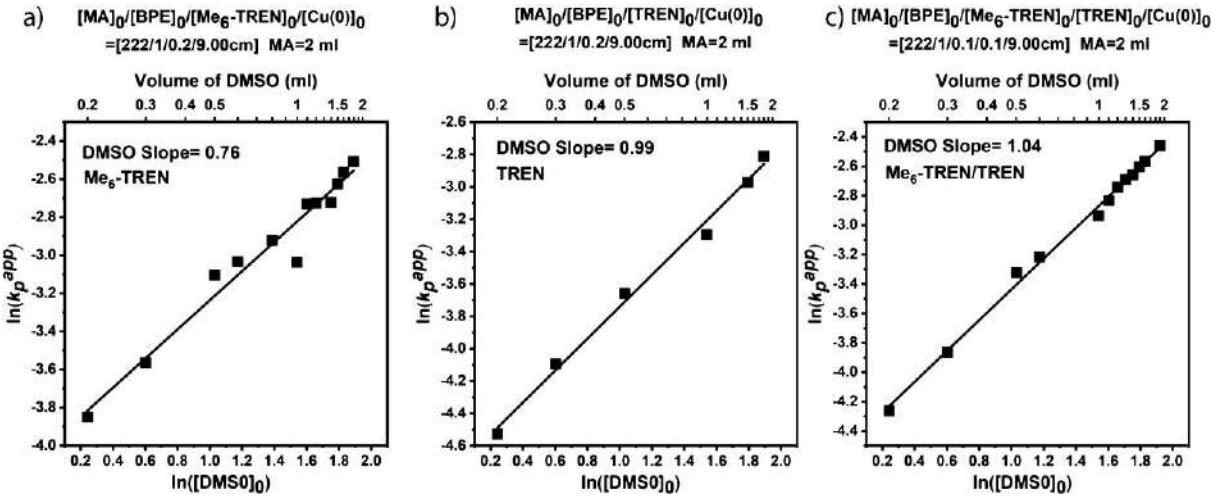

Figure 4.2.1. Determination of the external order of reaction in $[DMSO]_0$ for the Cu(0) wire/ligand-catalyzed polymerization of MA in DMSO at 25 °C, initiated with BPE. $\ln(k_p^{app})$ *vs* $\ln([DMSO]_0)$ with DMSO varied from 0.2 to 1.9 mL, with 2 mL of MA for (a) $[MA]_0/[BPE]_0/[Me_6\text{-TREN}]_0/[Cu(0)]_0$ = 222/1/0.2/9 cm; (b) $[MA]_0/[BPE]_0/[TREN]_0/[Cu(0)]_0$ = 222/1/0.2/9 cm; (c) $[MA]_0/[BPE]_0/[Me_6\text{-TREN}]_0/[TREN]_0/[Cu(0)]_0$ = 222/1/0.1/0.1/9 cm.

In any organic or polymerization reaction the decrease in the reactants concentration generated by increasing the solvent concentration results in a decrease of the rate of reaction. This unexpected trend that consists of the increase in rate of polymerization with the decrease of the monomer concentration demonstrates the catalytic activity of DMSO in SET-LRP. This result is in agreement with the experiments reported with Cu(0) powder as catalyst.[11a] The determination of the external order of reaction in DMSO was calculated by plotting the $\ln(k_p^{app})$ vs $\ln([DMSO]_0)$ (Figure 4.2.1a–c). The slope of these dependencies provided the external order of reaction in DMSO for the different ligands used in these SET-LRP experiments. An external order of reaction in DMSO of 0.76 was obtained in the presence of Me_6-TREN, while in the presence of TREN and the mixed-ligand Me_6-TREN/TREN (1/1 molar ratio), the external orders of reaction in DMSO were 0.99 and 1.04, respectively.

Mixed-Ligand Effect During Cu(0)-mediated SET-LRP

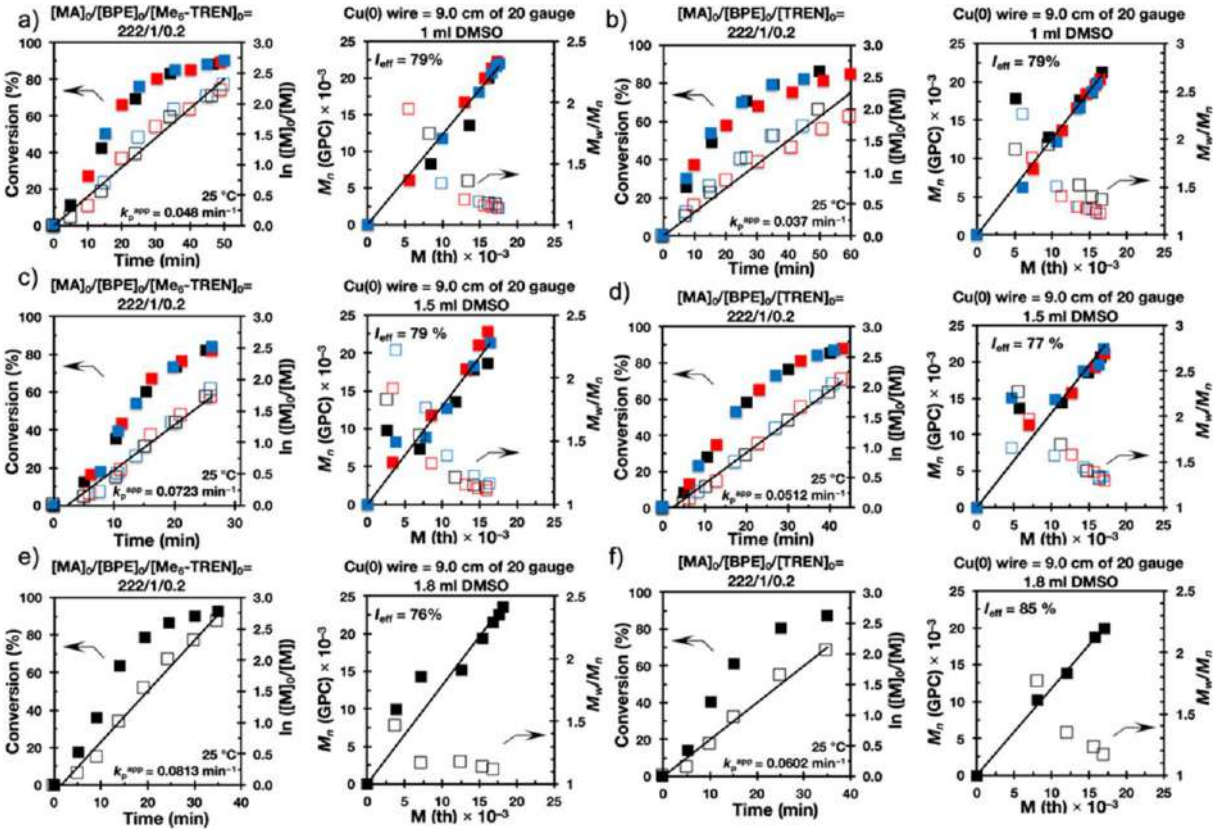

Figure 4.2.2. Kinetic plots, molecular weight and dispersity evolutions for the SET-LRP of MA in DMSO initiated with BPE and catalyzed with 9.0 cm nonactivated Cu(0) wire at 25 °C. Data in different colors were obtained from different kinetics, performed by different researchers. k_p^{app} and I_{eff} are the average values of three experiments. k_p^{app} vs $[DMSO]_0$ with DMSO varied from 1.0 mL (a) to 1.5 mL (c) to 1.8 mL (e) with 2 mL of MA for $[MA]_0/[BPE]_0/[Me_6\text{-TREN}]_0/[Cu(0)]_0$ = 222/1/0.2/9 cm. Identical experiments in which Me_6-TREN was replaced with TREN are in (b), (d), and (f).

Potential mechanism for the catalytic activity of DMSO

In order to address the catalytic activity of DMSO, first it must be considered that SET-LRP experiments were performed in a mixture of two solvents, DMSO and the monomer, MA. Both DMSO and MA are good solvents that mediate the disproportionation of Cu(I)Br into Cu(0) and Cu(II)Br_2.[19a] While both solvents MA and DMSO mediate the disproportionation in the presence of these two ligands, MA and DMSO, only DMSO is a good solvent for Cu(I)Br and Cu(II)Br_2 obtained during the activation and disproportionation and is also a better solvent that mediates this disproportionation. MA mediates

disproportionation mostly by a surface effect. Therefore, it is expected that by increasing the ratio between DMSO and MA in the reaction mixture, the extent of disproportionation will increase. At the same time it has been demonstrated that DMSO stabilizes Cu(0) nanoparticles, while MA does not. Figure 4.2.3 presents disproportionation experiments that support this hypothesis. An increase in the amount of Cu(0) obtained by disproportionation is observed at the transition from MA/DMSO = 3/1 to 2/1. This increase continues to the transition to MA/DMSO = 1/1. However, in addition to this trend, at a 1/1 ratio, the stabilization of Cu(0) nanoparticles by the higher concentration of DMSO is also visible (see left vial in Figure 4.2.3). Increasing the stability of nanoparticles decreases the crystallization process and provides smaller but more active Cu(0) nanoparticles of the catalyst.[19b] It is well established that faster SET-LRP is mediated in more disproportionating solvents and in their mixtures.[19c-e] In addition, mixtures of solvents can display also a cooperative and synergistic effect that was not yet investigated for the case of MA/DMSO.[19e] Last but not least, since DMSO is one of the best solvents for SET processes, an increased concentration of DMSO also is expected to increase the rate of SET-LRP.[19f]

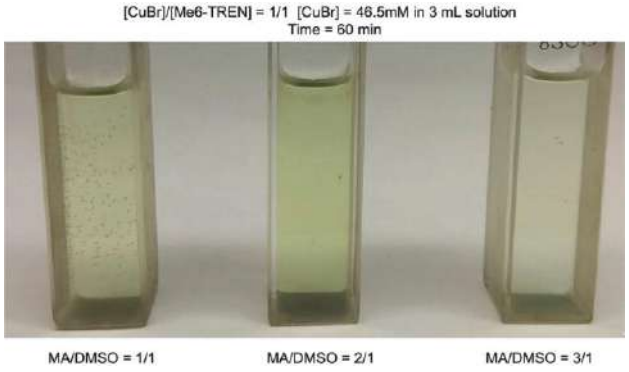

Figure 4.2.3. Visual observation of CuBr/Me_6-TREN complex dissolved in DMSO/MA. Conditions: [CuBr] = 46.5 mM, solvent = 3.0 mL, $[CuBr]_0/[Me_6\text{-TREN}]_0$ = 1/1. Pictures were taken 60 min after mixing the reagents.

Therefore, all these factors, the extent of disproportionation that determines the concentration of Cu(0) produced by disproportionation, the Cu(0) particle size generated by

disproportionation and their different reactivities, the solubility of Cu(I)Br and Cu(II)Br_2 compounds in the MA/DMSO solvent, and the quality of the MA/DMSO solvent for SET reactions, contribute to the catalytic effect of DMSO reported here, even if the most reactive Cu(0) species employed in the SET-LRP are atoms.[46]

Mixed-ligand methodology during the SET-LRP of 2 mL of MA in 1 mL of DMSO using Me_6-TREN, Me_6-TREN/TREN, and TREN as ligands

The detection of the mixed-ligand effect for Me_6-TREN/TREN was first observed and reported for SET-LRP performed in water/organic solvents biphasic systems.[10b] In the current series of experiments, the ratio between Me_6-TREN and TREN was changed from 1:0 to 0:1 while keeping the ratio of ligand to initiator constant at 10 mol%. The ratio between MA and DMSO was also kept constant (2 mL of MA to 1 mL of DMSO; Scheme 4.2.1 and Figure 4.2.4).

Interestingly, all tested mixed-ligand compositions generated higher k_p^{app} values than those obtained in control experiments carried out in the presence of either Me_6-TREN or TREN. These results will be discussed later. The partial replacement of Me_6-TREN with TREN increased the k_p^{app} while retaining first-order kinetics (Figure 4.2.4). The best catalytic activity was observed at a 1:1 molar ratio of the two ligands (compare Figure 4.2.4a, b, and c), suggesting the H-bonded new ligand from Scheme 4.2.1. Under these conditions, the SET-LRP of MA proceeded faster than control experiments with Me_6-TREN (Figure 4.2.4a) and TREN (Figure 4.2.4e), respectively.

This mixed-ligand methodology also provided the highest conversion and an improved control over molecular weight distribution (Figures 4.2.5 and 4.2.6). The summary of results is in Table 4.2.1. Representative GPC data plotted in Figure 4.2.6 illustrate the dependence of molecular weight *vs* conversion. GPC data show monomodal peak distributions shifting to higher molar mass at high conversion. The most relevant result was observed at the 1:1 molar ratio between the two ligands. In this case, the I_{eff} was found to be above 80%.

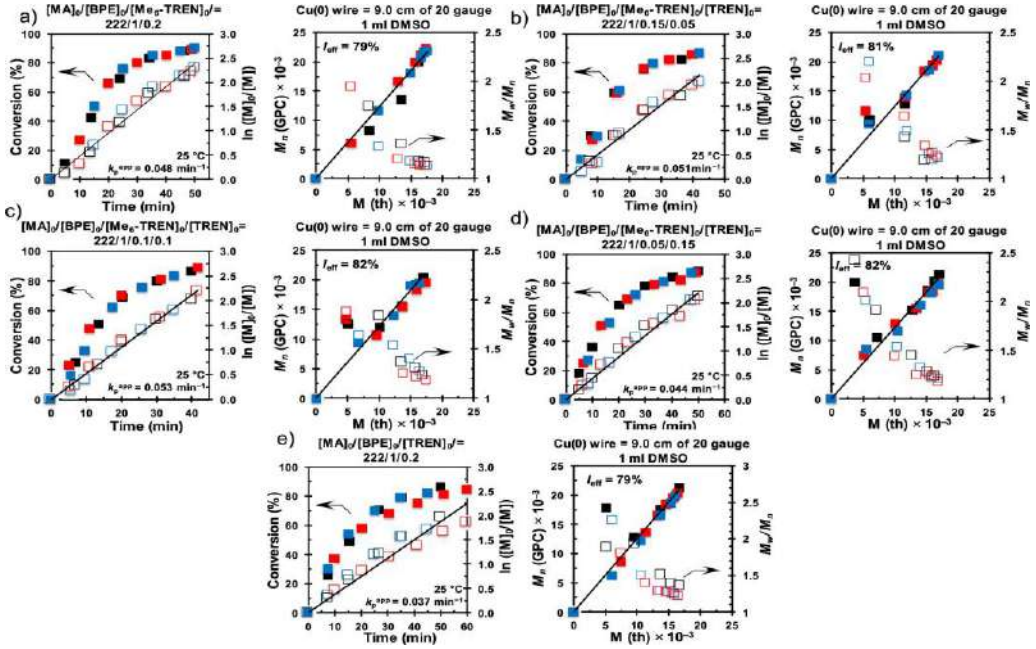

Figure 4.2.4. Kinetic plots, molecular weight, and dispersity evolutions for the SET-LRP of MA in DMSO initiated with BPE and catalyzed by the 9.0 cm nonactivated Cu(0) wire at 25 °C in the presence of (a) Me_6-TREN and (b–d) different ratios of Me_6-TREN/TREN and (e) TREN. Experimental data in different colors were obtained from different kinetics experiments, sometimes performed by different researchers. k_p^{app} and I_{eff} are the average values of three experiments. $[MA]_0/[BPE]_0/[ligand]_0/[Cu(0)]_0$ = 222/1/0.2/9 cm.

Table 4.2.1. Dependence of k_p^{app} on the dimension of the Cu(0) wire in the SET-LRP of MA initiated with BPE in DMSO at 25 °C[a].

entry	wire length (cm) 20G	reaction condition	k_p^{app} (min^{-1})	k_p^{app}/k_p^{app} (TREN)	M_w/M_n	I_{eff} (%)
1	9.0	[MA]/[BPE]/[Me_6-TREN] 222/1/0.2	0.048	1.3	1.14	79
2	9.0	[MA]/[BPE]/[Me_6-TREN]/[TREN] 222/1/0.15/0.05	0.051	1.4	1.21	81
3	9.0	[MA]/[BPE]/[Me_6-TREN]/[TREN] 222/1/0.1/0.1	0.053	1.4	1.23	82
4	9.0	[MA]/[BPE]/[Me_6-TREN]/[TREN] 222/1/0.05/0.15	0.044	1.2	1.20	82
5	9.0	[MA]/[BPE]/[TREN] 222/1/0.2	0.037	1.0	1.23	79

[a] Reaction conditions: monomer = 2 mL; solvent = 1 mL.

Mixed-Ligand Effect During Cu(0)-mediated SET-LRP

These data demonstrate that the mixed-ligand catalyst consisting of nonactivated Cu(0) wire and Me_6-TREN/TREN is an effective new catalytic system for the SET-LRP of MA in DMSO.

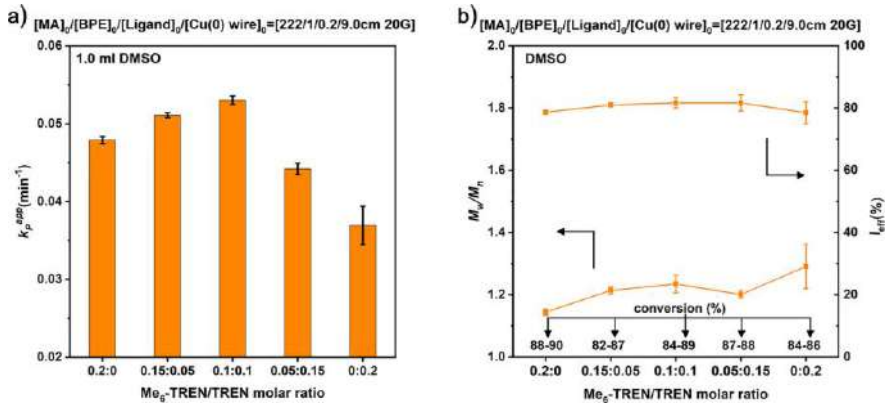

Figure 4.2.5. Evolution of k_p^{app} for the SET-LRP of MA (2 mL) initiated with BPE in DMSO (1 mL) mediated with different ratios between Me_6-TREN and TREN at 25 °C (a). Initiator efficiency (I_{eff} (%)) and dispersity (M_w/M_n) as a function of the ratio between Me_6-TREN and TREN.

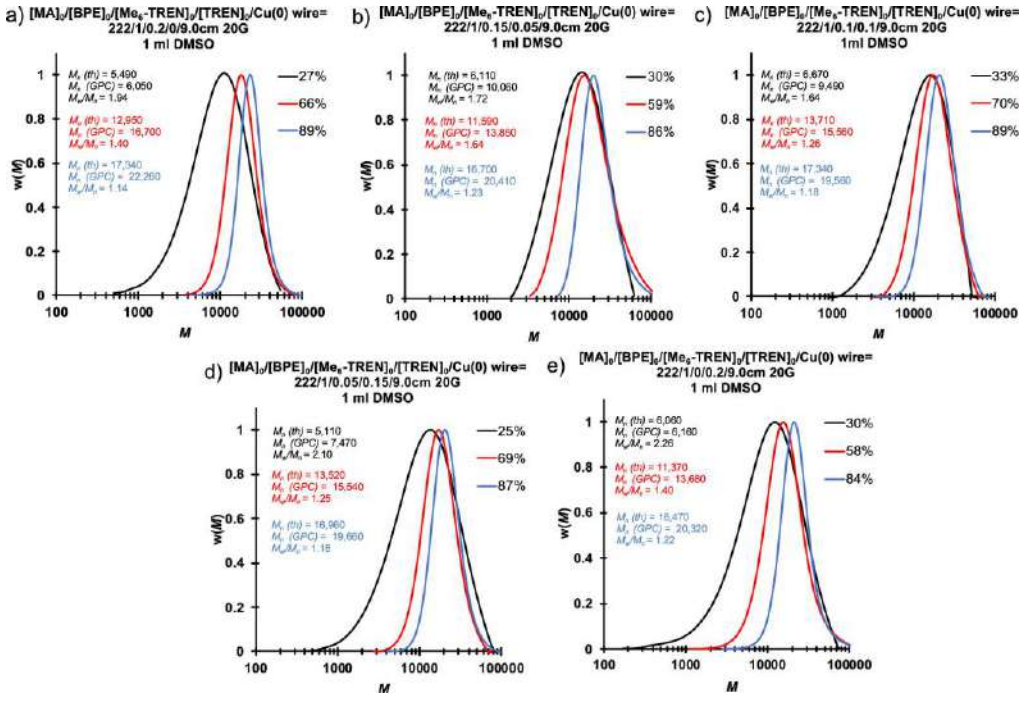

Figure 4.2.6. Representative GPC traces of the evolution of molecular weight as a function of conversion for the SET-LRP of MA in a mixture of 2 mL MA with 1 mL DMSO catalyzed by 9.0 cm nonactivated Cu(0) wire at 25 °C in the presence of various ligand compositions, as mentioned on top of the GPC curves. Reaction conditions: MA = 2 mL, DMSO = 1 mL, $[MA]_0/[BPE]_0/[L]_0$ = 222/1/0.2.

Visualization of the polymerization reaction at high conversion

The images in Figure 4.2.7 reveal an almost undetectable increase in the blue color of the reaction mixture as the concentration of TREN increased. This trend most probably indicates a negligible increase in the extent of bimolecular termination that is too low to be detected by NMR and MALDI-TOF. A similar result was observed during the mixed-ligand effect observed in biphasic water–organic solvent systems.[10b]

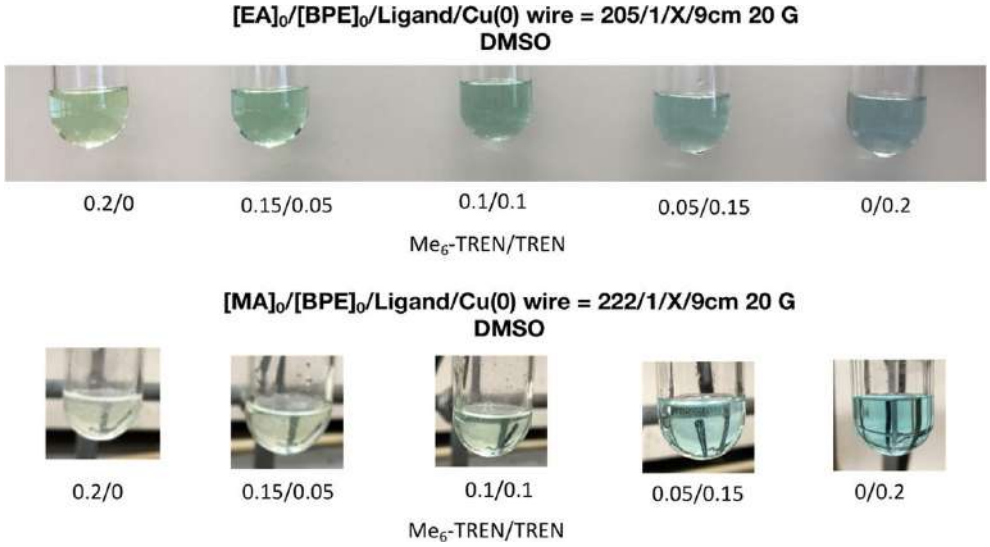

Figure 4.2.7. Visualization of the reaction mixture of SET-LRP of MA initiated with BPE in DMSO using various ligand ratios (X) shown under the Schlenk tube. Reaction conditions are on top of each series of experiments.

Structural analysis of PMA before and after thio-bromo "click" reaction

A combination 400 MHz ^{1}H NMR and MALDI-TOF methods before and after reacting the -Br end-groups of PMA with thiophenol via thio-bromo "click" reaction[47] were employed to estimate the living character of SET-LRP performed at various molar ratios between Me_6-TREN and TREN and compare them with Me_6-TREN and TREN. Low molecular weight polymers were synthesized for these investigations. Figures 4.2.8 and 4.2.9 show representative ^{1}H NMR spectra of PMA isolated at high conversion of SET-LRP in DMSO in the presence of Me_6-TREN (Figures 4.2.8a and 4.2.9a), Me_6-TREN/TREN (Figures 4.2.8b and

4.2.9b), and TREN (Figures 4.2.8c, 4.2.9b) before and after thio-bromo "click" reaction. Within experimental error, the chain end functionality (FBr, FSPH %) of all PMA samples is 100%.

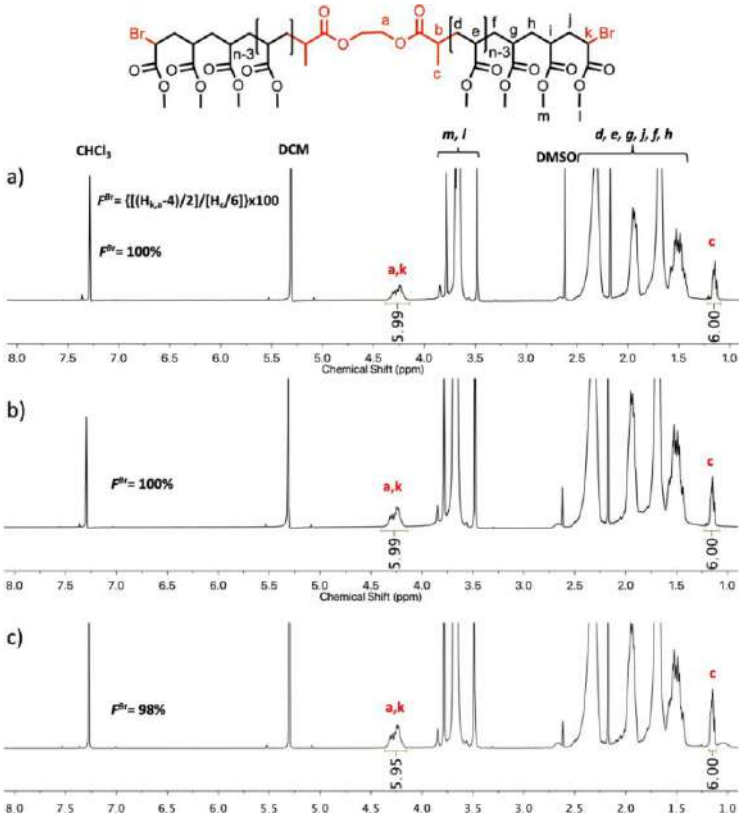

Figure 4.2.8. ^{1}H NMR spectra at 400 MHz of α,ω-di(bromo)PMA at (a) 94% conversion (M_n = 8,620 and M_w/M_n = 1.22; $[MA]_0/[BPE]_0/[Me_6\text{-TREN}]_0$ = 60/1/0.2); (b) 90% conversion (M_n = 9,090 and M_w/M_n = 1.41; $[MA]_0/[BPE]_0/[Me_6\text{-TREN}]_0/[TREN]_0$ = 60/1/0.1/0.1); (c) 96% conversion (M_n = 7,384 and M_w/M_n = 1.23; $[MA]_0/[BPE]_0/[TREN]_0$ = 60/1/0.2); Polymerization conditions: MA = 2 mL, DMSO = 1.0 mL, and nonactivated 9 cm Cu(0) wire of 20 gauge. The signals at 7.26 and 5.30 ppm are due to partially nondeuterated residue of $CDCl_3$ and dichloromethane, respectively. FBr values refer to chain-end functionality of PMA before thio-bromo "click" reaction (%).

This remarkable result demonstrates that the catalytic activity of DMSO increases the ligand activity of TREN and transforms it into an excellent ligand.

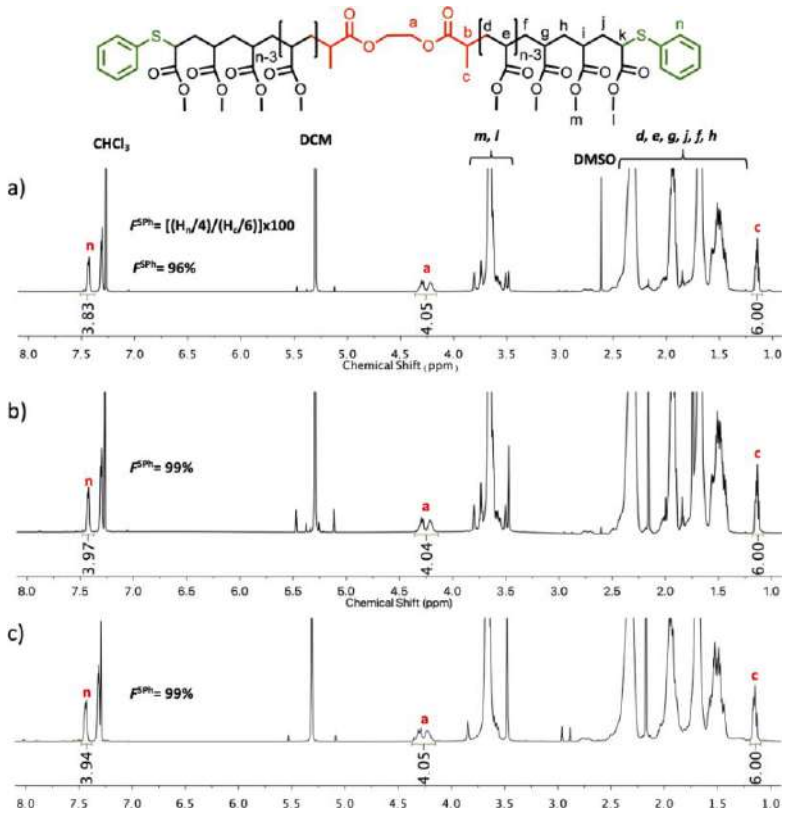

Figure 4.2.9. ^{1}H NMR spectra at 400 MHz of α,ω-di(phenylthio) PMA at (a) 94% conversion (M_n = 8,620 and M_w/M_n = 1.22; $[MA]_0/[BPE]_0/[Me_6\text{-TREN}]_0$ = 60/1/0.2); (b) 90% conversion (M_n = 9,090 and M_w/M_n = 1.41; $[MA]_0/[BPE]_0/[Me_6\text{-TREN}]_0/[TREN]_0$ = 60/1/0.1/0.1); (c) 96% conversion (M_n = 7380 and M_w/M_n = 1.23; $[MA]_0/[BPE]_0/[TREN]_0$ = 60/1/0.2); Conditions: MA = 2 mL, DMSO = 1.0 mL, and nonactivated 9 cm Cu(0) wire of 20 gauge wire. The signals at 7.26 and 5.30 ppm are due to a partially nondeuterated residue of $CDCl_3$ and dichloromethane, respectively. FSPh values refer to chain-end functionality of PMA after a thio-bromo "click" reaction (%).

Structural analysis by MALDI-TOF before and after thio-bromo "click" reaction

Representative MALDI-TOF spectra of PMA synthesized using Me_6-TREN, TREN, and equimolar amounts of Me_6-TREN and TREN isolated in between 90% and 96% conversion were analyzed before and after thioetherification (Figures 4.2.10, 4.2.11, and 4.2.12). The polymers isolated after SET-LRP at very high conversions showed one molecular weight distribution that was assigned to the bromine-terminated PMA ionized with Na^+.

Mixed-Ligand Effect During Cu(0)-mediated SET-LRP

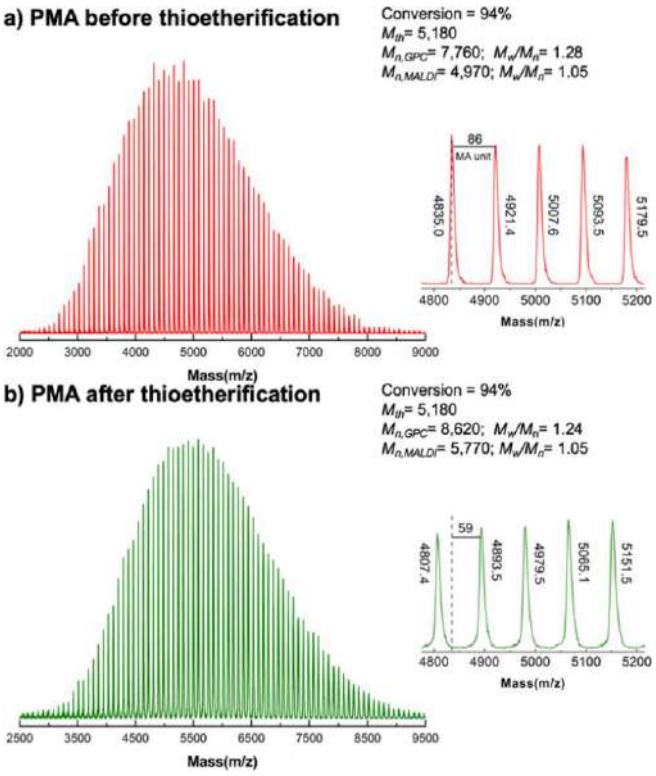

Figure 4.2.10. MALDI-TOF of PMA-Br isolated at 94% from SET-LRP of MA in DMSO solution initiated with BPE and catalyzed by nonactivated Cu(0) wire at 25 °C. (a) Before "thio-bromo click" reaction. (b) After "thio-bromo click" reaction. Reaction conditions: MA = 2 mL, DMSO = 1.0 mL, $[MA]_0/[BPE]_0/[Me_6\text{-TREN}]_0$ = 60/1/0.2, 9.0 cm of 20 gauge Cu(0) wire. The dotted line in expansion after thioeterification shows the original peak from before thioeterification, while 59 represents the increase in molar mass after thioeterification, that is, 2*[SC_6H_5 (109, 2)–Br (79, 9)] = 58.57 for each chain-end.

After thioetherification, the original peaks disappeared and reappeared at 59 mass units higher mass values. This is the expected mass difference value for the replacement of −Br atoms (2 × 79.9) by −SPh moieties (2 × 109.2) at both polymer chain-ends. MALDI-TOF analysis of PMA prepared using Me_6-TREN and TREN showed also high levels of chain-end functionality (Figures 4.2.10, 4.2.11, and 4.2.12, respectively). This demonstrates again the role of the catalytic activity of DMSO in transforming the neglected TREN into an excellent ligand for SET-LRP.

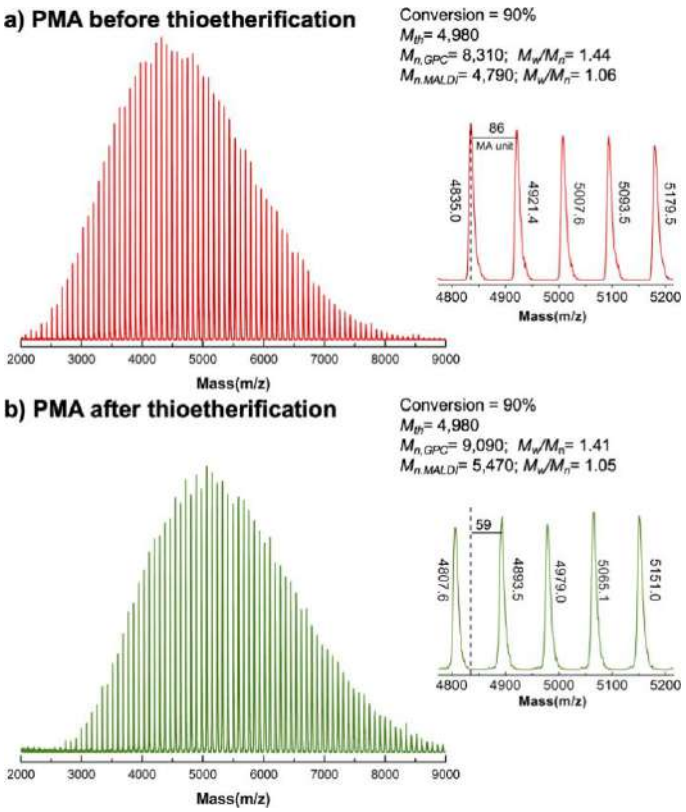

Figure 4.2.11. MALDI-TOF of PMA-Br isolated at 90% from SET-LRP of MA in DMSO solution initiated with BPE and catalyzed by a nonactivated Cu(0) wire at 25 °C: (a) Before the "thio-bromo click" reaction; (b) After the "thio-bromo click" reaction. Reaction conditions: MA = 2 mL, DMSO = 1.0 mL, $[MA]_0/[BPE]_0/[Me_6\text{-}TREN]_0/[TREN]_0$ = 60/1/0.1/0.1, 9.0 cm of 20 gauge Cu(0) wire. The dotted line in expansion after thioetherification shows the original peak from before thioetherification, while 59 represents the increase in molar mass after thioetherification, that is, 2*[SC_6H_5 (109, 2)-Br (79, 9)] = 58.57 for each chain end.

Mixed-Ligand Effect During Cu(0)-mediated SET-LRP

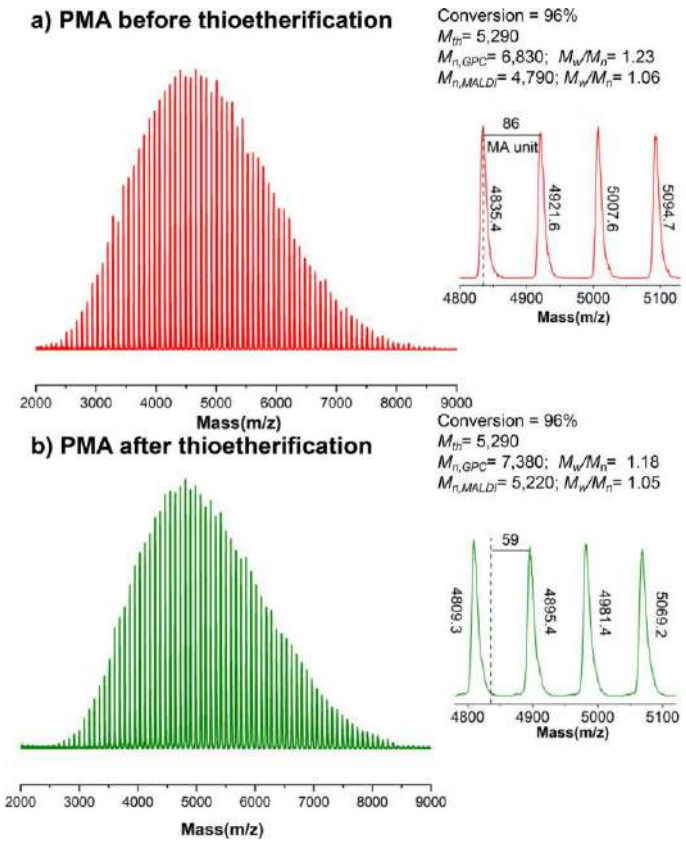

Figure 4.2.12. MALDI-TOF of PMA-Br isolated at 96% from SET-LRP of MA in DMSO solution initiated with BPE and catalyzed by nonactivated Cu(0) wire at 25 °C: (a) Before the "thio-bromo click" reaction; (b) After the "thio-bromo click" reaction. Reaction conditions: MA = 2 mL, DMSO = 1.0 mL, $[MA]_0/[BPE]_0/[TREN]_0$ = 60/1/0.2, 9.0 cm of 20 gauge Cu(0) wire. The dotted line in expansion after thioetherification shows the original peak from before thioetherification, while 59 represents the increase in molar mass after thioetherification, that is, 2*[SC_6H_5 (109, 2)–Br (79, 9)] = 58.57 for each chain end.

Mixed-ligand effect observed during SET-LRP of 2 mL of MA in 1.5 mL of DMSO using Me_6-TREN, Me_6-TREN/TREN, and TREN as ligands

Kinetic experiments for the SET-LRP of 2 mL of MA in 1.5 mL of DMSO performed with the mixed-ligand Me_6-TREN/TREN under similar reaction conditions to the experiments performed with 2 mL of MA in 1 mL of DMSO from Figure 4.2.4 are reported in Figure 4.2.13.

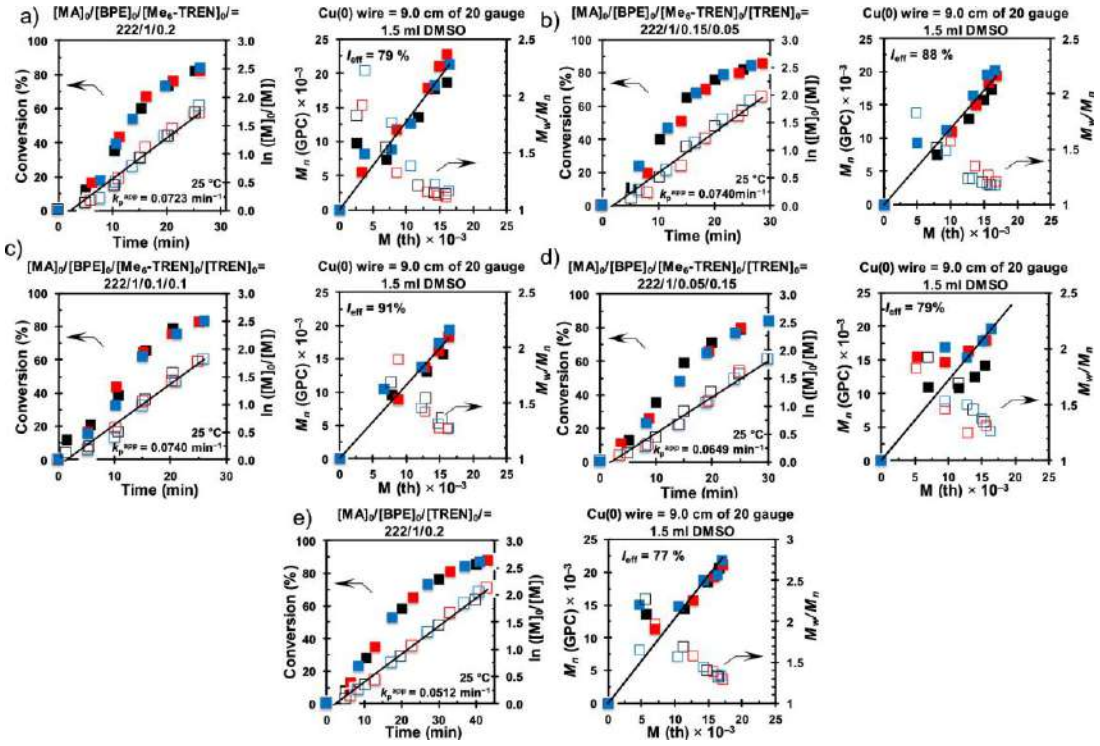

Figure 4.2.13. Kinetic plots, molecular weight, and dispersity evolutions for the SET-LRP of MA in DMSO, initiated with BPE and catalyzed by the 9.0 cm nonactivated Cu(0) wire at 25 °C. Experimental data in different colors were obtained from different kinetics experiments, carried out by different research. K_p^{app} and I_{eff} are the average values of three experiments ($[MA]_0/[BPE]_0/[ligand]_0/[Cu(0)]_0$ = 222/1/0.2/9 cm); MA = 2 mL; DMSO = 1.5 mL.

The freeze-though process was identical in both series of experiments, and therefore, due to the larger scale of the experiments reported in Figure 4.2.13, a small induction period was observed in a few cases. All experiments from Figure 4.2.13 were performed as triplicates. A comparison of the k_p^{app} values from Figure 4.2.4 with the data from Figure 4.2.13 indicates an increase in the k_p^{app} values by increasing the concentration of DMSO. An increase in the concentration of DMSO corresponds to a decrease in the concentration of MA and is expected to provide, under normal kinetic conditions, a decrease in the rate of polymerization. Therefore, the increased k_p^{app} values correspond to the catalytic effect of DMSO. Representative GPC experiments for the kinetics from Figure 4.2.13 are reported in Figure 4.2.14.

Mixed-Ligand Effect During Cu(0)-mediated SET-LRP

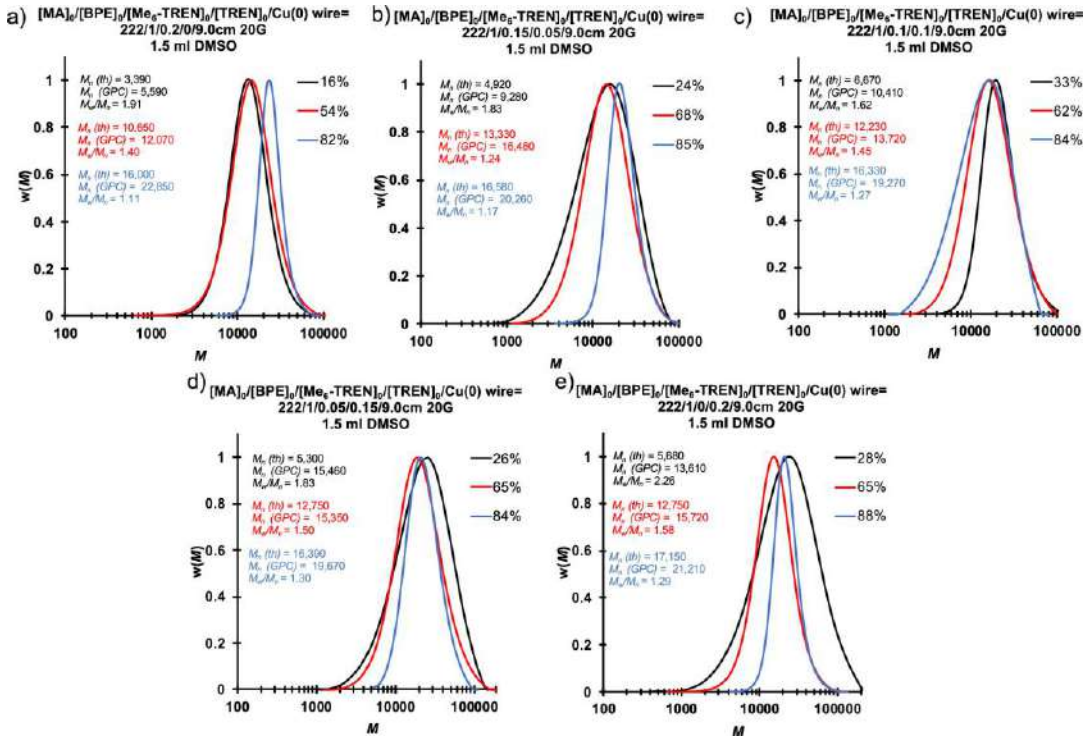

Figure 4.2.14. Representative GPC traces of the evolution of molecular weight as a function of conversion for the SET-LRP in a mixture of 2 mL of MA and 1.5 mL of DMSO catalyzed by 9.0 cm nonactivated Cu(0) wire at 25 °C in the presence of various ligand compositions. Reaction conditions: MA = 2 mL, DMSO = 1.5 mL, $[MA]_0/[BPE]_0/[L]_0$ = 222/1/0.2.

The GPC traces from Figure 4.2.14 provide the same trend with the corresponding data from Figure 4.2.6. Control experiments for the kinetic data reported in Figure 4.2.13 are reported in Figure 4.2.15. Their GPC data are shown in Figure 4.2.16, while the summary of all results is reported in Table 4.2.2. Figure 4.2.17 illustrates the results of the mixed-ligand effect performed with 2 mL of MA and 1.5 mL of DMSO. The control experiment data are also included in Figure 4.2.17 to support the mixed-ligand effect. The most remarkable series of results come from the comparison of the data from the mixed-ligand effect carried out with 2.0 mL of MA and 1.0 mL of DMSO versus 2.0 mL of MA and 1.5 mL of DMSO (compare Figure 4.2.4 with Figure 4.2.13 and Figure 4.2.5a with Figure 4.2.17).

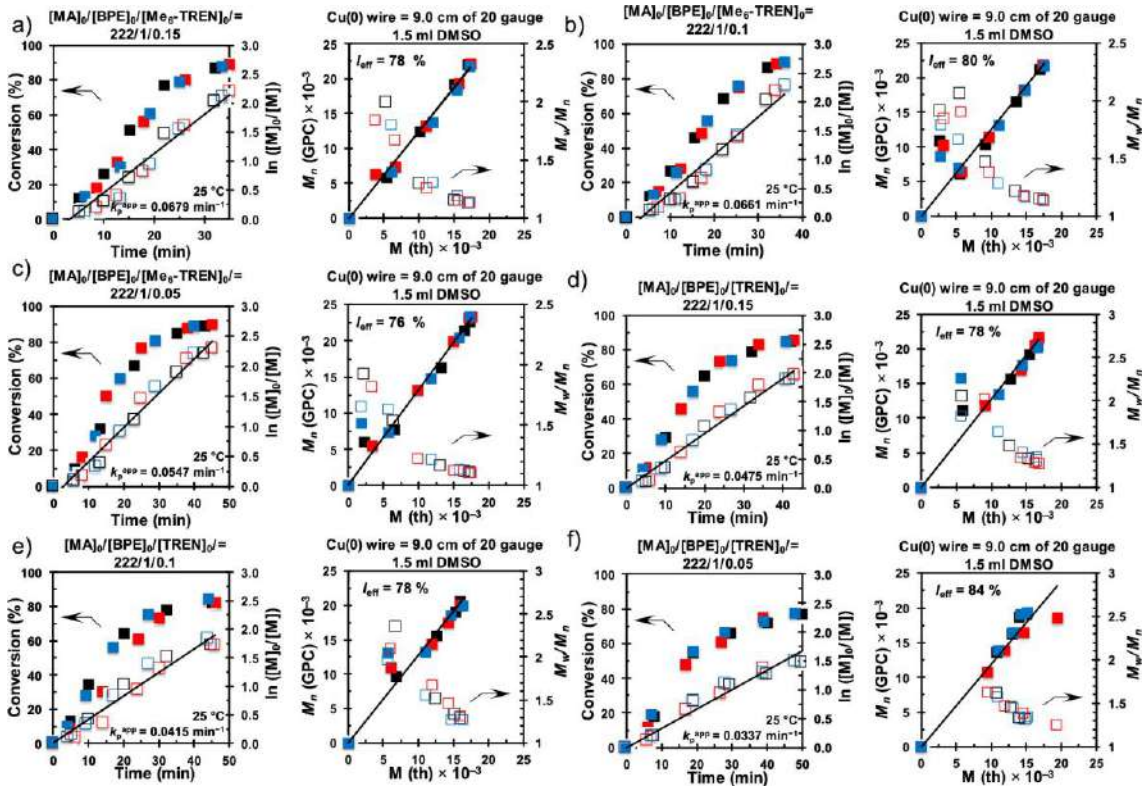

Figure 4.2.15. Control experiments: Kinetic plots, molecular weight, and dispersity evolutions for the SET-LRP of MA in DMSO, initiated with BPE and catalyzed by the 9.0 cm nonactivated Cu(0) wire at 25 °C. Experimental data in different colors were obtained from different kinetics experiments and generated by different research. K_p^{app} and I_{eff} is the average value of three experiment ($[MA]_0/[BPE]_0/[ligand]_0/[Cu(0)]_0$ = 222/1/0.15 to 0.05/9 cm); MA = 2 mL.

This comparison is also made in Table 4.2.3. The most representative result from this comparison is that, while the k_p^{app} value for Me_6-TREN at 1 mL of DMSO is 1.30, the value of k_p^{app} for TREN at 1.5 mL of DMSO is 1.38. Therefore, TREN becomes at 1.5 mL of DMSO more efficient than Me_6-TREN at 1 mL of DMSO.

This result explains the revitalization of TREN and its transformation into an excellent ligand by the catalytic effect of DMSO.

Mixed-Ligand Effect During Cu(0)-mediated SET-LRP

Table 4.2.2. Dependence of k_p^{app} on the dimension of the Cu(0) wire in the SET-LRP of MA-initiated with BPE in 1.5 mL of DMSO at 25 °C[a].

entry	wire length (cm) 20G	reaction condition	k_p^{app} (min^{-1})	M_w/M_n	I_{eff} (%)
1	9.0	[MA]/[BPE]/[Me_6-TREN] 222/1/0.2	0.0723	1.11	79
2	9.0	[MA]/[BPE]/[Me_6-TREN]/[TREN] 222/1/0.15/0.05	0.0740	1.17	88
3	9.0	[MA]/[BPE]/[Me_6-TREN]/[TREN] 222/1/0.1/0.1	0.0740	1.26	91
4	9.0	[MA]/[BPE]/[Me_6-TREN]/[TREN] 222/1/0.05/0.15	0.0649	1.26	79
5	9.0	[[MA]/[BPE]/[TREN] 222/1/0.2	0.0512	1.28	77
6	9.0	[MA]/[BPE]/[Me_6-TREN] 222/1/0.15	0.0679	1.13	78
7	9.0	[MA]/[BPE]/[Me_6-TREN] 222/1/0.10	0.0661	1.13	80
8	9.0	[MA]/[BPE]/[Me_6-TREN] 222/1/0.05	0.0547	1.10	76
9	9.0	[MA]/[BPE]/[TREN] 222/1/0.15	0.0475	1.27	78
10	9.0	[MA]/[BPE]/[TREN] 222/1/0.10	0.0415	1.27	78
11	9.0	[MA]/[BPE]/[TREN] 222/1/0.05	0.0337	1.24	84

[a] Reaction conditions: monomer = 2 mL; solvent = 1.5 mL.

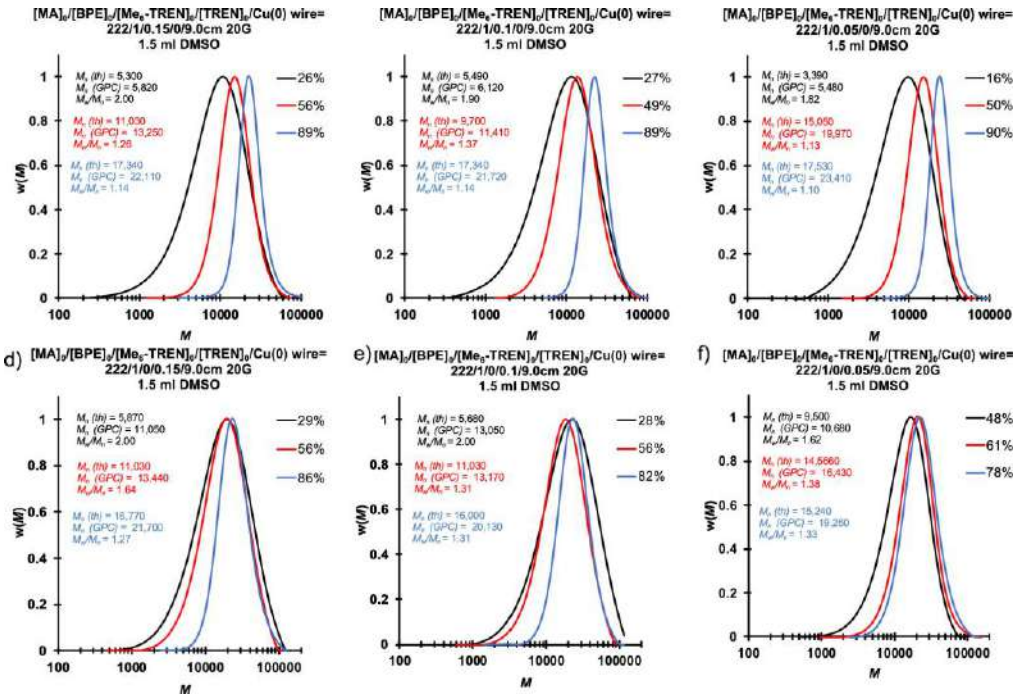

Figure 4.2.16. Representative GPC traces of the evolution of molecular weight as a function of conversion for the SET-LRP in a mixture of 2 mL of MA and 1.5 mL of DMSO catalyzed by the 9.0 cm nonactivated Cu(0) wire at 25 °C in the presence of various ligand compositions. Conditions: MA = 2 mL, DMSO = 1.5 mL, ($[MA]_0/[BPE]_0/[ligand]_0/[Cu(0)]_0$ = 222/1/0.15 to 0.05/9 cm); MA = 2 mL.

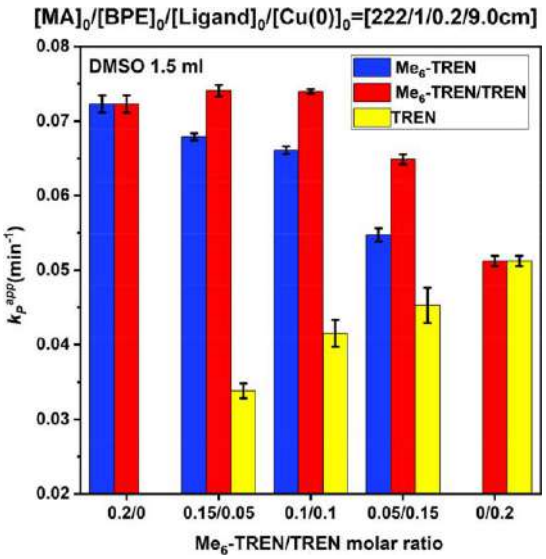

Figure 4.2.17. Evolution of k_p^{app} for the SET-LRP of MA (2 mL) initiated with BPE in DMSO (1.5 mL) mediated with different ratios between Me_6-TREN and TREN at 25 °C (in red). Control experiments performed only with Me_6-TREN (in blue) and only with TREN (in yellow) are also incorporated.

Mixed-Ligand Effect During Cu(0)-mediated SET-LRP

Table 4.2.3. Dependence of k_p^{app} on the 9 cm 20 G of the Cu(0) wire in the SET-LRP of MA initiated with BPE in DMSO at 25 °C[a].

entry	vol of DMSO (mL)	reaction condition	k_p^{app} (min^{-1})	k_p^{app}/ k_p^{app} (entry 10)	M_w/M_n	I_{eff} (%)
1	1.5	[MA]/[BPE]/[Me_6-TREN] 222/1/0.2	0.072	1.95	1.11	79
2	1.0	[MA]/[BPE]/[Me_6-TREN] 222/1/0.2	0.048	1.30	1.14	79
3	1.5	[MA]/[BPE]/[Me_6-TREN]/[TREN] 222/1/0.15/0.05	0.074	2.00	1.17	88
4	1.0	[MA]/[BPE]/[Me_6-TREN]/[TREN] 222/1/0.15/0.05	0.051	1.38	1.21	81
5	1.5	[MA]/[BPE]/[Me_6-TREN]/[TREN] 222/1/0.1/0.1	0.074	2.00	1.26	91
6	1.0	[MA]/[BPE]/[Me_6-TREN]/[TREN] 222/1/0.1/0.1	0.053	1.43	1.23	82
7	1.5	[MA]/[BPE]/[Me_6-TREN]/[TREN] 222/1/0.05/0.15	0.065	1.76	1.26	79
8	1.0	[MA]/[BPE]/[Me_6-TREN]/[TREN] 222/1/0.05/0.15	0.044	1.19	1.20	82
9	1.5	[MA]/[BPE]/[TREN] 222/1/0.2	0.051	1.38	1.28	77
10	1.0	[MA]/[BPE]/[TREN] 222/1/0.2	0.037	1.00	1.23	79

[a] Reaction conditions: MA = 2 mL.

Structural analysis of PMA before and after thio-bromo “click” reaction

Structural analysis was performed by a combination of ^{1}H NMR and MALDI-TOF before and after thio-bromo “click” reaction (Figures S6–S10 in Annex E). The chain-end functionality of the PMA is 97% before thio-bromo “click” reaction and 98% after thio-bromo “click” reaction, respectively, regardless of the structure of the ligand employed during SET-LRP (Figures S7 and S8 in Annex E). These excellent results are confirmed by the MALDI-TOF analysis performed before and after thio-bromo “click” reactions (Figures S6, S9, and S10 in Annex E).

4.2.3. Conclusions

DMSO exhibits a catalytic effect when used as solvent during SET-LRP of MA initiated with BPE and catalyzed with nonactivated Cu(0) wire both in the presence of Me_6-TREN and TREN and in mixtures of Me_6-TREN with TREN. A mixed-ligand effect was observed when mixtures of Me_6-TREN with TREN were used as ligands. The catalytic activity of DMSO can be exploited, as demonstrated here, to enhance the reactivity of TREN and of its 1/1 mixture with Me_6-TREN, while decreasing the basicity of the ligand and eliminating side reactions mediated by it. The most fundamental question related to this topic that must be addressed is the following: do all disproportionating solvents display a catalytic effect in SET-LRP or only DMSO? Research to address this question is in progress.

4.2.4. Experimental section

Materials

Methyl acrylate (MA; 99%, Acros) was passed over a short column of basic Al_2O_3 to remove its radical inhibitor. Tris(2-aminoethyl)amine (TREN; 99%, Acros), Cu(0) wire (20 gauge wire, 0.812 mm diameter from Fisher), and dimethyl sulfoxide (DMSO; 99.8%, Sigma-Aldrich) were used as received. Triethylamine (NEt_3; >99.5% Chemimpex) was distilled under N_2 from CaH_2. Bis(2-bromopropionyl)ethane (BPE) was synthesized by esterification of ethylene glycol with 2-bromopropionyl bromide in the presence pyridine.[48] Hexamethylated tris(2-aminoethyl)amine (Me_6-TREN) was synthesized by a literature procedure.[49]

Methods

^{1}H NMR (400 MHz) spectra were recorded on a Bruker AVANCE NEO 400 NMR instrument at 27 °C in $CDCl_3$ containing tetramethylsilane (TMS) as internal standard. Gel permeation chromatography (GPC) analysis of the polymer samples was performed using a Shimadzu LC-20AD high-performance liquid chromatograph pump, a PE Nelson Analytical 900 Series integration data station, a Shimadzu RID-10A refractive index (RI) detector, and

three AM gel columns (a guard column, 500 Å, 10 μm and 104 Å, 10 μm). THF (Fisher, HPLC grade) was used as eluent at a flow rate of 1 mL·min^{-1}. The number-average (M_n) and weight-average (M_w) molecular weights of PMA were determined with poly(methyl methacrylate) (PMMA) standards from American Polymer Standards. MALDI-TOF spectra were obtained on a Voyager DE (Applied Biosystems) instrument with a 337 nm nitrogen laser (3 ns pulse width). The accelerating potential was 25 kV, the grid was 92.5, the laser power was 2200–2500, and a positive ionization mode was used. The sample analysis was performed with 2-(4-hydroxyphenylazo) benzoic acid as the matrix. Solutions of the matrix (25 mg/mL in THF), NaCl (2 mg/mL in deionized H_2O), and polymer (10 mg/mL) were prepared independently. The solution for MALDI-TOF analysis was obtained by mixing the matrix, polymer, and salt solutions in a 5/1/1 volumetric ratio. Subsequently, 0.5 μL portions of the mixture were deposited onto three wells of sample plate and dried in air at room temperature before being subjected to MALDI-TOF analysis.

Standard procedure for SET-LRP of MA in DMSO using Me_6-TREN, TREN, and the mixed-ligand Me_6-TREN/TREN methodology

Stock solutions prepared with different ratios of Me_6-TREN to TREN such as 0.02/0 M, 0.015/0.005 M, 0.01/0.01 M, 0.005/0.015 M, and 0/0.02 M in DMSO were first made. The monomer (MA, 22.2 mmol, 2.00 mL), organic solvent (DMSO if necessary), DMSO stock solution (0.02 mmol ligand, 1 mL), and initiator (BPE, 0.1 mmol, 33.2 mg) were added in this order to a 25 mL Schlenk tube. The mixture was deoxygenated by six freeze–pump–thaw cycles. Subsequently, the Schlenk tube was opened under a positive flow of nitrogen to add the Cu(0) wire wrapped around a Teflon-coated stir bar. Two more freeze–pump–thaw cycles were carried out while holding the stir bar above the reaction mixture with the help of an external magnet. The Schlenk tube was filled with N_2, and the reaction was placed in a water bath at 25 °C. Then, the stir bar wrapped with the Cu(0) wire was dropped gently into the reaction. The introduction of the Cu(0) wire defines t = 0. Samples were taken at different times by purging the side arm of the Schlenk tube with nitrogen for 2 min using a deoxygenated syringe and stainless steel needles. Samples were dissolved in $CDCl_3$ and

quenched by air bubbling. After that, the monomer conversion was measured by ^{1}H NMR spectroscopy. In order to determine the molecular weight and polydispersity of the samples, the solvent and the residual monomer were removed under vacuum. Finally, samples were dissolved in THF and passed through a short small basic Al_2O_3 chromatographic column to remove any residual copper and analyzed by GPC. The resulting PMA was precipitated in cold methanol and dried under vacuum until constant weight to perform chain-end analysis by ^{1}H NMR spectroscopy, before and after the thioetherification of the chain ends.

General method for the chain-end thioetherification of PMA *via* thio-bromo "click" reaction

In a 10 mL test tube sealed with a rubber septum, thiophenol (0.05 equiv) and distilled triethylamine (NEt_3, 0.05 equiv) were added into a solution of the corresponding polymer (0.01 equiv) in acetonitrile (1 mL) under a nitrogen flow. The mixture was stirred at room temperature for 3 h. Then, the resulting modified PMA was precipitated in cold methanol and washed with methanol several times. The resulting polymer was dried under vacuum to a constant weight.

4.2.5. References

[1] Reetz, M. T.; Sell, T.; Meiswinkel, A.; Mehler, G. *Angew. Chem., Int. Ed.* **2003**, *42*, 790-793.

[2] Duursma, A.; Hoen, R.; Schuppan, J.; Hulst, R.; Minnaard, A. J.; Feringa, B., L. *Org. Lett.* **2003**, *5*, 3111-3113.

[3] Fors, B. P.; Buchwald, S. L. *J. Am. Chem. Soc.* **2010**, *132*, 15914-15917.

[4] Fan, Y.; Xia, Y.; Tang, J.; Ziarelli, F.; Qu, F.; Rocchi, P.; Iovanna, J. L.; Peng, L. *Chem. - Eur. J.* **2012**, *18*, 2221-2225.

[5] Cong, M.; Fan, Y.; Raimundo, J. M.; Xia, Y.; Liu, Y.; Quéléver, G.; Qu, F.; Peng, L. *Chem. - Eur. J.* **2013**, *19*, 17267-17272.

[6] (a) Percec, V.; Golding, G., M.; Smidrkal, J.; Weichold, O. *J. Org. Chem.* **2004**, *69*, 3447-3452. (b) Wilson, D. A.; Wilson, C. J.; Rosen, B. M.; Percec, V. *Org. Lett.* **2008**, *10*, 4879-4882. (c) Moldoveanu, C.; Wilson, D. A.; Wilson, C. J.; Corcoran, P.; Rosen, B. M.; Percec, V. *Org. Lett.* **2009**, *11*, 4974-4977. (d) Wilson, D. A.; Wilson, C. J.; Moldoveanu, C.; Resmerita, A. M.; Corcoran, P.; Hoang, L. M.; Rosen, B. M.; Percec, V. *J. Am. Chem. Soc.* **2010**, *132*, 1800-1801. (e) Leowanawat, P.; Resmerita, A. M.; Moldoveanu, C.; Liu, C.; Zhang, N.; Wilson, D. A.; Hoang, L. M.; Rosen, B. M.; Percec, V. *J. Org. Chem.* **2010**, *75*, 7822-7828. (f) Moldoveanu, C.; Wilson, D. A.; Wilson, C. J.; Leowanawat, P.; Resmerita, A. M.; Liu, C.; Rosen, B. M.; Percec, V. *J. Org. Chem.* **2010**, *75*, 5438-5452. (g) Leowanawat, P.; Zhang, N.; Resmerita, A.-M.; Rosen, B. M.; Percec, V. *J. Org. Chem.* **2011**, *76*, 9946-9955. (h) Leowanawat, P.; Zhang, N.; Safi, M.; Hoffman, D. J.; Fryberger, M. C.; George, A.; Percec, V. *J. Org. Chem.* **2012**, *77*, 2885-2892. (i) Leowanawat, P.; Zhang, N.; Percec, V. *J. Org. Chem.* **2012**, *77*, 1018-1025. (j) Zhang, N.; Hoffman, D. J.; Gutsche, N.; Gupta, J.; Percec, V. *J. Org. Chem.* **2012**, *77*, 5956-5964. (k) Leowanawat, P.; Zhang, N.; Safi, M.; Hoffman, D. J.; Fryberger, M. C.; George, A.; Percec, V. *J. Org. Chem.*

2012, *77*, 2885-2892. (l) Malineni, J.; Jezorek, R. L.; Zhang, N.; Percec, V. *Synthesis* **2016**, *48*, 2795-2807. (m) Malineni, J.; Jezorek, R. L.; Zhang, N.; Percec, V. *Synthesis* **2016**, *48*, 2808-2815.

[7] Li, K. -T.; Shieh, D. C. *Ind. Eng. Chem. Res.* **1994**, *33*, 1107-1112.

[8] Matyjaszewski, K.; Wei, M.; Xia, J.; McDermott, N. E. *Macromolecules* **1997**, *30*, 8161-8164.

[9] Lizuka, E.; Wakioka, M.; Ozawa, F. *Macromolecules* **2015**, *48*, 2989-2993.

[10] (a) Percec, V.; Guliashvili, T.; Ladislaw, J. S.; Wistrand, A.; Stjerndahl, A.; Sienkowska, M. J.; Monteiro, M. J.; Sahoo, S. *J. Am. Chem. Soc.* **2006**, *128*, 14156-14165. (b) Feng, X.; Maurya, D. S.; Bensabeh, N.; Moreno, A.; Oh, T.; Luo, Y.; Lejnieks, J.; Galià, M.; Miura, Y.; Monteiro, M. J.; Lligadas, G.; Percec, V. *Biomacromolecules* **2020**, *21*, 250-261.

[11] (a) Percec, V.; Guliashvili, T.; Ladislaw, J. S.; Wistrand, A.; Stjerndahl, A.; Sienkowska, M. J.; Monteiro, M. J.; Sahoo, S. *J. Am. Chem. Soc.* **2006**, *128*, 14156-14165. (b) Percec, V.; Popov, A. V.; Ramirez-Castillo, E.; Monteiro, M.; Barboiu, B.; Weichold, O.; Asandei, A. D.; Mitchell, C. M. *J. Am. Chem. Soc.* **2002**, *124*, 4940-4941.

[12] Rosen, B. M.; Percec, V. *Chem. Rev.* **2009**, *109*, 5069-5119.

[13] Zhang, N.; Samanta, S. R.; Rosen, B. M.; Percec, V. *Chem. Rev.* **2014**, *114*, 5848-5958.

[14] Lligadas, G.; Grama, S.; Percec, V. *Biomacromolecules* **2017**, *18*, 2981-3008.

[15] Boyer, C.; Corrigan, N. A.; Jung, K.; Nguyen, D.; Nguyen, T. K.; Adnan, N. N.; Oliver, S.; Shanmugam, S.; Yeow, J. *Chem. Rev.* **2016**, *116*, 1803-1949.

[16] Anastasaki, A.; Nikolaou, V.; Nurumbetov, G.; Wilson, O.; Kempe, K.; Quinn, J. F.; Davis, T. P.; Whittaker, M. R.; Haddleton, D. M. *Chem. Rev.* **2016**, *116*, 835-877.

[17] Anastasaki, A.; Nikolaou, V.; Haddleton, D. M. *Polym. Chem.* **2016**, *7*, 1002-1026.

[18] Rosen, B. M.; Jiang, X.; Wilson, C. J.; Nguyen, N. H.; Monteiro, M. J.; Percec, V. *J. Polym. Sci., Part A: Polym. Chem.* **2009**, *47*, 5606-5628.

[19] (a) Levere, M. E.; Nguyen, N. H.; Leng, X.; Percec, V. *Polym. Chem.* **2013**, *4*, 1635-1647. (b) Jiang, X.; Rosen, B. M.; Percec, V. *J. Polym. Sci., Part A: Polym. Chem.* **2010**, *48*, 403-409. (c) Lligadas, G.; Percec, V. *J. Polym. Sci., Part A: Polym. Chem.* **2008**, *46*, 6880-6895. (d) Nguyen, N. H.; Kulis, J.; Sun, H.-J.; Jia, Z.; van Beusekom, B.; Levere, M. E.; Wilson, D. A.; Monteiro, M. J.; Percec, V. *Polym. Chem.* **2013**, *4*, 144-155. (e) Jiang, X.; Fleischmann, S.; Nguyen, N. H.; Rosen, B. M.; Percec, V. *J. Polym. Sci., Part A: Polym. Chem.* **2009**, *47*, 5591-5605. (f) Bunnett, J. F.; Scamehorn, R. G.; Traber, R. P. *J. Org. Chem.* **1976**, *41*, 3677-3682.

[20] Rosen, B. M.; Percec, V. *J. Polym. Sci., Part A: Polym. Chem.* **2007**, *45*, 4950-4964.

[21] Sienkowska, M. J.; Rosen, B. M.; Percec, V. *J. Polym. Sci., Part A: Polym. Chem.* **2009**, *47*, 4130-4140.

[22] Hatano, T.; Rosen, B. M.; Percec, V. *J. Polym. Sci., Part A: Polym. Chem.* **2010**, *48*, 164-172.

[23] Percec, V.; Popov, A. V.; Ramirez-Castillo, E.; Weichold, O. *J. Polym. Sci., Part A: Polym. Chem.* **2003**, *41*, 3283-3299.

[24] Nguyen, N. H.; Levere, M. E.; Percec, V. *J. Polym. Sci., Part A: Polym. Chem.* **2012**, *50*, 35-46.

[25] Nicol, E.; Derouineau, T.; Puaud, F.; Zaitsev, A. *J. Polym. Sci., Part A: Polym. Chem.* **2012**, *50*, 3885-3894.

[26] Nguyen, N. H.; Levere, M. E.; Percec, V. *J. Polym. Sci., Part A: Polym. Chem.* **2012**, *50*, 860-873.

[27] Voorhaar, L.; Wallyn, S.; Du Prez, F. E.; Hoogenboom, R. *Polym. Chem.* **2014**, *5*, 4268-4276.

[28] Simula, A.; Nikolaou, V.; Alsubaie, F.; Anastasaki, A.; Haddleton, D. M. *Polym. Chem.* **2015**, *6*, 5940-5950.

[29] Moreno, A.; Grama, S.; Liu, T.; Galià, M.; Lligadas, G.; Percec, V. *Polym. Chem.* **2017**, *8*, 7559-7574.

[30] Moreno, A.; Galià, M.; Lligadas, G.; Percec, V. *Biomacromolecules* **2018**, *19*, 4480-4491.

[31] Moreno, A.; Liu, T.; Galià, M.; Lligadas, G.; Percec, V. *Polym. Chem.* **2018**, *9*, 1961-1971.

[32] Moreno, A.; Jezorek, R. L.; Liu, T.; Galià, M.; Lligadas, G.; Percec, V. *Polym. Chem.* **2018**, *9*, 1885-1899.

[33] Moreno, A.; Liu, T.; Ding, L.; Buzzacchera, I.; Galià, M.; Möller, M.; Wilson, C. J.; Lligadas, G.; Percec, V. *Polym. Chem.* **2018**, *9*, 2313-2327.

[34] Jezorek, R. L.; Enayati, M.; Smail, R. B.; Lejnieks, J.; Grama, S.; Monteiro, M. J.; Percec, V. *Polym. Chem.* **2017**, *8*, 3405-3424.

[35] Smail, R. B.; Jezorek, R. L.; Lejnieks, J.; Enayati, M.; Grama, S.; Monteiro, M. J.; Percec, V. *Polym. Chem.* **2017**, *8*, 3102-3123.

[36] Enayati, M.; Jezorek, R. L.; Smail, R. B.; Monteiro, M. J.; Percec, V. *Polym. Chem.* **2016**, *7*, 5930-5942.

[37] Enayati, M.; Smail, R. B.; Grama, S.; Jezorek, R. L.; Monteiro, M. J.; Percec, V. *Polym. Chem.* **2016**, *7*, 7230-7241.

[38] Enayati, M.; Jezorek, R. L.; Monteiro, M. J.; Percec, V. *Polym. Chem.* **2016**, *7*, 3608-3621.

[39] Grama, S.; Lejnieks, J.; Enayati, M.; Smail, R. B.; Ding, L.; Lligadas, G.; Monteiro, M. J.; Percec, V. *Polym. Chem.* **2017**, *8*, 5865-5874.

[40] Nguyen, N. H.; Rosen, B. M.; Jiang, X.; Fleischmann, S.; Percec, V. *J. Polym. Sci., Part A: Polym. Chem.* **2009**, *47*, 5577-5590.

[41] Lligadas, G.; Rosen, B. M.; Bell, C. A.; Monteiro, M. J.; Percec, V. *Macromolecules* **2008**, *41*, 8365-8371.

[42] Nguyen, N. H.; Rosen, B. M.; Lligadas, G.; Percec, V. *Macromolecules* **2009**, *42*, 2379-2386.

[43] Ahrland, S.; Rawsthorne, J.; Haaland, A.; Jerslev, B.; Schaffer, C. E.; Sunde, E.; Sørensen, N. A. *Acta Chem. Scand.* **1970**, *24*, 157-172.

[44] Ciavatta, L.; Ferri, D.; Palombari, R. *Chem.* **1980**, *42*, 593-598.

[45] Nguyen, N. H.; Sun, H.-J.; Levere, M. E.; Fleischmann, S.; Percec, V. *Polym. Chem.* **2013**, *4*, 1328-1332.

[46] (a) Negrel, J. C.; Gony, M.; Chanon, M.; Lai, R. *Inorg. Chim. Acta* **1993**, *207*, 59-63. (b) Julliard, M.; Chanon, M. Photoelectron Transfer Catalyst. *Chem. Scr.* **1894**, *4*, 11-21. (c) Timms, P. L. *Proc. R. Soc. London, Ser. A* **1984**, *396*, 1-19. (d) Klabunde, K. J. *Acc. Chem. Res.* **1975**, *8*, 393-399. (e) Klabunde, K. J.; Li, Y. X.; Tan, B. J. *Chem. Mater.* **1991**, *3*, 30-39.

[47] (a) Rosen, B. M.; Lligadas, G.; Hahn, C.; Percec, V. *J. Polym. Sci., Part A: Polym. Chem.* **2009**, *47*, 3931-3939. (b) Rosen, B. M.; Lligadas, G.; Hahn, C.; Percec, V. *J. Polym. Sci., Part A: Polym. Chem.* **2009**, *47*, 3940-3948.

[48] Lligadas, G.; Percec, V. *J. Polym. Sci., Part A: Polym. Chem.* **2007**, *45*, 4684-4695.

[49] Ciampolini, M.; Nardi, N. *Inorg. Chem.* **1966**, *5*, 41-44.

Chapter 5

Overall Conclusions

5. Overall conclusions

During the course of this thesis, it has been demonstrated that controlled/living RP techniques such as Cu(0) wire-catalyzed SET-LRP, RAFT polymerization and Cu(II)Br_2-mediated photopolymerization are promising tools to deliver BCPs derived from bio-available lactic acid-derived solvents (i.e. EL, BL, DML) in combination with other renewable monomers. Some of the targeted biobased AB and ABA copolymers were useful in technological applications such as pressure sensitive adhesives (PSAs) and stabilizers in emulsion polymerization. Furthermore, it has been demonstrated that the "mixed-ligand" concept can be exploited to obtain improved polymeric materials *via* SET-LRP.

The general conclusions of this thesis are the following:

- The SET-LRP of the bio-based acrylate monomers based on EL, and homologous structures with methyl and n-butyl alkyl chains, in alcohols, homogeneous mixtures of alcohols and water, and biphasic mixtures of alcohols with water provided excellent control over the molecular weight, polydispersity and chain end functionality of the resulting linear polymers. These results create the basis for the synthesis of polymers with more complex architecture.

- Low T_g polyacrylates derived from ELA in combination with a high T_g modelic biobased polymers, based on pinene acrylate, have been shown suitable for the preparation of BCPs with phase-separated morphology. When the bio-available glycerol acrylate was used instead of pinene acrylate, an amphiphilic BCP capable to self-assemble into micellar nanoparticles in water was obtained.

- EL and DML derived acrylics are well-behaved monomers under Cu(II)Br_2-mediated LR photopolymerization to generate amphiphilic AB BCPs that could self-assemble in water to generate nanoaggregates with different morphologies such as LCMs, worm-like micelles, and vesicles.

Overall conclusions

- Some of these amphiphilic AB BCPs, exhibited an efficient performance as nonionic surfactants in the preparation of PMMA and PSt latexes *via* aqueous emulsion polymerization, demonstrating their practical significance for technological applications.

- The combination of BLA with other biobased monomers such as isosorbide acetate- and vanillin- acrylates is promising to deliver PSAs based on ABA-type BCPs prepared by RAFT polymerization. Some of the developed triblocks possess competitive adhesive performance when compared to commercial pressure-sensitive tapes.

- SET-LRP successfully created polyMnA using TFE and TFP with a range of targeted degrees of polymerization (DP 25-200) in moderate reaction times (< 7 hours), regardless of the bulkiness and hydrophobicity of the biobased MnA.

- The combination of ^{1}H NMR and MALDI-TOF analysis performed before and after the modification of bromine terminus *via* "thio-bromo" click chemistry and *in situ* reinitiation copolymerization experiments supported the high end-group fidelity of the prepared biobased polymers.

- A "mixed-ligand" effect was observed when mixtures of Me_6-TREN with TREN were used as ligands for the Cu(0)-mediated SET-LRP of MA in both homogeneous and "programmed" biphasic systems based on dipolar aprotic solvents and water.

- During the SET-LRP of MA in 8/2 (v/v) aqueous mixtures of NMP, DMF, and DMAc with H_2O, the use of the "mixed-ligand" system enhanced the rate of polymerization, and improved monomer conversion and molecular weight control. A Me_6-TREN/TREN 1/1 molar ratio was demonstrated to be the most efficient system.

- DMSO exhibits a catalytic effect when used as solvent for the SET-LRP of MA initiated with BPE initiator and catalyzed with nonactivated Cu(0) wire both in the presence of Me_6-TREN and TREN and in a "mixed-ligand" system. Also in this case, the most important effect was observed at 1/1 molar ratio between both ligands. These results

suggest that, in addition to a fast exchange between the two ligands, a new single dynamic ligand, generated by hydrogen-bonding, should be considered in future mechanistic investigations.

Annexes

Annex A

Supplementary Information for

Polyacrylates derived from bio-based ethyl lactate solvent *via* SET-LRP

Table of contents:

Supporting information for Chapter 2.1

1. Structural characterization of ELA

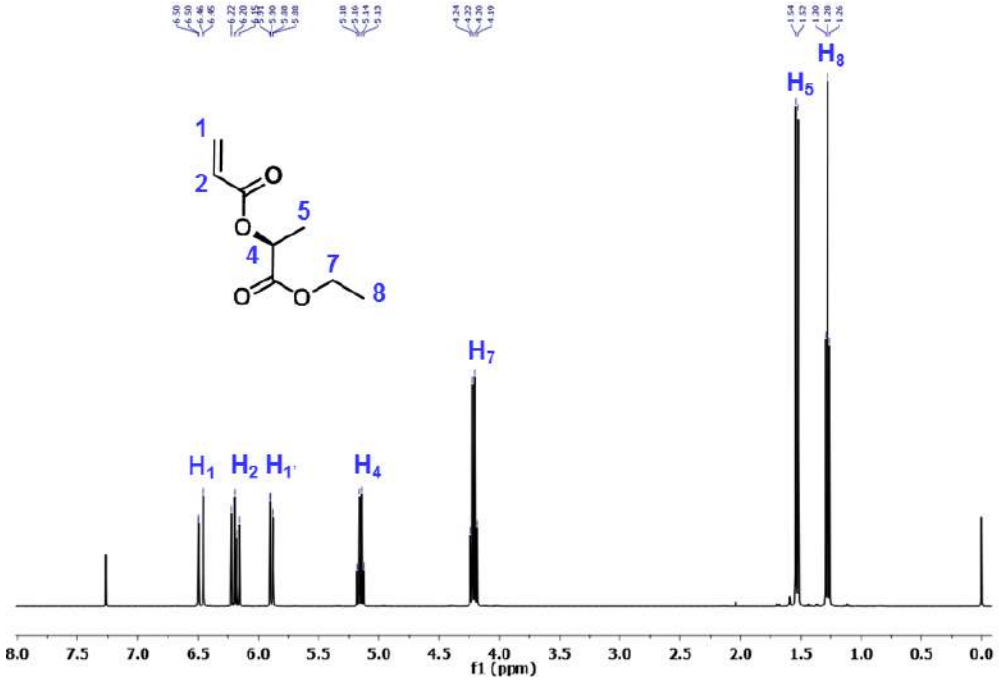

Figure S1. ^{1}H NMR spectrum of ethyl lactate acrylate (ELA) in $CDCl_3$.

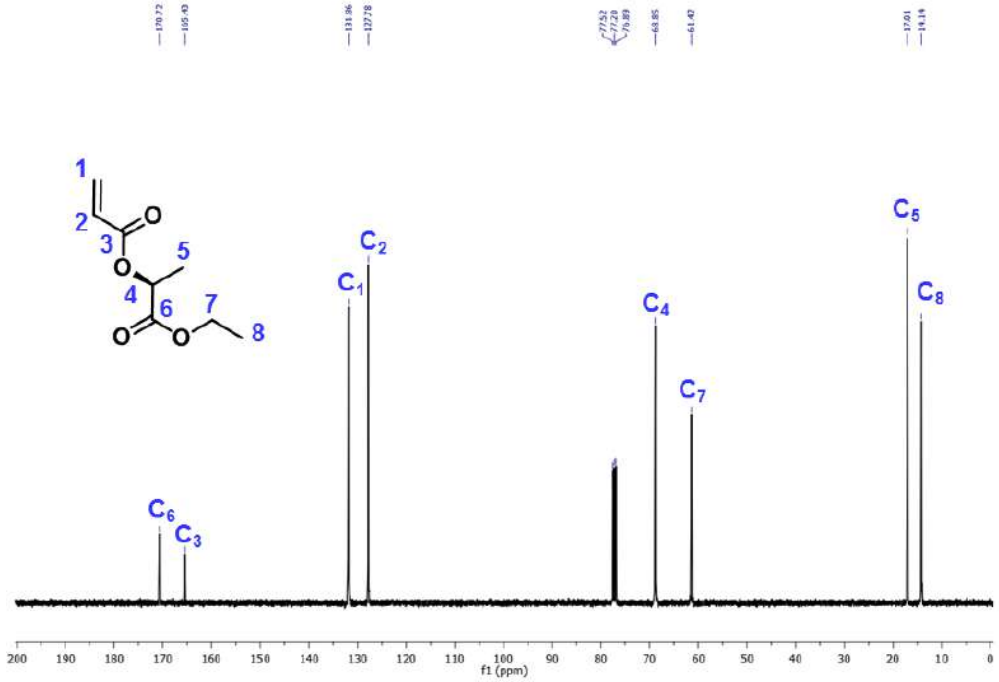

Figure S2. ^{13}C NMR spectrum of ELA in $CDCl_3$.

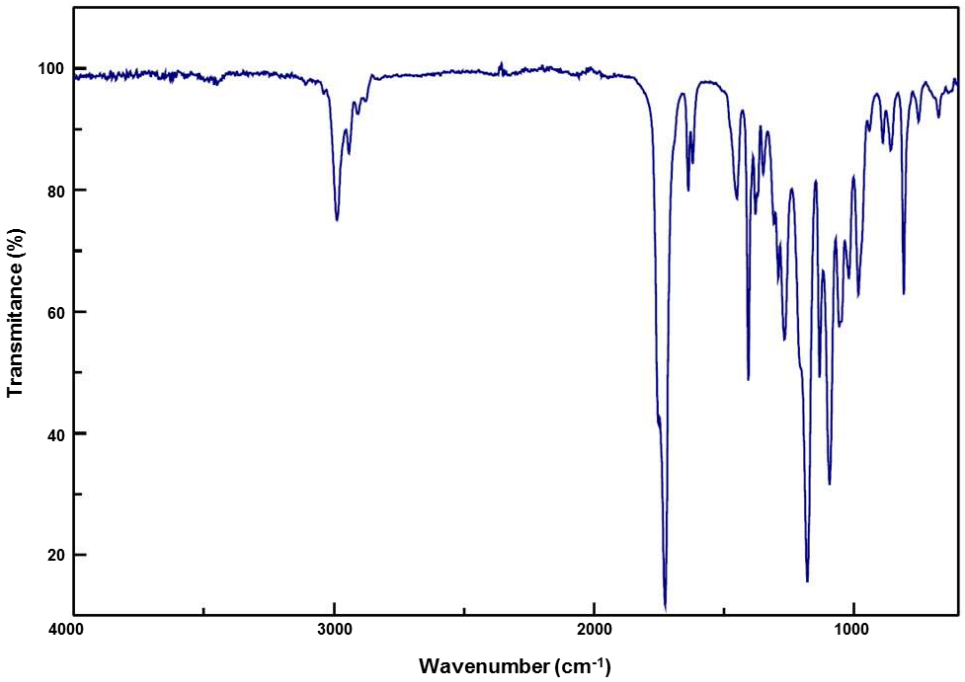

Figure S3. FTIR spectrum of ELA.

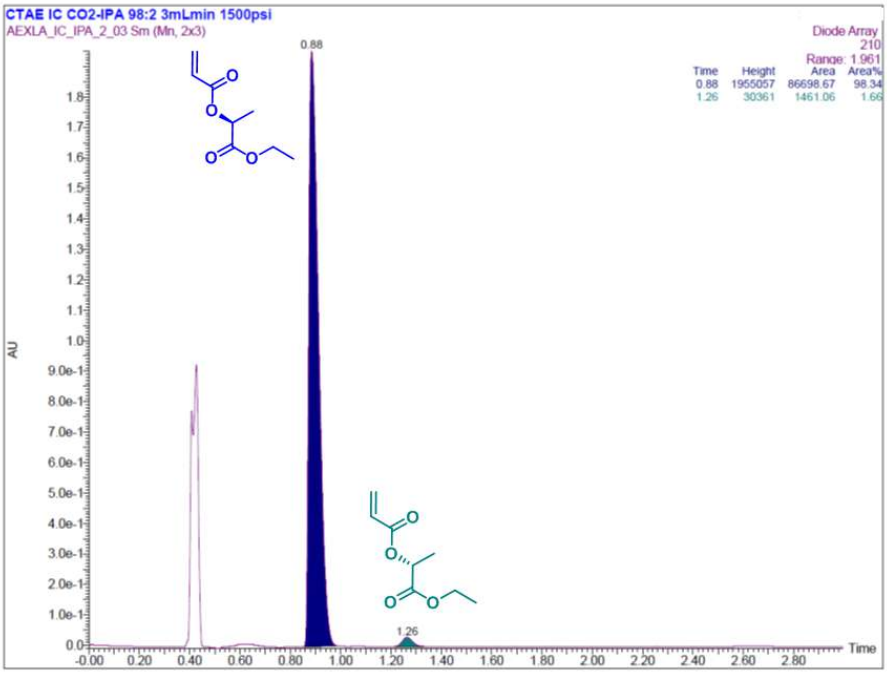

Figure S4. SFC chromatogram of ELA synthesized from natural ethyl lactate (EL) purchased from Sigma-Aldrich.

Supporting information for Chapter 2.1

2. SET-LRP of ELA

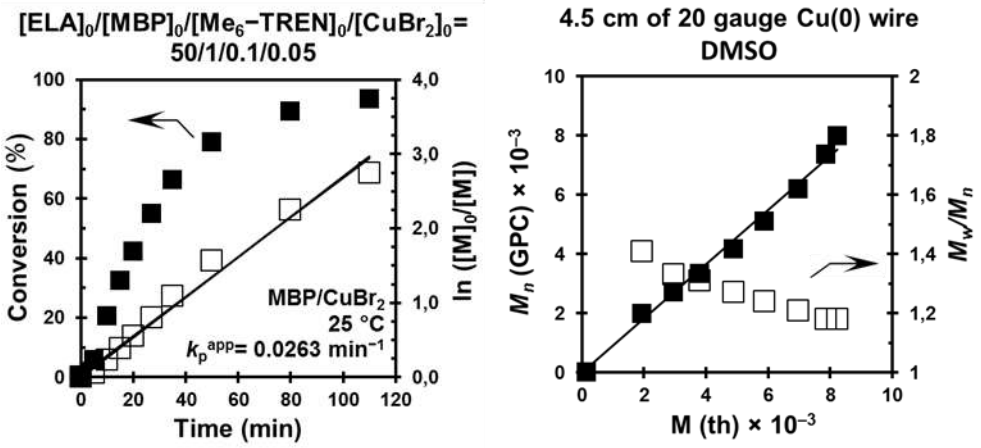

Figure S5. Monomer conversion, kinetic plot and evolution of molecular weight and polydispersity for the Cu(0) wire-catalyzed SET-LRP of ELA in DMSO initiated with methyl α-bromopropionate (MBP) at 25 °C in the presence of externally added $Cu(II)Br_2$. Reaction conditions: ELA = 1 mL, DMSO = 0.5 mL, 4.5 cm hydrazine- activated Cu(0) wire and $[ELA]_0/[MBP]_0/[Me_6\text{-}TREN]_0/[CuBr_2]_0$ = 50/1/0.1/0.05.

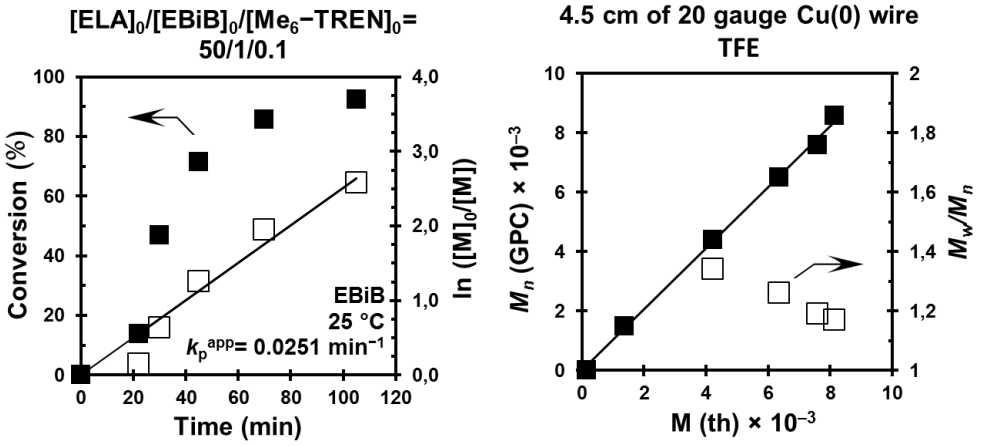

Figure S6. Monomer conversion, kinetic plot and evolution of molecular weight and polydispersity for the Cu(0) wire-catalyzed SET-LRP of ELA in TFE initiated with ethyl α-bromoisobutyrate (EBiB) at 25 °C. Reaction conditions: ELA = 1 mL, TFE = 0.5 mL, 4.5 cm hydrazine-activated Cu(0) wire and $[ELA]_0/[EBiB]_0/[Me_6\text{-}TREN]_0$ = 50/1/0.1.

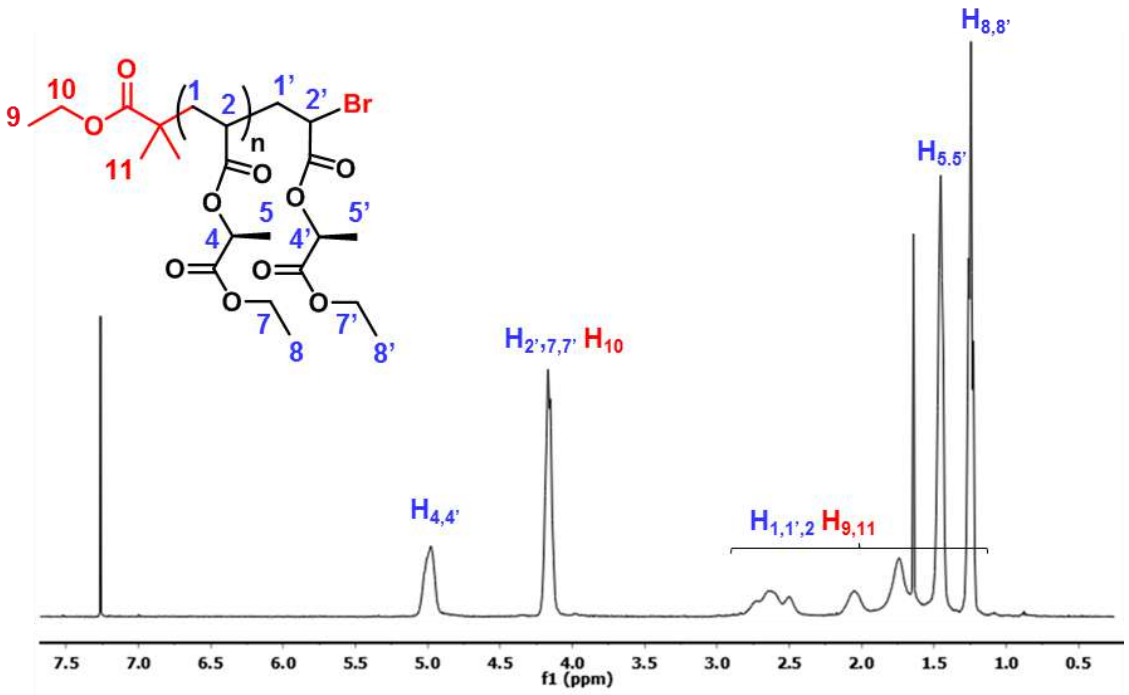

Figure S7. ^{1}H NMR spectrum of poly(ELA) ($M_{n,GPC}$ = 4,120 and M_w/M_n = 1.22) in $CDCl_3$.

3. Thermal and chiroptical characterization of poly(ELA)

The thermal properties of poly(ELA) ($M_{n,GPC}$ = 34,700 and M_w/M_n = 1.20) were evaluated using thermogravimetric analysis (TGA, Figure S8a red trace) and differential scanning calorimetry (DSC, Figure S8b red trace). Compared to PMA ($M_{n,GPC}$ = 38,850 and M_w/M_n = 1.22) of approximately the same molar mass prepared also by SET-LRP, poly(ELA) showed 5% mass loss ($T_{5\%}$) at lower temperature (307 °C compared to 359 °C). The TGA thermogram of poly(ELA) shows one dominant degradation step with a maximum weight loss (T_{max}) at 379 °C. This process, ascribed to the thermal decomposition of polymer, occurs 33 °C higher for PMA (T_{max} = 412 °C). As expected, DSC analysis confirmed that poly(ELA) is amorphous. Compared to PMA, the T_g of this polymer shows a significant decrease possibly associated to the presence of EL pendant groups limiting chain packing and consequently increasing segmental motion (T_g = 16 °C compared to -1 °C). The T_g of poly(ELA) was not much different for a lower molar mass sample (T_g = -2.6 °C for $M_{n,GPC}$ = 4,120) but dropped to

Supporting information for Chapter 2.1

-28 °C for poly(BLA) of similar molecular weight ($M_{n,GPC}$ = 5,000). On the other hand, contact angle measurements demonstrated that polyacrylates with ethyl lactate pendant groups are hydrophobic polymers (Figure S8c). Note that compared to PMA, PELA is more hydrophobic. Furthermore, the chirality which is to be expected for poly(ELA) was confirmed by circular dichroism (CD) analysis optical rotation measurements. In contrast to PMA which does not contain any chiral center, poly(ELA) ($M_{n,GPC}$ = 34,700 and M_w/M_n = 1.20) exhibited intense CD signal around 215 nm (Figure S9). However, the fact that the specific optical rotation of poly(ELA) was approximately the same than that of the corresponding monomer precursor supports that the optical activity of the polymer arises only due to the configurational chirality in the side chain and not from a conformational chirality (Table S1).

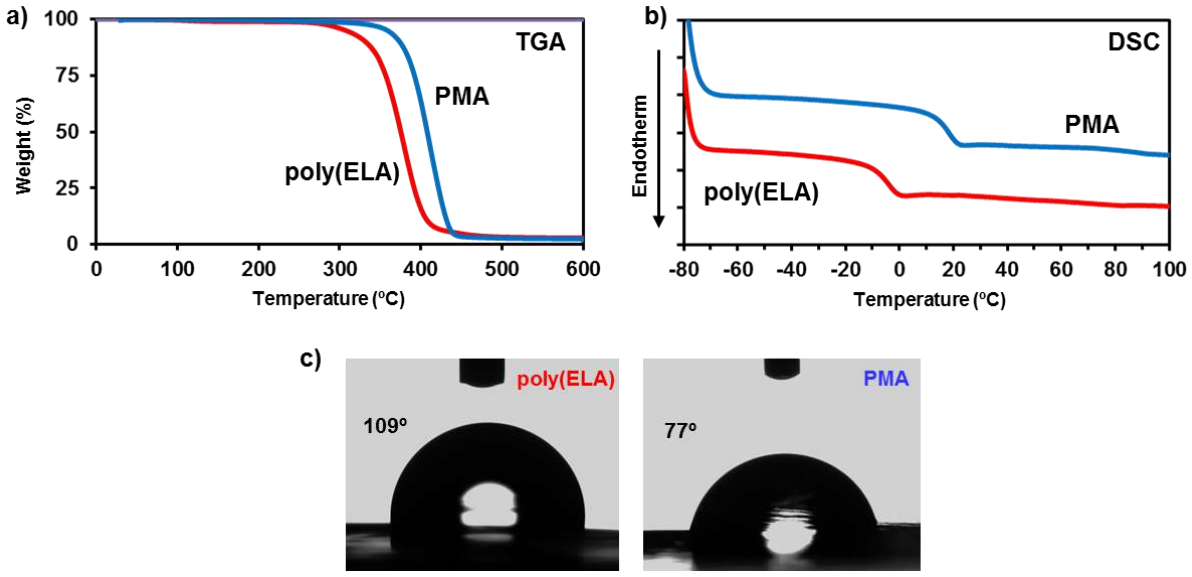

Figure S8. Analysis of thermal properties and contact angle for poly(ELA) in comparison with PMA. (a) TGA thermograms, (b) DSC thermograms and (c) contact angle images for droplets of water on polymer surface.

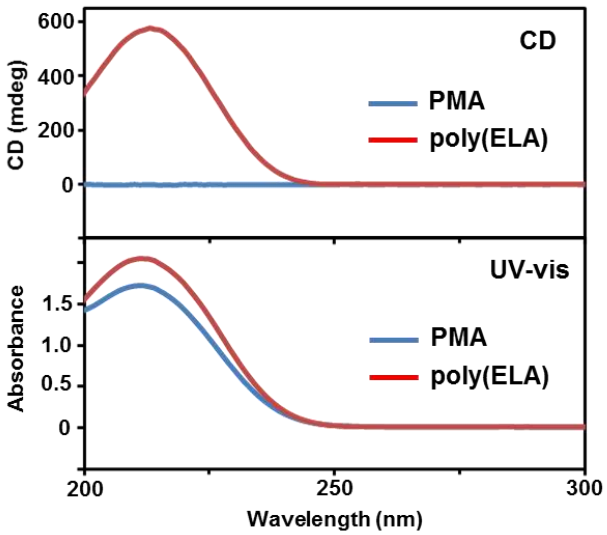

Figure S9. UV-vis and CD spectra of poly(ELA) and PMA in acetonitrile at 25 °C. Concentration: 1.3 mg/mL for all measurements.

Table S1. Optical rotation of ELA, MA, poly(ELA) and PMA.

entry	compound	M_n [a]	M_w/M_n [a]	$[\alpha]_D$ degrees [b]
1	ELA	-	-	-53.9
2	poly(ELA)	34,700	1.20	-54.3
3	MA	-	-	-1.5
4	PMA	38,850	1.22	-0.5

[a] Determined by GPC using PMMA standards. [b] Optical rotation measurements were performed at 25 °C with a 1 dm cuvette in acetonitrile with a concentration of 1mg/mL.

Supporting information for Chapter 2.1

4. SET-LRP of αPA

The ethanolic SET-LRP of αPA at DP= 25 showed perfect LP behaviour as indicated by linear time evolution of ln([M]$_0$/[M]) and M_n(GPC) *vs* M(th) plots (Figure S10). The synthesized polymers were well-defined as indicated by narrow and perfectly symmetric GPC peaks (Figure S11). Interestingly, the hydrophobicity of this monomer forced this SET-LRP system to proceed through a self-generated biphasic system (Figure S12). However, this does not compromise the achievement of outstanding control of molecular weight and chain ends as illustrated in the MALDI-TOF spectra of the polymer isolated after the kinetic experiment (Figure S13).

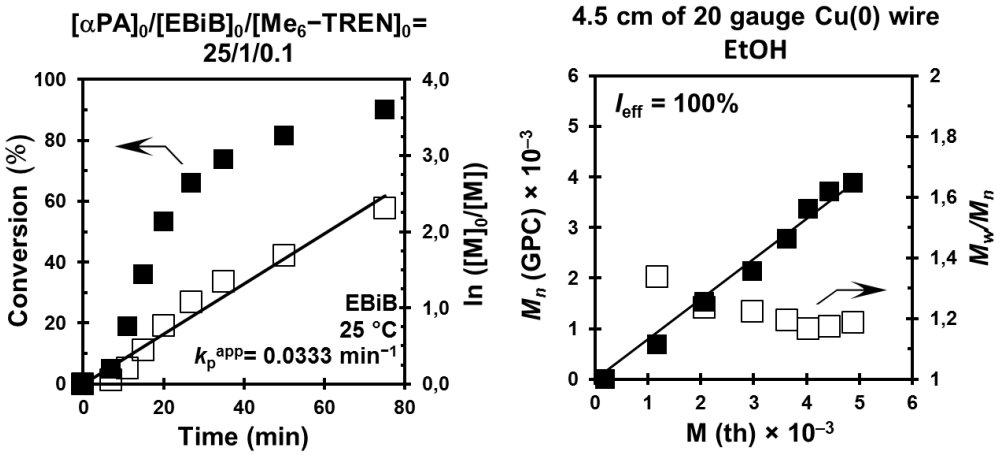

Figure S10. Monomer conversion, kinetic plot and evolution of molecular weight and polydispersity for the Cu(0) wire-catalyzed SET-LRP of αPA in EtOH initiated with EBiB at 25 °C. Reaction conditions: αPA = 1 mL; EtOH = 0.5 mL; 4.5 cm hydrazine- activated Cu(0) wire; [αPA]$_0$/[EBiB]$_0$/[Me$_6$-TREN]$_0$= 25/1/0.1.

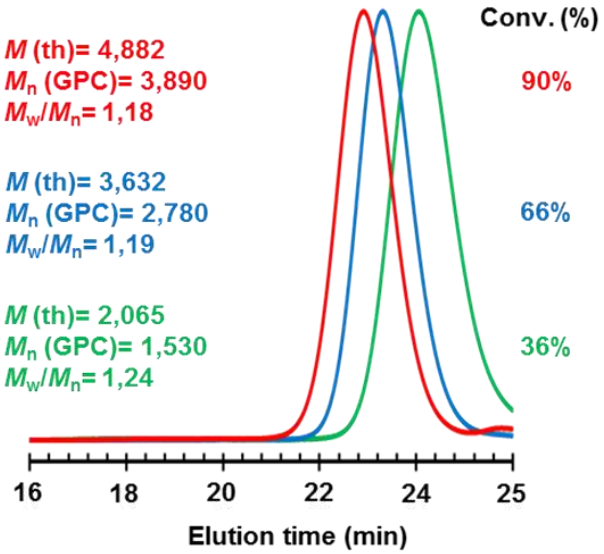

Figure S11. Representative GPC traces (normalized to peak height) of poly(αPA) obtained from kinetic experiment shown in Figure S10.

Figure S12. Digital image of the biphasic reaction mixture self-generated thorough the SET-LRP of αPA in EtOH. The image was captured at 90 % conv. Reaction conditions: αPA = 1 mL; EtOH = 0.5 mL; 4.5 cm hydrazine- activated Cu(0) wire; $[\alpha PA]_0/[EBiB]_0/[Me_6\text{-TREN}]_0$= 25/1/0.1.

Supporting information for Chapter 2.1

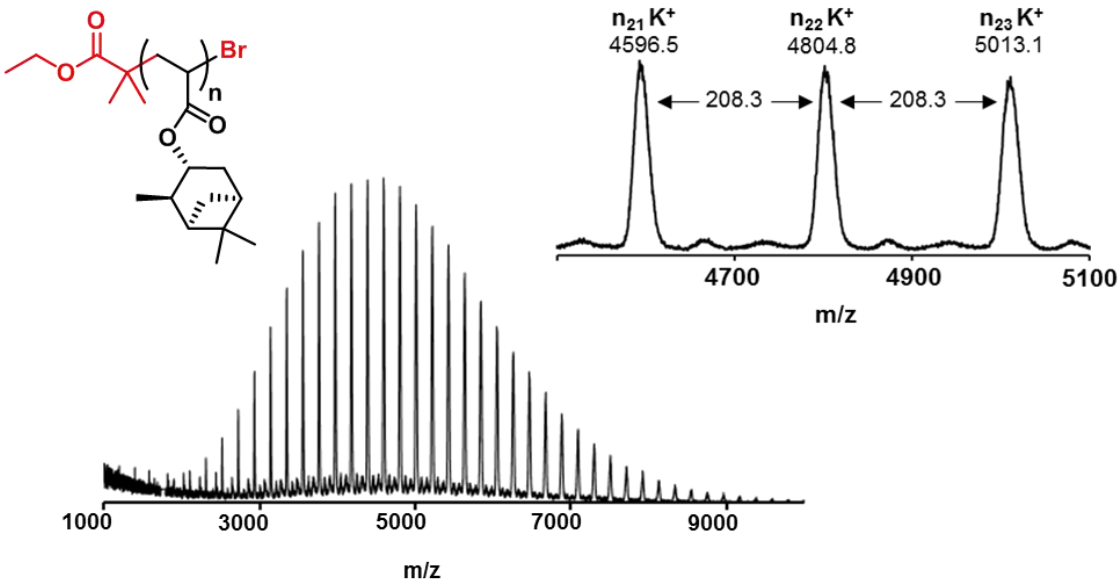

Figure S13. MALDI-TOF spectrum of poly(αPA) obtained at 90% monomer conversion after kinetic experiment shown in Figure S10.

Annex B

Supplementary Information for

Photoinduced upgrading of lactic acid-based solvents to block copolymer surfactants

Table of contents:

Supporting information for chapter 2.2

1. Structural characterization of ELA and DMLA

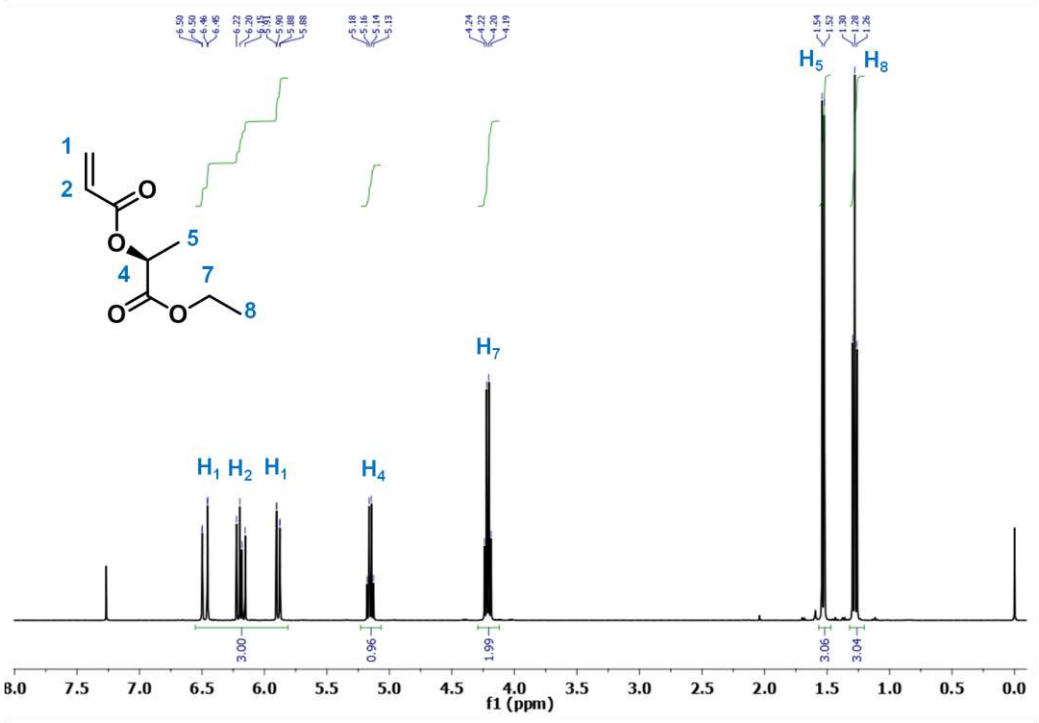

Figure S1. ^{1}H NMR spectrum of ELA in $CDCl_3$.

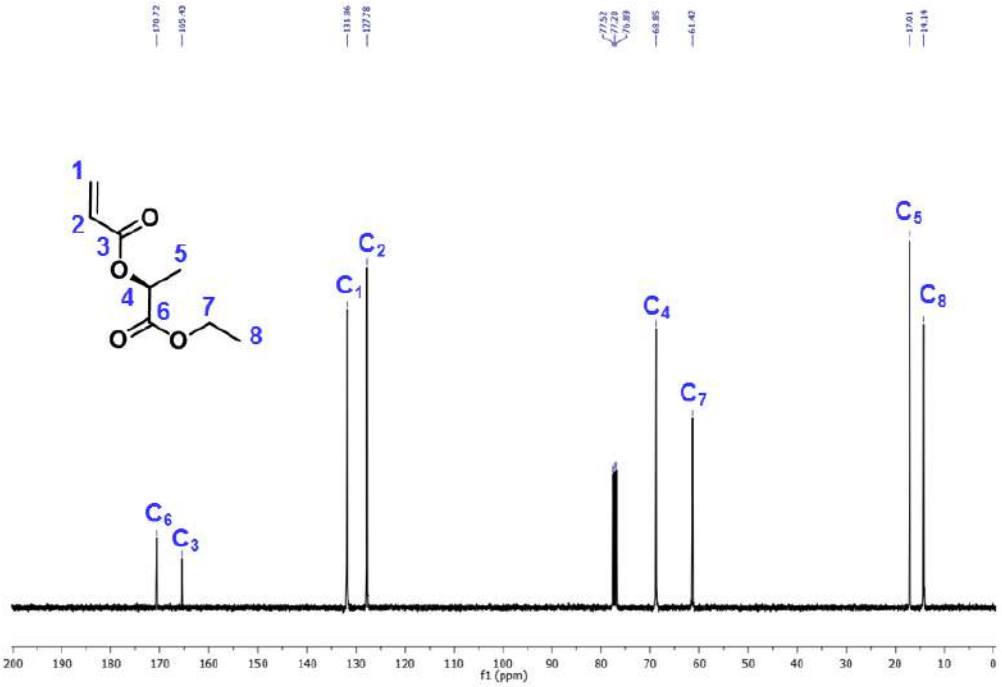

Figure S2. ^{13}C NMR spectrum of ELA in $CDCl_3$.

Annex B

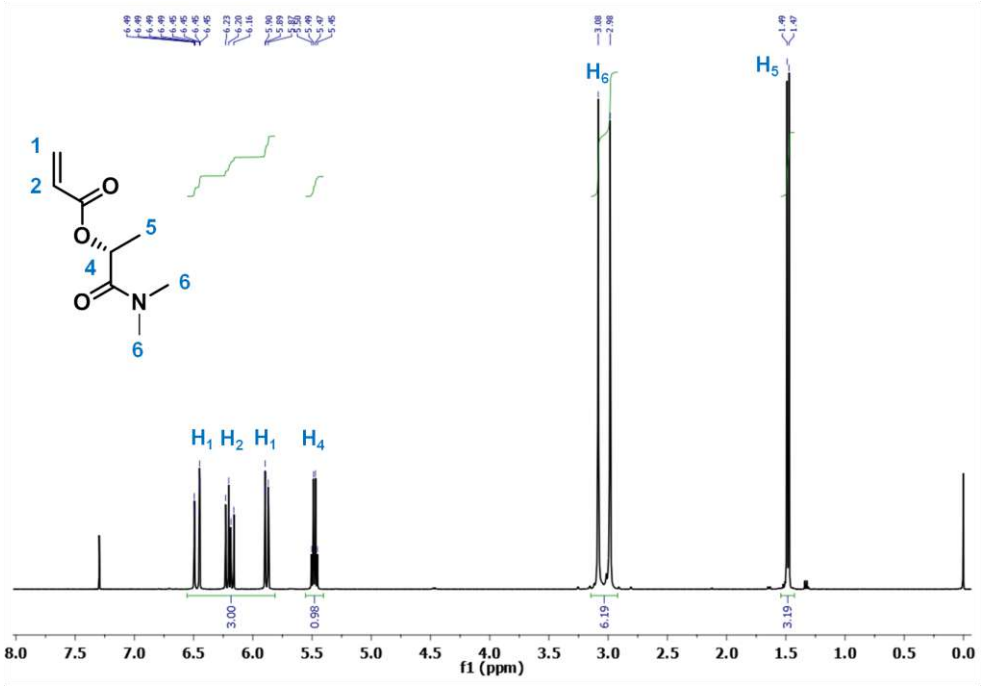

Figure S3. ^{1}H NMR spectrum of DMLA in $CDCl_3$.

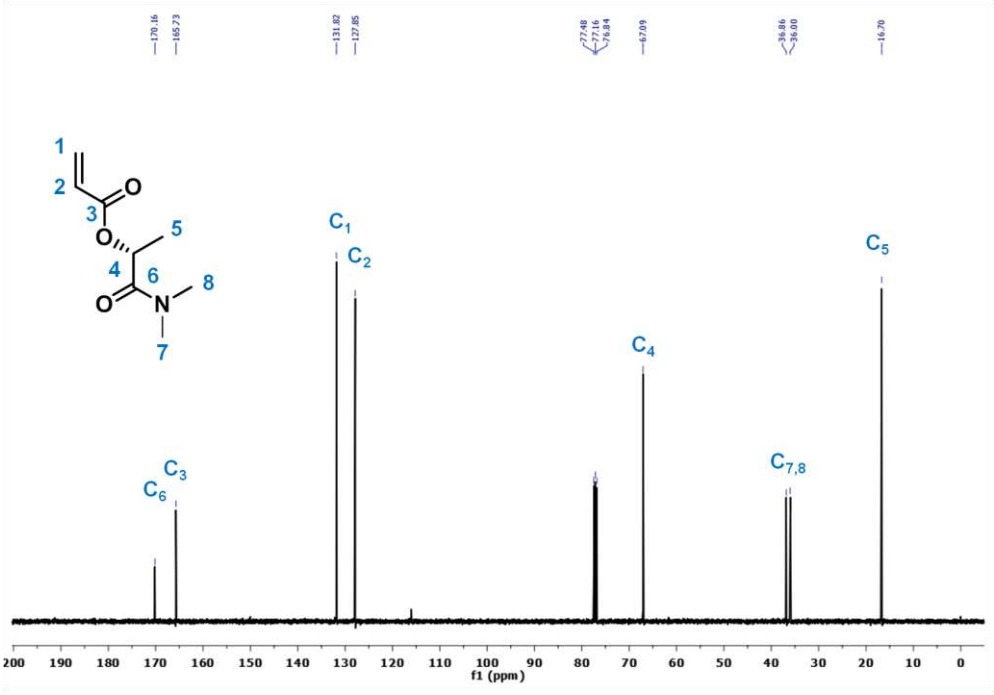

Figure S4. ^{13}C NMR spectrum of DMLA in $CDCl_3$

Supporting information for chapter 2.2

2. Characterization of PDMLA synthesized by FRP

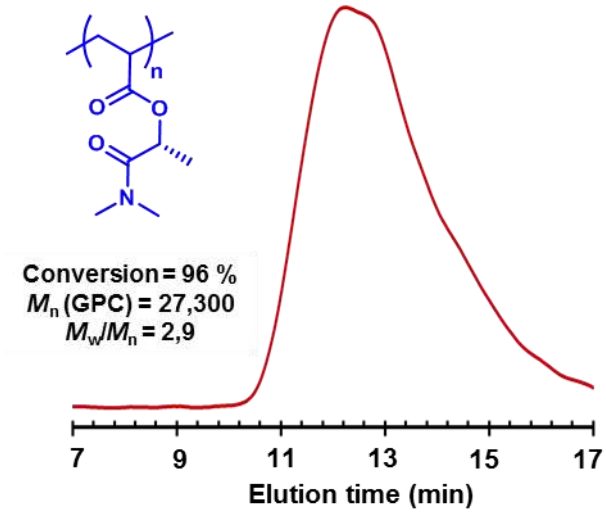

Figure S5. GPC trace of PDMLA synthesized by FRP at 90 °C using AIBN as initiator.

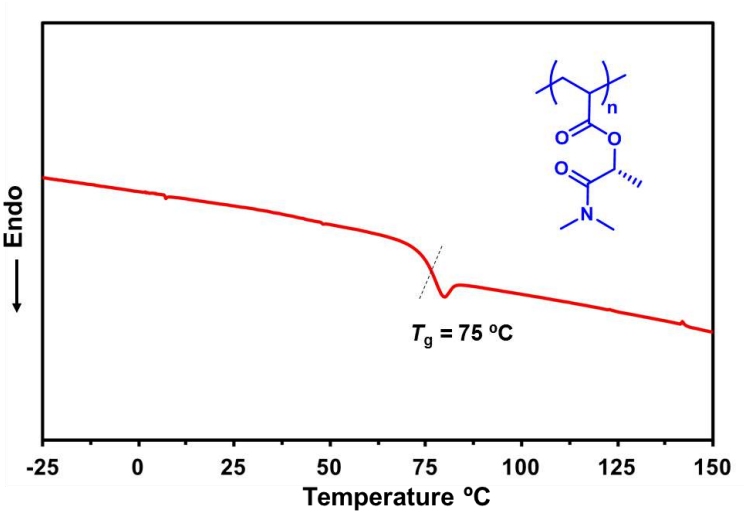

Figure S6. DSC analysis of PDMLA synthesized by FRP at 90 °C using AIBN as initiator.

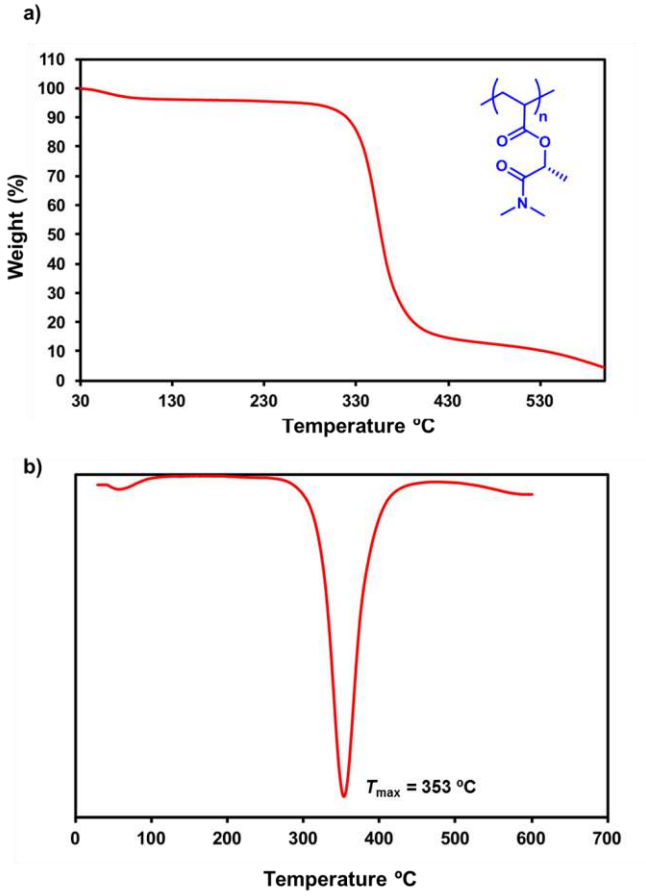

Figure S7. (a) TGA analysis and (b) DTGA of PDMLA synthesized by FRP at 90 °C using AIBN as initiator.

Supporting information for chapter 2.2

3. Cu(II)-mediated radical photopolymerization of DMLA and ELA

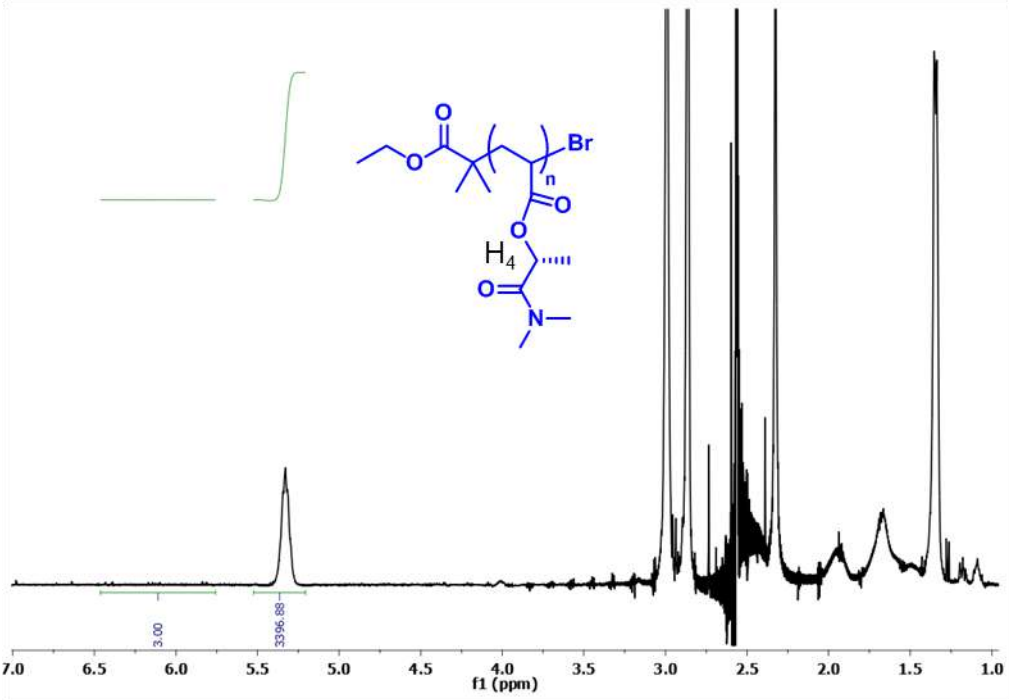

Figure S8. ^{1}H NMR spectrum in $CDCl_3$ of the reaction mixture after Cu(II)Br_2-mediated radical photopolymerization of DMLA using EBiB as an initiator at a targeted DP = 50 (irradiation with UV-light for 3 h).

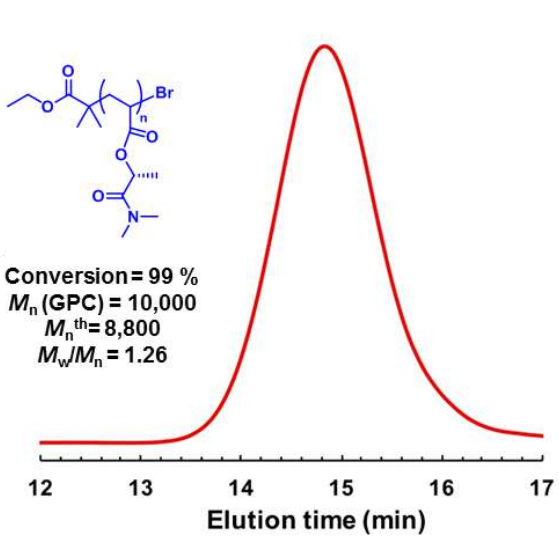

Figure S9. GPC analysis of PDMLA isolated after Cu(II)Br_2-mediated radical photopolymerization of DMLA in DMSO using EBiB as an initiator at a targeted DP = 50 (irradiation with UV-light for 3 h).

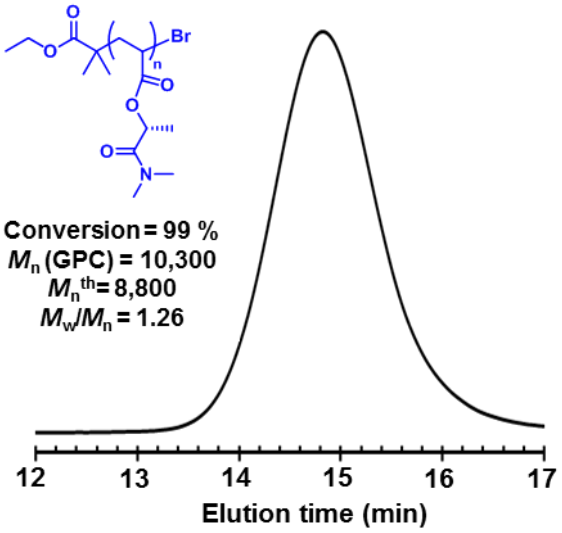

Figure S10. GPC analysis of PDMLA isolated after Cu(II)Br_2-mediated radical photopolymerization of DMLA in DML using EBiB as an initiator at a targeted DP = 50 (irradiation with UV-light for 3 h).

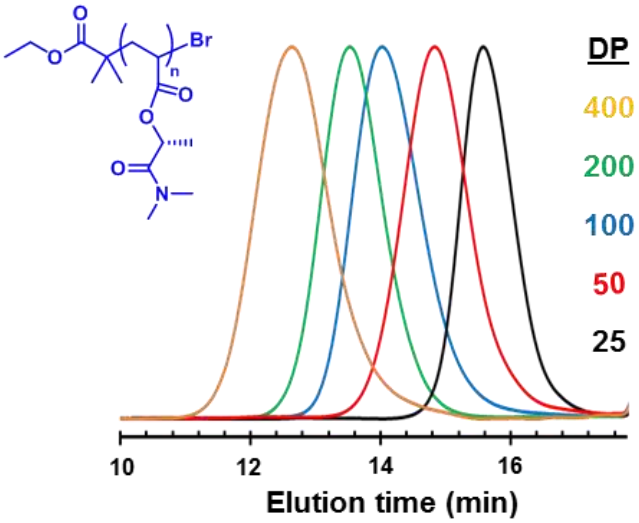

Figure S11. GPC traces (normalized to peak height) of PDMLA isolated after Cu(II)Br_2-mediated radical photopolymerization in DMSO with different targeted DPs (25-400).

Supporting information for chapter 2.2

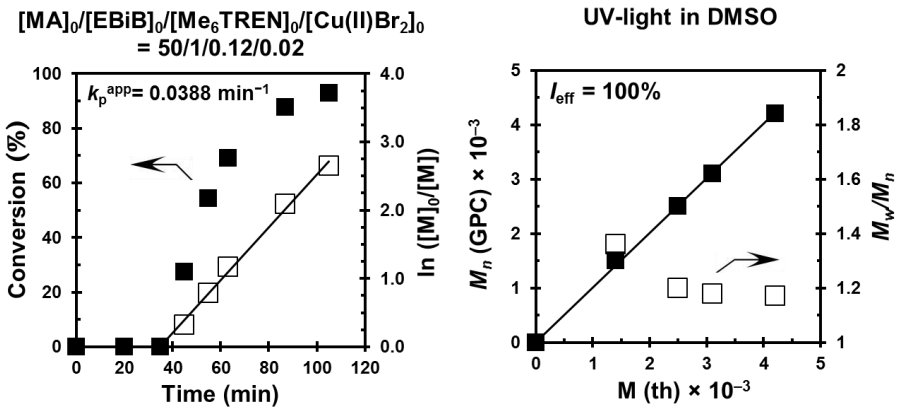

Figure S12. Kinetics plots and evolution of experimental M_n (GPC) and M_w/M_n versus theoretical $M_{n,th}$ for the Cu(II)Br_2-mediated living photopolymerization of MA in DMSO. Reaction conditions: 1 mL MA, 0.5 mL DMSO, $[MA]_0/[EBiB]_0/[Me_6\text{-TREN}]_0/[Cu(II)Br_2]_0$= 50/1/0.12/0.02.

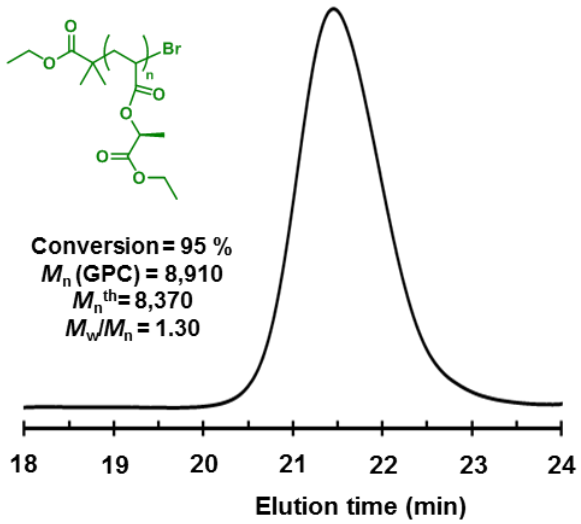

Figure S13. GPC analysis of PELA isolated after Cu(II)Br_2-mediated radical photopolymerization of ELA in EL using EBiB as an initiator at a targeted DP = 50 (irradiation with UV-light for 3 h).

4. Synthesis and characterization of amphiphilic BCPs

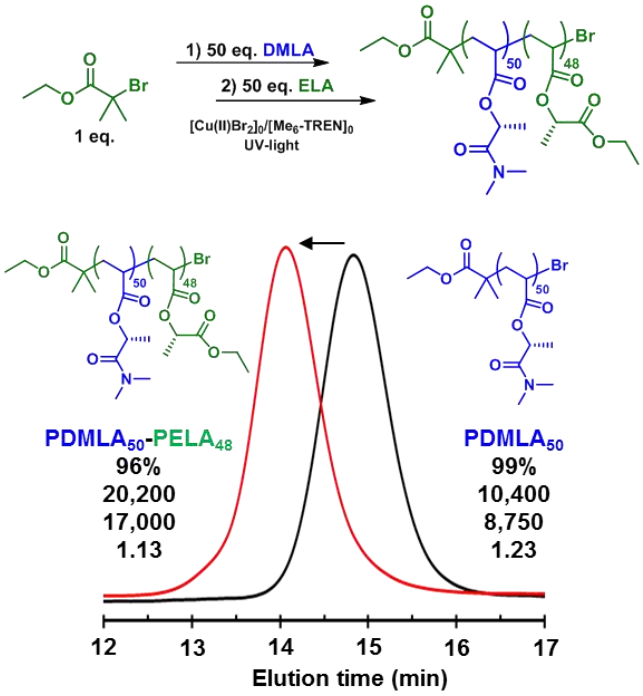

Figure S14. GPC analysis of the *in situ* block copolymerization *via* Cu(II)Br_2-mediated photopolymerization of PDMLA with ELA. Reaction conditions for the synthesis of PELA macroinitiator: $[DMLA]_0/[EBiB]_0/[Me_6\text{-}TREN]_0/[Cu(II)Br_2]_0$= 50/1/0.12/0.02 in DMSO (50 vol%) followed by the addition of deoxygenated ELA (50 equiv) in DMSO *in situ*.

Supporting information for chapter 2.2

5. Self-assembly of amphiphilic BCPs in water

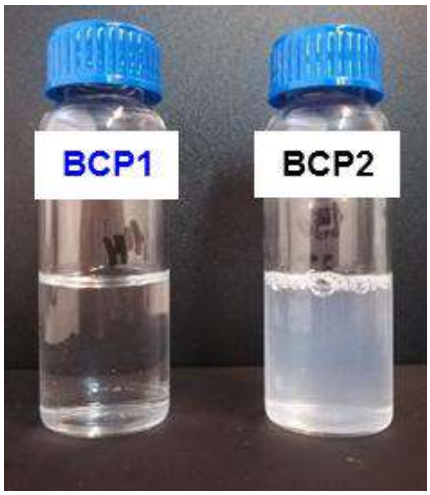

Figure S15. Digital images of images of self-assemblies from BCP1 (1 mg·mL^{-1}) and BCP2 (0.5 mg·mL^{-1}) in water.

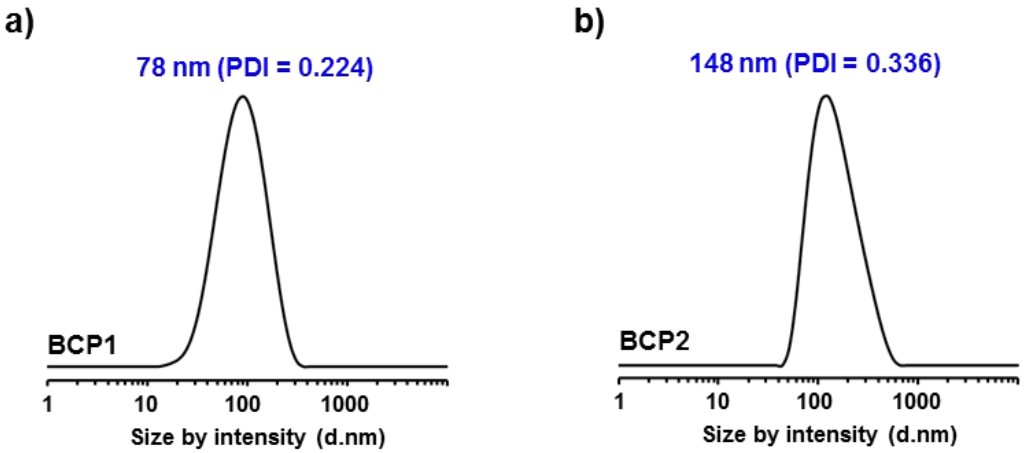

Figure S16. DLS size distribution by intensity for (a) BCP1 self-assembled in water by direct dissolution and (b) BCP2 self-assembled by fast injection of the copolymer (dissolved in THF) into water at 25 °C.

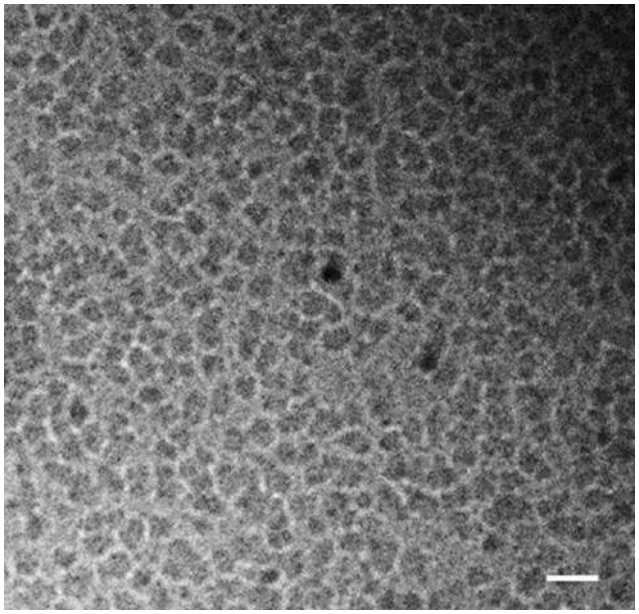

Figure S17. Low magnification cryo-TEM images for BCP1 self-assembled in water by direct dissolution. Scale bar is 100 nm.

Supporting information for chapter 2.2

6. Characterization of PMMA and PSt latexes

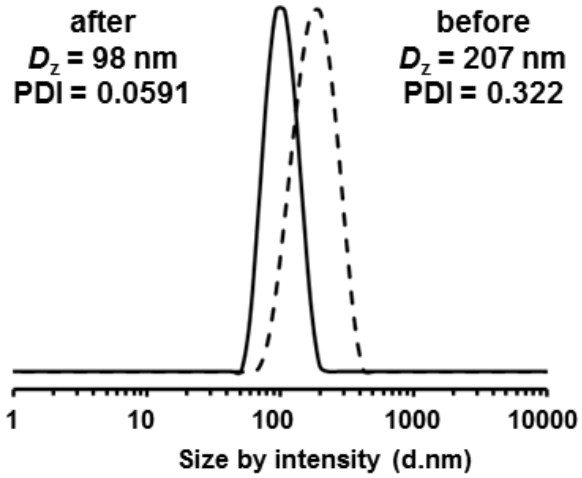

Figure S18. Droplet (before polymerization) and particle-size distributions (after polymerization) by intensity for emulsion polymerizations of MMA at 75 °C.

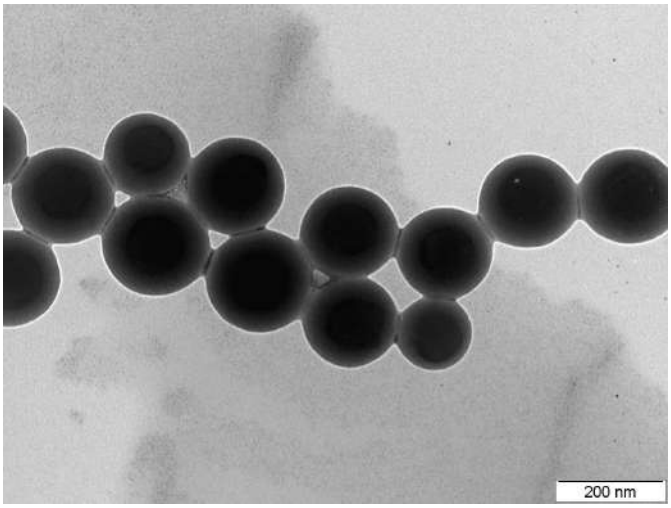

Figure S19. TEM image of PSt latex stabilized by BCP1.

Annex C

Supplementary Information for

Biosourced all-acrylic ABA block copolymers with lactic acid-based soft phase

Table of contents:

Supporting information for chapter 2.3

1. Structural characterization of PBLA-2Z

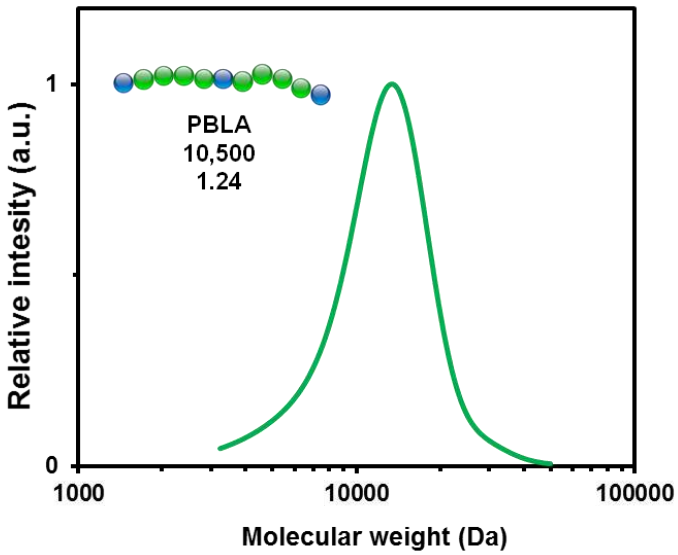

Figure S1. GPC analysis PBLA-2Z. Numbers shown correspond to $M_{n,GPC}$, and M_w/M_n, from top to bottom.

2. Structural characterization of PIA-PBLA-PIA

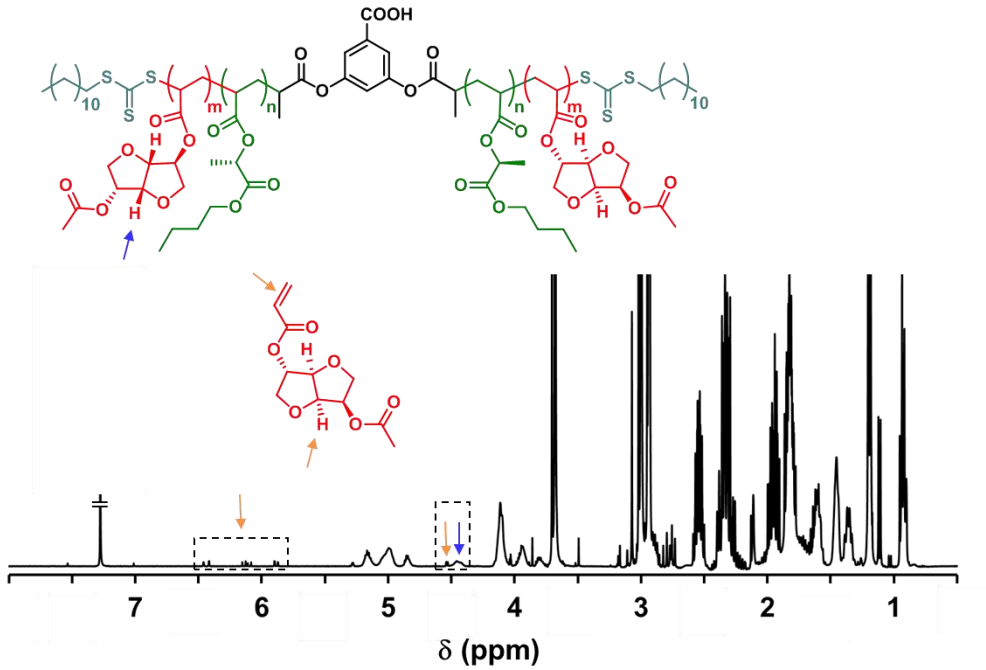

Figure S2. ^{1}H NMR spectrum in $CDCl_3$ of the reaction mixture after the chain extension of PBLA-2Z macro-RAFT agent with IA monomer at 70 °C in Rhodiasolv® PolarClean solvent. Monomer conversion was determined to be 86% by integration of the monomer/polymer signals marked with arrows.

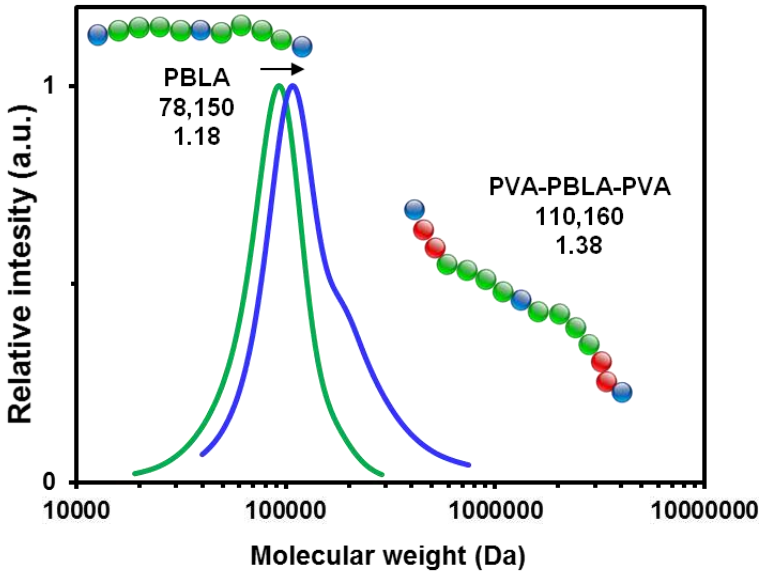

Figure S3. GPC traces of the chain extension of PBLA-2Z macro-RAFT agent with VA monomer at 70 °C in Rhodiasolv® PolarClean solvent. Numbers shown correspond to $M_{n,GPC}$, and M_w/M_n, from top to bottom.

3. Thermomechanical characterization of PVA-PBLA-PVA and PIA-PBLA-PIA BCPs

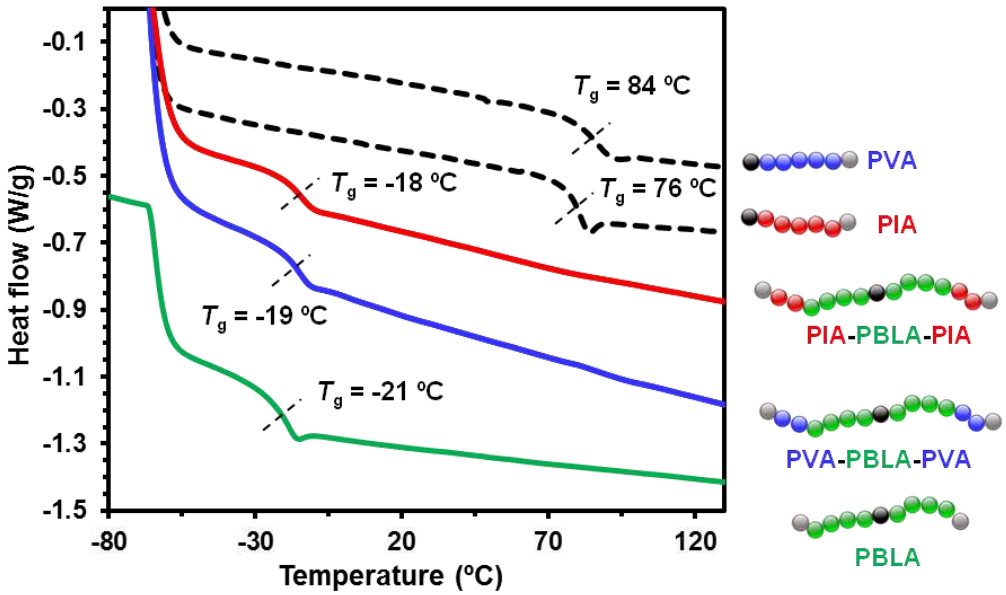

Figure S4. DSC thermograms of PVA ($M_{n,GPC}$ = 14,460 g·mol^{-1}), PIA ($M_{n,GPC}$ = 13,830 g·mol^{-1}), and PBLA-2Z ($M_{n,GPC}$ = 78,150 g·mol^{-1}) homopolymers and triblock copolymers PIA-PBLA-PIA ($M_{n,GPC}$ = 103,500 g·mol^{-1}) and PVA-PBLA-PVA ($M_{n,GPC}$ = 110,150 g·mol^{-1}).

Supporting information for chapter 2.3

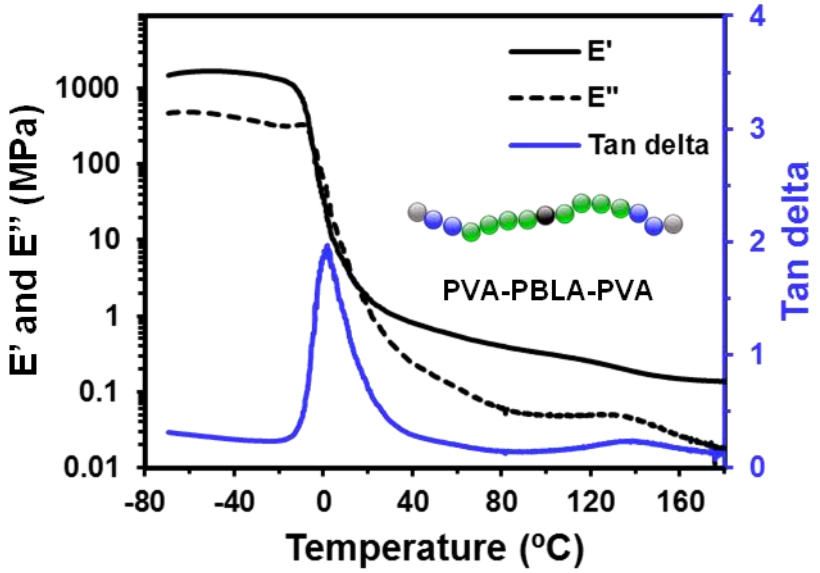

Figure S5. Dynamic tensile storage (E') and loss (E'') moduli and tan δ (= E''/E') as a function of temperature of PVA-PBLA-PVA triblock.

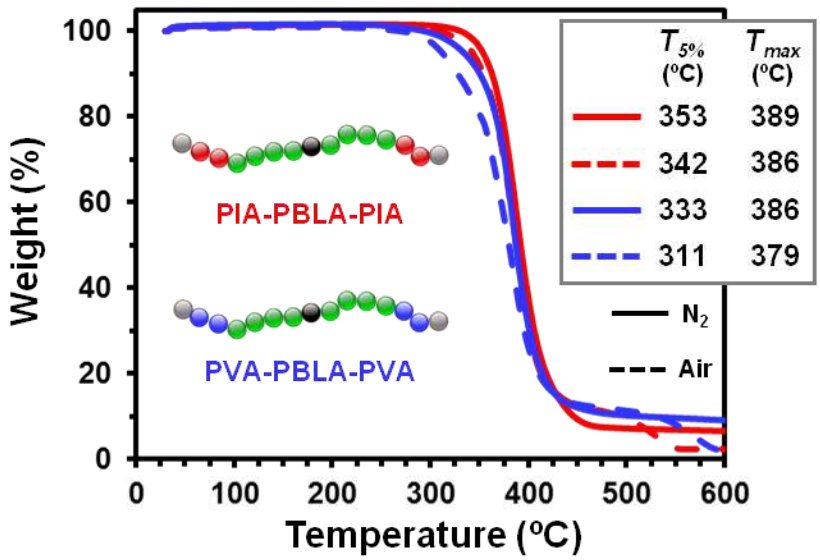

Figure S6. TGA for PIA-PBLA-PIA (red lines) and PVA-PBLA-PVA (blue lines) under nitrogen and air atmosphere.

Annex D

Supplementary Information for

Replacing Cu(II)Br_2 with Me_6-TREN in biphasic Cu(0)/TREN catalyzed SET-LRP reveals the mixed-ligand effect

Table of contents

Supporting Information for Chapter 4.1

1. Kinetic plots, molecular weight and polydispersity evolution for the SET-LRP of MA

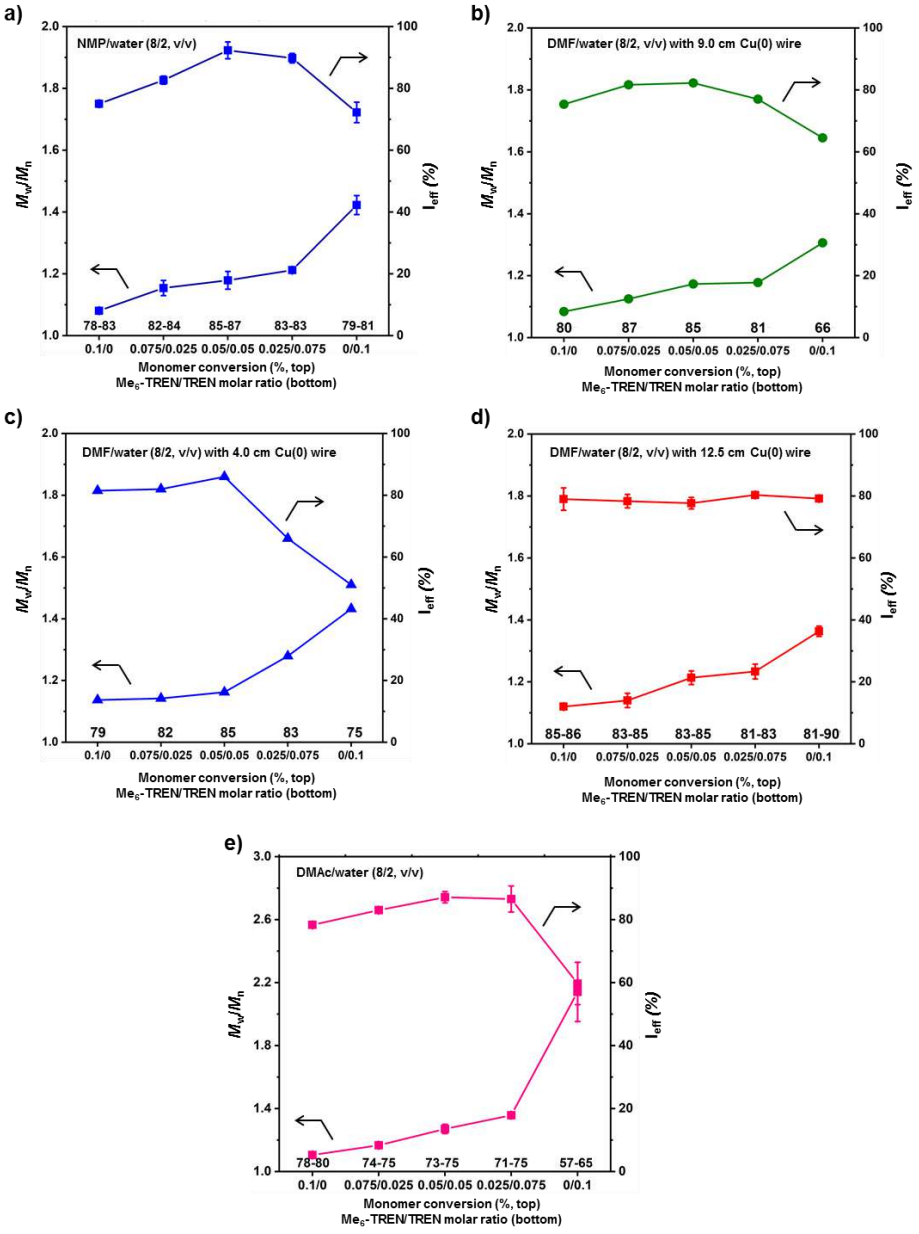

Figure S1. Evolution of M_w/M_n and I_{eff} for the SET-LRP of MA initiated with BPE in various "programmed" biphasic reaction mixtures at 25 °C. (a) NMP/water mixture (8/2, v/v) using 9.0 cm nonactivated Cu(0) wire as catalyst. (b) DMF/water mixture (8/2, v/v) using 9.0 cm of nonactivated Cu(0) wire as catalyst. (c) DMF/water mixture (8/2, v/v) using 4.0 cm of nonactivated Cu(0) wire as catalyst. (d) DMF/water mixture (8/2, v/v) using 12.5 cm of nonactivated Cu(0) wire as catalyst. (e) DMAc/water mixture (8/2, v/v) using 9.0 cm of nonactivated Cu(0) wire as catalyst. Reaction conditions: MA = 1 mL, organic solvent = 0.4 mL, water = 0.1 mL, and $[MA]_0/[BPE]_0/[L]_0$ = 222/1/0.1.

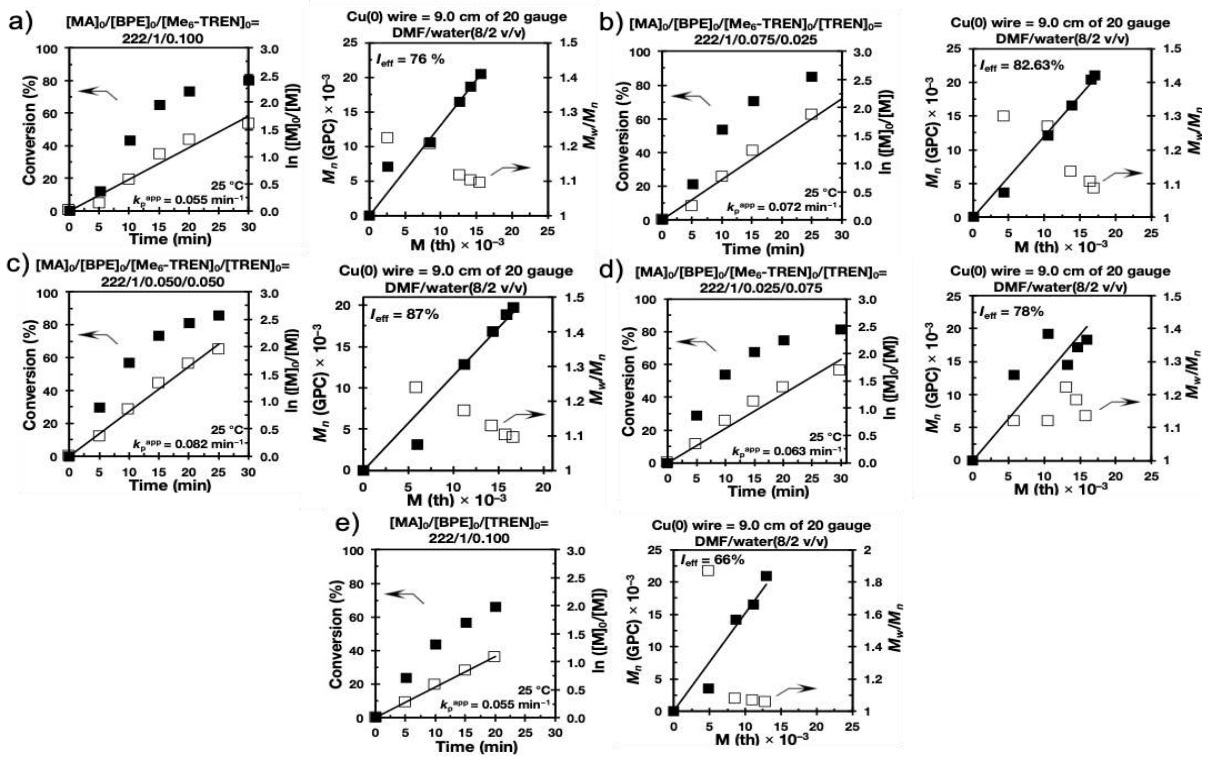

Figure S2. Kinetic plots, molecular weight and polydispersity evolution for the SET-LRP of MA in DMF/water mixture (8/2, v/v) initiated with BPE and catalyzed by 9.0 cm nonactivated Cu(0) wire at 25 °C. Experimental data in different colors were obtained from different kinetics experiments sometimes performed by different researches. k_p^{app} and I_{eff} are the average values of three experiments. Reaction conditions: MA = 1 mL, DMF = 0.4 mL, water = 0.1 mL, $[MA]_0/[BPE]_0/[L]_0$ = 222/1/0.1.

Supporting Information for Chapter 4.1

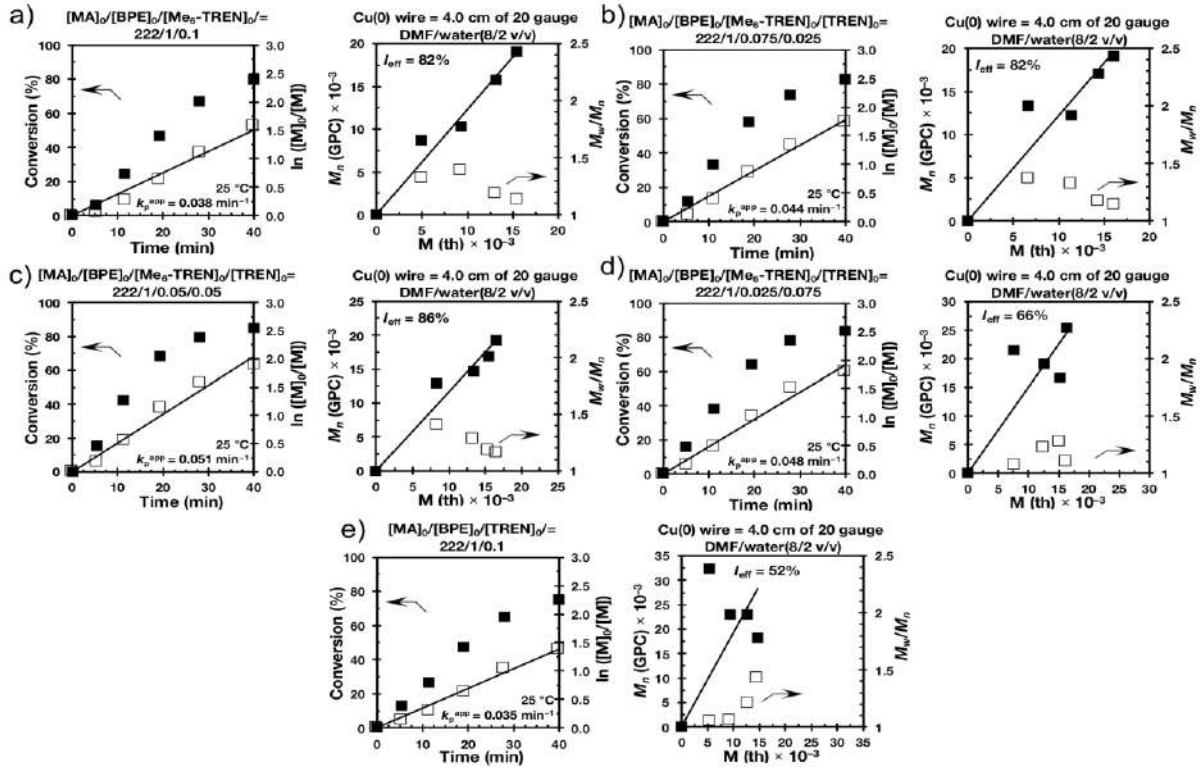

Figure S3. Kinetic plots, molecular weight and polydispersity evolution for the SET-LRP of MA in DMF/water mixture (8/2, v/v) initiated with BPE and catalyzed by 4.0 cm nonactivated Cu(0) wire at 25 °C. Experimental data in different colors were obtained from different kinetics experiments sometimes performed by different researches. k_p^{app} and I_{eff} are the average values of three experiments. Reaction conditions: MA = 1 mL, DMF = 0.4 mL, water = 0.1 mL, $[MA]_0/[BPE]_0/[L]_0$ = 222/1/0.1.

Annex D

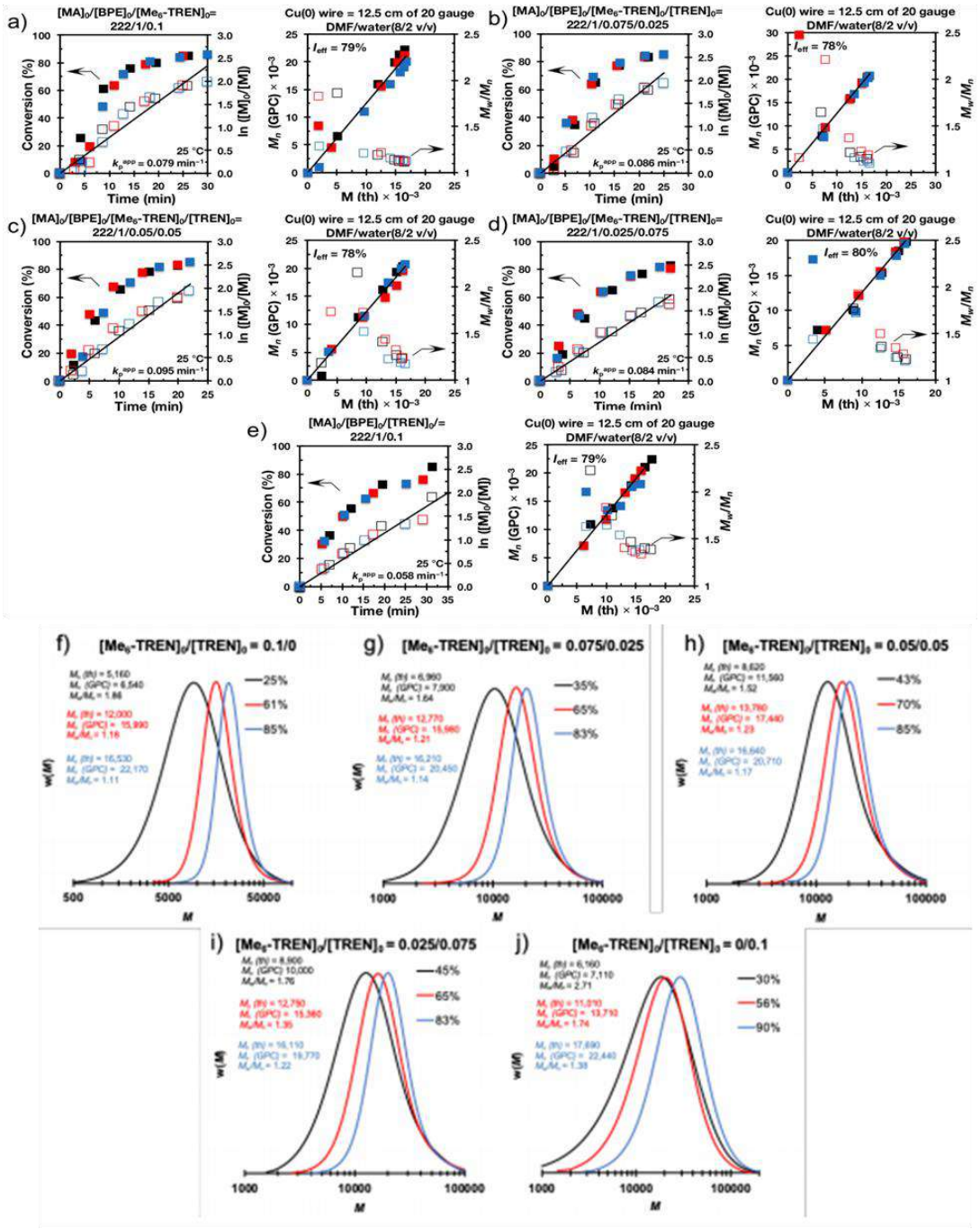

Figure S4. Kinetic plots, molecular weight, polydispersity evolution and representative GPC traces of the evolution of molecular weight as a function of conversion for the SET-LRP of MA in DMF/water mixture (8/2, v/v) initiated with BPE and catalyzed by 12.5 cm nonactivated Cu(0) wire at 25 °C. Experimental data in different colors were obtained from different kinetics experiments sometimes performed by different researches. k_p^{app} and I_{eff} are the average values of three experiments. Reaction conditions: MA = 1 mL, DMF = 0.4 mL, water = 0.1 mL, $[MA]_0/[BPE]_0/[L]_0$ = 222/1/0.1.

Supporting Information for Chapter 4.1

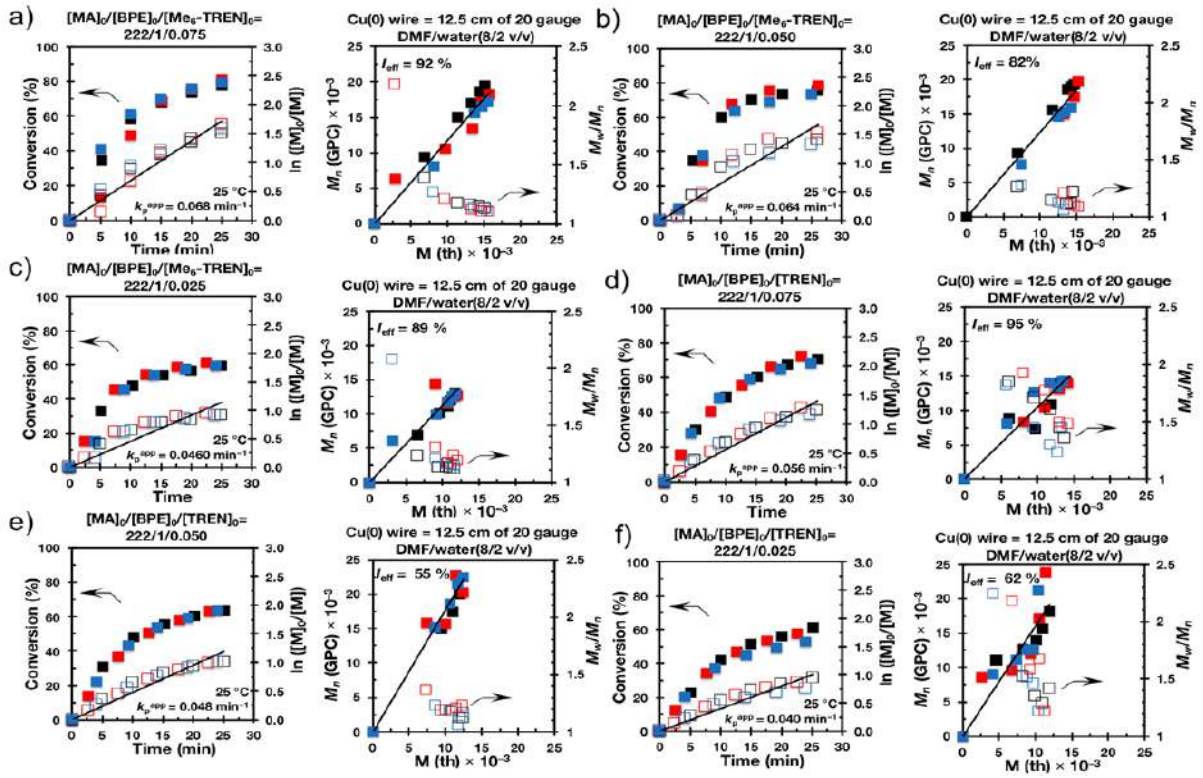

Figure S5. Kinetic plots, molecular weight and polydispersity evolution for the SET-LRP of MA in DMF/water mixture (8/2, v/v) initiated with BPE and catalyzed by the 12.5 cm nonactivated Cu(0) wire at 25 °C. Experimental data in different colors were obtained from different kinetics experiments sometimes performed by different researches. k_p^{app} and I_{eff} are the average values of three experiments. Reaction conditions: MA = 1 mL, DMF = 0.4 mL, water = 0.1 mL, $[MA]_0/[BPE]_0/[L]_0$ = 222/1/0.075 (panels a,d), $[MA]_0/[BPE]_0/[L]_0$ = 222/1/0.05 (panels b,e), $[MA]_0/[BPE]_0/[L]_0$ = 222/1/0.025 (panels c,f).

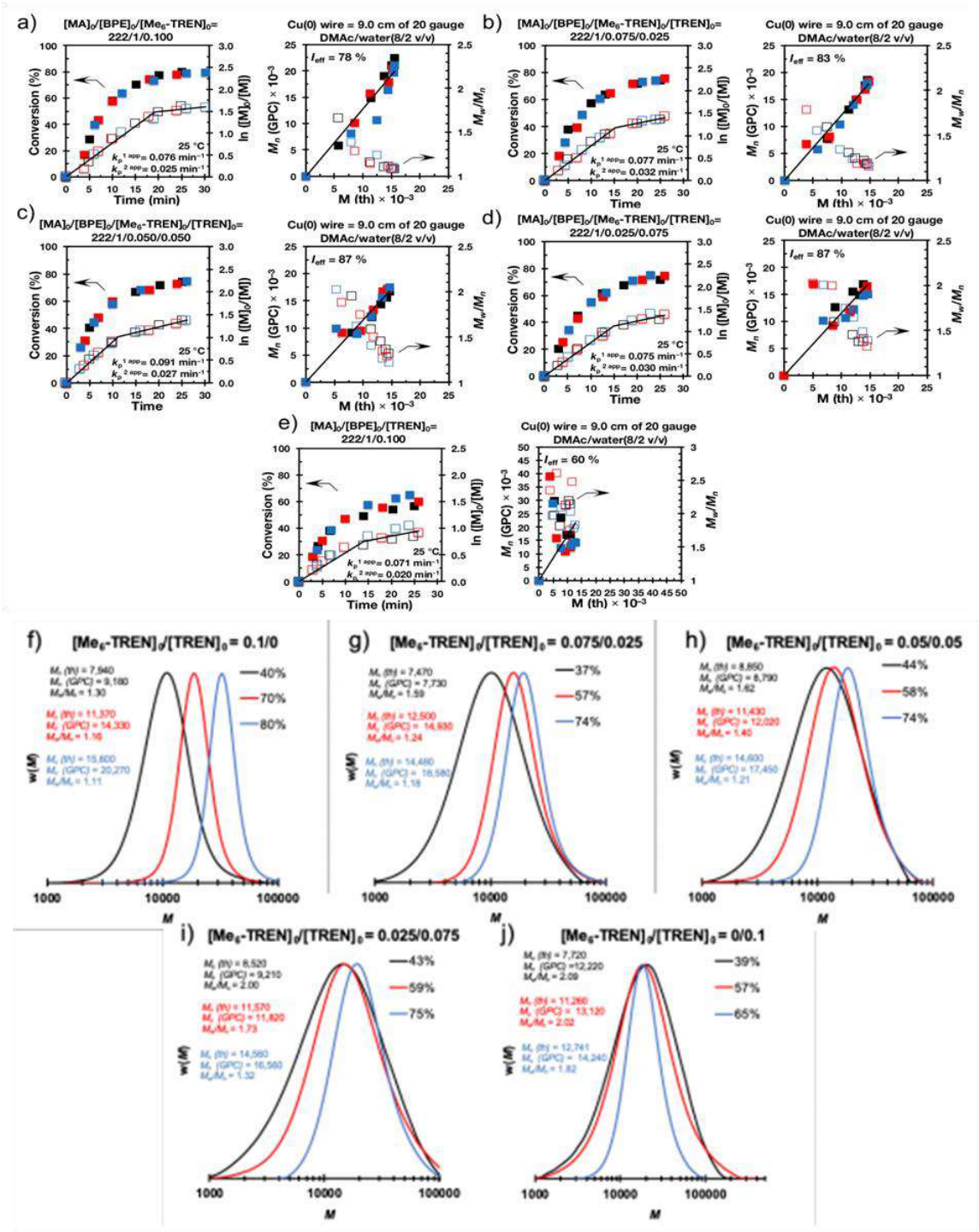

Figure S6. Kinetic plots, molecular weight, polydispersity evolution and representative GPC traces of the evolution of molecular weight as a function of conversion for the SET-LRP of MA in DMAc/water mixture (8/2, v/v) initiated with BPE and catalyzed by the 9.0 cm nonactivated Cu(0) wire at 25 °C. Experimental data in different colors were obtained from different kinetics experiments sometimes performed by different researches. k_p^{app} and I_{eff} are the average values of three experiments. Reaction conditions: MA = 1 mL, DMAc = 0.4 mL, water = 0.1 mL, $[MA]_0/[BPE]_0/[L]_0$ = 222/1/0.1.

Supporting Information for Chapter 4.1

2. Digital images of control experiments

Figure S7. Visualization of the reaction mixture for the control experiments performed under the conditions placed at the top of each series of experiments. EA is the short name used for ethyl acetate employed to mimic an inert compound resembling MA.

3. ^{1}H NMR and MALDI-TOF MS of PMA after SET-LRP

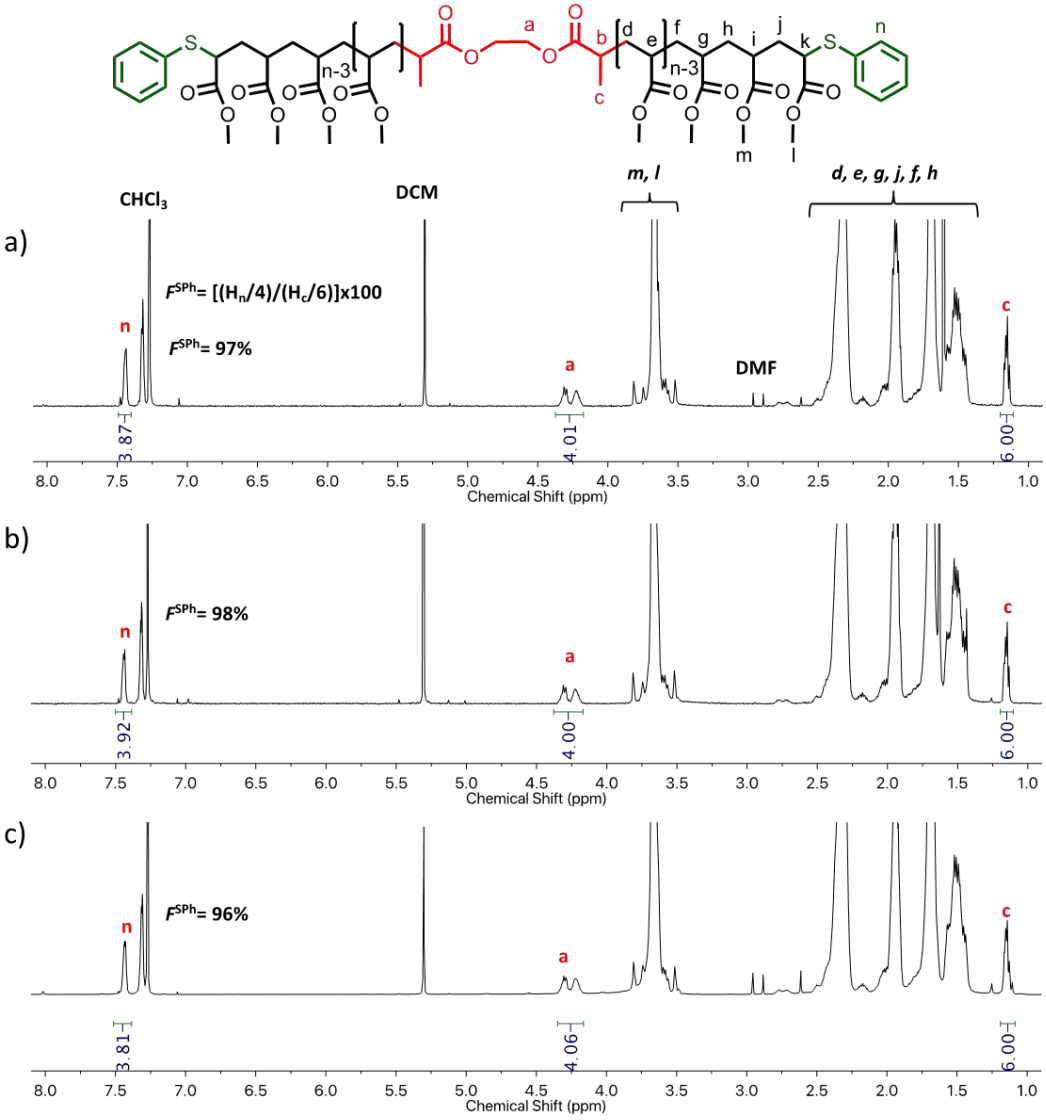

Figure S8. ^{1}H NMR spectra at 400 MHz of α,ω-di(phenylthio)PMA at (a) 93% monomer conversion (M_n= 7,420 and M_w/M_n= 1.15) ([MA]$_0$/[BPE]$_0$/[Me$_6$-TREN]$_0$ = 60/1/0.1); (b) 91% monomer conversion (M_n = 8,260 and M_w/M_n= 1.17) ([MA]$_0$/[BPE]$_0$/[Me$_6$-TREN]$_0$/[TREN]$_0$ = 60/1/0.05/0.05); (c) 94% monomer conversion (M_n= 6,090 and M_w/M_n =1.34) ([MA]$_0$/[BPE]$_0$/[TREN]$_0$ = 60/1/0.1). Polymerization conditions: MA = 1 mL, DMF = 0.4 mL, water = 0.1 mL using 12.5 cm of nonactivated Cu(0) wire 20-gauge wire. The signals at 7.26 ppm and 5.30 ppm are due to partially nondeuterated residue of $CDCl_3$ and dichloromethane, respectively.

Supporting Information for Chapter 4.1

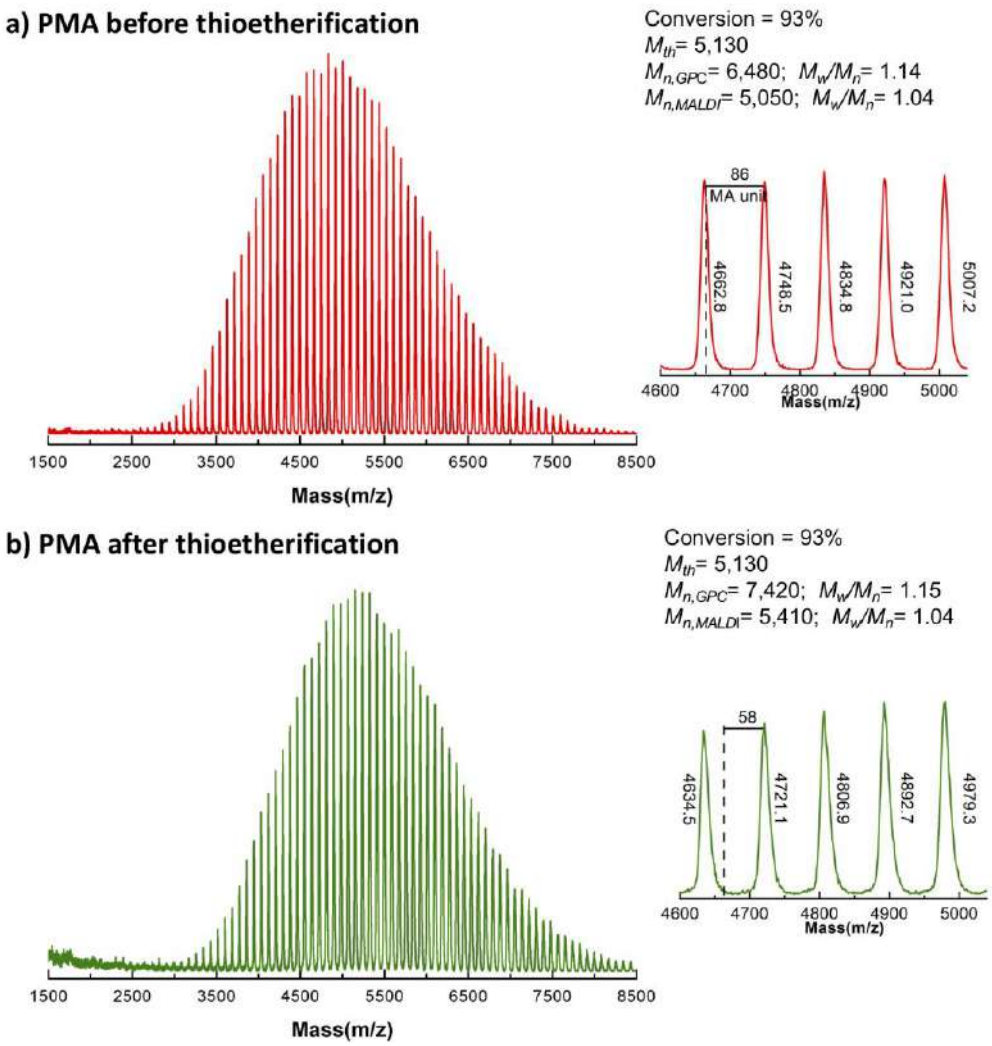

Figure S9. MALDI-TOF of α,ω-di(bromo)PMA isolated at 93% monomer conversion from SET-LRP of MA in DMF/water (8/2, v/v) mixture initiated with BPE and catalyzed by nonactivated Cu(0) wire at 25 °C: (a) before and (b) after "thio-bromo "click". Polymerization conditions: MA = 1 mL, DMF = 0.4 mL, water = 0.1 mL using 12.5 cm of nonactivated Cu(0) wire 20-gauge wire ($[MA]_0/[BPE]_0/[Me_6\text{-}TREN]_0$ = 60/1/0.1). The dotted line in expansion after thioetherification shows the original peak from before thioeterification, while 58 represents the increase in molar mass after thioeterification i.e., 2x[SPh (109. 2) - Br (79.9)] = 58.57 for each chain end.

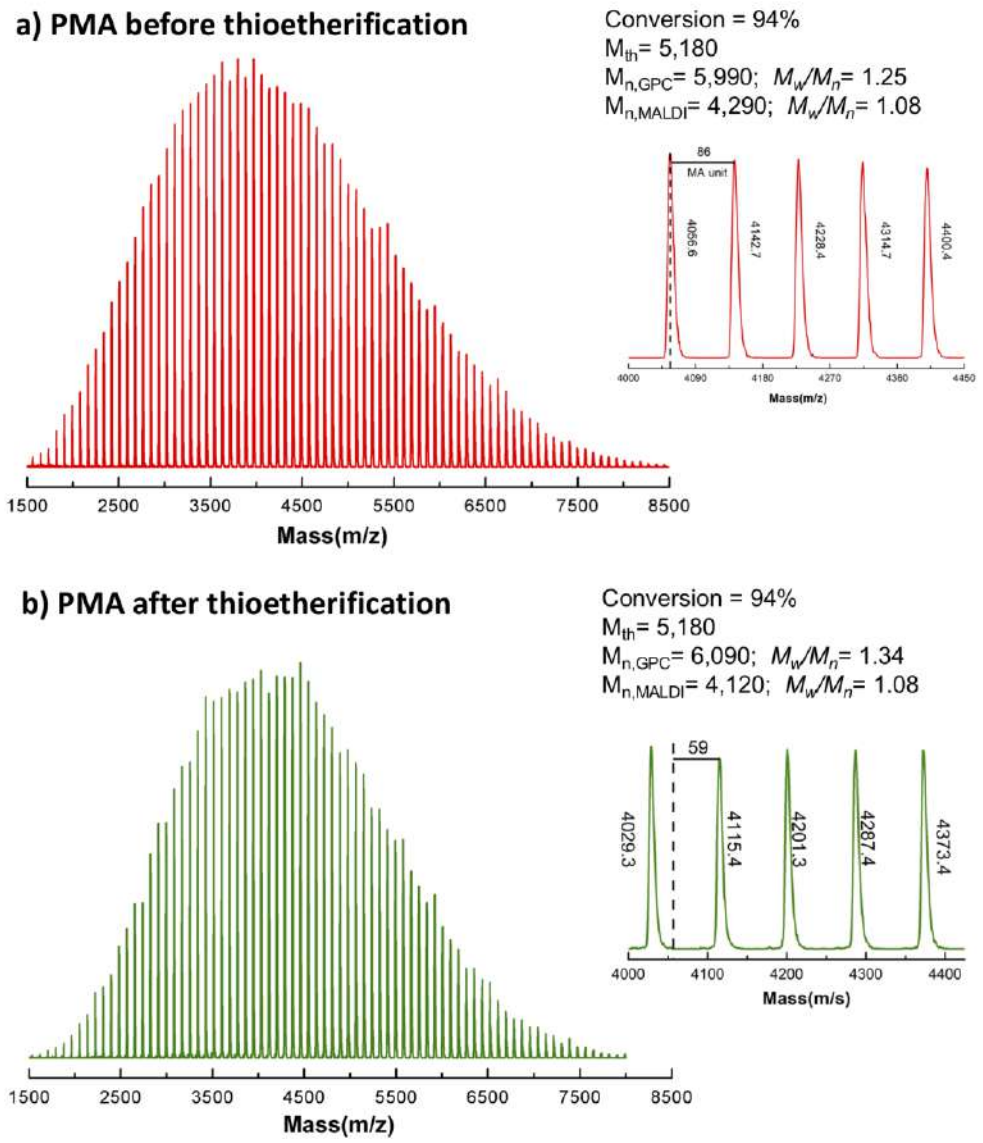

Figure S10. MALDI-TOF of α,ω-di(bromo)PMA isolated at 94% monomer conversion from SET-LRP of MA in DMF/water (8/2, v/v) mixture initiated with BPE and catalyzed by nonactivated Cu(0) wire at 25 °C: (a) before and (b) after "thio-bromo "click". Polymerization conditions: MA = 1 mL, DMF = 0.4 mL, water = 0.1 mL using 12.5 cm of nonactivated Cu(0) wire 20-gauge wire ($[MA]_0/[BPE]_0/[TREN]_0$ = 60/1/0.1). The dotted line in expansion after thioetherification shows the original peak from before thioeterification, while 58 represents the increase in molar mass after thioeterification i.e., 2x[SPh (109. 2) - Br (79.9)] = 58.57 for each chain end.

Supporting Information for Chapter 4.1

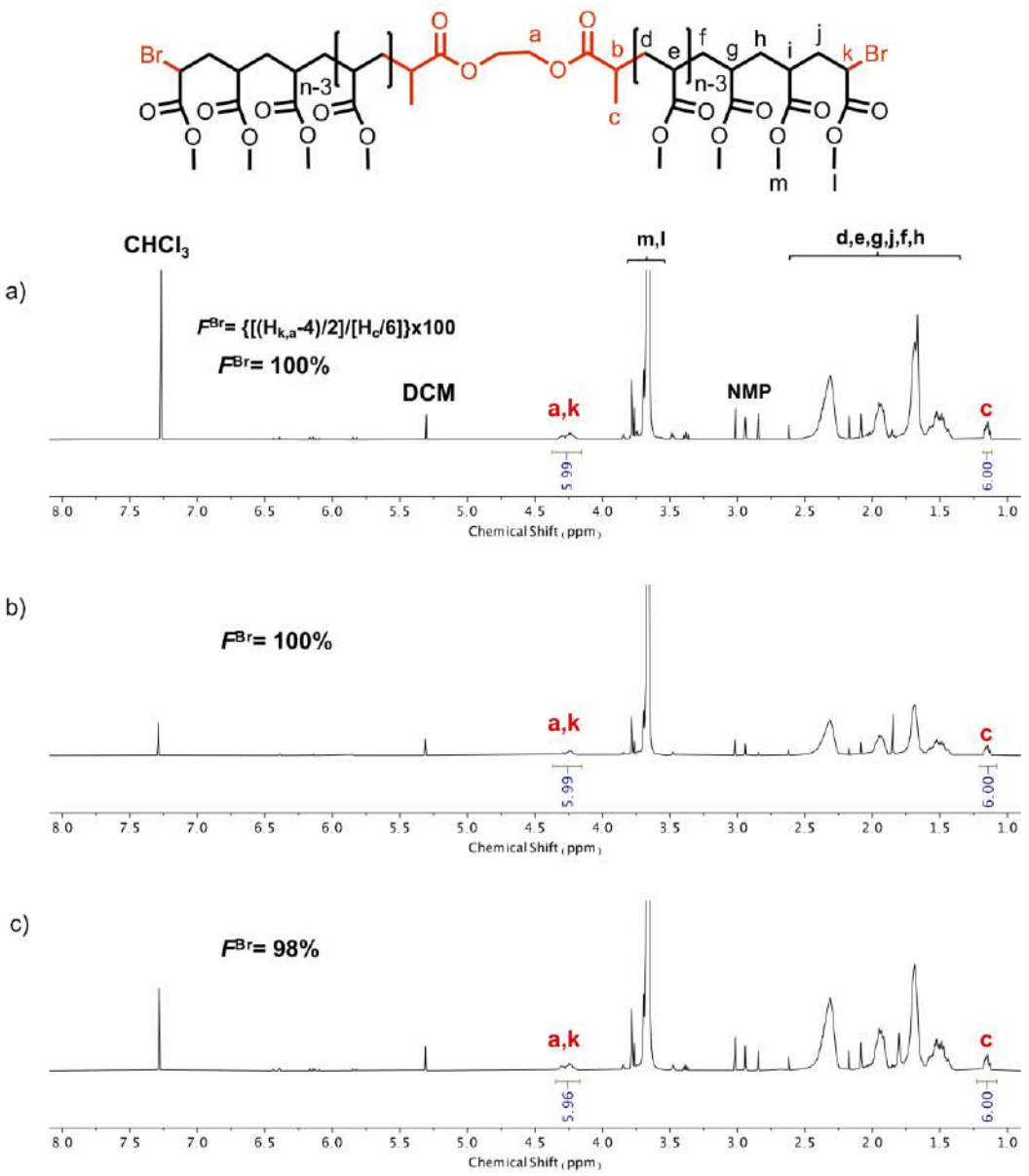

Figure S11. ^{1}H NMR spectra at 400 MHz of α,ω-di(bromo)PMA at (a) 98% monomer conversion (M_n= 6,850 and M_w/M_n= 1.17) ($[MA]_0/[BPE]_0/[Me_6\text{-TREN}]_0$ = 60/1/0.1); (b) 98% monomer conversion (M_n = 4,750 and M_w/M_n= 1.25) ($[MA]_0/[BPE]_0/[Me_6\text{-TREN}]_0/[TREN]_0$ = 60/1/0.05/0.05); (c) 99% monomer conversion (M_n= 6,470 and M_w/M_n =1.33) ($[MA]_0/[BPE]_0/[TREN]_0$ = 60/1/0.1). Polymerization conditions: MA = 1 mL, NMP = 0.4 mL, water = 0.1 mL using 9.0 cm of nonactivated Cu(0) wire 20-gauge wire. The signals at 7.26 ppm and 5.30 ppm are due to partially nondeuterated residue of $CDCl_3$ and dichloromethane, respectively.

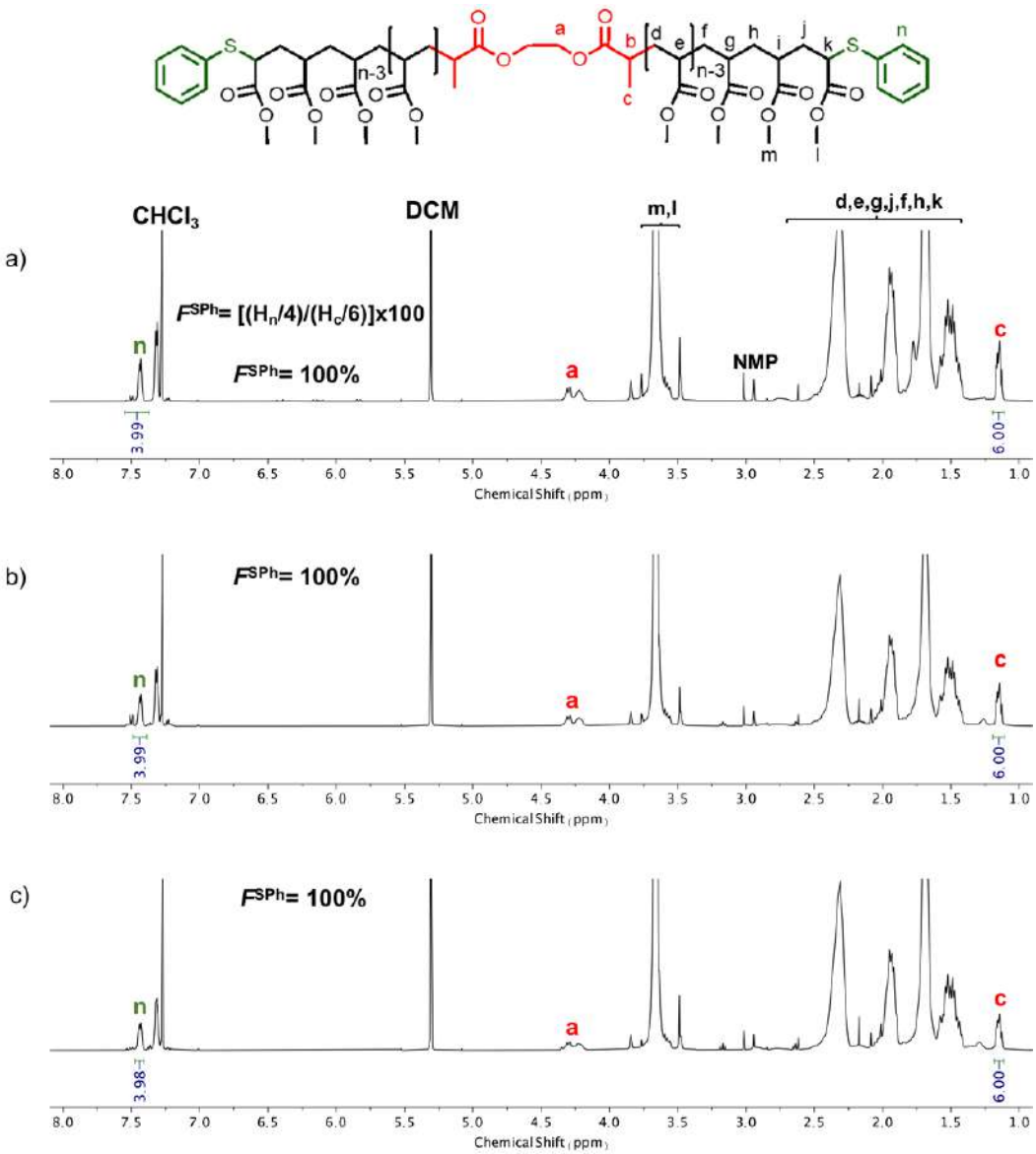

Figure S12. ^{1}H NMR spectra at 400 MHz of α,ω-di(phenylthio)PMA at (a) 98% monomer conversion (M_n= 7,340 and M_w/M_n= 1.17) ($[MA]_0/[BPE]_0/[Me_6\text{-TREN}]_0$ = 60/1/0.1); (b) 98% monomer conversion (M_n = 5,890 and M_w/M_n= 1.29) ($[MA]_0/[BPE]_0/[Me_6\text{-TREN}]_0/[TREN]_0$ = 60/1/0.05/0.05); (c) 99% monomer conversion (M_n= 7,400 and M_w/M_n =1.35) ($[MA]_0/[BPE]_0/[TREN]_0$ = 60/1/0.1). Polymerization conditions: MA = 1 mL, NMP = 0.4 mL, water = 0.1 mL using 9.0 cm of nonactivated Cu(0) wire 20-gauge wire. The signals at 7.26 ppm and 5.30 ppm are due to partially nondeuterated residue of $CDCl_3$ and dichloromethane, respectively.

Supporting Information for Chapter 4.1

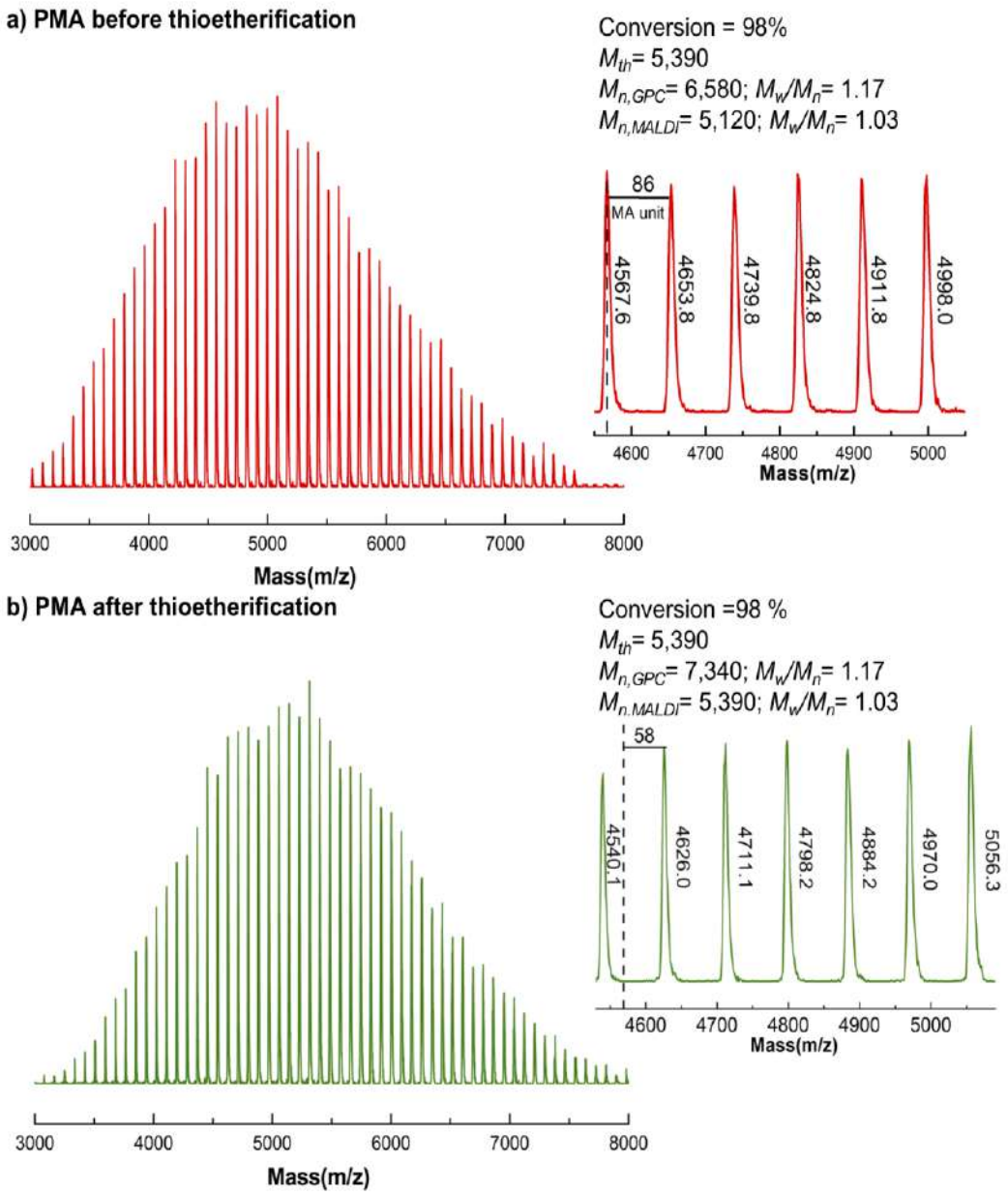

Figure S13. MALDI-TOF of α,ω-di(bromo)PMA isolated at 98% monomer conversion from SET-LRP of MA in NMP/water (8/2, v/v) mixture initiated with BPE and catalyzed by nonactivated Cu(0) wire at 25 °C: (a) before and (b) after "thio-bromo "click". Polymerization conditions: MA = 1 mL, NMP = 0.4 mL, water = 0.1 mL using 9.0 cm of nonactivated Cu(0) wire 20-gauge wire ($[MA]_0/[BPE]_0/[Me_6\text{-}TREN]_0$ = 60/1/0.1). The dotted line in expansion after thioetherification shows the original peak from before thioeterification, while 58 represents the increase in molar mass after thioeterification i.e., 2x[SPh (109. 2) - Br (79.9)] = 58.57 for each chain end.

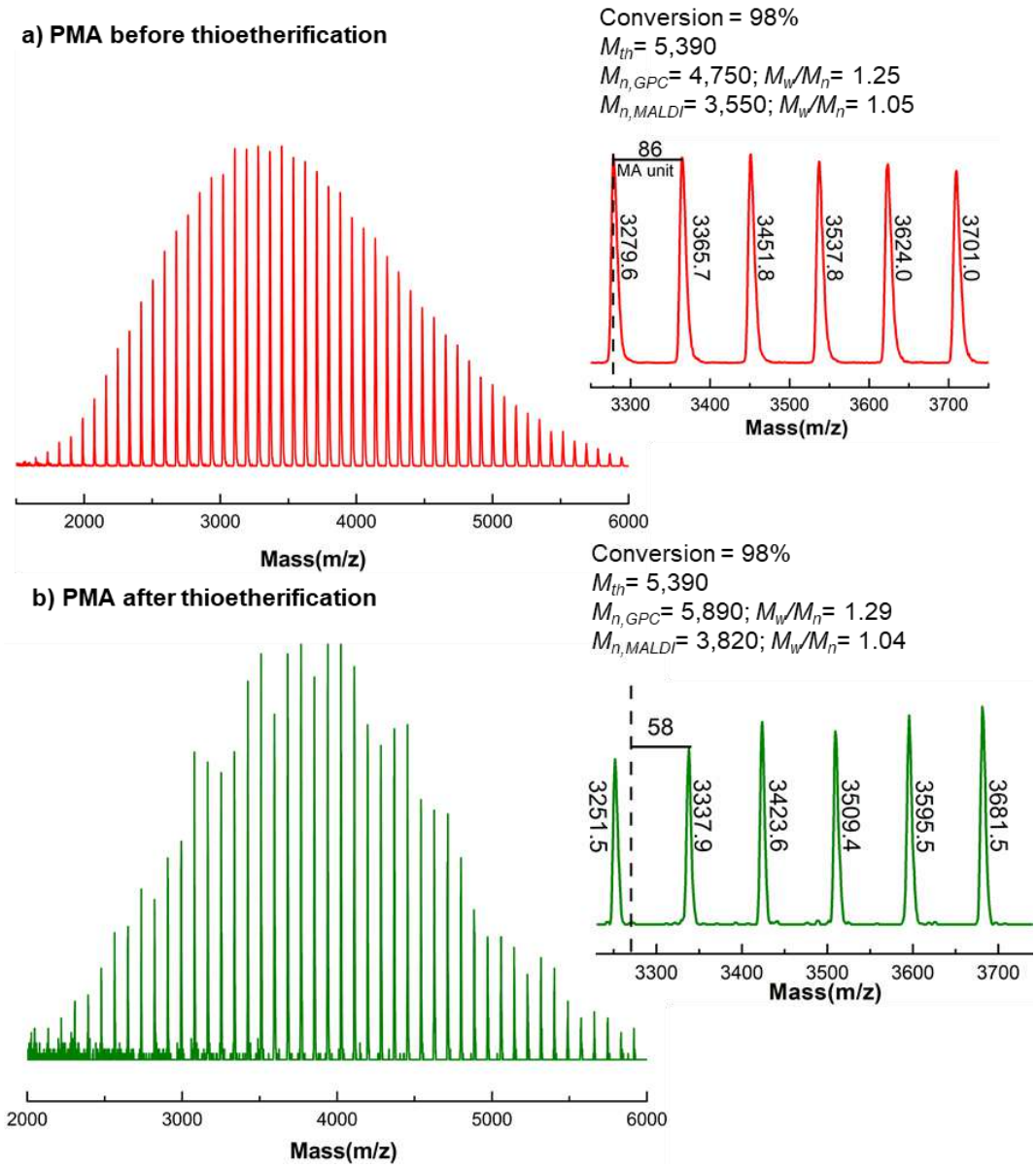

Figure S14. MALDI-TOF of α,ω-di(bromo)PMA isolated at 98% monomer conversion from SET-LRP of MA in NMP/water (8/2, v/v) mixture initiated with BPE and catalyzed by nonactivated Cu(0) wire at 25 °C: (a) before and (b) after "thio-bromo "click". Polymerization conditions: MA = 1 mL, NMP = 0.4 mL, water = 0.1 mL using 9.0 cm of nonactivated Cu(0) wire 20-gauge wire ($[MA]_0/[BPE]_0/[Me_6\text{-}TREN]_0/[TREN]_0$ = 60/1/0.05/0.05). The dotted line in expansion after thioetherification shows the original peak from before thioeterification, while 58 represents the increase in molar mass after thioeterification i.e., 2x[SPh (109. 2) - Br (79.9)] = 58.57 for each chain end.

Supporting Information for Chapter 4.1

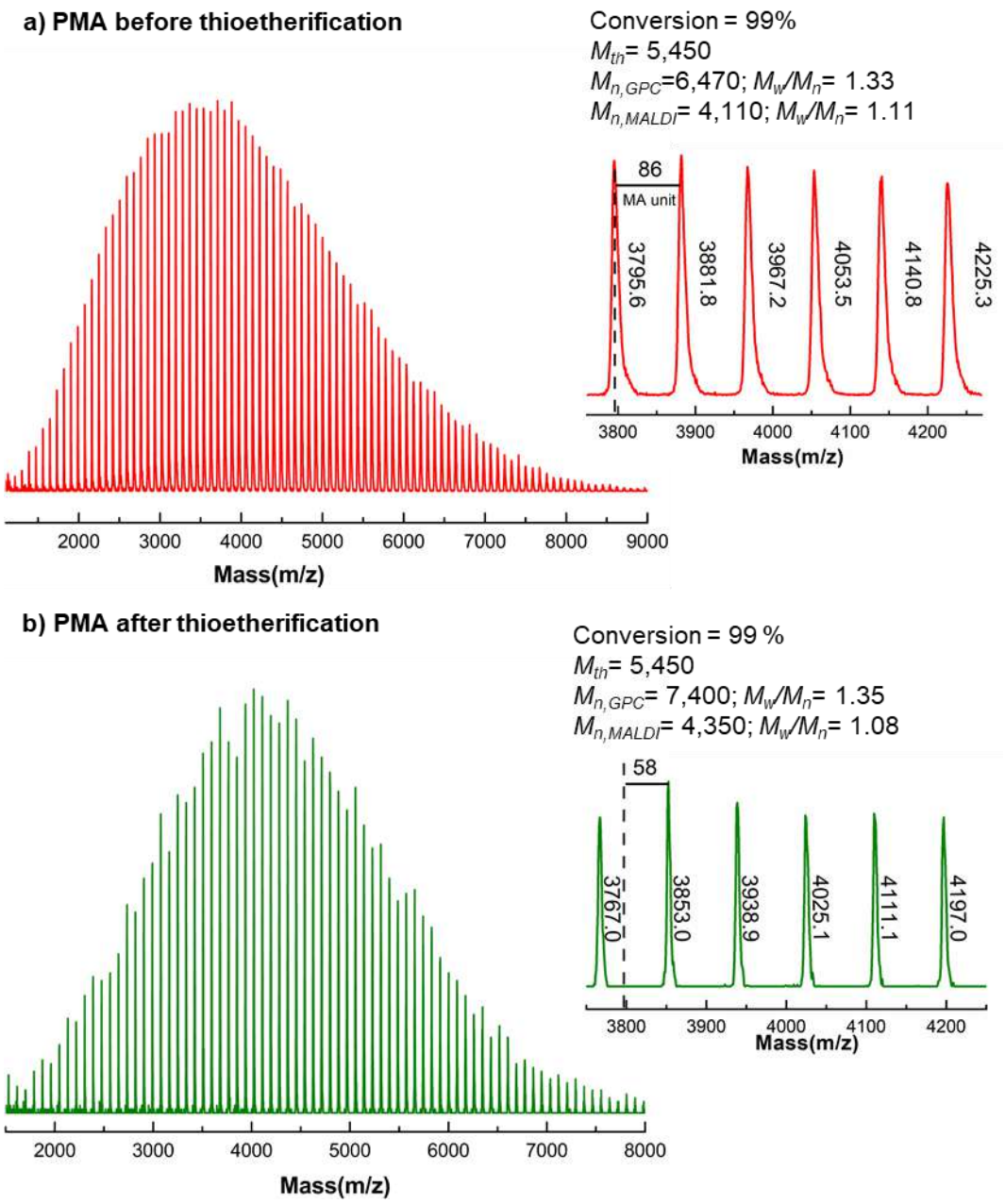

Figure S15. MALDI-TOF of α,ω-di(bromo)PMA isolated at 99% monomer conversion from SET-LRP of MA in NMP/water (8/2, v/v) mixture initiated with BPE and catalyzed by nonactivated Cu(0) wire at 25 °C: (a) before and (b) after "thio-bromo "click". Polymerization conditions: MA = 1 mL, NMP = 0.4 mL, water = 0.1 mL using 9.0 cm of nonactivated Cu(0) wire 20-gauge wire ($[MA]_0/[BPE]_0/[TREN]_0$ = 60/1/0.1). The dotted line in expansion after thioetherification shows the original peak from before thioeterification, while 58 represents the increase in molar mass after thioeterification i.e., 2x[SPh (109. 2) - Br (79.9)] = 58.57 for each chain end.

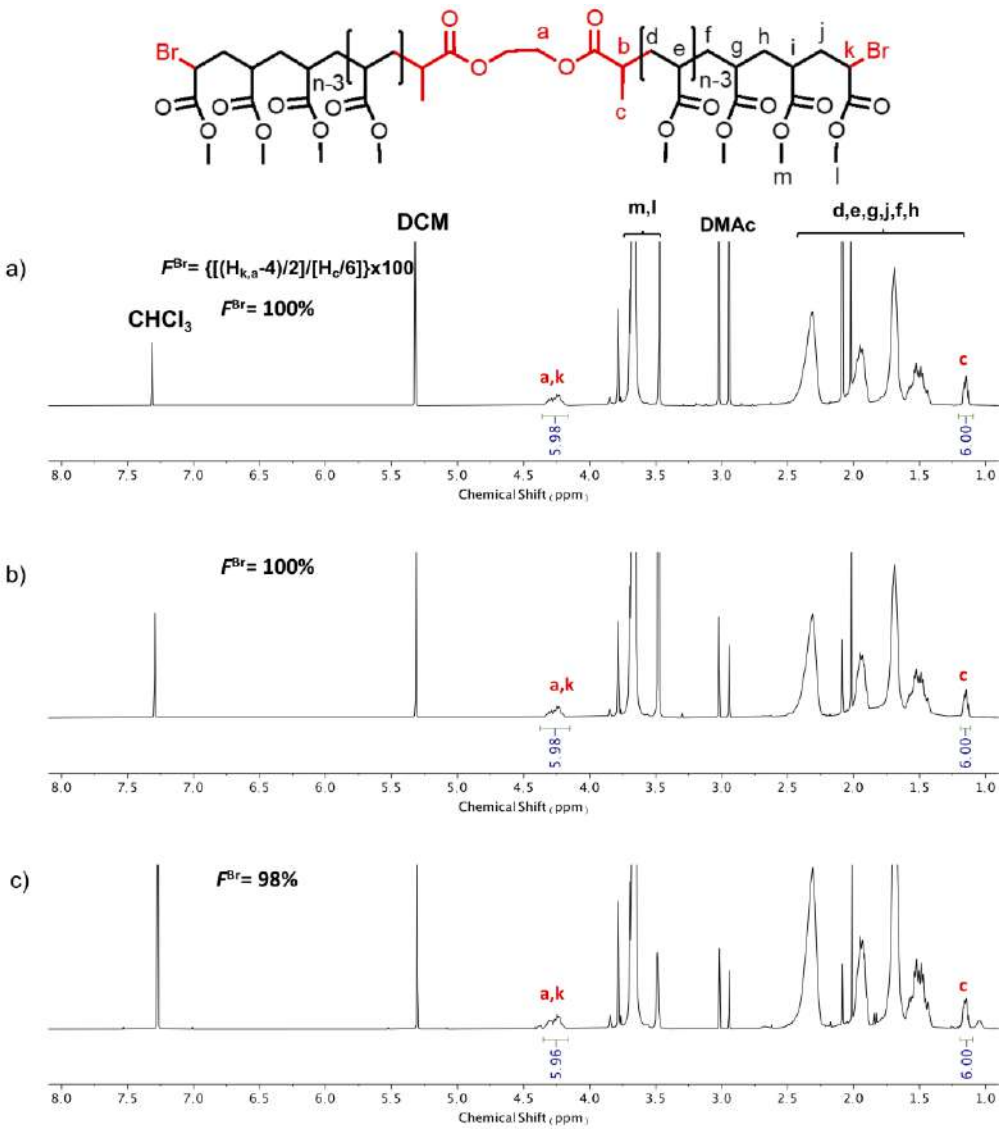

Figure S16. ^{1}H NMR spectra at 400 MHz of α,ω-di(bromo)PMA at (a) 96% monomer conversion (M_n= 6,280 and M_w/M_n= 1.16) ([MA]$_0$/[BPE]$_0$/[Me$_6$-TREN]$_0$ = 60/1/0.1); (b) 98% monomer conversion (M_n = 6,150 and M_w/M_n= 1.29) ([MA]$_0$/[BPE]$_0$/[Me$_6$-TREN]$_0$/[TREN]$_0$ = 60/1/0.05/0.05); (c) 83% monomer conversion (M_n= 4,870 and M_w/M_n =1.95) ([MA]$_0$/[BPE]$_0$/[TREN]$_0$ = 60/1/0.1). Polymerization conditions: MA = 1 mL, DMAc = 0.4 mL, water = 0.1 mL using 9.0 cm of nonactivated Cu(0) wire 20-gauge wire. The signals at 7.26 ppm and 5.30 ppm are due to partially nondeuterated residue of $CDCl_3$ and dichloromethane, respectively.

Supporting Information for Chapter 4.1

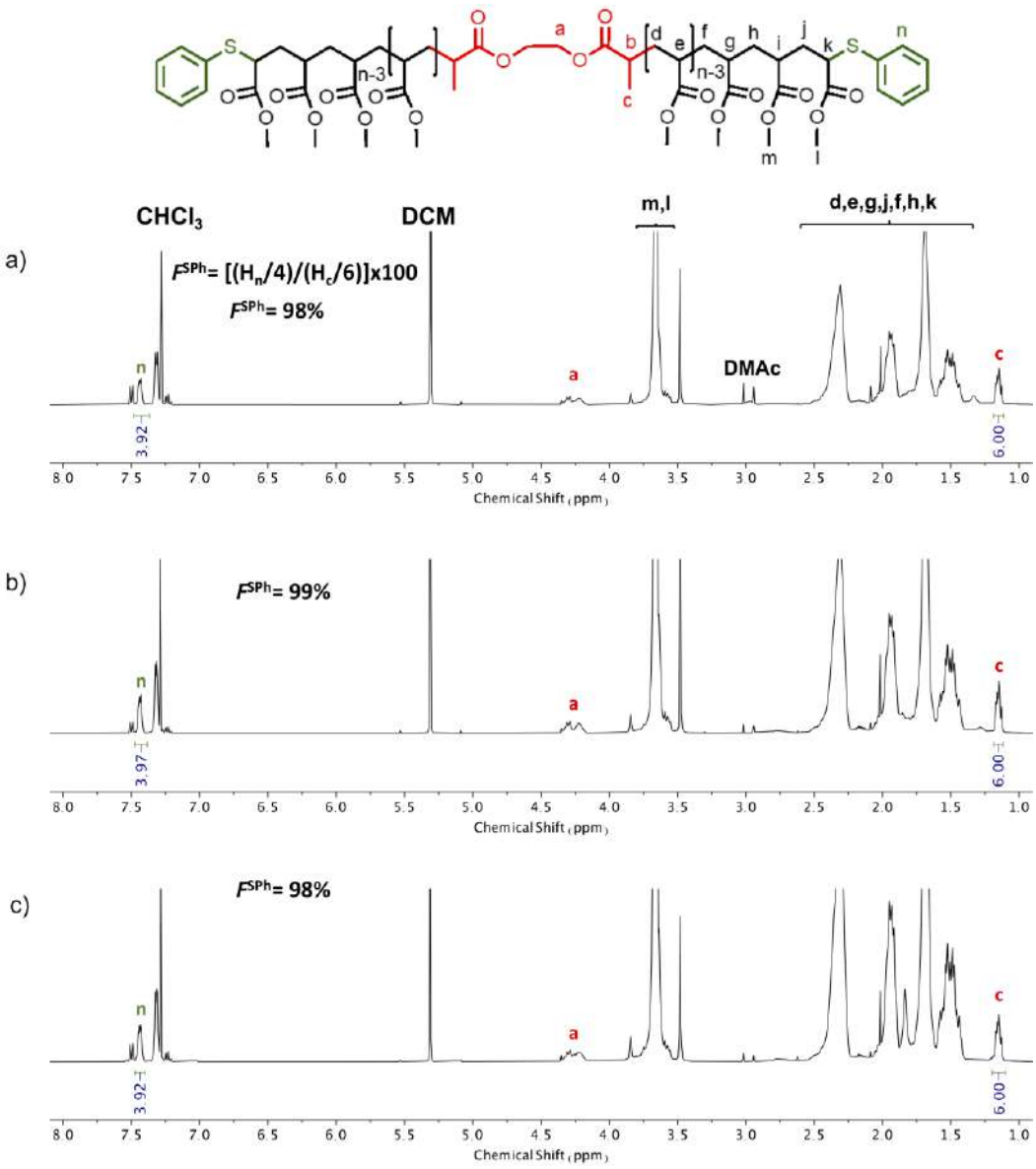

Figure S17. ^{1}H NMR spectra at 400 MHz of α,ω-di(phenylthio)PMA at (a) 96% monomer conversion (M_n= 6,460 and M_w/M_n= 1.17) ($[MA]_0/[BPE]_0/[Me_6\text{-TREN}]_0$ = 60/1/0.1); (b) 98% monomer conversion (M_n = 6,560 and M_w/M_n= 1.30) ($[MA]_0/[BPE]_0/[Me_6\text{-TREN}]_0/[TREN]_0$ = 60/1/0.05/0.05); (c) 83% monomer conversion (M_n= 7,380 and M_w/M_n =1.69) ($[MA]_0/[BPE]_0/[TREN]_0$ = 60/1/0.1). Polymerization conditions: MA = 1 mL, DMAc = 0.4 mL, water = 0.1 mL using 9.0 cm of nonactivated Cu(0) wire 20-gauge wire. The signals at 7.26 ppm and 5.30 ppm are due to partially nondeuterated residue of $CDCl_3$ and dichloromethane, respectively.

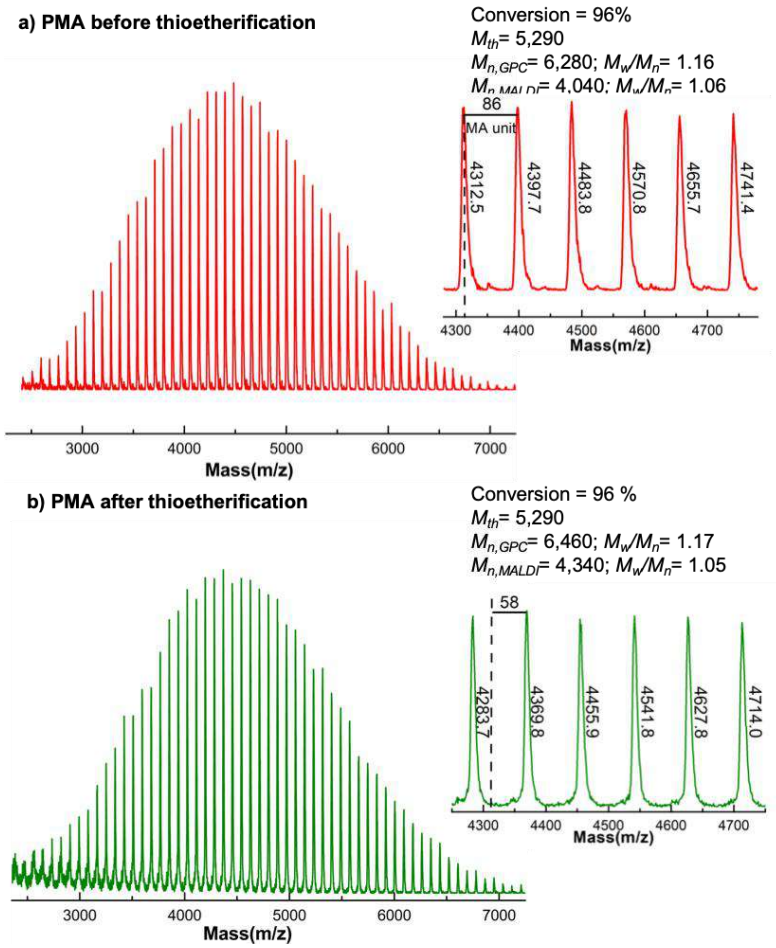

Figure S18. MALDI-TOF of α,ω-di(bromo)PMA isolated at 96% monomer conversion from SET-LRP of MA in DMAc/water (8/2, v/v) mixture initiated with BPE and catalyzed by nonactivated Cu(0) wire at 25 °C: (a) before and (b) after "thio-bromo "click". Polymerization conditions: MA = 1 mL, DMAc = 0.4 mL, water = 0.1 mL using 9.0 cm of nonactivated Cu(0) wire 20-gauge wire ($[MA]_0/[BPE]_0/[Me_6\text{-}TREN]_0$ = 60/1/0.1). The dotted line in expansion after thioetherification shows the original peak from before thioeterification, while 58 represents the increase in molar mass after thioeterification i.e., 2x[SPh (109. 2) - Br (79.9)] = 58.57 for each chain end.

Supporting Information for Chapter 4.1

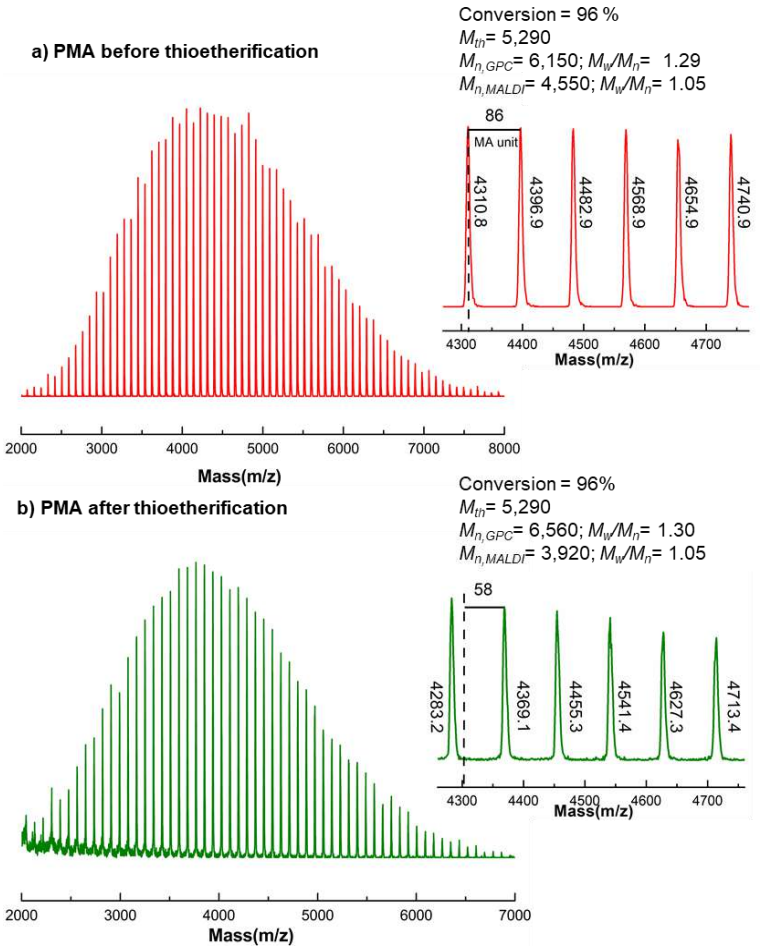

Figure S19. MALDI-TOF of α,ω-di(bromo)PMA isolated at 96% monomer conversion from SET-LRP of MA in DMAc/water (8/2, v/v) mixture initiated with BPE and catalyzed by nonactivated Cu(0) wire at 25 °C: (a) before and (b) after "thio-bromo "click". Polymerization conditions: MA = 1 mL, DMAc = 0.4 mL, water = 0.1 mL using 9.0 cm of nonactivated Cu(0) wire 20-gauge wire ($[MA]_0/[BPE]_0/[Me_6\text{-}TREN]_0/[TREN]_0$ = 60/1/0.05/0.05). The dotted line in expansion after thioetherification shows the original peak from before thioeterification, while 58 represents the increase in molar mass after thioeterification i.e., 2x[SPh (109. 2) - Br (79.9)] = 58.57 for each chain end.

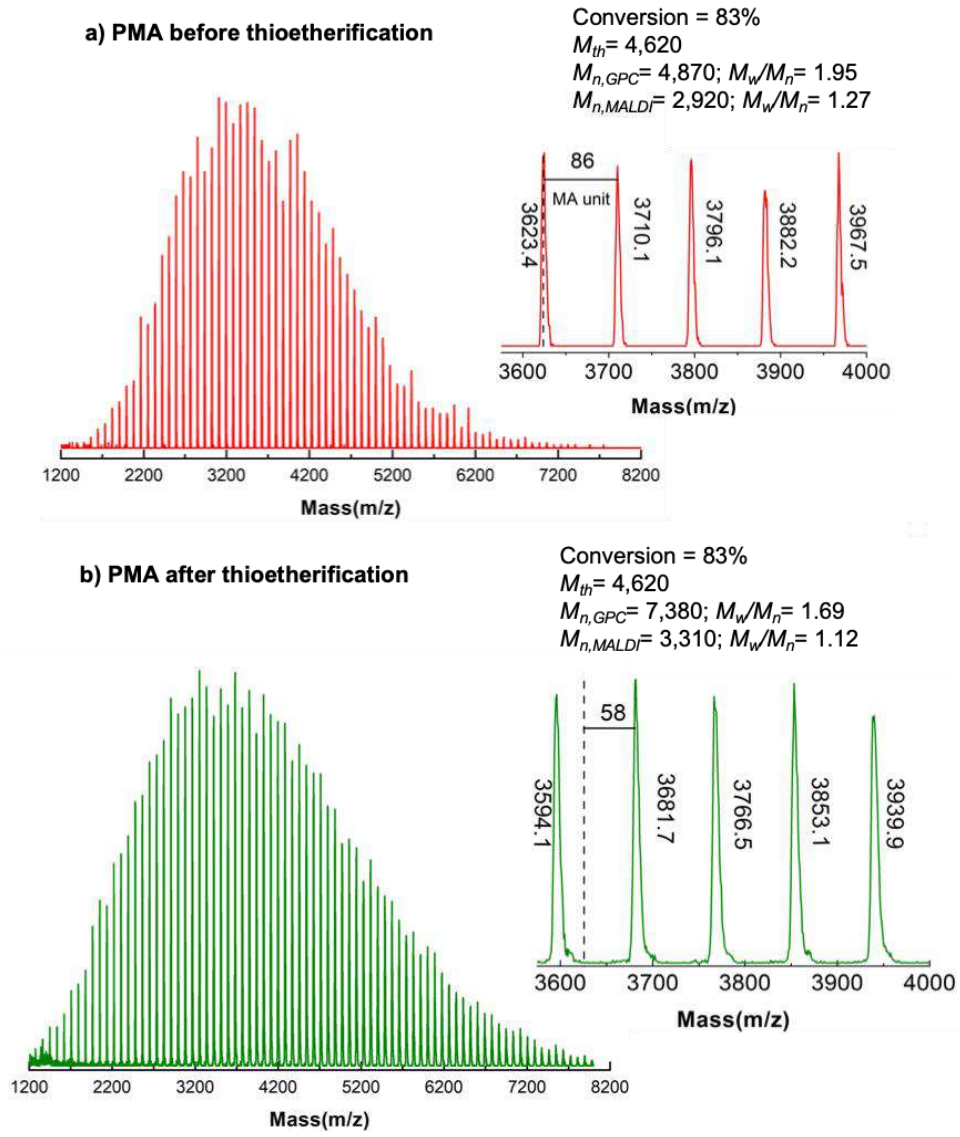

Figure S20. MALDI-TOF of α,ω-di(bromo)PMA isolated at 83% monomer conversion from SET-LRP of MA in DMAc/water (8/2, v/v) mixture initiated with BPE and catalyzed by nonactivated Cu(0) wire at 25 °C: (a) before and (b) after "thio-bromo "click". Polymerization conditions: MA = 1 mL, DMAc = 0.4 mL, water = 0.1 mL using 9.0 cm of nonactivated Cu(0) wire 20-gauge wire ($[MA]_0/[BPE]_0/[Me_6\text{-}TREN]_0$ = 60/1/0.1). The dotted line in expansion after thioetherification shows the original peak from before thioeterification, while 58 represents the increase in molar mass after thioeterification i.e., 2x[SPh (109. 2) - Br (79.9)] = 58.57 for each chain end.

Supporting Information for Chapter 4.1

4. Summary of SET-LRP of MA

Table S1. Dependence of k_p^{app} on the dimension of the Cu(0) wire in the SET-LRP of MA initiated with BPE in DMF/water (8/2,v/v) at 25 °C.[a]

entry	wire length (cm)	reaction conditions	k_p^{app} (min^{-1})	k_p^{app}/ k_p^{app} (TREN)	M_w/M_r	I_{eff} (%)
1	12.5	[MA]/[BPE]/[Me_6-TREN]= 222/1/0.1	0.079	1.4	1.12	79
2	12.5	[MA]/[BPE]/[Me_6-TREN]/[TREN]= 222/1/0.075/0.025	0.086	1.5	1.14	78
3	12.5	[MA]/[BPE]/[Me_6-TREN]/[TREN]= 222/1/0.05/0.05	0.095	1.6	1.21	78
4	12.5	[MA]/[BPE]/[Me_6-TREN]/[TREN]= 222/1/0.025/0.075	0.084	1.4	1.23	80
5	12.5	[MA]/[BPE]/[TREN]= 222/1/0.1	0.058	1.0	1.36	79
6	9.0	[MA]/[BPE]/[Me_6-TREN]= 222/1/0.1	0.055	1.0	1.09	76
7	9.0	[MA]/[BPE]/[Me_6-TREN]/[TREN]= 222/1/0.075/0.025	0.057	1.0	1.08	82
8	9.0	[MA]/[BPE]/[Me_6-TREN]/[TREN]= 222/1/0.05/0.05	0.082	1.5	1.09	87
9	9.0	[MA]/[BPE]/[Me_6-TREN]/[TREN]= 222/1/0.025/0.075	0.063	1.1	1.13	78
10	9.0	[MA]/[BPE]/[TREN]= 222/1/0.1	0.055	1.0	1.25	66
11	4.0	[MA]/[BPE]/[Me_6-TREN]= 222/1/0.1	0.038	1.1	1.14	81
12	4.0	[MA]/[BPE]/[Me_6-TREN]/[TREN]= 222/1/0.075/0.025	0.044	1.3	1.14	82
13	4.0	[MA]/[BPE]/[Me_6-TREN]/[TREN]= 222/1/0.05/0.05	0.051	1.4	1.16	86
14	4.0	[MA]/[BPE]/[Me_6-TREN]/[TREN]= 222/1/0.025/0.075	0.048	1.4	1.28	66
15	4.0	[MA]/[BPE]/[TREN]= 222/1/0.1	0.035	1.0	1.40	51

[a] Reaction conditions: monomer = 1 mL; solvent + water = 0.5 mL. The v/v ratio must be multiplied by 10 to obtain % solvent/% water. The value of v + v must be divided by 20 to obtain the total volume of solvents, 0.5 mL.

Table S2. Dependence of k_p^{app} on the dimension of the Cu(0) wire in the SET-LRP of MA initiated with BPE in NMP/water(8/2,v/v) at 25 °C.[a]

entry	wire length (cm) 20 G	reaction conditions	k_p^{app} (min^{-1})	k_p^{app}/ k_p^{app} (TREN)	M_w/M_r	I_{eff} (%)
1	9.0	[MA]/[BPE]/[Me_6-TREN]= 222/1/0.1	0.068	1.1	1.08	75
2	9.0	[MA]/[BPE]/[Me_6-TREN]/[TREN]= 222/1/0.075/0.025	0.078	1.3	1.15	87
3	9.0	[MA]/[BPE]/[Me_6-TREN]/[TREN]= 222/1/0.05/0.05	0.080	1.3	1.18	85
4	9.0	[MA]/[BPE]/[Me_6-TREN]/[TREN]= 222/1/0.025/0.075	0.076	1.3	1.21	96
5	9.0	[MA]/[BPE]/[TREN]= 222/1/0.1	0.060	1.0	1.42	77

[a] Reaction conditions: monomer = 1 mL; solvent + water = 0.5 mL. The v/v ratio must be multiplied by 10 to obtain % solvent/% water. The value of v + v must be divided by 20 to obtain the total volume of solvents, 0.5 mL.

Table S3. Dependence of k_p^{app} on the dimension of the Cu(0) wire in the SET-LRP of MA initiated with BPE in DMAc/water(8/2,v/v) at 25 °C.[a]

entry	wire length (cm)	reaction conditions	k_p^{app} (min^{-1})	k_p^{app}/ k_p^{app} (TREN)	M_w/M_r	I_{eff} (%)
1	9.0	[MA]/[BPE]/[Me_6-TREN]= 222/1/0.1	0.076	1.1	1.11	78
2	9.0	[MA]/[BPE]/[Me_6-TREN]/[TREN]= 222/1/0.075/0.025	0.077	1.1	1.16	83
3	9.0	[MA]/[BPE]/[Me_6-TREN]/[TREN]= 222/1/0.05/0.05	0.091	1.3	1.29	87
4	9.0	[MA]/[BPE]/[Me_6-TREN]/[TREN]= 222/1/0.025/0.075	0.075	1.0	1.36	87
5	9.0	[MA]/[BPE]/[TREN]= 222/1/0.1	0.071	1.0	2.14	60

[a] Reaction conditions: monomer = 1 mL; solvent + water = 0.5 mL. The v/v ratio must be multiplied by 10 to obtain % solvent/% water. The value of v + v must be divided by 20 to obtain the total volume of solvents, 0.5 mL.

Annex E

Supplementary Information for

The Me_6-TREN/TREN mixed-ligand effect during SET-LRP in the catalytically active DMSO revitalizes TREN into an excellent ligand

Table of contents

Supporting Information for Chapter 4.2

1. Kinetic plots, molecular weight and polydispersity evolutions for the SET-LRP of MA

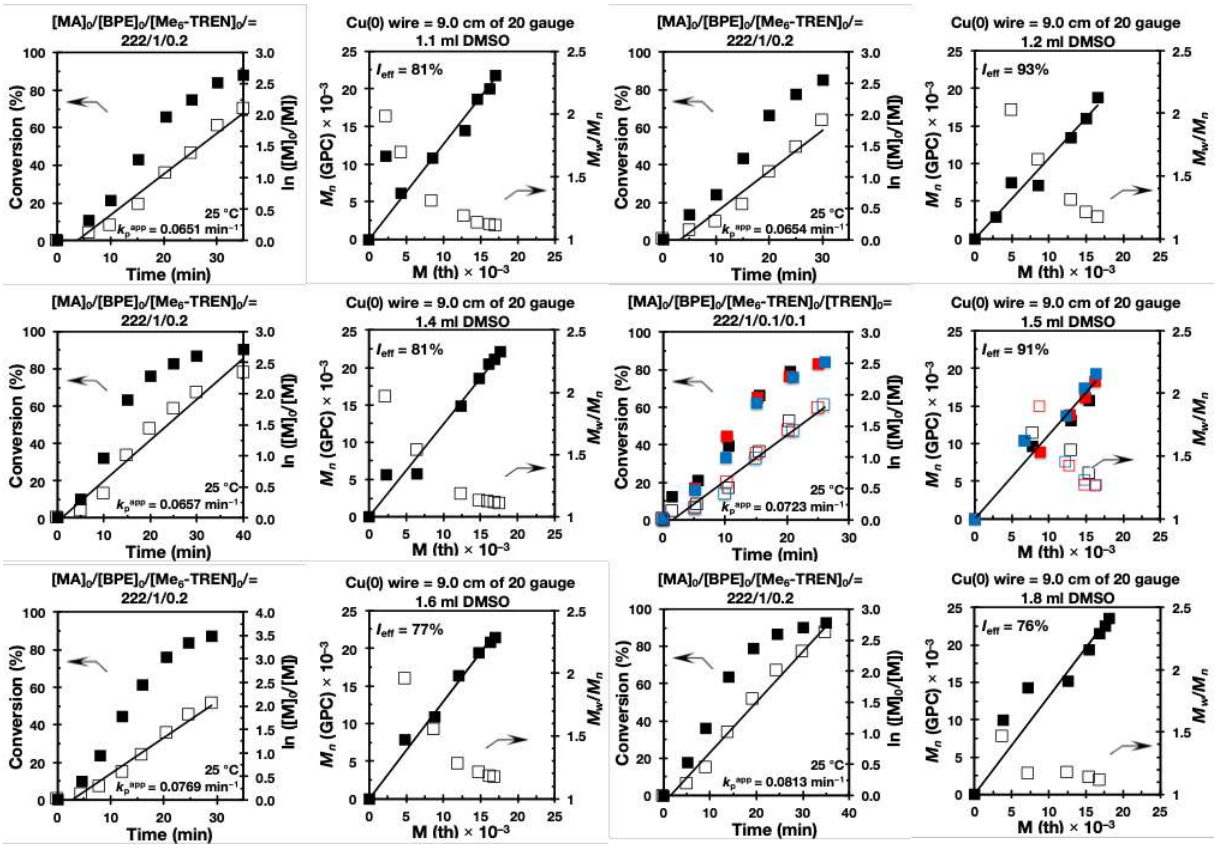

Figure S1. Kinetic plots, molecular weight and dispersity evolutions for the SET-LRP of MA in DMSO, initiated with BPE and catalyzed by 9.0 cm non-activated Cu(0) wire at 25 °C. Experimental data in different colors were obtained from different kinetics experiments, sometimes performed by different researchers. k_p^{app} and I_{eff} are the average values of three experiments. ln(k_p^{app}) *vs* ln([DMSO]$_0$), DMSO was varied from 1 to 1.8 mL with 2 mL of MA. [MA]$_0$/[BPE]$_0$/[Me$_6$-TREN]$_0$/[Cu(0)]$_0$ = 222/1/0.2/9cm.

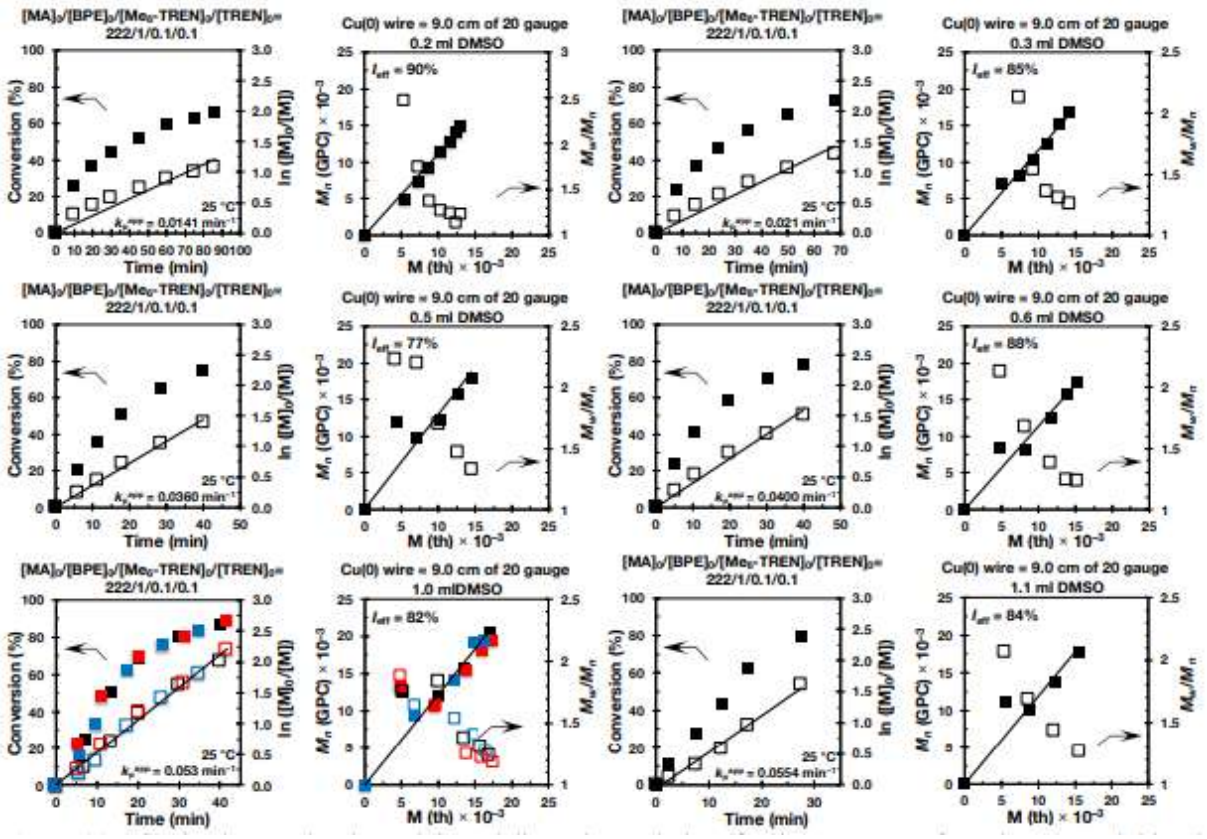

Figure S2. Kinetic plots, molecular weight and dispersity evolutions for the SET-LRP of MA in DMSO, initiated with BPE and catalyzed by 9.0 cm non-activated Cu(0) wire at 25 °C. Experimental data in different colors were obtained from different kinetics experiments, sometimes performed by different researchers. k_p^{app} and I_{eff} are the average values of three experiments. $\ln(k_p^{app})$ *vs* $\ln([DMSO]_0)$, DMSO was varied from 0.2 to 1.1 mL with 2 mL of MA. $[MA]_0/[BPE]_0/[Me_6\text{-}TREN]_0/[TREN]_0/[Cu(0)]_0$ = 222/1/0.1/0.1/9 cm.

Supporting Information for Chapter 4.2

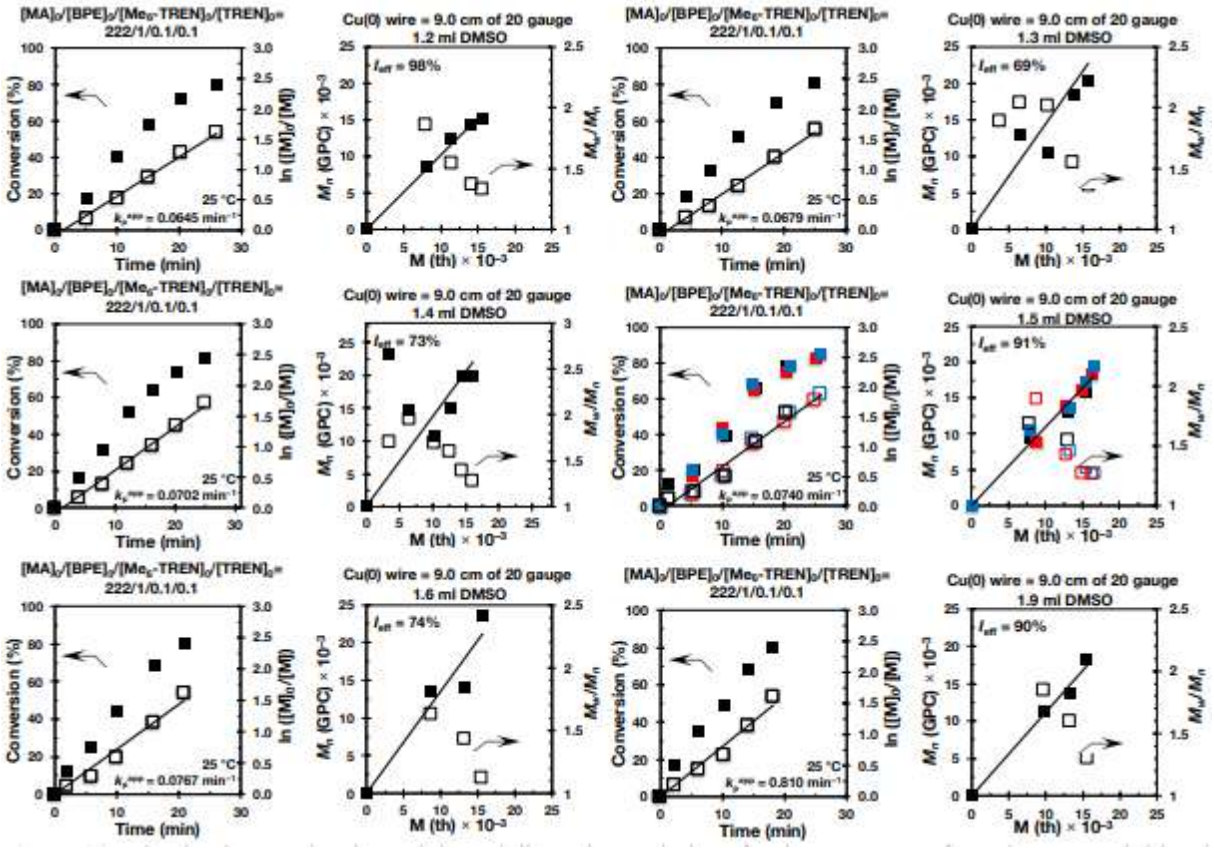

Figure S3. Kinetic plots, molecular weight and dispersity evolutions for the SET-LRP of MA in DMSO, initiated with BPE and catalyzed by 9.0 cm non-activated Cu(0) wire at 25 °C. Experimental data in different colors were obtained from different kinetics experiments, sometimes performed by different researchers. k_p^{app} and I_{eff} are the average value of three experiments. ln(k_p^{app}) *vs* ln([DMSO]$_0$), DMSO was varied from 1.2 to 1.9 mL with 2 mL of MA. [MA]$_0$/[BPE]$_0$/[Me$_6$-TREN]$_0$/[TREN]$_0$/[Cu(0)]$_0$ = 222/1/0.1/0.1/9cm.

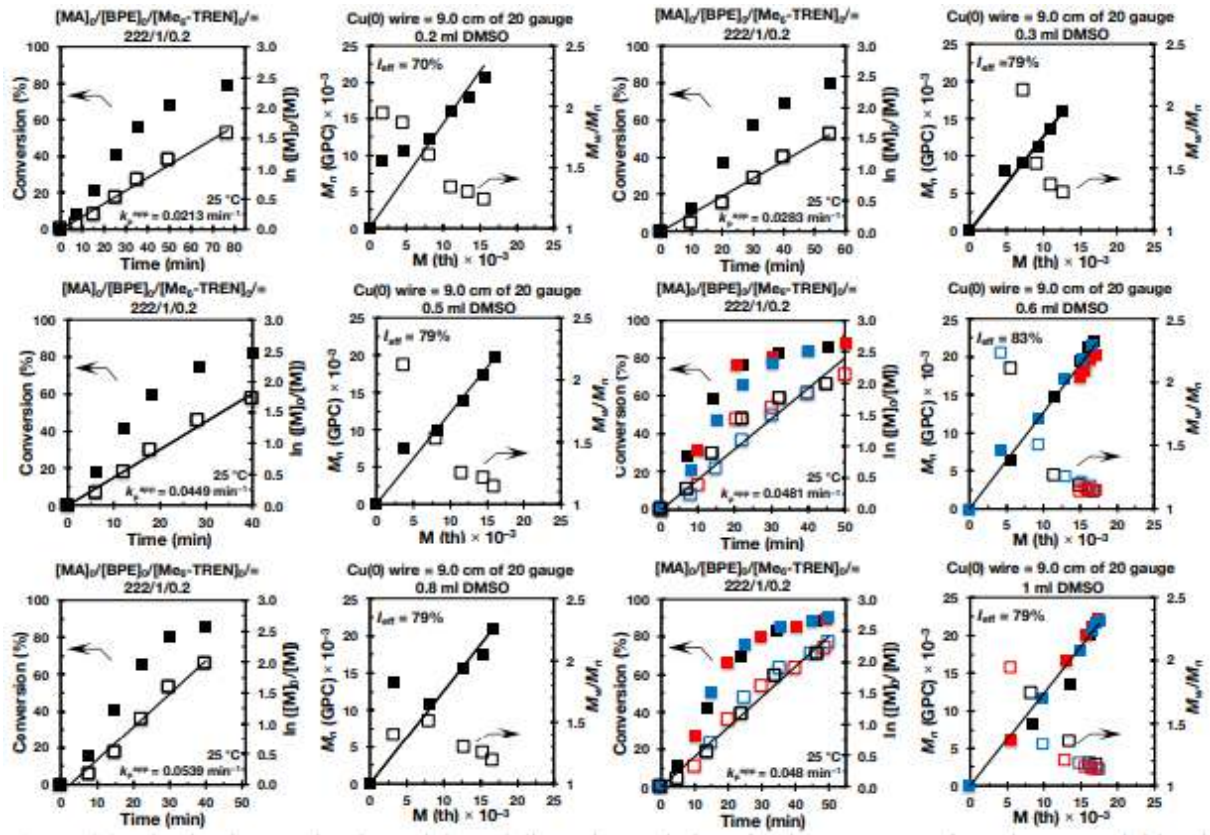

Figure S4. Kinetic plots, molecular weight and dispersity evolutions for the SET-LRP of MA in DMSO, initiated with BPE and catalyzed by 9.0 cm non-activated Cu(0) wire at 25 °C. Experimental data in different colors were obtained from different kinetics experiments, sometimes performed by different researchers. k_p^{app} and I_{eff} are the average value of three experiments. ln(k_p^{app}) vs ln([DMSO]$_0$), DMSO was varied from 0.2 to 1 mL with 2 mL of MA. [MA]$_0$/[BPE]$_0$/[Me$_6$-TREN]$_0$/[Cu(0)]$_0$ = 222/1/0.2/9cm.

Supporting Information for Chapter 4.2

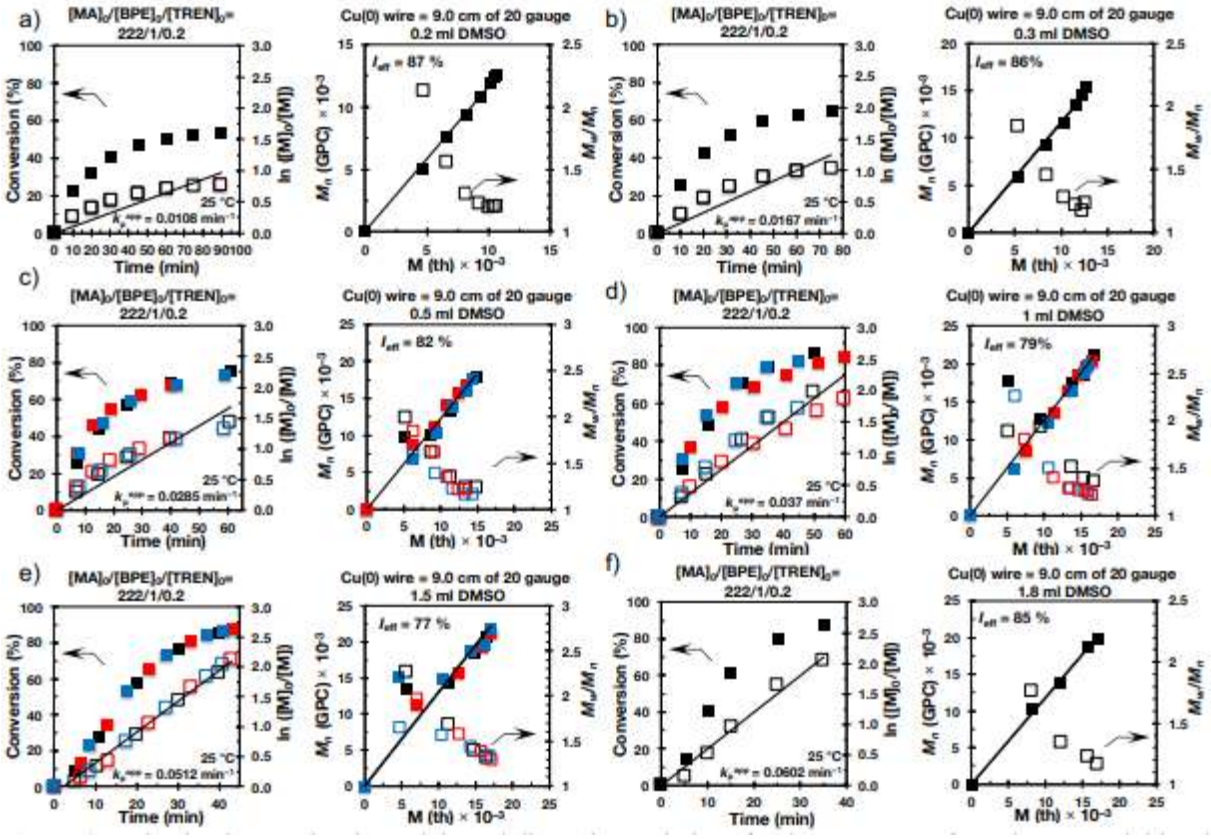

Figure S5. Kinetic plots, molecular weight and dispersity evolutions for the SET-LRP of MA in DMSO, initiated with BPE and catalyzed by 9.0 cm non-activated Cu(0) wire at 25 °C. Experimental data in different colors were obtained from different kinetics experiments, sometimes performed by different researchers. k_p^{app} and I_{eff} are the average value of three experiments. ln(k_p^{app}) vs ln([DMSO]$_0$), DMSO was varied from 0.2 to 1.8 mL with 2 mL of MA. [MA]$_0$/[BPE]$_0$/[TREN]$_0$/[Cu(0)]$_0$ = 222/1/0.2/9cm.

2. ^{1}H NMR and MALDI-TOF spectra of PMA obtained by SET-LRP

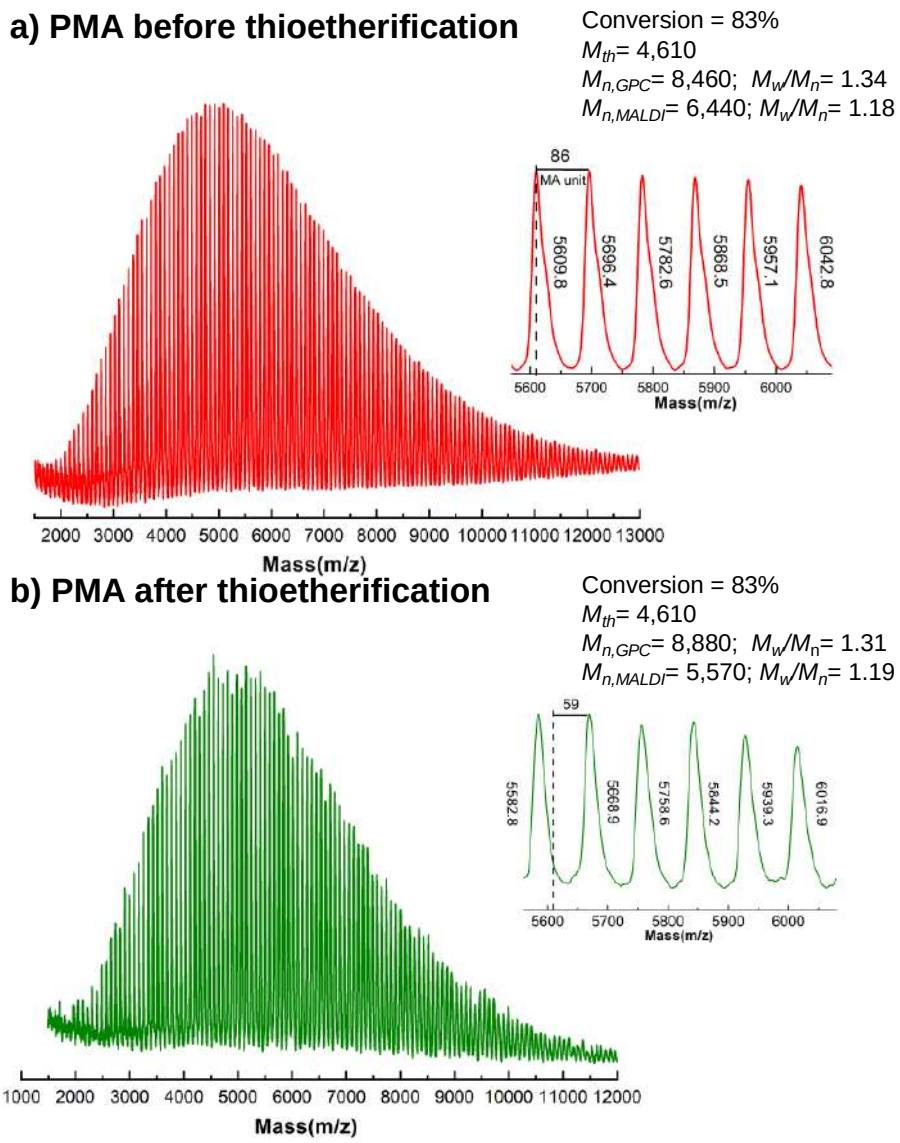

Figure S6. MALDI-TOF of PMA-Br isolated at 83% from SET-LRP of MA in DMSO solution initiated with BPE and catalyzed by non-activated Cu(0) wire at 25 °C; (a) before thio-bromo "click" reaction; (b) after thio-bromo "click" reaction. Reaction conditions: MA = 2 mL, DMSO = 1.50 mL, $[MA]_0/[BPE]_0/[Me_6\text{-TREN}]_0$ = 60/1/0.2, 9.0 cm of 20 gauge Cu(0) wire. The dotted line in expansion after thioeterification shows the original peak from before thioeterification, while 59 represents the increase in molar mass after thioeterification i.e., 2*[SC_6H_5 (109, 2)–Br (79, 9)] = 58.57 for each chain end.

Supporting Information for Chapter 4.2

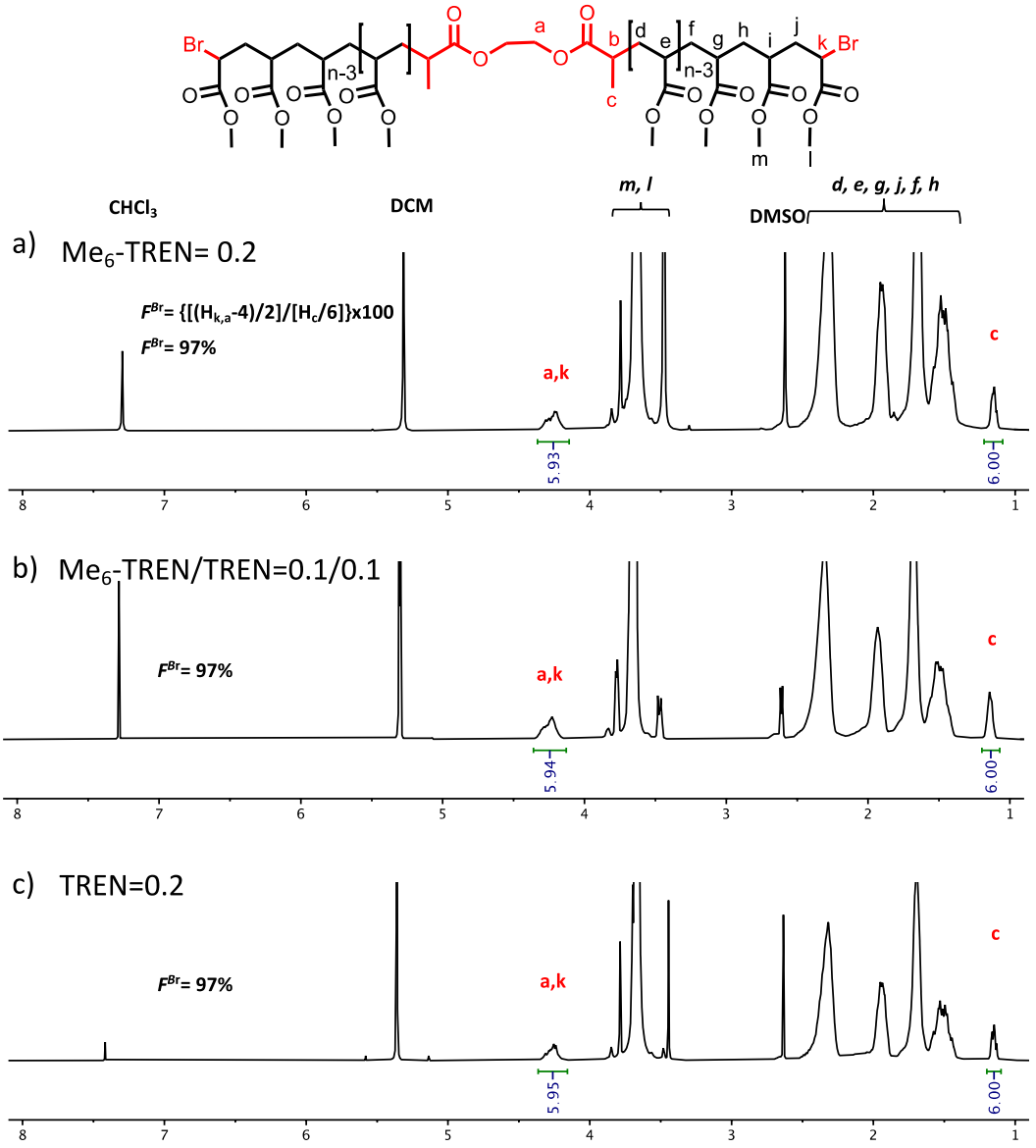

Figure S7. ^{1}H NMR spectra at 400 MHz of α,ω-di(bromo)PMA at: (a) 83% conversion (M_n= 8,460 and M_w/M_n= 1.34), ([MA]$_0$/[BPE]$_0$/[Me$_6$-TREN]$_0$ = 60/1/0.2); (b) 92% conversion (M_n = 6,420 and M_w/M_n= 1.27) ([MA]$_0$/[BPE]$_0$/[Me$_6$-TREN]$_0$/[TREN]$_0$ = 60/1/0.1/0.1); (c) 95% conversion (M_n= 7,690 and M_w/M_n =1.15) ([MA]$_0$/[BPE]$_0$/[TREN]$_0$ = 60/1/0.2); Polymerization conditions: MA = 2 mL, DMSO = 1.5 mL and non-activated 9 cm Cu(0) wire of 20 gauge. The signals at 7.26 ppm and 5.30 ppm are due to the partially non-deuterated residues of $CDCl_3$ and dichloromethane, respectively.

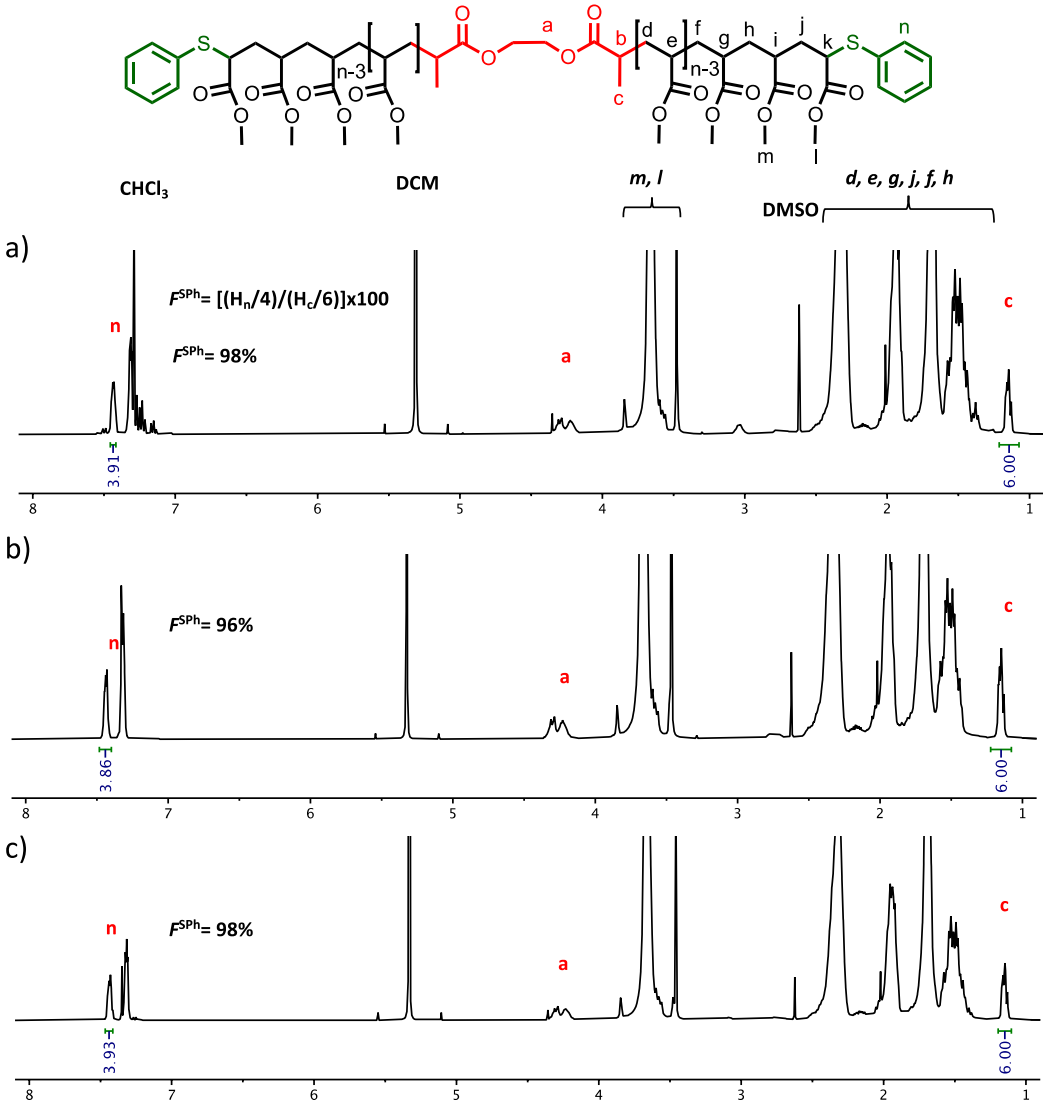

Figure S8. ^{1}H NMR spectra at 400 MHz of α,ω-di(phenylthio)PMA at: (a) 83% conversion (M_n= 8,880 and M_w/M_n= 1.19), ($[MA]_0/[BPE]_0/[Me_6\text{-TREN}]_0$ = 60/1/0.2); (b) 90% conversion (M_n = 7,140 and M_w/M_n= 1.27), ($[MA]_0/[BPE]_0/[Me_6\text{-TREN}]_0/[TREN]_0$ = 60/1/0.1/0.1); (c) 96% conversion (M_n= 8,180 and M_w/M_n =1.13), ($[MA]_0/[BPE]_0/[TREN]_0$ = 60/1/0.2); Polymerization conditions: MA = 2 mL, DMSO = 1.5 mL and non-activated 9 cm Cu(0) wire of 20 gauge. The signals at 7.26 ppm and 5.30 ppm are due to the partially non-deuterated residues of $CDCl_3$ and dichloromethane, respectively.

Supporting Information for Chapter 4.2

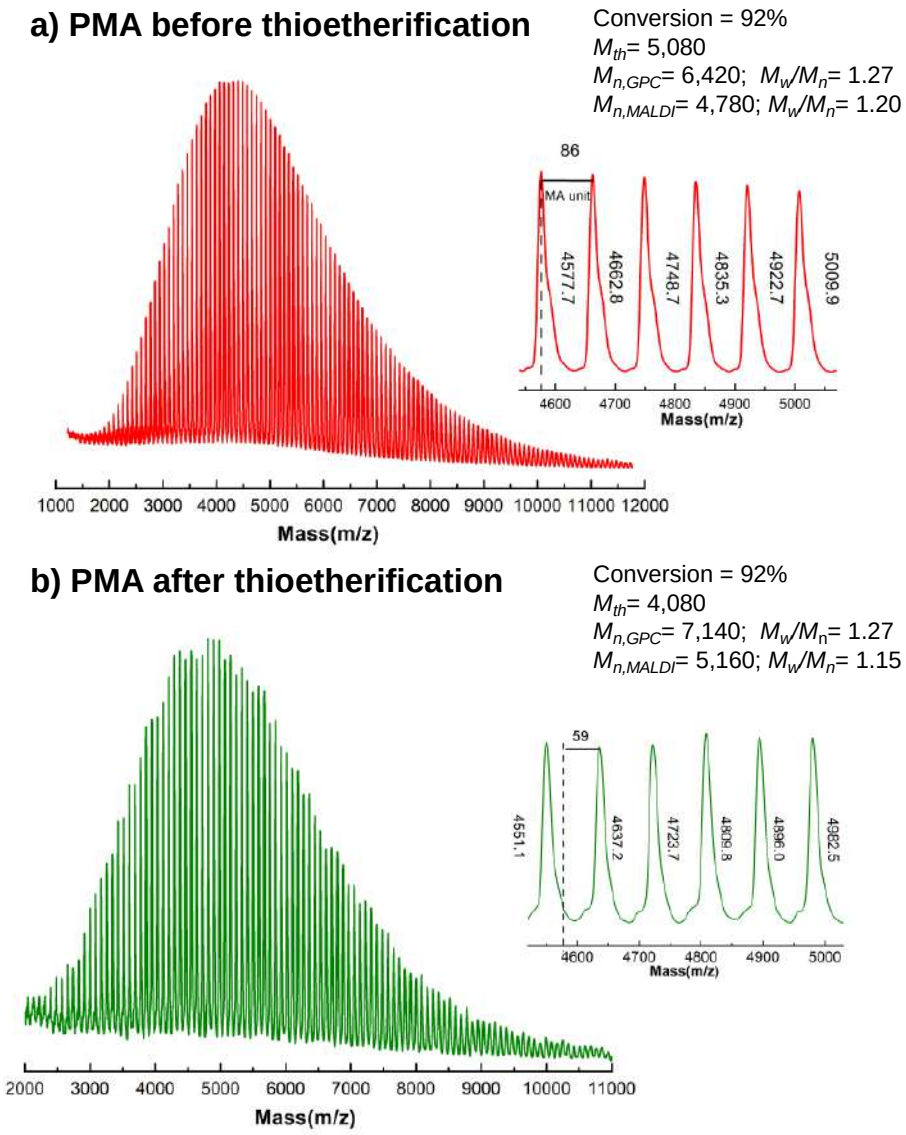

Figure S9. MALDI-TOF of PMA-Br isolated at 92% from SET-LRP of MA in DMSO solution initiated with BPE and catalyzed by non-activated Cu(0) wire at 25 °C; (a) before thio-bromo "click" reaction; (b) After thio-bromo "click" reaction. Reaction conditions: MA = 2 mL, DMSO = 1.50 mL, $[MA]_0/[BPE]_0/[Me_6\text{-TREN}]_0/[TREN]_0$ = 60/1/0.1/0.1, 9.0 cm of 20 gauge Cu(0) wire. The dotted line in expansion after thioeterification shows the original peak from before thioeterification, while 59 represents the increase in molar mass after thioeterification i.e., 2*[SC_6H_5 (109, 2)–Br (79, 9)] = 58.57 for each chain end.

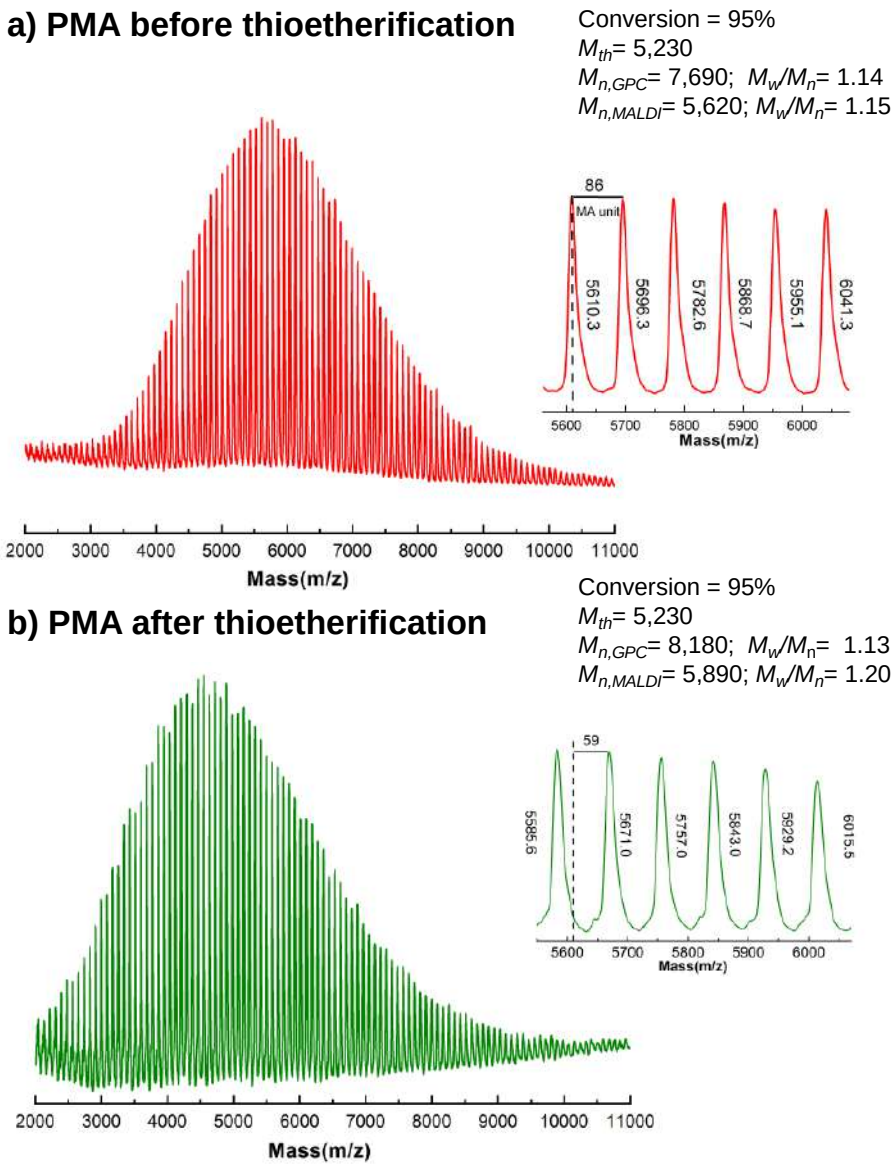

Figure S10. MALDI-TOF of PMA-Br isolated at 95% from SET-LRP of MA in DMSO solution initiated with BPE and catalyzed by non-activated Cu(0) wire at 25 °C; (a) before thio-bromo "click" reaction; (b) after thio-bromo "click" reaction. Reaction conditions: MA = 2 mL, DMSO = 1.50 mL, $[MA]_0/[BPE]_0/[TREN]_0$ = 60/1/0.2, 9.0 cm of 20 gauge Cu(0) wire. The dotted line in expansion after thioeterification shows the original peak from before thioeterification, while 59 represents the increase in molar mass after thioeterification i.e., 2*[SC_6H_5 (109, 2)–Br (79, 9)] = 58.57 for each chain end.

UNIVERSITAT
ROVIRA i VIRGILI